Aalto University School of Science and Technology
Faculty of Engineering and Architecture
Department of Applied Mechanics **Series AM**
Aalto Yliopisto Teknillinen korkeakoulu
Insinööritieteiden ja arkkitehtuurin tiedekunta
Sovelletun mekaniikan laitos **Sarja AM**
Espoo 2010 TKK - AM - 16

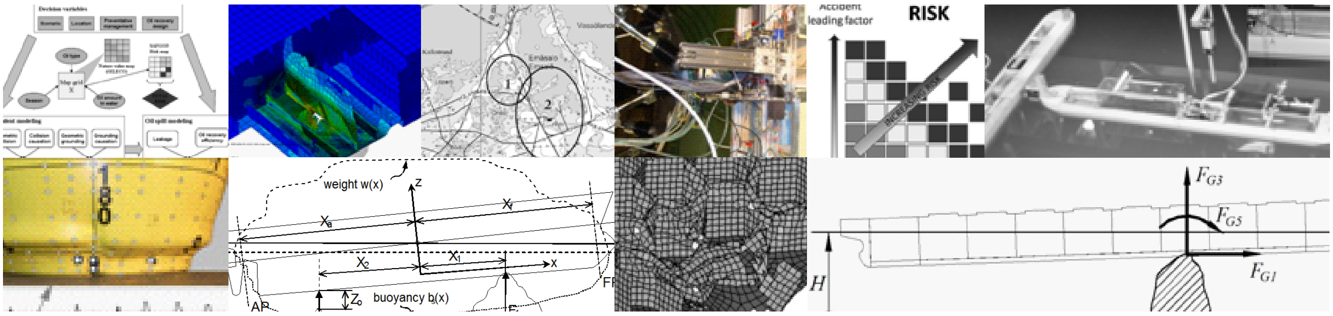

5th International Conference on Collision and Grounding of Ships

June 14th - 16th 2010 Espoo, Finland

Edited by
Sören Ehlers, Jani Romanoff

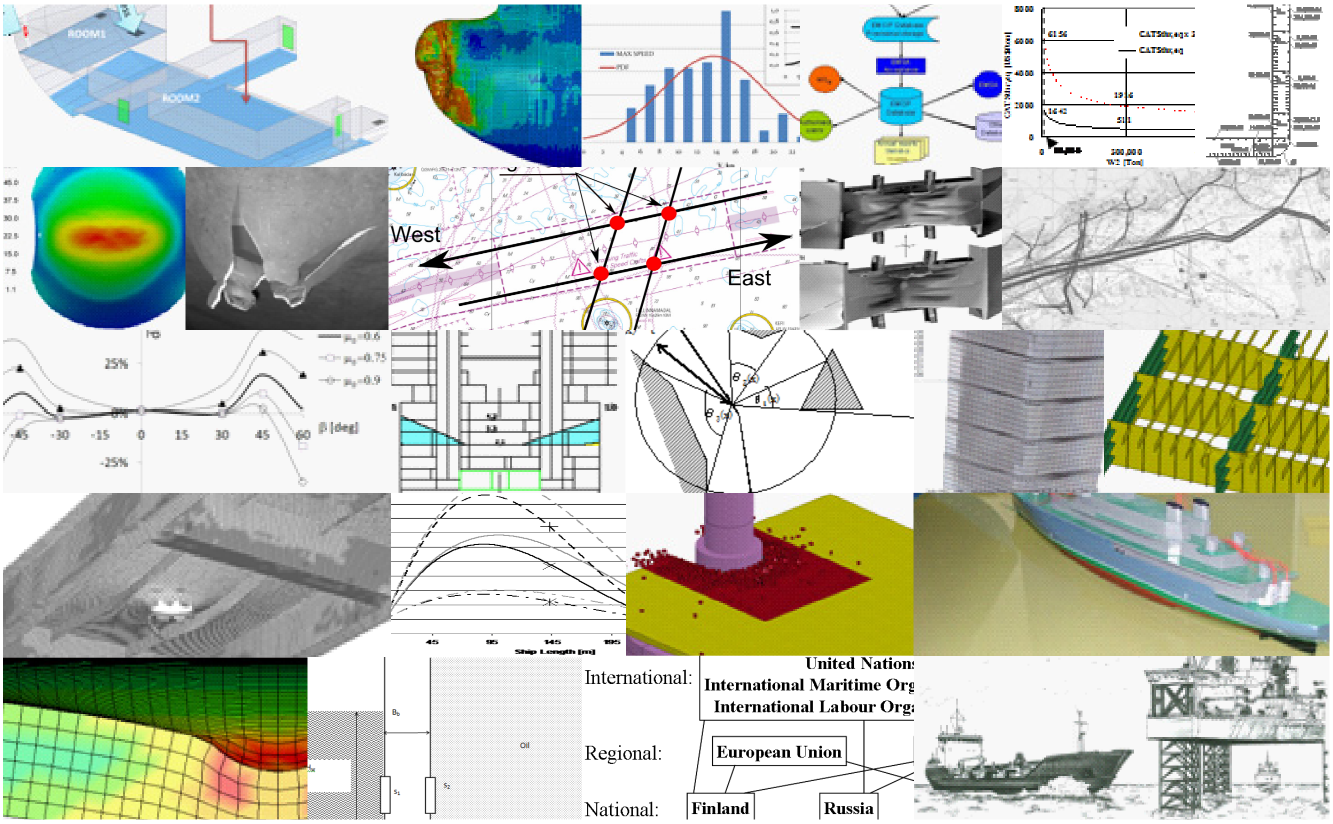

Aalto University
School of Science
and Technology

TKK - AM - 16

5th International Conference on Collision and Grounding of Ships
June 14th - 16th 2010 Espoo, Finland

Edited by
Sören Ehlers, Jani Romanoff

A grateful thanks to all our reviewers!

Conference steering committee

Prof. Preben Terndrup Pedersen, Denmark
Prof. Petri Varsta, Finland
Prof. Eike Lehmann, Germany
Mr. Fujio Kaneko, Japan
Prof. Jorgen Amdahl, Norway
Mr. Jaideep Sirkar, USA

Local organizing committee from the Marine Technology Group of the Aalto University:

Prof. Petri Varsta
Prof. Jerzy Matusiak
Prof. Pentti Kujala
D.Sc. Sören Ehlers
D.Sc. Jani Romanoff

Aalto University
School of Science and Technology
Faculty of Engineering and Architecture
Department of Applied Mechanics

Aalto yliopisto
Teknillinen korkeakoulu
Insinööritieteiden ja arkkitehtuurin tiedekunta
Sovelletun mekaniikan laitos

cover layout by:
Markus Ahola
proceedings layout by:
as2con - alveus ltd.
research & consulting

Aalto University
School of Science and Technology
Faculty of Engineering and Architecture
Department of Applied Mechanics
P.O. Box 15300
FI - 00076 Aalto
FINLAND
Tel. +358-9-47023501
Fax +358-9-47024173
E-mail: leila.silonsaari@tkk.fi

© 2010 Aalto University

ISBN 978-952-60-3211-5
ISBN 978-952-60-3212-2 (PDF)
ISSN 1797-609X
ISSN 1797-6111 (PDF)
URL: http://lib.tkk.fi/Reports/2010/isbn9789526032122.pdf

Multiprint Oy
Espoo 2010

Foreword

In my work related to the topic of collisions and groundings in the past 12 years I have always considered this conference and the resulting proceedings to be of great value for everyone in of scientific community. It is my pleasure to participate in the 5th International Conference on Collision and Grounding of Ships organized in Finland. These proceedings comprise a careful state of the art collection of current collision and grounding related research activities. The conference serves and will serve in the years to come, as an excellent opportunity to disseminate our research findings and to outline future research areas. I would like to thank all contributors to the conference and to the proceedings.

Petri Varsta

Sponsored by:

www.stxeurope.com
www.napa.fi
www.lr.org
www.merenkulunsaatio.fi
www.erab.se
www.tsv.fi

Table of contents

Goal Based Ship Safety Application in large cruise ship design

Kai Levander

STX Europe Cruise & Ferries (Retired), SeaKey Naval Architecture, Turku Finland

Abstract:
New, innovative ship designs often fall outside the rulebook safety framework. IMO has responded by developing goal-based ship construction standards. For passenger vessels this goal is that "the ship itself is its best lifeboat". This means that in case of collision, grounding or fires both passengers and crew can stay onboard as the ship proceeds to port. This goal based safety approach has been applied in the design of the world's largest cruise ship "Oasis of the Seas".

Introduction

Safety is a key element in the design of all passenger vessels like cruise ships or passenger-car ferries. Traditionally safety rules have been developed empirically, based on experience from ships in operation. Today naval architects have powerful, computer based tools, like 3D-CAD for "drawing" work, but also many different calculation programs for system optimisation and simulation. This makes it possible to evaluate a new design in detail already during the design phase. Also IMO, flag state authorities and class societies have seen the benefits of theoretical calculations and simulations both for rule development and for evaluation of new innovative ship solutions. This paper presents the application of goal base safety philosophy in the design of the world's largest cruise ship "Oasis of the Seas". The ship was designed and built by STX Europe for Royal Caribbean International in 2009. A sister ship will follow in the autumn 2010.

The cruise business

Rapid Growth in Cruise Ship Size

The cruise operation as we see it today started back in the early 1970's. The size and the capacity of the vessels have been doubled every ten years, as can be seen from the example of vessels designed and built by STX Europe in Finland for Royal Caribbean Cruises Ltd. (Fig 1). These six generations of ships built for RCCL are not unique, but similar examples can be presented for other major cruise operators, like Carnival Cruise Lines and Norwegian Cruise Line. The strong development of the cruise market and the passenger base, especially in North America, has supported this growth. The cruise vessels built at STX Europe yard in Turku are 225 000 GT in size and carry 5 400 passengers in double occupancy. The two "Oasis" – class vessel were contracted at a cost of 900 Million Euro per vessel and represent an important business decision both for the ship owner and the yard. The rules and regulations for passenger vessels have been intended for much smaller vessels and the increase in size means that instead of applying traditional prescriptive rules equivalent safety principles had to be used in the design and construction.

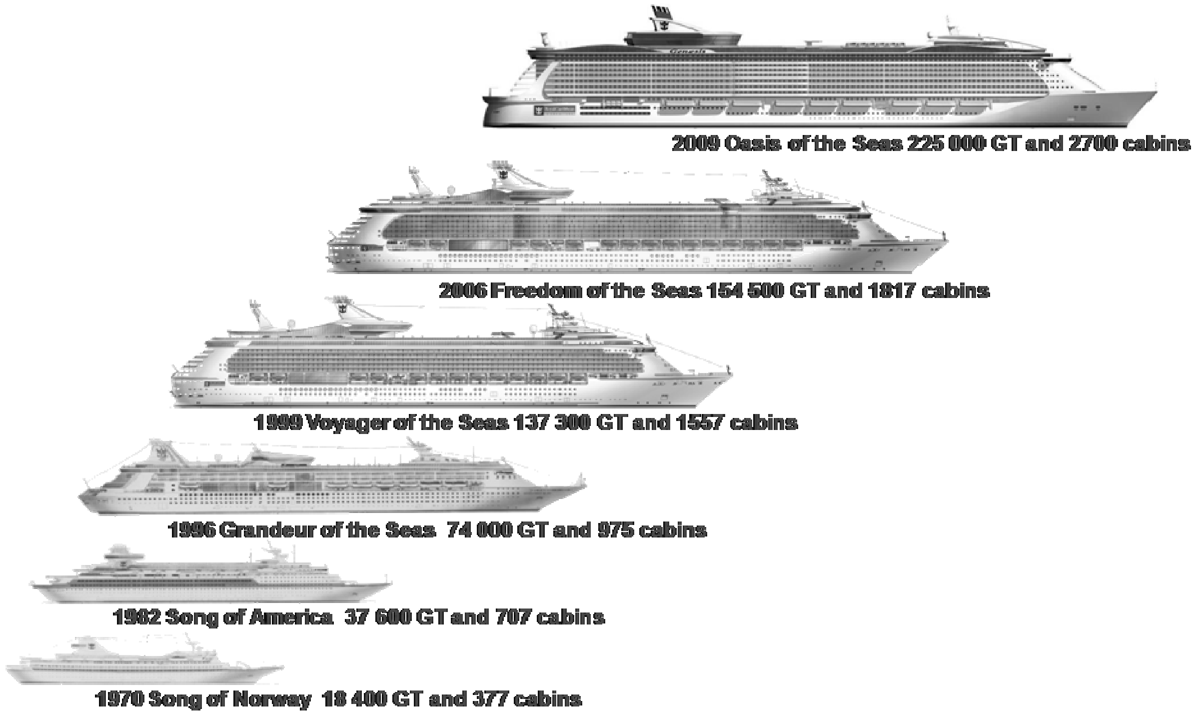

Figure 1: The growth in cruise ship size and capacity

Goal Based Ship Safety

Passenger ships have been operating with excellent safety records, but a few fatal accidents have turned public opinion on the safety of cruise ships and passenger-car ferries. IMO, flag state authorities and class societies have responded by evaluating the possibilities to further increasing the safety standards for large vessels with several thousands of persons onboard. Now IMO introduces a new SOLAS regulation II-1/3-10 on "*Goal-based ship construction standards for bulk carriers and oil tankers*".

For passenger vessel the IMO goal is that "*Ship is its best lifeboat and in the event of any casualty persons can stay safely on board as the ship proceeds to port*".

Cruise ship performance indicators

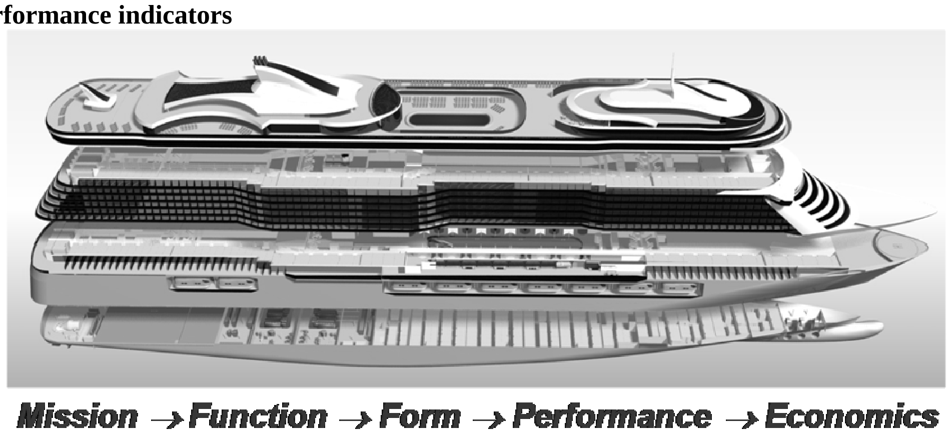

The naval architect must understand the technical and economical factors that are guiding both cruise ship building and cruise operation (fig 2). The cruise ship owner always first asks about the ship price and compares it to the price per passenger for other newbuildings and for the ships in the existing fleet. Shipyard building cost is more related to Gross Tonnage than to the passenger capacity. For European yards, building cost is in Euro, the owners are more tied to US dollars. More important than the building cost is the money making potential for the vessel. What will the average ticket income be and the onboard revenue? Cruise ships have very large crews, but labour costs are low and partly based on tips. Bunker cost has been a very small part of the total operating cost, but has rapidly increased during 2008. CO2 emission is also important and passengers ask about the carbon footprint of their cruise vacation. Safety, reliability and environmental friendliness have become basic requirements for all cruise ships. If a new design concept cannot fulfil these demands, no ship owner will be interested.

Impact Area	Technology Drivers	Goal	Indicator
Construction	Design Concept Standard Solutions Modular Construction Supplier Networking	Construction Efficiency	Building Price [$ / D.O.] Building Cost [EUR / GT]
Payload Functions	Passenger Capacity Cabin Standard Public Spaces Entertainment & Activities	Ticket Revenue Onboard Revenue	Money making potential [$ / paxday]
Hotel Service	Food & Beverage Cabin Cleaning Onboard Service	Pax Satisfaction	Pax / Crew Ratio Hotel crew cost [$ / Year]
Ship Service	Hull Form & Propulsion Power Plant Fuel Type & Consumption	Energy Saving -20% CO2	Bunker Cost [$ / Year] Carbon Footprint
	Navigation Machinery Operation	Automation	D & E crew cost [$ / Year]
	Planned Maintenance Condition Monitoring	Reliability	Keep cruise schedule
	Fire prevention Grounding prevention Collision Prevention	Safety	Casualties Insurance cost Repair & replacement cost
Social Values	Smoke & Emissions Waste, Sewage, Ballast Wake & Noise Recycling & Scrapping	Environmental Friendliness	Health Risk Environment fees & fines Disposal cost

Figure 2: Key performance indicators

Development trends

Panamax and Post Panama Cruise Ships

The Panama Canal has affected cruise ship design for many years. The maximum beam of 32,2 m allowed in the locks made ships long and narrow. To increase the number of outside balcony cabins more decks were added in the superstructure, but stability then became a problem. This problem was solved by making the superstructure narrower than the hull, with balcony cabins on both sides of a centre casing. This reduces the top weight of the vessel and allows more decks to be added. The old locks restrict the size of Panamax vessels to below 100 000 GT.

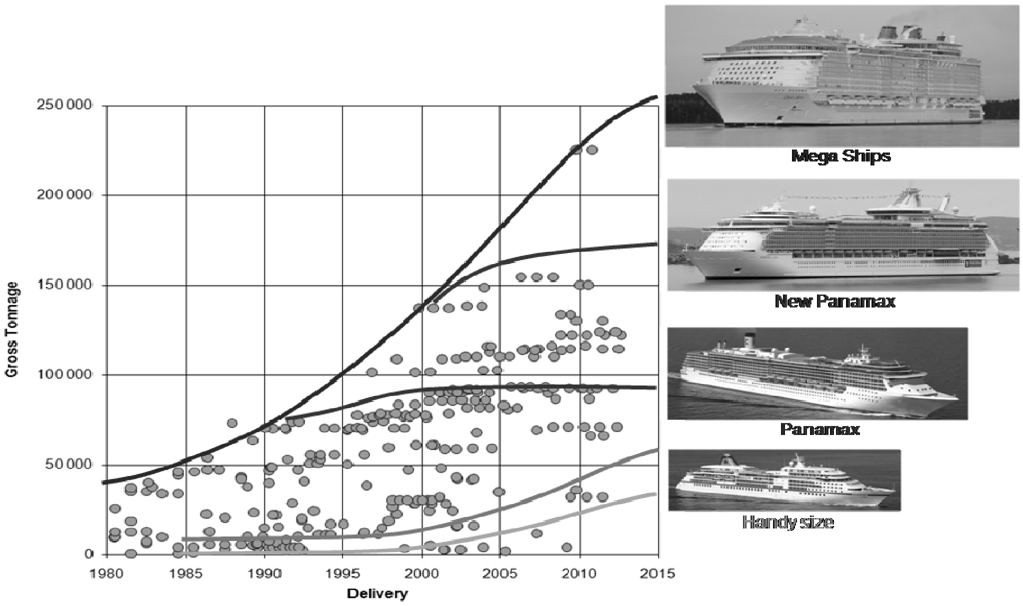

Figure 3: Cruise ship development trends

Panama Canal Authority has started the construction of a third row of locks, with impressive dimensions. The increased size is not introduced for the cruise industry, but to enable large container vessels to transit. Much larger cruise ships will also be able to pass from the Caribbean to the West Coast. The new locks are scheduled to be completed by 2014. The new locks will be large enough to allow today's Post Panama ships, like "Freedom of the Seas" to pass (fig 4). Air draught is restricted by the free height under the Bridge of Americas and will demand some innovative funnel arrangement. A new cruise ship size, New Panamax class, will develop for the bigger locks replacing the existing Panamax size. Mega Ships, like "Oasis of the Seas" are, however, too large even for the new Panama locks (fig 3).

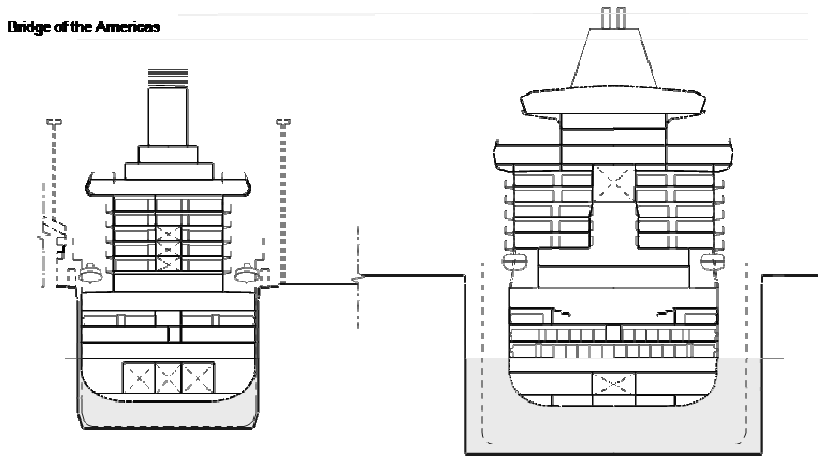

Figure 4: Old and new Panama lock dimension

New Cruise Ship Types

When cruise ships grow in size and beam increases there are more and more inside decks areas in the vessel. To maintain and preferably increase the number of passenger cabins with windows or balconies special layouts must be used. In the Panamax ships more decks could be added by narrowing the superstructure . In the Post Panama ships of "Voyager" and "Freedom" type some inside cabins have windows overlooking the indoor promenade. The new locks in Panama Canal make it possible to increase the hull beam and add more decks in the superstructure, increasing from 4…5 cabin decks in old Panamax ships to 6…7 in new contemporary NPX designs. In ships of mega size, the superstructure can be longitudinally split in two halves with an outdoor promenade deck in between, like in the "Oasis of the Seas" (fig 5 and 6). The traditional prescriptive SOLAS rules were not intended for this type of innovations and a new approach needed for ship safety assessment.

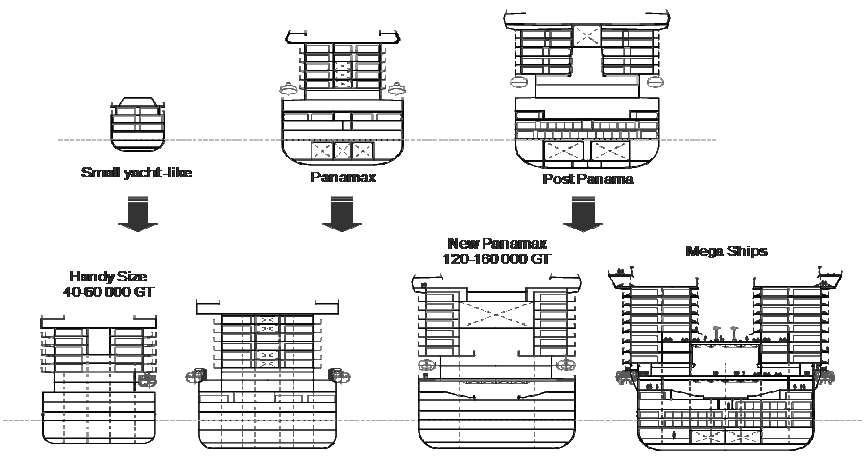

Figure 5: Size and type evolution

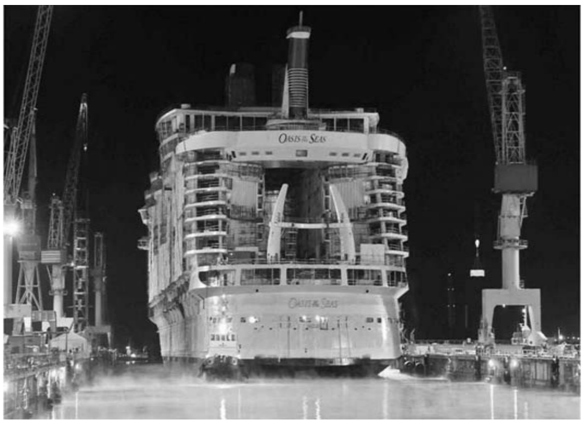

Figure 6: "Oasis of the Seas" with split superstructure

Safe and reliable
IMO Goal Based Standard

The goal-based ship standards are developed on the basis of a five-tier system, consisting of goals (Tier I), functional requirements (Tier II), verification and acceptance criteria (Tier III), rules and regulations for ship design and construction (Tier IV) and industry procedures and quality systems (Tier V).

IMO has defined as the goal for passenger vessels that "the ship itself is its best lifeboat". This means that in case of casualty both passengers and crew can stay safely onboard as the ship proceeds to port. Safe areas shall be available onboard for passengers and crew after a fire, collision or grounding as long as the casualty threshold has not been exceeded. Fire detection and fire fighting shall prevent the fire from spreading in the ship to adjacent fire zones. For damage stability, the new IMO probabilistic rule is applied. Partial power for propulsion and hotel load shall be available also after the casualty, as well as essential safety and comfort systems. Only if the casualty exceeds the threshold an evacuation and abandonment of the ship is necessary (fig 7).

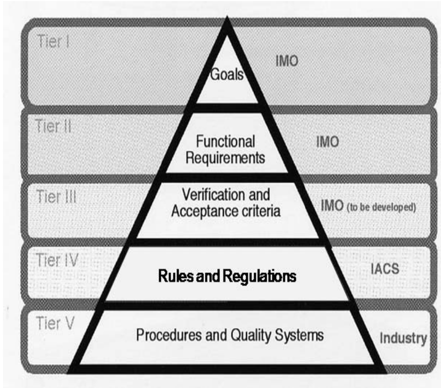

Figure 7: IMO Goal "Ship is its best lifeboat"

Fire safety
Alternative Design

The increasing size and passenger capacity of cruise ships mean that also the public spaces must increase in size. In the prescriptive SOLAS rule the max length of the main fire zones is 40 m, but up to 48 m can be used in certain cases. The area should be less than 1600 m^2. In many vessels the size of the main dining room and the show theatre has been limited by this rule even after extending the fire zone length to 48 m. In the "Voyager" and "Freedom" class cruise ships the indoor promenade reaches through several main fire zones. Here fire doors are installed at each main fire bulkhead. On the promenade floor deck level, where passengers walk, sliding doors are used, but in the three deck high upper part of the promenade atrium big, vertically hinged folding doors are installed.

In "Oasis of the Seas" Alternative Design (SOLAS Ch. II-2 Reg.17) has been applied. The ship is much wider than 40 m and the average size of the fire zones is well above 1600 m^2. Extensive simulations and fire hazard analysis were used to verify that "equal safety" were achieved in selected, representative areas (fig 8). Also the indoor promenade is much larger than in previous vessels and doubled roller shutters are used as fire dampers in the main fire bulkheads. In addition normal size fire doors in the bulkheads are installed on the escape routes (fig 9).

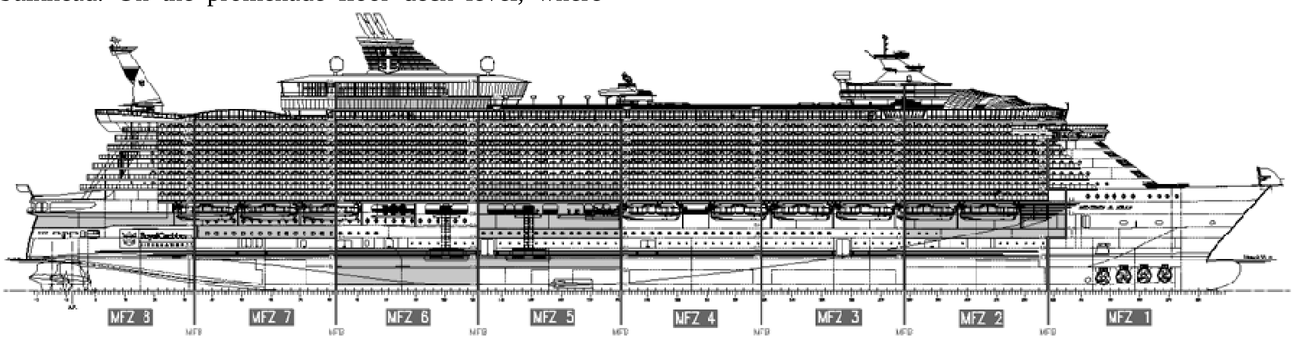

Figure 8: The "Alternative Design" principle was used for representative areas in large fire zones

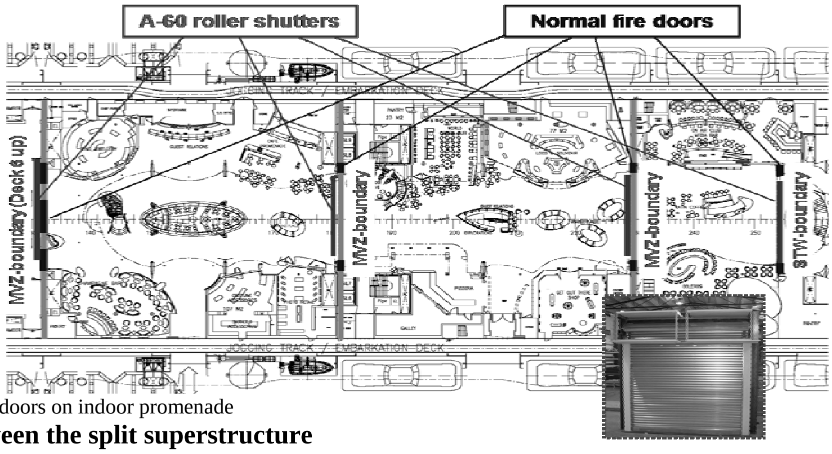

Figure 9: Fire shutters and doors on indoor promenade

Outdoor spaces between the split superstructure

Outdoor spaces between the split superstructure introduced a new fire safety concern (fig 10 and 12). Fire loads were simulated and different solutions tested to demonstrate equal safety with SOLAS. Fire break areas were introduced in the lay out to slow down spread of fire.**Longitudinal fire break** hinders fire spread from one side to another in the split superstructure. This should be at least 3 m wide. Use of all combustibles is prohibited in this area, except deck-covering with low-flame spread characteristics (fig 11).**Transverse fire breaks** slow down spread of fire due to any possible wind effects. These are 6m long zones in the vicinity of the MVZ boundaries. Low (<0,5m) living vegetation is allowed, but no combustible furnishings**.**

Figure 10: “Board Walk” aft

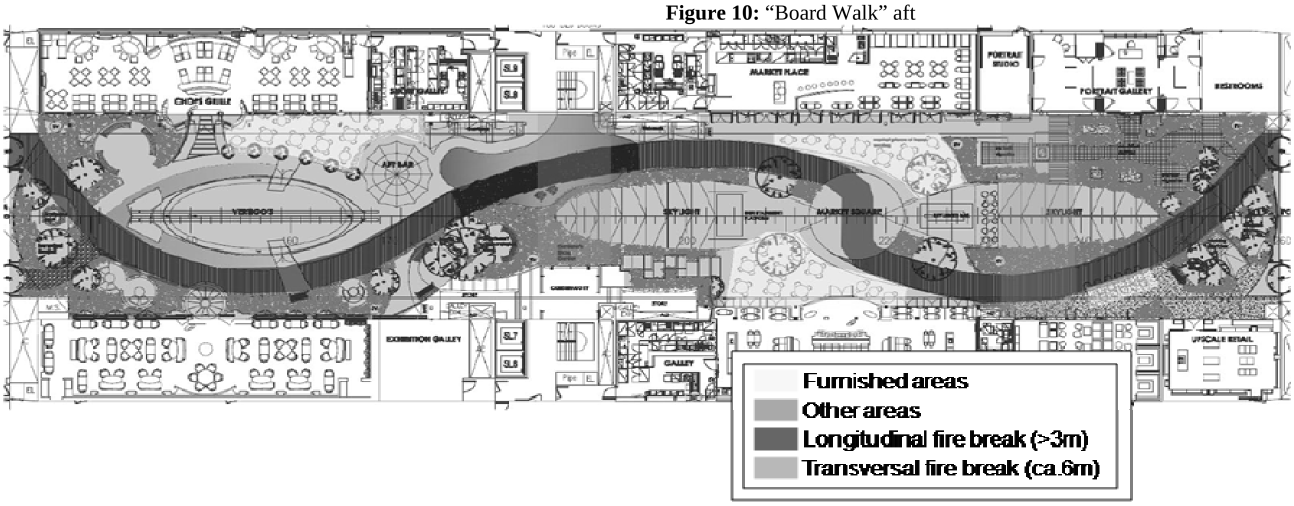

Figure 11: Fire breaks in “Central Park”

Figure 12: “Central Park” between the split superstructure in “Oasis of the Seas”

Figure 13: Survivability after grounding or collision

Damage stability

Probabilistic Damage Stability Rule

The new rule is based on the probability for damages to the hull, found by analyzing the length, penetration and vertical extent of damages reported by ship collisions and groundings (fig 13). The probability that the ship will survive is calculated for several thousand different damage cases to get the attained index. This must be bigger than the required index specified in the IMO rule. Required index increases with the number of persons onboard and the length of the ship. The number of persons includes both passengers and crew. The index also depends on the lifeboat capacity. Most cruise ships are built for long international voyages with lifeboat capacity for 75% of all persons onboard. For the remaining 25% life rafts or marine evacuation stations are provided. For a cruise ship of Panamax size, the required index is about 0,8 and for a Mega Size vessel it approaches 0,9 (fig 14).

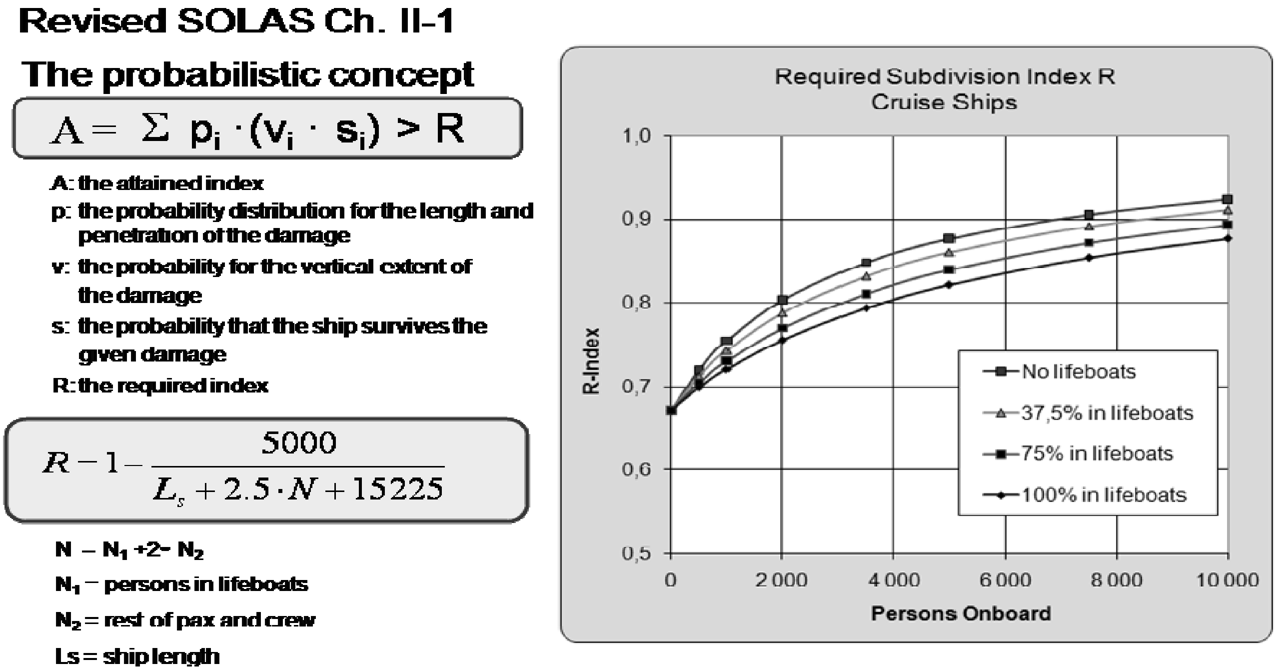

Figure 14: Required subdivision index

Probabilistic Damage Stability Rule

The new probabilistic rule requires a lot of calculation work. The rule is technically complicated and the interpretation is still not fully established. In cruise ships where the beam is not restricted by any canal locks or similar, the required index can be attained by using a “wide body” concept. Increased hull beam gives high initial stability and this improves the attained index. In cruise ships, the internal water tightness is improved by installing partial watertight bulkheads at the ship sides to prevent down flooding from compartment to compartment when the ship heels.

The survival probability can be further investigated using numerical simulation of flooding events and model testing.

For “Oasis of the Seas” the IMO probabilistic rule was applied ahead of entry into force (fig 15, 16 and 17)

- 9000 damage cases calculated
- The Required Index R = 0,88 and Attained Index A = 0,91
- Numerical simulations and model tests using a performance based approach suggest survival probability of 0,99

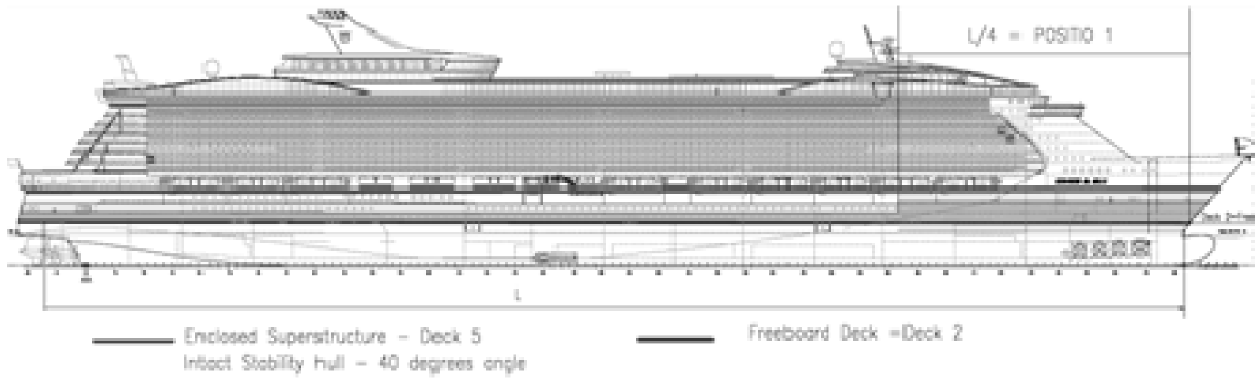

Figure 15: Watertight integrity and freeboard deck

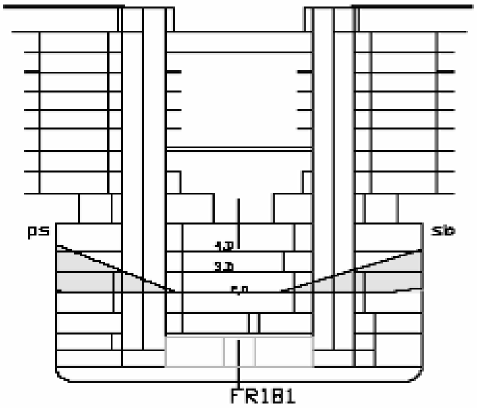

Figure 16: Watertight integrity to 40 deg

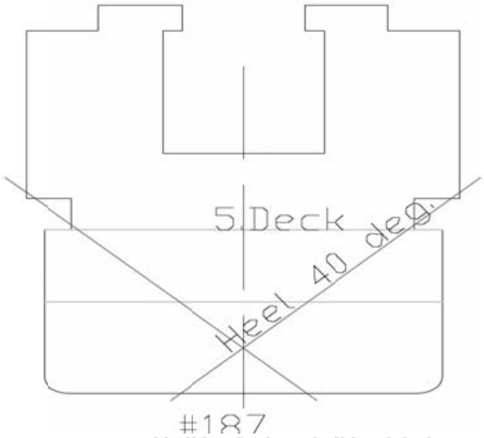

Figure 17: Partial bulkheads above bulkhead deck

Safe return to port

Redundant Power Supply and Propulsion

The IMO new rule also requires that passengers and crew in the case of casualty should stay onboard as the ship proceeds to port. This demands a redundant power supply and propulsion. With diesel-electric machinery, this can be secured by locating the diesel-generators in two or more engine rooms separated by watertight and fire insulated bulkheads (fig 18). All auxiliary systems must be divided in the same way. A safe solution is to place the diesel-generators in two separate main fire zones and have separate engine casings all the way to the funnel. Also the propulsion should consist of at least two units, located in protected compartments (fig 19). All essential safety system must also remain in use and some basic comfort maintained for passengers and crew.

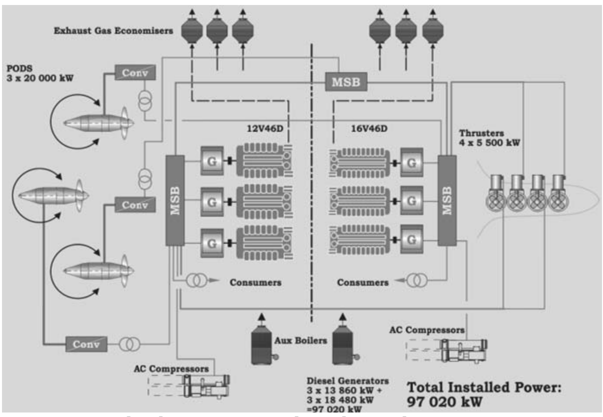

Figure 18: Redundant power supply and propulsion

Figure 19: Triple pod propulsion, all units steerable

Casualty threshold exceeded

Evacuation

If, the damage from the casualty exceeds the survival threshold the ship must be evacuated. Extensive work was carried out to optimize the evacuation from any space onboard. Evacuation traffic simulations were based on MSC Circular 1033 and representative passenger demographics used. Assembly stations are in protected spaces, well-known by all passengers, close to the lifeboat embarkation areas. Assembly time must be less than 60 minutes (fig 19).

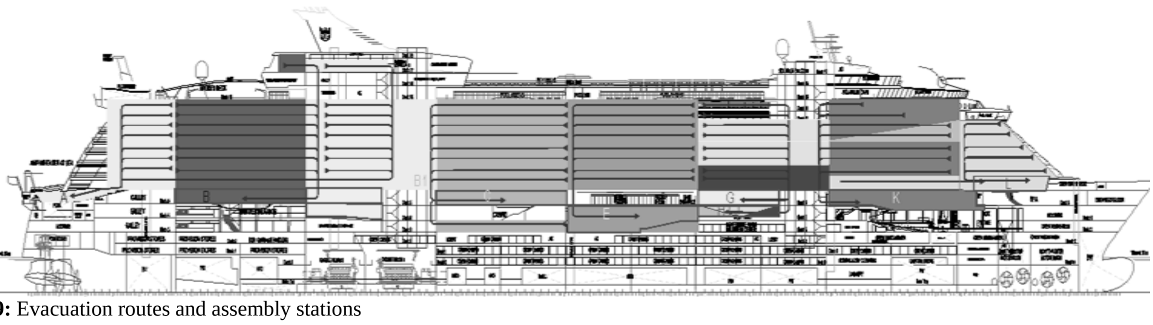

Figure 19: Evacuation routes and assembly stations

Life Saving Appliances

The lifeboats and life raft stations occupy much space along the embarkation deck in a large cruise ship. Passenger capacity grows proportionally more than the ship length when size is increased. In a cruise ship of 200 000 GT with 6000 passengers and 2000 crew onboard there is not enough length along the embarkation deck if traditional 150 person lifeboats are used. If two 150 person lifeboats are combined into one rescue vessel for 300…400 persons the space demand along the lifeboat deck is reduced and the LSA capacity can be increased to the required 8000…9000 persons. The use of larger life boats must be approved by class and flag state following the “equal safety principle”. If life boats are stowed in launching position outside the ship side, embarkation is fast and the davit system simplified. Reinforcement needed for the wave loads on the life boats in extreme seas must be evaluated by model testing (fig 20).

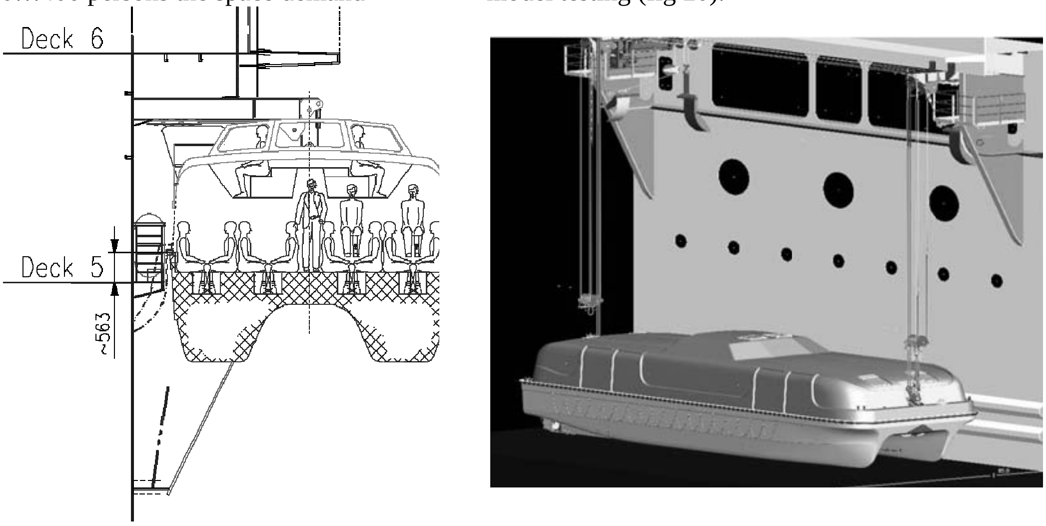

Figure 20: Large life boat for 370 persons and launching system

Operation safety

Designing and building ships to the traditional prescriptive rules or following the new goal based approach does not automatically guarantee safe and reliable cruise for the passengers. Also the operation must follow the same safety philosophy. Safer operation of a large cruise ship demands both skill and dedication from the officers and crew. All control system onboard should support and guide the crew on the day to day operation, but especially when accidents or causalities demand special actions. In “Oasis of the Seas”, the following solutions were used (fig 21):

Bridge fully dedicated for navigation

- Safety Centre adjacent to the bridge
- Integrated and redundant navigation system
- Improved ability to manage safety and security incident
- Same principle adopted for the Engine Control Centre
- Video broadcasting from bridge to large screens at assembly stations for effective communication
- Reliable passenger and crew count system at assembly stations
- Public address system extends to the life boats
- Surveillance system for enhanced monitoring of evacuation, over 1300 CCTV cameras

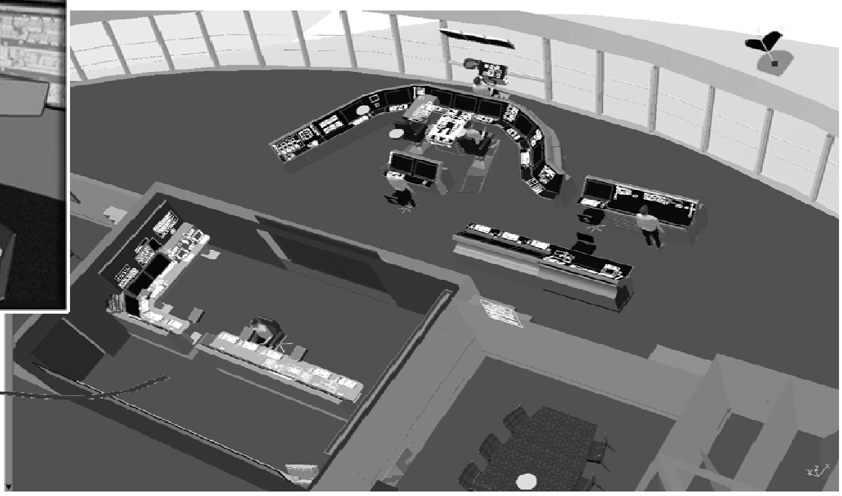

Figure 21: Safety centre adjacent to the bridge

Conclusion

Cruise operators have been optimistic and invested in more ships for further growth of the cruise business. But the competition in the vacation market is hard, especially after the crises in the financial market. Potential passengers have been reluctant to go on a cruise and have evaluated also other vacation alternatives. But the cruise market is recovering and now is the right time to plan new ships when shipyard order books are empty and building cost has been reduced. To create a new successful generation of cruise ships, cruise operators, naval architects and interior designers must work together to find the ideal solution. They must learn from the problems in previous designs and look for new technical possibilities that can improve the performance, environmental friendliness and safety of the new ships. How can the passenger capacity be increased? What layout should be used for maximum balcony ratio? Can the fuel consumption be reduced? What hull form has the best sea keeping characteristics? What is the building cost per passenger in the new design? Can a large ship be delivered in less than 3.5 years?

But most important will be to understand the passengers, their demands and expectations. Both the naval architect and the interior designer must look at the ship from the passenger's point of view to be able to create a winning design for the next 25 years. Tankers, bulk carriers and container vessels are "heavy industry" business, building standard vessel types in long series at competitive prices. Success in the cruise business demands different skills. We must provide a unique experience for the passengers to fulfil their expectations and make them come back again for more cruises during their next vacations.

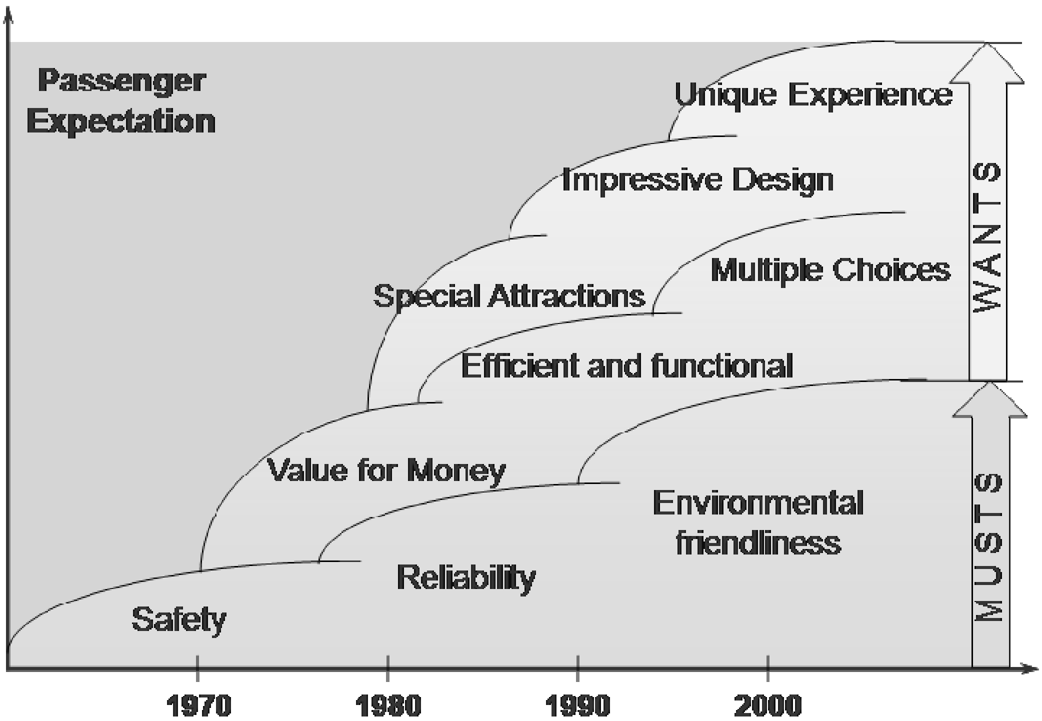

Figure 22: Cruise passengers expect unique experiences in a safe, reliable and environmental friendly ship

References:

Levander , K. "Cruise Ships – Success factors for the design", IMDC 2009

IMO "SOLAS 2004" Chapter II-2 Regulation 17 Alternative Design

IMO "SOLAS 2009" Revised Chapter II-1 Subdivision and Damage Stability Regulations Explanatory Notes from SLF 51/7

IMO "SOLAS 2010" New Chapter II-1 System capabilities after flooding casualty on Passenger Ships

IMO "SOLAS 2010" New Chapter II-2 Safe Return to Port for Passenger Ships

Royal Caribbean Cruises http://www.royalcaribbean.com and http://www.oasisoftheseas.com

STX Europe "Cruise Ship R&D and Newbuilding Projects" http://www.stxeurope.com

European Marine Casualty Information Platform a common EU taxonomy

Paulo Correia

European Maritime Safety Agency (EMSA)

Abstract:
A comprehensive and common marine casualty taxonomy is a fundamental factor for statistics, risk analysis and the facilitation of cooperation between States when investigating marine casualties and incidents. This paper will present the structure and the taxonomy behind the database of the European Marine Casualty Information Platform (EMCIP), developed by the European Maritime Safety Agency (EMSA - was set up by the Regulation (EC) N° 1406/2002, with the main objective to provide technical and scientific assistance to the European Commission and Member States in the development and implementation of EU legislation on maritime safety, pollution by ships and security on board ships. http://www.emsa.europa.eu/). The database, using this common taxonomy, went live on October 2009 and is being used by a number of European Member States, on a voluntary basis. Populating EMCIP will become mandatory after the transposition period established by the Directive 2009/18/EC, on 17 June 2011

Introduction

The Directive 2009/18/EC[1], in establishing the fundamental principles governing the investigation of accidents in the maritime transport sector, puts an end to the absence of rules governing the conduct of safety investigations in Europe.

The main principles of the Directive are: the implementation of independent maritime casualty safety investigations; cooperation among the investigative bodies and obligation to report accidents. To achieve these goals, permanent and independent investigative bodies should be created.

Independence can be achieved by the separation of safety from judicial investigations, while still allowing the sharing of some factual information. It is worth contrasting the two types of investigations. The aim of a judicial investigation is to deliver justice by apportioning blame or liability in the case of any violation of the regulations in force. A safety investigation, meanwhile, by establishing a non-blame culture and preserving the confidentiality of the witnesses' testimony, is in a better position to illustrate possible lessons and issue safety recommendations to prevent future accidents.

Cooperation between the lead investigating State, other Member States and third countries involved in an accident, is an important factor for the effectiveness of the investigation. Parallel investigation should be avoided, although the views of the various investigative bodies involved should be taken into account.

The obligation to investigate a certain type of casualty, based on the risk or the lessons that can be extracted from the investigation and also issuing safety recommendations as a follow up are also important pillars of the Directive.

Finally, commitments to report all the marine casualties or incidents to EMCIP publishing any safety investigation reports produced are also important elements for the transparency and quality of the process and for the public and for shipping industry awareness.

European marine casualty information platform

EMCIP is a web-based platform constituted up to now a Database, a Portal and an Admin tool. The development of further tools is also foreseen.

The Admin tool allows organisations to access to their assigned repository on the EMCIP system in order to create users and to attribute roles.

The EMCIP Portal is used to support the investigation process, and to help investigators, by providing support documents and information: e.g. user manuals, lists of contacts, 24-hour contacts, news, events and reporting problems and changes.

The EMCIP database provides the means to store data and information related to marine casualties involving all types of ships and occupational accidents. It also enables the production of statistics and analysis of the technical, human, environmental and organisational factors involved in accidents at sea.

The database taxonomy has been developed by EMSA in consultation with the Member States, on the basis of European research[2] and international recommended practice and procedures[3]. The EMCIP technical platform makes use of a similar software platform developed for the aviation industry by the IPSC - JRC[4] of the European Commission.

At the present stage, EMSA promotes voluntary participation in EMCIP population by the investigation authorities of the Member States, during a transitional period until the Member States bring into force the laws, regulations and administrative provisions necessary to comply with Directive 2009/18/EC. This voluntary participation phase anticipates the future

[1] http://eur-lex.europa.eu/LexUriServ/LexUriServ.do?uri=OJ:L:2009:131:0114:0127:EN:PDF

[2] Such as: Casualty Analysis Methodology for Maritime Operations (CASMET) project.

[3] Such as: MSC-MEPC.3/Circ.3 - harmonized reporting procedures, International Maritime Organisation (IMO).

[4] Institute for the Protection and Security of the Citizen – Joint Research Centre

framework proposed by the legislative initiative of the Commission. In addition to helping to achieve an overall European objective that is, a single repository of information on maritime accidents in the EU the national competent authorities will be able to store, process and use data for their own particular needs.

Reporting

The accident investigation Directive considers that the submission of data to, and the general use of, the European Marine Casualty Information Platform (EMCIP) to be an integral part of the overall safety investigation system. It requires that according to the database scheme:

All marine casualties and incidents shall be notified in accordance with the format described in Annex II of the Directive, as well as, data resulting from safety investigations;

Data on marine casualties and incidents shall be stored and analysed by means of EMCIP

The EMCIP database is structured to enable the storage and processing of ship casualty related data, as well as data relating to occupational accidents covering all types of ships no matter its severity (very serious, serious, less serious and incidents).

The database is populated by the national competent authorities of the Member States acting as data providers, who in turn are supported by the system itself in their notifying, reporting and search tasks, as well as in their preparatory work for conducting safety investigations. EMSA manages the system and accepts the communicated data before it is finally stored.

EMSA and the national competent authorities operate the system within a culture of 'no blame and no liability' and in accordance with personal data protection.

EMSA manages the system and, through an acceptance procedure, monitors the quality of the data before it is finally stored. This is an important task when a new system is used by many different organisations.

Figure 1 shows EMCIP workflow which is based on the concept of notifications and additional (investigative) data that could be the result of safety investigations.

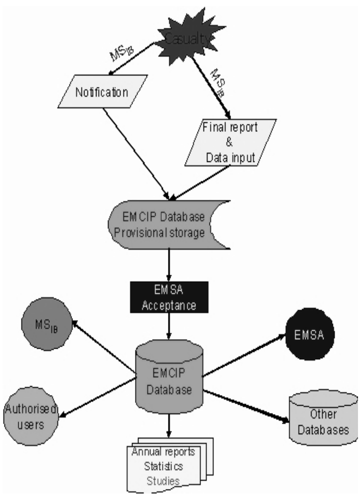

Figure 1

Event representation

The database is prepared to collect unsafe events in a sequence order following the approach of the STEP[1] method (Figure 2):

- multi-linear events; and
- events in sequence order and related to each other

There are two types of events: casualty and accidental events. Casualty events which express some kind of energy release or conversion are listed in the Annex. The accidental events[2] seen as the immediate causes can be: equipment failure, environmental effect, external agent, hazardous substances and human erroneous actions[3].

The accidental events can be associated with two periods of the accident process: at the casualty or emergency stage.

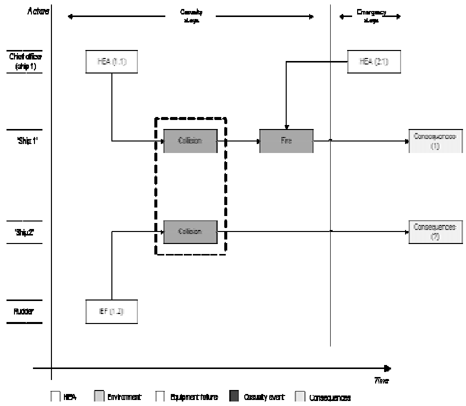

Figure 2

According to this approach, an event is one actor performing one action and an actor was in a certain place doing something at the time of the accident. The actors can be a person, a thing (e.g. goods or equipment) or a natural element involved in the accident.

Each accidental event may have associated organizational factors, called contributing factors: these are shipboard operations and shore management. Figure 3 presents a schematic example of the interaction between events and events and associated contributing factors.

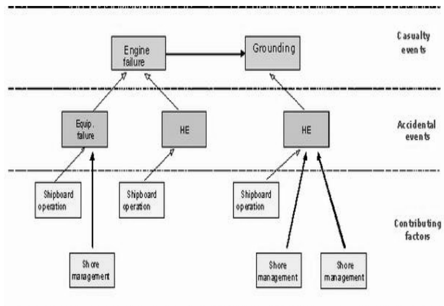

Figure 3

[1] Sequential timed events plotting procedures

[2] From Casualty Analysis Methodology for Maritime Operations (CASMET)

[3] Following the terminology proposed by Cognitive Reliability and Error Analysis Method (CREAM)

There are also related precursor events associated to each type of accidental event, that can be seen in a dimension perpendicular to the picture, and covering for example human factors and failure modes.

Taxonomy

The development of a marine casualty taxonomy for Europe is a fundamental factor in facilitating cooperation between Member States when investigating marine casualties or incidents.

The use of the same coded language (taxonomy) will diminish the risk of having different investigators using different representations of the same event and associated information. The taxonomy is supported by the definitions of the fields and its values, regular investigator training on EMCIP, together with assessment of the quality of the data.

Based on a common taxonomy, 27 Member States plus Norway and Iceland will be populating the EMCIP database, which means that a large amount of data will be available to carry out statistical and risk analysis.

The EMCIP taxonomy or the classification scheme is constituted by extensive coded information, allowing its translation and incorporation in the system if requested by Member States.

There are also text fields such as: description of the accident, where free text can be inserted, keywords and text fields for contributing factors and safety recommendations.

Associated to each occurrence, the investigators can also attach several files such as: the investigation report, pictures, movies and other relevant source material.

The taxonomy can be divided across factual data, such as, ship details or interpretation data such as the fatigue factors of a particular actor.

The database taxonomy took into account the conclusions of the CASMET project and using its proposed codes for contributing factors (causal factors). Other sources include the categories of cognitive factors and permanent and temporary person-related functions of CREAM, and also some annexes of the IMO on harmonised procedures for reporting marine casualties and incidents.

Human errors and organisational factors are an important aspect of the EMCIP taxonomy. As an example, Figure 4 shows the groups of information that might be stored for human error actions.

Tree structure

The following tree, Figure 5, represents the main structure of the basic entities in the EMCIP taxonomy. The main entity of each report is the occurrence (casualty with a ship, or occupational accident, or incident). Entities are created below the main entity because they may exist in multiple instances (e.g. more than one vessel may be involved in a casualty occurrence).

Occurrence

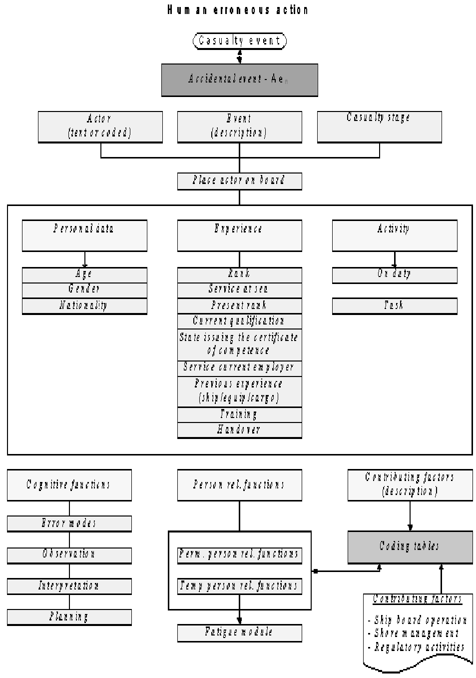

Figure 4

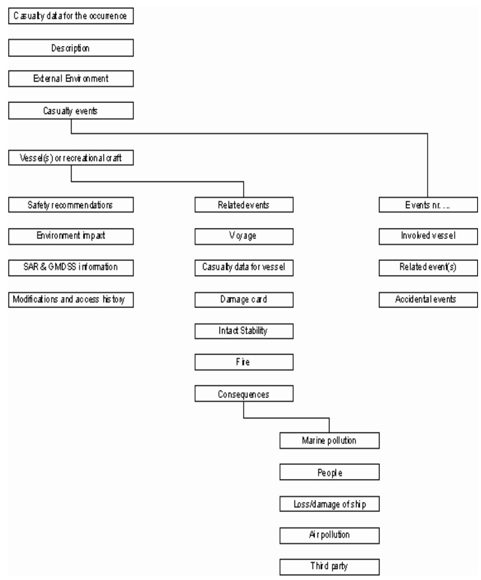

Figure 5

The investigator builds this tree according to the type of the casualty, number of ships involved, number and type of accidental events, contributing factors, safety recommendations and other information available.

Main functions

Query, Statistics, Export and Graph are functions allowing users to interrogate the EMCIP database.

The Query Builder, the function that will be explained in more detail here, supports the creation of query libraries in which predefined queries can be stored, exchanged and executed. Users have complete freedom in defining their own queries.

The Query Builder accepts criteria involving any attribute (field), which is part of the EMCIP taxonomy. These criteria can be combined using logical operators AND, OR and brackets [ ], { }. Using these queries and query libraries, the identification and retrieval of specific selected safety data out of a repository becomes easy and flexible.
A query is a command sent to the database server to identify a set of occurrences from the database based on a criterion or a number of logically combined criteria.
The marine investigators have direct access through the Internet to all EMCIP data for their Member State that are not barred by special arrangement, and are able to produce statistics, safety studies and other reports for safety related purposes using pre-defined and open query tools.
For example a query can be created to search the occurrences - collisions that have occurred involving passenger vessels (Ro-ro), crossing or approaching or leaving a TSS, where there was at least one passenger injured, in 2009, see figure 6.

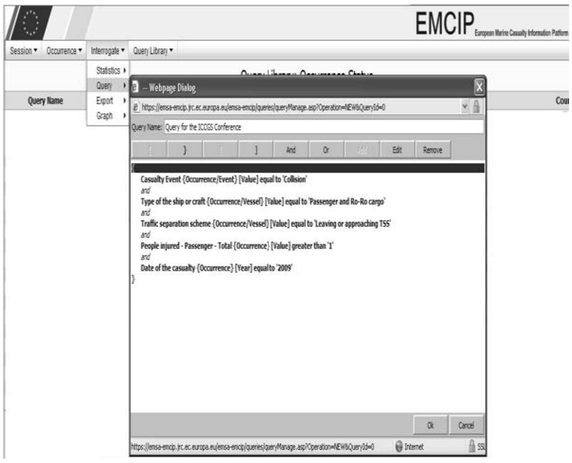

Figure 6

It is possible to query the text fields by words or group of words which is an important tool to search a particular facet of the accident that is not covered by the taxonomy.

Therefore, this open search tool enables EMSA and the national competent authorities to produce statistics, safety studies and other reports based on objective, reliable and comparable data. This enables the Commission and the Member States to take the necessary steps to improve maritime safety and prevention of pollution by ships and to evaluate the effectiveness of existing measures.

Conclusion

The fundamental principles contained in the Directive 2009/18/EC on accident investigation, the common methodology and EMCIP system ensure that an effective safety investigation system can exist across Europe.

The EMCIP database allows:

•The frequency and consequences of each casualty type to be obtained. Additionally, consequences relating to people, environment and material damages and those of the emergency response following it can be obtained separately.

•The frequency of accidental events and contributing factors associated with particular casualty types to be obtained as well as the safety recommendations issued.

•The frequency and/or consequence related to particular circumstantial information (e.g. relating to all "actors" and the respective factual information concerning dangerous goods, damage records, intact stability, fire-fighting equipment, SAR intervention, fatigue and pollution response) to be obtained.

EMCIP thus adds quantitative, qualitative and economic value to the investigation of marine casualties, incidents and occupational accidents. It achieve this by streamlining and consolidating the acquisition and storage of notification and investigation data received from all Member States. EMCIP uses a common taxonomy, and by effective analysis of that data, this enables general risk identification and marine casualty and incident prevention at the national, European and global level.

References

Hollnagel, Erik (1998) Cognitive Reliability and Error Analysis Method.

European project (1999) Casualty Analysis Methodology for Maritime Operations.
http://www.emsa.europa.eu/end185d007d003d002d005.html

MSC-MEPC.3/Circ.3 - harmonized reporting procedures – reports required under SOLAS/MARPOL.
http://www.emsa.europa.eu/end185d007d003d002d003.html

ANNEX

Casualty event

Capsizing/Listing
- Capsizing
- Listing

Collision
- With other ship
- With multiple ships
- Ship not underway

Contact
- Floating object
  - Cargo
  - Ice
  - Other
  - Unknown
- Fixed object
- Flying object

Damage to ship or equipment

Grounding/stranding
- Drift
- Power

Fire/Explosion
- Fire
- Explosion

Flooding/Foundering
- Foundering
- Flooding
  - Progressive
  - Massive

Loss of control
- Loss of electrical power
- Loss of propulsion power
- Loss of directional control
- Loss of containment[1]

Hull failure

Missing

[1] This includes for example any cargo damage or cargo lost overboard, oil spills and atmospheric pollution not caused by any other casualty event.

Numerical and Experimental Investigation on the Collision Resistance of the X-core Structure

Sören Ehlers, Kristjan Tabri, Jani Romanoff and Petri Varsta

Aalto University - School of Science and Technology, Department of Applied Mechanics / Marine Technology

Abstract

This paper analyses the collision resistance of the X-core structure. The analyses includes a detailed investigation of the non-linear plate and laser weld material behaviour using optical, full-field strain, measurements. The resulting material relations are implemented into the Finite Element model. Furthermore the Finite Element model includes the influence of the ships motions to predict the collision resistance accurately. The verification of the numerical results is done by a comparison of the experimental and numerical force versus penetration curves and by a comparison of the deformed geometries. The latter is achieved through a digitized three-dimensional model of the post experimental X-core structure. As a result the accuracy of the collision simulations is presented and discussed.

Introduction

The continuous growth in worldwide sea traffic increases the risk of ship to ship collisions. Therefore, demands for novel crashworthy ship side structures exist which have superior energy absorption capabilities than conventional ship side structures. Hence, based on the steel sandwich structural concept and laser welding, a sandwich side structure with multiple "x" shaped core elements has been developed and tested in large scale, see Wolf (2003).

Commonly structural collision analyses are carried out using the non-linear finite element method in a quasi static fashion with a power law based material relation, a failure criterion for simulating rupture and rigid connections between structural elements neglecting the actual weld. However, the quasi static simulation does not consider the motions of the vessels and can thereby not predict the available energy to deform the X-core structure. The power law based material relation and common failure criteria are not dependent on one another, and can therefore not predict the non-linear material behaviour with sufficient accuracy, see Ehlers et al. (2008a). Furthermore, the rigid connections between structural elements are not representing the true behaviour of the laser weld, and thus cannot be used to predict the structural behaviour accurately, especially if the laser weld fails.

Therefore, this paper investigates the influence of the laser weld including weld failure on the energy absorption of the X-core structure subjected to a ship collision. The laser weld was analysed with optical measurements to identify the local material behaviour by means of failure strain and force by Jutila (2009). His findings are implemented into the finite element model of the X-core structure to simulate the correct behaviour of the laser weld. The non-linear plate material behaviour is considered using an element length dependent material relation including failure according to Ehlers and Varsta (2009). The collision simulation is carried out in a dynamic fashion considering the motions of the colliding vessels as described in Pill and Tabri (2009). The importance of these fully dynamic simulations will be presented through a comparison to a series of quasi static collision simulations. Furthermore, the post experimental large scale X-core structure which was formerly tested for collision resistance by TNO (Wolf 2003) was digitalized with a topometric sensor system to obtain a full 3D reference model. This reference model will be compared with the results of the numerical simulations. Thereby the influence of the laser weld behaviour, respectively laser weld failure, will be identified and presented.

The X-core structure

The laser welded X-core structure has been designed in the EU Sandwich project and tested in the EU Crashcoaster project (Wolf 2003). Figure 1 shows a cross section of the X-core structure. The section consists of four "x" shaped core elements, which are joined by laser welding. The total thickness of the sandwich structure is 360 mm with a height of 1.5 m and a total length of 5.5 m. The thickness of the outer shell is 6 mm, the X-core and the inner shell thickness is 4 mm. The sandwich structure is conventionally welded to a support structure which itself is welded and joined to the struck vessel, see Figure 2.

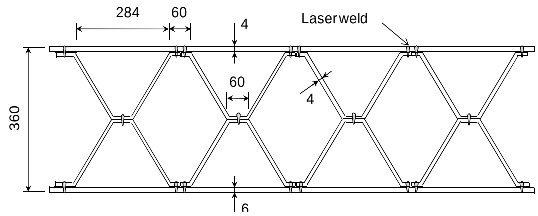

Figure 1. Laser welded X-core cross-section (dimensions are in mm)

Figure 2. Experimental overview

The striking ship, which was equipped with a rigid bulbous bow, impacted the struck ship at amidships on a course perpendicular to the struck ship. Hence, very small yaw motions occurred. The struck vessel is a barge with 14 tanks. As only one of the tanks was partially filled, the effect of sloshing neglected in the analysis, however its influence is discussed briefly. In order to enable the striking ship to hit the test section to the right spot, the struck ship was kept in a fixed position by two spud poles. The poles were connected to the ship by pivoting mechanism, which was opened just before the contact took place. Opened the pivot allowed poles to rotate and therefore their resistance to the ship motions was not considered. The main dimensions for both ships are given in Table 1. At the moment of the first contact, the velocity, v_0, of the striking ship was 3.33 m/s.

Table 1. Main dimensions and loading conditions of the ships

	Striking ship	Struck ship
Length, *L*	80 m	76.4 m
Beam, *B*	8.2 m	11.4 m
Depth, *D*	2.62 m	4.67 m
Draft*, *T*	1.3 m	3.32 m
Displacement, □	721 tons	2465 tons
Added mass of prevailing motion component*	a_{11} = 36 tons	a_{22} = 715 tons
Number of tanks	2 x 5	2 x 7
Ballast water with free surface	44.6 tons	0 tons

* a_{11} -surge added mass, a_{22} -sway added mass.

The penetration depth was evaluated as a relative displacement between the ships. The ship motions were recorded in the centre of gravity (COG) of the ships and thus, the penetration does not consider small local displacements, which might occur due to finite stiffness of the structures connecting the impact bulb and the test structure to the rest of the ship. Figure 2a presents the penetration as a function of time and Figure 3b shows the collision force as a function of the penetration. These figures will serve as comparative measures to verify the numerical collision simulations. The deformed X-core structure is shown in Figure 4a. The outer plating shows an 18 cm long vertical fracture close to the centre of the striking location. Furthermore, the laser welds connecting the "x" shaped core elements and the outer plating are torn at several locations, see for example Figure 4b.

(a)

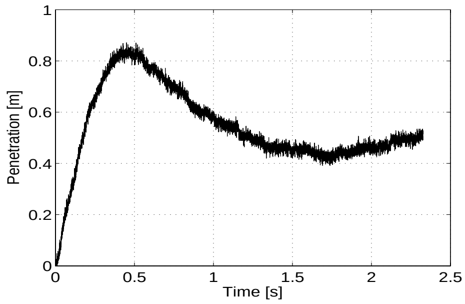

(b)

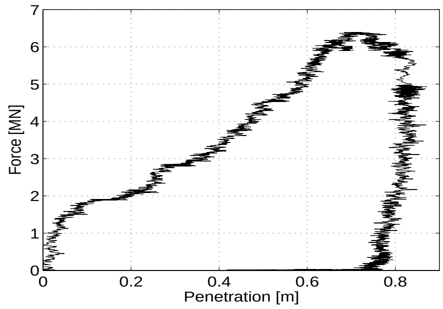

Figure 3. Penetration as a function of time (a) and force as a function of penetration (b) (Wolf 2003)

(a)

(b)

Figure 4. Deformed X-core structure (a) and failed laser weld (b)

Numerical modelling of the X-core collision

General and introduction

The explicit solver LS-DYNA version 971, see Hallquist (2007), is used for the collision simulations. These collision simulations are carried out dynamically, both considering actual ship motions in a coupled approach and prescribed displacement-controlled motions in a quasi-static (QS) approach. The coupled analyses are conducted with the actual velocities and accelerations occurring during the collision while the quasi-static simulations are conducted with a constant prescribed velocity assuming a certain penetration path. Thus, the dynamic effects in collision and the exact penetration path are more precisely modelled in the coupled approach. The comparison of these two approaches will present the influence of the ship motions on the simulation results. The ANSYS parametric design language is used to build the finite element model of the supported X-core structure; see Figure 5 and Ehlers et al. 2008a. The structure is modelled using 515328 four noded, quadrilateral Belytschko-Lin-Tsay shell elements with 5 integration points through their thickness. In the contact area, the element length is 4.4mm, whereas the remaining elements have a length of 26.4mm, see also Figure 5.

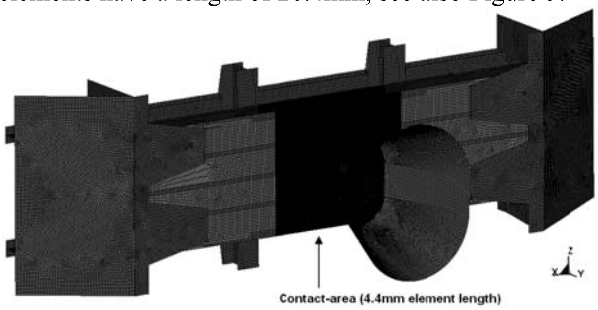

Figure 5. Meshed X-core structure

Standard LS-DYNA hourglass control is used for the simulations. The automatic single surface contact of LS-DYNA is used to treat the contact occurring during the simulation with a static friction coefficient of 0.3. The reaction forces between the striking bow and the side structure are obtained by a contact force transducer penalty card.

Quasi-static collision simulations

The quasi-static collision simulations are carried out to investigate the influence of the laser weld failure strain on the force and penetration predictions. Therein the rigid striking bow impacts the X-core structure with a constant displacement of 2.4 m/s at a straight penetration path. This displacement speed is taken to be the approximate average from the large scale experiment, see Figure 3a. The translational degrees of freedom are fixed for the indicated nodes, see Figure 6.

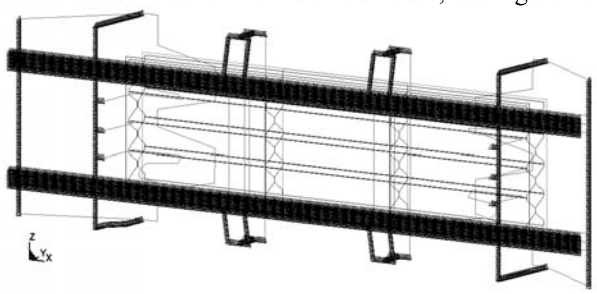

Figure 6. Supported X-core structure, translational degrees of freedom are fixed for the indicated nodes

Coupled dynamic collision simulations

In coupled dynamic collision simulations, the ships are allowed to move and the exact penetration history is defined from the collision dynamics and mechanics. The structural deformations are affecting and are evaluated under the actual physical motions occurring during the collision, thus the name coupling. For dynamic simulations the mass, inertia and hydrodynamic properties of the ships are included in the finite element model. This paper utilizes the coupled method proposed by Pill and Tabri (2009), which allows dynamic collision simulations with LS-DYNA. The ship motions are limited to the plane of water surface and thus the restoring forces are not included. Furthermore, the forces associated with the hydrodynamic damping and frictional resistance are neglected as their inclusion is not straight forward and as their share in the energy balance is relatively low, less than 10% of the total available energy, see Tabri (2010). Hence, the model concentrates on the accurate modelling of the main force components – the contact and the inertial forces.

In the finite element model, the masses and inertias of the colliding ships are modelled by using a small number of mass points, see Figure 7. The striking ship consists of a modelled bow region and three mass points. Correspondingly, the struck ship consists also of three mass points and a part of the side structure. The mass points are constrained to move together with the boundary nodes of the modelled structural parts and are thereby acting as boundary conditions, see also Figure 6. The mass nodes of the striking ship are given the initial velocity v_0=3.33 m/s.

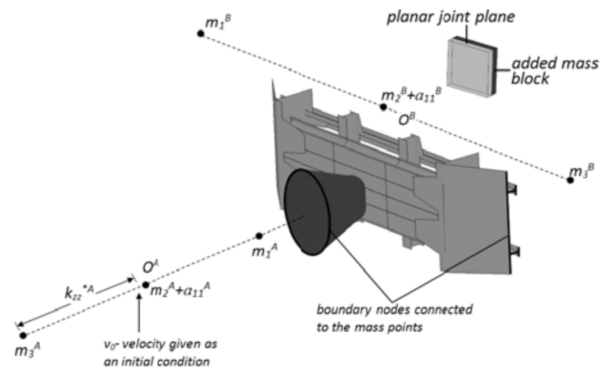

Figure 7. Calculation setup for dynamic collision simulations

Furthermore, the hydrodynamic added mass components associated with translational motions are included in certain directions only. The surge added masses of the striking and struck ships are marked as a_{11}^A and a_{11}^B in Figure 7. These added masses are positioned in the centres of gravity of the ships. The added mass associated with the sway motion is included only for the struck ship as the motions of the striking ship are predominantly in the surge direction. For the struck ship the sway added mass is modelled as a single block of additional mass that is located on the opposite side of the striking location, see Figure 7. This added mass block is constrained to the mass points through a planar joint, which restricts relative movement in sway direction and allows the joined entities to move in the surge direction. Thus, this mass becomes active only if the struck ship undergoes sway motion.

Plate material modelling

The aim of the dynamic and quasi-static X-core collision simulations presented in this paper is to predict the non-linear material behaviour until fracture with sufficient accuracy and to identify the influence of the laser weld behaviour on the results. Therefore, this paper uses the element length dependent true strain and stress relation until fracture identified by Ehlers and Varsta (2009) for NVA steel; see Figure 8. This element length-dependent NVA material relation is identified on the basis of optical measurements. The Norske Veritas Grade A (NVA) steel is a certified and common normal shipbuilding steel. This material relation is assumed to represent the material behaviour of the large scale X-core specimen sufficiently, because the exact material relation of the X-core specimen is unknown. Furthermore, Ehlers and Varsta obtained their results of 4 mm thick plate material, which is equal to the thickness of the X-core elements and the inner plating, the outer plating is 6 mm thick and thereby in sufficiently close range. The elastic modulus is 206 GPa, the Poisson ratio is 0.3 and the measured yield stress is 349 MPa.

This failure strain and element length relation is implemented in the ANSYS parametric design language model generation via material 24 of LS-DYNA (Hallquist 2007) and allows failing elements to be removed at the critical strain. This failure strain is set to 0.66 and 0.39 for the element size of 4.4mm and 26.4 mm respectively, see also Figure 8. The constant strain failure criterion is justified due to the close ranges of triaxiality at failure for 4 mm and 6 mm thick plates, see Ehlers (2010). The strain rate sensitivity is not included in this material relation, as no influence on the ultimate tensile force and failure strain for different displacement speeds are found, see Figure 9 and Figure 10. The difference in both strain and force was found to be below three percent.

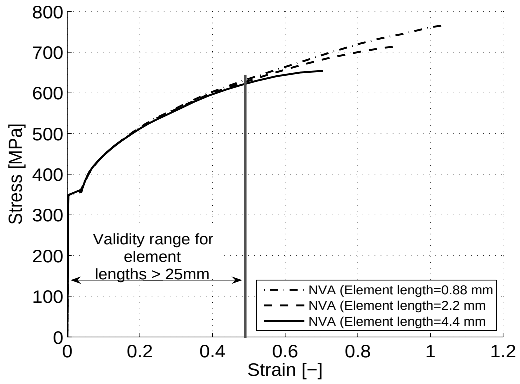

Figure 8. Element-length dependent NVA material relation until failure

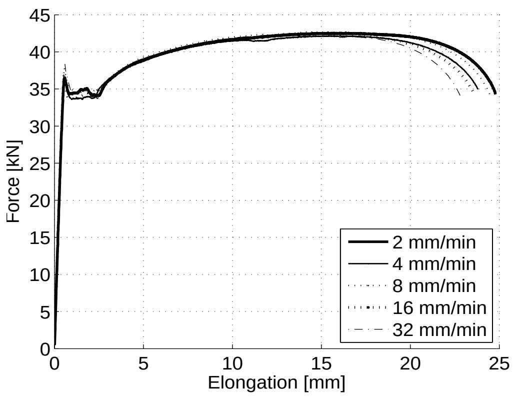

Figure 9. Force versus elongation for different displacement speeds

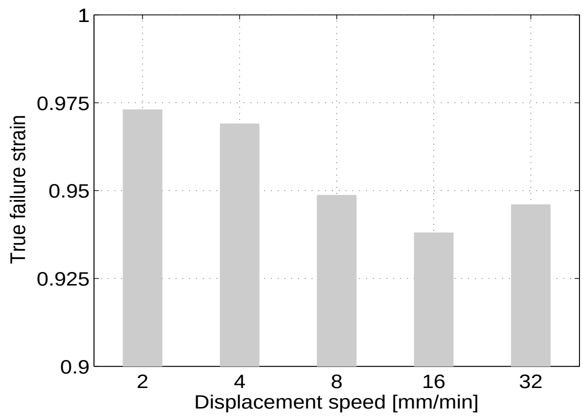

Figure 10. Local failure strain versus displacements speed

Weld modelling

The weld dimension-dependent material behaviour is obtained based on optical measurements, see Jutila (2009). The average width of his laser welds was 1.496 mm. Furthermore, he obtained a normal weld failure force from where the failure stress, $\sigma_{N(weld\,failure)}$, equal to $0.947\,kN/mm^2$, can be found. Jutila's local surface displacement measurements lead to logarithmic weld failure strain of 0.1. His measurements are in accordance with literature findings; see for example Çam et al. (1999) and Boroński (2006). Furthermore, this local weld failure strain is obtained on the basis of the discrete pixel dimensions from the optical measuring system whereby the strain reference length is clearly defined. This strain reference length is equal to 0.256 mm. Therefore, the gap between the X-core structures steel plates is set to 0.256 mm and the constraint spot weld model of LS-DYNA (Hallquist 2007) is used to represent the laser weld with a weld failure strain of 0.1, see Figure 11. The weld failure force in normal direction is set to 6.236 kN and 37.41 kN for the 4.4 mm and 13.2 mm element sizes respectively. The spot weld fails if the failure strain or force is reached. The entire model consists of 10305 spot welds, or 227 spot welds per meter of laser weld, being sufficiently dense to represent a continuous laser weld. Furthermore, the choice of the constraint spot weld model is justified as it assumes that the mass less spot weld is torn out of the adjacent plates once the critical state is reached. This behaviour is in line with the experimental observations of the laser weld failure, see Figure 12. To study the sensitivity of the weld failure strain on the overall failure process, a series of quasi-static collision simulations are carried out with a weld failure strain value ε_{ef} of ∞, 0.1, 0.05, 0.01 and 0.001.

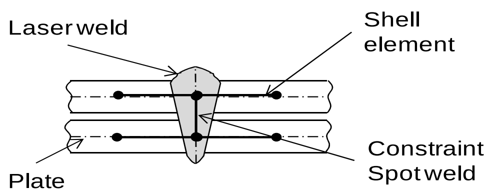

Figure 11. Constraint spot weld location representing the laser weld

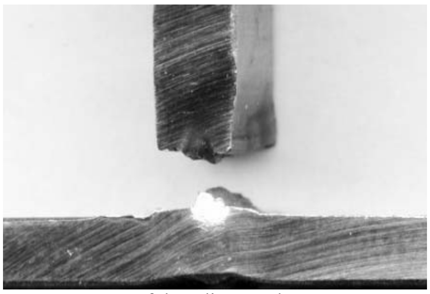

Figure 12. Laser torn out of the adjacent plate

Results and verification

Digitalization of the deformed X-core structure

The X-core structure shown in Figure 4a is digitized with the Tritop and Atos optical system produced by Gesellschaft für Optische Messtechnik (GOM). Thereby a full 3D reference model of the deformed shape after the collision experiment is obtained for a comparison with the results of the numerical simulations. The digitalization is done in two steps, at first the Tritop photogrametric system is used to capture a set of coded and uncoded measuring points which are applied randomly throughout the X-core specimen. The Tritop system consists of a digital camera which captures the coded measuring points from different angles and can thereby position them in a coordinate system for reference of the Atos measurements. The Atos system consists of two digital cameras and a fringe projection source which can digitalize within a measuring volume of 2 x 2 x 2 m³ in one view. The digitalization takes place through the fringe recording of the two digital cameras positioned in an angle to one another. Thereby the location of the fringe is known following the object grating principle.

(a)

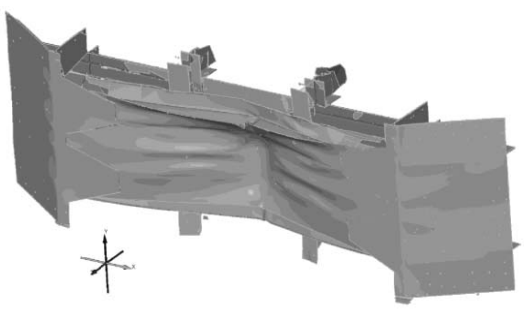

(b)

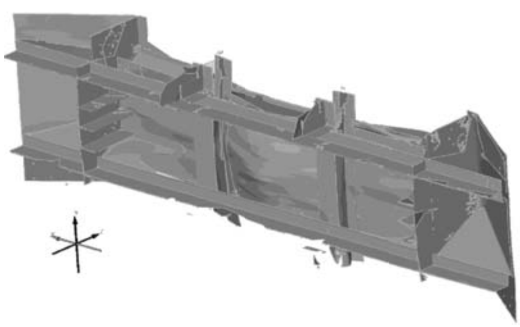

Figure 13. Digitalized X-core structure, front side (a) and back side (b)

Due to the large overall dimensions of the supported X-core structure the measuring point recordings from the Tritop system serve as a basis to position the Atos recordings with reference to the coded measuring points in one global coordinate system. By doing so, at least 3 coded measuring points need to be within the Atos digitalization view. As a result, the following 3D model is obtained, see Figure 13. This digital model of the X-core structure will be used to produce an overlay figures with the resulting deformed geometry from the dynamic finite element simulations. Thereby, and by comparing the force versus penetration curves, the numerical simulations will be verified.

Results of the numerical simulations

The resulting force versus penetration curve from the dynamic collision simulation is shown in Figure 14 together with the experimental result and a series of quasi-static simulations. These quasi-static simulations are obtained until a predefined penetration close to 1m is reached. The simulated penetration versus time from the dynamic simulation is compared to the experimental curve in Figure 15. The simulated penetration history is in good correspondence with the experimental curve. The peak penetration is predicted accurately, however slightly earlier. For comparison, the applied constant displacement of the quasi-static simulations is plotted in Figure 15 too.

Overall the dynamic simulations corresponds well to the experimental curve, the peak force at maximum penetration is however over estimated by the simulation. The quasi-static simulations present the influence of the failure strain on the force versus penetration curve. The simulated force becomes smaller with decreasing weld failure strain values.

The choice of constant strain failure criterion for the laser weld is justified, because initially only 1% of the welds fail due to the force criterion and all subsequent welds fail due to the strain limit. Furthermore, it is interesting to note, that the structural response for an infinite weld failure strain value is approximately equal to the response with a failure strain value of 0.1.

Fracture in the outer plating of the X-core structure, as found in the experiment, was not observed at the corresponding stage of penetration for the dynamic or quasi-static simulations. However, up to 96% of the plate failure strain value is reached in the striking location, and thus indicating that rupture would occur in a subsequent step. The latter was observed in subsequent steps of the quasi-static simulations.

The overlays of the digitalized and deformed geometry of the quasi-static and dynamic simulation using a weld failure strain of 0.1 are shown in Figure 16. The compliance of the deformed geometry is very good. The distributions of the deviations shown next to the legend in Figure 16 indicate that most of the deviations are between 0 and -25mm. In other words the numerical simulations over predict the deformations slightly. However, the contact region is represented sufficiently. Furthermore, the presence of rigid body motions seem to influence the results slightly, because the deviations show that the X-core specimen is twisted along the x-axis, which might be a result of the post-experimental transport.

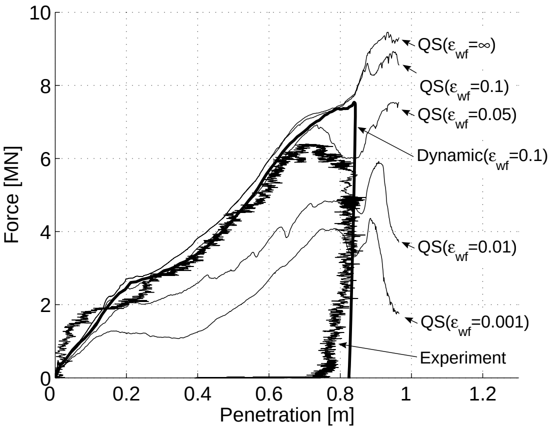

Figure 14. Dynamic and quasi-static (QS) collision simulation force versus penetration curves compared to the experimental result

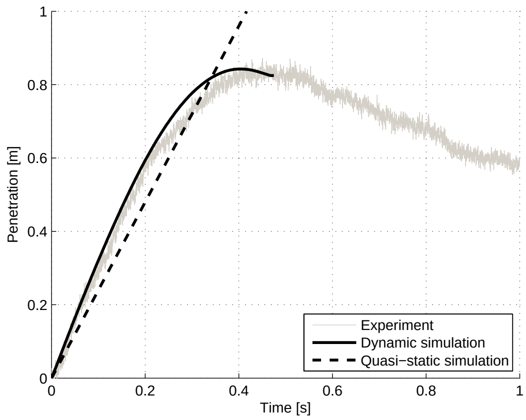

Figure 15. Quasi-static (QS) and dynamic penetration versus time versus exp

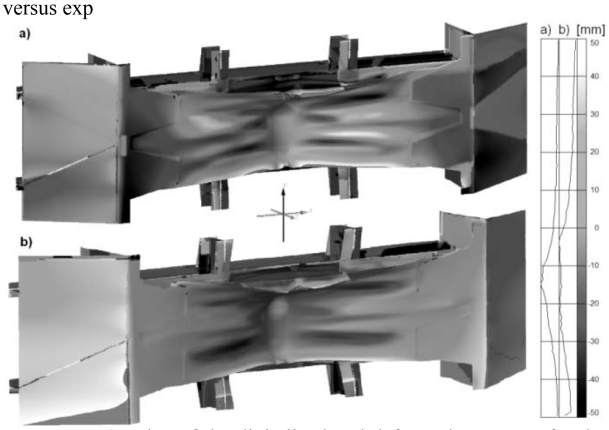

Figure 16. Overlay of the digitalized and deformed geometry for the quasi-static (a) and dynamic simulation (b)

Discussion

The maximum force is slightly over estimated with the dynamic and quasi-static simulations using a laser weld failure strain value of 0.1, see Figure 14. However, the results of the quasi-static simulations using a laser weld failure strain value of 0.05 are significantly closer to the maximum experimental curve. This indicates that the assumption of homogenous laser weld properties along the laser weld length throughout the X-core specimen is not entirely correct. Furthermore, this indicates that local deviations in the laser weld strength are quite probable, and thus reducing the maximum force. Additionally, the global bending of the hull girder and the presence of a very small amount of sloshing in the ballast tanks can contribute to the reduction in maximum experimental force compared with the simulations. However, the overall good correspondence of the force versus penetration curves indicates that the material relation, both for the plate- and weld material, obtained with optical measurements suffices for the presented collision simulations. Additionally, it can be said that the presented numerical implementation of the laser weld and the choice of constant strain weld failure criterion produces reasonable results.

The similar response of the X-core structure using an infinite failure strain and a failure strain of 0.1 indicates that this structure is not particularly sensitive to the laser weld properties, being in a reasonable range however. Hence, the local failure of the laser welds in the contact region does not reduce the global response for failure strain values of at least 0.05.

In general the influence of the ship motions on the force penetration curve is visible, because they cause a slight reduction in collision force. However, the corresponding quasi-static simulation is in very close range and represents a fair approximation, see Figure 14. This is expected, as in a scenario where the striking ship is colliding at a right angle to the struck ship, the influence of coupling is small as the penetration path can be prescribed rather precisely for the quasi-static simulations. More important however, is the fact that only the dynamic simulation is able to predict the correct end-point of the force versus penetration curve, respectively the available energy to deform the X-core structure.

The overlay of the finite element results with the digitalized deformed X-core structure served as an advanced tool for identifying the correct striking location and appropriate boundary conditions. Thereby the boundary conditions, respectively restrictions of translational degrees of freedom, of the support structures edges could be positioned only at the straight edges which where needed to obtain a similar deformation shape, see Figure 16.

Furthermore, it adds another option to verify the numerical results besides the force versus penetration curve alone, see Figure 14 and 16. Thereby it contributes to the strengthening of the reliability and accuracy of the numerical simulations. However, this is only applicable if the deformed shape is experimentally investigated.

Summary

A dynamic ship collision experiment is simulated with the non-linear finite element method. The laser weld of the investigated X-core structure is successfully integrated into the numerical model. A material relation, both for the plate- and weld material, based on optical measurements represented the non-linear material behaviour with sufficient accuracy. The comparison of the simulated and experimental results by means of the force versus penetration curve and by the digitalized deformed test structure shows good correspondence. Furthermore, the digitalized model served to verify the simulations on a new accuracy level and thereby contributes to the quality and reliable of non-linear collision simulations.

Acknowledgements

This paper has been funded by the project ‘Closed, filled steel structures – SUTERA’ by the 100-Year Foundation of the Federation of Finnish Technology Industries.

References:

Boroński D. Cyclic material properties distribution in laser-welded joints. International Journal of Fatigue. 2006; 28;346–354.

Çam G, Erim S, Yeni Ç, Koçak M. Determination of Mechanical and Fracture Properties of Laser Beam Welded Steel Joints. Supplement to the Welding Journal, June 1999; 193s-201s.

Cummins WE. The impulse response function and ship motions. Schiffstechnik 1962;9;101-109.

Ehlers S. A procedure to optimize ship side structures for crashworthiness. Journal of Engineering for the Maritime Environment. 2010;224;1-12.

Ehlers S, Broekhuijsen J, Alsos HS, Biehl F, Tabri K. Simulating the collision response of ship side structures: A failure criteria benchmark study. Int Ship Progress 2008a; 55; 127-144.

Ehlers S, Klanac A, Kõrgesaar M. A design procedure for structures against impact loading. Jahrbuch Schiffbautechnische Gesellschaft, 2008b.

Ehlers S, Varsta P. Strain and stress relation for non-linear finite element simulations. Thin-Walled Structures 2009, doi:10.106/j.tws.2009.04.005.

Hallquist JO. LS-DYNA keyword user’s manual, Version 971, 2007. Livermore Software Technology Cooperation, California.

Jutila M. Failure mechanism of a laser stake welded T-joint. Master of Science Thesis. Helsinki University of Technology. Department of Applied Mechanics 2009.

Pill I, Tabri K. Finite element simulations of ship collisions: A coupled approach to external dynamics and inner mechanics. In proceedings of Analysis and Design of Marine Structures 2009, pp. 103-109.

Wolf, M. Full scale collision experiment, X-type Sandwich side hull. EU Sandwich project report Deliverable TRD448, 2003, p. 21.

Examples of selected research efforts made on characteristics of material, ship side structure response and ship survivability in ship collisions

Jonas W. Ringsberg, Erland Johnson, Martin Schreuder and Per Hogström

Division of Ship Design, Department of Shipping and Marine Technology, Chalmers University of Technology, SE-412 96 Göteborg, Sweden

***Abstract*:**
The conditions for damage stability and survivability of a struck ship in arbitrary sea-state are, from a structural point of view, determined by the size and shape of the damage opening in the struck ship. To be able to make realistic simulations and draw conclusions on these topics, it is of outmost importance that research on ship collision investigate in detail the features of structural integrity, characteristics and failure phenomena that interact during, for example, a collision. A contribution to the field is presented in the current article which summarises research experiences from a group that is working with ship collision safety, using both experiments and numerical simulations by finite element (FE) analysis. Results are presented from tensile and forming limit tests, followed by FE analyses of these with the objective of predicting material rupture using appropriate constitutive material models and damage criteria. An example of an innovative design of a side-shell structure that is considered being more intrusion-tolerant than most side-shell structures used today is demonstrated. Finally, results from a research project which has a holistic approach on the assessment of survivability of a struck ship are presented. In the project, a methodology has been developed which combines structural analysis, damage stability analysis followed by risk analysis. Examples of results are presented where the probability of survival is calculated for various sea-state conditions.

Introduction

Collision and grounding constitute a significant part of ship losses in modern time. For that reason, large research efforts are being put on prevention and mitigation of the consequences by simulation of these events. Being a compound problem, it involves numerous disciplines of research which traditionally have been treated separately with limited interaction. The potentially costly consequences of a lost ship in the form of fatalities, property, cargo and related industries, as well as pollution of the environment in the form of oil spill, etc., are in the public view one of the driving forces that motivates research on collision and grounding. The trend in worldwide shipping is that total freight at sea is growing and that its role in the logistic transport chain of many types of cargoes is indispensable. Accordingly, the number of ships at sea and the sizes of these are increasing continuously. As a result, the risk of collision between vessels has increased, in particular for short sea shipping close to shore where sea-traffic density is high and the sea routes may be narrow. Several numerical procedures have been established which are suitable for novel structural evaluation of large ship structures on, for example, the collision between two ships (see, for example, Alsos 2008; ISSC 2003; Wang et al. 2002).

This article presents an overview of the achievements made by the Division of Ship Design at Chalmers University of Technology, Sweden, within the research on ship collision safety (see, for example, Hogström et al. 2009; Karlsson 2009; Karlsson et al. 2009; Ringsberg 2009; Schreuder et al. 2009). Examples are presented for calculations of structural damage by means of nonlinear finite element (FE) analysis, experimental and numerical analysis of prediction of rupture, and an example of a crashworthy design. A holistic approach on the assessment of survivability of a struck ship is presented where the probability of survival can be calculated for various sea-state conditions and damage opening configurations.

Experiments

This section presents results from the three types of experiments which provide the engineer and researcher, working on ship collision and grounding, with valuable information in model-making and validation of models using, for example, the FE method: uniaxial tensile tests, forming limit diagram tests and a ship-like structure small-scale test. The two former tests are necessary for the definition of material constitutive model characteristics, and for the choice and tuning of material parameters of the failure or fracture criterion used in the analysis. The last experiment takes a step from simple laboratory specimen geometry to a small-scale-realistic ship structure and challenges the selection of model parameters, FE-solver and simplifications made. Hence, it can be used for verification or validation of established numerical models which can subsequently serve as a guidance to model an even larger structure, such as the entire ship. Figure 1 shows the work flow that is necessary for having full control in a situation where one wants to make realistic and reliable analyses of the last step of large (global) ship structures which cannot be verified by testing due to large dimensions.

Figure 1: Illustration of range in scales (approx. resolution in FE mesh) in material testing and numerical simulation of a ship collision and grounding.

Uniaxial tensile tests

The influence of the element size of the FE mesh, the well-known length scale dependence on the failure limit, and utilisation of damage evolution models available in commercial FE software can be studied in detail using tensile test results. Additional topics of interest are the influence of multiaxial strain state on failure, see Alsos et al. 2008, and the applicability and reliability of the criteria studied in numerical investigations of ship-ship collisions; see the following “Forming limit diagram tests” section for more details.

In Hogström et al. (2009), novel uniaxial tensile tests are presented using the ARAMIS (2009) optical strain measuring system. This system enables a very accurate monitoring of displacements on the specimen surfaces and therefore also material characteristics. Three materials were tested: the NVA mild steel (DNV, 2007), the Domex 355 high strength steel (SSAB, 2009), and the NV5083 aluminium material (DNV, 2007). The NVA material is a material that is commonly used in shipbuilding today, while the Domex 355 and NV5083 materials have lately become more frequently used as a consequence of the demands on weight reduction and lighter ship structures. The thickness of the specimens was 4 mm and they were manufactured from hot-rolled steel plates and cold-rolled aluminium plates. The experimental setup fulfilled the requirements in the DNV rules (DNV, 2007).

The data obtained from the ARAMIS recordings allow for an analysis of the displacements over length scales defined by the engineer. As a result, the “Aramis” strain of the test rod can be measured using virtual extensometers (VE) that represent various length scales. A VE is defined as the distance between two points along the length of the test rod that are positioned at an equal distance from the point of fracture. Figure 2 presents the results from the ARAMIS recordings made on the NVA mild steel: a long VE corresponds to a strain value measured over the entire length of the test rod (see the bold line in Figure 2a), while a small value of the VE corresponds to more local strain behaviour (see the dotted line in Figure 2a). The “Aramis” stress in Figure 2 was calculated using the force recorded by the load cell in the test machine divided by the actual area of the cross-section where fracture (eventually) occurred; see Hogström et al. (2009) for details. This area was calculated using the displacement information recorded on the specimen. In addition, the curve fitted to the fracture points in Figure 2b is the Barba law formulation proposed by Yamada et al. (2005); see also Paik (2007) who presents important practical techniques for finite element modelling to simulate among others ship collision and grounding.

Forming limit diagram tests

Forming limit tests can be carried out in order to study the multiaxial strain behaviour of the material in terms of necking and fracture. In numerical analysis of ship structures subjected to impact loading conditions, the multiaxial strain behaviour and characteristics ought to be incorporated in the failure criterion used in order to properly mimic the damage degradation and fracture of the structure. Consequently, such tests were conducted in

(a)

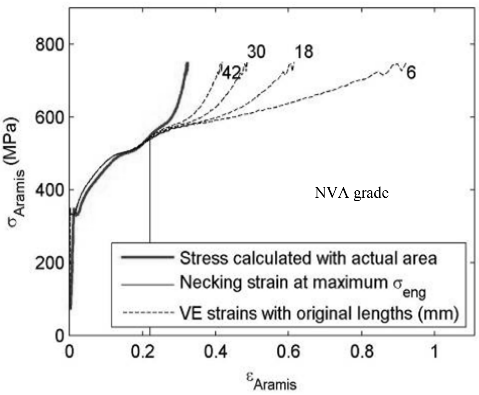

(b)

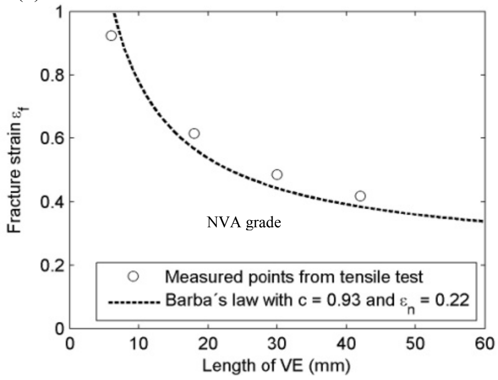

Figure 2: Results from the tensile tests on the NVA mild steel material. (a) The stress is calculated based on the actual area of the test specimen and the strain is measured in accordance with the length of the virtual extensometer (given in mm). (b) Presentation of the fracture strain as a function of the length of the virtual extensometer together with Barba’s relation fitted to the measured points.

(a)

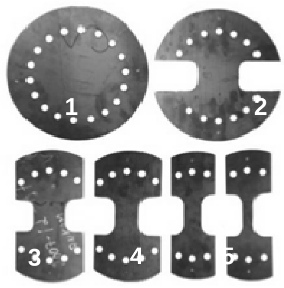

(b)

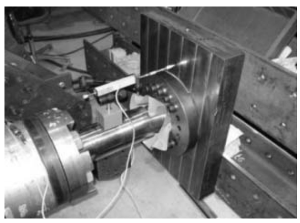

Figure 3: (a) The six test geometries: each of them corresponds to one strain state in the forming limit diagram. Geometry 1 is the circular plate (upper left) and geometry 6 is the narrowest of the geometries (lower right). (b) Test setup: the punch goes into the hold in which the specimen is clamped, the teflon lubrication sheets can be seen between them. Also, the displacement gauge can be seen, fixed on top of the punch.

Hogström et al. (2009). The tests were carried out on the NVA steel grade in accordance with the ISO 12004-2 standard and the ARAMIS system was used to monitor the surface displacements of the test specimens. Six different geometries were tested, see Figure 3, corresponding to six data points in the forming limit diagram (FLD). Three samples of each geometry were tested.

A summary of the results from the forming limit tests can be presented in the principal strain space shown in Figure 4. Here, the mean values of each specimen are presented and the error bars denote the standard deviations in test results between test specimens for the test geometries 1 to 6, respectively. It is to be noted that, even though the evaluation procedure is designed to reduce the scatter, there is larger scatter in results from the measurements for fracture in the ε1 direction in contrast to the ε2 direction; see Hogström et al. (2009) for discussion. The curve corresponding to the Bressan-Williams-Hill (BWH) criterion proposed by Alsos et al. (2008) is also shown in the figure.

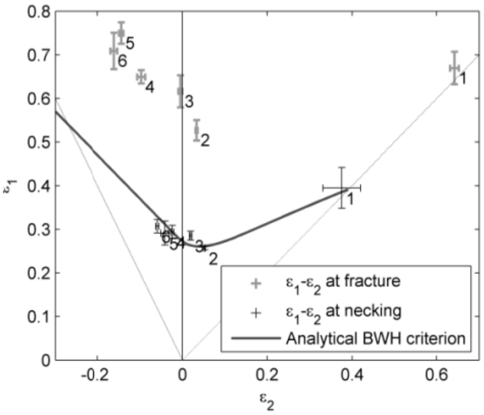

Figure 4: Results from forming limit tests of the six geometries (based on five sections on three test samples for each geometry): mean values and standard deviations (denoted by the error bars) in the principal strain space (ε1 and ε2 directions), for necking and fracture. The analytical solution of the BWH criterion fitted to the experimental values is also included.

Bulb impact with ship-like structure in small scale

Karlsson et al. (2009) studied the structural characteristics of a ship side-shell structure subjected to bulb impact. The experimental ship side-shell structure tested was developed from a double-bottom side-shell structure. The function and possible structural collapse of each of the elements during simulation with a bulb impact load was considered as part of the experimental structure development process.

In order to fit the testing object to the testing machine, the dimensions of the structure had to be scaled down by a factor of 3 compared to a similar type of full-scale structure. Figure 5 shows the dimensions of the structure and its structural elements. The structure was made of the 240 steel grade material with the roll direction oriented in the x-direction as shown in Figure 5. The L-profiles are running-through. To facilitate this, L-shaped holes were made in the vertical plates and in the T-beam web plate, around which the L-profiles were welded. The welds were made according to welding standards.

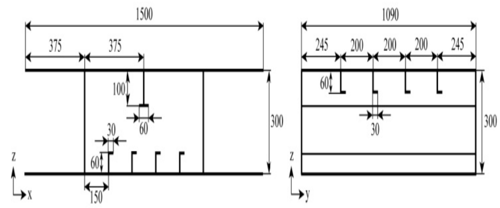

Figure 5: The side-shell structure used in the bulb-structure impact test (mm).

A reinforcing frame was designed and welded around the structure along its edges to create clamped boundary conditions to ensure well-controlled failure modes of the structure. The lower part of the frame was welded to a rigid fixture, see Figure 6. Four displacement transducers were positioned in two directions at the supporting frame and fixture in order to register the frame's deformation and to make sure that the fixture's deformation during the tests was negligible.

A solid indenter (half-sphere) with a radius of 135 mm represented a solid bulb geometry during testing. It was mounted in a press machine with a 20 MN load capacity, and its moving speed and direction was 4 mm/s perpendicular to the sheet's surface with the collision point in the centre of the sheet, see Figure 6. The indenter was moved until penetration of the lower plate occurred. Two similar structures were tested and before each test, the indenter was pushed against the structure followed by unloading, at low speed ten times, for relaxation of the residual stresses caused by welding of the sheet to the frame. The load magnitude in this loading sequence was within the elastic region of the material. The results from the experiments are presented together with the FE analyses of them.

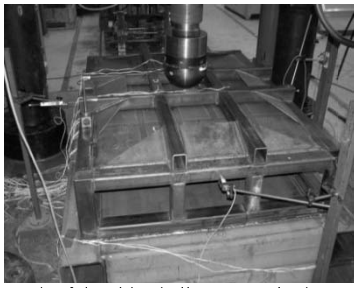

Figure 6: Photograph of the side-shell structure in the test rig.

Finite element analyses of the experiments

The FE analyses of the experiments were carried out using the commercial software Abaqus/Explicit (Dassault Systèmes, 2007). All geometries were modelled using four-node shell elements with reduced integration (S4R in Abaqus/Explicit) and 5 section points through the thickness. The resolution and size of elements in the models was determined by normal convergence analysis.Generally, shell elements that are thick in relation to their side lengths give poor results in bending, since this type of element has a plane stress formulation and thus they are unable to resolve stress gradients in their thickness direction. In the uniaxial tensile tests, no bending is present and in the forming limit tests, membrane and bending stresses are present but the membrane stresses are regarded as being dominant, making the use of shell elements feasible. In addition, results in the elements are taken in the through the thickness mid section point, i.e. in the neutral axis, and thus bending stresses are disregarded.

For the modelling of different physical phenomena leading to failure of a material, Abaqus/Explicit offers several models that handle initiation and evolution of damage. For damage initiation (DI) in ductile metals, either the ductile criterion, a phenomenological model for the nucleation, growth and coalescence of voids, or the shear criterion that models shear band localization, may be used. In addition, the most frequently used criteria for predicting material failure are based on effective plastic strain. Such criteria have gained in popularity due to their simple and effective formulation and have been proved to give results with satisfying accuracy by, among others, Karlsson et al. (2009). However, these criteria neglect the influence of strain state and recently criteria which take this into account have been proposed and applied, see, for example, Ehlers et al. (2008) and Hong et al. (2007). An example of such a criterion, which was compared with the experiments, is the BWH criterion proposed by Alsos et al. (2008).After the damage initiation, a damage evolution model describes the degradation of the material up to the point of fracture. In Abaqus/Explicit, the evolution is defined either through the displacement at fracture, uf, or the energy dissipated during the failure process, Gf. The former alternative was used in the current study. The displacement at fracture is defined as uf = L×εf where L is a characteristic element length and εf is the plastic strain at fracture taking into account the influence of the length scale, cf. Barba's law. In the post-necking region, the element size of the mesh has a great influence on the solution. Consequently, this dependency has to be accounted for when the damage evolution parameter is defined. In Abaqus/Explicit, damage evolution may be defined as linear, bilinear/piecewise linear, or following an exponential behaviour, see Hogström et al. (2009).

Uniaxial tensile tests

The FE simulations of the tensile tests were conducted in order to study the damage evolution law in terms of mesh dependency (element size or length scale) and choice of damage evolution function. Several element sizes (between 1 and 8 mm) were compared to investigate its influence on the solution and results. Up to the point of damage initiation, no dependence from the element size could be seen between different FE models and simulations. However, after the initiation of damage, the influence from the element size became significant. This could be compensated for by using Barba's law through adjustment of the uf-parameter, as seen in the previous section, according to the characteristic element length in the FE model.

The material in the FE analysis was the NVA mild steel material that was represented by an isotropic hardening model with piecewise linear isotropic hardening characteristics for the plastic behaviour. A Young's modulus of 210 GPa and a yield stress of 310 MPa were used, see Hogström et al. (2009) for details.

In Hogström et al. (2009), the ductile criterion was used to model the damage initiation in the FE simulation of the tensile tests using the necking strain from the tests, εn = 0.22, as the plastic strain at the onset of damage. The FE simulations were interrupted at a point that had a similar definition as the experimental point of interruption of a test, i.e. when the gradient of the stress-strain relation increased rapidly and fracture was a fact. The displacement at fracture, uf, used in the FE simulations was calculated using εf according to Barba's law.

Figure 7 shows a comparison in results between a tensile test and an FE simulation of it. Figure 7a shows the major principal strain in the facets on the specimen's surface and it was calculated using the data recorded by the ARAMIS measurement system. The corresponding result from an FE simulation is shown in Figure 7b where the bilinear damage evolution relationship was used. The results are presented at the time, T, which is 95% of the total time to fracture, Tf. There is very good agreement in results between the experiment and the FE simulation with respect to magnitude of the major principal strain and the contours of its distribution.

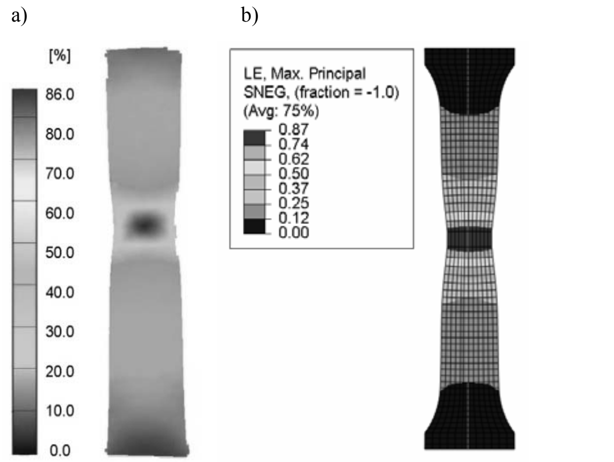

Figure 7: Major principal strain results for a tensile test presented at T = 0.95Tf: (a) results from an experiment using the ARAMIS system and (b) results from an FE simulation using Abaqus/Explicit.

Forming limit diagram tests

In the simulation of the forming limit tests, zero friction was assumed and the contact conditions between the punch and the specimen were modelled using the "general contact condition" in Abaqus/Explicit. Only half of the test specimens were modelled because of symmetry. In addition, the material in the FE analysis was the NVA grade material that was represented by an isotropic hardening model with piecewise linear isotropic hardening characteristics for the plastic behaviour. A Young's modulus of 210 GPa and a yield stress of 310 MPa were used.

Several criteria for simulating instability of sheet metal are available in Abaqus/explicit, such as the "FLD criterion" which was used in the simulation of the forming limit tests. In the FE simulations of the forming limit tests, all six geometries in Figure 3a were assessed. To define damage initiation, representing the necking in the experiments, the FLD criterion was used with tabular values of ε1 and ε2 taken from the BWH curve presented in Figure 4 as input. Degradation due to evolution of damage was represented in the FE model using the bilinear damage evolution law also used in the FE simulation of the tensile test. The results from the FE simulations were evaluated similarly to the evaluation of tests; see Hogström et al. (2009).

The results in Figure 8 show that the trends of both the necking and fracture are captured by the FE simulated values; however, some discrepancies are present. The points representing necking for test geometries 2-6 are collected around the major principal strain axis, while the corresponding simulated points are more separated in the ε1-ε2 space. A similar trend can be seen with the points representing fracture. One reason for this effect may be that the specimens (4 mm thick) were manufactured from hot-rolled steel plates, which induced pre-straining (and anisotropy) in the material, and this effect was not represented in the FE material model.

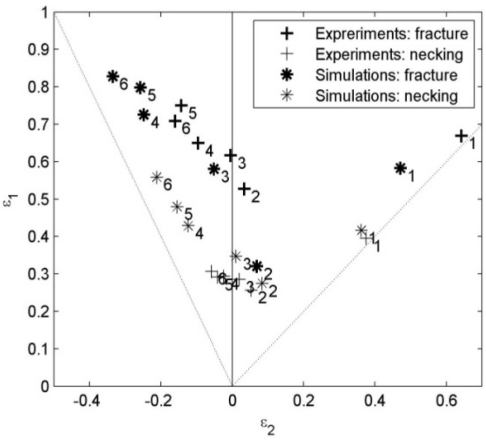

Figure 8: Results presented in principal strain space from the experiments and FE simulations of the forming limit tests.

Figure 9 shows a comparison in results of the major principal strain in a test specimen of geometry 2 and the FE simulation of the same geometry. The results are presented at a time, T, which is 95% of the total time to fracture, Tf. There is very good agreement in results, both with respect to magnitude of the major principal strain and the contours of its distribution.

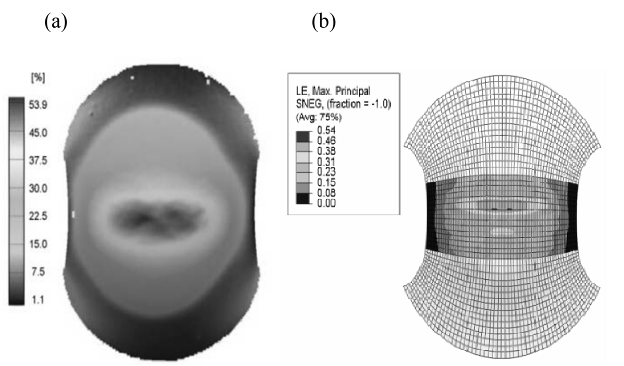

Figure 9: Major principal strain results for an FLD test on geometry 2 at T = 0.95Tf: (a) results from an experiment using the ARAMIS system and (b) results from an FE simulation using Abaqus/Explicit.

Bulb impact with a ship-like structure in small scale

A detailed description of the FE simulation of the bulb impact with the ship-like structure test is presented in Karlsson et al. (2009). In the simulations, large deformations, nonlinearity in material properties, multiaxial stress-strain conditions and material rupture were also accounted for.

The shear failure criterion model in Abaqus/Explicit was used in conjunction with von Mises plasticity model. Note that despite the fact that the shear failure model criterion has known limitations, for example during compressive loading conditions or its inability to simulate the fracture process accurately, see Alsos (2008), this criterion is still often used by ship design engineers and can be considered as being sufficient in certain types of analyses. Note, however, that it is recommended to compare this criterion with a similar analysis (if possible) using the FLD criterion and damage evolution modelling presented in a previous section. If necking is the defined limit of failure, either the FLD or BWH criterion can be used alone. Figure 10 presents the results from the best calibration that could be achieved against the test results: mesh size 15 mm and true failure strain 39%. The agreement was considered as being satisfactory, since the FE model mimics the bulb reaction force-displacement curve from the tests until the second peak, and most of the failure modes of parts of the structure correspond very well between tests and FE simulation. However, one possible cause for the poor prediction of the penetration of the lower plate is the residual stresses caused by welding. Even though the residual stresses were relaxed in the test structure in advance of the testing, it was done only for the upper plate and not for the lower one.

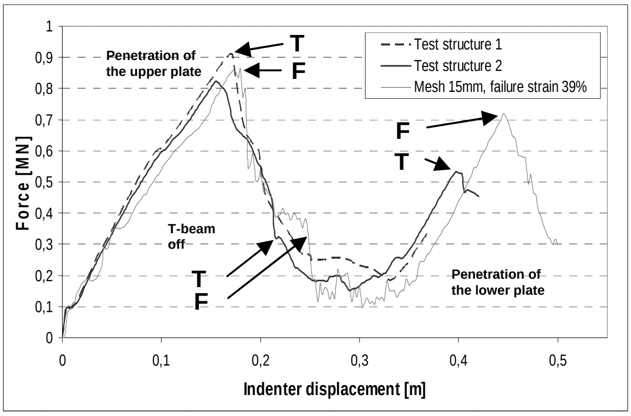

Figure 10: Results from tests and the best calibrated FE model (FEA): a mesh size of 15 mm and a true failure strain of 39%.

Safer structures against collision by innovative designs

When a ship strikes another ship in the side-shell structure, the majority of the momentum energy of the striking vessel is transformed into energy absorption in both ships' structures; some of the energy is transferred to the water, due to damping effects. The most structural damage will be found in the struck ship because of the structure's characteristics for this type of loading and also the bulb of the striking ship. The striking ship's bulb and bow may be severely damaged, but often not as critically as for the struck ship.

The way the energy is absorbed is mainly determined by the structural arrangement and the material properties of the struck hull section and the striking bow's geometry. Wang et al. (2000) demonstrated that the energy absorption and fracture initiation of a hull in a collision differs greatly for different bow forms, as the geometry of the striking bow has a direct influence on the response of the struck ship's side-shell structure. A small spherical bow will cause fracture in the contact area whereas a large bow will cause fracture in adjacent hard points.

A variety of attempts to vary the structural arrangements and scantlings of double side-shells has been made in order to improve the energy absorption capabilities in collisions (Ehlers et al. 2007; Klanac et al. 2005; Kitamura 1997; Kim and Lee 2001). Large-scale crash tests using sandwich structures with X and Y-shaped core geometries have shown good results (Peschmann 2001; Tabri et al. 2004; Wevers and Vredeveldt 1999). Hong et al. (2007) and Tavakoli et al. (2007) conclude that an effective way to improve the energy absorption capacity of an FPSO is to reduce the frame spacing and to increase the plate thickness. Another way of increasing the collision safety was presented by Yamada et al. (2005), who, instead, made the bulb weaker in order to deform easier on impact, absorbing a larger part of the energy. Tautz (2007) introduced a new solution where the idea is to make a deeper intrusion possible before leakage by arranging perforations of the web frames, where the inner shell can separate from the web in a collision.

Karlsson (2009) describes a conceptual thinking behind a new innovative side-shell structure whose inner side-shell will postpone or delay failure to a large extent, during a collision scenario, in contrast to most commonly used side-shell structures used today. In the study, a side-shell structure was developed which has considerably improved structural characteristics when subjected to a ship-ship collision scenario as compared with most side-shell structural designs existing today. A Systems Engineering design methodology was adapted together with the project partners to go forward in the process of finding a successful design solution; see Karlsson (2009) for detailed description.

The development of the new innovative structure, hereafter referred to as the "corrugated" structure, meaning that the inner side-shell has a horizontal-corrugated geometry, relied to a large extent on nonlinear explicit FE simulations. The reference structure was the side-shell of the ship developed in the European fifth framework programme, EU project INTERMODESHIP (The Intermodal Ship). This ship is a "Trollhättemax" ship which is a shore-ship for RoRo cargo and designed for traffic in the Trollhätte Canal in Sweden and in the inland waterways in Germany (Duisburg).

The most successful design of the side-shell structure that was simulated by FE analysis was a structure with a horizontally-corrugated inner side-shell that is welded to vertical webs with a spacing of 2400 mm. As the bulb of the striking ship impacts with this side-shell structure, the bulb penetrates the outer side-shell before it reaches the inner side-shell. A substantial part of the initial energy momentum has been consumed by the striking vessel at this instance in time, but a lot remains to be transferred to the struck structure. With the following penetration of the striking ship's bulb into the struck ship's structure, the corrugated panel separates from the webs and, because of its geometric shape, it develops like an accordion without breaking and more energy is absorbed by the already fractured structure without the occurrence of penetration of the inner side-shell.

The FE-simulations of the "flexible" inner side-shell structure show that it can increase the energy absorption considerably more than the stipulated 100%, at the same time as the stakeholders' interests are fulfilled. The range in intrusion depth of ten collision positions of the reference design was 1.50-2.04 m. With the new crashworthy structure, i.e. the "flexible" inner side-shell structure, the range in intrusion depth is increased to 2.98-3.96 m; see Karlsson (2009) for details. This corresponds to approximately B/5 of the ship's breadth. The deep intrusion made results possible with an increase of the amount of absorbed energy of between 206%- 295% of the struck ship without breaking! In Figure 11, a comparison of the collision-resistance between the reference and corrugated side-shell structures is presented, here illustrated as the maximum penetration of the striking ship into the struck ship when the inner side-shell of both structures have fractured in the lower compartment. The new side-shell structure design has not yet been tested in a laboratory and it may need to be further optimised.

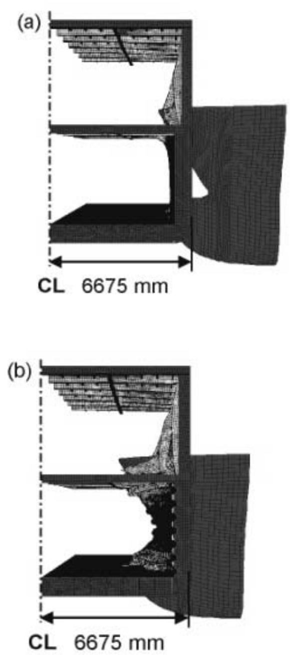

Figure 11: A comparison of the collision-resistance between the (a) reference and (b) corrugated side-shell structures illustrated as the maximum penetration of the striking ship into the struck ship when the inner side-shell of both structures have fractured in the lower compartment. Note the larger penetration depth of the corrugated side-shell structure.

A holistic assessment of ship survivability

In the HASARD project (Holistic assessment of ship survivability and risk after damage), a comprehensive calculation procedure has been developed useful for quantitative assessment of the survivability of damaged ships (incorporating structural collision resistance, structural stability and collapse, and time simulation of ship flooding and stability in waves). The connection and interaction between nonlinear structural damage analysis and seakeeping/stability is a unique feature of the project, i.e. to treat the entire system and chain of sequences and consequences that may risk the survivability of a struck ship. It can be used directly in the ship design process for studying the consequences of plausible collision scenarios; hence, necessary actions and design considerations can be identified before the ship is built. Enhancement of the understanding of the physical processes involved in the chain of events following a collision between ships will also be obtained in the project.

The project constitutes two tracks, structure and stability. Deliverables from the former include, among other things, phenomenological models, which, with satisfying reliability, can mimic the collapse and rupture phenomena in ship-ship collision simulations using the FE method. Deliverables from the stability track include, among other things, further enhancement of a computer code developed for the analysis of transient ship instability conditions, see Schreuder (2005), and a formulation of procedures which may quantify the ability of a damaged ship to stay upright. This computer code is called SIMCAP and it has been validated and successfully used in the research study on the sinking sequence of MV Estonia (Schreuder, 2008). In summary, these procedures can be used for the analysis or as a measure of the safety performance of, for example, RoPax ferries.

The two tracks of the project operate in close collaboration through the exchange of information, which leads them towards a common aim: to develop a calculation procedure for becoming a useful tool for risk analysis (structural collapse and ship stability) of the survivability of a collided and flooded ship, see Figure 12 for a schematic representation of the iterative procedure between tracks. The collision event is discretisized in time to enable the transfer of information between models, such as collision damage/pattern, ship flooding and stability in waves, and global and local loads acting on the structure.

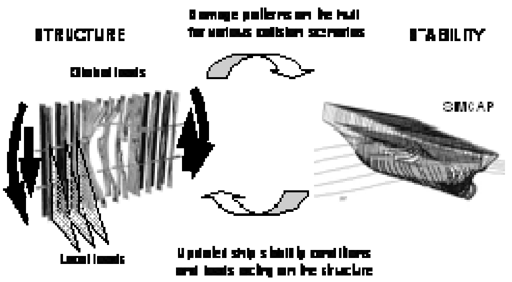

Figure 12: Iteration scheme between structure and stability tracks. The stability track delivers the collision-structural damage to the stability track, which calculates the ship's condition of stability. The more the struck ship penetrates the side-shell of the struck ship, the larger the collision damage is and an instability condition may occur.

Because of the complexity of the numerical models, the experiments and experiences from FE simulations are valuable for the validation of some of the models and calculation procedures, especially collision impact, energy absorption, material rupture and damage pattern. These necessary tests determine material and structural characteristics for a loading situation similar to that of a ship-ship collision event.

In a case study using the holistic approach used in the HASARD project, the behaviour of a ship after a collision damage resulting in a loss of the watertight integrity was studied. The studied vessel is a RoPax ferry that has been struck amidships by a similar sized ship at a right angle, resulting in a two-compartment damage (worst SOLAS damage), see Figure 13. The static angle of equilibrium for the damage case is about 3 degrees. A large opening to the vehicle deck will, however, allow for an accumulation of water due to the wave action, and finally a capsizing of the ship.

The damaged space is situated below the bulkhead deck close to amidships. The damage opening was generated by FE analysis and represents a bulbous bow penetration of the struck hull. The capsize mode of this damage case is governed by the amount of floodwater on the vehicle deck. The time to capsizing, Tcap, is defined as the time when the floodwater volume reaches 2000 m3. This will be a simple and robust definition, since the floodwater volume is monotonically increasing above approx. 1800 m3, as opposed to, for example, the fluctuating roll angle. The ship will always capsize within a few wave encounters after this amount has been reached.

Simulations were made for two different wave spectra, Jonswap with Tp = 8 s and $\gamma = 3.3$ and Pierson-Moskowitz (P-M) with Tp = 12s, 11 different significant wave heights (between 3 m and 8 m) and 8 different headings (every 45 deg) resulting in a total of 176 simulation runs. The ship had no forward speed and the simulation time was 30 minutes (1800 s) for all runs. Figure 13 shows the time series of one single simulation which resulted in a ship capsizing after 324 s. The very rapid process, from 30 to 180 degrees of roll, is partly due to the absence of a superstructure and hence buoyant volumes of the hull model in the simulations. However, a non-watertight superstructure cannot prevent capsizing. It can only slow down an inevitable event.

(a) (b)

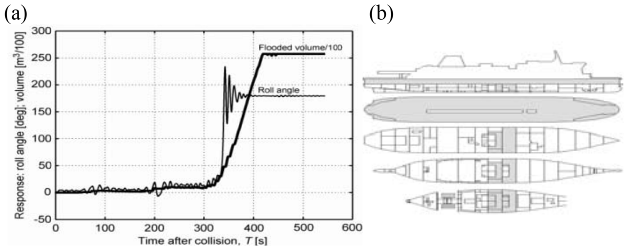

Figure 13: (a) Time series of a typical capsizing simulation with significant wave height 6.0 m. (b) The RoPax ferry with damaged compartments shaded.

The time to capsize is collected from the time series of all simulations. In Figure 14, Tcap is plotted against the significant wave height for all Jonswap spectrum simulations (data at Tcap = 1800 s means that there was no capsizing at the end of the simulation). The appearance of the graphs for the different headings suggests the existence of a survival limit, as also reported by e.g. Spanos and Papanikolaou, 2007; a wave height below which capsizing will never occur. This corresponds to a steady state floodwater volume (below ~2000 m3) on the vehicle deck. For sufficiently small waves there will be no flooding of the vehicle deck at all, due to the residual freeboard.

For more accurate results, several wave train realizations are needed and it is currently under investigation in the project. This allows for a quantitative risk analysis, where each single graph in Figure 14 can be transformed into a region with increasing cumulative probability of capsizing as the wave height increases.

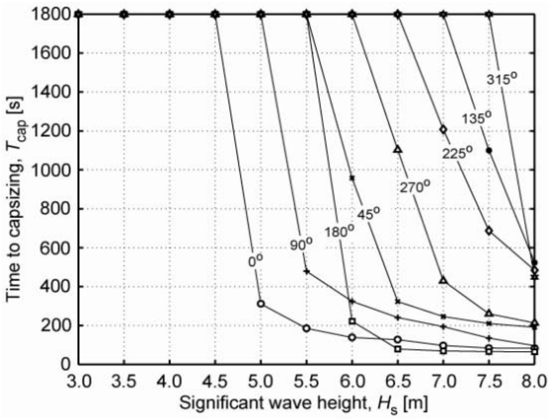

Figure 14: Example of results from all Jonswap spectrum simulations: influence of the heading angle on the time to capsizing.

It is also of interest to study the influence of wave seeds. A first set of simulations have been carried out for the two compartment damage in Figure 13 and with a loading condition that corresponds to a vertical centre of gravity (KG) equal to 12.89 m for the current ship. In the simulations, the sea states were represented by both the Jonswap spectrum (peak period Tp = 4·sqrt(Hs) and peak enlargement factor γ = 3.3) and the P-M spectrum with Tp = 12 s. The significant wave height, Hs, was varied between 3 and 8 m with an increment of 0.5 m. In the Jonswap spectrum simulations, 16 heading angles were used, i.e. every 22.5°, while in the P-M simulations, 8 heading angles were used, i.e. every 45°.

The time to capsizing, Tcap, is collected from the time series of all simulations. Figure 15 presents an example of the time to capsizing, Tcap, against the significant wave height for head sea conditions using the Jonswap spectrum. In the figure, the traces from the eight wave seeds also suggest the existence of a survival limit. Note the scatter band in time to capsizing as a consequence of the variation in wave seeds.

The area enclosed by the traces in Figure 15 constitutes a capsizing band, see Jasionowski et al. (2003), i.e. the probability of capsizing increases within the band as the wave height or time increases. This is illustrated in Figure 16 where the cumulative density function of capsizing probability versus Tcap is presented for the three significant wave heights 5.5 m, 6.0 m and 6.5 m.

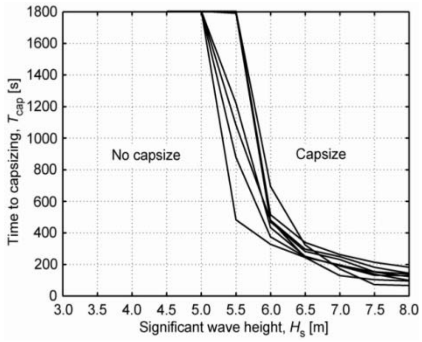

Figure 15: Scatter in time to capsizing obtained by simulation of 8 wave seeds with the Jonswap spectrum and head sea conditions.

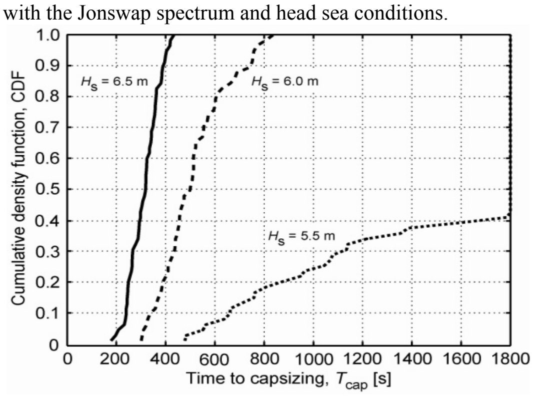

Figure 16: Cumulative density functions of capsizing probability versus Tcap for Hs = 5.5 m, 6.0 m and 6.5 m.

Conclusions

Today, material rupture of laboratory specimens and small-scale ship-like structures can be simulated with satisfying accuracy; only computer capacity and acceptable computational effort are limitations. Nevertheless, there are of course challenges when it comes to the computer capacity required when the larger full-scale ship structures with a high degree of detail complexity is a matter for the analysis. This calls for further development of more simplistic models and also criteria that capture damage degradation phenomena appropriately without being too detailed.

An example of a crashworthy structure was presented, which, by numerical simulations, shows very promising results and could be used already today in ships under construction. This structure must, however, be further assessed and also tested in a laboratory. The development of this type of structure is a good example of the fact that there is still room and large potential for contributing to safer shipping if a more open-minded thinking and acceptance for innovation approaches are adopted, not only by the researchers.

The holistic approach utilised in the HASARD project has shown the importance of combining a structural analysis with a damage stability analysis, both in the early stages of safety assessment of ship structures, but also in the future for development of guidance in collision-scenario-based decision making systems. One of the conclusions this far in the project is that the high degree of accuracy a researcher on structure analysis strives for actually has a minor influence on the characteristics in the following damage stability analysis; this yields also for the researcher within the area of damage stability analysis.

Consequently, by adoption of a holistic approach, where structure integrity and damage stability research are combined, using a systematic parameter (sensitivity) and collision-scenario-based analysis, simplified models and criteria can be developed more efficiently and with higher precision. It will also be clearer which variables that are the most important to focus on when it comes to, for example, the survivability or risk for capsizing that is of greatest concern in the HASARD project.

References:

Alsos H.S. 2008. Ship grounding – analysis of ductile fracture, bottom damage and hull girder response [dissertation]. [Trondheim, Norway]: Norwegian University of Science and Technology.

Alsos H.S, Hopperstad O.S, Törnqvist R, Amdahl J. 2008. Analytical and numerical analysis of sheet metal instability using a stress based criterion. International Journal of Solids and Structures. 45(7-8):2042–2055.

ARAMIS. 2009. http://www.gom.com/EN/index.html [2009-04-30].

Dassault Systèmes. 2007. Abaqus version 6.7 documentation.

et Norske Veritas (DNV). 2007. Rules for classification of ships/high speed, light craft and naval surface craft.

Ehlers S, Klanac A, Tabri K. 2007. Increased safety of a tanker and RoPax vessel by implementing a novel sandwich structure. In: Lehmann E, Biehl, F. Proceedings of the 4th International Conference on Collision and Grounding of Ships (ICCGS2007); September 9–12; Hamburg, Germany. Elbe-Werkstätten GmbH, Hamburg, Germany:109–115.

Ehlers S, Broekhuijsen J, Alsos H.S, Biehl F, Tabri K. 2008. Simulating the collision response of ship side structures: A failure criteria benchmark study. International Shipbuilding Progress, 55(1-2):127–144.

Hogström P, Ringsberg J.W, Johnson E. 2009. An experimental study of the effects of length scale and strain state on the necking and fracture behaviours in sheet metals. International Journal of Impact Engineering, 36 (10-11):1194–1203.

Hong L, Amdahl J, Alsos H.S, Klaebo F. (2007). Damage assessment and impact resistant design of FPSOs with respect to supply vessel collisions. In: Basu R.I, Belenky V, Wang G and Yu Q. Proceedings of the 10th International Symposium on Practical Design of Ships and Other Floating Structures (PRADS2007); September 30 – October 5; Houston, Texas, U.S.A. ABS, Houston, Texas, U.S.A.: 622–630.

Jasionowski A, Vassalos D, Guarin L. 2003. Time-based survival criteria for passenger Ro/Ro vessels. Marine Technology. 40(4):278–287

Karlsson U.K. 2009. Improved collision safety of ships by an intrusion-tolerant inner side-shell. Chalmers University of Technology, Department of Shipping and Marine Technology, Göteborg, Sweden. Report No.: R-09:113. (Submitted for publication, under review.)

Karlsson U.K, Ringsberg J.W, Johnson E, Hoseini M, Ulfvarson A. 2009. Experimental and numerical investigation of bulb impact with a ship side-shell structure. Marine Technology. 46(1):16–26.

Kim J.Y, Lee J.W. 2001. A comparative study of the double hull structures for the collision energy absorption systems. Journal of Ship and Ocean Technology, 5(4): 19–28.

Kitamura O. 1997. Comparative study on collision resistance of side structure. Marine Technology, 34(4):293–308.

Klanac A, Ehlers S, Tabri K, Rudan S, Broekhuijsen J. 2005. Qualitative design assessment of crashworthy structures. In: Soares C.G, Garbatov Y, Fonseca N. Proceedings of the 11th International Congress of the International Maritime Association of the Mediterranean (IMAM2995); September 26–30; Lisboa, Portugal. Taylor and Francis, London, U.K.:461–471.

Schreuder M, Hogström P, Ringsberg J.W, Janson C-E, Johnson E. 2009. Holistic assessment of ship survivability and risk after damage. In: Kvamsdal T, Pettersen B, Bergan P, Oñate E, García J. Proceedings of the International Conference on Computational Methods in Marine Engineering III (MARINE2009); June 15-17; Trondheim, Norway. International Center for Numerical Methods in Engineering (CIMNE), Barcelona, Spain:347–351.

ISO 12004-2. 2007. Metallic materials-Sheet and strip-Determination of forming limit curves - Part 2: Determination of forming limit curves in laboratory.

ISSC Committee V.3. 2003. Collision and Grounding. 15th International Ship and Offshore Structures Congress, Vol. 2, Chapter 3, San Diego, U.S.A.

Paik J.K. 2007. Practical techniques for finite element modelling to simulate structural crashworthiness in ship collisions and grounding (Part I: Theory). Ships and Offshore Structures, 2(1):69–80.

Peschmann J. 2001. Calculation of the energy absorption of the steel structure of ships during collision and grounding. [dissertation].

[Hamburg, Germany]: Technical University of Hamburg-Harburg.

Ringsberg J.W. 2009. Characteristics of material, ship side structure response and ship survivability in ship collisions. Ships and Offshore Structures. (In Press).

Schreuder M. 2005. Time simulation of the behaviour of damaged ships in waves [licentiate degree thesis]. [Göteborg, Sweden]: Chalmers University of Technology.

Schreuder M. (2008). Research study on the sinking sequence of MV Estonia. SSPA, Göteborg, Sweden. Research Report No.:134.

SSAB. 2009. http://www.ssabdirekt.com. [2009-04-30].

Spanos D, Papanikolaou A. 2007. On the time to capsize of a damaged RoRo/passenger ship in waves. In: Proceedings of the 9th International Ship Stability Workshop; August 30–31; Hamburg, Germany.

Tabri K, Broekhuijsen J, Matusiak J, Varsta P. 2004. Analytical modelling of ship collision based on full scale experiments. In: Proceedings of the 3rd International Conference on Collision and Grounding of Ships (ICCGS2004); October 25–27; Izu, Japan. Society of Naval Architects of Japan:302–311.

Tautz I. 2007. Predetermined breaking points in a ship's double hull – an innovative design concept to enhance collision safety. In: Lehmann E, Biehl, F. Proceedings of the 4th International Conference on Collision and Grounding of Ships (ICCGS2007); September 9–12; Hamburg, Germany. Elbe-Werkstätten GmbH, Hamburg, Germany:171–175.

Tavakoli M.T, Amdahl J, Alsos H.S, Klaebo F. 2007. Analysis of supply vessel stern impacts with an FPSO. In: Lehmann E, Biehl, F. Proceedings of the 4th International Conference on Collision and Grounding of Ships (ICCGS2007); September 9–12; Hamburg, Germany. Elbe-Werkstätten GmbH, Hamburg, Germany:19–28.

Wang G, Arita K, Liu D. 2000. Behaviour of a double hull in a variety of stranding or collision scenarios. Marine Structures, 13(3):147–187.

Wang G, Spencer J, Chen Y. 2002. Assessment of a ship's performance in accidents. Marine Structures, 15(4-5):313–333.

Wevers L.J, Vredeveldt A.W. 1999. Full scale ship collision experiments 1998. TNO, Delft, The Netherlands.

Yamada Y, Endo H, Terndrup-Pedersen P. 2005. Numerical study on the effect on buffer bow structure in ship-ship collision. In: Proceedings of the 15th International Offshore and Polar Engineering Conference (ISOPE15); June 19–24; Seoul, Korea. ISOPE, Massachusetts, U.S.A.:604–611.

Review and Application of Ship Collision and Grounding Analysis Procedures

Preben Terndrup Pedersen

Technical University of Denmark, Department of Mechanical Engineering

Abstract:
It is the purpose of the paper to present a review of prediction and analysis tools for collision and grounding analyses and to outline a probabilistic procedure whereby these tools can be used by the maritime industry to develop performance based rules to reduce the risk associated with human, environmental and economic costs of collision and grounding events. The main goal of collision and grounding research should be to identify the most economic risk control options associated with prevention and mitigation of collision and grounding events.

The full paper can be found in:

Marine Structures (2010), doi:10.1016/j.marstruc.2010.05.001

Survivability of grounded and damaged ships

George Zaraphonitis and Manolis S. Samuelides

National Technical University of Athens, Greece

Abstract:
Accidents such as collisions and groundings have an effect not only during the incident but also after the impact. On one hand, the damage decreases the strength of the ship hull and on the other hand the ship after the accident may be subjected to unfavorable loading conditions. These may be static, as a result of change in the weight distribution and the external static loads - for example because of the grounding forces, or dynamic, under the action of incident waves. The paper addresses the strength of the damaged structure and the loading induced on damaged hulls of bulk carriers. The determination of the loading includes the influence of dynamic effects due to waves loading and the interaction of the hull with the sea bed in the grounding area. The strength of the steel structure in the corresponding damaged condition is assessed and the safety margin of the damaged ship is calculated by comparing it to the bending moment that is expected to be applied to the grounded ship. Results are generated for the case of a 175,000 dwt bulk-carrier in full load condition.

Introduction

Ship groundings may cause both local damage around the contact area between the hull of the ship and the sea bed, as well as high global loads that may cause failure of the ship girder and subsequent breakage of the hull. These detrimental effects of grounding actions are not limited during the incident or within a short time after it, but cause structural damage to the hull and present a hazard to the environment for days, weeks or even longer after the ship is set aground (Samuelides et al 2007).

When the hull sits on the sea bed, the bottom structure is generally subjected to transverse loading. This mode may occur statically, when for example the ship sits on a pinnacle, supporting its weight, or dynamically under the wave action causing relative motion of the ship with respect to the sea bed, which in extreme cases (e.g. when the ship is relatively lightly loaded and under heavy weather conditions) may result in a repeated impact of the bottom structure (pounding impact). Example of actual grounding that has caused pounding action is the case of bulk carrier New Carissa (http://www.shipstructure.org). As an example to high static loads we refer to the case of a 304 m long, 273,000 dwt single skin oil tanker that rode over the Buffalo Reef off the coast of Singapore (Tikka 2000). Transverse loading on the bottom plate that cause high forces on floors and girders also occur when the ship is forced towards the sea bed as a result of tidal actions.

Grounding loads in combination with the changes in the weight and buoyancy distributions that are subsequent to groundings have an effect on the static bending moments that are exerted on the ship's hull.

Under these conditions high shear forces are expected in the vicinity of the contact area of the hull with the sea bed, whereas static bending moments may exceed the maximum allowable thresholds. Further, wave action causes wave bending moment distributions that when superimposed to the static loading may be detrimental for the grounded vessel.

Investigations related to global loads during groundings have been reported among others by Pedersen (1994), Wang et al (1992), Brown et al (2004), Hussein et al (2009) and Luis et al (2009). Pedersen (1994) developed a mathematical model for a ship that rides on a slope and found that the longitudinal strength of the ship defined on the basis of the section modulus according to the IACS requirements may not be sufficient to withstand the static loads that are applied in a severe grounding. Wang et al (2002) developed a formula to derive the hull girder strength of damaged hulls and applied it to 67 commercial ships built in the 80ies and 90ies and were in service when the article was written. Brown et al (2004) presented an analysis of the motions and loads in six-degrees of freedom of a grounded ship in waves, with an appropriate soil reaction model to estimate dynamic ground reaction forces. In the analysis, the steady-state grounded motion of the stranded ship in waves around the quasi-equilibrium position is treated as a steady-state linear dynamic problem. Recently Hussein et al (2009) reported a study on the residual strength of double hull tankers built according to the CSR, under various damaged scenarios and Luis et al (2009) conducted a longitudinal strength reliability of a stranded tanker hull. The loading on the tanker was defined on the basis of the extremes that the ship could find during operation for both still-water and wave induced loads. Example of a study on the global wave loads acting on a damaged Ro-Ro vessels is presented by Korkut et al. (2005).

Zaraphonitis et al (2009) presented an investigation that aims to evaluate the ability of a damaged hull of a 175,000 dwt bulk carrier to withstand the combined global static and wave loads, when she sits on a pinnacle of the sea bed. The static vertical bending moment is calculated using the equations of static equilibrium under the assumption that a) the weight of the ship, b) the draughts of the grounded ship, and c) the location of the reaction force from the sea bed are known. Wave loads are derived using potential flow calculations, assuming that the hull is attached to the sea bed where she is set aground. Further, the authors calculated the ultimate strength capacity of the ship hull under vertical bending moments using a Smith-type approach, for both the intact and damaged cross-sections. Subsequent to the above mentioned calculations, the demand, i.e. the loads that act on the ship, is compared to the capacity, i.e. the ultimate strength of the ship in damaged condition.

The present paper extends the work of Zaraphonitis et al (2009) in that the wave bending moments are calculated for irregular sea waves taking into account that the ship rests in contact with the sea-bed on the location of grounding. Calculations have been performed for a typical modern Bulk Carrier, designed in accordance with the Common Structural Rules. The Main Characteristics of the vessel are summarized in Table 1. The construction materials of the primary structural elements are high tensile steel having a yield stress of 315 MPa and 355 MPa. A sketch of the cargo loading of the intact vessel is presented in Figure . The Midship Section of the ship is presented in Figure 2 and the Body Plan in Figure 3.

Global loads due to grounding

Static loads

The vessel is considered traveling at a full load condition, carrying 169,000 t of ore in holds number 1, 3, 5, 7 and 9 (see Figure) at a mean draught of 18.031 m and at practically zero trim. The vessel's displacement is equal to 200,230 t with a DWT of 174,730 t. The maximum bending moment is equal to 568.45 kt·m at 177.0 m from After Peak (hogging). The maximum shear forces are 16.27 kt at x=63.5 m from AP and -16.75 kt at x=244.8 m from AP. The distribution of weights (WD curve), buoyancy (BD curve), shear forces (SHEAR curve) and bending moments (BEND curve) along the ship length are presented in Figure 4.

Table 1: Main Characteristics of the vessel

Length BP [m]	[m]	281.0
Beam	[m]	45.0
Draught (Scantling)	[m]	18.0
Draught (Design)	[m]	16.5
Depth	[m]	24.7
Number of Holds		9
Lightship	[t]	25,500.0
DWT (Scantling Draught)	[t]	175,000.0
Service Speed (Design Draught)	[kn]	16.5
Propulsion Power (MCR)	[kW]	18,650.0
Section Modulus at Midship	[m^3]	45.6

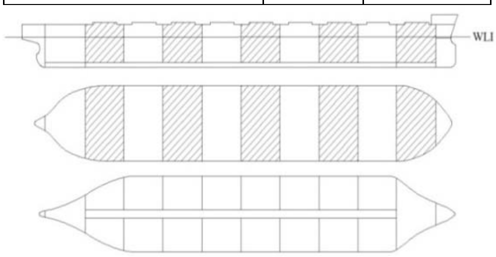

Figure 2. Cargo loading

At this condition, a grounding accident is assumed, after which, the fore peak tank, the pipe tunnel and the double bottom tanks beneath the Holds 1, 2, 3 and 4 are breached and flooded with water. The vessel is considered floating in contact with the sea-bottom at the middle of Hold 4, 180.5 m from the Aft Peak. The vessel's draught at the point of contact is assumed equal to 18.0m (i.e. at the initial draught, before the accident). Under this condition, i.e. 18m draught at contact point and weight distribution as in flooded condition, hydrostatic balance results in a static vertical force equal to 22,080 t is acting on the ship at the point of grounding, while the corresponding pitching moment is assumed equal to zero (the ship is assumed free to trim about a transverse axis through the point of contact with the sea bottom). The mean draught of the vessel is found equal to 17.736 m with a trim of 1.938 m by the bow, when the ship is assumed free to trim about a transverse axis through the point of contact so that the corresponding pitching moment equals to zero.

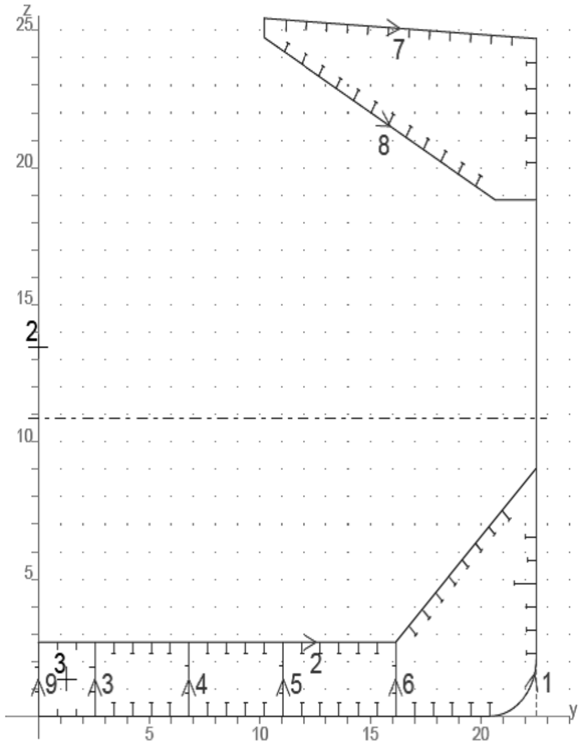

Figure 2. Midship of the studied vessel.

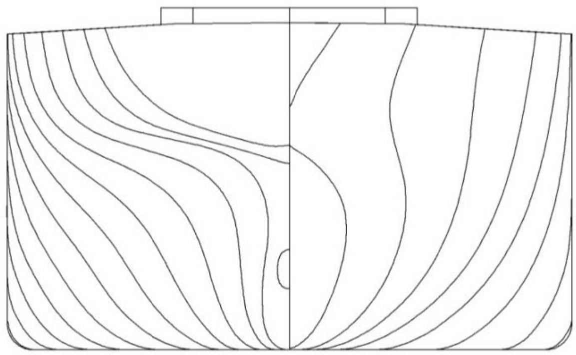

Figure 3. Body plan of the studied vessel.

The distribution of weights (WD curve), buoyancy (BD curve), shear forces (SHEAR curve) and bending moments (BEND curve) along the ship length for the grounded ship are presented in Figure 5. In this figure, the grounding force has been added to the buoyancy curve, resulting in a sharp peak that may be clearly observed in the middle of the 4th Hold. The maximum bending moment after the grounding accident is equal to 1,211.55 kt·m at x=178.4 m from AP (hogging). The maximum shear forces are 18.99 kt at x=63.5 m from AP and -23.77 kt at x=193.0 m from AP. According to these results, the maximum shear force and bending moment have been increased by 42% and 113% respectively, in comparison with the intact case. For the shake of comparison, the corresponding maximum bending moment and shear force for the freely floating ship and for the same damage case (i.e. without the grounding force) are equal to 726.43 kt·m and 18.09 kt respectively, indicating that at least for the particular case, a grounding accident results in a considerable increase of the static loads exerted on the hull structure.

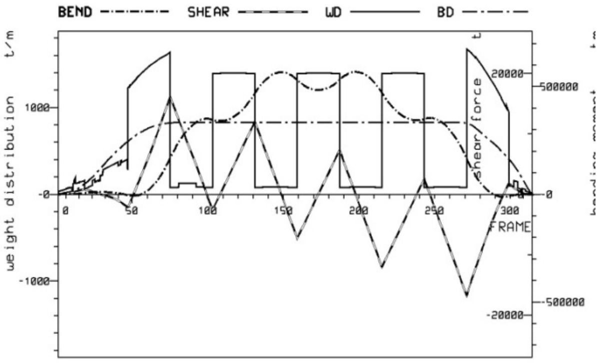

Figure 4. Distribution of forces and moments-intact condition.

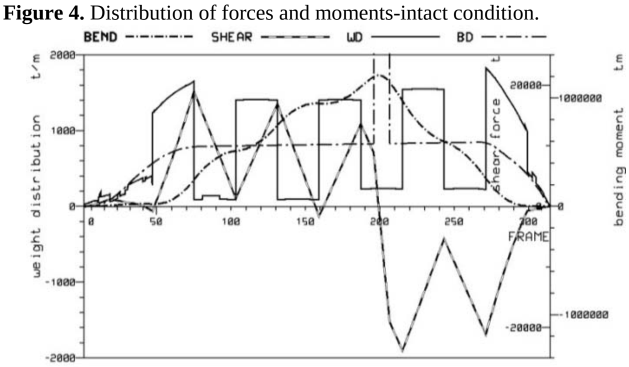

Figure 5. Distribution of forces and moments, after grounding.

Wave loads in regular waves

The analysis of the hydrodynamic interaction of a vessel freely floating at zero forward speed with an incoming regular wave has been discussed in detail by Papanikolaou (1985). The distribution of zero-speed pulsating Green sources over the wetted surface of the body is used to express the radiation and diffraction potentials, and the resulting integral equation is solved to derive the corresponding source strengths. The above procedure and the related computer software was extended by Papanikolaou et al. (1990) for the calculation of bending moments and shear forces acting on the transverse sections of a ship floating on the free surface with zero forward speed, or when advancing with a constant forward speed, subject to incident regular waves.

For the calculation of the vertical bending moments and shear forces acting on the transverse sections of a grounded vessel the above procedure has been modified accordingly. The sea-bottom is assumed horizontal with a water depth H. The ship is assumed to be grounded on a reef, resulting in a new floating position under the action of a (steady) vertical motion G. Under the action of an incoming regular wave of amplitude a_w and frequency ω, additional dynamic forces and moments are acting on the vessel. Within the limits of the linear theory these forces are considered sinusoidal, oscillating with frequency ω, while their amplitude is proportional to the wave amplitude a_w. The forces and moments acting on the ship at the point of grounding in the longitudinal plane are shown in Figure 6. Let F_{G1} and F_{G3} be the complex amplitudes of the forces acting on the ship in the longitudinal and vertical direction respectively, and F_{G5} the amplitude of the pitching moment around the transverse axis passing through the centre of the contact area (in the following for simplicity reasons the contact area is reduced to a single point). Additional forces and moments, i.e. a transverse force F_{G2}, a horizontal (yawing) moment F_{G6} about the vertical axis passing through the collision point and a torsional moment F_{G4} about the longitudinal axis may be also acting on the ship, although not shown in Figure 6.

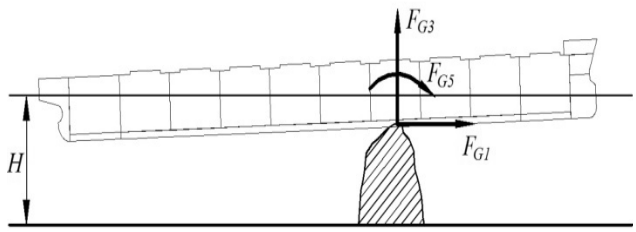

Figure 6. Forces and moments acting on the vessel at the point of grounding.

For the sake of simplicity, in the following we assume that the damage case due to grounding is symmetric and that the vessel remains in a vertical position after the damage. In addition, we consider only the cases of head and following waves, therefore the transverse force F_{G2}, the torsional moment F_{G4} and the yawing moment F_{G6} are set equal to zero. However, the extension of the developed model to the case of oblique wave direction is straightforward. We introduce a coordinate system with it's origin on the free surface, directly above the point of grounding with the x axis towards the bow, the y axis towards the port side of the ship and a vertical axis z pointing upwards. The equations of motion may be expressed as follows:

$$\sum_{k=1}^{6}\left[-\omega^2(M_{ik}+A_{ik})-j\omega B_{ik}+C_{ik}\right]\xi_k = F_i + F_{Gi} \qquad (1)$$

where i=1,2,..6, ξ_k is the complex amplitude of motion k, M_{ik} are the components of the generalized mass matrix of the ship, A_{ik}, B_{ik} and C_{ik} are the added mass, damping and restoring coefficients in the i direction due to the motion of the ship in the k direction and F_i is the wave force in the i direction. Assuming that the reef is rigid enough to withstand the reaction forces, the ship is considered fully restrained in the longitudinal direction, therefore the amplitude of the surge motion ξ_1 is set equal to zero. The downwards heaving motion of the vessel at the point of contact with the reef is also considered fully restrained, while a wave of very high amplitude could cause an upwards heaving motion, resulting in a severe loading of the hull structure due to pounding. This would require a heaving force amplitude F_{G3} just higher than the calculated static vertical force due to grounding G. In our analysis we assume limited wave heights, so that F_{G3} is always smaller than G. Therefore the heaving motion of the ship at the point of grounding is also fully restraint, while in addition the wave amplitude resulting in $F_{G3}=G$ is also calculated. According to the obtained results it would take a very high wave for F_{G3} to become greater than G. For example, with a wave length of 250 m, for which the maximum bending moments have been calculated, the required wave amplitude resulting in $F_{G3}=G$ is up to 10 m (or 20 m wave height). For the pitching moment F_{G5} we may consider two opposite limiting cases:

- A pitching moment of adequate magnitude is acting on the ship at the point of contact, resulting in zero pitching motion.
- The pitching moment is equal to zero, with the vessel pitching freely about the point of contact.

In the first case, the ship is totally restrained in all modes of motion and the resulting dynamic grounding forces and moments can be calculated from eq. (1), setting the ship motions equal to zero:

$$F_{Gk} = -F_k, \quad k = 1,3,5 \tag{2}$$

In the second case, since the surge and heave motions are assumed totally restrained and the pitching moment due to grounded (F_{G5}) is assumed equal to zero, the pitch motion can be directly calculate:

$$\xi_5 = \frac{F_5}{-\omega^2 (M_{55} + A_{55}) - j\omega B_{55} + C_{55}} \tag{3}$$

Substituting ξ_5 in the corresponding equations for the heave motion and setting $\xi_3=0$, the vertical grounding force F_{G3} is calculated by:

$$F_{G3} = [-\omega^2 (M_{35} + A_{35}) - j\omega B_{35} + C_{35}]\xi_5 - F_3 \tag{4}$$

The horizontal grounding force F_{G1} may be calculated by a similar expression. In a real case of grounding, the actual situation would be somewhere between these two limiting cases, depending on the particular details of the accident and the mechanical properties of the sea bottom. The calculations presented herein were performed for the second case, i.e. assuming zero pitching moment, with the vessel free to pitch.

The calculation of the hydrodynamic interaction of the ship with incoming regular waves and of the corresponding dynamic shear forces and bending moments exerted along the vessel's length have been performed by a modified version of the fully three-dimensional software code NEWDRIFT, developed by the Ship Design Laboratory of NTUA. The wetted surface of the ship in the state of static equilibrium following the grounding has been discredited by 2x839 plane quadrilateral elements (Figure 7). The sea-bottom is assumed horizontal with a water depth H=30 m. The obtained results for the wave bending moments vs. the wave length for incoming regular head waves of unit amplitude are presented in Figure 8. Each curve in Figure 8 corresponds to the bending moment calculated at the longitudinal position of a transverse bulkhead. The variation of the wave bending moment along the length of the vessel for a series of wave lengths is presented in Figure 9. The corresponding results for the vertical shear forces are presented by Zaraphonitis et al (2009).

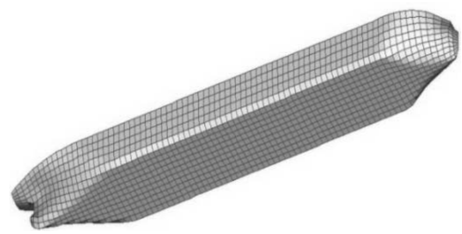

Figure 7. Discretization of wetted surface

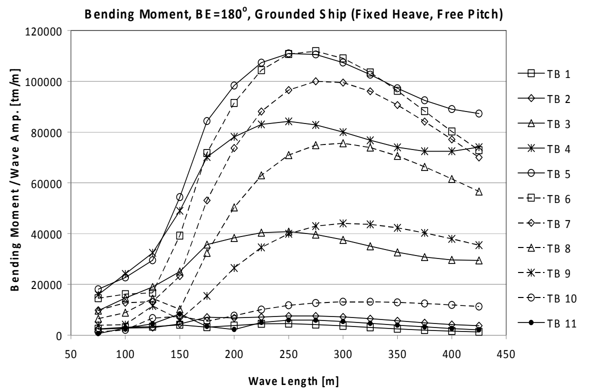

Figure 8. Wave bending moments at transverse bulkheads vs. wave length, head waves.

Figure 9. Wave bending moments along the ship length for selected wave lengths, head waves.

Wave loads in irregular waves

The calculated wave loads in regular waves provided the basis for the analysis of the loading in more realistic irregular seaways. Calculations are performed assuming long crested seaways characterized by JONSWAP two parameters spectra, with a heading of 180 deg (head waves). The already calculated wave bending moments in regular waves have been divided by the product of $\rho g L^2 B a_w$ to obtain the non-dimensional responses. The spectra of the non-dimensional bending moments have been calculated for various combinations of significant wave heights and modal periods T_0. Since a linear dependency between the wave induced loads and the wave amplitude is assumed, in the following results are presented only for a significant wave height of 1.0 m. From the presented results, the corresponding wave loads for different wave heights can be readily calculated. The calculated wave bending moment spectra at the longitudinal positions of bulkheads no 4, 5 and 6 for two modal periods (6 sec and 10 sec) are presented in Figure 11 and Figure 12. Short term predictions for the various responses may be performed based on the characteristics of the corresponding response spectra. In the present study we are particularly interested in estimating extreme wave bending moment values with the vessel being exposed in specified sea conditions and for a given period of time in the order of a few hours, for which it may be assumed that the wave conditions remain constant.

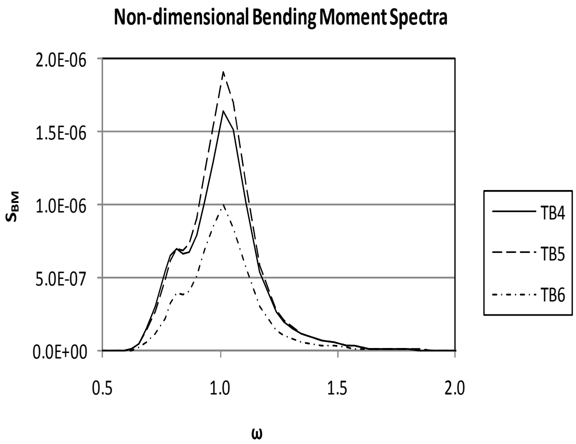

Figure 10. Wave bending moment spectrum for $H_{1/3}$=1 m and T_o=6 sec (BE=180°).

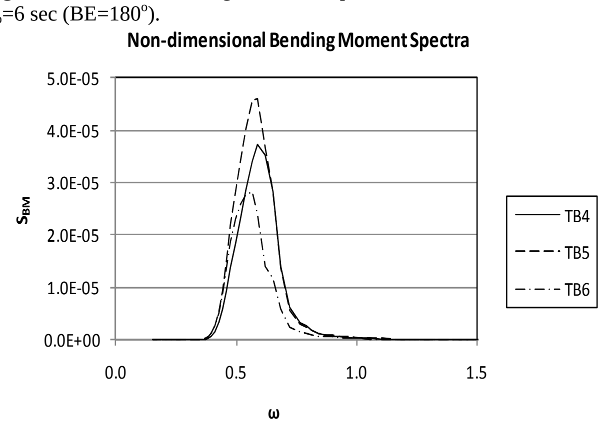

Figure 11. Wave bending moment spectrum for $H_{1/3}$=1 m and T_o=10 sec (BE=180°).

Let M_w be the non-dimensional wave bending moment acting on a transverse section of the ship. For a given sea state, we seek to find an extreme value $\hat{M}_w$ of the wave bending moment, for which the probability of been exceeded in a given time T is less than α, where α is an acceptable small positive number. Following Ochi (1973) $\hat{M}_w$ may be calculated:

$$\hat{M}_w = \sqrt{2 m_0 \ln\left[\frac{3600\ T}{2\pi\alpha}\sqrt{\frac{m_2}{m_0}}\right]} \tag{5}$$

where m_0 and m_2 are the zero and second moments of the corresponding response spectrum and T is the time interval in seconds. Applying equation (5) the extreme wave bending moments acting on the vessel at the longitudinal position of the transverse bulkheads have been calculated. Table 2 summarizes the obtained results for the extreme wave bending moments at the transverse bulkhead no. 4 assuming a significant wave height of 1.0 m and for a range of modal periods. The presented values correspond to probabilities of exceedance of 0.1%, 0.5% and 1.0%. The corresponding results for transverse bulkhead 5 (i.e. the first intact bulkhead) are presented in Table 3.

Table 2: Extreme wave bending moments (in t.m) at bulkhead 4

α \ T_0	4sec	6sec	8sec	10sec	12sec	14sec
0.1	4,525	11,430	13,540	42,020	63,350	74,760
0.05	4,677	11,820	24,380	43,560	65,720	77,590
0.01	5,013	12,700	26,240	46,960	70,910	83,790
0.001	5,460	13,860	28,700	51,420	77,740	91,940

Table 3: Extreme wave bending moments (in t.m) at bulkhead 5

α \ T_0	4sec	6sec	8sec	10sec	12sec	14sec
0.1	4,656	12,010	23,790	46,470	76,550	94,500
0.05	4,812	12,430	24,640	48,190	79,410	98,080
0.01	5,158	13,350	26,520	51,950	85,700	105,930
0.001	5,610	14,570	29,000	56,900	93,960	116,250

Vertical bending capacity

Allowable still water bending moment

The allowable still water bending moments at sea $M_{SEA,i}$ are given by:

$$M_{SEA,i} = SM \cdot \sigma_{ALL} - M_{WAVE,i} \tag{6}$$

where SM is the actual minimum section modulus of the ship based on net scantlings, which equals to 45.6 m^3, σ_{ALL} is the allowable normal stress due to vertical bending, which equals to 264 MPa for HTS with yield stress 360 MPa, $M_{WAVE,i}$ is the design wave bending moment and subscript i denotes hogging or sagging. The design wave bending moments are given in kt·m by:

$$M_{WAVE,HOG} = 190 \cdot C \cdot L^2 \cdot B \cdot c_b / 9810$$
$$M_{WAVE,SAG} = -110 \cdot C \cdot L^2 \cdot B \cdot \left(c_b + 0.7\right) / 9810 \quad (7)$$

From (6) and (7) it is determined that the allowable still water bending moments at sea are 564 kt·m for the sagging and 596 kt·m for the hogging case.

Ultimate strength

The ultimate strength under vertical bending conditions may be calculated using an iterative Smith – type approach or FE. The Smith type iterative approach is based on the assumption that plane sections remain plane and it is conducted in steps. In each step the user assumes a curvature and performs iterations to determine the position of the neutral axis, which results in zero axial force and the applied bending moment. In the case of symmetric hull section, either intact or damaged, the neutral axis remains parallel to the bottom and deck of the hull. However when the damage is asymmetric, the position of the neutral axis needs to be updated both by translation and rotation.

For the present study it has been assumed that the damage is symmetric and the ultimate strength of the hull is determined using the MARS software that is available from the site of Bureau Veritas. Figure 2 shows the cross-section of the bulk carrier as designed by MARS and Figure 12 shows the bending moment-curvature curve obtained by the program. As it may be seen the maximum value of the bending moment that the hull may carry is 1,824 kt·m in hogging and in 1,483 kt·m in sagging condition. These values refer to the intact hull, i.e. without considering the damage due to grounding. Should the damaged structural elements are removed it is possible to obtain the ultimate bending moment capacity of the hull after grounding. In the present case it has been assumed that the damage is symmetrical with respect to the longitudinal plane of symmetry and its transverse extent is such, that both the duct tunnel and the double bottom ballast tanks are breached. It is therefore considered that the keel plates as well as the centre girder and the side girders that are located to the right and to the left of the centre girder are damaged and therefore do not contribute to the strength of the hull (Figure 13). Based on the above

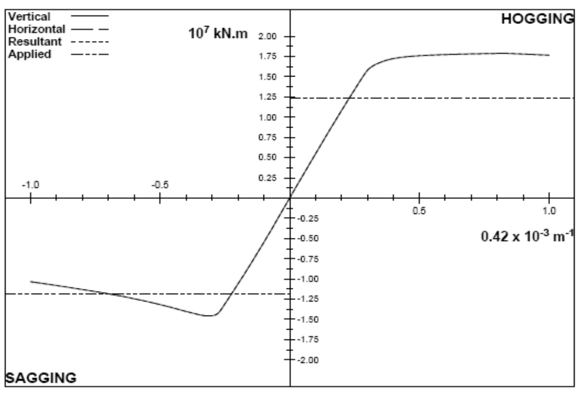

Figure 12. Bending moment vs. curvature for intact hull

description the total width of the damage is 10 m, which is a realistic value for ships that ground. In this case the ultimate bending moment capacity is 1,692 kt·m for hogging condition and 1,446 kt·m for sagging condition, i.e. 7.8% lower in hogging condition and marginally different – 2,6% - in sagging condition with respect to the corresponding values of the intact hull. The bending moment versus curvature curve for the damaged hull is presented in Figure 14.

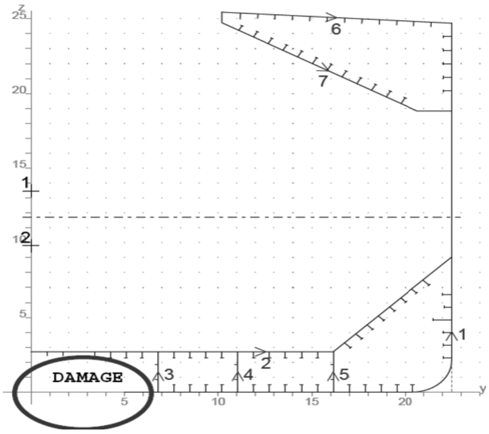

Figure 13. Damaged hull

Discussion of results

An example of the comparison of the demand, i.e. maximum bending moment that is expected to be applied to the hull of the grounded bulk carrier, and capacity, i.e. the ultimate bending moment that the hull may withstand is shown in Figure 15. In particular the values of the demand are based on the assumption that the ship remains for 3 hours on a pinnacle, subject to an incident long crested irregular seaway characterized by a JONSWAP wave spectrum characterized by its significant wave height and modal period. The sea-bottom is assumed horizontal with a water depth H=30 m and the wave heading is equal to 180 deg (head waves). Further, it is observed that the wave bending moment obtains its maximum value at the same cross section were the maximum static bending moment occurs when the ship rests on the sea bed, i.e. between bulkheads 4 and 5. A more thorough approach would require considering the exposure of the ship for a larger duration, while a storm is gradually developing and decaying and calculate the probability of exceeding bending moment values comparable to the vessel's ultimate strength.

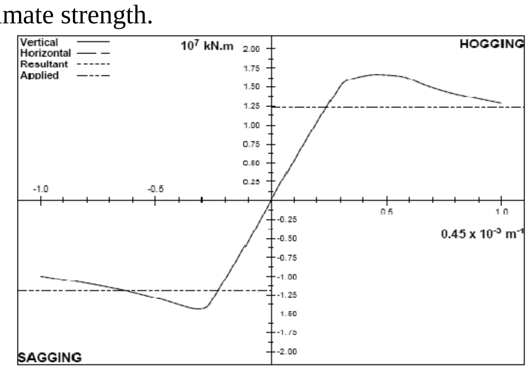

Figure 14. Bending moment vs. curvature for damaged hull

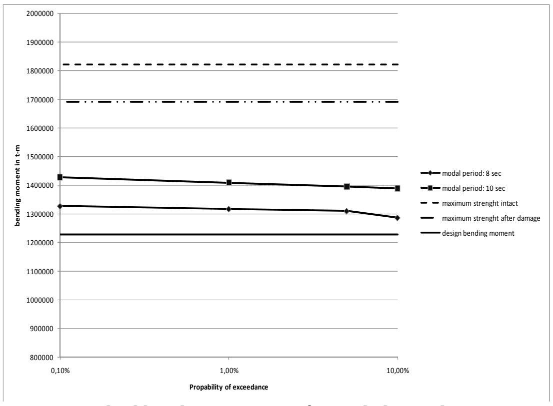

Figure 15. Applied bending moment of stranded vessel

Figure 15 presents the applied bending moment on the stranded vessel versus the probability of exceedance for in the case of significant wave height of 4 m and modal periods of 8 sec and 10 sec. As it can be seen when the modal period is 10 sec the bending moment of 1,428 kt·m has a probability of exceedance of 0.1%. The value of 1,428 kt·m exceeds by more than 19% the design bending moment of the ship, i.e. the section modulus times the allowable stress, and it is 16% lower than the ultimate bending moment capacity of the damaged hull. If the ultimate bending capacity is determined by considering also the partial safety factor 1.1 according to the CSR, the demand is 7% lower than the respective capacity, i.e. 1692 kt·m/1.1=1538 kt·m, of the hull.

Conclusions

The paper presents a methodology to assess the survivability of a ship that rest on a pinnacle of the sea bed as a result of a grounding. In stranded condition the ship is assumed to be in contact with the sea-bed, i.e. there is always a reaction force between the ship and the ground. The assessment is based on the comparison of the demand, i.e. the bending moment, which the ship is expected to encounter under irregular wave conditions while she rests on the pinnacle versus the capacity, i.e. the ultimate bending moment capacity of the damaged hull. The action of the waves is determined assuming that the ship is attached at a certain point to the sea bed and may freely pitch with respect to that point. The ultimate bending capacity is calculated using the software MARS of Bureau Veritas. The methodology is applied in the case of grounding of a 175,000 dwt bulk carrier, built according to the CSR. An on-going study investigates the effect of the grounding scenarios, location of point of contact, flooding condition, reduction of draught, location and transverse extend of the damage on the results.

References

Brown A.J., Simbulan M., McQuillan J. & Gutierrez M. 2004. Predicting Motion, Structural Loads and Damage in Stranded Ships Phase I, *Ship Structures Committee Report SSC-434*.

Hussein, A.W. & Soares, C. G. 2009. Reliability and Residual Strength of Double Hull Tankers Designed According to the new IACS common Structural Rules, *Ocean Engineering*, doi:10.1016/j.oceaneng.2009.04.006.

Korkut, E., Atlar, M. & Incecik, A. 2005. An Experimental Study of Global Loads Acting on an Intact and Damaged Ro-Ro Ship Model, *Ocean Engineering* 32, 1370-1403.

Luis, R.M., Texeira, A.P. & Soares C.G. 2009. Longitudinal strength reliability of a tanker hull accidentally grounded, *Structural Safety* 31, pp. 224-233.

Ochi, M.K. 1973. On Prediction of Extreme Values. Journal of Ship Research, vol. 17, no. 1.

Ochi, M.K. 1982. Stochastic Analysis and Probabilistic Prediction of Random Seas, Advances in Hydroscience, 13, Academic Press, pp. 217-375.

Papanikolaou, A. 1985. On Integral Equation Methods for the Evaluation of Motions and Loads of Arbitrary Bodies in Waves, *Ingenieur-Archiv,* Vol. 55, pp. 17-29.

Papanikolaou, A., Schellin, T. and Zaraphonitis, G. 1990. A 3D Method to Evaluate Motions and Loads of Ships with Forward Speed in Waves, *in Proceedings of 5th Int. Congress on Marine Technology, IMAEM 90, pp 452-457, Athens, Greece*.

Pedersen, P.T. 1994. Ship Grounding and Hull girder Strength, *Marine Structures* 7 (1994) 1-29.

Samuelides, M.S., Amdahl, D. & Dow, R. 2007. Studies on the behaviour of bottom structures during grounding, *Proceedings of MARSTRUCT 2007,* Glasgow, Scotland.

Tikka, K.K. 2000. Risk-based Life Cycle Management of Ship Structures, *Ship Structures Committee Report SSC-417*.

Wang, G., Chen, Y., Zhang, H. & Peng, H. 2002. Longitudinal Strength of Ships with Accidental Damages, *Marine Structures* 15 (2002) 1190138.

Zaraphonitis, G. & Samuelides M. 2009. Behavior of Ship Structures in Damage, *in Proceedings of 13th Congress of* International Maritime Association of Mediterranean, IMAM 2009, Istanbul, Turkey.

Environmental risk of collision for enclosed seas: Gulf of Finland, Adriatic, and implications for tanker design

Alan Klanac [1,2,3], Teuta Duletić [1,3], Sandro Erceg [1,3], Sören. Ehlers [2], Floris Goerlandt [2] and Darko Frank [1,2]

[1] *as2con-alveus ltd. research & consulting, Rijeka, Croatia,* [2] *Aalto University, Dept. Applied Mechanics, Espoo, Finland,*
[3] *University of Rijeka, Faculty of engineering, Ship Design and Construction Dept., Rijeka, Croatia*

Abstract:

The paper describes collision risk analysis for the enclosed sea areas, namely the Gulf of Finland as a part of the Baltic Sea and the Adriatic as a part of the Mediterranean Sea. The analysis focuses on the environmental risk of tankers. Three characteristic tanker sizes are observed: HANDYMAX, AFRAMAX and VLCC. The specific observed geographical areas are chosen for their similarities, precisely for their importance to the welfare of local communities, for their geographical characteristics, i.e. long and narrow bays, and for their intensive maritime traffic. The analysis consists of the evaluation of the available deformation energy, assessment of hull crashworthiness applying non-linear FEM, and risk calculations. The results lead to some interesting findings, e.g. risk is higher in the enclosed sea areas than in the worldwide navigation, AFRAMAX exhibits the least amount of risk, etc.

Introduction

Nowadays, the public is becoming less tolerant towards environmental spoiling. In the marine environment, oil spills present a high risk to a sustainable future. They can have the disastrous consequences as the oil spills may render large areas of sea unusable for several years. See some examples in Figure 1. Ship collisions, besides groundings and hull failures are the most relevant causes of these adverse events (IOPC 2009).

Figure 1: Examples of oil spills with disastrous consequences (left: Torrey Canyon, right: Exxon Valdez)

Especially sensitive to this harm are the enclosed waters of the seas, like the Gulf of Finland or Adriatic, which are also the prime focus in this study. Comparing past incidents like that of Exxon Valdez, which happened in the enclosed sea area, with those that occurred in the open ocean, like ABT Summer (Hook 1997), clearly indicate the sensitivity of the geographical location to the environmental damage. Furthermore, the actual quantity of the spilled oil had a secondary role to the overall consequences.

Rapid increase of the quantities of oil transported in the Gulf of Finland in the last decade due to Russian oil exports, as well as the importance of the Adriatic Sea to the economic livelihood of the Public, indicate these two enclosed sea areas as especially interesting for the minimization of the environmental risk of the maritime transport. Furthermore, the problem of ship collisions in these narrow bays is more severe than average, since tankers meet denser traffic conditions as well as the crossing traffic especially in the Gulf of Finland.

Table 1. Main dimensions of the example ships

	HANDYMAX	AFRAMAX	VLCC
Length between perpendiculars, L_{BP}	180,0 m	238,0 m	320,0 m
Beam, *B*	32,20 m	42,48 m	70,00 m
Depth, *D*	15,00 m	20,70 m	25,60 m
Draught, *T*	11,50 m	15,50 m	19,00 m
Deadweight	40 000 t	110 000 t	314 000 t
Webframe spacing	3,56 m	3,50 m	4,00 m
Transverse bulkheads spacing	17,80 m	35,00 m	60,00 m

To help minimize the environmental risks of collision in these enclosed waters, the aim of this paper is to understand the contribution to the risk exerted by the tanker size and the accorded size of the transported cargo. To reach the aim, three characteristic sizes of tanker, HANDYMAX, AFRAMAX and VLCC, are considered in the analysis, with their details provided in Table 1.

The analysis of environmental collision risk builds on the methodology of collision risks assessment as presented in Figure 2 (Ritvanen 2006). The methodology draws on the momentum-conservation collision model, statistical sampling and analysis, and on the numerical simulations of collisions. In detail, traffic data are input to the ship-to-ship collision model to establish the available collision deformation energy. The available energy is thus established through its distribution for the particular geography area, depending also on the size of the struck tanker. It is also compared with the tanker's hull capacity to absorb collision energy prior to breach of the inner hull evaluated in the numerical collision simulations.

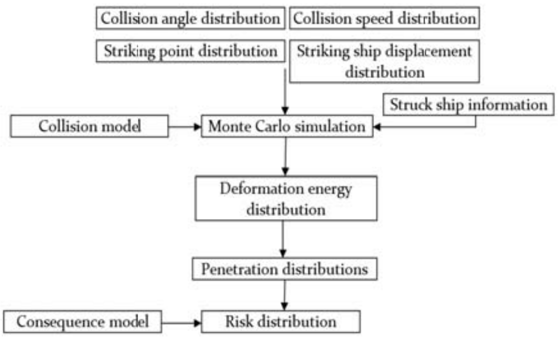

Figure 2: Adopted procedure for the computation of environmental risk of collision.

If the available deformation energy is higher than the capacity of the hull to tolerate collision impact, a spillage can then be expected resulting in pollution, and finally in clean-up and economic compensation costs. Multiplying these costs with the probability of their occurrence in the end determines the risk. Environmental risk is also observed as distributed over the relevant stakeholders of themaritime industry. According to the established conventions on liability to to costs of pollution damage, CLC'92 and IOPC'92 (IOPC 2005), these stakeholders are ship owner/operators and oil receivers. However, their liability is limited according to the convention rules, as it depends on the size of the vessel, and not on the severity of damage. Thus, part of the risk is transfered to the public, and the public is considered also as a stakeholder.

Klanac and Varsta (2010) show that between these three stakeholders, environmental risk are unequally distributed. And since the first two stakeholders have direct influence to determine the size of the tanker for charter, it is relevant to see how does a particular share of the environmental risk for each of the considered stakeholders depends on this size.

Klanac and Varsta (2010) show that between these three stakeholders, environmental risk are unequally distributed. And since the first two stakeholders have direct influence to determine the size of the tanker for charter, it is relevant to see how does a particular share of the environmental risk for each of the considered stakeholders depends on this size.

Risk analysis has been used often when assessing risk associated to the maritime traffic on a certain geographical area. There exist significant contributions in the literature, which form the basis of contributions brought by this paper. We mention here a notable few. Brown (2002) examined how collision random variables influence the extent of predicted collision damage. He generated collisions with Monte Carlo simulation using simplified ship collision model SIMCOL (Chen, 2000) and carried out a sensitivity analysis on four different ships. Lützen (2001) analysed ship collisions on different ship types and damage scenarios. She used a collision database collected within the European research project HARDER (Laubenstein *et al.* 2001, Lützen 2003) and applied it in Monte Carlo simulation to achieve distributions for damage sizes to establish a proposal for the new damage stability regulations. Hence she did not concentrate on the material losses or environmental effects of a collision nor take into account the financial consequences. Otto *et al.* (2002) studied the financial consequences of collision and grounding accidents. They linked the collision risk, the probability functions for the collision damage length, depth and height, and the monetary values for material damage to achieve a financial risk value without taking into account the environmental risk or loss of human life. Ravn and Friis-Hansen (2004) performed a collision risk analysis study, where the extent of damage on ship hull in collision is estimated using regression analysis, namely the Neural Networks. Using FEM-based non-linear numerical simulations of collision (Klanac *et al.* 2005, Shillo 2006, Ehlers *et al.* 2007), Ritvanen (2006) assessed the performance and made comparison of different tanker side structures in a collision. The material, environmental and total risk values as a function of deformation energy were also presented.

Kujala *et al.* (2009) summarise the accident statistics in the Gulf of Finland from 1997 to 2006. According to the collision accident modelling made in the study, the most risky crossing is the one between Helsinki and Tallinn. Most of the ship-to-ship collisions had happened in February or March, which is congruent with the fact that most of the ship–ship collisions had happened in ice channels.Similarly to this paper, Montewka (2009) argues also the relevance of collision risk assessment for tankers in the Gulf of Finland.

For the Adriatic, no conslidated databased of traffic accidents exist, including the risk of collision. However, Buksa and Zec (2005) have considered the present and future estimated traffic in the Bay of Rijeka,in the northern Adriatic Sea, and by means of traffic model simulation have analyzed the present risk considering also the future increase. Zec *et al.* (2005) had performed scenario analysis of the potential oil spills for the same areas of the Adriatic.

Relevance of the environmental risk to the Adriatic and Gulf of Finland

In Figure 3 we can notice the location and characteristic shapes of the observed seas. The Adriatic Sea is a part of the Mediterranean Sea that separates the Italian Peninsula from the Balkans. The western coast is Italian, while the eastern coast belongs mostly to Croatia, and then to Montenegro, Albania, Slovenia and Bosnia and Herzegovina. The Adriatic has an extreme length of about 378 Nm. It has an average width of about 87Nm. Its total surface area is about 160 000 km². Average depth is 444 meters. From a total of 8300 km of the Adriatic coast, Croatia spreads on about 6200 kilometres, or in other words, approximately 75 % of the length of the hole Adriatic coast.

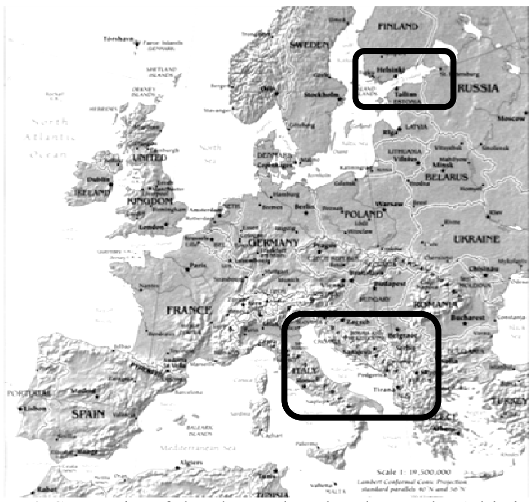

Figure 3 Geography of the observed enclosed seas, the Adriatic and the Gulf of Finland

Gulf of Finland represents an eastern arm of the Baltic Sea. It is 231 Nm long, and maximum 65 Nm wide. It contains many islands, especially in front of the City of Helsinki. Gulf of Finland is located between Finland, Russia and Estonia. On very harsh winters the Gulf can be frozen entirely from December throughout March, while more regularly freezing occurs from late January till March. It is very shallow and groundings occur regularly, but for this reason traffic is intensively regulated and monitored. Furthermore, the winter conditions add to the risks.

Alongside the Mediterranean, Adriatic experiences very intense tanker traffic. Mediterranean Sea, which represents only 1% of the world sea area, takes 30 % of the world trade, and more than a quarter of global oil traffic. More than a thousand tankers and 70 million tons of oil enter Adriatic every year. Croatia holds 75 %of the Adriatic coast, while Italy holds 75 % of the tanker traffic in its ports, mostly in Trieste, in the very north of the Adriatic. Adriatic is also extremely important for the tourism and fishing, and economies of Croatia and Montenegro heavily depend on these.

The Gulf of Finland is one of the densest sea areas in the world. In the maritime traffic in the Gulf of Finland were transported 263 million tonnes of cargoes of which the share of oil products was 56%. 23% of the cargoes were loaded or unloaded in the Finnish ports, 60% in the Russian ports and 17% in the Estonian ports. Characteristically, the traffic in the Gulf of Finland consists of east-west and north-south traffic. East–west traffic, leading to and from the Russian harbours, relates mostly to the cargo shipping, while the transverse traffic connects passengers on their route between Helsinki in Finland and Tallinn in Estonia.

Deformation collision energy

Ship-to-ship collision phenomenon is typically split between ship dynamics and structure deformations. The overall kinetic energy of both vessels is thus split onto deformation energy absorbed by the structure and the residual kinetic energy that induces ship motions. How the overall kinetic energy is split depends on a multiple of factors, among others the vessels' displacements, their speeds, collision angle and location along the hull, and to a lesser extent the vessels' structural arrangement.

For this reason Zhang (1999) defines a simplified collision model based on the momentum conservation originally by Minorsky (1959). The model is able to well estimate the amount of deformation energy, without considering the colliding vessels' structure. Therefore, deformation energy is decoupled computationally from the residual kinetic energy, and the effect of collision onto damage of vessels can be observed more easily. Furthermore, for this reason, deformation energy can be established for a desired geography area, or for an observed ship, or for their combination, e.g. see Lützen (2001). Such is the case here, where using the Monte Carlo Simulation method we establish effectively the available deformation energy for the observed enclosed waters, and for the considered three tankers.

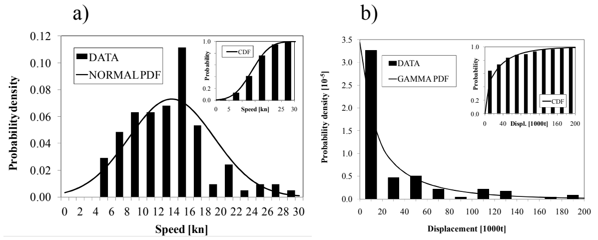

Figure 4. Vessel speed (a) and displacement (b) probability desity distributions (CDF in window) in the Adriatic sea

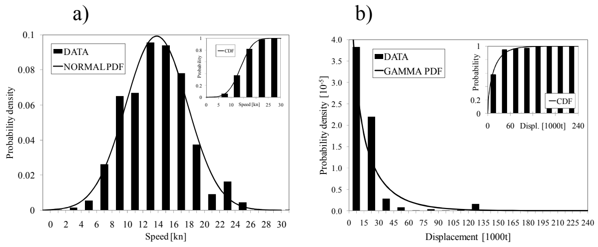

Figure 5. Vessel speed (a) and displacement (b) probability desity distributions (CDF in window) in the Gulf of Finland

The particulars of striking vessel are defined statistically based on the traffic data. Traffic data of the Adriatic and the Gulf of Finland, classified over annual distributions of vessels' speed and displacement, is presented in Figure 4 and 5. The data is collected using Automatic Identification System (AIS). Specifically for the Gulf of Finland, it refers to the open water navigation, i.e. the winter navigation in ice-bound conditions is excluded. The traffic data is fitted with Normal and Gamma probability distributions for vessel speed and displacement respectively. Goodness of fit can be verified visually observing the cumulative probability distribution given in smaller windows of Figures 4 and 5.

Collision speed of the striking vessel is conditional to the service speed provided in the data. According to the data obtained from the previous worldwide collisions (Lützen 2001), collision speed can be uniformly distributed between the zero speed and 75% of the service speed, after which it triangularly decreases to zero at service speed. The speed of the observed struck tanker on the other hand is assumed to be triangularly distributed between zero and her service speed, with the most likely value equal to zero.

Collision angle and collision location along the struck vessel are assumed also on the basis of previous worldwide collision accidents data, as presented by Tuovinen (2005). Their distributions are defined as normal for the collision angle, with the mean of 93° and a standard deviation of 42°, while the distribution of collision location is uniform. Ståhlberg (2010) recently presented new arguments that could raise doubts in the applicability of the worldwide data of collision angle distribution to the enclosed sea areas, indicating that this distribution is fairly location-dependent. Being so recent, the results of this study should be however further explored with respect to actual sea areas considered, especially in the case of the Adriatic sea.

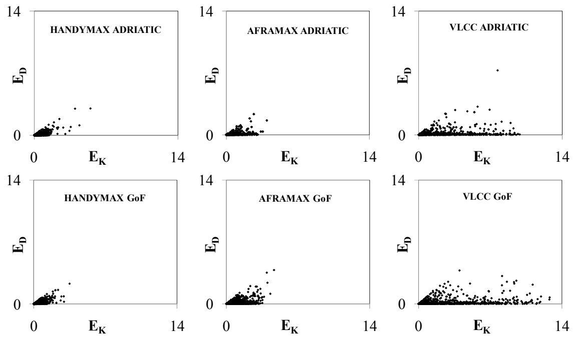

Figure 6. Computed deformation energies E_D against kinetic energies E_K during collisions simulations using Monte Carlo method. Energy values are given in Giga Joules.

Figure 6 depicts the values of deformation energy attained from the Monte Carlo collision simulations plotted against the kinetic energy. We can see how the overall kinetic energy increases with the size of the vessel. It is also higher for the Gulf of Finland in comparison with the Adriatic, but the maxima of the attained deformation energies for each case differs much less. This can be addressed to the known fact that high-energy collisions incite much more ship motions than deformations, see e.g. Tabri (2010).

The number of collision simulations proves to be sufficient to achieve a reasonable convergence of deformation energy frequency distributions. The probability distributions can be seen in Figures 7a and b. for a couple of combinations – the vessel size and the considered sea area. In the same figures we can see also that in both situations, the discrete distribution can be sufficiently accurately approximated with a continuous Gamma distribution.

Assuming that the Gamma distribution of the deformation energy is applicable generally, for the sake of comparison Figure 7c brings also the distribution of the available deformation energy in the worldwide traffic for the observed AFRAMAX, established based on the calculations by Lützen (2001). Evidence of this applicability can be indirectly confirmed by a solid fit of a cumulative Gamma distribution through the 25, 50, 75 and 90 percentiles.Depiciting of distributions for other tankers and navigation areas is omitted in order to maintain paper brevity.

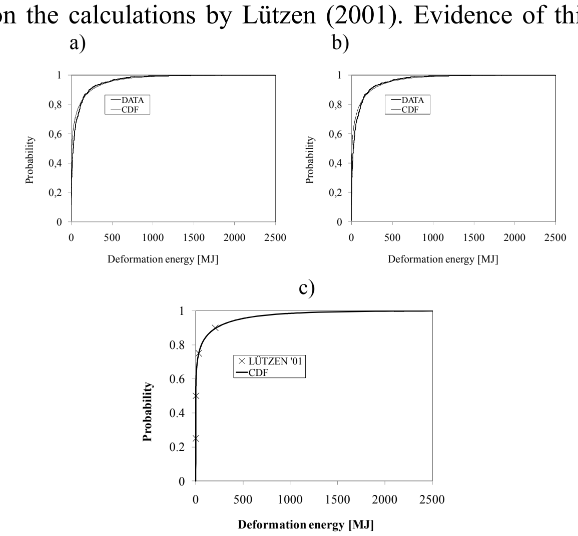

Figure 7: Probability distribution of the available deformation energies given for a few exemplary cases. Namely for the a) HANDYMAX tanker in the Adriatic Sea, b) VLCC tanker in the Gulf of Finland, and c) AFRAMAX tanker in the worldwide traffic

Table 2: Mean and standard deviation of computed available deformation energies

	Adriatic Sea			Gulf of Finland			the World		
Tanker type	**Handy**	**Afra**	**VLCC**	**Handy**	**Afra**	**VLCC**	**Handy**	**Afra**	**VLCC**
μ [MJ]	84	111	149	118	142	192	60	80	100
σ [MJ]	196	253	424	200	284	393	170	245	325

Table 2 presents the mean and standard deviation for the Gamma distributions of the deformation energy attained from the Monte Carlo collision simulations.

Hull crashworthiness

After establishing the available deformation energies for the observed three tankers operating in the Adriatic, the Gulf of Finland, but also worldwide, we need to define the nominal capacity of their hull to tolerate this energy without breaching of the cargo tanks. This capacity, defined as such, is effectively assumed to represent the crashworthiness of the tankers independently of the geographic location of operations, or striking ship size and speed of collision.

Crashworthiness is established using the non-linear Finite Element Method (FEM) through numerical simulations of the structural deformations of tankers' hulls during collision. The simulations determine the required deformation energy to initiate the breach of the inner hull of the vessel.

Physically, these simulations consist of computing energy required to push a rigid indenter into the side structure of the observed tankers, until the indenter breaches the inner hull. The rigid indenter resembles a bulbous bow, with a tip diameter of 3.2m, while its length is 6.85 m and base radius 5.6 m. It has been noticed that in many collision cases striking bow sustains only a minor damage compared with the side structure of the struck ship, striking bow can be defined as rigid in these types of calculations (Zhang *et al.* 2004).

Collision is a very localized phenomenon due to differing size of striking bulbous bow and the extension of the side structure (Wevers and Vredevelt 1999, Ehlers *et al.* 2008). As such, hull's crashworthiness will depend significantly on the location of contact. Since the probability of collision location is difficult to estimate, hull crashworthiness will be established for a number of characteristic locations over the hull side.

Structural arrangement of the three tankers with scantlings is given in Figures 8 to 10 depicting their midship cross-sections. All ship are built from normal shipbuilding steel Grade A with 235 MPa yield strength.

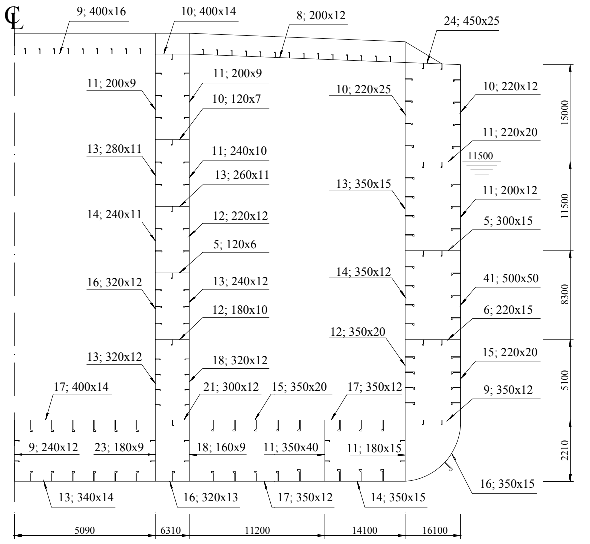

Figure 8: HANDYMAX tanker midship cross-section

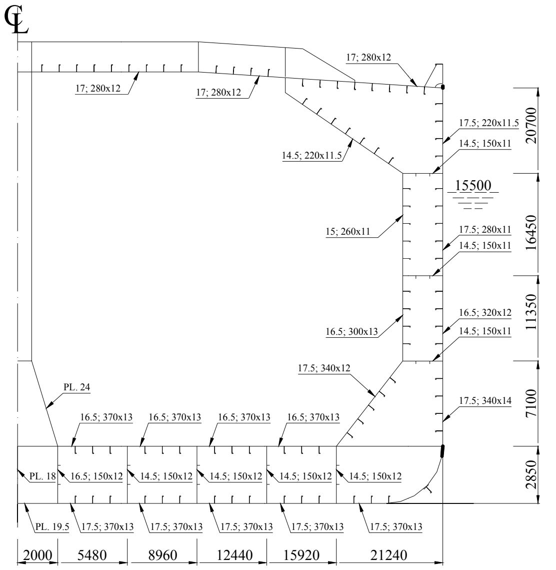

Figure 9: AFRAMAX tanker midship cross-section

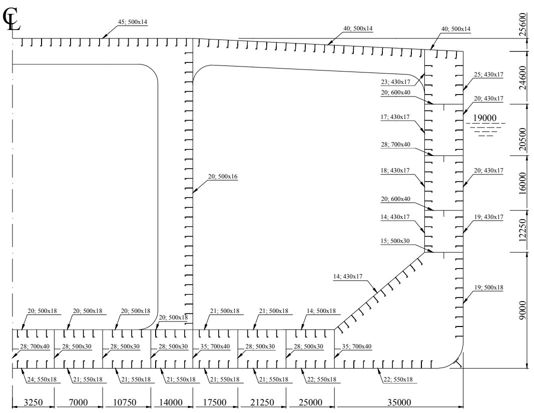

Figure 10: VLCC tanker midship cross-section

Non-linear finite element model

Structural collision simulations are performed using the commercial solver LS-DYNA version 971. ANSYS parametric design language is used to build the finite element model for the tankers' cross-sections, see (Ehlers *et al.* 2008b). The structure is modelled using four nodded, quadrilateral Belytschko-Lin-Tsay shell elements with 5 integration points through their thickness. Following the criterion for crashworthiness, i.e. that the inner hull should remain intact, only the significant structural membersare included in the finite element model, thus also saving computation time. Longitudinally, FEM models extend between the two transverse bulkheads, and transversely, the models extend until the first internal longitudinal bulkhead, as seen in Figure 11,which gives enough distance between the relevant deformed area and the model boundaries. This is verified by visual control of the plastic strains in the edges of the models. Model is restrained at the transverse bulkheads by fixing the translational degrees of freedom. All remaining edges in the model are free.

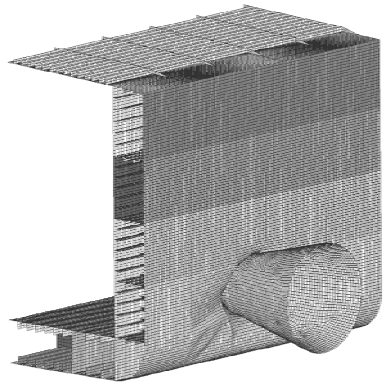

Figure 11: Non-linear FEM simulation of a HANDYMAX in a collision with rigid bulbous bow

The collision simulations are displacement-controlled, i.e. that the rigid bulbous bow is moved into the tanker side structure at a constant velocity of 10 m/s. This velocity is reasonably low so as not to cause inertia effects resulting from the ships' masses; see Konter *et al.* (2004). The ship motions are not considered in this analysis, since we are interested to evaluate crashworthiness. After all, they have been considered indirectly in the analysis of deformation energy described in the previous chapter. Standard LS-DYNA hourglass control is used for the simulations; see (Hallquist 2007).

The time step is controlled by the bar-wave speed and the following length measure: the maximum of the shortest element side or the element area divided by the minimum of the longest side or the longest diagonal of the element. Instabilities for this time step measure could not be found. Additionally, the solution is moderately mass-scaled, however, without causing inertial effects that could influence the results.

The automatic single surface contact of LS-DYNA see (Hallquist 2007) is used to treat the contact occurring during the simulation with a static friction coefficient of 0.3. The reaction forces between the striking bow and the side structure are obtained by a contact force transducer penalty card; see (Hallquist 2007, Ehlers*et al.* 2008). Integrating the contact force over the penetration depth leads to the energy absorbed by the conceptual design alternative.

a)

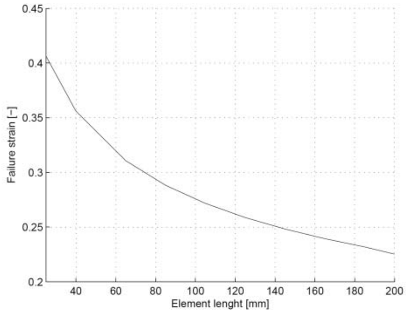

b)

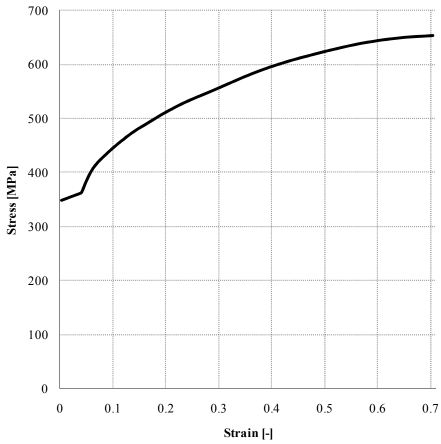

Figure 12: a) Fracturing strain and element length relation,b) NVA true strain and stress relation applied

Non-linear behaviour of the hull material is modelled using the true strain and stress relation until fracture identified by Ehlers and Varsta (2009) and Ehlers (2009), as seen in Figure 12. The fracturing strain and element length relation is implemented into the model via material 24 of LS-DYNA (Hallquist 2007). The elements surpassing fracturing are in the end removed from the model during simulation.

Collision Cases

Structural collision simulations are very time-expensive, thus the most critical collision scenario is generally applied to computationally determine the hull crashworthiness; see Zhang *et al.* (2004). Here, the collision scenario is designed in a way that a striking and a struck ship collide at the angle of 90°. Such a scenario is generally considered critical since in most of the cases it results in the extensively large damages.

As noted above, the amount of energy prior to the breach of the inner hull of the struck ship changes with respect to the striking position. In other words, different configurations of side structural elements of the struck ship in longitudinal direction generate different energies prior to the breach of the inner hull. As a consequence, there are two characteristic striking positions in longitudinal direction, see Figure 13:

i. Position amid web frames, i.e. within 800 mm (half of the radius of the cone-shaped bulbous bow) from each one,
ii. Position directly on the web frame, with span of 800 mm from both, fore and aft side of web frame.

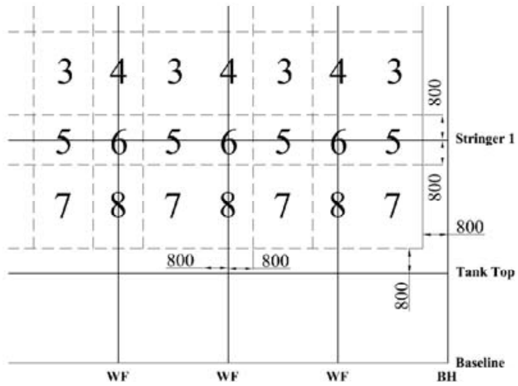

Figure 13: Striking positions concept/determination

Two more characteristic positions in transversal direction are defined:

iii. Position amid stringers, i.e. within 800 mm from each one,
iv. Position directly on the stringer, bounded with lines 800 mm offset from each one.

To increase the precision of averaging the energy prior to the breach of the inner hull, four described positions are duplicated and vertically arranged. Using of eight striking positions surely affects on getting the final amount of averaged energy. Probability of occurrence of each striking position is calculated according to their areal contribution to the surface bounded with tank top and waterline in vertical direction, and horizontally between two bulkheads, Figure 14.

Amounts of energy prior to the breach of the inner hull for all striking positions as well as averaged values of energy are given in Table 3, and are applied in further considerations.

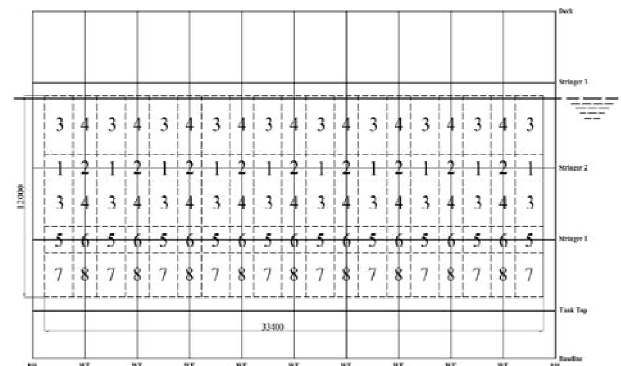

Figure 14: Striking positions on the AFRAMAX tanker

Table 3: Calculated energies, penetration lengths and probabilities of occurrence for each striking position

		HANDYMAX			AFRAMAX			VLCC		
Striking Position		Energy, MJ	Penetration Length, m	p	Energy, MJ	Penetration Length, m	p	Energy, MJ	Penetration Length, m	p
1	⊖	8,31	3,0	0,178	49,14	3,0	0,076	82,83	4,0	0,136
2	⌖	8,58	3,0	0,116	35,51	2,5	0,057	89,57	3,5	0,085
3	○	11,39	3,0	0,178	38,41	3,0	0,292	50,56	3,5	0,183
4	ϕ	12,34	3,0	0,116	38,28	3,0	0,221	60,48	3,5	0,114
5	⊖	8,19	3,0	0,178	43,36	3,0	0,076	53,53	3,5	0,068
6	⌖	5,08	2,5	0,116	68,31	4,0	0,057	71,11	3,5	0,042
7	○	7,27	3,0	0,072	60,22	4,5	0,126	63,57	5,0	0,230
8	ϕ	4,54	2,5	0,047	61,99	4,5	0,095	82,35	5,0	0,143
E_{avg}		**8,71**			**46,11**			**67,98**		

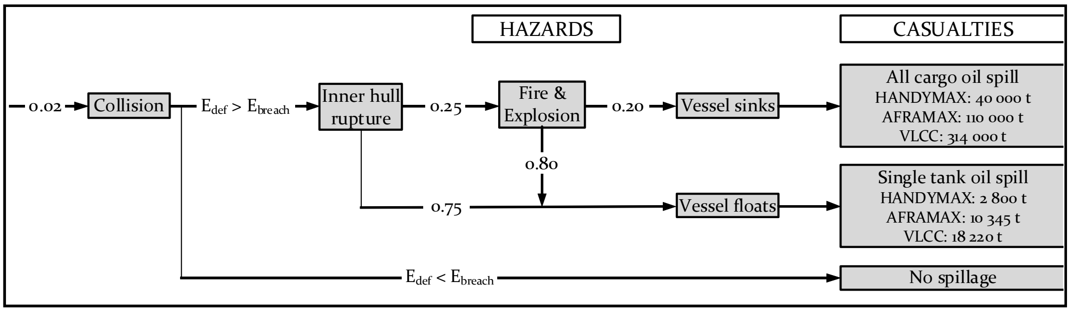

Figure 15: Collision event tree

Computation of Risk

Having established the available deformation energy, and the energy required to breach the inner hull of the tankers, we can now estimate the environmental risk for each of the observed sea areas, as well as for the worldwide navigation.

We evaluate here the risk following a standard definition of value of loss under uncertainty, i.e. risk is a sum of products of probabilities of occurrence of certain damages. Thus it is necessary to estimate well the damages instigated by the collision consequences, as well as the corresponding probabilities.

In this paper it is assumed that the breach of the inner hull occurs once the available deformation energy surpasses the capacity of the hull to absorb collision energy, i.e. if $E_{def}>E_{breach}$.

Probabilities of environmental damage

Probability of occurrence of a collision is assumed to be p_{coll} = 0.02. Several studies indicate this figure both for the worldwide navigation (Lützen 2001) and for local sea areas, namely the Gulf of Finland (Kujala *et al.* 2009, Ylitalo 2010). It is also adopted here for the Adriatic, as no better estimates exist in the literature for this sea area.Lately, other values had been also proposed for the worldwide navigation, but no general consensus has been noticed in the literature. Furthermore, it is assumed that the tankers sail 60% of time fully laden, which is a very conservative estimate.

If inner hull rupture appears, various hazards show up. Performed risk calculation includes only fire and explosion as an event, which may lead to the oil spillage from all tanks. Probability of fire and explosion on the vessel is taken as 0.2. However, it is assumed that vessel will sink in only 20 % of fire and explosion cases, and thus lose and spill the complete oil cargo.

Here we consider two casualties that the oil spill emerges from a single tank, or from all tanks. Considered collision scenarios are represented in Figure 15, and the probabilities adopted are assumed according to IMO (2001, 2002, 2004, 2005, 2005b), Tuovinen (2006), Papanikolaou *et al.*(2005), Grey (1999).

Costs of the environmental damage

Regarding collisions of tankers, environmental damage is the most relevant casualty for all the maritime stakeholders, and it considers here all direct consequences to the economy of the affected coastal area. This considers then not only oil spill clean-up costs, but also direct damages to the business, e.g. fisheries, tourism, etc. Secondary effects to the economy in the national level are not considered. Generally, they belong more under consideration of standard business risk.

Environmental damage, i.e. the costs of oil spillage can be conveniently estimated utilizing the probabilistic model of Friis-Hansen and Ditlevsen (2003). The model is based on the recorded major spills damage data (IOPC 2009), which is represented through the probability of the environmental damage cost *C*, defined with the expected cost of spillage $E[\log C]$ and its dispersion $D[\log C]$, and the expected volume of the oil spilled *S*, defined similarly with $E[\log S]$ and $D[\log S]$, where μ_s represents the expected volume of oil to be spilled, e.g. the tank volume, and *c* is the random variable of damage cost. In brief, the probability distribution of the environmental damage cost as defined by the model is defined with the following normal distribution:

$$F_C(c,\mu_s)=\int_0^1 \Phi\left(\frac{\log c-\varsigma-\eta\log(-\mu_s\log\upsilon)}{\theta}\right)d\upsilon \qquad (1)$$

in which:

$$\varsigma = E[\log C]-\eta E[\log S], \qquad (2)$$

$$\eta=\rho[\log C,\log S]D[\log C]/D[\log S], \qquad (3)$$

$$\theta = D[\log C]\sqrt{1-\rho[\log C,\log S]^2}\ . \qquad (4)$$

Since the original publication of this damage model several new accidents have occurred, e.g. the likes of m/t Prestige and m/t Hebei Spirit, the original damage data is thus updated. The new consolidated data is seen now in Figure 16. Furthermore, since the original damage data has been considered in the value of USD of year 2000, the financial valuation is also updated, and also converted to EUR. The mean values and standard deviations of distributions of amount of oil spilled and the amount of damage costs are changed then accordingly. These are then based on the linear regression of the data presented in Figure 16. Furthermore, since the original damage data has been considered in the value of USD of year 2000, the financial valuation is also updated, and also converted to EUR. The mean values and standard deviations of distributions of amount of oil spilled and the amount of

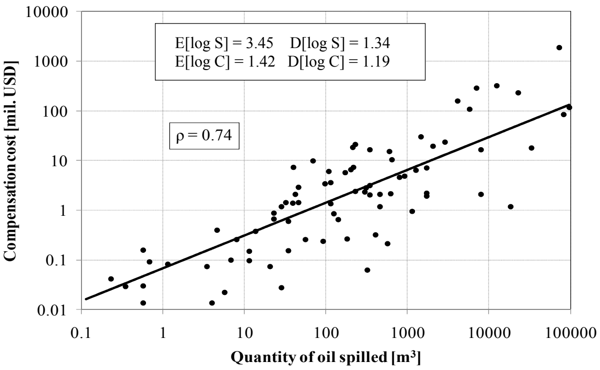

Figure 16: Double logarithm scatter plot of reported oil spill volume and corresponding environmental damage costs with logarithms of the expected spill volume and damage costs E[.] and respective dispersions D[.]

damage costs are changed then accordingly. These are then based on the linear regression of the data presented in Figure 16.

The expected damage cost$C$ is computed for two characteristic adverse events following the considered event tree, i.e. the spillage of a single tank of oil, and the spillage of the overall cargo; see Fig.15. The damages are split over each of the relevant three maritime stakeholders, i.e. the ship owner/operator, oil receiver(s) and the public. Their expected costs are established by using the following expression that formalizes liabilities of each of the three stakeholders according to the established maritime conventions, i.e. CLC'92 and IOPC'92.

$$C(stakeholder, \mu_S) = \int_0^\infty c \cdot f_C(c, \mu_S) \cdot I(stakeholder) dc \tag{5}$$

$$I(stakeholder) = \begin{cases} f_C(c, \mu_S) & c_{\min} < c < c_{\max} \\ 0 & \text{otherwise} \end{cases} \tag{6}$$

where $I(stakeholder)$ filters the inapplicable costs and $f_C(c, \mu_S)$ is a PDF of probability distribution given in Eq. (1). The financial value of liabilities, $c_{min}$and c_{max}, for each stakeholder are specified in Table 4 based on the observed tanker size, in this case the her gross tonnage(IOPC 2005), while the expected environmental damage costs in a collision for a stakeholder are specified accordingly in Table 5.

Table 4: Limits of liability for environmental damage costs

		C_{min}			C_{max}		
	[M€]	Handy	Afra	VLCC	Handy	Afra	VLCC
Stakeholder	Owner	0	0	0	10	29	84
	Receiver	10	29	84	1037	1037	1037
	Public	1037	1037	1037	∞	∞	∞

Table 5: Expected costs in M€ of the environmental damage in a collision per considered stakeholder and tanker.

	Ship Type	Handymax		Aframax		VLCC	
	Ship Volume	One tank 2200 [m^3]	All cargo 40000 [m^3]	One tank 12000 [m^3]	All cargo 127000 [m^3]	One tank 21000 [m^3]	All cargo 309000 [m^3]
Stakeholder	Owner	1	1	4	5	7	10
	Receiver	12	31	19	38	20	41
	Public	70	550	229	1197	384	2202

Calculation of the environmental risk

Risk is evaluated on the annual basis, due to considered traffic data. Risk is given for each of the observed tankers and also for each of the relevant maritime stakeholders. Risk is calculated by integrating over the random variable of the available annual deformation energy of all the probable collision consequences, and by multiplying that value with the probability of collision occurrence, p_{coll}, and a probability of the fully laden tanker voyage

$$u_{risk,j} = p_{coll} \cdot p_{laden} \int_{E_{def}} \sum_i p_i(E_{def}) \cdot C_{i,j}(E_{def}) dE_{def} \tag{7}$$

where the consequences costs and corresponding probabilities are calculated as

$$\sum_i p_i\left(E_{def}\right) C_{i,j}\left(E_{def}\right) = \begin{cases} 0, & \text{if } E_{def} < E_{breach} \\ p_{fire}\left[p_{loss} C_{total,j} + \left(1-p_{loss}\right) C_{tank,j}\right] + \\ +\left(1-p_{fire}\right) C_{tank,j}, & \text{if } E_{def} \geq E_{breach} \end{cases} \tag{8}$$

based on the numbers provided in Figure 15 for ther probabilities and Table 5 for the cons

The annual value of risk for the three tanker sizes, three stakeholders and three geographical areas is given finally in Table 6. The same table brings also the annual risks averaged per day of operations since vessels do not operate constantly in the enclosed sea area.

Discussion

Observing the risk given in Table 6 we can make a few conclusions on attained findings. Annual risks averaged per day of operations are higher in the enclosed waters than in the worldwide navigation, as much as double. This relates obviously to the higher available deformation energy in the enclosed waters, emerging from differences in traffic, see the mean and standard deviation given in Table 2. Thus also, the risk is the highest in the Gulf of Finland, about 80% higher than for the worldwide navigation if comparing daily

Table 6: The annual (a) and averaged per day (b) risk for the three tankers, three stakeholders and three navigation areas

a)

	Adriatic Sea			Gulf of Finland			World		
Risk [M€]	Handymax	Aframax	VLCC	Handymax	Aframax	VLCC	Handymax	Aframax	VLCC
Owner	0.006	0.014	0.023	0.009	0.018	0.036	0.005	0.010	0.017
Receiver	0.077	0.081	0.065	0.110	0.102	0.101	0.058	0.054	0.049
Public	1.510	1.107	1.489	2.296	1.389	2.291	1.213	0.733	1.120
TOTAL	1.593	1.202	1.577	2.415	1.509	2.428	1.276	0.797	1.186

b)

	Adriatic Sea			Gulf of Finland			World		
Risk [1000€]	Handymax	Aframax	VLCC	Handymax	Aframax	VLCC	Handymax	Aframax	VLCC
Owner	0.016	0.039	0.063	0.023	0.049	0.097	0.012	0.026	0.048
Receiver	0.211	0.222	0.178	0.301	0.279	0.277	0.159	0.148	0.134
Public	4.137	3.033	4.079	6.290	3.805	6.277	3.323	2.008	3.068
TOTAL	4.364	3.294	4.321	6.615	4.134	6.651	3.495	2.182	3.250

averaged values. In the Adriatic, the risk is higher about 50%.

These results justify in the end the premise that navigation in the enclosed waters is riskier with respect to collision and environment than the worldwide navigation. However, it should be noted that vessels do not spend equal amounts of time in the worldwide and enclosed water navigation, nor these observed tankers take the same routes. For example, if we consider a typical journey of an AFRAMAX from the Arabian Gulf, e.g. Kuwait to the Trieste harbour in the Adriatic, that lasts abt. 15 days (excluding the anchorage in Suez), the open water, i.e. the worldwide navigation, can be realistically assumed to exist only between the Gulf of Oman and the Gulf of Aden, and between Suez and the Strait of Otranto. This is about 1 900 nm out of total 5 000 nm, i.e. about 5 to 6 days or 30 to 35% of total time, since the vessel, besides the Adriatic, sails through the Gulf of Aden and the Red Sea. Some of the typical VLCCs, on the other hand, cannot pass through Suez Canal fully laden, and when they take a journey, e.g. to Rijeka harbour in the Adriatic they might need to take a longer route around the Cape of Good Hope, which means that the risk of collision in the worldwide navigation becomes much more relevant.

Besides these findings and conclusions, itis very important to bring attention to the difference in risk between stakeholders. While the risks for ship owner/operator on an annual basis are fairly small, for oil receivers these are abt. 10 times as high. Yet these values are minor in comparison with the risk faced by the public, which measure 10 to 20 times that of oil receivers, and correspondingly 100 to 200 times that of owner/operator.

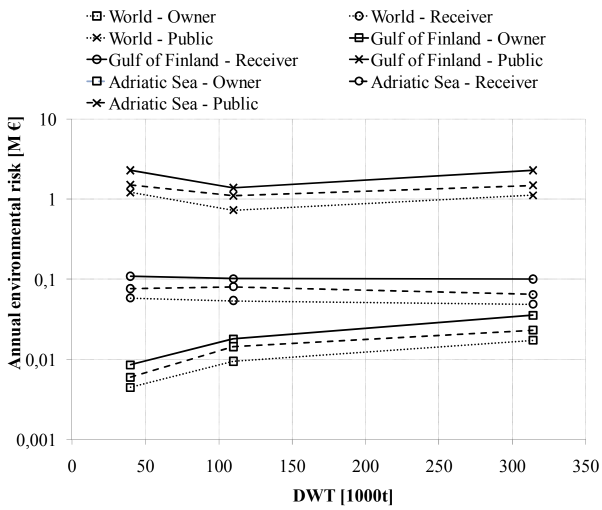

Figure 17: Distribution of the anual environmental collision risk per stakeholder, per tanker and and geographic area.

Further conclusions based on the findings of this study can be made if we analyse the effect of ship size to the environmental collision risk. If considering total risk, the riskiest tankers are interestingly the HANDYMAX (40'000DWT) and VLCC (313'000DWT), the smallest and the largest vessels considered, while the risk is significantly reduced with AFRAMAX (110'000DWT) tankers, see Table 6. Figure 17 thus presents the calculated risk against the tankers' deadweight.

This result is caused by the ratio between the hull crashworthiness and the amount of oil transported onboard. From Figure 18 we can notice a quick rise in crashworthiness between HANDYMAX and AFRAMAX tankers in comparison to the rise in the size of the expected oil spill, i.e. the size of their tanks, or the amount of transported cargo.

From Figure 17 we can also notice the distribution of risk between different stakeholders. The ship owner/operator thus experiences the smallest risk with the smallest tanker, i.e. HANDYMAX, while their risk is increasing with the size. Obviously then, the owner/operator would prefer to invest and operate the smallest tanker, but if we consider that this collision risk is almost negligible, size of the preferred tanker will be determined probably on other, more commercial factors. Oil receivers, on the other hand, seem not to be affected by vessel size. This means that could base their preferences on oil transport on other economical attributes, or other kinds of risk. The public is best off with the medium sized tanker, the AFRAMAX, as she shows the least risk in comparison with the other two considered vessel sizes. Commonly, all stakeholders do not experience significant difference in risk variations due to tanker size between the navigational areas considered in this study.

Conclusion

This paper brought a series of comparative analysis of environmental risk of collisions. Focus of the analysis was on the enclosed sea areas, the Gulf of Finland and the Adriatic, and on a three tanker sizes, HANDYMAX, AFRAMAX and the VLCC. Evaluated risks of collisions for these three tanker types were also compared for the worldwide navigation.

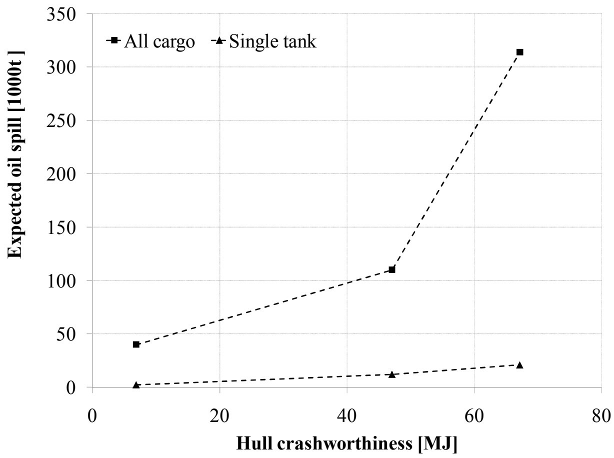

Figure 18: Expected oil spill size against hull crashworthiness

The analysis considered evaluation of the available deformation collision energies for the enclosed sea areas and for the observed tankers. Evaluation of the expected costs of environmental damage was also performed. In the end, the risks were distributed over three relevant stakeholders, the ship owner/operators, oil receivers and the public.

Results brought a series of findings. The following three are possibly the most relevant to be repeated here. Navigation in the enclosed sea areas is more risky than in the open, worldwide regime. The least risky tanker out of three considered seems to be the AFRAMAX due to good combination of her hull crashworthiness and cargo capacity. The risk is very unevenly shared between the stakeholders, where the public faces the very biggest share of the total environmental risk, i.e. more than 90%.

These findings need further investigations however. Firstly, more vessel sizes could be analysed, like PANAMAX and SUEZMAX, which would fill in the gaps in the curves presented. All elements of the analysis presented could also benefit from improvements in methodology and the data considered. This specifically refers to the collision model to estimate the deformation energy. Recent works of Tabri (2010) could be applied for example to better estimate the deformation energy considering also the hull crashworthiness. Furthermore, the probabilities of adverse events can be studied more, especially if they can be sensitive to the geographical areas, using methods such as that of Goerlandt F. (2010)

More enclosed sea areas could also be considered, like the Danish Straits, the Strait of Dover, Sea of Marmara, Gulf of Bothnia, etc. Such a data could be eventually used to establish a GIS-based map of world environmental risk, especially if other adverse events are to be considered, firstly the groundings, and later on hull breakings due to service conditions.

References

Brown, A.J. Collision scenarios and probabilistic collision damage. Marine Structures, 15:335–364, 2002.

Buksa, J., Zec, D. Model procjene pomorskih rizika u ograničenom plovnom području. Pomorstvo, god. 19., str. 173-193. (in Croatian), 2005.

Chen, D. Simplified ship collision model. Master's thesis, Virginia Polytechnic, Institute and State University, Blacksburg, Virginia, USA, 2000.

Ehlers, S. Strain and stress relation until fracture for finite element simulations of a thin circular plate. Submitted to the Journal of Thin-Walled Structure, 2009.

Ehlers, S., Broekhuijsen, J., Alsos, H.S., Biehl, F., Tabri, K. Simulating the collision response of ship side structures: A failure criteria benchmark study. International Shipbuilding Progress, Volume 55, Number 1-2, p. 127-144, 2008.

Ehlers, S., Klanac, A., Kõrgesaar, M. A design procedure for structures against impact loading. STG Yearbook 2008b, in press.

Ehlers, S., Klanac, A., Tabri, K. Increased safety of a tanker and a RO-PAX vessel by implementing a novel sandwich structure. Proc fourth International Conference on Collision and Grounding of Ships. p. 109-115. Hamburg, 2007.

Ehlers, S., Varsta, P. Strain and stress relation for non-linear finite element simulations. Thin-Walled Structures, doi:10.106/j.tws.2009.04.005, 2009.

Friis-Hansen, P., Ditlevsen, O. Nature preservation acceptance model applied to tanker oil spill simulations. Structural safety, 25:1-34, 2003.

Grey CJ. The cost of oil spills from tankers. In: Proc Int Oil Spill Conference. 1999. Available at: http://www.itopf.com/_assets/spilcost.pdf, accessed on 11 Oct 2009.

Goerlandt F, Kujala P. Modeling of ship collision probability using dynamic traffic simulation. In: Soares G (ed.) Proceedings of ESREL conference. London: Taylor and Francis; 2010.

Hallquist, J.O. LS-DYNA. Keyword User's Manual, Version 971. Livermore: Livermore Software Technology Corporation, 2007.

Hooke, N. Maritime casualties, 1963-1996. 2nd edition, LLP Limited, London, 1997.

International Maritime Organization. Casualty statistics and investigations: Very serious and serious casualties for the year 2000. FSI.3/Circ.3, 2002; Available at: http://www.imo.org/includes/blastDataOnly.asp/data_id%3D5118/3.pdf, accessed on: 4 Aug 2008.

International Maritime Organization. Casualty statistics and investigations: Very serious and serious casualties for the year 2001. FSI.3/Circ.4, 2004; Available at: http://www.imo.org/includes/blastDataOnly.asp/data_id%3D8934/4.pdf, accessed on: 4 Aug 2008.

International Maritime Organization. Casualty statistics and investigations: Very serious and serious casualties for the year 2002. FSI.3/Circ.5, 2005; Available at: http://www.imo.org/includes/blastDataOnly.asp/data_id%3D11539/5.pdf, accessed on: 4 Aug 2008.

International Maritime Organization. Casualty statistics and investigations: Very serious and serious casualties for the year 2003. FSI.3/Circ.6, 2005; Available at: http://www.imo.org/includes/blastDataOnly.asp/data_id%3D11540/6.pdf, accessed on: 4 Aug 2008.

International Maritime Organization. Casualty statistics and investigations: Very serious and serious casualties for the year 1999. FSI.3/Circ.2, 2001; Available at: http://www.imo.org/includes/blastDataOnly.asp/data_id%3D5397/2.pdf, accessed on: 4 Aug 2008.

IOPC Annual report 2008. International oil pollution compensation funds, London, 2009.

IOPC Liability and Compensation for Oil Pollution Damage: Texts of the 1992 Conventions and the Supplementary Fund, IOPC 2005.

Klanac, A., Ehlers, S., Tabri, K., Rudan, S., Broekhuijsen, J. Qualitative design assessment of crashworthy structures, Proceedings of International Maritime Association of Mediterranean, p. 461-9, IMAM, Lisboa 2005.

Klanac, A., Varsta, P. Design of marine structures with the improved safety for environment. Submitted to journal of Reliability Engineering and System Safety, 2010.

Konter, A., Broekhuijsen, J., Vredeveldt, A. A quantitative assessment of the factors contributing to the accuracy of ship collision predictions with the finite element method. In Proc Third Int Conf Collision and Grounding of Ships, p. 17-26. Japan, 2004.

Kujala, P., Hänninen, M., Arola, T., Ylitalo, J. Analysis of the marine traffic safety in the Gulf of Finland, Reliability Engineering & System SafetyVolume 94, Issue 8, Pages 1349-1357, August 2009.

Laubenstein, L., Mains, C., Jost, A., Tagg, R., Bjørneboe, N. Updated probabilistic extents of damage based on actual collision data. In Proceedings of 2nd International Conference on Collision and Grounding of Ships ICCGS, Lyngby, Technical University of Denmark, 2001.

Lützen, M. Ship Collision Damage. In Proceedings of 8th International Marine Design Conference, Athens. Greece, May 2003.

Lützen, M. Ship Collision Damage. PhD thesis. Lyngby: Technical University of Denmark, 2001.

Minorsky, V.U. An analysis of ship collisions with reference to protection of nuclear power plants. Journal of Ship Research, 3(2), 1959.

Montewka, J. Predicting risk of collision for oil tankers in the Gulf of Finland. Journal of KONBiN, 3-4 (11-12), 2009, pp.17-32.

Otto, S., Pedersen, P.T., Samuelides, M., Sames, P.C. Elements of risk analysis for collision and grounding of RoRo passenger ferry. Marine Structures, 15:461–474, 2002.

Papanikolaou, A, Eliopoulou, E, Alissafaki, A, Aksu, A, Tuzcu, C, Delautre, S, and Mikelis, N. Critical review of AFRAMAX tankers incidents. In: Proc 3rd Int Conf Marine Science and

Technology for Environmental Sustainability ENSUS. Newcastle upon Tyne, 2005.

Protocol, international oil pollution compensation funds, London, 2005.

Ravn, E.S., Friis-Hansen, P. Predicting collision damage and resulting consequences. In Proceedings of 3rd International Conference on Collision and Grounding of Ships ICCGS, Izu, Japan, 2004.

Ritvanen, H. A Crashworthy Ship: Comparative Risk Analysis of AFRAMAX–tanker Side Structures, Master's thesis, Helsinki University of Technology, Department of Mechanical Engineering, Ship Laboratory, 2006.

Schillo, N. Comparison of two ship side structures under simplified collision with LS–Dyna. Master's thesis, TU Kaiserslauten, Germany, 2005.

Ståhlberg, K. Estimating deformation energy in ship-ship collisions with stochastic modelling. Master's thesis, Aalto University School of Science and technology; 2010.

Tabri, K. Dynamics of ship collision. D.Sc. thesis, Aalto University School of Science and technology; 2010.

Tuovinen, J. Statistical Analysis of Ship Collision. TKK master thesis. Espoo, 2006.

Wevers L.J, Vredeveldt A.W. Full Scale Ship Collision Experiments 1998. TNO Delft, 1999.

Zec, D., Francic, V., Buksa J. Ocjena djelotvornosti uklanjanja onečišćenja mora primjenom analize predložaka. Pomorski zbornik 43, 63-84. (in Croatian), 2005.

Zhang, L., Egge, E.D., Bruhms, H. Approval procedure concept for alternative arrangements. In: Proc Third Int Conf Collision and Grounding of Ships. p. 87-97, Japan, 2004.

Zhang, S. The Mechanics of Ship Collisions. PhD thesis, Technical University of Denmark. Department of Naval Architecture and Offshore Engineering, Lyngby, 1999.

Ylitalo J. Modelling marine accident frequency. Master's thesis, Aalto University School of Science and technology, 2010.

An Experimental Investigation of the Intermediate Flooding Phases in Internal Compartments of an ITTC Damaged Passenger Ro-Ro Ferry

Chadi Khaddaj-Mallat, Bertrand Alessandrini, Jean-Marc Rousset and Pierre Ferrant

Équipe Hydrodynamique et Génie Océanique, Laboratoire de Mécanique des Fluides, École Centrale de Nantes, France

Abstract:
Damaged Ro-Ro ferries have proved to be extremely vulnerable regarding their hydrostatic stability. After an abrupt ingress of water caused by a maritime accident, the spaces below the car deck can experience dangerous intermediate flooding stages, and the ship can sink earlier than predicted.
These stages depend upon many factors pertaining to the vessel, the accident, and the environment. Some of these factors interact during the flooding. An experimental investigation using an ITTC Ro-Ro ferry was devoted to provide a thorough insight to the flooding physics by following the Design of Experiments methodology.
Both transient and progressive phases are found highly dependent upon water and air behaviours. The damage area, the time of damage creation, and the air ventilation level inside damaged compartments are key factors in determining the final ship state. We encourage the application of DOE method to statistically analyse the data and reveal interactions between entailed factors.

Nomenclature

C	Wave velocity (m/s)
CD	Cross Duct
DBA	Double Bottom Aft
DBF	Double Bottom Forward
EB	Engine Block
ER	Engine Room
g	Gravitational acceleration (m/s^2)
GR	Generator Room
IFS	Intermediate Flooding stages
OM	Opening Mechanism
p_{atm}	Atmospheric pressure (Pa)
P_{ij}	Level j of design factor P_i
PS	PortSide
SB	StarBoard
SR	Storage Room
T	Wave period (s)
T_Φ	PRR02 natural period
WT_PS	Wing Tank of the DBF PS
WT_SB	Wing Tank of the DBF SB
ρ	Water density (Kg/m^3)

Introduction

Ro-Ro and Ro-Pax ferries have been growing for decades. Despite the global economic downturn, their industry continues to show positive signs. This is evident by the scheduled launch of some humongous new Ro-Pax vessels by 2012 (as Stena Superferry 1 and 2, 1st and 2nd Stena Seabridger Class MKII, etc.). The safety of such vessels remains of the utmost importance in their design, and operation, when accidents of a varying nature (collision, grounding, etc.) can occur. Thus, advantage should be taken of the available maritime accident data; to foster a better understanding of the underlying physics, and to prevent the occurrence of more accidents in the future. The commercial use of passenger Ro-Ro ferries has proven to be successful. This is due to undivided car decks that reduce the time required for onboard operations. However, it is well known that this characteristic is the main contributor to the sinking of these vessels, as the reserve of buoyancy above the bulkhead deck has completely vanished when the ship shell was damaged. Therefore, efforts have been made by researchers and ship designers, to contribute to confirming the vulnerability of these vessels regarding their stability (Braund 1978; Dand 1989). On the other hand, the geometry of the spaces below the bulkhead deck is also of great importance indeed. It has proved to be a key parameter in the determination of the final state of such vessels when damaged. During the investigation of the sinking of the European Gateway (1982), reported in (Spouge 1985), the "Transient Asymmetric Flooding" phenomenon was discovered, and 80% of the total heeling moment produced during sinking was attributed to the newfound phenomenon. Reinforced by an abrupt ingress of water right after the damage creation, large free surface effects, as well as inertia effects regarding roll motion, render the IFS potentially dangerous, as shown in (Journée et al. 1997; TNO 1997). Thus, the heeling moment exceeds the residual restoring one, and; therefore, the ship heels violently and eventually becomes on the verge of capsize as concluded in (Santos and Guedes Soares 2000).The effect of the IFS on ships' damaged survivability has been studied based on parametric investigations (Chang and Blume 1998; Chang 1999). The floodwater behaviour in the IFS has been extensively investigated and well documented (de Kat et al. 2000; Vassalos 2000; Santos and Guedes Soares 2000, etc.), although the air behaviour and its interaction with water have attracted considerably less attention (Palazzi and de Kat 2002; SSPA 2008). Generally, parametric investigations have provided a better understanding of the basic flooding physics' fundamentals, and have assisted in identifying some significant parameters of the assessed phenomena. Nonetheless, it was stated in (Santos et al. 2002), that: "Very few attempts have been made to ascertain exactly what happens during the IFS and its influence in the capacity of a damaged ship to survive under given environmental conditions". The IFS depend upon hosts of factors related to the vessel hydrostatical and geometrical characteristics, the accident that caused the damage, and the environmental conditions. Besides, what actually characterise these phases are the inherent interdependencies linking these factors that could become strong interactions (Khaddaj-Mallat et al. 2009, 2010). However, it is worth noting that there has not yet been a study to reveal interdependencies and interactions between implicated factors. This is the primary motivation for this work.

Philosophy

One particular research project of the Hydrodynamics and Ocean Engineering Team of the Fluid Mechanics Laboratory of the Ecole Centrale de Nantes in France is devoted to assessing the dynamic behaviour and survivability in waves of damaged Ro-Ro ferries. Supported by intuitive means and preliminary examinations, a rich state-of-the-art-research has assisted in determining the steps to come gradually, for both experimental and computational investigations. As the complex floodwater behaviour and its interaction with the damaged vessel motion limit the effectiveness of the numerical prediction attempts, it was a requisite to perform physical model tests. Three main ideas established the guidelines of the experimental work. They are as follows.

1) Physically, "Ship motion and flooding are distinct but intrinsically interrelated and highly interacting processes", as stated in (Vassalos and Letizia 1998).
2) Experimentally, we do believe in iterative experimentation. Thus, both experimental and computational works progress gradually and in parallel.
3) The measurement of hydrodynamic efforts is required for the validation of numerical models, in particular for those phenomena whose mathematical representation is difficult to formulate, as the flooding we intend to examine. Thus, we measured the hydrodynamic efforts for captive tests, as well as forced-oscillation tests.

Moreover, the project's first step, whose outcomes are partially reported in (Khaddaj-Mallat et al. 2009, 2010), has culminated in two important findings:

1) The adequacy of calm water investigation to assess the IFS of Ro-Ro ships.
2) The requisite of applying statistical approaches to Design of Experiments methodologies (simply called nowadays DOE), in order to identify the main contributing factors and reveal their main effects, existing interdependencies, and possible interactions.

The aforementioned key points determined the extent of innocuous simplifications the investigation in the project's second step is going to have with respect to a real damage scenario. Hence, rather than embarking with the more general damage scenario of a passenger Ro-Ro ferry advancing in waves and, consequently, involving both water ingress/egress through the damage hole and ship motion processes, we first considered the assessment, in calm water, of the flooding of a Ro-Ro ferry. We applied the DOE methodology for designing the plan of experiments, as well as for analysing the data. Two series of distinct tests were performed:

- Flooding experiments in which the model is kept fixed. These tests are performed to assess the influence of the entailed factors on hydrodynamic efforts exerted on the model during the IFS. Moreover, they help better understand the behaviour of both implicated fluids, i.e. water and air.
- Forced oscillation tests performed for realistic combinations between the six degrees of freedom. These tests permit to quantify the influence of external excitations on the measured quantities and sloshing.Based on the background mentioned previously, the objective of the experimental investigation into the IFS was twofold, *viz.*:

1) To find a model characterising the transient phase, that accounts for the involved factors and elucidate their interactions. To this end, a statistically-based experimental design method was employed.
2) To provide test data for calibration and validation of a numerical model based on SPH method (Smooth Particles Hydrodynamics), under development at the moment of writing this paper, as well as numerical results of past investigations that dealt with the same ship (24th and 25th ITTC benchmarks; European research project Harder 2000-2003; Cho et al. 2005; Santos and Guedes Soares 2009).

In addition to the main objective, secondary purposes are listed as follows.

- Better understand flooding physics.
- Test the efficiency of DOE methodology to deal with ocean-engineering problems, particularly vessel's stability.
- Verify the adequacy of calm water condition to assess the IFS of Ro-Ro ferries, and identifying the factors whose trends remain similar or less-changing whether assessed in calm water or in waves.
- Optimise the layout of Ro-Ro engine rooms.

To meet these goals, the PRR02 - ITTC/SiW passenger Ro-Ro ferry was used. The data of this vessel were elaborated within the ITTC studies and are limited to the single case of two compartments damage amidships. Furthermore, as we aim at investigating the flooding far from its strong interaction with ship response and motion, we dealt with the midsection of the ship and tested it for two distinct test series.

In the present paper: IFS refers to both transient and progressive phases. The term "wave" is used to categorise the flooding water behaviour occurring at the free surface, inside the model. The experimental quantities and results are presented in model scale.

The remainder of this paper is organised as follows. After presenting the physical background and the way to achieving our goals, section 3 describes the preparation of the experimental investigation. Sections 4 and 5 are devoted to presenting the adopted experimental methodology and the testing programme, respectively. Then, section 6 presents some first findings, not relevant to any DOE design plans. Finally, conclusions are drawn in Section 7.

Experimental Investigation Model

Model Design and Scale

PRR02 is a modern passenger Ro-Ro ferry of SOLAS 90 stability standards. The main dimensions of the model (the PRR02 midsection) are given in Table 1, and the PRR02 body plan is shown in Figure 1. The model was designed for side damage investigations. It was constructed at a 1:38.25 scale, in compliance with (ITTC 2005). As it can be seen in Figure 2, the model extends to the car deck and comprises two double bottoms containing a cross-flooding arrangement in the forward one above which a generator room then a storage room are located. A large compartment representing the ER and including two EBs is located above the aft double bottom. The permeability of the ER was insured by fitting intact plane-parallel foam blocks. These dummy blocks, made removable for model testing purposes, were glued on the bottom of the ER at different transversal positions. In the DBF, a 3B/5-length CD connects the tank WT_SB to WT_PS. Void spaces, coloured in light black in Figure 2, surround the CD, and remain intact after damage.

Table 1. Main dimensions of the PRR02 midsection.

Length, L(m)	26.714
Beam, B(m)	25.000
Draft, T(m)	6.400
Car deck above baseline (m)	9.100
Model scale	1:38.25
PRR02 Length, L_{pp}(m)	174.800

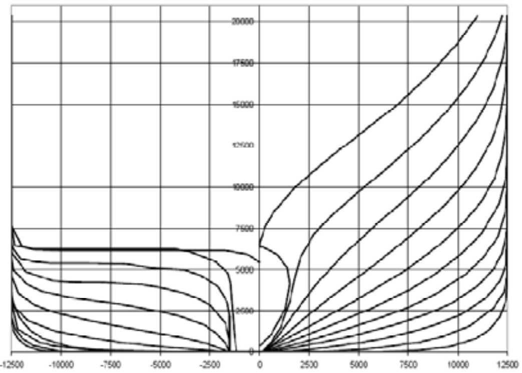

Figure 1. PRR02 body plan (dimensions in mm real scale).

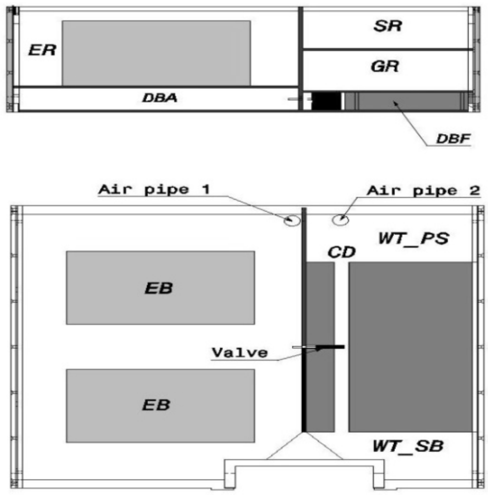

Figure 2. Model general arrangements.

Model Construction

Generally, the selected materials for the construction of the model (midsection ship hull and internal compartments) should ensure:

1) A high degree of global rigidity and a negligible flexural response particularly when the model is subjected to forced oscillations.
2) Setting the OM, with ensuring water and air tightness between the OM and the ship hull.
3) Possible visual analysis of the flooding process and air behaviour in the compartments below the car deck.

Therefore, the vessel shell, the internal decks, and the central bulkhead were manufactured in PVC.

However, the aft and forward bulkheads, as well as the upper deck were made in see-through Plexiglas to allow visualisation and video recordings. In the DBF, a CD connected the two wings double bottom tanks. A valve was mounted at the midpart of the CD. It was either opened (On) or closed (Off) during the experiments. The access to this valve was gained through a hole performed in the aft bulkhead.

Two air pipes were included in the model, to reproduce air pressure fluctuations expected in full-scale ship. They extended from the decks limiting the double bottoms upwards to outside the model. Thus, air pipe 1 was placed in the PS corner of the ER, near the central bulkhead, and air pipe 2 was positioned in the centreline of the CD as PS as possible. As the parameter "air ventilation" has essentially two levels (fully-ventilated and partially-ventilated), the diameters of both air pipes were changed during the tests.

Damage Characteristics

The flooded compartments were chosen according to the worst SOLAS 90 damage scenario. The damage characteristics were as follows.

1) A longitudinal extent in the outer shell, based on the total subdivision length in meters, equal to MIN (($3\%L_{pp}$+3m), 11m) in real scale.
2) A rectangular shape in side, reproducing the real bilge shape. Two damage areas pertaining to different types of accidents were tested. To do so, the vertical extent of the damages was varied while keeping its longitudinal one constant.
3) Concerning the shape of the damage opening in the decks, we tried to reproduce as practically as possible a collision with a V-shape-penetrating-bow striking ship, i.e. to make isosceles-triangles notches in all decks penetrating to the B/5 lines. Because of the hull bilge part and the opening door, the performed notch had the shape shown in

Opening Mechanism

Conceiving the OM was governed by the flooding cases to be tested. Thus, several constraints affected the conception of the OM. They are listed as follows.

- The OM should enable testing the two damage areas indicated previously.
- It should enable testing different times of damage creation: instantaneous damage, and damage created in a duration function of the vessel natural period.
- It should be mechanically powerful to create "instantaneous damage".
- The opening door should fit the bilge part of the model.
- The contact of the ship shell with the opening door should be watertight, thus reducing as much as possible possible water leakage.
- The measured hydrodynamic efforts should never be influenced by the mechanism of damage creation, particularly the moment generated when opening the door.
- Visual observation and analysis of the flooding through the damage opening are requested.

Based on the above-mentioned constraints, the OM shown in Figure 3 was conceived. It comprises a vertical door, made by Altuglas, that appropriately fits with the hull shape. An electrical motor, mounted on the deck along with a rope-pulley system, opened the door and let it run on rails up alongside the hull and over the deck. The motor is controlled in both course (position of the bottom edge of the door) and velocity (relevant to a fixed time of damage creation). Thus, the motor was calibrated in terms of opening velocity versus time of damage creation. Water leakage through the opening door was significantly reduced by means of resin and rubber seal. From the predetermined door course and the input velocity, the time duration between the start and the stop of the door was calculated.

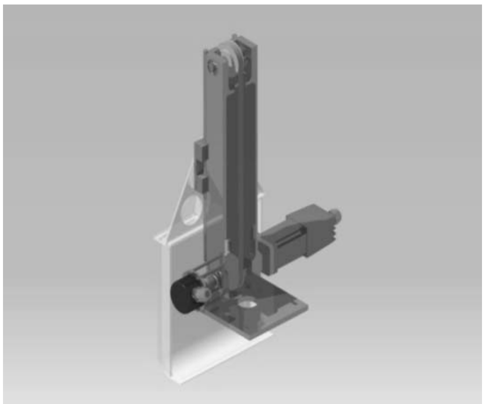

Figure 3. The OM and door.

Experimental Set up

Once the goals are determined, an appropriate experimental set up should be conceived to obtain sound conclusions. We were planning to investigate the IFS, by performing flooding tests in which the body is kept fixed as well as forced-oscillation tests. To this end, the conceived experimental set up chiefly relies on the use of a 6-DOF-motion platform "Hexapod" settled upside down, as well as a custom-made 6-DOF dynamometer attached to its movable plate.

The "Hexapod"

It consists of an actuator body, actuator/bracket joints, upper and lower frames, and AC servomotors and drivers. Its body is linked by universal joints to a moving platform which is actuated by six actuators and operated by six electric servomotors. The maximal velocity and acceleration of each servomotor are 600 mm/s and 12 m/s^2, respectively. The range of frequency of the dynamic movements is [0, 3] Hz, depending on the movement amplitude. The measurements of the positions of the "Hexapod" motions in the six degrees of freedom were performed at the same sampling rate (1 kHz), and they were acquired in outputs. This "Hexapod" can be used upside down.

The Dynamometer

It is based on 4 piezo-resistive 3D transducers (Kistler 9251A) located between 2 adjusted horizontal plates made of Aluminium 4G. One of the plates is bolted on a stiff steel base which is fastened to the Hexapod during the experiments. The 12 transducers channels are connected to 6 high precision charge amplifiers (Kistler 5011B) delivering 6 independent signals to the acquisition system. The "Hexapod" and the dynamometer mounted on its movable plate are shown in Figure 4.

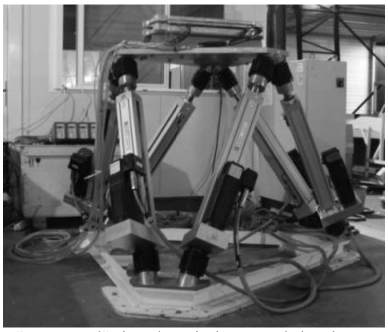

Figure 4. The "Hexapod", its electric box, and the dynamometer

Mounting the Experimental Set up

We remind that the model was manufactured in several parts. The main part, i.e., the PRR02 midsection shell was joined, as shown in Figure 5, by means of PVC welding to the decks and the central bulkhead located at the axis of the damage hole. The aft and forward bulkheads as well as the upper deck composed of 3 plates were joined with screws to the main part. Then, the OM was set up after being assembled aside and its conditions of opening controlled. Doing so, the equipped model was ready to join the remaining parts of the experimental set up. Then, the model and the dynamometer were joined end to end by means of steel bars, as shown in Figure 6.

Figure 5. The model at an early stage.

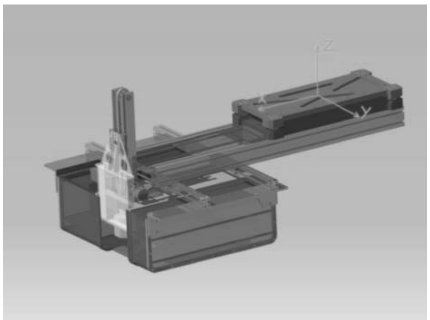

Figure 6. The model attached to the dynamometer.

The resulted structure was then fastened to the "Hexapod" settled upside down, itself affixed to a 3-leg framed structure (Tripod) built on the basin floor. Then, the equipped body was placed at its appropriate draught in the basin. The operability and structural rigidity of the whole experimental set up and particularly of the investigated body constituents, as bulkheads, decks, etc. were studied and found to be correct and sufficient when hydrostatic and then hydrodynamic efforts will propagate into the body components. The conceived experimental set up is shown in Figure 7, and, Figure 8 shows the experimental set up mounted in the basin.

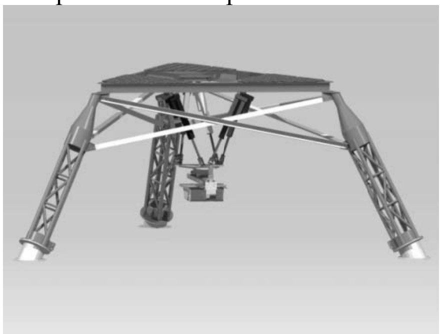

Figure 7. The conceived experimental set up

Figure 8. The experimental set up in the basin.

A zoom in on the experimental set up and on the equipped model are also shown in Figure 9 and Figure 10, respectively.

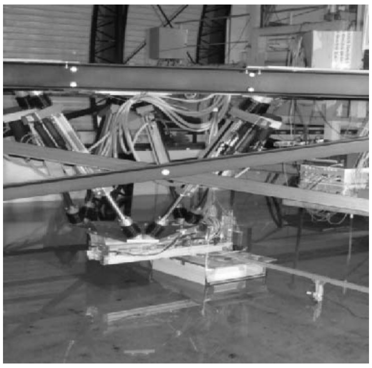

Figure 9. Zoomed experimental set up.

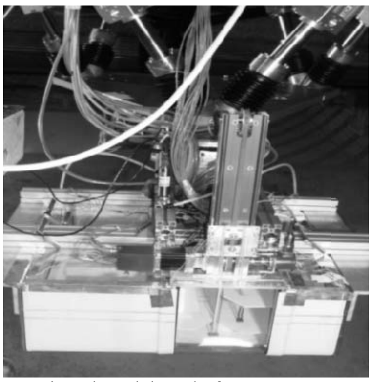

Figure 10. The equipped model ready for test.

1 kHz-sampling frequency was used since it was very important to manage to capture expected peaks in the behaviours of the air pressures, particularly during the transient flooding phase, as well as those of water heights and hydrodynamic efforts.

Instrumentation
The instrumentation system consisted of the following.

Air Pressures' Measurements
Two configurable pressure transducers (Honeywell, Model FP2000) were used to measure the air over-pressure in the double bottoms DBA and DBF. They are one-psi-range gauges (7000 Pa), with infinite resolution, and a frequency response equal to the natural frequency. As the sensors cannot be practically mounted where the measurements were intended to be taken, i.e. close to the double bottom bulkheads immerged in water at the PS, they were put close to the location of air pressure measurements; see Figure 11.

Water Heights' Measurements
The amount of accumulated water needs to be determined in order to assess the residual stability of a damaged ship. Therefore, water height probes were mounted in every room, as shown in Figure 11. They were at all 20 probes inside the model, as well as one mounted in the basin in front of the damage opening. Equipping the model by water heights was challenging, particularly for those in the double bottoms. The probes were constructed by means of two parallel stainless steel wires distant of 2 mm. However, probes 9 to 14 were flat copper gauges attached to either the hull or the central bulkhead.

Water heights' calibration was performed twice using the basin water. Obtained results were very close, and no one probe has shown a correlation factor, calculated over at least 10 different levels per compartment, less than 99.9%.

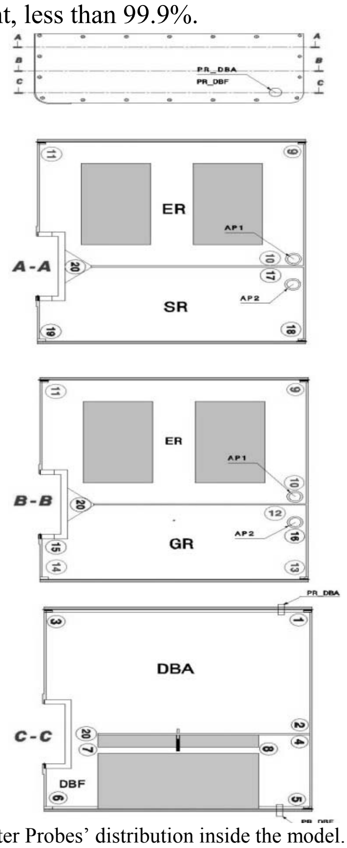

Figure 11. Water Probes' distribution inside the model.

Video Recordings
A high speed video camera of 120 Hz-sampling rate was installed on the carriage in front of the damage opening. It viewed the damage creation process, the flooding, as well as the air escape through the opening hole. This allowed visual analysis of the flooding process and quantification of the system water tightness, especially at the bottom and side edges of the sliding door. Furthermore, two underwater cameras were installed in the forward and aft ends of the model. For this reason, the aft and forward bulkheads were made transparent. These cameras permitted to film the behaviour of the water surface inside the flooded compartments. A fourth camera of 30 Hz-sampling rate was installed on the tank side viewing a big part of the experimental setup and also the body from its aft SB corner.

Experimental Methodology
Why DOE Methodology?
Traditionally, the study of damaged stability has been conducted using the one-factor-at-a-time approach, where the effect of each factor is investigated separately. When lots of factors intervene, this approach implies a significant amount of experiments. Moreover, it is unable to estimate the magnitude of interactions and might often miss important conclusions about the dependence of the effect of one factor on the level of another one.

Statistical approaches to experimental design are necessary to obtain sound conclusions from the data in less time and budget. These methods, simply called nowadays Design of Experiments or DOE, reduce the number of experiments needed for the analysis of factors' main effects. Moreover, the interpretation behind takes account of both the coupling between the factors' effects and the natural variability of the assessed phenomenon, whose ignorance might fault the whole analysis. A detailed explanation of conducting such experiments, as well as a wide variety of experimental designs can be found in (Schimmerling et al. 1998; Ryan 2006).

Hence, the guidelines for designing the experiment based on DOE methodology are as follows.

Choice of Factors, Levels, and Ranges
After stating the problem and fixing the objectives, the challenging task is to properly determine the design factors, their ranges, and their levels, as the model we plan to build will not be valid outside these ranges. Therefore, several measures have been taken. First, we screened initial heel and trim, as their influence on the IFS is relatively small. In addition, the metacentric height GM was not considered in the current experiment, as the experimental set-up is conceived to measure hydrodynamic efforts. Thus, the design factors for this study as well as their selected levels were determined and are presented in Table 2. It is worth to mention that this study deals with a large number of factors influencing the IFS; the metacentric

height is the only factor influencing these stages that is not taken into account.

Table 2. Designed factors and their levels.

Factor designation	Factor	Level 1	Level 2
P_1	Initial draught	LC1 (167mm)	LC2 (140mm)
P_2	Damage area	Small damage	Large damage
P_3	Cross-flooding	On	Off
P_4	Air ventilation level	Fully-ventilated	Partially-ventilated
P_5	ER permeability μ	0.70	1.00 (No EBs)
P_6	Transversal position of EBs	217.86 mm	EBs at the centerline
P_7	Time of damage creation	0 sec	$4T_{\Phi}/3$
P_8	External excitation	No excitations	Forced oscillations

The factors' levels depend on the DOE plan we applied. As we are going to present the first findings not relevant to any DOE plans, the considered number of levels is that related to the parametric investigations we are going to deal with in this paper. Every factor possesses two levels. It is herein worth to mention that, in the philosophy of DOE experiments, a plan based on design factors possessing two levels each is recommended to quantify all factors' main effects. The selected factor's levels should be neither close nor far approaching the limits of the range of a factor's variation.

P_1 levels are the operational draughts of the ship. P_{21} extends to the deck that limits the DBF. This damage case represents in fact a grounding accident. Whereas, P_{22} deals with a collision accident in which the damage extends with unlimited vertical extent. P_{31} and P_{32} are set when the valve located at the CD midpart is open or closed, respectively. P_4 deals with the degree of air ventilation in the model. It is actually the ratio of the air pipe cross sectional area divided by that of the CD that determines whether fully or partially-ventilated the model is going to be. Thus, according to (Ruponen and Routi 2007), the compartments are considered fully-ventilated for a percentage larger than 10. Experimentally, we positioned air pipes corresponding to 15% and 6% area ratios when setting P_{41} and P_{42} levels, respectively. The locations of the air pipes' inlets in the horizontal plan are shown in Figure 11. The permeability of a space is the percentage of that space which can be occupied by water. Thus, when there are no EBs in the ER, P_{52} is set. P_{61} is set when the transversal distance between the one EB plane parallel side to the board, measured longitudinally at the central bulkhead, is equal to 217.86 mm. P_{71} is set when an instantaneous damage is created. Experimentally, the average of P_{71} calculated over all performed tests was roughly 110 ms, a value that demonstrates the reliability of the conceived OM. P_{81} is relevant to flooding tests and P_{82} to forced-oscillation tests.

Selection of the Response Variables

After conducting tests to assess the repeatability and the reproducibility of our experiment, we found that the experimental uncertainty is relatively small (<3.5%) and that our measurement system is reliable. Therefore, based on the quantities we measured, we have determined the following response variables.

- For Fx, Fy, and Mx: The maximum amplitude, the time to reach it with respect to the start of the damage creation, and the amplitude after the IFS ends.
- For Fz and My: The maximum amplitude, the time to reach it with respect to the start of the damage creation, the amplitude after the IFS ends, the slope during the event of damage creation (the door vertical movement), the amplitude when the door movement ceases.
- The flooding rates and the discharge coefficient through the damage opening.
- For air pressures in DBA and DBF: the peak and its correspondent time of occurrence, the values at the end of the door movement and after the IFS ends.
- For water heights: the peak, time to reach it, and the slope during the water accumulation.

These quantities were evaluated for each test. Analysing the results of all the performed tests will determine the response variables that really characterise the IFS.

Performing the Experiment

Prior to conducting the tests, we checked some technical aspects of the system, as that all components and measurement system conveniently work. Between two consecutive tests, we also checked that both water and air tightness were still ensured, and that the damaged compartments were dry. As recommended in (Coleman and Montgomery 1993), we conducted some trial runs with different factors' combinations. These runs assisted in verifying the consistency of the experimental material, in obtaining a rough idea of the experimental errors, and in revisiting the decisions made in previous steps (factors' levels and ranges…).

As the model operated in air and in water during the tests, the air pressures in DBA and DBF were measured by means of air pressure transducers always operating in air. Thus, the recorded pressures differ from actual ones, and should; therefore, be corrected. The correction procedure is formulated hereunder; see Figure 12.

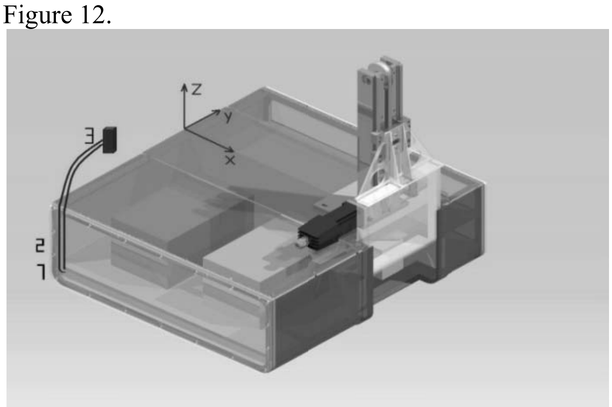

Figure 12. The model with its DBA equipped for air pressure measurement

In Figure 12: 1 is the point where we want to measure the air pressure; 2 is the highest point the water might reach in the tube; 3 is the point where the air pressure is measured, i.e. the contact between the tube and the transducer. L is the tube length (distance between points 1 and 3), and ε is the distance between points 1 and 2.

Therefore, p_3 is the measured pressure indicated by the air pressure transducer. It will be corrected to p_1 (the air pressure we want to measure) by taking both air and water behaviours inside the tube into account.

The air compressibility inside the tube lets the product of pressure and volume remains constant during the studied phenomenon. Thus, we can evaluate ε:

$$\varepsilon = L.\left(1 - \frac{p_{atm}}{p_{atm} + p_3}\right) \quad (1)$$

Hydrostatics allows writing:

$$p_1 = p_3 + \rho_{water}.g.\varepsilon \quad (2)$$

The numerical application of Equation (1) provides the ratio ε/L (it was found to be less than 12% for all tests). Then, p_1 is evaluated based on Equation (2).

As we are going to present the first experimental findings, not the DOE results, we shall not continue to present the further steps in applying the DOE methodology. Thus, for the work presented in this paper, we have taken advantage of the DOE methodology to perform the experiments as effectively as possible.

The test runs we are going to analyse in this paper are indicated in Table 3. The test related to the selected combination (believed "realistic and moderate") was performed twice (F001&F002).

Table 3. Tests' configurations

Test Run	P_1	P_2	P_3	P_4	P_5	P_6	P_7	P_8
F001 & F002	1	2	1	1	1	1	2	1

Experimental Results

The performed tests provide a great deal of important information on the influence of the entailed factors on the IFS. The tests we treat in this paper can highlight the physics of flooding; quantify the repeatability for all measured data and the reproduction of relevant aspects and sub-phenomena. The coordinate system is previously indicated in Figure 12; Y-axis is positive towards the forward ship part along its longitudinal dimension.

Hydrodynamic Efforts

The times of damage creation (P_7) for tests F001 and F002 are 3.602 s and 3.590 s, respectively. The curves of Fx, Fy, and Mx for the two tests are very close. They oscillate from the start of the door movement to approximately six times the time of damage creation. Three peaks can be identified during these oscillations: PEAK1 occurring at 37%.P_7, PEAK2 occurring at 78%.P_7, and PEAK3 occurring at 177%.P_7. It is worth to mention that the maximums of Fx, Fy, and Mx occur at the same time, 78%.P_7 corresponding to PEAK2. Figure 13 shows the trimming moment Mx for the two tests, and identifies the 3 PEAKS. Mx tends to an asymptote with a value of zero after the IFS end, indicating that the floodwater is equally distributed along the model longitudinal direction.

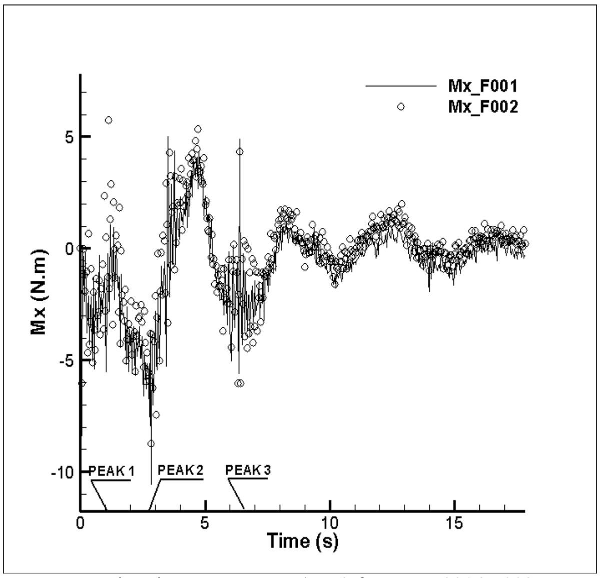

Figure 13. Trimming moment Mx (N.m) for tests F001&F002.

The response variables relevant to the vertical force Fz (previously defined in §4.3) are very close between the two tests; see Figure 14. Even at their maximums synchronised with PEAK3, the vertical forces Fz show similar oscillations. After the transient flooding ceases, Fz is approximately 463 N. This value is in correspondence with the floodwater mass. Furthermore, the difference between the maximum Fz value and the one it reaches after the transient flooding ceases is not more than 23 N (a difference of 5% of the maximal Fz magnitude). However, the Fz slope during the damage creation is about 136 N/s, highly influenced by the levels P_{22} and P_{72}.

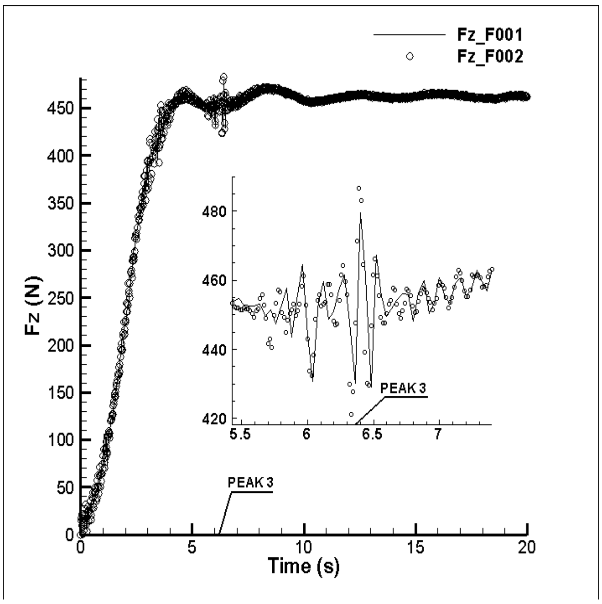

Figure 14. Vertical force Fz (N) for tests F001&F002.

The response variables relevant to the heeling moment My are also very close between the two tests; see Figure 15. Even at their maximums synchronised with PEAK3, My show similar oscillations. The value that My takes after the transient flooding ceases is approximately 43 N.m towards the PS. Furthermore, the difference between the maximum Fz value and the one it reaches after the transient flooding ceases is not more than 7N.m (a difference of 14% of the maximal My magnitude). However, My slope during the damage creation is about 11 N.m/s, highly influenced by the levels P_{22} and P_{72}.

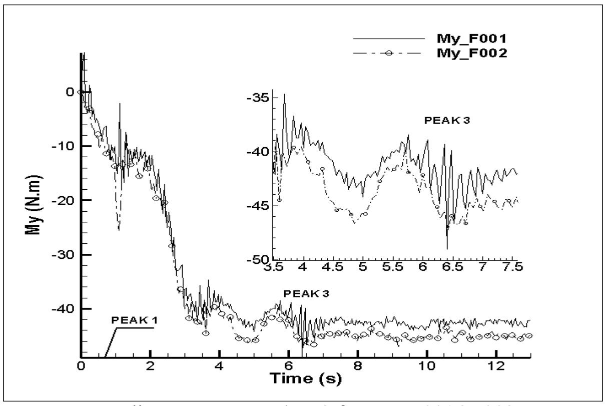

Figure 15. Heeling moment My (N.m) for tests F001&F002.

Behaviours of floodwater and air

The air over pressure measured in DBA for the two tests, depicted in Figure 16, corresponds to fully-ventilated compartments. Once again, the three PEAKS previously identified are found. An exceptional reproduction is observed during the IFS, particularly for PEAK1 and PEAK3. Thus, PEAK3 is the maximum value for Fz, My, and the air pressure in DBA. The slight delay at PEAK2 is believed to be influenced by the stop of the OM. This reproduction reveals the reliability the tests have in reproducing the assessed physical phenomenon and the intrinsic chemistry that relates both floodwater and air behaviours to the hydrodynamics. It is also obvious that this air pressure is a non-negative quantity.

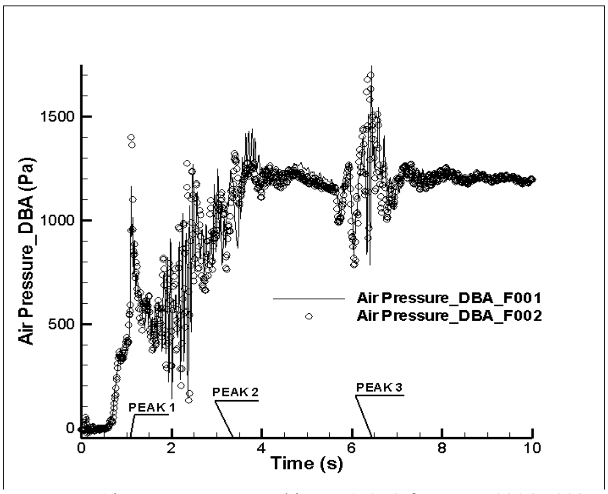

Figure 16. Air pressure measured in DBA (Pa) for tests F001&F002.

The interaction between water and air behaviours is illustrated in Figure 17. Right after the damage creation, the air pressure inside the DBA starts to increase. Water first makes contact with Probe1 after less than 1 s. At the moment corresponding to PEAK1, water at Probe1 reaches its maximal value for the first time after a fast flooding.

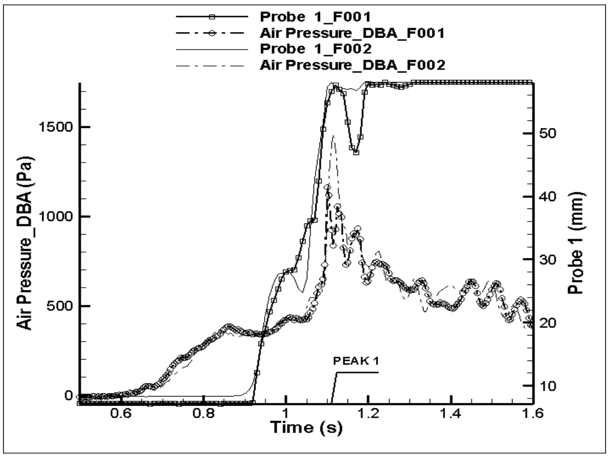

Figure 17. Air pressure measured in DBA (Pa) and water height indicated by Probe1 for tests F001&F002.

The air pressures measured in DBA and DBF for the two tests are depicted in Figure 18. On the contrary of the air pressure measured in DBA, the one measured in DBF presents negative values, i.e. a pressure less than the atmospheric pressure, during the transient flooding. This could be explained by the air compression in WT_PS, much more intense than in DBA, as the allowable space for the water to flood decreases because of the void spaces that occupy roughly 60% of the DBF. The maximal peak of the air pressure measured in DBF is 3 to 4 times greater than that measured in DBA. Moreover, the air pressure in DBF strongly fluctuates and reaches higher peaks than those observed in DBA. This is related to the DBF geometry. However, both air pressures take approximately the same time delay to begin to build up, and, at the end of the IFS, tend to a similar value, roughly to that of the hydrostatic pressure.

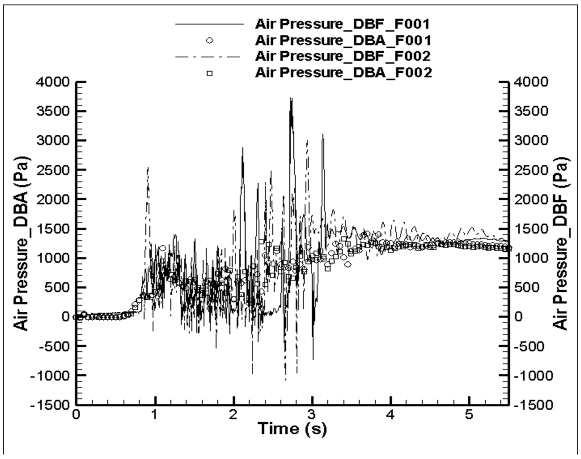

Figure 18. Air pressure measured in DBA and DBF for tests F001&F002.

Therefore, PEAK1 is attained when the wave front of the first travelling wave inside the DBA reaches the PS, thus the air becomes strongly compressed. PEAK2 is highly influenced by the cease of the OM. PEAK3 presents at the same time a maximum of the hydrodynamic efforts, particularly the vertical force and the heeling moment, as well as a maximum of the air pressure over the whole IFS. The exceptional correspondence between the detected three PEAKS, on one hand, and the vertical force Fz, the heeling moment My, and the air pressure in DBA, on the other hand, is depicted in Figure 19. Besides, the snapshots related to the three PEAKS, taken by the submarine camera that visualises the model from aft (the DBA and the ER), as well as those taken by the high speed camera placed in front of the damage hole, are depicted in Figure 20(a,b,c). Left-side and right-side snapshots are taken by the submarine camera and the high speed one, respectively. Based on these camera videos, we notice, particularly for test F001, that the DBA will become completely flooded 434 ms before the damage creation ceases, and generally, that the DBA usually becomes completely flooded between the time correspondent to PEAK2 and the stop of the creation of the large damage (P_{22}). Furthermore, after the first wave front within the DBA reaches the PS, we observe air bubbles trying to escape through the damage opening while other water particles continue to flood inside the model.

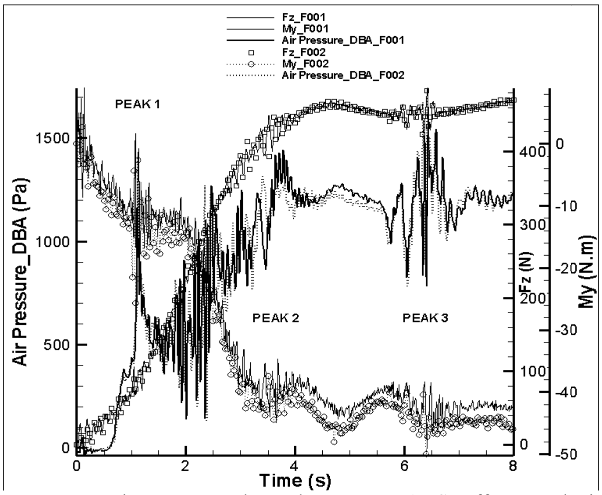

Figure 19. The correspondence between PEAKS, efforts, and air pressure in DBA for tests F001&F002.

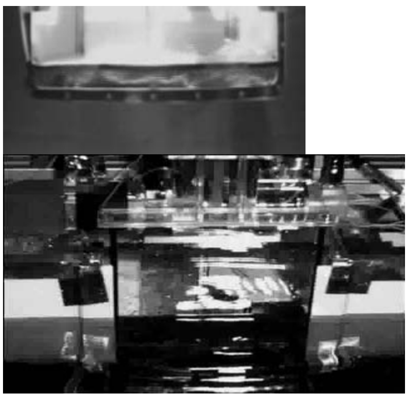

Figure 20 (a). Snapshots relevant to PEAK1 of test F001.

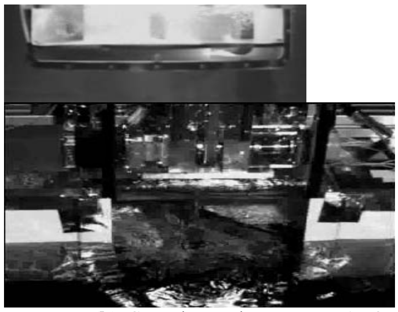

Figure 20 (b). Snapshots relevant to PEAK2 of test F001.

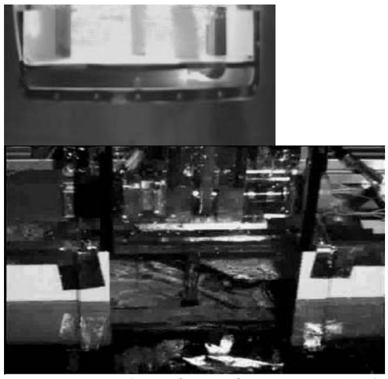

Figure 20 (c). Snapshots relevant to PEAK3 of test F001.

After the start of the damage opening, it is noticed, that the near the probe in the double bottom is from the opening, the fast water first makes contact with it. This is independent of the angle that determines its position with respect to X-axis, but depends on the obstructions the water will face on its way. Thus, water first makes contact with double bottom probes as time goes up in the following order: probe 20, probe 7, probe 6, probe 3, probe 8, probe 2, probe 4, probe 1, and finally probe 5. Then, it is in the following order that the start of the fast water accumulation at a probe happens in the other compartments: probe 14, probe 15, probe 11, probe 16, probe 12, probe 13, probe 10, probe 9, probe 17, probe 19, probe 18. The water heights measured by the probes located at the PS of the double bottoms are depicted in Figure 21. Water first makes contact with Probe4 before it first makes it with Probe1, confirming that the cross-flooding through CD is very fast. Because of the void spaces, water will take more time to reach Probe5, and will fill the WT_PS slowly.

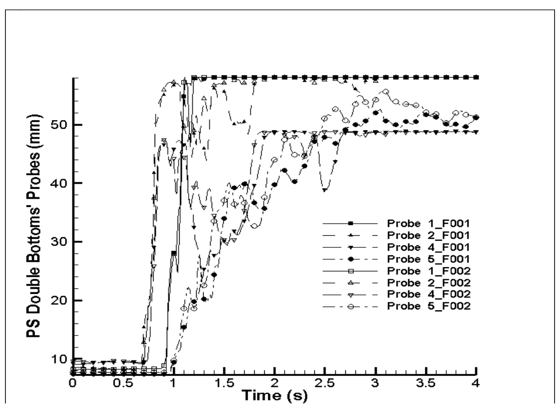

Figure 21. Water heights measured by PS probes in the double bottoms for tests F001&F002.

The water heights measured by means of probes 9, 10, and 11 mounted inside the ER are depicted in Figure 22. These water heights show a similar twofold-behaviour that comprises a "relatively-low-frequency" and a "relatively-high-frequency" behaviours.

The former is pseudo-periodic, and damps relatively fast, as the EBs contribute to slowing down the floodwater. These low-frequency oscillations, occurring at a pseudo-period of 3.8s, represent the harmonic motion of a mechanical oscillator, initially excited by the inflow of water through the damage hole. Its characteristic length is related to the ER dimensions. As the ER is partially submerged, the shape of this behaviour is also determined by the air compressibility,

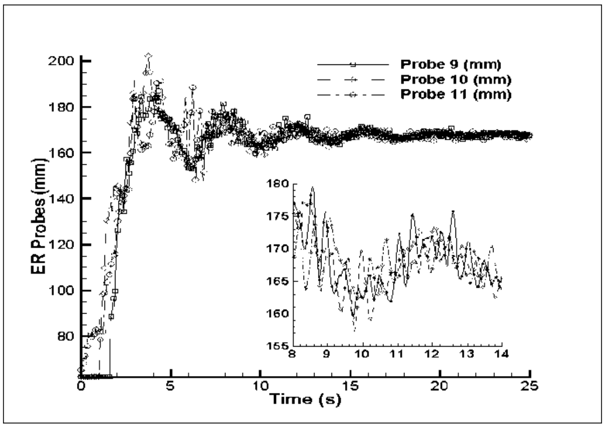

Figure 22. Water heights measured by ER Probes for test F001.,

and the air tries to escape from the ER outside the model through the damage hole, as the video recordings show. Moreover, this behaviour is influenced by the quantity of floodwater entering the ER (factor P_2), as well as the ER's permeability (factor P_5).It was observed that the pseudo-period of these oscillations diminishes in the case of an ER without blocks (P_{52}), as without EBs it will take much more time for the oscillations to stop. As the ER passes from a state in which it is dry to another in which water will flood inside, we shall assume that non-stationary waves could be generated inside this room. This let us relate such waves' velocity to their theoretical period (of 0.25s) by:

$$\frac{\omega C}{g} = \frac{1}{4} \; with \; \omega = \frac{2\pi}{T} \qquad (3)$$

The application of Equation (3) provides a velocity of 1.48 m/s for the waves propagating inside the E.R. Considering Probe11, water will first make contact with it after approximately 0.32s, and the hypothesis of non-stationary waves seems acceptable to better understand these low-frequency oscillations.

On the other hand, the "high-frequency" behaviour is characterised by oscillations of relatively small amplitudes that occur at high frequencies. The pseudo period of the oscillations of Probe9 (located SB) is roughly 377 ms. That of Probes 10 and 11 (both located PS) is the same and equals about 309 ms. These oscillations are highly influenced by the obstructions inside the ER, and their characteristics, i.e. amplitude and pseudo-period, are determined by the interaction between the floodwater and the EBs, as well as that between floodwater and the ER sides. The characteristic length of the high-frequency oscillations is that of the passages between the ER obstructions and sides. However, the periods of these oscillations will increase when no obstructions exist inside the ER. What actually help explain the "high-frequency" behaviour in the ER is the shape of the water behaviour observed in the SR, itself also partially submerged; see Figure 23. It is clear that the "high-frequency" behaviour in the SR is strongly damped, as no obstructions exist in the way of water. However, the "low-frequency" behaviour is observed in the SR.

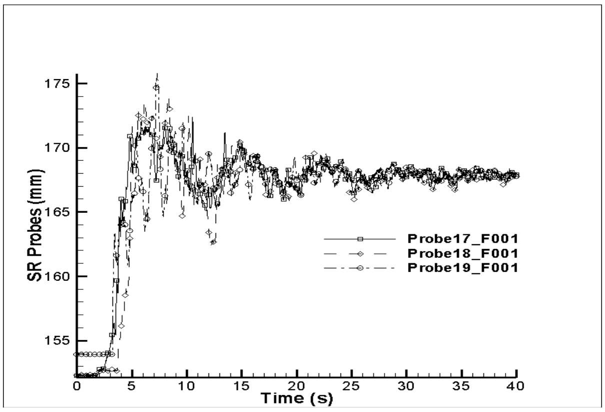

Figure 23. Water heights measured by SR Probes for test F001.

Nonetheless, the twofold-behaviour observed in the ER is completely absent in the GR, as it is completely submerged; see Figure 24. Water first makes contact with GR's probes located SB (as they are the nearest to the damage hole), then spreads inside the GR with a relatively-high speed. Thus, the GR's probes located PS fill relatively very fast, and reach approximately their maximum values. Then, as there will be no place for the air in the PS, it will escape outside the model through the damage hole. Thus, the GR's probes located SB begin to be filled and do this also rapidly.

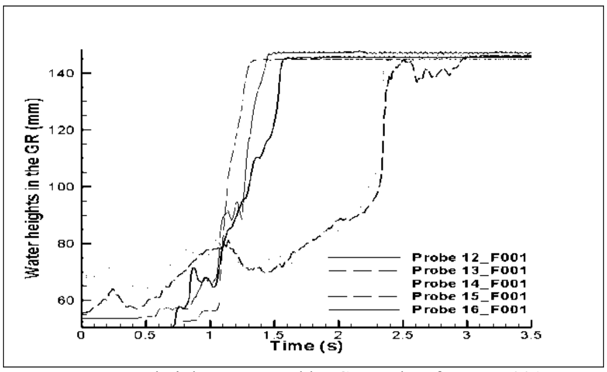

Figure 24. Water heights measured by GR Probes for test F001.

Discharge coefficient

Evaluating the flooding rate through the damage hole depends on:

- the size and shape of the damage hole,

- the magnitude of flow velocity that depends on the relative positions of water surfaces,
- the time of damage creation,
- the degree of air ventilation inside the model,
- the model scale, and
- the discharge coefficient.

Based on the vertical force Fz, the flow rate through the damage opening can be evaluated during a test following the relationship:

$$Q(t) = \frac{1}{\rho g}\frac{\partial F_z}{\partial t} \tag{4}$$

The application of Equation (4) evaluates Flow rate1 (L/s) for test F001; see Figure 25. The flow rate reaches a maximum of about 19 L/s before the damage creation ceases. After this peak, the flow rate oscillates around zero before it asymptotically tends to zero after the IFS end. We believe that the water egress through the damage opening results in negative values of the flow rate (noticeable in Figure 20(b)).

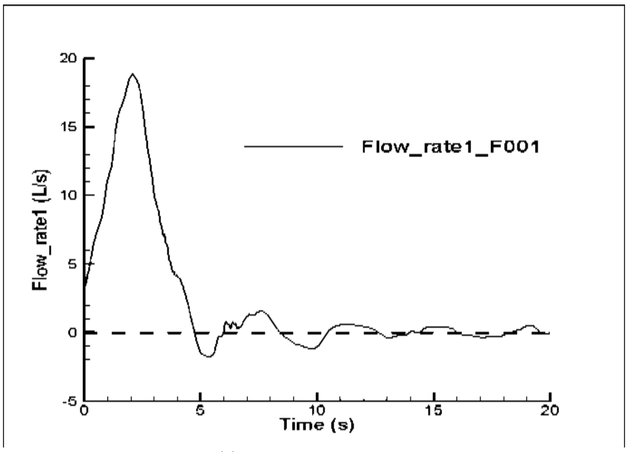

Figure 25. Flow rate1, $Q(t)$, for test F001.

An estimation of the flow rate through the damage opening can be obtained based on the traditional formulation mainly established for stationary flows:

$$\tilde{Q}(t) = C_d.A_{open}(t).sign(\Delta h(t)).\sqrt{2g.|\Delta h(t)|} \tag{5}$$

where :

$$sign(x) = \begin{Bmatrix} -1\ if\ x < 0 \\ 0\ if\ x = 0 \\ 1\ if\ x > 0 \end{Bmatrix} \tag{6}$$

and C_d is the discharge coefficient that equals 0.55 for the current flooding case (Katayama and Ikeda (2005)); $A_{open}(t)$ is the damage area; and $\Delta h(t)$ is the difference between the external water level (the appropriate draught) and the internal one (estimated by the water height indicated by Probe20). The application of Equation (5) results in evaluating the Flow rate2 (L/s) for test F001 depicted in Figure 26. An experimental uncertainty in the estimation of the flow rate2 arises from relying on the signal that Probe20 delivers to evaluate $\Delta h(t)$. This is obvious in the fluctuations Flow_rate2 shows which are less amplified for Flow_rate1. When applied to the flooding process, the traditional flow rate estimation, i.e. by means of

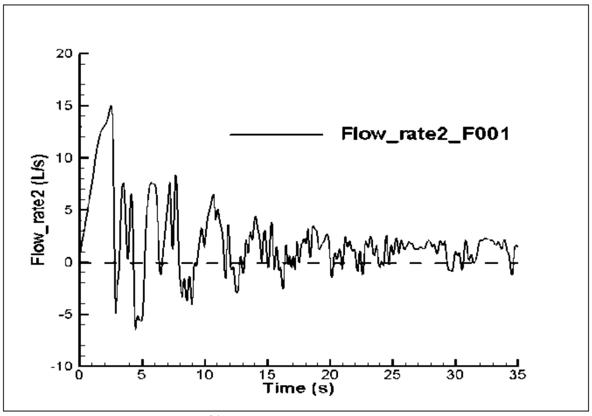

Figure 26. Flow rate2, $\tilde{Q}(t)$, for test F001.

equation (5), manages to provide an acceptable global shape. However, it underestimates the maximal flow rate, highly related to the estimated discharge coefficient C_d.

The discharge coefficient, as a function of time, can be experimentally evaluated, for the flooding situation we are dealing with, by means of the following formula:

$$C_d(t) = Q(t)/\left[A_{open}(t).\sqrt{2g.\Delta h(t)}\right] \tag{7}$$

The discharge coefficient for test F001 is depicted in Figure 27.

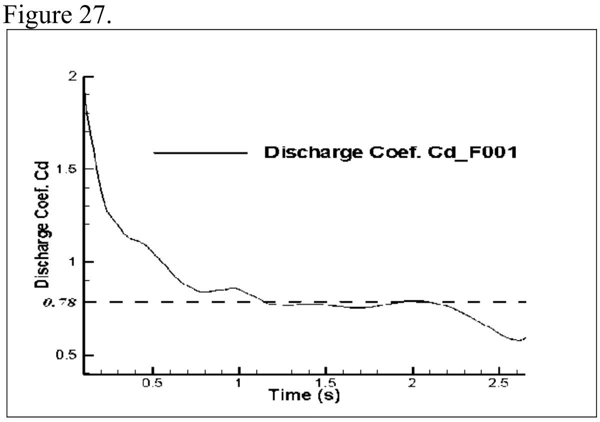

Figure 27. Discharge Coefficient, $\tilde{Q}(t)$, for test F001.

At the start of the damage opening, a fast flooding occurs that results in a high discharge coefficient. Then, the discharge coefficient reaches a constant value (between 0 and 1, but slightly higher than that determined in (Katayama and Ikeda (2005)) before the damage creation ceases. Thus, we believe the hypothesis of considering a constant discharge coefficient when evaluating the flow rate in case of flooding is simplified, and a reliable estimation of the flow rate should be based on a discharge coefficient function of time.

Conclusion

After the state-of-the-art-research conducted in the first part of this project revealed the necessity of quantifying the degree of interaction between the main contributing factors during the IFS, a comprehensive experimental investigation based on DOE methodology had been performed. In this work, the fundamental physics of flooding are studied through systematic model tests. This contribution presents the preparation of the experiment as well as the first findings not relevant to any DOE plans. Ensuring both water and air tightness, and selecting the design factors, their levels, and their ranges, were the most two challenging steps in the technical and theoretical phases of this campaign, respectively.

The results of the first two tests reported herein demonstrate the applicability of the presented methodology of experimental investigation into the complicated behaviour of the IFS. What physically renders this behaviour complex is the strong coupling between the ship motion and the flooding process. Both water Ingress/Egress through the damage hole and water accumulation procedure inside the damaged compartments contribute to complicating the flooding process.

The experiments demonstrate that, during the IFS, a strong interaction is found between, on one hand, both implicated fluids, i.e. water and air, and, on other hand, the model behaviour. The former is assessed by measuring the water heights in several locations inside all damaged compartments, as well as the air pressure in the double bottoms.

The latter is assessed by the measured hydrodynamic efforts. The detection of three PEAKS highlights this interaction during the transient inflow. These PEAKS are found particularly related to the damage area, the time of damage creation, and the air ventilation level. Moreover, a two-fold behaviour is observed in the ER partially submerged. These behaviours are drawn by the air compressibility, the water surface, as well as the non-basic sloshing occurring inside this room.

The tests also confirmed that the discharge coefficient for realistic flooding situations is not constant during the IFS, and estimates it experimentally as function of time. Once the variation of the discharge coefficient is evaluated during the flooding, the traditional formulation provides reliable assessment of the flow rate without measuring the hydrodynamic efforts.

The proposed experimental approach applied in the frame of the philosophy previously explained also constitutes a very good basis for the verification of time-domain simulation programs, especially the numerical code based on SPH method we are currently developing, as well as many computational works carried out in the past.

On the basis of the foregoing analysis of the tests' results, it is believed that conveniently considering the air behaviour is indispensable in the computational approaches. Furthermore, the DOE methodology seems useful to assessing such complicated problems. Hence, further research will concentrate on proving the efficiency of DOE methodology in data analysis and its capability to reveal interactions between involved and also evolved factors to eventually build a model characterising the IFS of Ro-Ro ferries.

Acknowledgements

Mr. Jean-Luc Toularastel and Mr. Bruno Pettinotti have contributed in designing the experimental set up, and in conducting and preparing the tests, respectively. The authors would like to express their gratitude to them. Sincere thanks are also extended to Dr. Pekka Ruponen from Napa Ltd, Finland, for his interest in the present project, as well as to Dr. Gérard Delhommeau for his valuable advice. We also acknowledge the reviewers for their valuable comments that help improve the scientific quality of this contribution.

References:

Braund NA. 1978. Damage Stability; Research for the Future. In: Safe Ship / Safe Cargo Conference; 1978; London, U.K.

Chang BC. 1999. On the Damage Survivability of Ro-Ro Ships Investigated by Motion Simulation in a Seaway. Ship Technology Research – Schiffstechnik. 46 (4):192–207.

Chang BC, Blume P. 1998. Survivability of Damaged Ro-Ro Passenger Vessels. Ship Technology Research – Schiffstechnik. 45 (3):105–112.

Cho SK, Hong SY, Kim YH, Lee KJ. 2005. Investigation of Dynamic Characteristics of the Flooding Water of the Damaged Compartment of an ITTC Ro-Ro Passenger Ship. In: Proceedings of the 8th International Ship Stability Workshop; 2005 October 6–7; Istanbul, Turkey.

Coleman DE, Montgomery DC. 1993. A Systematic Approach to Planning for a Designed Industrial Experiment (with discussion). Technometrics. 35:1–27.

Dand IW. 1989. Hydrodynamic Aspects of the Sinking of the Ferry 'Herald of Free Enterprise'. Transactions of the Royal Institution of Naval Architects. 131:145–165.

de Kat JO, Kanerva M, van 't Veer R, Mikkonen I. 2000. Damage Survivability of a New Ro-Ro Ferry. In: Proceedings of the 7th International Conference on Stability of Ships and Ocean Vehicles; 2000 February 7–12; Launceston, Australia.

[ITTC] International Towing Tank Conference. 2005. Testing and Extrapolation Methods Loads and Responses, Stability Model Tests on Damage Stability in Waves; Recommended Procedures and Guidelines 7.5-02-07-04.2.

Journée JMJ, Vermeer H, Vredeveldt AW. 1997. Systematic Model Experiments of Flooding of Two Ro-Ro Vessels. In: Proceedings of the 6th International Conference on Stability of Ships and Ocean Vehicles; 1997 September 22–27; Varna, Bulgaria.

Katayama T, Ikeda Y. 2005. An Experimental Study of Fundamental Characteristics of Inflow Velocity from Damaged Opening. In: Proceedings of the 8th International Ship Stability Workshop; 2005 October 6–7; Istanbul, Turkey.

Khaddaj-Mallat C, Rousset JM, Ferrant P. 2009. On Factors Affecting the Transient and Progressive Flooding Stages of Damaged Ro-Ro Vessels. In: Proceedings of the 10th International Conference on Stability of Ships and Ocean Vehicles; 2009 June 22–26; Saint-Petersburg, Russia.

Khaddaj-Mallat C, Rousset JM, Ferrant P. 2010. The Transient and Progressive Flooding Stages of Damaged Ro-Ro Vessels: A Systematic Review of Entailed Factors. Submitted to Journal of Offshore Mechanics and Arctic Engineering. ASME 2010 Transactions.

Palazzi L, de Kat JO. 2002. Model experiments and simulations of a damaged ship with air-flow taken into account. In: Proceedings of the 6th International Ship Stability Workshop; 2002 October 13–16; Webb Institute, New York, U.S.A.

Ruponen P, Routi AL. 2007. Time Domain Simulation of Cross-Flooding for Air Pipe Dimensioning. In: Proceedings of the 9th International Ship Stability Workshop; 2007 August 30–31; Hamburg, Germany.

Ryan TP.2006. Modern Experimental Design. New York: Wiley.

Santos TA, Guedes Soares C. 2000. The Influence of Obstructions on the Transient Asymmetric Flooding of Ro-Ro Ships. In: Proceedings of the 7th International Conference on Stability for Ships and Ocean Vehicles; 2000 February 7–12; Launceston, Australia.

Santos TA, Guedes Soares C. 2009. Numerical assessment of factors affecting the survivability of damaged ro-ro ships in waves. Ocean Engineering. 36:797–809.

Santos TA, Winkle IE, Guedes Soares C. 2002. Time Domain Modeling of the Transient Asymmetric Flooding of Ro-Ro Ships. Ocean Engineering. 29.667–668.

Schimmerling P, Sisson JC, Zaïdi A. 1998. Pratique des Plans d'expériences. Paris : Lavoisier. In French.

Spouge JR. 1985. The Technical Investigation of the Sinking of the Ro-Ro Ferry "European Gateway". Transactions of the Royal Institution of Naval Architects. 128:49–72.

[SSPA] Statens SkeppsProvnings Anstalt (Sweden). 2008. Final

Report – Research Study on the Sinking Sequence of MV Estonia; Research Report No. 134 of a study by SSPA Consortium. 2008; Göteborg, Sweden.

Vassalos D. 2000. The Water on Deck Problem of Damage Ro-Ro Ferries. Contemporary Ideas on Ship Stability. Oxford :Elsevier Science Ltd. 163–185.

Vassalos D, Letizia L. 1998. Characterisation of the Flooding Process of a Damaged Ro-Ro Vessel. International Journal of Offshore and Polar Engineering. 8(3):11–18.

[TNO] Netherlands Organisation for Applied Scientific Research (The Netherlands). 1997. Damage Stability, A Review of Research in The Netherlands; TNO Report no. 97-CMC-R0291 of a study by Vredeveldt AW, Uwland JJ. 1997 July; Delft, The Netherlands.

Use of Level Sensors in Breach Estimation for a Damaged Ship

Paavo Penttilä and Pekka Ruponen

Onboard-Napa Ltd, Napa Ltd

Abstract:
The flow of flood water from a breach in the hull into a ship is studied. The problem of estimating the size and location of the breach is discussed from the point of view of reliable flooding simulations and predictions in a real situation onboard a damaged ship. An inverse method is introduced for detecting a breach. The method is tested with a large passenger ship design by calculating a large set of randomly generated single breach damages with various combinations of sensor density, noise and filter length. The results and applicability of breach detection and flooding simulation as a part of decision support system are discussed.

Introduction

The concern for ship safety has risen as the number of passengers has increased onboard commercial vessels. The safety of passengers on a large cruise ship is a top priority. Ships have therefore become widely populated with various safety systems, namely for fire, stability, evacuation and of course flooding control. This study will focus on flooding and more specifically on breach detection. Progressive flooding in passenger vessels has been studied for several years and some very good methods have been developed during that time. However, these tools are yet to be fully utilized, especially in decision support on commercial vessels. So far *Ölcer and Majuner (2006)* have presented a method that is based on pre-calculated simulations and recently another flooding simulation tool, based on the actual initial conditions has been implemented in the Onboard-NAPA software (*The Naval Architect, 2008*).

The IMO regulations, *IMO MSC 77/4/1 (2003)*, require that all watertight spaces below the bulkhead deck should have a system to evaluate and/or quantify water ingress. Nowadays most new large passenger ships have been equipped with flooding sensors in cabin areas, machinery spaces and void spaces. A recent IMO report of a correspondence group, *IMO SLF-51/11 (2008)*, recognizes that all information used in the operational decisions should be as accurate as possible and be based upon the actual damage, flooding extent and the rate of flooding. Regarding day to day operation and decisionmaking in actual conditions, this means calculating the expected or simulated results of the flooding. In order to calculate a prediction, the initial condition, namely the location and size or area of the breach, has to be determined.

In this study the word “breach” is used to describe an opening that connects a damaged room to sea. There may be several breaches with several damaged rooms in different compartments forming one large breach but in this text the word breach is used only to mean a single opening involving one damaged room. It is assumed that if the area and location of all breaches can be calculated automatically (without human intervention) from flooding sensor output, it is then possible to calculate how the flood water will progress, thus enabling a powerful decision support system that is able to produce accurate predictions. The target of this study is to find out whether a breach can be calculated purely from the flooding sensor measurements.

The required sensor accuracy for measuring a breach was discussed in *Penttilä (2008)* and the accuracy of typical sensors was considered to be sufficient for the purpose of breach estimation. A general approach for solving the breach properties from level sensor signals was also introduced in *Penttilä (2008)*. The approach involves an inverse method for breach calculation, which is an attempt to determine the breach by matching progressive flooding simulation parameters to the measured results. The principles of this method are presented briefly. This study continues to examine the applicability of the inverse method in breach detection using a statistical set of different damages. A typical flood sensor arrangement on a large passenger ship is used and a case study of 433 random damages is used to get an approximation of the applicability of the inverse method.

Flooding Prediction Method

This study uses a time-domain flooding simulation method, described in *Ruponen (2007),* which is based on the conservation of mass and Bernoulli’s equation with semi-empirical discharge coefficients for each opening. The implicit scheme ensures numerical stability even with long time steps. The simulation method has been extensively validated against experimental results. A principal assumption is that the water levels inside the vessel are flat and horizontal. This is considered to be very reasonable for passenger ships with dense non-watertight subdivision. The simulation method can also deal with air compression, but in this study it is assumed that all flooded rooms are fully ventilated.

Based on Bernoulli’s theorem for an incompressible flow, the rate of flooding through an opening with an area A and discharge coefficient C_d is:

$$\frac{dV}{dt} = A \cdot C_d \cdot \operatorname{sign}\left(H_{w,out} - H_{w,in}\right) \cdot \sqrt{2g\left|H_{w,out} - H_{w,in}\right|} \qquad (1)$$

where g is the acceleration due to gravity and H_w is the water level height. This equation forms the basis for both flooding simulation and breach detection.

Due to the inviscid nature of equation (1), Ruponen’s applied method of solving progressive flooding is relatively fast and enables calculation of multiple simulations within a reasonable time with current computing power. Another advantage of this simulation method is that when the real *measured* breach is used, the results are then based on the real initial condition. This effectively eliminates the interpolation problems related to applications based on pre-calculated cases, such as *Ölcer and Majunder (2006)*. When calculation is directly based on the actual initial condition, it is not necessary to make additional assumptions regarding the routes for floodwater progression, which are required when results are interpolated within a limited set of pre-calculated results.

In Ruponen’s applied method, also the leaking and collapsing of non-watertight structures, such as closed fireproof doors, are taken into account. But at the time of writing, the critical pressure heads are still based on rough estimations, presented in *IMO SLF47.INF6 (2004)*. In addition a constant discharge coefficient 0.6 is used for all openings. Within the ongoing project FLOODSTAND (see acknowledgements), comprehensive experimental and numerical studies will be carried out in order to increase the reliability of the applied parameters in the flooding simulation method. This is important also for the inverse method, because when the reliability of the simulation method is increased, consequentially as a side effect, the reliability of the inverse method is also increased.

Inverse Method for Breach Analysis

Principles

Determining the source of the flooding constitutes as an inversion problem and in this section the inverse method for breach analysis is briefly introduced. A more comprehensive description on the principles of the method is given in Penttilä (2008).The method is based on the assumption that if the hull of a ship is breached below the waterline, water starts to flood in and the flood water flows in a deterministic and usually non-reversible way. Therefore all measurable water levels inside the ship have an explicit dependency on time. The ship’s floating position is also a function of time. Whatever happens is assumed to be the consequence of the breach and the breach only. This means that each breach or a set of breaches forms a unique and recognizable pattern. However the pattern is unique only in respect to the measurement accuracy. The problem is to find the right set of breaches that result in matching flooding simulation results with the observations within the measurement accuracy. In general an inverse problem is to determine the parameters that produce the known outcome. In this case the outcome is the group of measured flood water levels and the parameters are the breach set properties, like the number of damaged rooms (or the number of flood water sources), the corresponding areas of all flood water entry points and also the ship’s initial loading condition. The initial loading condition is usually known due to regulations and onboard loading computers. However because of the complexity of the inverse problem, the number of flood water sources is limited in this study to a single breach.Inversion problems typically have more than one solution. The number of solutions can be reduced, by limiting the degrees-of-freedom for the breach location and changing the level of abstraction in the ship model (less detailed). The X-coordinate is ignored in this study and the Y- and Z-coordinates can be connected with the valid assumption that the breach is always located at the hull surface (Figure 1). According to *Penttilä (2008)* the Z-coordinate has the greatest significance, but only near the waterline. In this study the approximation described in *Penttilä (2008)* is used in both direct and inverse calculations and the exact location of the breach in the joint hull area (JHA) of a damaged room is not studied. At the level of abstraction of this study, the most critical task is to determine from flooding sensors which rooms are damaged. The exact location and area are secondary. The success of determining the correct damaged room depends highly on the sensor arrangement; how many, and where, the flood water sensors are installed inside the vessel. The degrees-of-freedom can be great if there is no possibility to measure the flood water in the rooms, which are primarily flooded. Such cases are more likely to fail.

If the number of different possibilities for flood water entry points can be limited, so that each combination can be calculated within a reasonable time, the breach can be solved literately by comparing the results of each possible breach to the actual measurement so that the “best-fit” results determine the breach.

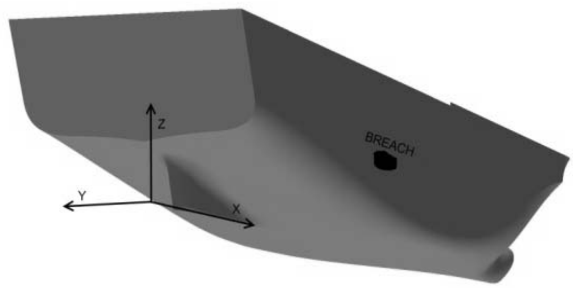

Fig. 1 Applied co-ordinate system and location of the breach

Description of the Method

In this study a number of different cases are calculated. Each case is calculated with various amounts of added random noise. The amount of noise is considered to be known. It is expected that in further studies this can be derived from the applied sensor type. In order to calculate the breach origin from level measurement a specific algorithm has been developed. This is illustrated in Figure 2. Each case contains a specific known amount of added noise and the expected correlation can be calculated from this. From the detected water levels in rooms and the known connections between watertight structures, all possible entry points for flood water are derived.

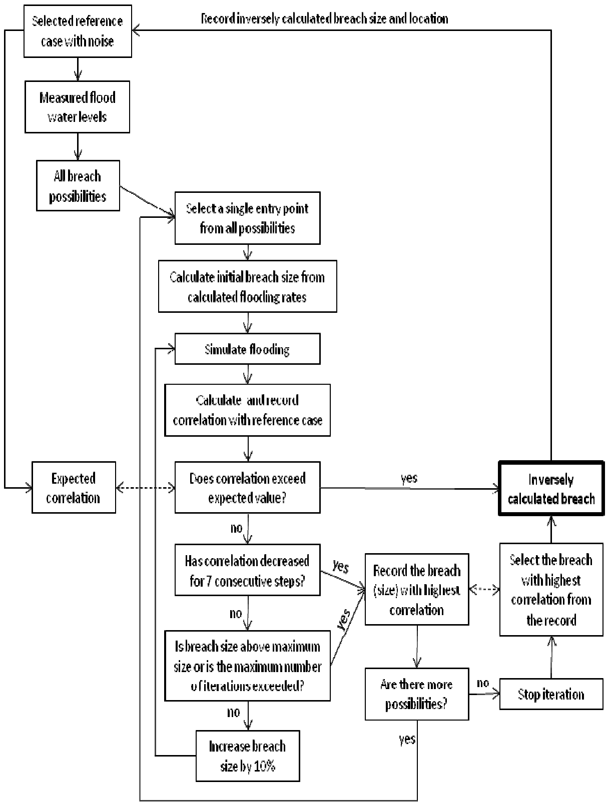

Fig. 2 Process description of the inverse iteration algorithm

The flood water can penetrate through non watertight structures and the number of different entry points can be very great. Each entry point is calculated with different breach areas from the initial area upwards in 10% increments until maximum size 2 m^2 is reached. The initial area was estimated from the flooding rates calculated from the reference data. Because the iteration works upwards from a small breach towards a larger breach size, the calculated initial size was divided by 3, to make sure the initial guess is smaller the actual size.

The iteration proceeds until the calculated correlation exceeds the expected value or until maximum number of iterations is exceeded. The expected correlation is estimated from the amount of added noise by:

$$c_{expected} = \frac{1}{\left(1 + \frac{noise}{2.5}\right)} - 0.01 \qquad (2)$$

The purpose of the expected correlation is simply to reduce the required calculation time in the iteration. The constants in equation (2) are empirical coefficients and further research is still needed.

The iteration also stops if the calculated correlation decreases for 7 consecutive steps. The correlation is calculated by comparing the relative mean difference in water levels in compartments and the relative mean differences in trim and list between the simulated results and the reference case.

After iteration of a specific breach has stopped, the next possible case is selected and the process continues until all possibilities have been calculated or until the expected correlation value is exceeded. The size and location of the breach with the highest correlation is recorded for further analysis.

Case Study

Large Passenger Ship Design

A modern Panamax size cruise ship design of 90 000 GT was used as a test case. The main dimensions of the ship are listed in Table 1.

Table 1. Case study ship data

Gross tonnage	90 000
Length over all	290 m
Breadth	32 m
Draft	7.7 m
Initial GM	2.0 m

The ship is divided into 19 watertight compartments extending to the bulkhead deck. The NAPA-model has a total of 312 openings, which connect 170 rooms. A room is always by definition watertight and water can only spread to other rooms through openings. An example of the 3D model rooms and openings is presented in Figure 3.

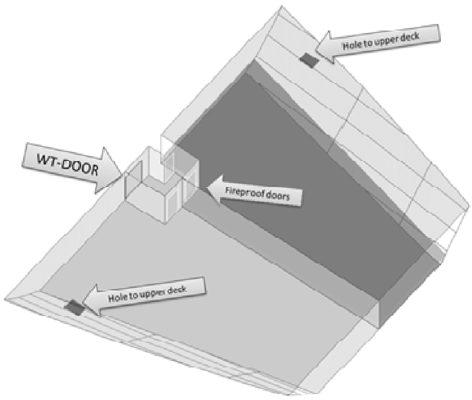

Fig. 3 Example of the 3D model and level of detail during flooding

Damage Cases

A set of 433 damage cases were generated by Monte Carlo simulation on the basis of damage statistics for collisions. However, cases with high penetration/length ratio were ignored since in those damage cases the colliding ship is likely to have a notable effect on the flooding through the breach. Each damage case was limited to a single breached room and the area of the breach was limited between 0.01 – 2.0 m^2. The limitation is necessary due to current measurement capabilities. If the breach was very large, the damaged compartments would fill with such speed that neither the selected time step for simulation nor a real flooding sensor would be able to measure the flooding rate. The applicability of the inverse method for very large breaches is not included in this study. However, in general it is considered that the damage location is easier to detect if the damage extent is large.

Each damage case was calculated using the NAPA software, which implements Ruponen's method (see Ruponen, 2007 and The Naval Architect, 2008), assuming a calm sea state. Total of 225 cases were calculated with all doors closed and 208 cases were calculated with all fireproof doors (total of 167) open. Most cases resulted in progressive flooding through various openings in the ship. On average 2.3 rooms were flooded during the simulation time (120 s) when all fireproof doors were closed and an average 2.7 rooms were flooded when the fireproof doors were open. All watertight openings were always defined as closed.

After each case was simulated the results were stripped in order to make the comparison for an authentic case. All data which would not be available in a real situation was removed. The available data after the stripping consists of the floating position and flood water levels in the rooms with sensors as functions of time. The entire process of testing the inverse method is illustrated in Figure 5.

Added noise in reference results

A true measurement always contains some measurement errors or noise. Possible sources for error in level measurement are discussed in *Penttilä* (*2008*). In this study two different amounts of random noise were added to the reference data. The Figures 4a and 4b illustrate the added noise to the measurement of 4 flooded rooms.

(a)

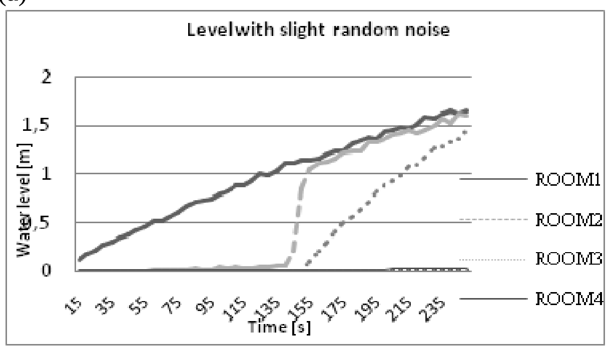

(b)

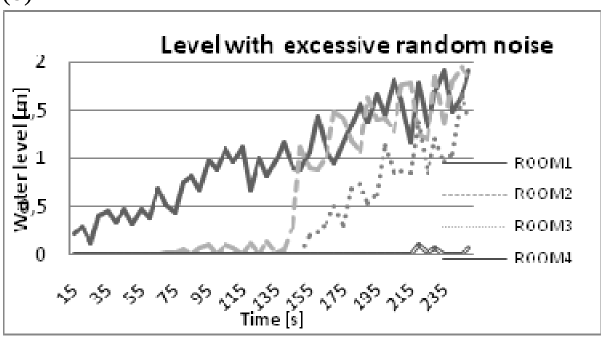

Fig. 4 (a) Level with slight added noise

The purpose of the generated random noise was to simulate disturbances in the flood water level measurements. The added noise makes it more difficult to calculate the initial flooding rate and the origin of the breach and makes the case more realistic. However, It should be noted that the added noise does not correspond to disturbances due to sloshing and is only an approximation of random measurement distubances. Typical flooding sensors described in *Penttilä* (*2008*) may also react to changes in air pressure due to flooding, but this effect is not studied in this text. All flooded spaces are assumed to be freely ventilated. The added noise is expected to decrease the likehood of determining the correct breach succesfully.

Inverse calculation

In this study the generated damage cases with various combinations of noise and time spans were fed in to an algorithm applying the inverse method to determine the location and area of the breach. The algorithm tries to determine the correct breach by iterating through different simulations and comparing the results to the available data. The available simulation data was limited to selected time spans. These time spans are referred to as "filter lengths" from the measurement analogy. The breach is being filtered from the level data. The purpose of adding noise and changing the time span of the available data was to study the effect of noise and filter length on the inverse method (discussed in *Penttilä 2008*). Same opening statuses were used in both direct and inverse calculation. The process of applying the inverse method to generated reference results is illustrated in Figure 5.

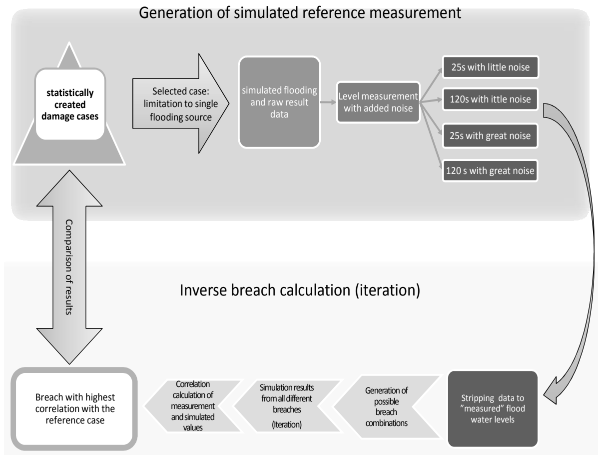

Fig. 5 Process diagram illustrating the method of testing the inverse method

The specific algorithm used in this study is optimized for a wide range of solutions and is expected to solve most cases which have a single breach solution. If the algorithm fails to produce the correct answer the reason may either be in the algorithm design or in the theoretical limitations of the method. These cases are not distinguished in this study. Research for improving the efficiency of the algorithm continues.

Inverse breach calculation is always done for a selected time span or filter length. In this study we assume that in a real damage scenario, the breach should be calculated as early as possible within the first minutes (if possible). Theoretically the inverse method is expected to determine the correct breach always if the available data is infinitely long and noiseless. However in real cases there is always some noise and the time available for measurement and calculation is limited.

The problem is similar to signal processing where a long filter is slow less susceptible to noise, whereas a short filter is fast but more sensitive to noise. The problem of breach measurement is similar to filtering also in the sense that the time span of the reference data has to be selected prior to the inverse calculation. Therefore the selected period is called in this text the *filter length*. In this study filter lengths of 25 s and 120 s are studied. These lengths fit the expected breach area (between 0.01 – 2.0 m^2). A more detailed description of the filter length selection criteria is described in *Penttilä* (*2008*). Time step used in the simulations and inverse calculation was 5 s.

Table 2. Summary of generated damage cases

	All doors closed	***Fireproof doors open***
Total number of generated damage cases	235	228
Flooding not detected by flooding sensors	11	22
Breach too small (no noticeable flooding)	70	61
Total number of remaining suitable damage cases	154	145
Average breach size	0.21 m^2	0.21 m^2
Average distance from waterline	0.98 m	1.17 m
Average number of flooded rooms (within 120 s)	2.29	2.66

Sensor arrangement

The ship is equipped with 57 flooding sensors in total of 245 rooms/tanks. 170 rooms are subject to progressive flooding and remaining 75 are closed and not connected to any other rooms by openings. There are 45 flooding sensors in the 170 rooms, of which 33 are located in rooms that are larger than 300 m^3. The "density" of the sensor arrangement in potential areas of progressive flooding is calculated by

$$\rho_{sensors} = \frac{n_{sensors}}{n_{connected\_rooms}} \quad (3)$$

In this case the density of the sensor arrangement is approximately 0.26.

The calculations were performed for two sensor arrangements. All cases were calculated first with the assumption that all rooms are equipped with a sensor (sensor density 1.0) and then with the sensor density 0.26. When each room is equipped with a sensor the success rate of calculating the correct breach is expected to be 100% and less for the case where only selected rooms are equipped with a flooding sensor.

In the case of a sparse sensor density (0.26), noise levels of 2% and 10% were considered realistic and were used in the calculation. But in the case of the high sensor density (1.0) noise levels were 5% and 35%. The higher noise levels were used because solving a breach with a very tight sensor arrangement is considered to be almost a trivial task. Therefore excessive noise was added in order to really test the method.

Results

A summary of the damage cases is presented in Table 2. Some of the generated damages resulted in too small a breach compared to the distance from the waterline. These damages did not result in noticeable flood water amounts and a total of 131 cases were left out from the inverse calculations because of this. It should be noted that with longer filter lengths also these damages could have been included. Also some damages did not result into flooding which could be detected by the flooding sensors. There were a total of 33 of these cases. It is not known whether flood water would have spread to rooms with flooding sensors if the time span had been longer. The final number of suitable cases for the inverse calculation was 299. Table 2 lists the cases in more detail.

The success rate of the inverse method was measured by checking whether the method was able to determine the correct damaged room (breach location) from detected flood water and whether the calculated breach area corresponds to the reference case within a ±30% margin. The general arrangement and the sensor arrangement of the ship model were such that in 64.6% of the cases the flood water was detected by a flooding sensor in the primarily flooded room.

Table 3 shows the results of the study for all 299 inversely calculated cases with the assumption that all rooms are equipped with a flooding sensor and Table 4 shows the results with a typical sensor arrangement of sensor density 0.26.

Table 3 Success rate of calculating the correct breach with sensor density 1

	All doors closed		***Fireproof doors open***	
	Location	Area	Location	Area
Filter 120s				
Noise 5%	99.6 %	60.7%	99.0 %	61.1%
Noise 35%	97.3 %	21.9%	98.1 %	25.0%
Filter 25s				
Noise 5%	100.0 %	68.0%	98.6 %	64.4%
Noise 35%	97.8 %	37.7%	98.1 %	41.1%

Table 4 Success rate of calculating the correct breach with a sensor density 0.26

	All doors closed		***Fireproof doors open***	
	Location	Area	Location	Area
Filter 120s				
Noise 2%	69.5%	64.5%	76.6%	65.8%
Noise 10%	67.5%	56.7%	74.5%	41.7%
Filter 25s				
Noise 2%	67.5%	31.7%	74.5%	41.7%
Noise 10%	68.2%	20.1%	70.3%	28.4%

Table 3 shows that the method used in this study is very likely to find the correct location for the breach even with high amounts of noise in the measurement data as long as each room is equipped with a sensor. The average success rate in finding the primarily flooded room was 98.6%. This is slightly less than the expected success rate of 100%. The success rate of calculating the correct breach area within the margin was more dependent on the filter length and noise than the success rate on locating the breach correctly.

Table 4 shows that the same method, when used for a sparse sensor arrangement, is less likely to find the correct breach. The average success rate in determining the primarily damaged room was 71.1%. Again the effect of noise and filter length is more noticeable for the calculation of the breach area than the location. It should be noted that the two result sets were calculated with different amounts of noise and are not directly comparable. Naturally the opening status of the fireproof doors has a greater impact on the results when the sensor arrangement is sparse. When all fireproof doors are open, the method was 8.5% more likely to determine the breach correctly.

The inverse method is based on comparing correlations of the results of different breaches to the reference results. The correlation r between the simulated and the measured levels was calculated by:

$$r = 1 - \sigma_{rel} \tag{4}$$

where σ_{rel} is mean relative deviation between measured and simulated level. Also trim and list were included in the correlation calculation.

An example of a successful case is presented in Figure 6, showing a good correlation between the results with the predicted damage size and location and the generated measurement data with very significant amount of noise.

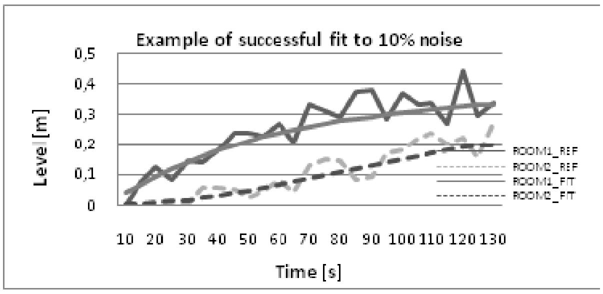

Fig. 6 Example of successful fitting of breach to level data

Also one failed case was analyzed in detail. In this case there was a breach in ROOM1 but there was an open pathway for the flood water to progress directly onto the lower deck. This case failed because there is no way to distinguish a breach in ROOM1 from a breach in ROOM2. The situation is illustrated in Figure 7.

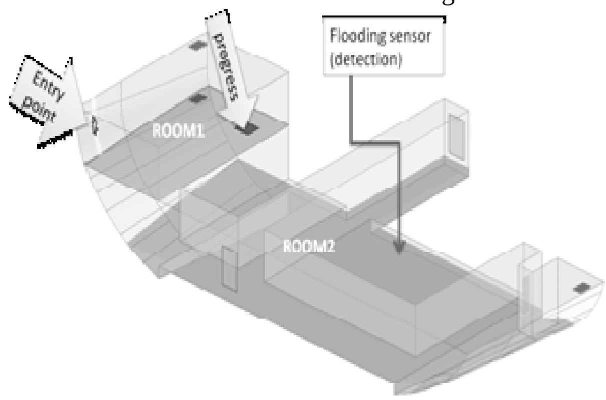

Fig. 7 Example of flooding from adjacent compartment

Flood water flows almost instantaneously through the open staircase to the lower deck and flooding remains symmetrical. There is no listing and the difference between the results of a breach in ROOM1 and ROOM2 is negligible as long as the flooding rates match. It should be noted however, that in this case, the errors in predictions due to a wrong breach location are minimal because the wrong breach produces very similar results to the correct breach. This is referred to as the “problem of similarities”. Figure 8 illustrates how the fit seems to imply that the breach is correct.

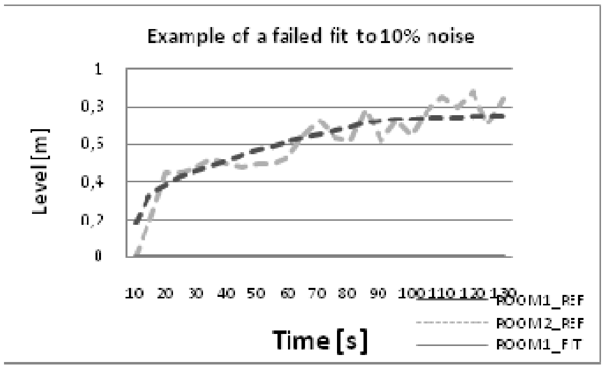

Fig. 8 Example of failed fitting of breach to level data (note the zero-level in ROOM1 in both the reference and fitted case)

Discussion

The results of the 299 inversely calculated damage cases with two different sensor arrangements strongly suggest that the inverse approach is applicable in breach detection but that the reliability of the method depends greatly on the sensor arrangement. The average likelihood of determining the breach correctly by using the inverse method was 71.1%. This is a good result compared to the sensor density of the vessel (0.26). But on the other hand the results in this study can be slightly too optimistic as such, because the number of breaches was limited to a single breach. The sensor arrangement of the vessel was considered typical.

The flooding sensor density of the ship was 0.26, which might suggest that flood water would be undetected in approx. 74% of the cases. However due to the progressive nature of flooding the flood water in most cases progressed to rooms which were equipped with flooding sensors. In 71.1% of these cases the flooding resulted in sufficiently recognizable patterns for the inverse method to work. The method resulted in almost 100% success rate when all rooms were simulated to have a flooding sensor. This does not necessarily mean that all rooms need to be equipped with flooding sensors for the inverse method to work, but it is unclear which sensors are critical. Another result is that when all fireproof doors were set open, the method more likely to find the correct breach. Fireproof doors are generally advised to be kept open during flooding in order to minimize asymmetrical flooding, but when the sensor arrangement is sparse this has also a positive effect on breach detection.

The effect of noise and filter length to the success rate is as expected. The method is more likely to find a correct solution if there is very little noise or the filter length is long. The change from little noise to excessive noise seems to decrease the success rate of finding the correct location on average by 2 percentage units. The effect of the filter length is less clear. The results would seem to indicate that 25 s filter length is in some cases not enough, but that 120 s filter length does not significantly increase the likelihood of finding the correct breach. Optimal filter length depends on the flooding rate and measurement accuracy.

The average success rate of determining the area of the breach within a reasonable margin was fairly low. On average the calculated breach size was within ±30% margin in 47% of the cases with sensor density of 1.0, and within margin in 44% of the cases with the sensor density of 0.26. Such low success rate on calculating the correct breach area indicates that the algorithm used in this study could be further developed.

Even though a more advanced algorithm is expected to increase the success rate of the inverse method, the maximum theoretical success rate is not known. It is believed by the authors that with 10% noise and 120 s filter length the theoretical maximum might be as high as 90% even with such a sparse sensor density. The example of the failed case shows that not all cases can be solved correctly even with a very dense sensor arrangement. This is because all sensors always have a specific zero-limit, which has to be exceeded before flood water is detected. If flood water does not rise up to the sensor and flows directly to another room, any method will surely fail. However if the difference in vertical location is not very great compared to the breach immersion, the actual location of a breach is not a real problem. This is because the prediction results would still remain the same. From this point of view, the results could be analyzed from the point of view of similar results and not by correct breach. The problem of similarities is however not studied in this text but it should be noted that this subject should be included in the study of optimal sensor arrangements.

The case of multiple breaches was not included in this study. Real damage situations are likely to involve multiple breaches flooding at the same time or at different times. Therefore the limitation to a single breach is a rough approximation. The problem of multiple breaches was excluded from this initial study due to the complexity. When a more advanced algorithm, able to solve multiple breaches, is developed, the same study can be repeated without the single breach limitation. It is believed by the authors that the resulting success rates would be similar or slightly less.

In this study the sensor accuracy was simulated by adding random noise to the measurement. However, real flood water sensor have another limitation, which is the minimum liquid level, that can be measured. Typical level sensors measure air pressure at 3 cm from the floor and because the air pressure in the room may change slightly there must be some zero-limit for the sensor to avoid false flooding detection. In this study the zero-limit for the sensors was 0 cm, which means that it is assumed that the sensors can measure flood water level with infinite accuracy down to 0 m. In real case the zero-limit is of order 10 cm and raising the zero-limit from 0 to 10 cm may have a decreasing effect on the success rates. However this effect was not studied in this text.

In addition to designing a suitable algorithm to solve cases with multiple breaches, another difficulty is trying to calculate the breach properties from flooding sensor output when all breaches are not yet immersed. Flooding sensors can never detect a breach, which has not yet started flooding and if there are multiple breaches, some may start to flood later on after sufficient changes in floating position. No method based on flooding sensors can solve such cases successfully with a short filter length.

Conclusions

The target of this study was to find out whether it is possible to determine the location and size of a breach purely from flooding sensor output without human intervention. A total number of 2392 cases (299 cases with two different sensor arrangements and combinations of 2 different filter lengths and 2 different amounts of random noise) were calculated inversely and the results strongly indicate that the inverse method is applicable in determining the breach from the water level data only if the sensor arrangement is dense enough. When calculated with a typical sensor arrangement, the method was able to successfully determine the correct floodwater origin in 71.1% of the cases. However the method was only able to derive the correct breach size within a reasonable margin in 44% of the cases.

It is believed by the authors that the inverse method can be developed further so that it can (if the sensor arrangement is dense enough) successfully solve a very high percentage of damage cases inversely and determine the breach size more accurately. However any method with sufficient noise will fail if the sensor arrangement is too sparse, therefore it should be noted that if a valid method can be produced, it has a theoretical maximum depending on how the flooding sensors are placed. A good method could therefore be used to study the optimal sensor placement. Well-placed sensors in a ship enable much higher precision decision support systems than what is possible today with current sensor arrangements.

An inverse method for determining the breach location and size from flooding sensor output was extensively tested. Unfortunately the results of this study are still somewhat inconclusive due to the limitation of a single flood water origin (single breach). However, so far the inverse approach in breach detection has proven to have great potential and it is believed that the general case would have similar results. Further development and testing of the presented method for the breach detection will be carried out within the FP7 Research Project FLOODSTAND.

Finally, it should be noted that even with a sophisticated breach detection analysis and carefully validated flooding simulation tools, the final outcome of any real flooding may always be different from the prediction. This is mainly because currently, the various applied parameters for openings, like collapsing pressure of a fireproof door, are not known very accurately. Furthermore, it is possible that the water will find unpredicted progression routes, such as pipes and ducts that may not be included in the simulation model. The result of any computer based decision support tool is always a prediction based on best approximations, intended to help in the decision making. The actual decision (e.g. to evacuate or to proceed to the nearest port) should always be made based on the real situation, including available support tools, visual observations and expertise of the crew and emergency response service.

Acknowledgement

The research leading to these results has received funding from the European Community's Seventh Framework Programme (FP7/2007-2013) under grant agreement n° 218532 (project FLOODSTAND). The financial support is gratefully appreciated.

Reference:

IMO MSC 77/4/1 (2003) Maritime Safety Committee: Large Passenger Ship Safety, Cruise Ship Safety Forum Recommendations, 20 March 2003

IMO SLF47/INF.6 (2004). Large Passenger Ship Safety: Survivability Investigation of Large Passenger Ships, submitted by Finland, 11. June 2004.

IMO SLF-51/11 (2008) Stability and Seakeeping Characteristics of Damaged Passenger Ships in a Seaway When Returning to Port by Own Power or Under Tow, 10 April 2008

Ölcer, A. I., Majuner, J. (2006) A Case-based Decision Support System for Flooding Crises Onboard Ships, Quality and Reliability Engineering International; 22:59-78

Penttilä, P. (2008) Use of Level Sensors in Breach Estimation for a Damaged Ship, Master’s Thesis, Helsinki University of Technology

Ruponen, P. (2007) Progressive Flooding of a damaged passenger ship, Doctoral Dissertation, Helsinki University of Technology

The Naval Architect (2008) Decision Support for Flooding Control, The Naval Architect, May 2008, pp. 32-33

Analytical and numerical modelling of oil spill from a side damaged tank

Mohammad Taghi Tavakoli, Jørgen Amdahl and Bernt J. Leira

Department of Marine Technology, Norwegian University of Science and Technology,Otto Nielsens v10, 7491, Trondheim, Norway

Abstract:
The objective of this paper is to study the oil spill from damaged tank in collision. The work comprises development of analytic models for fast estimation of oil spill, and CFD simulation with the FLUENT software for verification of the simple models. In the previous papers the oil leakage from damaged tank with an opening in the bottom is investigated.
The purpose of the present study is to extend the scope to cover oil spills in collision cases where openings occur in the sides. In such cases, the gravity force is important as in the grounding scenario. In collision scenarios, however, there is a local imbalance due to different densities of the fluids while the internal pressure is equal to external pressure. A combination of water inflow/oil outflow through the opening may occur. Analytical calculations and time domain simulations are applied to calculate the volume of oil outflow and outflow rate versus time. Good agreements are obtained between the simplified analytic model and CFD of the oil spill.

Introduction

Most tankers are loaded such that the internal pressure at the tank is larger than the external sea pressure. Thus, if the tank is damaged, cargo flows out. If the tanker carries somewhat less cargo, so that hydrostatic balance is established at - or several meters above the tank bottom, water tends to enter the ship through the hole in the hull as long as the highest point of damage is below the hydrostatic balance level. This presupposes equal atmospheric pressures at the surfaces of both seawater and oil cargo. If there is overpressure, oil outflow will increase in a ruptured tank. Conversely, reduced ullage space pressure will reduce oil outflow. This suggests that reduced internal pressure is a potential means of controlling oil outflow in grounding (Tanker Spills, 1991).

If the density of the cargo in the damaged tank is lower than that outside sea water, but the hydrostatic pressure is higher over the opening, then outflow will occur, which produces a gravity current. The hydrostatic pressure is the key factor in analyzing the leak rate. Hydrostatic pressure is an isotropic phenomenon, i.e. at any given point in a fluid the pressure will be the same, regardless of the direction in which it is measured. Oil will run out of a damaged tank if the interior hydrostatic pressure of the oil at the opening is greater than the exterior hydrostatic pressure of the sea at the same point. The flow continues at an ever decreasing rate until the inside and outside pressures are equalized. In order to calculate the theoretical outflow rate and spill volume, the Bernoulli's principle is utilized for this condition (Tavakoli et al. 2008, Tavakoli et al. 2009).
If the opening is in the side of the tank, and the pressures on the average are equal over the opening between oil and water, there is still local imbalance and the flow will cease only when the lower lip of the hole are water. So, the side leak is divided into two stages. The analytical models have been developed based on the integrated Bernoulli’s equation for the fluid flow in the first phase.

Phase 1: Gravity current

In the grounding case and in the first phase of side damage, there are two governing principles; namely the Bernoulli's principle and ideal gas law.

Bernoulli's principle

Based on the Bernoulli's principle, the sum of pressure, potential energy and kinetic energy per unit volume is constant at any point. In its original form, for incompressible flow in a uniform gravitational field, it reads:

$$\frac{\partial}{\partial S}\left(\rho g h+\frac{1}{2}\rho v^2+P\right)=0 \tag{1}$$

$$\frac{dP_u}{dt}=\rho_o v\frac{dv}{dt}-\rho_o g.\frac{d(H_o-h_h)}{dt} \tag{2}$$

$$if\ h=H_o-h_h\rightarrow\frac{dP_u}{dt}=\rho_o v\frac{dv}{dt}-\rho_o g.\frac{d(h)}{dt} \tag{3}$$

Where p_u, ρ_o, H_o and h_h are respectively, ullage pressure, density of oil, height of oil in the cargo tank and puncture height from the bottom.

The ideal gas law

Fthenakis (1999) described a scenario where the vessel is closed at the top and vapor and air fill the gas space. The initial pressure is atmospheric, but as the liquid level sinks, the pressure in the gas-space is reduced. The ideal gas law is given by:

$$P_u=\frac{n_a R T}{V_u}+\frac{n_o R T}{V_u}=(n_a+n_o)\frac{R T}{V_u} \tag{4}$$

where n_a and n_o are the number of moles of air and oil respectively, R is the gas constant, T is the absolute temperature, and V_u is the ullage volume.

$$\frac{dP_u}{dt} = -(n_a + n_o)\frac{RT}{V_u^2}\frac{dV_u}{dt} + \frac{dn_o}{dt}\frac{RT}{V_u} \qquad (5)$$

The last term Eq. 5 represents vaporization of the oil inside the tank. The change of the ullage volume inside the vessel depends on the rate of outflow.

Bernoulli's principle and the ideal gas law:

While the oil outflow velocity is *v* and puncture area s, the change of volume is obtained by eq. 6.

$$v\,s = \frac{dV_u}{dt} = -\frac{d(A_t h)}{dt} = -A_t\frac{d(h)}{dt} \qquad (6)$$

where s and A_t are hole area and tank area respectively. By combination Eqs.'s 3, 5 and 6 there is obtained:

$$\frac{dv}{dt} = \frac{s}{A_t}\left[g + \frac{RTA_t}{V_u^2\rho_o}(n_a + n_o) + \frac{dn_b}{dt}\frac{RT}{V_u\rho v}\right] \qquad (7)$$

This equation can be solved numerically for given values of V_u. For analytical solution it is necessary to introduce a simplification. The equation can be solved by simplifying and taking a mean value of the ullage volume during the discharge.

$$V_u = \frac{V_u(t_1) - V_u(0)}{2} \qquad (8)$$

where V_u is ullage volume, t_1 is the time for completion of phase 1, $V_u(0)$ is initial ullage volume $V_u(t_1)$ is the final ullage volume. The solution of Eq.7 by taking the mean value of the ullage volume is as follows:

$$v = \left[g\frac{s}{A_t} + \frac{P_u(0)V_u(0)s}{V_u^2\rho_o} + \frac{dn_b}{dt}\frac{RT}{V_u\rho v}\right]t + v(0) \qquad (9)$$

$$v(0) = \sqrt{2g(h-h_h) - \frac{2\rho_w}{\rho_o}g(T-h_h)} \qquad (10)$$

In case of venting from the ullage space, the pressure in the ullage space will be equal to the atmospheric pressure. It can also be pressurized to a constant value, for example by pumping. In this condition, the efflux rate is a function of the oil height, puncture point location and ullage pressure. It decreases when the height is reduced and is obtained by the following equation:

$$P_u + \rho_o g(H_o - h_h) - \frac{1}{2}\rho_o v^2 = P_{atm} + \rho_w g(D - h_h)$$

$$v(h) = \sqrt{\frac{2(P_u - P_{atm})}{\rho_o} + 2g(h-h_h) - \frac{2\rho_w}{\rho_o}g(T-h_h)} \qquad (11)$$

where *h* is the height of oil in the cargo tank. The rate of outflow through the hole is:

$$\dot{Q} = C_d\, v\, ds \qquad (12)$$

If the opening is in the side, the velocity varies as a function of the height (b) in the opening.

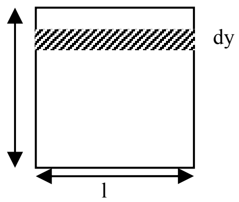

Figure 1. Outflow from rectangular opening

The approximate volume flow rate through a strip of height dy and width l is:

$$Q = c_d\, v\, l\, dy\, dt$$

$$\frac{dQ}{dt} = c_d v l\, dy = c_d l\int_{H_2}^{H_1}\sqrt{\frac{2(P_u - P_{atm})}{\rho_o} + 2g(y-h_h) - \frac{2\rho_w}{\rho_o}g(T-h_h)}\,dy \qquad (13)$$

If the opening is - rectangular, H_1=H-b/2 and H_2=H+b/2, integration over the height yields;

$$\frac{dQ}{dt} = c_d v b\, dy = c_d b\frac{1}{3g}\left[\left(\frac{2(P_u - P_{atm})}{\rho_o} + 2g(y-h_h) - \frac{2\rho_w}{\rho_o}g(T-h_h)\right)^{\frac{3}{2}}\right]_{H-b/2}^{H+b/2} \qquad (14)$$

Then the result can be written:

$$\dot{Q} = c_d s\sqrt{\frac{2(P_u - P_{atm})}{\rho_o} + 2g(y-h_h) - \frac{2\rho_w}{\rho_o}g(T-h_h)}\left[1 - \frac{1}{96}\left(\frac{b}{h-h_h}\right)^2 + \ldots\right] \qquad (15)$$

For a small opening (b<<h), the flow rate is:

$$\dot{Q} = c_d\, s\sqrt{\frac{2(P_u - P_{atm})}{\rho_o} + 2g(y-h_h) - \frac{2\rho_w}{\rho_o}g(T-h_h)} \qquad (16)$$

while,

$$Q_{Total} = \Delta h\, B\, L \qquad (17)$$

in which Δh is the ideal change in height and is given by:

$$\Delta h = (H_o - h_h) - \frac{\rho_w}{\rho_o}(d - h_h) \qquad (18)$$

C_d is the discharge coefficient, *s* is the opening hole area, and d is draft of ship.

The ideal outflow rate is given by equation (7):

$$T(h) = \frac{A}{c_d\, s\, g}(v_i - v_h) \qquad (19)$$

The outflow velocity can be expressed as a function of time:

$$v(t) = v_{initial} - \frac{c_d\, s\, g t}{A} \qquad (20)$$

The average outflow velocity can be represented by equation (3)

$$v_{ave} = \frac{1}{a-b}\int_b^a v(h)dh = \frac{v_i^3}{3\Delta h g} \tag{21}$$

where *a* and *b* are the initial and final height of oil in the cargo tank, and v_i is the initial oil outflow velocity. The theoretical oil spill volume is given by equation.4; Similarly, the oil height inside the wing tank is given by:

$$h(t) = \frac{c_d^2 s^2 g}{2A^2}t^2 - \frac{v_{initial} c_d s}{A}t + \left(\frac{v_{initial}^2}{2g} + \frac{\rho_w H_w}{\rho_o}\right) \tag{22}$$

The total outflow duration is obtained when hydrostatic equilibrium between oil and water is attained. It is given by:

$$T_{total} = \frac{A}{c_d s g}\sqrt{\frac{2(P_u - P_{atm})}{\rho_o} + 2g.(H_o - h_h) - \frac{2g\rho_w(D-h_h)}{\rho_o}} = \frac{v_{initial}}{c_d g}\frac{A}{s} \tag{23}$$

Phase 2. Two way flow

When the pressures on the average are equal over the water and oil interface in the opening, there is a local imbalance due to different densities of the fluids. A combination of water inflow/oil outflow through the opening may occur. The inflow-outflow through the opening must be equal from continuity, but the effective opening will gradually be reduced. To compute the process in all its details will be too complicated, but it is possible to estimate the initial flow rate. Fannelop (1994) introduces some basic assumptions: the volume flow rates are equal, the flow velocity is given by the hydrostatic pressure difference and the flow area is constant.

These assumptions can be expressed as follows for a rectangular cross section,

$$s_1 + s_2 = s \tag{24}$$

$$\int_{s_1} v_1 ds_1 + \int_{s_2} v_2 ds_2 = 0 \tag{25}$$

$$v_1 = v_2 = \sqrt{2g\frac{(\rho_w - \rho_o)}{\rho_w}|y|} \tag{26}$$

where s_1 and s_2 are the inflow and outflow areas. Refer fig.2. y is the height of the stream surface for each flow. For example in a rectangular or circular opening and with these assumptions, the interface is located at the midheight of the opening and y is half of the opening height. For a triangular opening, in order to satisfy the assumption, the interface is located at 32% of the height of the edge.

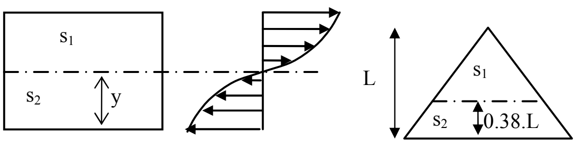

Figure 2. Flow through rectangular and triangle openings

The flow will cease when there is water on both sides of the breach. The oil outflow in this phase can be given by:

$$Q_{o2} = BLh_h \tag{27}$$

where B and L are breadth and length of the tank and h_h is the height of the opening from the bottom. The outflow time in the second phase is given by:

$$T = \frac{Q_{02}}{C_d s v_1} \tag{28}$$

Single hull design

The geometric parameters which are pertinent to the oil flow from a single hull design are depicted schematically in Figure 3. *s* is the opening area, L and B are the length and breadth of the ruptured cargo tank, respectively. Q is the theoretical oil spill volume, which equals the reduction of the cargo content. It is assumed that neither the inner nor the outer hull has undergone any structural deflections. The blockage effect is considered only in relation to the opening area and discharge coefficient. This paper does not examine the flow through and around structural members in the tank. The effects of viscosity and turbulence are neglected. By neglecting the effects of viscosity, it is implicitly assumed that the gravitational forces are much greater than the viscous forces (Schneekluth et al. 1998).

Case Study

Illustrative examples are presented in order to show the performance of the proposed method and to compare the predictions with numerical simulations. The vessel selected for the case study, is a FPSO with displacement of 170,000 tonnes. The principal dimensions of the FPSO and ruptured tank are shown in Figure 3.The opening area is 0.1 m^2, 1 meter length and 10 centimetres height. It is assumed that rupture occurs 4 meter higher than the bottom of the tank and has the shape of a rectangular prism.

In the numerical simulation, the model is 2D and it is assumed that the rupture geometry and resultant flow are longitudinally invariant. The height of the hole is 10 centimetres and has 10 grid points across. The model has 15000 and 10000 grid points in the vertical direction of the damaged tank and intact tank, respectively, and 5000 in the transverse direction in both tanks. The free water surfaces were set at atmospheric pressure. The Volume of Fluid CFD technique and laminar flow assumption are used in the simulations.

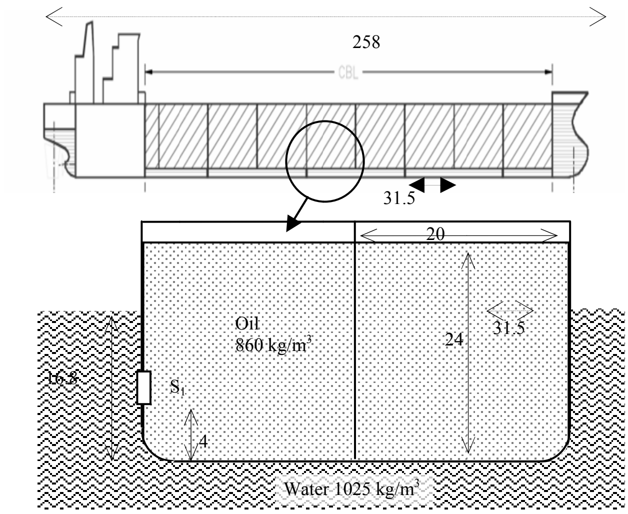

Figure 3. Principal dimensions of FPSO and damaged tank

Figure 4 to Figure 7 show the results obtained from Fluent. The oil height drops quickly in the first 8800 seconds and then remains constant. Figure 5 shows this phase and it attains equilibrium as shown in Figure 6. From the analytical results, it is observed that 2988 m3 oil flows to the sea in 8760 seconds. In the second phase, water is ingested into the tank, and this continues until approximately 4651 minutes. The flow finally stops when the hole is completely covered by water on both sides. Analytical results show 5534 m^3 oil spill in 5456 minutes. The discharge coefficients in the two phases are different. By comparing the results obtained with Fluent and analytical simulation, the discharge coefficient is estimated to 0.6 in the first phase and 0.45 in the second phase.

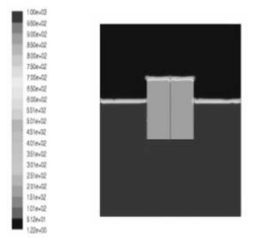

Figure 4. Initial condition

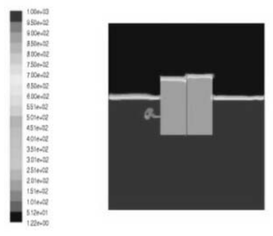

Figure 5. First phase

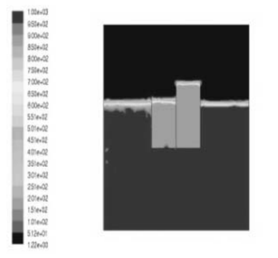

Figure 6. Second phase

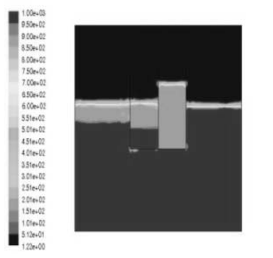

Figure 7. Final Condition

Phase 1: Gravity current

Using equations 6, 7 and 14, the initial and average outflow velocity of and the volume of oil loss can be calculated. 2988 m^3 (19.8% of the total oil) flows out in 8760 seconds (146 minutes) when the discharge coefficient is 0.6. Figure 8 shows the oil spill rate in the first phase according to analytical predictions and numerical simulations. Good agreement between the two sets of results is observed.

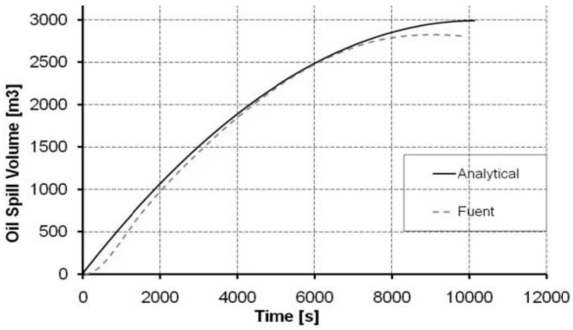

Figure 8. Oil spill volume versus time in the first phase

Phase 2: Two way flows

In the second phase, there is a combination of water inflow/oil outflow through the opening. In this phase, 2520 m^3 Oil spills to the sea in 279150 seconds (77 hours). Figure 9 shows and compares the oil spills versus time for two methods. The total oil spill in two phases is 5534 m^3 in 80 hours.

The volume and efflux rates of oil predicted with the suggested model are comparable to those obtained by means of numerical simulations.

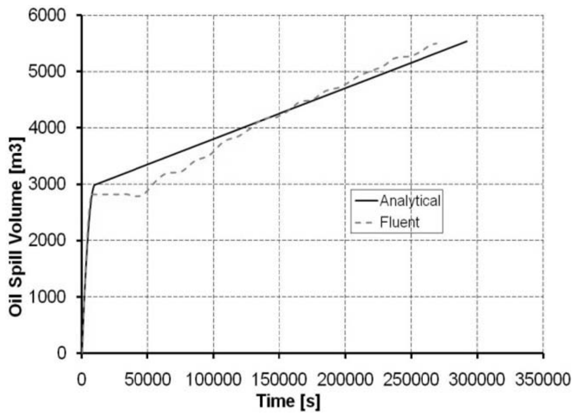

Figure 9. Oil spill volume versus time

Height of the puncture

The opening location on the side has a strong influence on the oil spill volume and rate. Figure 10 displays the effect of the puncture height on the oil spill volume in the both phases. If the opening is located in the bottom, the oil spill volume is zero in the second phase. As long as the puncture is below the waterline, the oil spill in both phase increases by increasing the height. The Oil spill volume increases by increasing the height of the puncture when the puncture is below the waterline In some cases, the opening is above the waterline. In these cases, the oil spills quickly to the sea just because of gravity. It ceases when the oil surface in the cargo tank reaches the opening as seen in Figure 10. The Oil spill volume decreases by increasing the height of the puncture when the puncture is above the waterline. Figure 11 presents the ratio of oil spill volume as a function of puncture height.

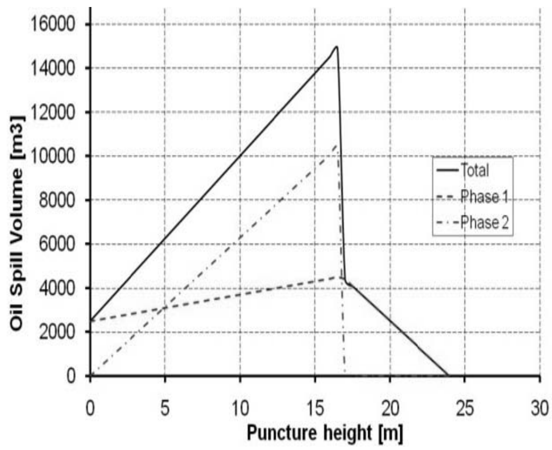

Figure 10. Oil spill volume versus the height of the opening in the side

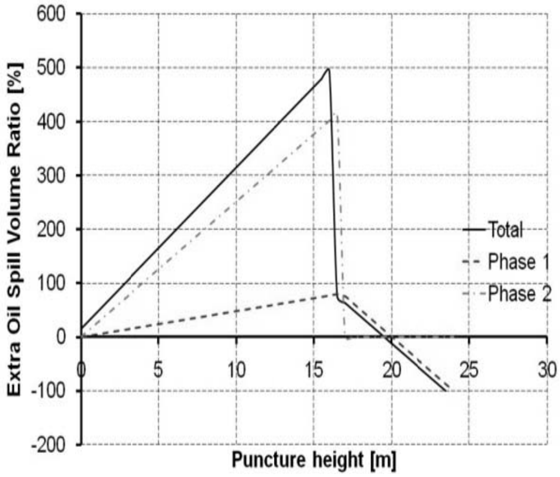

Figure 11. Extra oil outflow ratio vs. height of the puncture

Figure 12 shows the changes of the oil efflux rates by location of the puncture. It is seen that oil spills to the sea in a short time when the opening is either near the bottom or above the waterline.

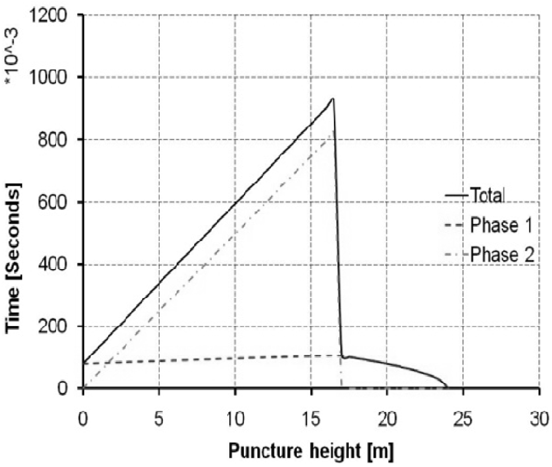

Figure12. Efflux time versus puncture height

Double side design

Double side designs are intended to provide protection for all collision scenarios, except those with the largest collision energy. Even for cases with serious damage, the double side structure should protect tanks in the periphery of the damage area.

Figure 13 shows the geometric parameters which are pertinent to the oil flows from double side design. It is assumed that rupture occurs in the side and has the shape of a rectangular prism. s is the opening area (l is the length and b is the width of the hole) and L and B are the length and breadth of the ruptured cargo tank, respectively.

It is assumed that neither the inner nor the outer hull has undergone any structural deflections. The blockage effect is considered only in relation to the opening area and discharge coefficient. This paper does not examine the flow through and around structural members in the tank. The effects of viscosity and turbulence are neglected. By neglecting the effects of viscosity, it is implicitly assumed that the gravitational forces are much greater than the viscous forces.

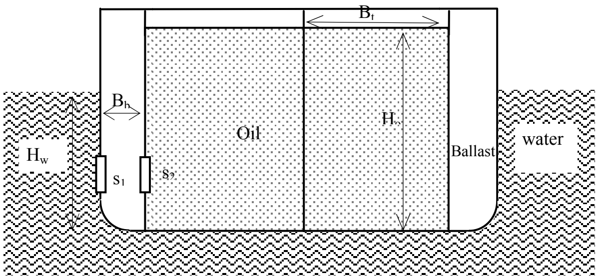

Figure 13. Geometry of the tanks, initial oil and water levels in double side design

In this model, it is assumed that the ballast tanks are empty. Oil flows out of the cargo tank to the ballast tank and water flows into the ballast tank from the sea. The oil and water jets occur simultaneously. There is no time lag between the initiation of the water and oil flow. The properties of oil and water do not change with time and are similar to those applied before.

The flow of oil and water is divided into three stages. In the two first stages, the flow is generated by different pressure around the openings. In the first stage, oil and water flow into the ballast tank. The second stage depends on the pressure in the cargo tank, the pressure in the ballast tank and the sea water pressure. These determine whether the oil runs out from the tank, or water flows into the cargo tank. The flow in the third one is caused by different densities of fluids. In the third step, a combination of water inflow/oil outflow through the opening may occur. When the opening is located in the side, there is a local imbalance due to different densities of the fluids, while there is hydrostatic equilibrium at the opening. The inflow-outflow through the opening must be equal from continuity, but the effective opening will gradually be reduced. This stage terminates when both holes are completely covered by water on both sides.

First stage: Filling of ballast tank

The oil and water convect through the ballast tank. The oil flows out from the cargo tank and water flows in from the sea into the ballast tank. The jet of oil is kept from leaving the hull by the jet of incoming water. This step ceases as soon as hydrostatic equilibrium occurs between oily-water and either sea water or cargo oil.

In relation to the interaction between oil and water in the ballast tank it assumed that oil and water are completely immiscible.

Oil inflow

The oil flows to the ballast tank with different trends. The outflow rate depends on the oil height in the cargo tank, draft of the ship, and height of mixture of oil-water in the ballast tank.

$$
\begin{aligned}
&If \quad h_{uow} \le h_h \rightarrow v_{ou1} = \sqrt{2g(h_{o1} - h_h)} \\
&If \quad h_{uow} > h_h \,\&\, h_{uw} \le h_h \rightarrow v_{uo1} = \sqrt{2g[(h_{o1} - h_h) - (h_{uow} - h_h)]} \\
&If \quad h_{uow} > h_h \,\&\, h_{uw} > h_h \rightarrow v_{uo1} = \sqrt{2g[(h_{o1} - h_h) - h_{uo} - (h_{uw} - h_h)\frac{\rho_w}{\rho_o}]} \qquad (29) \\
&Q_{O1} = \Delta h_{ou1} B L
\end{aligned}
$$

where h_{uow} is the height of the mixture of water and oil in the ballast tank, h_h is the height of the puncture, h_o is the height of the oil in the cargo tank, h_{uw} is the height of the water in the ballast tank, h_{uo} is the height of the oil and, Δh_{ou1} is the change in height of the oil in the cargo tank. The rate of outflow as a function of time can then be expressed as:

$$h_{o1} = \frac{c_{d1}^2 s_1^2 g}{2A_t^2} t_{o1}^2 - \frac{c_{d1} s_1}{A_t}\sqrt{2g(H_{o1} - h_h)}\, t_{o1} + (H_{o1} - h_h) \qquad (30)$$

$$Q_{o1} = A_t \Delta h_{o1} = -\frac{c_{d1}^2 s_1^2 g}{2A_t} t_{o1}^2 + c_{d1} s_1 \sqrt{2gH_{o1}}\, t_{o1}$$

The height of the oil in the ballast tank (h_{uo1}) is found as:

$$h_{uo1} = \frac{Q_{uo1}}{A_u} = -\frac{c_{d1}^2 s_1^2 g}{2A_t A_u} t_{o1}^2 + \frac{c_{d1} s_1 \sqrt{2gH_{o1}}}{A_u} t_{o1} \qquad (31)$$

Water inflow

The rate of water inflow to the ballast tank depends on the draft of the ship and the height of the oil-water inside the ballast tank while the ship's movements are neglected. By increasing the height of the mixture of oil-water, the rate of the water inflow will decrease. The rate of the incoming water can be obtained from the following equation:

$$
\begin{aligned}
&If \quad h_{uow} \le h_h \rightarrow v_{w1} = \sqrt{2g(d - h_h)} \\
&If \quad h_{uow} > h_h \,\&\, h_{uw} \le h_h \rightarrow v_{w1} = \sqrt{2g[(d - h_h) - \frac{\rho_o}{\rho_w}(h_{uow1} - h_h)]} \qquad (32) \\
&If \quad h_{ow} > h_h \rightarrow v_{w1} = \sqrt{2g[(d - h_h) - (\frac{\rho_o}{\rho_w} h_{uo1} + h_{uw1} - h_h)]}
\end{aligned}
$$

where d is the draft of the damaged ship. The height of the oil in the ballast tank is a function both of time and the height of the oil inside the cargo tank. In order to solve this equation, time domain simulations are performed. At each time step, the height of the oil is calculated, and then the height of the water is subsequently computed. The height of the water versus time is given by:

$$h_{uw1} = -(\frac{c_{d2} s_2}{A_u})^2 \frac{\rho_{ow} g}{2.\rho_w} t_{uw1}^2 + \frac{c_{d2} s_2 \sqrt{2g(d - h_h)}}{A_u} t_{uw1} \qquad (33)$$

and;

$$Q_{uw1} = -\frac{(c_{d2} s_2)^2 \rho_{ow} g}{2\rho_w A_{u1}} t_{uw1}^2 + c_{d2} s_2 \sqrt{2g(d - h_h)}\, t_{uw1} \qquad (34)$$

This stage is terminated once hydrostatic equilibrium between either the oil-water mixture and oil or water is attained.

Second stage: outflow and inflow to the ballast tank

The second stage depends on the height of the oil in the cargo tank, the ship's draft and the mixture of the oil-water in the ballast tank. Two different states may develop:

State 1

In the first state, the hydrostatic oil pressure at the inner opening (s_1) is greater than the hydrostatic pressure of the mixture of oil and water. If it is assumed that oil and water are immiscible, oil will run out of the cargo tank into the ballast tank and increase the hydrostatic pressure inside this tank and consequently push water or oil out to the sea.

State 2

In the second state, seawater flows into the ballast tank and oil or water flows into the cargo tank because the hydrostatic seawater pressure is greater than the pressure of the mixture of oil and water at the outer bottom opening. It is obvious that for the second state, there is no oil spill.This stage ceases as soon as second hydrostatic equilibrium occurs.

Third stage: Two way flows

The reason for oil outflow and water inflow in the third stage is different density of the fluids. This stage depends on the height of water inside the ballast tank and cargo tank. If the density of liquids is different at both sides of the holes, there is a combination of water inflow/oil outflow through the openings. The inflow-outflow through the openings must be equal from continuity reasons, but the effective opening will gradually be reduced.

Outer hole

Whereas the external side of the outer hole is always water, the height of the water in the ballast tank has a major impact on the flows. If the height of the water in the ballast tank is less than the height of the puncture, two way flows may happen. The water/oil flow to the ballast tank ceases when there is water on both sides of the two holes. The velocity of oil outflow/water inflow through the outer hole can be obtained:

$$If \quad h_{uw} < h_h \rightarrow v_{w2} = v_{o2} = \sqrt{2g\frac{(\rho_w - \rho_o)}{\rho_w}|y|} \tag{35}$$

y is the height of the stream surface for each flow, h_{uw1} is the height of the water in the ballast tank in the previous step. The flow will cease when there is water on both sides of the break. The oil outflow in this phase can be given by:

$$Q_{o3} = B_b\, L\,(h_h - h_{uw1}) \tag{36}$$

where B_b, L are breadth and length of the ballast tank and h_h is the height of the opening from the bottom and h_{uw1} is the height of the water in the ballast tank in the previous stage. The outflow time in the second phase is given by:

$$T = \frac{Q_{03}}{C_d s\, v_{o2}} \tag{37}$$

Inner hole

Whereas the fluid on the internal side of the inner hole is always oil, the height of the water in the ballast tank has a significant influence on the flow. If the height of the water in the ballast tank is higher than the height of the puncture, two way flows may occur. In this condition, there is a local imbalance due to different density of the fluids in the inner holes as well.

The water/oil flow to the ballast tank ceases when the height of the water in the cargo tank is equal to the height of the inner hole. The velocity of oil outflow/water inflow through the inner hole can be obtained from:

$$If \quad h_{uw} \geq h_h \,\&\, h_{cw} < h_h \rightarrow v_{w1} = v_{o1} = \sqrt{2g\frac{(\rho_w - \rho_o)}{\rho_w}|y|} \tag{38}$$

where y is the height of the stream surface for each flow, h_{uw} is the height of the water in the ballast tank, h_{cw} is the height of the water in the cargo tank in the previous step. The flow ceases when there is water on both sides of the inner break. The oil outflow in this phase is given by:

$$Q_{o4} = BL\,(h_h - h_{cw1}) \tag{39}$$

where B, L are breadth and length of the cargo tank, h_{cw1} is the height of the water in the ballast tank in the previous step.
The outflow time in the second phase is given by:

$$T = \frac{Q_{02}}{C_d s\, v_1} \tag{40}$$

Case study, double side design
Analytical Methods

In this case, there are rectangular openings 4 meter above the bottom of the tank. The opening is 1 meter long and 10 centimetre high.

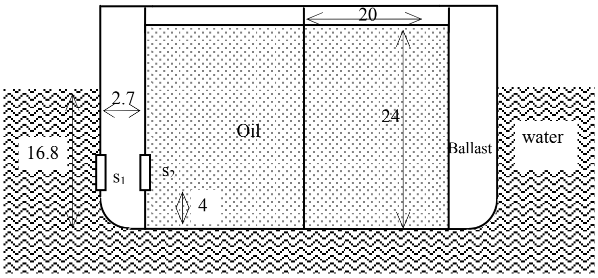

Figure 14. Principal dimensions of FPSO and damaged tank

First stage: Filling of ballast tank

In the beginning, the ballast tank is empty and oil and water flow in. Figure 15 shows the oil and water velocities through the two openings. The oil and water rates are constant if the free surface of mixture of oil and water in the ballast tank is below the openings. When the height of the mixture of oil and water is more than the height of the openings, the oil and water inflow rates decrease with time. In this case, at the end of this step, hydrostatic equilibrium takes place between the mixture of oil-water in the ballast tank and sea water.

The height of the oil and water in the ballast tank are shown in Figure 16. 1060 m^3 oil and 550 m^3 water flow into the ballast tank during 20 minutes.

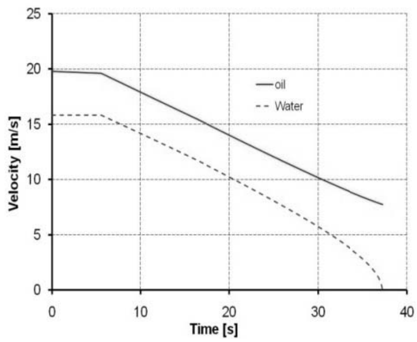

Figure 15. Oil and water flow rates through two openings

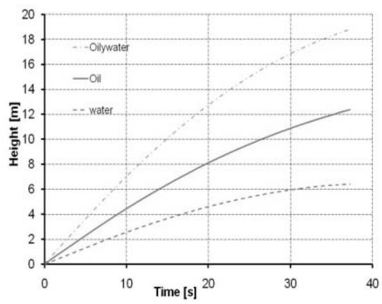

Figure 16. Height of water and oil in the ballast tank (first step)

Second stage: outflow and inflow to the ballast tank

The first stage ends once hydrostatic equilibrium occurs between sea water and oil-water in the ballast tank. But the hydrostatic oil pressure at the inner opening (S_1) is greater than the pressure of the mixture of oil and water in the ballast tank, so oil will run out of the cargo tank into the ballast tank. The inflow of oil to the ballast tank increases the hydrostatic pressure inside the ballast tank and pushes water or oil out to the sea. Figure 17. displays the height of the water and oil in the ballast tank in this step. As long as the height of the water in the ballast tank is larger than the height of the outer opening, the water runs out to the sea and the height of the oil increases.

This stage ceases as soon as hydrostatic equilibrium occurs for the second time.Figure 18 displays the outflow rate from the cargo tank to the ballast tank in both steps. It can be seen that at the end of this stage, the oil outflow velocity because of the gravity is zero. In the second stage, 1691 m^3 oil flows out to the sea in 154 minutes as shown in Figure 19.

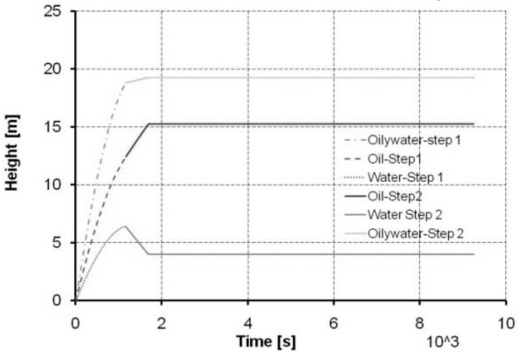

Figure 17. Height of water and oil in the ballast tank (first and second steps)

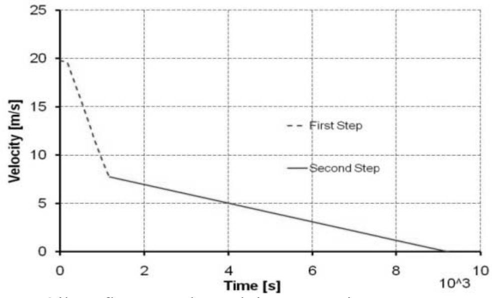

Figure18. Oil outflow rate through inner opening

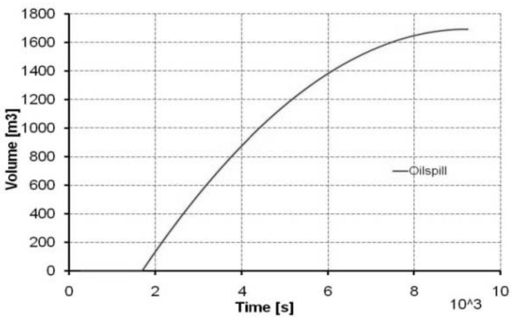

Figure 19. Oil spill volume

Third step: Two way flows

The reason for oil outflow and water inflow in the third step is different density of the fluids. The stage ceases when both sides of the openings are covered by water. At the end of the second step, both sides of the outer opening are almost covered by water. In this example, the water leaks through the inner opening into the cargo tank and oil flows out of the cargo tank simultaneously. The displacements of water and oil could also change the height of the water in the ballast tank. In order to maintain equilibrium, sea water is sucked into the ballast tank from the sea. In general, the height of the water and oil in the ballast tank is constant, while the height of the oil is reduced and the height of water is increased in the cargo tank. Figure 20. shows the height of the water in the cargo tank.

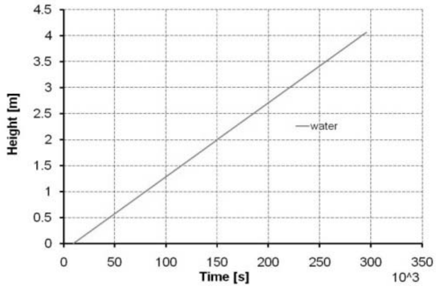

Figure 20. Height of the water in the cargo tank

Figure 21.shows the oil spill volume, 5550 m^3 oil flows out of the cargo tank in 4933 minutes. 4253 m^3 oil spills to the sea (28% of the total oil of the cargo tank) and 1297 m^3 oil retains in the ballast tank. Figure 22. and Figure 23. show the oil and water volume in the ballast and cargo tanks.

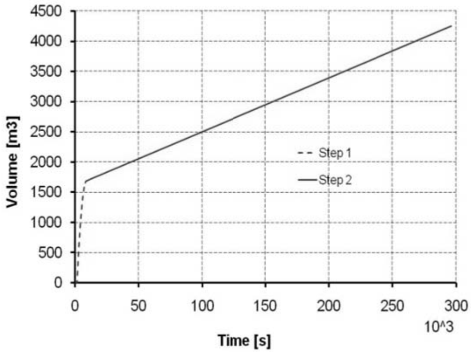

Figure 21. Oil spill volume

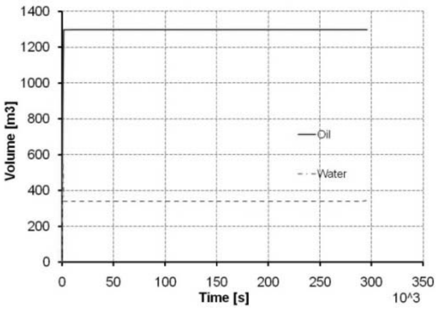

Figure 22. Oil and water in the ballast tank

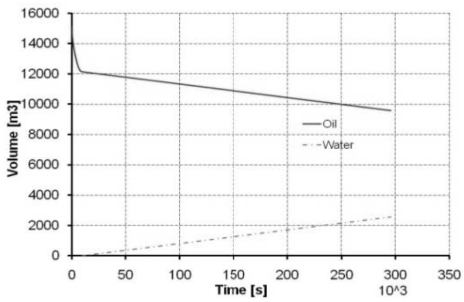

Figure 23. Oil and water in the cargo tank

Numerical Simulation

In order to test the validity of the suggested model with respect to oil spill predictions, a numerical simulation is performed with the computer software, Fluent (2007). The properties of the tanks, openings and liquids are similar to those of the previous examples.

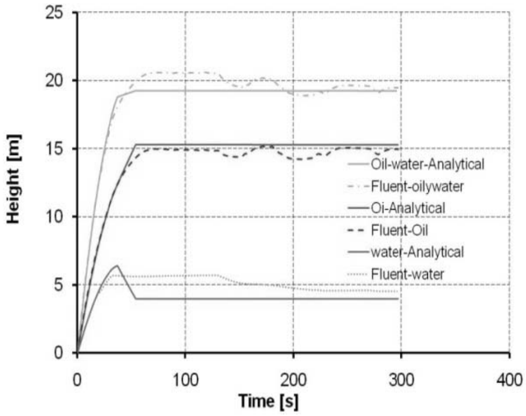

Figure 24. Comparison of oil and water in the ballast Tank

In Figure 24.the Fluent results are compared with analytical simulations. There is good agreement between results. In the analytical simulations, it assumed that the oil and water are perfectly immiscible. This assumption is the main reason why the results don't convergence completely at some points.Figure 25. compares the oil spill volume for the two simulations. It is seen that oil spills faster to the sea in the analytical simulation. Two causes are suggested. The first cause is the assumption about interaction between oil and water in the ballast tank. The second cause refers to the numerical model. In FLUENT, the released oil into the sea added to the water and increases the external pressure.

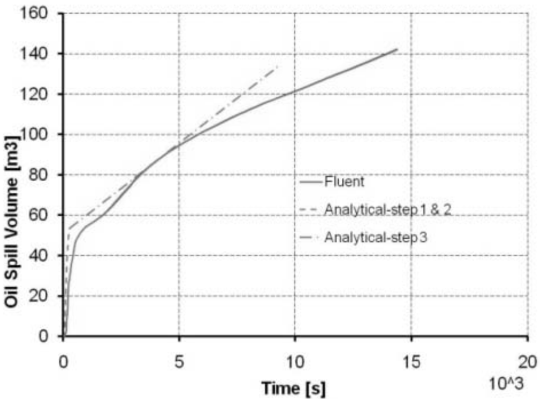

Figure 25. Oil spill volume

Conclusions

In this paper analytical methods are developed for analysis of the oil spill process for tanks with opening in the side. The crucial information is total oil spill and the temporal aspect. On the basis of calculations of oil-water flows, total spill and loss rate have been established. If the opening is in the side, the oil outflow process is different from the case with opening at the bottom. The location of the opening has a big influence on the oil spill volume and time. The oil spill volume and efflux time increase if the opening is in the side. The higher position of the opening, the more oil spills to the sea as long as the puncture is below the waterline. The effects of various hull configurations are analysed analytically. The results for different designs are confirmed with CFD simulations as well. The methods can also be extended to account for waves, tidal variations and buoyancy changes for the ship. The results show that some of the spilt oil from the cargo tank may be retained in the ballast tank for double side designs. The amount of oil captured depends on the damage size, and ballast tank space. The mixture of oil and water in the ballast tank delays oil drainage and effectively increases the oil spill time.

Acknowledgement

The present work is carried out within the scope of the program "ScenaRisC&G" at NTNU which is funded by the Norwegian Research Council. The support of the Research Council is gratefully acknowledged.

References:

FLUENT Inc., 2003 FLUENT Inc., 2003. FLUENT 6 User's Guide.

Fthenakis V.M. and Rohatgi U.S., A model of Liquid Releases from a Submerged Vessel, Journal of Loss Prevention, 12, 437-449, 1999.

M. Fingas, "The Basics of Oil Spill Cleanup", (Ed: J. Charles), 2. nd. ed.,. Lewis Publishers, Boca Raton, FL, USA 2001.

National Research Council, 1991,"Tanker Spills - Prevention by Design," National Research Council, National Academy Press, Washington, D.C.

Schneekluth, H., Bertram, V., "Ship Design for Efficiency and Economy – Second Edition", Butterworth-Heinemann, 1998.

Tavakoli, M.T., Amdahl, J., Ashrafian, A., Leira, B., 2008. "Analytical predictions of oil spill from grounded cargo tankers", Proceedings of the ASME 27th International Conference on Offshore Mechanics and Arctic Engineering, Estoril, Portugal.

Tavakoli, M.T., Amdahl, J., Leira, B., 2009. "Investigation of interaction between oil spills and hydrostatic changes", Proceedings of the ASME 28th International Conference on Offshore Mechanics and Arctic Engineering, Honolulu, USA.

T.K. Fannelop, "Fluid Mechanics for Industrial Safety and Environmental Protection", Elsevier, Amsterdam, 1994.

Evaluation of Critical Grounding Incidents

Bernadette Zipfel and Eike Lehmann

Hamburg University of Technology

Abstract:
A method is introduced to quickly measure the total bending moment and shear force for any ship due to soft groundings. Therefore the ship design program *e4* and the FE program *Ansys* are used and coupled. The grounding points respectively areas are combined with different load cases. These combinations are being considered for different water levels due to tide. The critical combinations that lead to an exceedance of the maximal allowable bending moment and shear force according to classification societies can be determined. The ship is modelled as rigid body and the sliding phase is not considered. The presented method is verified through existing formulas. Also the acting forces and moments as well as the sections at risk can be identified. The method is exemplary applied for a container vessel.

Introduction

The focus is being at soft grounding which happened more frequently in the last years. Especially because ship dimensions are continuously growing and the demurrage is reduced, the manoeuvring room is smaller in harbours. Grounding accidents can lead to the loss of human lives, severe environmental consequences and economical loss. Therefore assessing the influence of the additional forces and moments on the ship structure resulting from grounding is of main interest. For a pontoon, Östergaard et al. [6] developed formulas to calculate the additional vertical force and the bending moment caused by strandings. Pedersen [5] as well gave formulas for the additional shear force and the ending moment. He assumed that the breadth is constant over the length and that the waterplane area does not change while emerging. Lehmann et al. [4] published a formula to estimate the additional bending moment only at the main frame of any ship.

A method is developed to calculate the total bending moment, shear force and heeling angle due to grounding for any ship depending on the load case, the grounding point/area and the surface drawdown. The purpose is to find the critical combinations of grounding point/area, surface drawdown and load case which lead to an exceedance of the global bending moment and shear force requested by classification societies or/and lead to instability in the final position.

Furthermore the value of the additional forces and moments caused by grounding shall be determined. The method is performed for a container vessel.

Method

It is assumed that the ship does not suffer important damage between the initial contact with the ground and the final laying position.The hull behaves predominantly as a rigid body. Therefore the immersion of bow and stern when the ultimate resistance of the girder is reached is neglected.

A panmax container vessel with different load cases is chosen. Grounding of the vessel at certain points/areas including surface drawdowns due to tide is simulated with the ship design program *e4*. Then the resulting load forces and water pressure are applied onto a beam modelled in the finite element program *Ansys 11.0*.

As a result of the modelling of a predefined load case the total bending moment and the shear force caused by a grounding incident and changes in water level can be determined.

Dimensions and Load Cases of a Vessel

The relevant dimensions of the chosen vessel *Panmax-J* are given in table 1. *Panmax-J* is a ship design and fully implemented in *e4*.

Table 1: Dimension of *Panmax-J*

Length L_{oa}	294.1 m
Length L_{pp}	285.6 m
Breadth B	32.2 m
Height D	21.8 m
Design Draft T_d	12.04 m
Block Coefficient c_B	0.656
Mainframe Coefficient c_M	0.98
Speed v	24 kn

Three load cases are considered: the arrival (A), the ballast (B) and the departure case (C). All load cases are typical for estuary voyage. In the arrival case the ship has its design draft. Figure 1 shows the weight distribution, shear force and bending moment calculated for this load case at the centreline.The weight distribution is required for the FE calculations. *e4* gives all relevant weights as a line load distribution at the centreline.

During the ballast voyage the ships' draft is 6.26m. This load case has the largest bending moment and defines therefore the moments for the main frame design.

The vessel floats on the design draft while departing from a port. The still water bending moment is the smallest compared to the other two load cases.

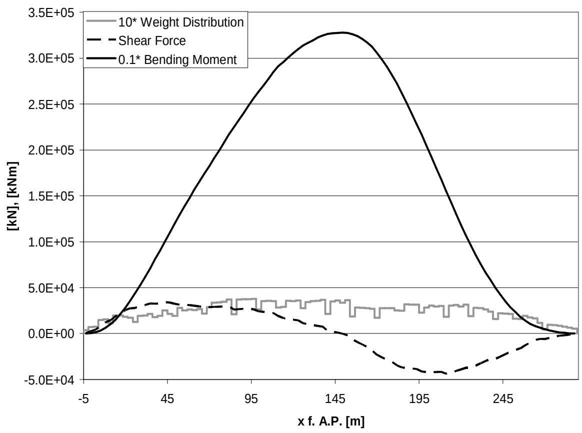

Figure 1: Load Case A: Weight Distribution, Shear Force and Bending Moment

Grounding Calculation in *e4*, Grounding Position and Tide

A subroutine was implemented in *e4*. So the user defines the position of grounding, surface drawdown and if the trim and the heel are fixed or free. The method generates a sheet of hydrostatic curves. Here the trim and the heel are always set free. They are automatically determined, so that the moments relative to the grounding location are equalized, see [3].

For each new floating condition, a sectional area curve is generated. The buoyancy at the centreline is converted in a line load distribution by integration of the sectional area curve.

The following table 2 gives an overview of the calculated cases.

In each grounding case the water level is changed. The initial position is calculated (no grounding, no tide) and then the surface is drawn down in one meter steps to a total change of five meters.

Table 2: Grounding Cases

Case	Description
A1	load case A, different grounding points, always y=0m
A2	load case A, different grounding areas, always y=0m
A1y	load case A, different grounding points, always y=8m
B1	load case B, different grounding points, always y=0m
C1	load case C, different grounding points, always y=0m

Finite Element Model

The total bending moments and vertical forces due to the grounding cases are calculated in *Ansys*.

The ship is modelled as a beam. The forces resulting from weight and buoyancy are applied as line loads onto the beam. The line load distribution from the floating condition generated in *e4* is in a ship-fixed coordinate system. For a correct FE calculation, the distribution should be in a ground-fixed reference system. A test with a pontoon (L=100m, B=1m, T=20m, trim angle=5°) reveals that the difference of the buoyancy distribution in a ship-fixed and a ground-fixed system are marginal. A difference in the distributions only occurs at the first meter of one end. After the first meter the difference is less than 0.4%. For a real ship, the difference is insignificant since ships have proportionally the fewest buoyancy at the bow and the stern.

The correct moment of inertia of the beam is not required for the method, because only the moments and forces are examined. For the cases A1, B1 and A1y five degrees of freedom are fixed at the grounding point. Only the rotation around y is free. Whereas the grounding area is modelled with springs to simulate an elastic foundation. The stiffness of the springs does not influence the result and is chosen to one.

In all cases a spring with a stiffness of one is placed at each end of the beam to prevent rigid body motions. The reaction forces in the springs are low and they do not have an influence on the results. A drawing of the beam and its boundaries is presented in figure 2 for each grounding case. The coordinate system is plotted and the vessel is sketchily shown in order to reach more clearness.

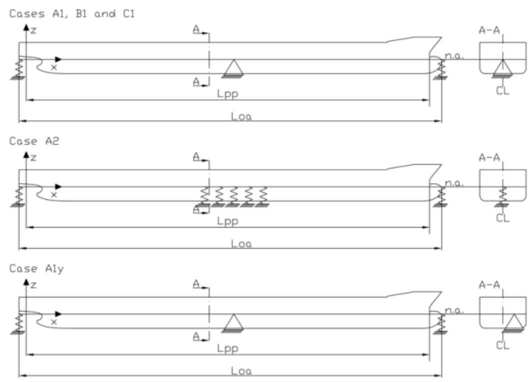

Figure 2: Beam (Idealized Ship)

Results of Method

Load case A is chosen for most calculations because its still water bending moment lies between the one of load case B and C.

Ground position is measured from aft perpendicular (A.P.). The cases A2, A1y, B1 and C1 are compared to case A1. For each case, the bending moments and shear forces for the five water levels are presented. The maximal allowable bending moments and shear forces which are determined according to the rules of Germanischer Lloyd (GL) [2] are always plotted with a dashed line as reference curves. The reference curves include the reserve between the still water and the seagoing conditions of the structure. The grounded vessel is probably not subjected to wave loads, [1],[5]. So if the curves are exceeded, the structure will take severe damage.

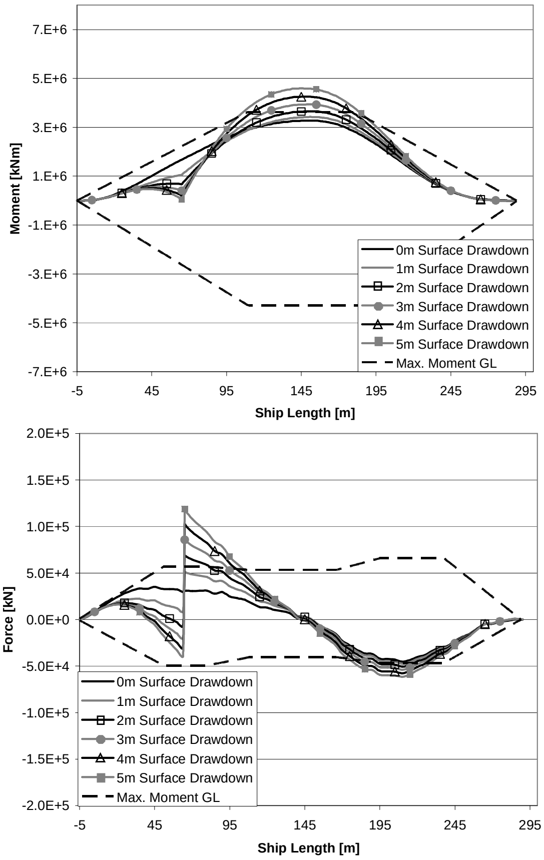

Figure 3: Bending Moments and Shear Forces due to Grounding at 65m A.P. (Case A1)

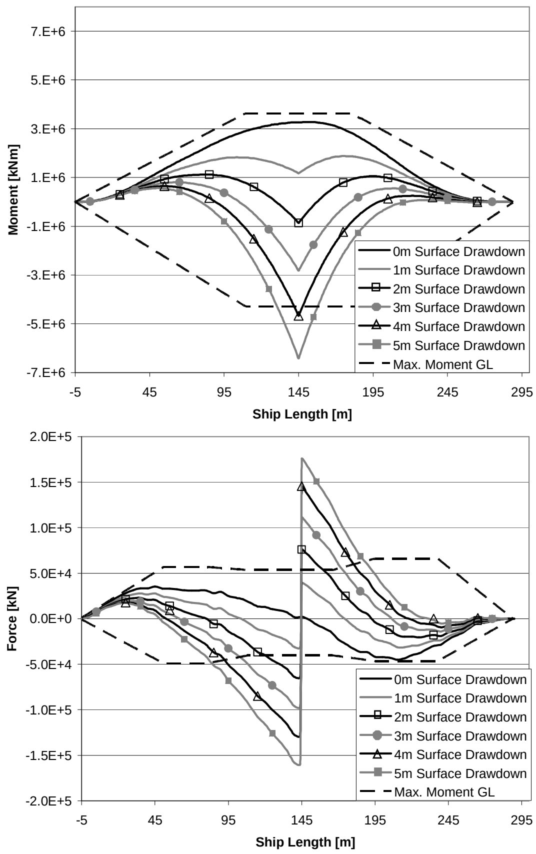

Figure 4: Bending Moments and Shear Forces due to Grounding at 145m A.P. (Case A1)

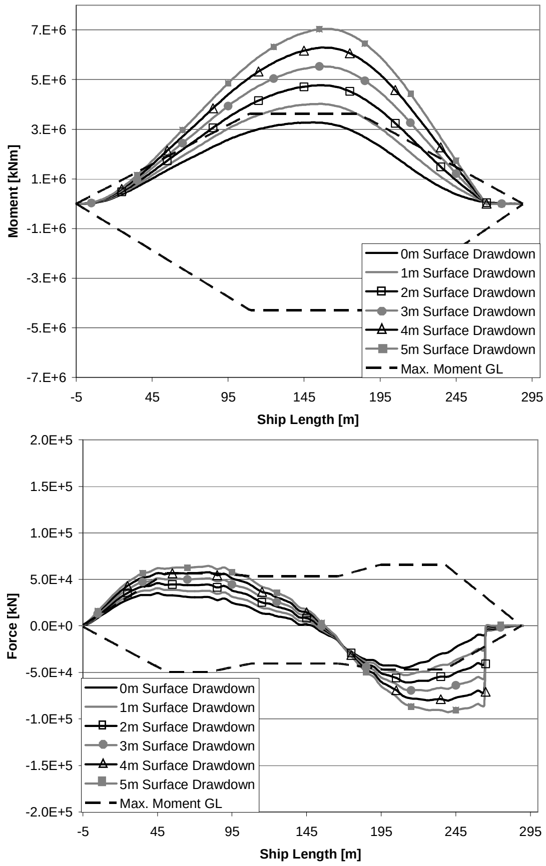

Figure 5: Bending Moments and Shear Forces due to Grounding at 265m A.P. (Case A1)

Grounding Case A1

Figures 3 to 5 exemplarily show the total bending moments and shear forces due to grounding at 65m, 145m and 265m A.P. for each surface drawdown. Except for four positions, most of the total bending moments exceed the allowable moment after GL. Only for running aground at 85m, 105m, 165m and 185m A.P., the moments of all water levels stay inside the envelope although they are reduced at the stranding position.

When the vessel strands in the area of the aft body (between -5m and 25m) or the fore body (between 225m and 285m A.P.), all tide levels lead to an exceedance of the maximal moment according to GL amidships. Accidents for two to five meters of surface drawdown which occur at 45m, 65m and 205m A.P. lead to an exceedance of the allowable bending moment. Running aground around midship section (125m and 145m) produces maximal bending moments for water drawdowns of 4m and 5m that lie outside the envelope (see fig. 3).

The highest positive bending moment out of all calculated positions occurs for grounding at the bow (285m: 7.3E6 kNm and 265m: 7.1E6 kNm, see fig.5).

The moment is measured amidships. However the effect is less for stranding at the stern (-5m: 6.3E 6kNm and 5m: 6.2E6 kNm) than for stranding at the bow. Due to stranding at 145m A.P., the maximal negative moment occurs with -6.4E6 kNm (see fig. 4). The shear force at the grounding position is remarkable high compared to the force in the initial floating condition. The effect of running aground can clearly be seen for every position by the large jump of the force value (see fig. 3 to 5).

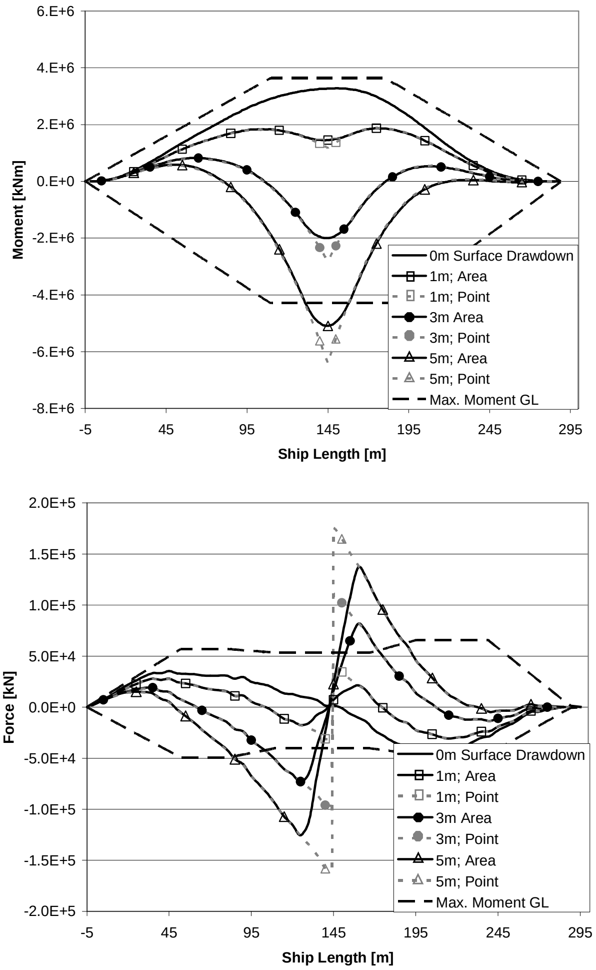

Figrue 6: Bending Moments and Shear Forces due to Grounding at 145m A.P. (Case A2

The whole course of the shear force also changes due to grounding. The maximal allowable vertical shear force according to GL is exceeded for each grounding incident and almost every water level. Just for one meter of surface drawdown and grounding at 65m, 105m, 125m and 145m A.P, the shear force stays inside the envelope (see fig. 3 and 4). The shear forces not only exceed the allowable value directly at the grounding position but also beyond it. Especially when the vessel grounds in the fore or aft body, the shear force is high at the area of the other end. However the maximal shear force often occurs at the same location as the maximal bending moment which takes place at the grounding position.
Stranding at 145m generates the highest shear force of 3.35E5 kN for 5m of surface drawdown out of all calculations. This is 100 times more than the shear force in the initial floating condition (see fig. 3).

Grounding Case A2

In grounding case A2 the reaction force is constantly distributed over 30m (ca. 10% of L_{oa}).
Figure 6 compares the total bending moments and shear forces for stranding at the area of 130-160m A.P. to grounding at the point 145m A.P. for three different tide levels.The bending moments and shear forces are explicitly smaller than for grounding at one point around midship. The average deviation between the moments of case A1 and case A2 measured at 145m A.P. is 31.93%.However the shear forces differ 30.07%. The reduction of forces and moments amidships decline for grounding in the area of the fore or aft body. The difference at 143m A.P. between point and area is only 2-2.5%. The deviation at the grounding position is still very high.

Grounding Case A1y

Stranding outside of the centreline primarily produces a heeling moment. The force due to stranding is small. Hence the resulting moments and forces do not differ much from the initial floating condition before grounding.

Table 3: Force, Heel and Trim Angle for Grounding at x=145m, y=8m

Δt	T_{AP} [m]	trim [m]	heel [m]	F_G [kN]
1	11.858	-0.007	5.86	7198.578
2	11.519	0.105	11.063	12397.878
3	11.083	0.249	15.767	17212.626
4	10.581	0.395	20.081	22353.066
5	10.026	0.536	24.084	28139.004

Table 3 gives the grounding force F_G, the trim and the heel angle for running aground at the point x=145m A.P. and y=8m.
In this case stability is the problem. The structure is only loaded with low forces and moments compared to case A1. Figure 7 reveals that the grounding force F_G of case A1 is ten-times higher than in case A1y.

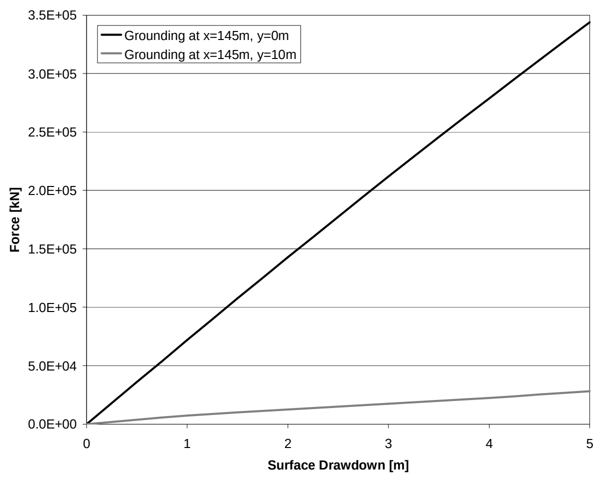

Figure 7: Grounding Force F_G: Case A1 vs. A1y

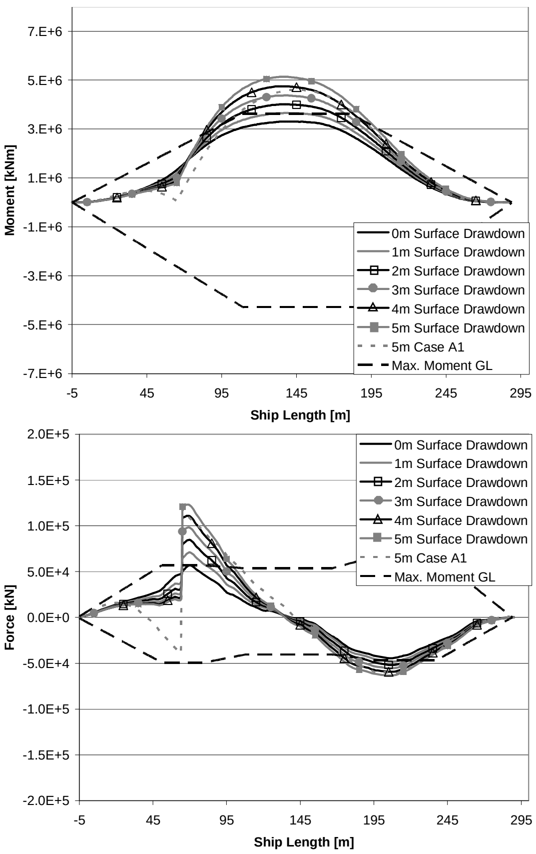

Figure 8: Bending Moments and Shear Forces due to Grounding at 65m A.P. (Case B1)

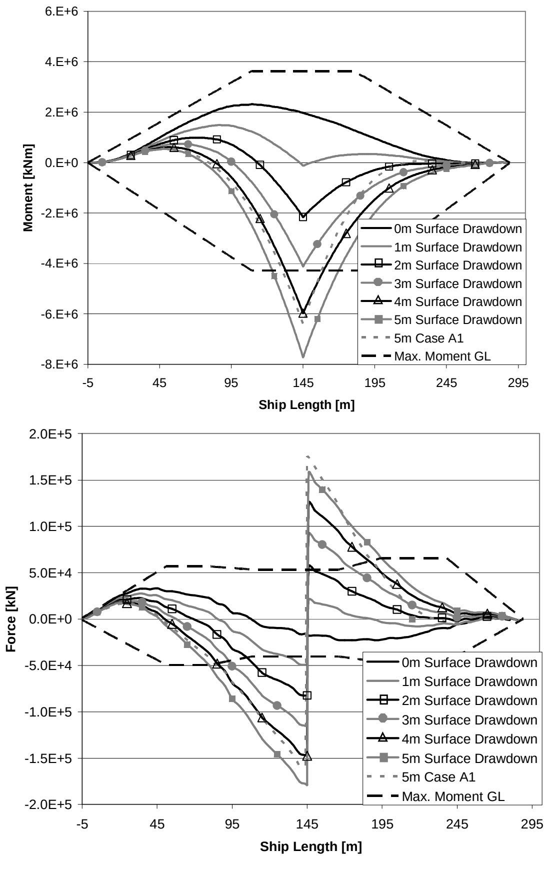

Figure 9: Bending Moments and Shear Forces due to Grounding at 145m A.P. (Case C1)

Grounding Case B1

When running aground at the aft part of the vessel the bending moments are higher than in case A1, see figure 8. An average deviation of 10.15% is measured at $\frac{L_{pp}}{2}$=143m. The shear forces are higher (10.52%) at the ground point but the jump is much smaller than in case A1.

If the ship strands amidships or in the fore body area, the moments and forces are clearly smaller. Especially for grounding at 145m A.P., all moments of case B1 are less than half the value of the moments in case A1. For stranding at 265m, the moments from case A1 are 15% higher amidships.

Grounding Case C1

In case C1 the moments and forces are higher than in case A1 when the vessel grounds amidships, see figure 9. For running aground in the area of the fore or aft body, the bending moments and the shear forces become smaller compared to case A1.

Verifying the Method

The grounding case A1 is also calculated with existing formulas of Lehmann et al. [4] and Östergaard et al. [6] to verify the method. The additional bending moment due to grounding is calculated at three points: 5m, 145m and 265m A.P. At all points, five moments are achieved, one for every meter of surface drawdown. Therefore a total of 15 moments with each formula are assessed and compared to the results of the described method.

In order to achieve more clarity the additional bending moments due to grounding which are calculated with three different methods/formulas are classified as shown below:

- $M_Z(x)$: additional bending moment at all length meters after Zipfel
- M_L: additional bending moment at 143m A.P. after Lehmann
- $M_Ö(x)$: additional bending moment at all length meters after Östergaard, multiplied by the coefficient of water plane c_{Wp}, see [1].

To attain $M_Z(x)$, the still water bending moment from load case A (see fig. 1) is subtracted from the calculated total bending moment due to the relevant grounding position.

First $M_Z(x=143m)$ is compared with M_L and afterwards compared to $M_Ö(x=143m)$. In the following,

the deviation from M_L respectively $M_Ö(x=143m)$ to $M_Z(x=143m)$ will be discussed. The percental differences of the moments resulting from each water level are averaged for the considered stranding point. Lehmann estimates the additional bending moment at the main frame due to different grounding positions for ships.

The required coefficients c_{Wp} and c_M are given by Lehmann estimates the additional bending moment at

the main frame due to different grounding positions for ships.
The required coefficients c_{Wp} and c_M are given by Lehmann [4] (pp. 924) for different block coefficients c_B. For c_B =0.7 the coefficients are given to c_{Wp} =0.8 and c_M =0.83.
The average deviation between M_Z(x=143m) and M_L for all 15 moments is 3.64%. The value of M_Z(x=143m) is frequently higher.
The maximum difference for grounding at 145m A.P. amounts to 6.85%. Here M_L is a conservative estimation compared to M_Z(x=143m). When the ship strands at 5m A.P., the value of M_L is 3.37% less than M_Z(x=143m). The moments M_Z(x=143m) and M_L are almost the same (difference: 0.7%) for ground point 265m A.P.
In total, the moments after Lehmann do not differ much to the moments achieved by the here presented method.
Östergaard developed formulas to calculate the additional vertical force $V(L^*, \tau)$ and the additional bending moment $M(L^*, \tau, x)$ caused by grounding of a pontoon.
It is difficult to compare a pontoon with a slender vessel. Nevertheless, the formula of Östergaard shall be used since no other simple formulations exist for the given problem. So the formula of Östergaard is multiplied by the water plane coefficient c_{Wp}, see [1]. This makes it possible to partly include the effect of the real water plane. The correct coefficient depends on the draft and the trim. For each grounding point and water level, the value c_{Wp} is taken out of the hydrostatic tables from *e4*. The achieved moment is called $M_Ö$(x). The moment $M_Ö$(x) is an approximation of reality.
For all 15 moments, the average deviation between M_Z(x=143m) and $M_Ö$(x=143m) is 25.63%.
Stranding at 145m A.P. gives a huge and conservative difference of 39.02% compared to M_Z(x=143m). For a grounding accident at 5m A.P., the moments are 33.44% higher than M_Z(x=143m). Again the least deviation can be seen when the vessel runs aground at 265m A.P. but the values of $M_Ö$(x=143m) are smaller than M_Z(x=143m).

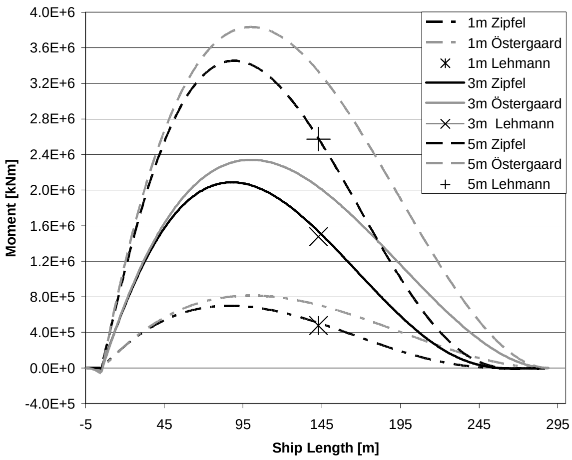

Figure 10: Additional Bending Moments due to Grounding at 5m A.P.

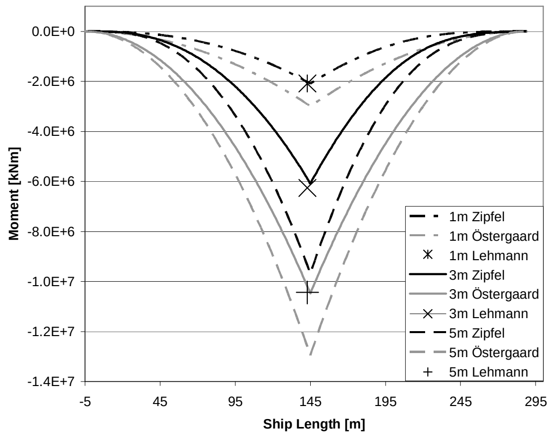

Figure 11: Additional Bending Moments due to Grounding at 145m A.P.

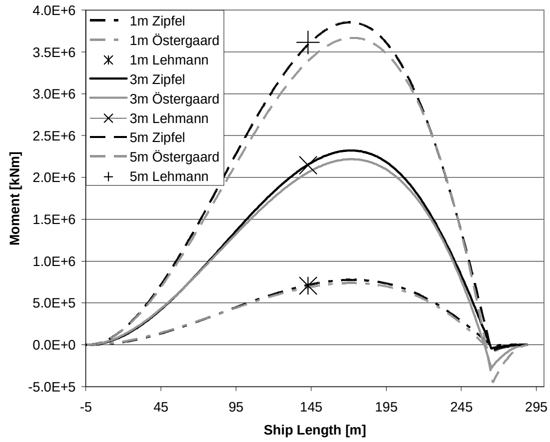

Figure 12: Additional Bending Moments due to Grounding at 265m A.P.

In figures 10 to 12 the additional bending moments M_Z(x), $M_Ö$(x) and M_L are plotted subject to three water levels (1m, 3m and 5m).
The formula of Östergaard does not produce good estimations for slender ships. Multiplying Östergaard's formula by the correct water plane coefficient reduces the moment. But the real buoyancy distribution of a slender ship is not included.
In all three cases the absolute value of the moments $M_Ö$(x) at the stranding point are explicitly higher than M_Z(x). For grounding at 145m and 265m A.P., the course of $M_Ö$(x) equals the course of M_Z(x) (see fig. 11 and 12). In the case shown in figure 11 the values are overestimated.
Östergaard's moments take good courses of the moment for running aground in the forward part (see fig. 12). Since the stern immerses which equals far more a pontoon than the bow. The value of the moment $M_Ö$(x=143m) amidships is less because at the grounding position the moment is overvalued. The vessels bow produces less overplus of buoyancy than a cuboid.
For grounding at 5m, the course achieved by Östergaard differs from M_Z(x) (see fig. 11). Now the bow immerses.
The bending moments M_Z(x), M_L and $M_Ö$(x) are also calculated for a full-bodied ship, because it equals more a pontoon. The bulk carrier *Bulker-B* as well is a ship

design (Studienarbeit Zipfel [7]) in *e4*. The bulker grounds at 10m, $\frac{L_{pp}}{2}$=110m and 210m A.P.

For the bulker, the formulas of Östergaard give better results than for the container vessel. The conservative estimation differs only 11.36% from M_Z(x=110m). The courses of $M_Ö$(x) for all position equal those of the method.
The moments M_L after Lehmann are then again almost the same as M_Z(x=110m).

Conclusion and Recommendations for Further Work

Conclusion

A method was introduced to measure the total bending moment, the shear force and the heel angle for any ship due to grounding. The critical combinations of grounding point/area, surface drawdown and load case that lead to an exceedance of the maximal allowable bending moment and shear force can be determined. The comparison with existing formulas showed that the presented method gives reasonable results which include all relevant effects as ship form and trim.
So the acting forces and moments as well as the sections at risk can be identified.
The method is quick and applicable for every existing vessel and every ship design.

The smaller the bending moment amidships resulting from the load case, the more the moment due to grounding in the middle of the ship leads to an exceedance of the allowable moment. However, when the vessel strands at the area of bow or stern and the initial bending moment is high, then a higher moment occurs amidships.

The shear force due to grounding for all positions is the most critical factor. Especially in combination with the maximal bending moment at the same position, the structure can take severe damage.
Not only the bending moment at the grounding position can be detrimental but also the moment amidships can exceed the allowable bending moment (for stranding in fore/aft body). This effect is not significantly reduced when the vessel runs aground on a sandbank.

Recommendations for Further Work

Knowing the acting forces and moments as well as the sections at risk, the next step is to reduce the simplification. The method can further be used to control the forces, moments and reactions.
At first, the ship should be considered as flexible. Therefore the structure of the whole ship or at least the interesting sections need to be modelled in the finite-element method. An adequate model with which includes the local and global failure by coinstantaneous guaranteeing a quick computing time, needs to be found.

Acknowledgements

The work was performed within the Research Training Group "Ports for Container Ships of Future Generations" located at Hamburg University of Technology. The project is financed by the German Research Foundation (Deutsche Forschungsgemeinschaft, DFG).

References

[1] Feddersen, G; Lehmann, E (2007). The Effects to a Container Ship due to Soft Grounding. ICCGS 2007
[2] Germanischer Lloyd (2009). Rules & Guidelines 2009; Chapter. http://www.gl-group.com
[3] Krüger, S (2009). Documentation of GROUND (in German). M-06, Hamburg University of Technology
[4] Meier-Peter, H; Bernhardt, F (2008). Compendium Marine Engineering. Seehafen Verlag
[5] Pedersen, PT (1994). Ship Grounding and Hull Girder Strength. Marine Structures, Vol.7
[6] Östergaard, C; Fricke, W; Pleß, E (1988). The Inland Vessel in Mouth of Rivers (in German). Jahrbuch der Schiffbautechnische Gesellschaft, Band 82
[7] Zipfel, B (2009). Design of a Bulk Carrier (in German). http://www.ssi.tu-harburg.de

Numerical simulation of transversely impacted, clamped circular aluminium plates

Richard Villavicencio, Leight Sutherland and Carlos Guedes Soares

Centre for Marine Technology and Engineering (CENTEC), Technical University of Lisbon, Instituto Superior Técnico, Lisboa, Portugal.

Abstract:
In this paper experimental and numerical results of a series of drop weight impact tests examining the dynamic response of fully clamped aluminium 5083/H111 circular plates struck transversely at the centre by a mass with a spherical indenter are presented. The impact velocity varied from 1.0 to 6.0 m/s. The plates showed no visible damage at the very lowest incident energies, but suffered both indentation damage and plastic deformation as incident energy was increased. The numerical modelling was performed using the LS-DYNA non-linear, dynamic finite element software. Both shell and solid element models of progressively refined mesh sizes were used and the results compared with the experimental data. The numerical calculations used can accurately predict the response of deflections, forces and absorbed energies, even for the models with coarse meshes. However, finer meshes and solid elements were required to obtain a satisfactorily accurate prediction of the deformed shape.

Introduction

Increased attention is being paid to the assessment of the collision strength of ship structures, and to developing more crashworthy designs. One approach to the problem is to use complex finite element models to calculate the energy absorbed during collision (Akita et al. 1972, Kajaste-Rudnitski et al. 2005). Another approach is to use simple models of energy absorption for each structural member and to calculate the absorbed energy as the collision progresses and the structural elements are subjected to large deformations (McDermott et al. 1974, Amdhal et al. 1995, Wang et al. 1997). The simplified models used to calculate energy absorption are based on rigid plastic theory, which has been shown to be appropriate for these predictions as described in Guedes Soares (1981), Jones (1989), Stronge and Yu (1993), and Yu and Chen (2000), among others. Concerning the behaviour of plates, a theoretical analysis that examines the dynamic plastic response of thin circular plates transversely and centrally struck by a mass with a conical head and a spherical nose has been summarized by Shen (1995). The analysis employs an interaction yield surface which combines the bending moment and membrane forces required for plastic flow. Approximate formulas for the load-deflection relationship of a rigid-plastic circular plate deflected by a rigid sphere were derived by Wang et al. (1998), which studied the behaviour at large deflection, neglecting the contribution from bending moments. Mechanics of the lateral indentation of a rigid sphere into a thin, ductile metal plate were studied by Simonsen and Lauridsen (2000) including experiments, analytical theories and finite elements calculations. The focus was the prediction of plate failure and the energy absorption until this point. Analytical theories were derived for the load-displacement behaviour of a plastic membrane up to failure. Experimental tests which examine the dynamic response and petalling failure of thin circular plates struck transversely by masses having conical heads were conducted by Shen et al. (2002) and the theoretical analysis which examines the petalling failure was proposed by Shen (2002).

The purpose of the present work is to compare the results of a series of experimental tests previously reported by Sutherland and Guedes Soares (2009) with a finite element analysis using different elements type and meshes size. The force-displacement curves of the different simulations are compared with the experimental results and the best approximations are selected for further calculations. The shape of the deformation is analyzed considering local indentation and global deflections.

Theoretical background

A theoretical analysis of the dynamic plastic response of thin circular plates struck transversely by non-blunt masses was proposed by Shen (1995) and is summarized as follows; The fully clamped circular plate in Figure 1 has a radius R, thickness H, mass density ρ and is struck by a mass G traveling with an initial velocity V_0 at the centre of the plate. After impact, the striker G is assumed to remain in contact with the plate. Therefore, the striker and the struck point of the plate have an initial velocity V_0 at the instant of contact and a common velocity throughout the entire response. The maximum total deformation W_t is divided into two parts: maximum local indentation W_i and maximum global deflection W. A quasi-static method is used to analyze the local deformation, while the global deflection is studied with a dynamic analysis. The local indentation and the central global deflection correspond to a common force magnitude between the striker and the impact point of the plate throughout the whole response. First the global deflection is calculated along with its corresponding force, and from this force the indentation is calculated. Thus, for example, the maximum force corresponds to the maximum centralglobal deflection and the maximum local indentation.

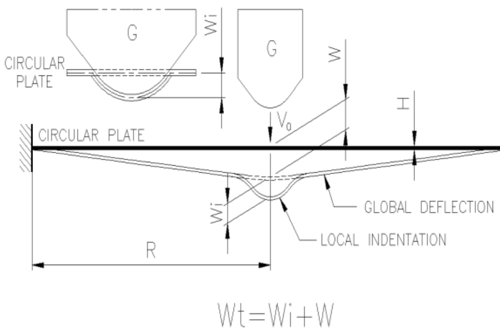

Figure 1: Clamped circular plate struck transversely at the centre by a mass.

The yield condition combines the bending moment and membrane force which cause the cross-section of a perfectly plastic structure to became fully plastic (Jones 1989). Material strain rate sensitive effects are considered with the aid of the Cowper-Simonds equation and Perrone and Bhadras approximation, which was further simplified by Jones (1989).

The indentation of the plate under the striker is observed to have the same shape as the head of the striker. It is assumed that any point in the un-deformed plate moves vertically without horizontal displacement in the deformed plate, as can be seen in the detail of Figure 1. For the global deflection the following two simplifications are introduced:

(a) The radial and circumferential membrane forces are equal and are independent of the radial coordinate.

(b) Plastic yielding is controlled independently by radial and circumferential bending moments and membrane forces.

In view of assumption (a) the normality requirement of plasticity associated with circumferential bending moment and membrane force is disregarded. Figure 1 shows the permanent total deformation of the plate, the shape of the un-deformed plate and the global deformation of the plate without local indentation. The local indentation plays an important role in the total response of the plate (W_i *and* W are generally of similar magnitude) and hence cannot be neglected.

Experimental details and summary of results

Impact testing was performed using a fully instrumented Rosand IFW5 falling weight machine. A small, light hemispherical ended cylindrical projectile was dropped from a known, variable height between guide rails onto clamped horizontally supported circular aluminium 5083/H111 plate targets. A much larger, variable mass was attached to the projectile and a load cell between the two gave the variation of impact force with time. An optical gate gave the incident velocity of the impact head, and hence the velocity, displacement and the energy it imparted could be calculated from the measured force-time data by successive numerical integrations, knowing the impact mass. The experimental set up can be seen in Figure 2. Specimen plates were 200 mm square and were fully clamped by four bolts between two thick 200 mm square steel plates with internal diameter D = 100 mm. The indenter was a hemi-spherically ended projectile of radius r = 5 mm. In order to investigate the effects of both global deformation and local indentation, tests were carried out for two plate thickness', 2.0 mm and 5.92 mm, (henceforth referred to as 'thin' and 'thick' respectively) using an impact mass of 3.103 kg and 4.853 kg respectively. Tests were carried out on virgin specimens for a range of impact velocities, from very low energies up to perforation where possible. Full experimental details and discussions of the experimental results may be found in Sutherland and Guedes Soares (2009).

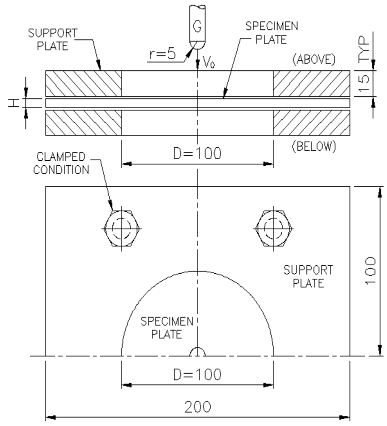

Figure 2: Circular plate specimen in clamped condition (dimensions in millimetres).

A representative sample of the full experimental results at low, medium and high incident energy for both thin and thick plates were selected for comparisons with the current numerical analyses, and are summarised in Table 1. The 'End' of the test is defined as when the contact force drops to zero, and occurs when the indenter first leaves the surface of the plate. Specimens suffering perforation were not considered here.

Table 1: Summary of experimental impact results.

Specimen	Impact Velocity (m/s)	Values at Peak Force Force (kN)	Defln (mm)	Energy (J)	Values at End Defln (mm)	Energy (J)
AL1-K	0.95	1.2	2.50	1.6	1.27	1.1
AL1-N	2.53	3.7	5.36	10.6	4.07	9.1
AL1-R	4.39	6.7	9.99	31.2	8.98	29.8
AL1-U	5.90	8.9	12.78	55.7	12.00	55.1
AL2-H	0.91	4.8	0.79	2.3	0.23	1.1
AL2-I	2.62	11.4	2.41	16.8	1.23	12.2
AL2-B	4.77	15.8	5.30	56.8	4.19	52.2
AL2-D	5.85	18.4	6.74	84.0	5.79	80.2

Numerical model

The computations were carried out using the LS-DYNA (version 971, Hallquist 2005) finite element package which is appropriate for non-linear explicit dynamic simulations with large deformations. The finite element model was designed with the following components (Figures 3 and 4): specimen plate, two support plates (one below and the other above the specimen plate) and the striking mass. The specimen plates were modelled with either shell or solid elements, the support plates with shell elements, and the striking mass with solid elements. The shell elements were 4-node with 5-integration points thought the thickness (Belytshko-Tsay formulation) and the solid elements were 8-node with 1-integration point (constant stress solid element formulation), both element formulations are the default in LS-DYNA.

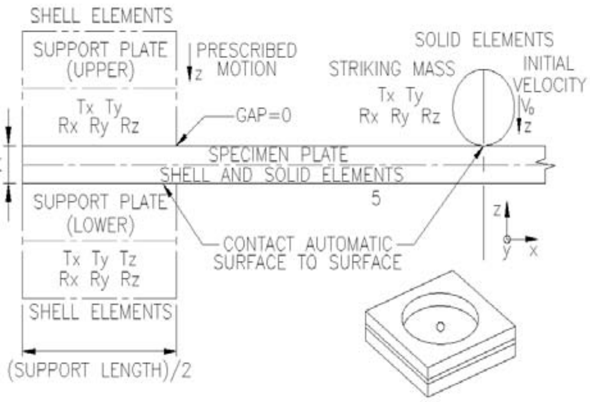

Figure 3: Details of finite element model.

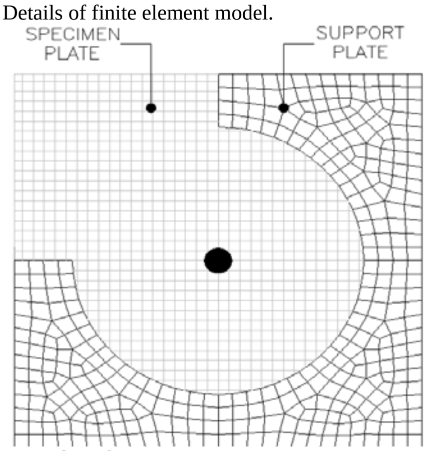

Figure 4: Typical mesh.

Mesh design

The type of element (shell or solid) and the mesh size used to model the plates were varied in order to optimise the agreement of the FE model with the experimental results. The meshing used in all cases was regular and square (Figure 4), meaning that the mesh was not finer neither at the point of impact nor at the supported perimeter. Initial calculations explored the use of different mesh configurations, some of them automatically generated and others with coincident nodes in the supports and radial orientation of the elements. Similar results were obtained in all cases and hence the simplest and cheapest mesh design was selected for all future calculations.The approach taken was to start with a mesh size equal to the plate thickness and then progressively decrease the mesh size until good correlation with the experimental maximum force and displacement results was achieved. It was also important to obtain a good approximation of the shape of the plate deformation, in terms of both local indentation and global deflection. The mesh size of the shell element models considered were 6x6, 4x4 and 2x2 mm for the thick plates (denoted by Shell6, Shell4 and Shell2 respectively), and 2x2, 1x1 and 0.5x0.5 mm for the thin plates (denoted by Shell2, Shell1 and Shell0.5 respectively). Care was taken to avoid an excessively high element side length to thickness ratio. The solid element model mesh sizes were 1x1x1mm for the thin plates (Solid1), and 2x2x2 and 1x1x1 mm for the thick plates (Solid2 and Solid1 respectively).

The finite element representation of the support plates was used to simulate the experimentally clamped boundary condition of the specimen plates using a relatively coarse mesh of shell elements with a side length of approximately 5 mm. The striking mass was modelled using solid elements since this simplified the definition of both the impact mass and the geometry, and in order to model the spherical geometry sufficiently accurately a mesh size of approximately 1.0 mm was chosen. The sphere was meshed to ensure that the face of a sphere element (as apposed to a single node 'corner') contacted with the plate, ensuring a more realistic simulation of the contact area.

The radius of the impacting mass is 5.0 mm, and hence the ratios of element size to indenter radius were 6/5, 4/5, 2/5, 1/5 and 1/10 for meshes with element side length 6, 5, 4, 2, 1 and 0.5 mm respectively. These ratios play an important role when the shape of the deformation is analyzed.

Boundary conditions

In the present finite element model the support plates simulate the boundary conditions of the specimen plate, compressing the specimen as occurred in the experiments (Figure 3). Only half of the support plate length compressing the specimen was modelled since this reduced the computational cost whilst previous numerical analyses showed that this did not affect the results. However, differences in the maximum displacement and absorbed energy were seen when the support plate thickness was reduced, and hence the full support plate thickness was modelled. No gap between the support plates and the specimen plate was modelled.

The lower support plate was constrained in all degrees of freedom (Figure 3). The upper support plate was constrained in all degrees of freedom except for vertical translation, because a prescribed vertical motion was imposed to compress the specimen plate to simulate the clamped condition. The value of the prescribed displacement was equal to $\varepsilon_y H/3$ (Ehlers 2010), where ε_y is the yield strain of the material and H is the thickness of the specimen. For the striking mass only the vertical translation was free, in which direction the initial impact velocity V_0 was assigned.

Contact definition

The contact between the striking mass and the specimen plate and between the support plates and the specimen plate were defined as "Automatic Surface to Surface" (Hallquist 2005). A static coefficient of friction of 0.3 in both cases was used and a dynamic coefficient of friction of 0.1 was included in the contact between the striking mass and specimen plate (Ehlers et al. 2007, Ehlers 2010).

Material

Both support plates were modelled as a rigid material to ensure no deformation. The 'Mat.020-Rigid' was selected from the material library of LS-DYNA, assigning mild steel mechanical properties (Young's modulus 210 GPa and Poisson's ratio 0.3) and a mass density of 7850 kg.

The striking mass was modelled using the same rigid un-deformable material and mechanical properties as the support plates. However, since the falling weight assembly was modelled as a simple sphere, an artificially large density was used to give the same mass as used in the experiments. The mass densities were 6.5E+6 and 10.0E+6 kg/m^3 for the striking mass of 3.103 and 4.853 kg respectively (a factor of 1.035 was included to allow for the small volume error since the sphere was modelled with a finite number of discrete flat elements).

The definition of the specimen plate material is most important, and thus the mechanical properties of the material used in the finite element models were obtained from in-house tensile tests carried out on material cut from the same panels from which the impact specimens were taken, and are summarized in Table 2. The material selected from the library of LS-DYNA was 'Mat.024-Piecewice linear plasticity', which allows the definition of a true stress-strain curve as an offset table.

Table 2: Mechanical properties of aluminium 5083/H111.

Property	Units	Aluminium 2.0 mm	Aluminium 6.0 mm
Mass density	kg/m^3	2710	2710
Young's modulus	GPa	65	65
Poisson's ratio	-	0.33	0.33
Yield stress	MPa	125	145
Rupture stress	MPa	285	290

Since the engineering stress-strain curve does not give a true indication of the deformation characteristics of a metal, it is necessary to use the true stress-strain curve that represents the basic plastic-flow characteristics of the material. The true stress must be based on the actual cross-sectional area of the specimen, but the true strain measurement is measured directly when, as is the case here, strain gauges are used (Dieter 1986).

In the true stress-strain curve until the onset of necking (for most materials, necking begins at maximum load at a value of strain where the true stress equals the slope of the flow curve) the true stress σ_t and the true strain ε_t are expressed in terms of engineering stress σ_e and engineering strain ε_e by:

$$\sigma_t = \sigma_e(\varepsilon_e + 1) \quad (1)$$

$$\varepsilon_t = \ln(\varepsilon_e + 1) \quad (2)$$

The tensile tests of these particular aluminum plates showed that the true stress at maximum load is almost coincident with the true fracture stress, and also noting that very little necking was observed in the tensile tests, the exact true stress-strain curve can be used as input in the numerical models. The true and engineering stress-strain curves for each thickness are shown in Figures 5 and 6. Since for the experimental impact tests considered here only plastic deformation was observed, failure strain was not required to define the material of the specimen plates.

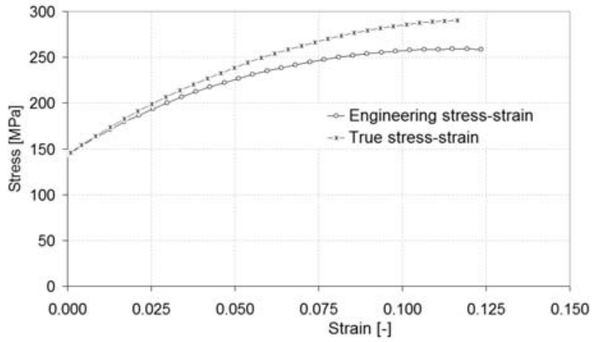

Figure 5: Engineering and true stress-stain curves (experimental). Thickness 5.92 mm.

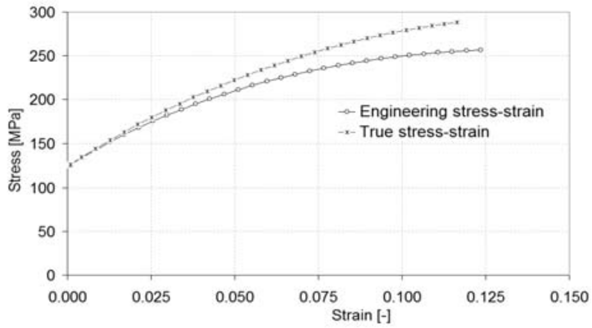

Figure 6: Engineering and true stress-stain curves (experimental). Thickness 2.00 mm.

The strain-rate sensitivity behaviour of materials in the finite element model may be included using the coefficients of the Cowper-Simonds constitutive equation (Jones 1989). However, published experimental results for aluminium alloy beams (Liu and Jones 1987) showed that they are essentially strain-rate insensitive, and for the circular plates considered here, including nominal strain-rate coefficients in the numerical simulations resulted in smaller displacements than seen in the experimental results. Hence, strain-rate sensitivity was not included in further numerical simulations here. It is important to note that for other materials, such as mild steel, the strain-rate sensitivity should be included (Liu and Jones 1987).

Tensile test simulation

As was mentioned in Section 4.4, since for the experimental impact tests considered here only plastic deformation was observed, failure was not required to define the material of the specimen plates. However, the experimental tensile tests used to obtain the material mechanical properties were modelled using LS-DYNA both in order to verify that the impact model gave the correct plastic deformation, and also to make an initial attempt at failure prediction. For a purely plastic response without necking or fracture, the plastic parameters of the material can be determined from the results of a tensile test. However, fracture and necking occur over a length which is much smaller than the side length of the elements considered here and so the elements used in the finite element model cannot capture such a local phenomenon, and so to model failure, LS-DYNA deletes elements when their average strain reaches a 'critical' value.

This 'critial' value must be calibrated against test data (since the F.E. models can not simulate the experimental failure event at a small enough scale) and is a function of the element size (Simonsen and Lauridsen 2000). The mesh sensitivity can be approached with an engineering method at the level of advanced industry practice (Simonsen and Lauridsen 2000) in which the 'critical' failure strain (in this case the average normal strain over the element) required to give the actual experimental material fracture strain is found through numerical simulations of the tensile tests using different failure strains and mesh densities. Here 'failure strain' denotes the strain value when fracture occurs.

In the numerical simulations, only the length of the tensile test specimens between the clamping edges was modelled (Figure 7) and the same mesh sizes used in the circular specimen plates (Shell elements) were considered. The translational degrees of freedom were restricted at one end and at the other end a constant displacement of 100 times the experimental speed was prescribed (Ehlers 2009). Default hourglass control was included. The true stress-strain curve used to define the material was the same as that used for the circular plate specimens (Figures 5 and 6).

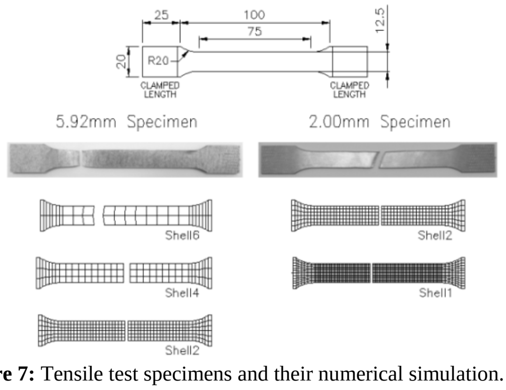

Figure 7: Tensile test specimens and their numerical simulation.

The material model for the tensile tests does not use a specific failure criteria in the purest sense, but the numerical simulation was 'calibrated' using the experimental data to give the 'critical' strain value (averaged over the element) that fitted the experimental results using a trial and error approach. For the tests carried out here, it was not difficult to estimate the first value of failure strain to be used since very little necking was observed in the experiments and thus the failure strain was close to the axial strain at the initiation of necking initiation. The force of the displaced nodes at the free end is obtained and this force plotted versus the applied prescribed displacement, and these values used to give the engineering stress-strain behaviour.

The results for different mesh sizes are presented in Figures 8 and 9 for thick and thin plates respectively. The 'critical' failure strain (used as input in the numerical model) represented in both graphs is 0.15. The dependences of the failure strain on the element size is evident from Figures 8 and 9 (a coarse mesh requires a minimum value of failure strain), showing that this parameter is not a true material property in this case. Most numerical simulations of tensile tests in the literature follow the engineering curve quite precisely until the point of necking independently of mesh size (even with relatively coarse meshes), but the post-necking behaviour is usually highly dependant on the mesh size (Simonsen and Lauridsen 2000, Tabri et al. 2007). For the aluminum 5083/H111 tensile tests carried out here, the stress at maximum load was almost coincident with the fracture stress and very little necking was observed (Figures 5 and 6). Hence, such post-necking modelling problems were avoided, and the plastic response could be equally well modelled using different mesh sizes.

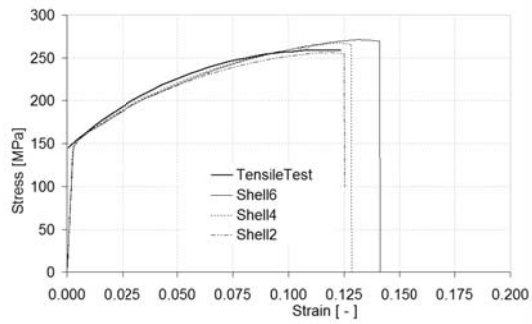

Figure 8: Numerical and experimental engineering stress-strain curves. Thickness 5.92 mm.

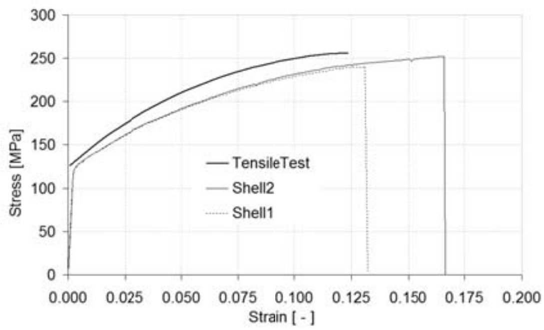

Figure 9: Numerical and experimental engineering stress-strain curves. Thickness 2.00 mm.

For the thick tensile test simulation, Figure 8 shows that all mesh sizes considered predicted well the plastic behaviour of the material. The fact that the Shell4 and Shell6 models overestimate the specimen failure strain show that a minimum value of the material failure strain would be required to be found for the coarser mesh sizes.

For the thin specimens the numerical simulation (Figure 9) for both mesh sizes considered give almost identical results, both giving approximately 8.0 % lower stress values than the experimental results. Again it is indicated that for the coarser mesh Shell2 model, a minimum value for the material failure strain should be obtained to give a more approximated response compared with the experimental results. It is worth noting that the numerical simulations all predicted a fracture perpendicular to the specimen axis whereas in the thin tests this fracture was inclined (Figure 7). This is due to the fact that the fracture process occurs at a molecular scale well below that of the mesh size, and may be due to adjacent layers of atoms sliding over each other, resulting in a shear failure.

Numerical results and comparison with experimental tests

Firstly various numerical models using the different mesh sizes and element type referred to in Section 4 were evaluated in terms of ability to predict the experimental results. In order to do this a 'high' and a 'low' velocity impact (Table 1, shaded rows) was modelled for each plate thickness. Figures 10 to 13 compare the experimental force-displacement curves with those from the finite element calculation. Then this information will be used to select the 'best' models to proceed to calculate the maximum force and displacement values for the whole range of experimental impact velocities considered here.

For the thick plates Figures 10 and 11 show that, for both velocities, the Shell2 model approximates well the experimental plastic response, and that the coarser meshed Shell4 and Shell6 are less accurate. For the solid element models very similar results were obtained using both mesh sizes, but in terms of force-displacement prediction they do not give better predictions than the computationally less demanding Shell2 model.

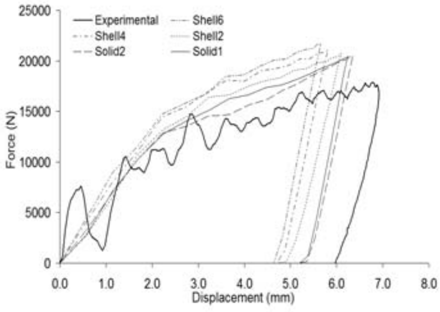

Figure 10: Force-displacement curves. Thick (5.92 mm) circular plates, impact velocity 5.85 m/s.

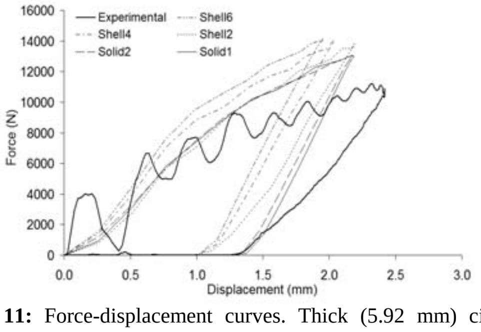

Figure 11: Force-displacement curves. Thick (5.92 mm) circular plates, impact velocity 2.62 m/s.

Again, for both impact velocities, the deflection at which this maximum force is reached is generally underestimated by the numerical models, consequently the maximum force is overestimated. Of the shell models, the Shell2 mesh gives the best prediction of this point, with both solid element models giving slightly better and very similar behaviour in this respect.

However, prediction of the impact response is not the only criterion; it is also beneficial to predict well the shape of deformation due to both local indentation and global deflection. Here it is relevant to remember that local 'indentation' can be thought of consisting of (i) local out of plane plate deformations (where the plate 'wraps around' the indenter) and also (ii) the actual indentation of the indenter into the thickness of the plate material.

Figure 14(a) shows that in this respect the Solid1 mesh gives a better definition of the shape of the deformation than does the Shell2 model. This is both because the finer mesh of the former is able to model more accurately the deformation around the indenter (c.f. (i) above), and because a solid element is able to model the change in thickness of the material due to the indentation (c.f. (ii) above).

Now considering the thin plates, Figures 12 and 13 show that all of the shell mesh sizes considered give a good representation of the plastic force-displacement behaviour, especially at the higher impact velocity, and that there is little to choose between them. The use of more computationally expensive solid elements gives a very good fit to the experimental data even at the low impact velocity, where the shell models over-estimate the force slightly.

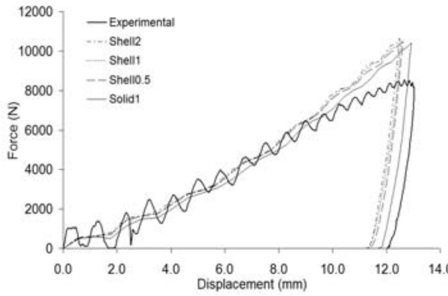

Figure 12: Force-displacement curves. Thin (2.00 mm) circular plates, impact velocity 5.90 m/s.

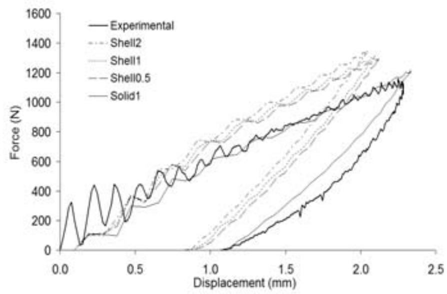

Figure 13: Force-displacement curves. Thin (2.00 mm) circular plates, impact velocity 0.95 m/s.

For the thin plates indentation is more significant in terms of out of plane plate deformation, but less significant in terms of indentation into the material thickness (Figure 14(b)). Hence, here the only requirement is a fine mesh to adequately model the local deformation, with shell or solid elements giving similar representations.

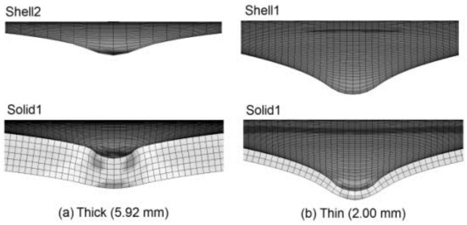

Figure 14: Shape of the deformation. (a) Thick (5.92 mm) circular plates, impact velocity 5.85 m/s. (b) Thin (2.0 mm) circular plates, impact velocity 5.90 m/s.

It should be noted at this point that though the experimental force-displacement curve is well but not always perfectly predicted by the numerical model, the time dependant curves of displacement and absorbed energy fit the experimental data very well.

The next step was to use the ‘best’ shell and solid models to simulate the remaining experimental impact velocities considered. As can be seen from figures 15 to 18 the models predict very well the maximum deflection and maximum force. It is also apparent that, *when considering maximum force and deflection values only*, there is little if any significant differences between the various models and hence little advantage in using a more computational expensive element model.

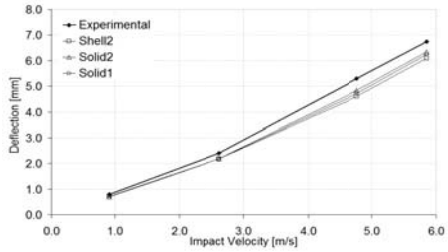

Figure 15: Maximum deflection vs. impact velocity. Thick (5.92 mm) circular plates.

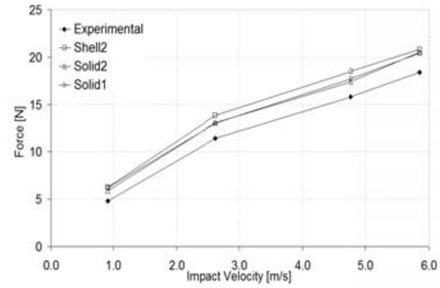

Figure 16: Maximum force vs. impact velocity. Thick (5.92 mm) circular plates.

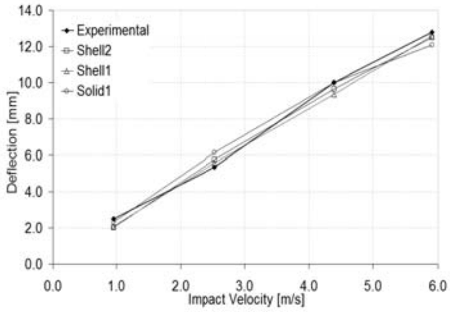

Figure 17: Maximum deflection vs. impact velocity. Thin (2.00 mm) circular plates.

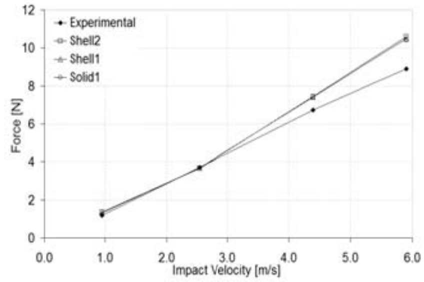

Figure 18: Maximum force vs. impact velocity. Thin (2.00 mm) circular plates.

The models showed that the maximum effective stress occurred on the lower surface opposite the impact point on both models shell and solid. The time variation of the effective stress is shown in Figure 19 for the thick circular plate with an incident velocity of 5.85m/s as an example. Stress is shown for elements on the upper and lower surface at both the impact point and at a point near the support. It can be seen from this figure that the maximum stress occurs on the surface opposite to the impact point, but that near the support the stresses are almost the same on both sides of the plate. The maximum effective stress distribution in the solid model is also plotted in Figure 20 for the same impact event.

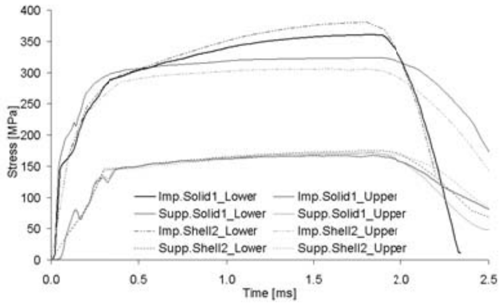

Figure 19: Effective stress with time. Thick (5.92 mm) circular plates, impact velocity 5.85 m/s.

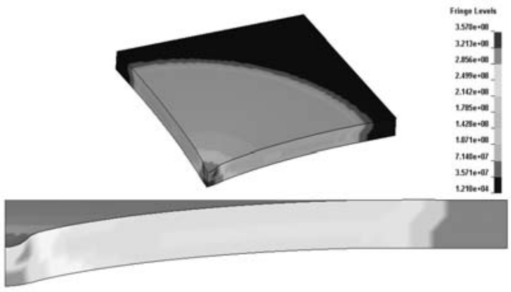

Figure 20: Maximum effective stress distribution. Thick (5.92 mm) circular plates, impact velocity 5.85 m/s.

The mass kinetic energy is dissipated as a combination of internal and sliding energies. For example, these values are plotted for the thick plate impacted at 2.62 m/s in Figure 21, where the magnitude of the sliding energy is about 13% of the dissipated kinetic energy using the Shell2 model, but only approximately 5% when either of the solid models are used. This implies that there is a small relative motion between the surface of the shell elements and the impacting mass, which is becoming less significant when solid elements are used. This could be because the indentation into the material thickness is modelled only in the case of solid elements, hence resisting sliding, but this is not clear and requires further investigation.

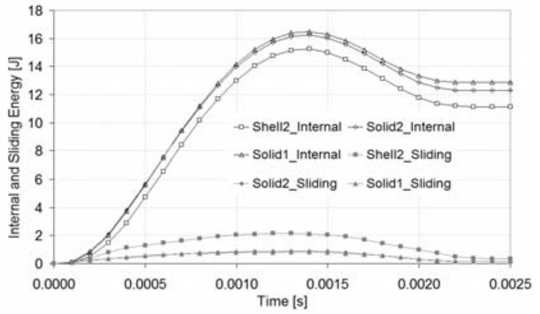

Figure 21: Internal and sliding energy dissipation. Thick (5.92 mm) circular plates, impact velocity 2.61 m/s.

Overall, good agreement between numerical and experimental results was obtained, especially for the thin plates. However, for the thick plates some discrepancies between theory and test results differences were noted, the possible reasons for which are discussed below:

It is possible that the actual experimental clamped condition was not as perfect as represented in the numerical model; it is quite possible that some slippage between the support plates was experienced by the specimen plate, and in fact all of the tested plates experienced greater displacements than predicted by the finite element models. The numerical clamped condition is affected by the static coefficient of friction in the contact definition between support and specimen plates, for example decreasing this coefficient gives greater displacements and lower forces, giving a better approximation between experimental and numerical results. Further work would be beneficial to further refine the model in terms of this coefficient.

The true stress-strain curve material definition input to the numerical model is also a possible source for discrepancies; here these values were obtained using tensile tests specimens cut from the same plates from which the impact specimens were taken, & the data differed from that supplied by the plate manufactures. Another possible material property source of errors is the strain-rate effect, which was not considered in the current numerical model. A search of the literature showed that Cowper-Symonds data for aluminium 5083/H111 is not available, and since these coefficients have been seen to vary greatly between specific aluminium alloys, values for other alloys could not be used. Preliminary studies into the effect of strain rate have showed that further work to obtain this data could improve the accuracy of the maximum displacement results calculated here.

A further possible source of differences between the finite element and experimental results is the oscillations seen during the impact response (experimental force-time curves), which were not separated from the mechanical loads. This effect could be due to vibrations in the striking mass assembly or material vibrations around the indentation stiffness, and the development of a more complex geometrical model would help to clarify the source of these effects.

Generally, in this study some of the parameters that affect the impact response were varied to optimise the finite element model (e.g. mesh size and element type), but others were set at constant values obtained from the literature or not included (e.g. static coefficient of friction and strain-rate parameters) in order to keep the size of the investigation practicable. However, further work could now investigate the effects of all of the parameters, especially if labour-saving techniques such as those of statistical experimental design (Sutherland and Guedes Soares 2003) were used to ensure a practical number of modelling runs and, importantly, to ensure that any interactions between these parameters are correctly identified.

Conclusions

Detailed information of the impact response of clamped aluminium 5083 circular plates has been obtained through non-linear explicit dynamic simulation using the LS-DYNA software package. The results obtained were in good agreement with those of previous experimental tests, indicating that even computationally inexpensive coarse meshes using shell elements are sufficient to predict the maximum deflections and forces. However, finer meshed shell and solid element models give better and best prediction of the force-displacement behaviour, respectively. Where small discrepancies between numerical and experimental results occurred, this was due to overestimation of the impact force; the variation of displacement with time is generally very well predicted.

The numerical simulations give a good understanding of the shape of the deformation in plates subjected to impact loading, and a fine meshed solid model is needed to give a good approximation of the deformation shape, especially where local indentation is significant. In the present work the study of the effect of mesh size showed that the ratio of element size to indenter radius should preferably be approximately 1/5 in order to satisfactorily define the shape of the deformation.

The material true stress-strain curve inputs to the numerical model were obtained from tensile tests on the actual material used to fabricate the impacted plates. This was simplified since the test maximum load was almost coincident with the rupture load, but for other materials is may be more difficult to define the true stress-strain curve and some approximations as the power law curve must be included.

The numerical models were successfully used to predict the impact response of Aluminium 5083 plates, and the next planned stage of this work is to see if the technique is also successful for steel plate impact tests. For example, strain-rate does not seem to play an important role in numerical simulation of these aluminium plates, however this may not be the case for other materials.

Acknowledgments

The work has been performed in the scope of the project MARSTRUCT, Network of Excellence on Marine Structures (http://www.mar.ist.utl.pt/marstruct/), which has been financed by the EU through the GROWTH Programme under contract TNE3-CT-2003-506141.

The first author has been financed by the Portuguese Foundation for Science and Technology (Fundação para a Ciência e Tecnologia), under contract SFRH/BD/46369/2008.

References

Akita Y, Ando N, Fujita Y, Kitamura K. 1972. Studies on collision-protective structures in nuclear powered ships. Nucl Engng Des. 19: 365 - 401.

Amdhal J, Kavlie D, Johansen A. 1995. Tanker grounding resistance. Proc. 6th Int. Symp. on Practical Design of Ships and Mobile Units (PRADS'95). 1072 - 1083.

Dieter GE. 1986. Mechanical behavior under tensile and compressive loads. ASM Handbook. 8: 99-10.

Ehlers S. 2010. Strain and stress relation relation until fracture for finite element simulations of a thin circular plate. Thin-Walled Structures. 48 (1): 1 - 8.

Ehlers S, Varsta P. 2009. Strain and stress relation for non-linear finite element simulations. Thin-Walled Structures. 47 (11): 1203 - 1217.

Ehlers S, Klanac A, Tabri K. 2007. Increased safety of a tanker and ropax vessel by implementing a novel sandwich structure. 4th International Conference on Collision and Grounding of Ships: Hamburg, Germany. 109 - 115.

Guedes Soares C. 1981. A Mode solution for the finite deflections of a circular plate loaded impulsively. Engineering Transactions. 29 (1): 99 - 114.

Hallquist JO. 2005. LS-DYNA Theory Manual. Livermore Software Technology Corporation.

Jones N. 1989. Structural Impact. Cambridge University Press.

Kajaste-Rudnitski J, Vastra P, Matusiak J. 2005. Some finite element estimates of ship collision event. Maritime Transportation and Exploitation of Ocean and Coastal Resources, Taylor & Francis Group, London. 447 – 453

Liu J, Jones N. 1987. Experimental investigation of clamped beams struck transversely by a mass. International Journal of Impact Engineering. 6 (4): 305 - 335.

McDermott JF et al. 1974. Tanker structural analysis for minor collision. Trans SNAME. 82: 382 - 407.

Shen WQ. 1995. Dynamic plastic response of thin circular plates struck transversely by nonblunt masses. Int. J. Solids Structures. 32 (14): 2009 - 2021.

Shen W.Q. 2002. A study on the failure of circular plates struck by masses. Part 2: theoretical analysis for the onset of failure. International Journal of Impact Engineering 27 (4): 413 - 432.

Shen WQ, Rieve NO, Baharun B. 2002. A study on the failure of circular plates struck by masses. Part 1: experimental results. International Journal of Impact Engineering. 27 (4): 399 - 412.

Simonsen BC, Lauridsen LP. 2000. Energy absorption and ductile failure in metal sheets under lateral indentation by a sphere. International Journal of Impact Engineering. 24 (10): 1017 - 1039.

Stronge WJ, Yu TX. 1993. Dynamic Models for Structural Plasticity. © Springer-Verlag London Limited.

Sutherland LS, Guedes Soares C. 2003. The effects of test parameters on the impact response of glass reinforced plastic using an experimental design approach. Composites Science and Technology. 63: 1 - 18.

Sutherland LS, Guedes Soares C. 2009. Impact behaviour of GRP, aluminium and steel plates. Analysis and Design of Marine Structures; Guedes Soares & Das (eds). Taylor & Francis Group: London. 293 – 300

Tabri K, Alsos H, Broekhuijsen J, Ehlers S. 2007. A benchmark study on ductile failure criteria for shell elements in multiaxial stress state. Advancements in Marine Structures, Guedes Soares & Das (eds). Taylor & Francis Group: London. 401-409.

Wang G, Ohtsubo H, Arita K. 1998. Large deflection of a rigid-plastic circular plate pressed by a sphere. Journal of Applied Mechanics. 65 (2): 533 - 535.

Wang G, Ohtsubo H, Liu D. 1997. A simple method for predicting the grounding strength of ships. J Ship Res. 41: 241 - 247.

Yu TX, Chen FL. 2000. Failure of plastic structures under intensive dynamic loading: Modes, criteria and thresholds. Int. J. of Mechanical Science. 42: 1531 - 1554

A material relation for numerical ship collision analysis

Sören Ehlers

Aalto University - School of Science and Technology, Department of Applied Mechanics / Marine Technology

Abstract:
Ship collisions can be assessed with the non-linear finite element method. Thereby the structural energy is calculated until a certain penetration or fracture limit is reached. Therefore, an appropriate non-linear strain and stress measure is needed to describe the material behaviour including fracture. Furthermore, this true strain and stress relation needs to be suitable for the finite element method. The latter is achieved through a determination of the material relation using optical measurements. As a result, a tanker collision is simulated out with the presented material relation, and for comparison with a standard power law based material relation. This comparison will present the difference in energy predictions using different material relations.

Introduction

Ship collision simulations are increasingly being performed to reveal the consequences from a structural point of view. These simulations are often carried out in a quasi-static fashion, commonly consisting of a struck model that is subjected to a rigid indenter. By this means, the deformations of the struck structure are alone in contributing to the crashworthiness. This approach results in the maximum energy being absorbed by a specific structure. Therefore, the absorbed energy can be used to compare different conceptual structures. In terms of a conceptual ship structure, the energy absorbed until inner hull rupture is of primary interest.

Finite element-based analysis of ship collision simulations has been performed in many commercial codes, such as LS-DYNA, ABAQUS, and MSC/DYTRAN, for example see Kitamura (1996). These simulations contain highly non-linear structural deformations, including rupture. Therefore, these finite element analyses require the input of the true strain and stress relation until failure. In other words, the material relation and a failure criterion determining the failure strain are needed. The true strain and stress relation of the material is commonly selected in the form of a power law; see, for example Ehlers et al. 2008. Power law parameters can be obtained from standard tensile experiments, see for example Joun et al. (2008). However, whether or not the chosen finite element length corresponds to the true strain and stress relation obtained remains questionable. For one selected finite element length, agreement between the numerical simulation and the tensile experiment may be achieved by an iterative procedure. Here the true strain and stress relation, i.e. the power material law, used as input for the simulation is changed until compliance with the corresponding tensile experiment is achieved, see for example Zhang et at. 1999. However, this iterative procedure can lead to wrong structural behaviour if the element size is changed, in which case the procedure needs to be repeated for each mesh size selected until compliance is reached. Therefore, the proper material relation until failure is of considerable importance, as it directly influences the accuracy of non-linear finite element simulations until fracture. Furthermore, the determination of the material relation alone does not necessarily suffice, as the failure strain, i.e. the end point of the stress versus strain curve, depends in turn on the material relation. However, a significant amount of research has been conducted to describe criteria to determine the failure strain and to present their applicability; see for example Ehlers et al. 2008. However, these criteria commonly use a standard or modified power law to describe the material behaviour, and a clear relation between the true strain and stress relation and the element length is not obtained. Relations to obtain an element length-dependent failure strain value are presented by various authors, see for example Alsos et al. 2009 and Ehlers et al. 2008. However, they define only the end point of the standard or modified power law. This inconsistent adjustment of the element length with respect to the chosen true strain and stress relation can lead to wrong structural behaviour, as no element length dependency of the true strain and stress relation including failure is obtained. A consistent material relation including failure is especially important in the case of collision simulation, because they are commonly carried out to compare different structural arangements and element dimensions.Therefore, this paper presents a material relation until failure for mild steel based on optical measurements. The finite element length-dependency of this strain and stress relation is achieved as the strain reference length is clearly identified. This strain reference length corresponds to the discrete pixel dimensions from the optical measurements. Hence, the finite element length has to correspond to this strain reference, and thereby an element length-dependent strain and stress relation until failure is achieved. It will be shown that this strain and stress relation can be used to simulate the deformation until rupture of a circular- and a stiffened plate and that it results in a better convergence of results with varying element size than a conventional power material law. A constant strain failure criterion is chosen to delete failing elements and to simulate rupture. As a result, a collision simulation is carried out for a tanker side structure using the presented and a power law based material relation until failure. The comparison of these simulation results will present the differences in energy prediction using different material relations.

Determination of the material relation

The determination of the material relation until failure, i.e. the true strain and stress relation, is shown on the basis of optical measurements, which measure the local displacements on the surface of the specimen. This dog-bone specimen has a length-to-breadth ratio (L/B) of 8 and consists of 4-mm-thick NVA steel. The displacement-controlled experiments are carried out with a tensile test machine at Växjö University, consisting of a MTS 322 Test Frame with Load Unit. The MTS Test Frame records the force and the resulting elongation of the specimens, in other words the force-elongation curve, which will be used to validate the proposed procedure. For details on the testing procedure and results see Ehlers and Enquist (2007).

The local strain is calculated from the local displacements obtained by the optical measurements on the basis of a discrete amount of pixel recordings, a so-called facet. The discrete pixel dimensions will clearly define the strain reference length. To determine the stress, the cross-sectional area at any given instant is calculated on the basis of the out-of-plane displacement measurements of the specimen. Therefore the local stress is determined on the basis of the minimum cross-sectional area of the specimen measured as a function of the strain reference length. The gauge length, i.e. the strain reference length, is shown to be a function of a discrete amount of pixel recordings from the optical measurements. As a result the true strain and stress relation until failure is obtained in a manner that is dependent on the choice of strain reference length. Furthermore, this strain reference length, ε_{ref}, is varied from 0.88 mm to 4.4 mm to show its sensitivity to the true strain and stress relation until failure. The obtained strain and stress relations are shown in Figure 2.

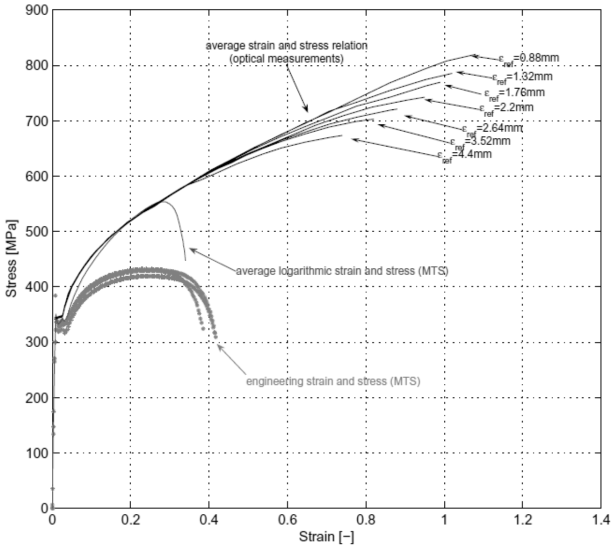

Figure 2: Measured true strain and stress relation (MTS measures are plotted for comparison)

Validation of the material relation

The true strain and stress relation until failure obtained with optical measurements is used to simulate a tensile-, plate- punching and stiffened plate indentation experiment with the finite element method. In this way, the novel material relation is validated, because the numerical results are compared with experimental results, see Ehlers and Varsta (2009), Ehlers (2009a/b). The experiments are simulated using the explicit time integration solver LS-DYNA version 971.

The structures are modelled using four nodded quadrilateral Belytschko-Lin-Tsay shell elements. The finite element length is equal to the strain reference length. The finite element length ranges from 0.88 mm to 4.4 mm and is equal to the strain reference length. For greater element lengths the true strain and stress relation is found to be independent of the element length, as the extent of the localisation becomes smaller than a single element. However, the element length-dependent failure strain is obtained according to experimental measurements. For small element lengths up to 4.4 mm, the failure strain is obtained with optical measurements, whereas the failure strain for greater element lengths up to 160 mm follows the natural logarithmic form of the well-known engineering strain at failure according to the gauge length of the specimen being 160 mm at a maximum, see Figure 3. This failure strain and element length relation allows the removal of failing elements at the correct strain. The initiation and propagation of fracture in the specimens is modelled in LS-DYNA by deleting the failing elements from the model. The element fails once the failure strain is reached. The failure strain serves as a criterion to delete elements to simulate rupture or to terminate the simulation at the point of rupture. The material is assumed to follow the von Mises flow rule, and the element is deleted once the equivalent plastic strain reaches the measured local failure strain. Furthermore, Ehlers and Varsta (2009) and Ehlers (2009a) showed that the choice of a constant strain failure criterion used for the simulations is justified as close ranges of triaxiality are obtained at the point of failure for tensile and plate specimens. The experimentally determined strain and stress relations are implemented via Material 124 of LS-DYNA. Standard LS-DYNA hourglass and time step control is used. For details of the modelling and simulation processes see Ehlers et al. (2007) and Hallquist (2005).

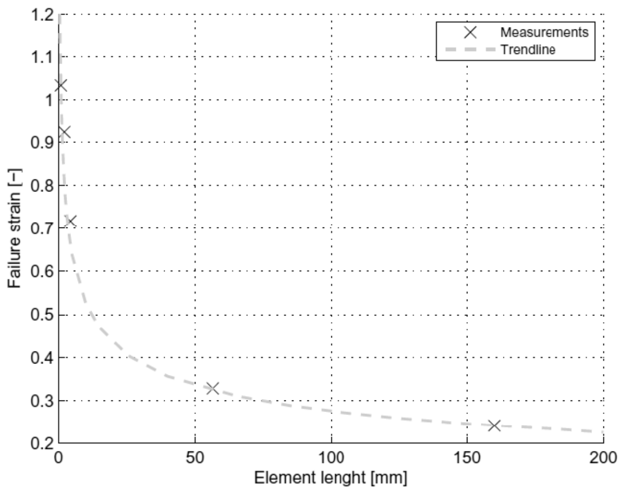

Figure 3: Experimental failure strain versus element length

The tensile specimen is modelled between the clamping wedges only. The translational degrees of freedom are prohibited at one edge, whereas the other edge is subjected to a constant displacement of 100x the experimental speed as no dynamic effects occur. Additionally, the simulation time remains desirably short. The force versus elongation curves from the tensile experiment simulation corresponds to the measurements with good agreement, see Figure 4. The simulation using the element length-dependent true strain and stress relation shows better convergence with changing element lengths, i.e. the strain reference lengths, until the point of failure than the common power law material relation according to ASM (2000); see Figure 4.

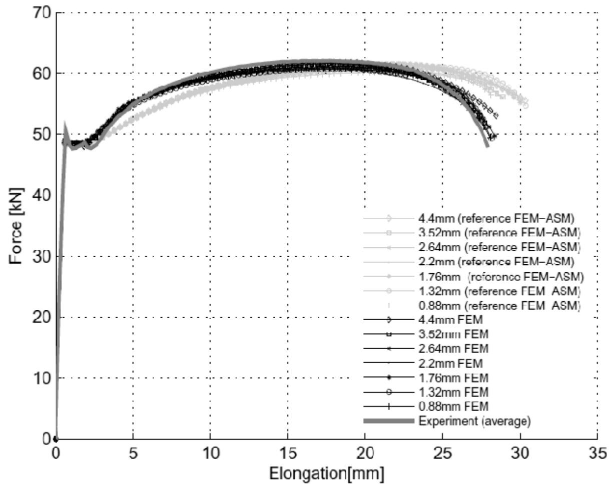

Figure 4: Finite element analysis results

The principle mesh of the plate specimen is shown in Figure 5, the rectangular mesh secures the correct element length for all elements in the fracture region, whereas the radial mesh secures the best contact in the clamping region, see Figure 6. The good correspondence between the numerical and experimental results indicates that the true strain and stress relation is suitable for plate deformation simulations until failure as it describes the non-linear behaviour using different element sizes sufficiently well; see Figure 7.

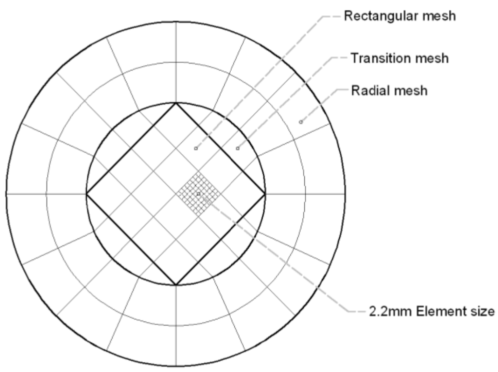

Figure 5: Principle finite element mesh of the plate specimen

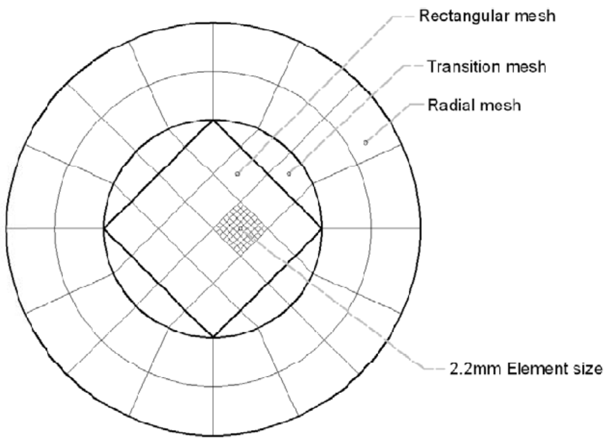

Figure 6: Principle experimental setup

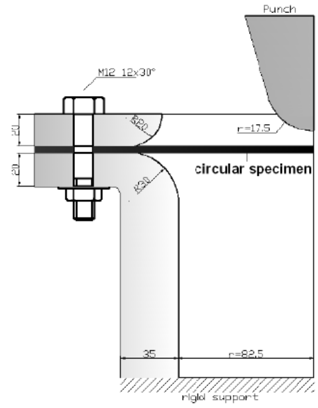

Figure 7: Finite element simulation results for the plate-punching experiment

Finite element simulation of a plate stiffened with two flat bars follows the model described by Alsos et al. (2009). The resulting force versus penetration curves using different element sizes for the stiffened plate are in good agreement with the existing experimental results see Figure 8.

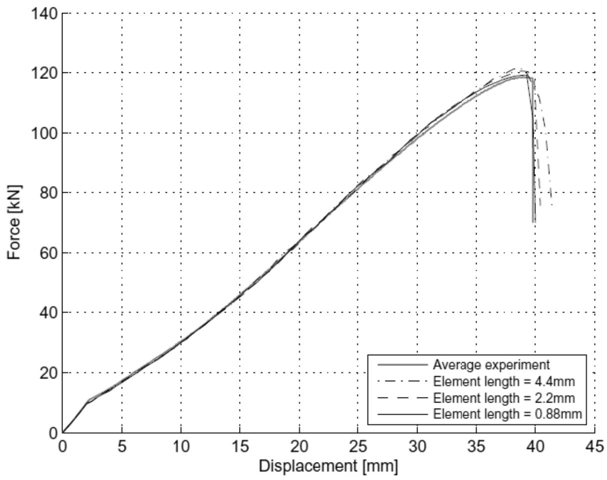

Figure 8: Finite element simulation of a stiffened plate and experimental results by Alsos et al. (2009)

Case study: A tanker collision simulation

This chapter presents a collision simulation using the non-linear finite element method to assess the crashworthiness of a tanker. The length of the tanker is

180 m and the beam is 32.2 m. The finite element model is build between two transversal bulkheads spaced 17.8 m with a webframe spacing of 3.56 m using the ANSYS parametric design language, see Figure 9 and Ehlers et al. (2008). The collision simulation is carried out for the optimised tanker concept presented by Ehlers (2009b). The cross section of the tanker is shown in Figure 10. A right-angle collision angle is chosen, because it allows a quasi-static simulation approach, because an arbitrary collision angle would reduce the energy available to deform the conceptual ship structure. Therefore, a rigid bulbous bow is moved into the ship side structure at a constant velocity of 10 m/s. This velocity is reasonably low so as not to cause inertia effects resulting from the ships' masses, see Konter et al. 2004.

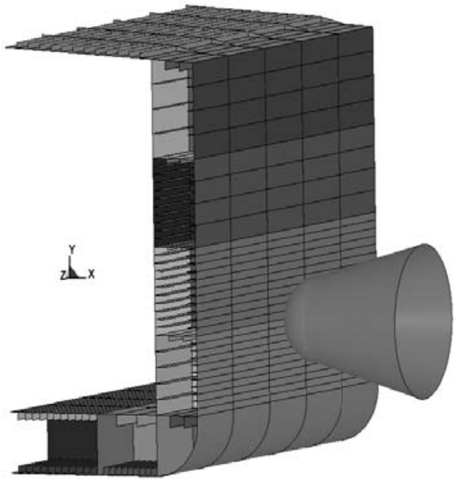

Figure 9: Finite element model and striking bulbous bow

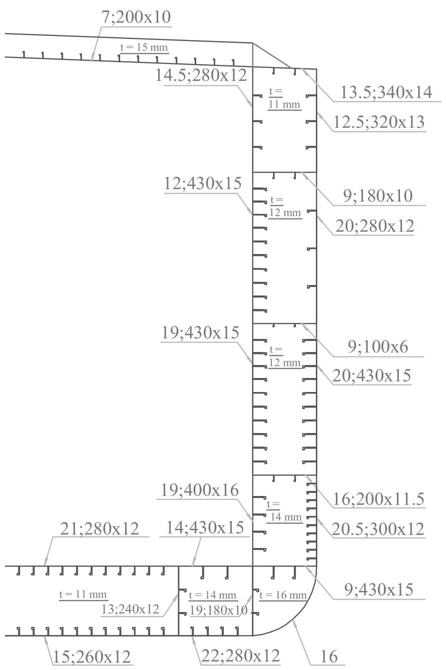

Figure 10: Tanker mainframe

Collision simulations need to predict the energy absorbed until inner plate rupture with sufficient accuracy. Therefore the novel true strain and stress relation until failure based on optical measurements is used for the simulations and implemented into the modelling procedure in order to assign the material relation according to the finite element size. For the coarse-mesh model, the same element distribution as in the stiffened plate simulation is used. Three elements per stiffener height and six elements between stiffeners are used, unless an element length of 40 mm is larger. The fine-mesh model is build with a constant 40 mm element length. For comparison the same finite element models are used with a power law ($K = 745, n = 0.22, \varepsilon_f = 0.92$) based failure criterion according to Zhang et al. (2004). The explicit non-linear solver LS-DYNA version 971 is used for the analysis.

The results of the collision simulation for the chosen boundaries are given in Table 2 and Figure 11. For a bettercomparison of the results, the values of Table 2 are normalised and made unit-less by dividing them by the energy value of the reference simulation using the novel material relation. The resulting difference in energy for the coarse- and the fine model is about 10% for the novel material relation. However, the power law based criterion shows a scatter of 252% in absorbed energy for the different element lengths.

Table 2: Collision simulation results

Material relation	Energy(coarse mesh)	Energy (fine mesh)
Power law based	0.46	1.16
Novel material relation	Reference	1.11

Conclusions

A novel finite element length-dependent material relation including failure is presented. A procedure to determine the true strain and stress relation experimentally until failure on the basis of optical measurements is given. The finite element simulations are carried out with the finite element length equal to the strain reference lengths. These comparative finite element simulations show very good agreement with experimental results.

Furthermore, a ship collision simulation of a tanker side structure is presented. This simulation is carried out using the novel element length-dependent true strain and stress relation including failure, and for comparison a power law based failure criterion. Thereby, the energy prediction using different material relations and failure criteria is presented. This difference is found to be up to 252% for different element sizes using the power law based criterion. The element length-dependent constant strain failure criteria and material relation proved to be sufficiently accurate with a scatter in energy of 10%.

In the future, this novel material relation can be used to obtain crashworthy ship structures confidentially.

Acknowledgements

The preparation of this paper is partial financially supported by the Finnish national project FIMECC/Light Research Program and is thankfully acknowledged.

References:

Alsos HS, Amdahl J, Hopperstad OS. On the resistance to penetration of stiffened plates, Part II: Numerical analysis. International Journal of Impact Engineering 2009;36;875-887.

ASM Handbook. Mechanical Testing and Evaluation. 2008.

Ehlers S. Strain and stress relation until fracture for finite element simulations of a thin circular plate. Thin-Walled Structures 2009a, doi:10.1016/j.tws.2009.08.004.

Ehlers S. A procedure to optimize ship side structures for crashworthiness. Journal of Engineering for the Maritime Environment 2009b, doi:10.1243/14750902JEME179.

Ehlers S, Broekhuijsen J, Alsos HS, Biehl F, Tabri K. Simulating the collision response of ship side structures: A failure criteria benchmark study. Int Ship Progress 2008; 55;127-144.

Ehlers S, Enquist B. Uniaxial tensile necking of steel dog-bone specimens. Helsinki University of Technology, Ship Laboratory 2007;M-303.

Ehlers S, Klanac A, Kõrgesaar M. A design procedure for structures against impact loading. STG Yearbook 2008.

Ehlers S, Tabri K, Schillo N, Ranta J. Implementation of a novel ship side structure into a tanker and a ropax vessel for increased crashworthiness. 6th European LS-DYNA Users' Conference, Gothenburg, Sweden 2007, 4.111-4.120.

Ehlers S, Varsta P. Strain and stress relation for non-linear finite element simulations. Thin-Walled Structures 2009, doi:10.106/j.tws.2009.04.005.

Hallquist JO. LS-DYNA Theory Manual. Livermore Software Technology Corporation. 2005.

Jalkanen J. Particle swarm optimization of load carrying structures. Journal of Structural Mechanics 2006;2;23-35.

Joun MS, Eom JG, Lee MC. A new method for acquiring true stress-strain curves over a large range of strains using a tensile test and finite element method. Mechanics of Materials 2008;40;586-593.

Kennedy J, Eberhart RC. Particle swarm optimization. In Proceedings of IEEE International Conference on Neural Networks, Piscataway, NJ. 1995;1942-1948.

Kitamura O. Comparative Study on Collision Resistance of Side Structure; International Conference on Design and Methodologies for Collision and Grounding Protection of Ships, San Francisco, California, USA, August 22-23, 1996. Also in Marine Technology, Vol. 34, No. 4, 293-308.

Konter, A., Broekhuijsen, J., Vredeveldt, A. A quantitative assessment of the factors contributing to the accuracy of ship collision predictions with the finite element method. In Proc Third Int Conf Collision and Grounding of Ships. Japan, 2004. p. 17-26.

Zhang, L., Egge, E.D., Bruhms, H. Approval procedure concept for alternative arrangements. In Proc Third Int Conf Collision and Grounding of Ships. Japan, 2004. p. 87-97.

Zhang ZL, Hauge M, Ødegård J, Thaulow C. Determining material true stress-strain curve from tensile specimens with rectangular cross-section. International Journal of Solids and Structures 1999;36(23);3497-3516.

The research on the flooding time and stability parameters of the warship after compartments damage

Waldemar Mironiuk

Naval University, Gdynia, Poland

Abstract:
Research on damage stability and unsinkability is a valuable source of knowledge of behaving a ship while flooding its compartments. In the paper, a short description of accidents and damages of Polish warships taking place in 1985-2004 is presented. The time when compartments are flooded (t_f) and stability parameters are one of the key elements which have influence on a rescue action. The knowledge of the time mentioned and a metacentric height (GM) are very important for a commanding officer making decisions while fighting for unsinkability and survival of the ship. To provide the information about the time t_f of a ship type 888 a new method was designed. The method was tested experimentally and results of the tests are presented in the paper. In the experiments, the flooding process of compartments was simulated. The next part of research was carried out on the laboratory stand bed, where the flooding time of damaged compartment of warship model was measured. The results of the experiments can be a base to define general rules to make proper decisions during the process of damage control.

Introduction

Even highly organized fleets struggle with accidents and technical breakdowns which cannot be completely eliminated. The breakdowns can be classified based on their causes. The basic causes of the breakdowns are: warfare, defects of materials and defects within the production process, constructional defects, technological defects in the process of renovation, material's wear and tear, not meeting the requirements in operating and servicing an equipment, not taking security measures while storing dangerous cargoes, e.g. explosive materials, petroleum products and other chemical components of serious fire hazard.

A partial or total loss in functionality of mechanisms and installations can occur both during warfare and during daily operating a ship.

Failures caused by navigational mistakes or wrong maneuverability represent a group of ship accidents and breakdowns which can lead to dangerous lost of floating of a ship due to flooding its compartments.

The statistical data prepared by the Polish Navy Commission of Warship Accidents and Breakdowns reveal 156 warship accidents and breakdowns between 1985 and 2004 year. The data mentioned are presented in Figure 1. (Korczewski & Wróbel, 2005). In a situation of a breakdown crew activities deciding about ability of a warship to fight should be directed to take a proper actions during the process of damage control and to protect stability, sinkability and maneuverability of the ship. Exercises within the confines of the process of damage control, apart from construction solutions, increase the safety of both a ship and crew. Training is carried out in well prepared training centers which are situated in the United Kingdom, Germany, Netherlands and Pakistan. The centers are equipped with ship models designed for simulating failure states which most frequently occur while operating a ship. The same models were also used in the experiments reported in the paper. One of the goals of the experiments mentioned was to determine the following parameters: t_f and GM

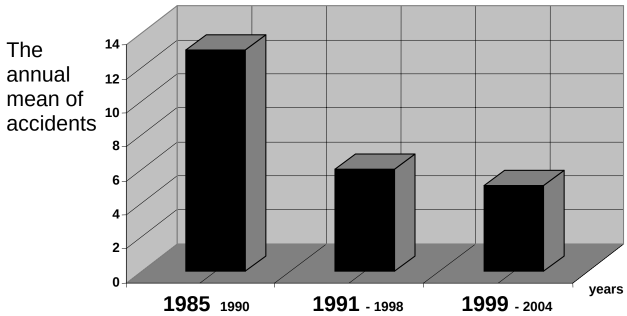

Figure 1. The overall structure of accidents and breakdowns between 1985- 2004

for the ship type 888. Presently, there is used only simplified method to calculate parameters above. The method presented in the paper has a distinctive difference compared to the existing, similar methods talk in some publications. The worked out method presents the permeability value depended on the water level inside the damaged compartment. Due to this, we can estimate more accurate quantity of the water in the compartment and finally more accurate the flooding time damaged compartment. The aim of presented method is to provide experimental validation.

The information about t_f and stability parameters is very important for a commanding officer. It enables him to make a proper decision during the process of damage control. The officer, based on the information should determine the point in time, when further fighting for unsinkability is senseless and when all effort should be directed to save the crew and documents (Miller, 1994).

Calculating the time of flooding ship's compartment

When calculating t_f, first, the velocity of water running through the damaged hull has to be determined.

The water flowing through a hole can be compared to liquid flowing from a tank of a surface A. The water velocity can be obtained from the following formula (Troskolanski 1961):

$$v_w = \sqrt{\frac{2 \cdot g \cdot h_z}{1 - \left(\frac{A_0}{A}\right)^2}} \quad (1)$$

where A_0 =cross section of a hole; A = horizontal cross section of a tank; g = acceleration due to gravity, and h_z = height of a liquid inside the tank.

Because the surface of a hole is much smaller than a sea surface, the water velocity can be obtained according to Torricelli's formula (Troskolanski 1961):

$$v_w = \sqrt{2 \cdot g \cdot h} \quad (2)$$

where h= depth of a hole.
For the real liquid the formula (2) can be presented as follows (Troskolanski 1961):

$$v_w = \varphi \cdot \sqrt{2 \cdot g \cdot h} \quad (3)$$

where $\varphi = 0{,}97 \div 0{,}98$ - the velocity coefficient dependant on the kind of liquid.
The equation (3) is applied when the water surface inside a hull is below a lower edge of a hole, i.e. for a constant pressure of the water. When the water pressure is changeable (the water surface inside a hull is above an edge of a hole and still grows up) the velocity of the water flowing to the compartment can be obtained according to the formula (Troskolanski 1961):

$$v_w = \varphi \cdot \sqrt{2 \cdot g \cdot (h - h_0)} \quad (4)$$

where h_0= height of liquid inside a tank above an edge of a hole.
The hole in the body can have a different shape and dimension dependant on the reason of damage. The shape of the hole influences a quantity Q of the water flowing to the compartment. The quantity Q depends on v, which in turn is a product of coefficient φ and narrowing coefficient $\chi = 0{,}61 \div 0{,}64$ (Troskolanski 1961). Therefore, the quantity of water Q flooded to the interior compartment can be obtained from the formula (Troskolanski 1961):

$$Q = A_0 \cdot v \cdot \sqrt{2 \cdot g \cdot h} \quad (5)$$

When the pressure of the water is changeable the quantity of water Q inside the compartment is calculatedfrom the formula (Troskolanski 1961):

$$Q = A_0 \cdot v \cdot \sqrt{2 \cdot g \cdot (h - h_0)} \quad (6)$$

The time t_f is as follows (Troskolanski 1961):

$$t_f = \frac{V}{Q} \quad (7)$$

where V= the volume of the water inside a compartment.

a)

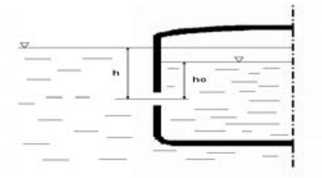

b)

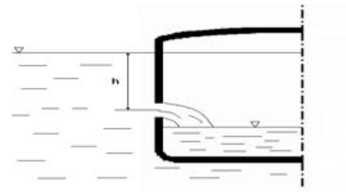

Figure 2. Compartment being flooded:
a) with constant water pressure,
b) with variable water pressure.

Calculating the volume of damaged compartments

The calculation of t_f was conducted for a damaged engine room of the ship type 888. The computer program was built to enable the calculations above. The program makes it possible to fix basic and necessary parameters to make a correct evaluation of the state of a ship. In turn, the information about the parameters mentioned above makes it possible to take proper decisions during the process of the damage control.

Computing the volume of damaged compartments

The volume of a damaged compartment is necessary to calculate the time t_f. The lines plan of the ship's hull is used to compute the theoretical volume v_t. Moreover, the plan was also used to have sections extracted at the place of ribs number 35, 40, 45, 50 where we can find the damaged compartment. The sections are shown in Figure 3 (Kowalke 2006).

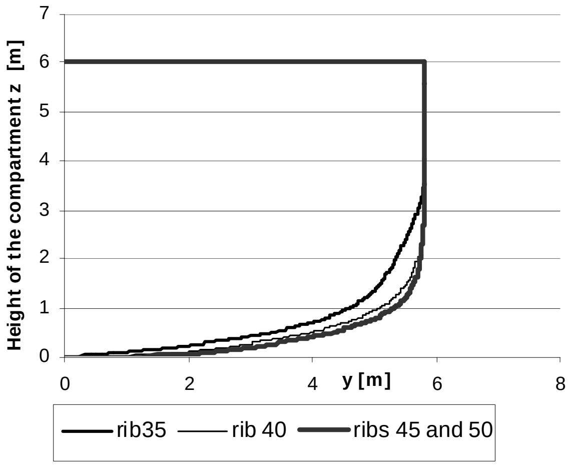

Figure 3. Sections of engine room

The area of the sections was calculated to estimate the accurate volume of the damaged compartment. Integral curves of sectional areas, obtained in this way, are presented in graphic form as a multinomial degree 7 in Figure 4.

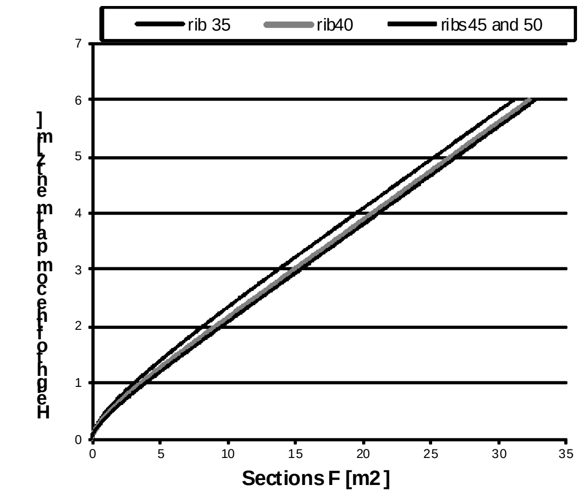

Figure 4. Integral curve engine room sectional areas

Using section areas and a distance between them, the theoretical compartment volume v_t can be calculated, by the formula (Deret 2003, Dudziak 2006):

$$v_t = \Sigma \frac{(F_i + F_{i+1}) \cdot l_w}{2} \tag{8}$$

where l_w = the distance between sectional areas, and F_i, F_{i+1} = section areas.

The permeability calculation

The volume of the empty compartment was calculated with the aid of the computer program. The real quantity of the water, flooding the compartment, is less than the theoretical volume of the compartment due to the volume of all mechanisms and devices inside the compartment. Usually, to calculate a real quantity of the water, the permeability of flooding compartment μ is used. Permeability is used in ship survivability and damaged stability calculations. In this case, the permeability of a space is a coefficient from 0 to 1. The permeability of a space is the percentage of volume of the space which may be occupied by seawater if the space is flooded. The remaining volume (not filled with seawater) being occupied by machinery, cargo, accommodation spaces, etc. The value of permeability for compartment is calculated by the formula (Deret 2003):

$$\mu = \frac{v}{v_t} \tag{9}$$

where v_t = theoretical compartment volume; v - real quantity of the water inside the compartment.

The numerical value of the permeability depends on both, a kind and destination of damaged compartment. The permeability of the compartment μ, which is announced in the SOLAS Convention, is usually used to calculate the real volume of the compartment. Typical values from the SOLAS Convention are:

- 0.95 for voids (empty spaces), tanks, and living spaces;
- 0.85 for machinery spaces;
- 0.60 for spaces allocated to stores.

This implies that for damaged stability calculation purposes, machinery spaces are only 15% full with machinery by volume (100% - 85% = 15%). In preliminary research presented in the paper, permeability of the engine room was estimated. Its value depends on the height of the water inside the compartment. The graph of the permeability is shown in Figure 5 **(Kowalke 2006)**.

The average value of the permeability for chosen compartments, obtained as a result of experiments, is comparable with the value of the SOLAS Convention and equals 0,84.

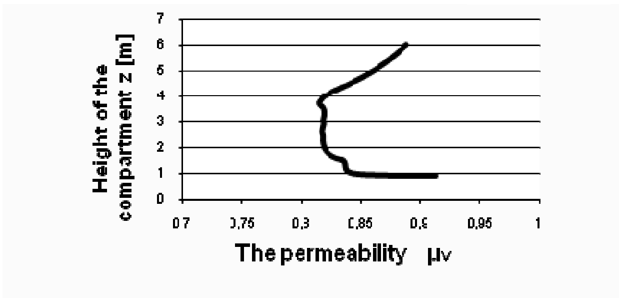

Figure 5. Graph of the engine room permeability μ_v

The model of simulation for damaged compartment

The simulation model of the engine room, equipped with all main mechanisms and devices, was made in the next part of the research. The view of the compartments being flooded is shown in Figure 6 **(Kowalke 2006)**.

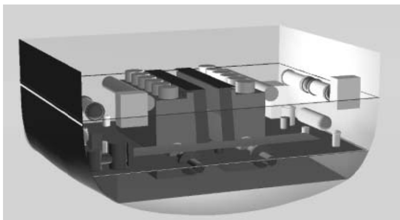

Figure 6. Engine room compartments being flooded

The analysis of the influence of damage parameters on the time t_f for the compartment ship type 888

The experimental research on t_f for engine room ship type 888 was carried out for different parameters of damages. In the research, the place and the dimension of damage were taken into consideration.

In the first stage of the research, t_f for the engine room was fixed. The calculations of t_f were made for the following example conditions: ship's draught T=4m, the dimension of damages R=0,03 m, R=0,05 m, R=0,1 m and R=0,2 m (R denotes radius). The holes were placed from 0,1m to 3,0 m below the surface of the sea. The results of the research are shown in Figure 7**.**

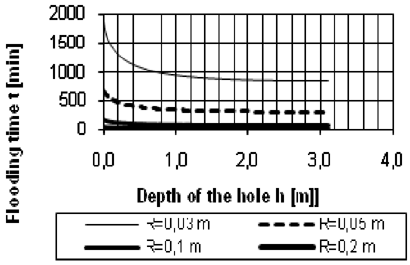

Figure 7. Flooding time t_f for the engine room

Figure 7 presents that t_f for the compartment with dimension of damage R=0,2m, placed 3 m below the surface of the sea, equals 3,4 minutes. This time is too short to seal the damage. Consequently, further activities of crew should be directed to protect spreading the water covering interior of the ship and to strengthen the construction of the watertight bulkhead.

The preliminary research on the flooding time on the stand bed

The flooding time calculation of damaged compartment, according to the method described in the paper, is verified on the laboratory stand bed. Thanks to a suitable construction and new concepts applied for the station, research on the ship reaction and position in the failure situations is possible. The main object of laboratory stand bed is ship's model type 888. The hull of model was made in accordance with the body plan. The elements of the superstructure and the ship equipment were simplified in the model but the appropriate scale 1:50 was kept. Main dimensions of the model are: length L-1,5 mbreadth B-0,25 m and draught T-0,08 m. This model is set up with specialized devices used for measurement of the position and for the analysis of the ship reaction during simulated damages. The shape of the model is shown in Fig.8 (Mironiuk 2006). The unsinkability research of the ship's model after having damaged one or more compartments will enable us to assess the flooding time of the model compartments and even whole model as well.

Figure 8. The laboratory stand bed

The engine room compartment was chosen to simulate. The compartment damage simulation can be done by opening the suitable valve situated inside the model. The scheme of the ship's model with a damaged compartment is shown in the computer window and presented in the Figure 9 (Mironiuk 2006).

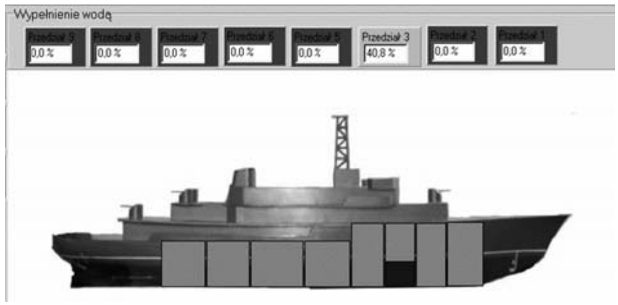

Figure 9. The scheme of ship's model with a partially flooded compartment

Within the framework of model research, the time of flooding the engine room of 888 type of vessel was determined. The research consisted in determination of time that will have passed from opening of the valve, making it possible to flood the compartment, until the outboard water level leveled with the liquid level in the compartment. The research was carried out using a sensor of water level in the compartment (pressure sensor) and a stopwatch. During the measurement two parameters were registered, i.e.:

- level of liquid in the compartment,
- flooding time.

Analysis of the performed measurement showed that level of the liquid in the compartment was approaching to 0,088 [m] of the liquid column and fixed itself after approximately 33 [min]. Knowing the scale of the model the real object's compartment flooding time assumed 2h45'. The flooding time obtained from the calculations was 1h59'. The compartment flooding time calculations were carried out for the leakage radius r=0,08 [m]. What was observed as a result of the research was a difference in the compartment flooding time at the level of 30%. The difference can be affected by, for example, imprecise physical model of the engine room. The computer model of engine room, which is used for flooding time calculation, is more accurate than physical model. Due to this, the permeability of damaged compartment of physical model has value different than permeability used by the computer program. Finally, the result of flooding time obtained from calculation is different than from research on the physical model. Presented results are obtained on the basis of experimental preliminary research and in the next step it will be corrected.

The metacentric height calculation

The next part of the research was devoted to estimate a metacentric height while flooding a damaged compartment. To calculate this parameter the added mass method was used. The result of calculations is shown in Figure 10.

To calculate the metacentric height the free surface effect was taken into consideration. Figure 10 implies that in the early stage of flooding the compartment, the metacentric height GupMu, is less than GM. In the later stages, GupMu increases and improves stability of a ship. This situation takes place due to adding a mass in the lower part of the ship.

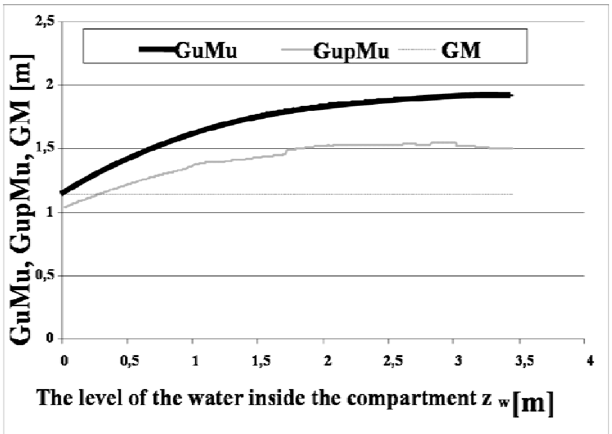

Figure10. Metacentric height GM- initial metacentric height (before demage);GuMu- metacentric height while flooding engine room; GupMu- metacentric height while flooding engine room with free surface.

Conclusions

The knowledge of the time t_f and metacentric height allows a commanding officer to make decisions while fighting for unsinkability and for the survival of the ship. The method of determining the permeability presented in the paper enables us to make calculating the time t_f more accurate. The modified method can be used to calculate the time t_f for ship type 888 with different types of hull damages. The method can be adopted for some other type of warships.

References:

Derett. D. R. 2003. Ship stability for Masters and Mates. BH. Oxford.

Dudziak, J. 2006. Teoria okrętu. WM: Gdańsk

Jakus, B., Korczewski, Z., Mironiuk, W., Szyszka, J., and Wróbel, R. 2001. Obrona przeciwawaryjna okrętu. Naval Academ:, Gdynia.

Korczewski, Z., Pawlędzio, A.and Wróbel, R. 2005. Analiza ilościowa wypadków i awarii na okrętach Marynarki Wojennej RP w latach 1985-2004. Przegląd Morski nr. Gdynia.

Kowalke, O. 2006. Komputerowa symulacja zatapiania przedziału siłowni okrętu typu 888. AMW: Gdynia.

Miller, D. 1994. Damage control - an insurance policy. International Defence Review nr 5.

Mironiuk, W., Pawlędzio, A., and Wróbel, R. 2004. Trenażer do walki z wodą. Gdynia, pp 14-30.

Mironiuk, W. 2006. Preliminary research on stability of warship models. COPPE Brazil: Rio de Janeiro.

Pawłowski, M. 2004. Subdivision and damage stability of ships Gdańsk.

Troskolanski, A. 1961. Hydromechanika Techniczna. Warszawa

A Method for Estimation of Grounding Frequency by Using Trajectories of Ships and Geometry of Seabed

Fujio Kaneko

Maritime Risk Assessment Department, National Maritime Research Institute(NMRI), Tokyo,Japan

Abstract

Until now by a lot of grounding accidents , severe environmental damages of sea areas were often caused. Therefore prevention of groundings has been a so important issue that several counter measures were developed and equipped to ships. To develop effective measures against grounding accurate estimation of grounding frequency is important. In this paper new methods for estimation of grounding frequency using ship trajectories and geometry of seabed in a considered sea area is presented.

Different from collision, grounding can be prevented by keeping a planned route which enables a ship to sail without grounding. However when a ship deviates from the planned route, grounding will occur sometimes.

Considering them grounding frequency of a ship is formulated in two ways. The one is assuming that grounding occurs by deviation from a planned route. The other is assuming that grounding occurs by deviation from trajectories without groundings, the cause of which is omission error at keeping modified route to cope with a deviation from the initially planned route. Moreover for verification of the method a number of grounding candidates or a number of groundings are estimated using ship trajectories in Akashi Channel and geometry of seabed of the channel. Furthermore comparing with a statistics of groundings caused in the channel, probability of failing to avoid grounding was estimated varying time without corrective action. Finally the effectiveness of shortening time interval of position fixings in Akashi Channel is indicated.

Introduction

The casualty and ship characteristics data(LRFP 1998-2007) indicate that grounding frequency has been as high as frequencies of collision and hull/machinery damage. (Figure 1, "WS" means "Grounding") In addition during 2009, 300 and above ships ground at sea area around Japan, and the number of groundings is the next highest to collision in Japan. Therefore grounding is not able to be neglected and effective safety measures should be considered urgently. For this purpose estimation of grounding frequency based on a rational and effective modelling and scientific approach for prevention of groundings are important.

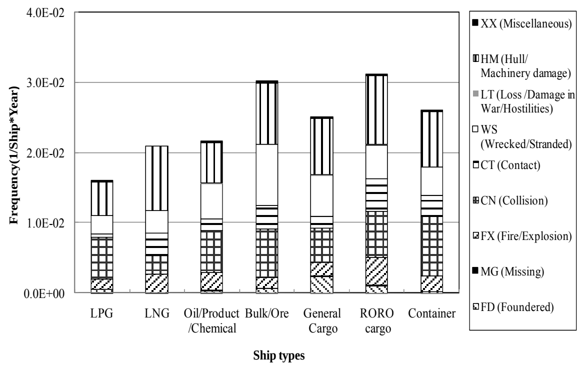

Figure 1 Accident frequencies of major cargo ship types of 500 GT and above (LRFP 1998-2007)

The method for estimating grounding frequency by modelling grounding from the relation between traffic flow and shoals and shore, was developed by Fujii et al.(Fujii 1974) A decades ago Pedersen developed methods for estimating grounding frequency from position distribution of a ship in the lateral direction to the ship's planned route. (Pedersen 1995) In many cases a ship can prevent grounding by keeping a route which are planned so as not to ground to shoals and shore before actual sailing. Therefore grounding is rather a problem caused by an individual ship's sailing than a problem caused by traffic flow. In case of treatment as an individual ship it should be noted that the position distribution along the lateral direction to a ship's planned route is thought to change as the distance between a ship and the target obstacle such as shoal and shore changes.

In this paper newly developed two methods for estimating grounding frequency are introduced. The one is assuming that grounding occurs by deviation from an initially planned route and probabilistic distribution of the deviation angle is a normal distribution, moreover probabilistic distribution of " time without corrective action" is a lognormal distribution. The other is assuming that grounding occurs by deviation from trajectories without groundings, the cause of which is omission error at keeping modified route to cope with a deviation from the initially planned route.

Besides for verification of those methods number of grounding candidates or a number of groundings are estimated using ship trajectories in Akashi Channel and geometry of seabed of the channel. Furthermore comparing with a statistics of grounding of the channel from 1989 to 1996 (Japan Coast Guard 1989-1996), probability of failing to avoid grounding was estimated varying time without corrective action. Finally the effectiveness of shortening time interval of position fixing is discussed.

Before introducing newly developed methods frequently used existing grounding model are summarized in chapter 2.

Existing grounding models

Two models as frequently used existing grounding models are explained briefly in this chapter. The literature (Mazaheri A. 2009) and (Jutta Y. 2008) and summarizes those models precisely.

A model based on traffic flow

Fujii's model (Fujii 1974) which is represented by Equation(1) is the representative model based on traffic flow. Figure 2 shows the concept of this model.

$$N = P(D + B)\rho V \qquad (1)$$

Where:
N is the number of ships which will ground
ρ is the average density of the traffic flow
V is the average speed of the traffic flow
D is the linear cross-section of the obstacle which is shallower than the draught of the ships
B is the average width of the ships
D+B is the effective width of the obstacle or shoal
P is the probability of mismaneuvering (probability of failing to avoid grounding)
$(D+B)\rho V$ represents a number of grounding candidates for ships in the traffic flow to ground to the target obstacle.
Then if number of groundings can be obtained by casualty statistics etc.,P is easily obtained by $N/(D+B)\rho V$. In case that there are large differences of speed among ships, the number of groundings can be obtained in this manner that after ships are grouped by speed, Equation(1) is applied to every such group, then all estimated grounding numbers of the groups are summed up.

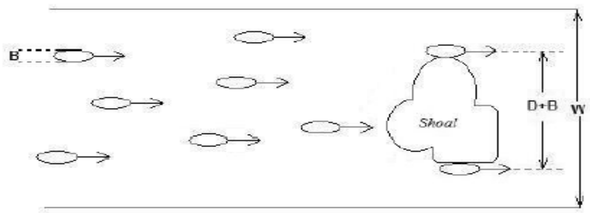

Figure 2 Grounding model by Fujii,Y. (Source (Mazaheri 2009))

An actual ship has a route to her destination, which was planned before sailing. Therefore though sometime direction of a ship turns toward a shoal at far area from the shoal, the direction is supposed to be changed not to ground to that. Therefore changing direction near a shore is not so much grounding avoidance maneuver as keeping planned route. Grounding is considered to occur because of deviation from planned route without corrective action after that.

A model based on position distribution of a ship in her route

Pedersen's model (Pedersen 1995) is the representative model based on lateral position distribution of a ship. Pedersen et.al. developed a method for estimating grounding frequency from position distribution of a ship in the lateral direction to the ship's planned route. In the model, a probability density function(p.d.f.) of position in the lateral direction to the ship's planned route are defined from the traffic on it. The p.d.f. is assumed to be the same all over her planned route. The grounding probability is obtained by multiplying some coefficients and the integral over the domain where ship's position has a grounding relation to the shoal. Figure 3 shows the concept of the second category of Pedersen's model.

This model categorizes grounding into 4 categories, which are explained below, and annual categorical frequency of grounding is estimated at each category, then annual grounding frequency is obtained by summing up annual frequencies of all categories.

- Ships following the ordinary, direct route at normal speed. Accidents in this category are mainly due to human error.
- Ships which fail to change course at a given turning point near the obstacle.
- Ships which take evasive action in the vicinity of the obstacle and as a result, collide with structure or ground on the shoal.
- All other track patterns than (1),(2) and (3) such as off-course ships and drifting ships.

As an example of the above categories, formulation in category (2) is shown in Equation (2)

$$F_{cat.2} = \sum_{ShipClass,i=1}^{n} P_{ci} Q_i P_0^{\frac{d-a_i}{a_i}} \int_L f_i B_i ds \qquad (2)$$

Where:

$F_{cat.2}$ is expected number of grounding per year of category 2
i is the number of ship class determined by vessel type and DWT or length
P_{ci} is the causation dependents on ship class(i) by the effect of the pilot since the probability of having a pilot during the passage increase with the vessel size
Q_i is the number of movements per year of ship class(i) in the considered lane
L is total width of considered area perpendicular to the ships' traffic
f_i is ship track distribution
B_i is grounding indication function, and is one when grounding occur, and zero when grounding does not occur.
P_0 is the probability of omission to check the position of the ship
d is the distance from obstacle to the bend in the navigation route, varying with the lateral position of the ship a_i is the average length between position checks by the navigator

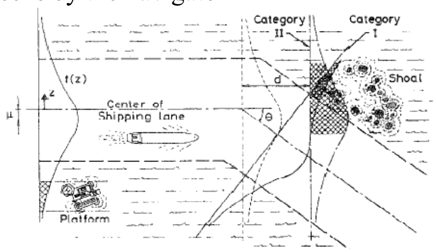

Figure 3 Grounding model by Pedersen,P.T.(Source (Pedersen 1995))

f_i is considered to be different if the distance from ship to a obstacle is different. Therefore to improve accuracy the change of f_i along the traffic route should be examined.

Grounding model using ships' trajectories and geometry of seabed

In the following newly developed grounding model is explained. In the following description it is assumed that a planned route is correctly set not to lead a ship to ground as long as she follows the route.

Outline

Collision candidate can be defined as a situation that ships collide each other if no evasive action will not be taken except keeping initially planned route. However grounding candidate can not be defined as the above definition of collision candidate. It is because planned route is set not to ground to obstacles such as shoal and shore. Whenever grounding occurs, a ship deviates from planned route if planned route is set using correct charts.

However even if a ship deviates from planned route, grounding scarcely occurs because of evasive action based on periodic position fixing for grounding avoidance. Then in this paper grounding candidate is defined as a situation that when a ship deviates from planned routes and she sails without corrective action such as changing course or speed a ship grounds. Therefore important things are number of deviations and time after beginning of deviation without corrective action.

Here the newly developed methods of estimating annual grounding candidate frequency or annual grounding frequency using trajectories of all ships in a considered sea area and geometry of seabed of the sea area is introduced. The methods are based on two different views on ships' trajectories.

A view that observed trajectories are almost the same as planned routes (View A)

This view is based on an assumption that number of deviations are not so many and large that differences between initial planned routes and trajectories are too small to decide that they are apparently different. Causes of deviations are the same as those by Pederson. They are thought to be listed holistically. On the contrary to the Pederson's method a ship is assumed to deviate from initially planned route to different direction at any point of the route in this method. Therefore the p.d.f. of deviation angle should be defined.

A view that observed trajectories are results after coping with deviations (View B)

In this view grounding is assumed to occur by more deviation from observed trajectories without groundings. In this case "deviation" means that a ship goes straight by failing to follow a modified route planned by a series of process for coping with a deviation from the initially planned route, in other word the deviation is assumed to occur by omission error in the process of following a modified route. Moreover the deviation by omission error assumed to occur at any point of modified route, that is observed trajectories, and it is also assumed that time interval of position fixing will be shorter than that of regular position fixing. In this assumption continuation of deviation after failure of position fixing is considered.

Observed trajectories and directional deviation at every point of trajectories

Trajectories obtained by analysis of radar images are serieses of points of fixed time interval. These points are called "trajectory points" here. Then at a considered sea area and to every ship type, a p.d.f. of a directional deviation which is the angle between successive elemental routes, edge points of which are successive trajectory points are made.(Figure 7) The observed trajectories are considered to include trajectory points which are the results of coping with deviations. Elemental route both edges of which are successive edges of a trajectory, called "unit trajectory" in the following description. Decision of grounding was made by comparing a draught of a ship with a depth of the position of the ship.

These views are similar to Pedersen's method of estimating grounding frequency based on a distribution of ship's position along the lateral direction to the ship's heading. Different from the Pedersen’s method these views are based on directional deviation. Moreover these grounding frequency estimation methods make it possible to calculate grounding of ships which have various draughts all together.

Methods for estimation of grounding frequency
Grounding model based on the view A(Model A)

For some reasons a ship is assumed to deviates with angle θ from her planned route at any points of it, and after that she is assumed to sail straight at the speed v(x) at the deviation point (x) for time (t) which is time without corrective action, then if there exist obstacles inside the circle, centre of which is the deviation point and radius of which is $v(x)\cdot t$, the ships grounds to those.(Figure 4) Here probability of combination of trajectory point (x) where deviation occurs and time without corrective action (t) is denoted as $H_i(x,t)$. $H_i(x,t)$ is called p.d.f. of time without corrective action at trajectory point (x) in the following. For $H_i(x,t)$ Equation(3) can be assumed .

$$\int_0^{T_{\max}(i)}\int_0^{L(i)} H_i(x,t)dxdt=1 \qquad (3)$$

Where L(i) is the length of planned route of ship(i).
$T_{max}(i)$ is the maximum time without corrective action from the beginning of deviation. Here for simplification, t and x are assumed to be mutually

independent, then $H_i(x,t)$ can be represented as Equation(4).

$$H_i(x,t) = h_i(t) g_i(x) \tag{4}$$

Where $h_i(t)$ is a p.d.f of time without corrective action of ship(i).
$g_i(x)$ is a p.d.f that deviation point of ship(i) is x.
$h_i(t)$ cannot be estimated from data such as trajectories, it would relate to time interval of position fixing.

Then the following variables are defined.
$f_i(\theta|x)$ is a p.d.f. of deviation angle when ship (i) deviates from planned route at x. it is called p.d.f. of directional deviation.
$\theta_{i\text{-}grd}(x,t)$ is a deviation angle when ship(i) deviates at point(x) on her planned route and after the deviation she sails at the speed and not changing direction for the time(t) she will ground.
$K_{out}(i,j)$ is a number of deviations in case that ship(i) will deviates when the cause of deviation is j.
j means one of the category numbers by Pedersen's categorization of grounding causes.
M is total number of ships sailing in a considered sea area.

Using the above definition, a number of grounding candidates($N_{grd-cd}(i)$) that ship(i) encounters in a navigation along the planned route is expressed as Equation(5).

$$N_{grd-cd}(i) = K_{out}(i,j) \int_0^{T_{max}(i)} \int_0^{L(i)} h_i(t) \left\{ \int_{\theta=\theta_{i-grd}(x,t)} f_i(\theta|x) g_i(x) d\theta \right\} dx dt \tag{5}$$

Then total number of grounding candidates($N_{grd-hz-total}$) which occurs in a considered sea area for a considered period is expressed as Equation(6).

Here if a number of grounding accidents during considered period and in the considered sea area, which is denoted as N_{grd-st} , is known, probability of failing to avoid grounding (P_{fail}) can be obtained as Equation (7).

After beginning of a deviation, position fixing is assumed to be carried out at every pre-determined time interval. Here time to the first position fixing after beginning of every deviation are assumed to distribute along log-normal distribution, the mean of which are normal time interval of position fixing. And it is assumed that if the first position fixing is done, any deviation will be corrected and grounding is successfully prevented. Therefore it is not considered that deviation continues after the first position fixing.

$$N_{grd-cd-total} = \sum_{i=1}^{M} N_{grd-cd}(i) \tag{6}$$

$$P_{fail} = \frac{N_{grd-st}}{N_{grd-cd-total}} \tag{7}$$

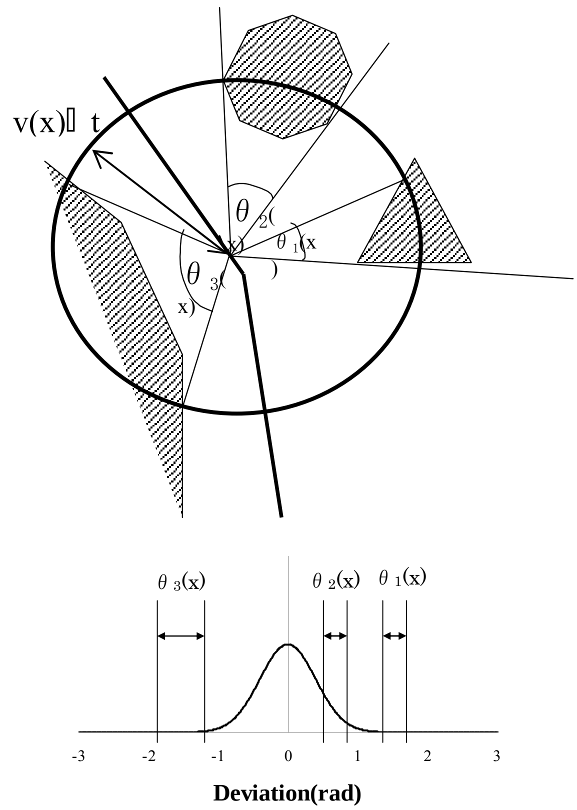

Figure 4 Grounding model based on deviation from a planned route (Model A)

Grounding model based on the view B(Model B)

In this case it is supposed that a ship will ground by omission error at position fixing or omission error at returning back to her trajectory just after position fixing at some time after deviation from her trajectory. (Figure 5) As mentioned above, in this case position fixing interval is thought to be shorter than that of regular sailing because this position fixing is assumed as the action on the way of keeping the trajectory by carrying out coping with the deviation from a planned route.

In this case number of grounding of ship(i) ($N_{grd}(i)$) can be expressed as Equation(8).

$$N_{grd}(i) = \int_0^{L(i)} \varepsilon^{\left\lceil \frac{T(x)}{\Delta t} \right\rceil} g_i(x) dx \tag{8}$$

Where

ε is omission error probability
Δt is position fixing interval
$g_i(x)$ is the same as $g_i(x)$ in Equation(4) and in Equation(5)
T(x) is the minimum time to the grounding of ship(i) when ship(i) sails to the direction of the unit trajectory just before a trajectory point (x) from point (x).
$\lceil y \rceil$ is the smallest integer above y (ceiling function of y).

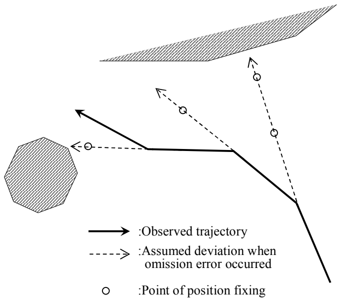

Figure 5 Grounding model based on omission error at keeping a trajectory (Model B)

Number of groundings which will occur in a considered sea area during considered period is expressed as Equation(9).

$$N_{grd-total} = \sum_{i=1}^{M} N_{grd}(i) \tag{9}$$

Application to Akashi Channel

Trajectories and groups of ships

Figure 6 shows ships' trajectories obtained by analyzing radar images of ships in Akashi Channel. Number of ships is 3,179. These ships are categorized into 26 groups by gross tonnage.(Table 1) Time interval between successive 2 points of trajectories, that is time length of a unit trajectory, ranges from 1 to 3 minutes at one minute interval. Ship's velocity was calculated at every unit trajectory. These data are 49 hours data of trajectories from 11:00 am, 30-Oct-1990 to 0:00 pm (noon), 1/Nov/1990.

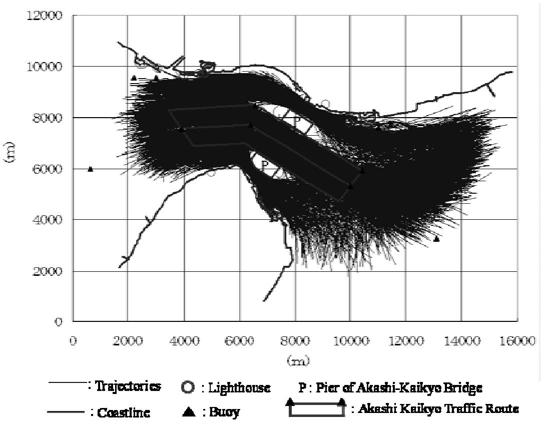

Figure 6 Ship trajectories in Akashi Channel (from 30/Oct. to 1/Nov./1990, during 49 hours)

p.d.f. of angles between successive unit trajectories used in Model A

Figure 7 shows the p.d.f. of angles between successive unit trajectories, which are called p.d.f. of directional deviation, that is $f_i(\theta|x)$. As mentioned above time length of a unit trajectory is from 1 minute to 3 minutes, and unit trajectories of 3 minute are more than that of 1 minutes. The shorter time length of unit trajectory becomes, the larger the probability at 0 degree will become, because the number of unit trajectories of straight trajectory becomes larger if the length of unit trajectory becomes shorter. However in this paper though p.d.f. of directional deviation depends on time length of unit trajectory, all unit trajectories are used for obtaining the p.d.f. of directional deviation.

The p.d.f. of directional deviation obtained from unit trajectories of all ship groups is thought to be approximated by a normal distribution. Moreover the p.d.f. of directional deviation of every group is mutually similar to each other.(Table 2) Therefore the p.d.f. of directional deviation obtained from unit trajectories of all ship groups is used as the p.d.f. of directional deviation of all trajectory points.

Here $g_i(x)$ is assumed as a constant at every trajectory point of ship(i), and is defined as $1/S_i$. S_i is a number of trajectory points of ship(i) - 1. $h_i(t)$ was approximated by lognormal distribution, the mean of which varies from 5 minutes to 15 minutes at 5 minutes intervals. This treatment of mean of position fixing interval is based on the literature (JDREA).

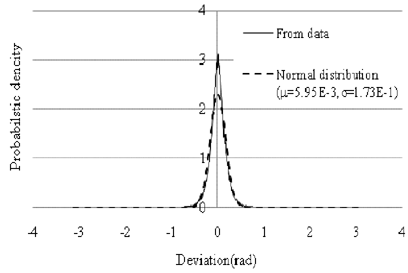

Figure 7 p.d.f. of deviation angle between successive unit trajectories of all ships

Table 1 Grouping of ships by gross tonnage and principal particulars of representative ship of every group of ships

Group No.	Range of Gross Tonnage	Number of ships	Gross Tonnage	Length overall (m)	Breadth (m)	Draught (m)
1	~ 20	827	10	10.7	3.4	0.96
2	~ 100	221	60	23.9	5.7	1.80
3	~ 200	611	150	36.0	7.5	2.49
4	~ 300	267	250	45.2	8.7	2.98
5	~ 400	60	350	52.6	9.5	3.35
6	~ 500	608	450	58.8	10.3	3.66
7	~ 1000	166	750	66.7	11.9	4.39
8	~ 1,500	179	1,250	78.1	13.8	5.58
9	~ 2,000	33	1,750	86.6	15.2	5.67
10	~ 2,500	50	2,250	93.6	16.4	5.75
11	~ 3,000	37	2,750	99.5	17.4	5.84
12	~ 4,000	47	3,500	107.2	18.7	5.96
13	~ 5,000	3	4,500	115.8	20.1	6.13
14	~ 6,000	3	5,500	123.2	21.3	6.30
15	~ 7,000	12	6,500	129.7	22.3	6.46
16	~ 8,000	5	7,500	135.6	23.3	6.63
17	~ 9,000	6	8,500	140.9	24.1	6.79
18	~ 10,000	7	9,500	145.8	24.9	6.95
19	~ 30,000	20	20,000	183.4	31.0	8.60
20	~ 40,000	6	35,000	218.0	36.5	10.76
21	~ 50,000	4	45,000	235.5	39.2	12.07
22	~ 70,000	3	60,000	257.4	42.6	13.85
23	~ 80,000	1	75,000	275.7	45.5	15.41
24	~ 90,000	1	85,000	286.5	47.2	16.32
25	~ 100,000	1	95,000	296.5	48.7	17.13
26	100,000～	1	150,000	341.3	55.7	19.78
Total		3,179				

Table 2 Parameter of p.d.f. of deviation angle between successive unit trajectories in every group of ships

Group No.	Data size	Mean (rad.)	Standard deviation (rad.)
1	11,731	2.74E-03	1.59E-01
2	3,887	4.25E-03	1.69E-01
3	10,095	1.42E-03	1.80E-01
4	4,824	7.92E-03	1.66E-01
5	1,064	1.07E-02	1.69E-01
6	11,044	8.95E-03	1.66E-01
7	2,730	1.27E-02	1.81E-01
8	2,423	-6.08E-03	2.41E-01
9	546	2.02E-02	1.66E-01
10	647	1.81E-02	1.91E-01
11	521	1.95E-02	1.80E-01
12	582	2.04E-02	1.89E-01
13	59	-3.08E-02	1.00E-01
14	38	2.89E-02	1.81E-01
15	157	3.52E-02	1.79E-01
16	63	2.77E-02	1.63E-01
17	80	5.68E-02	1.60E-01
18	68	5.23E-02	1.99E-01
19	249	5.08E-02	1.63E-01
20	84	-1.27E-02	1.29E-01
21	46	3.76E-03	1.54E-01
22	46	-2.73E-03	1.33E-01
23	13	6.07E-02	1.21E-01
24	6	1.92E-01	1.85E-01
25	11	-5.39E-02	8.68E-02
26	13	-1.36E-02	1.60E-01
All	51,027	5.95E-03	1.73E-01

Seabed geometry and contour lines at corresponding ship draughts of Akashi Channel

Here the geometry of seabed was defined as a polyhedron composed of triangles, vertex of which are depth measurement points. Therefore geometry of seabed is called seabed polyhedron in the following. A depth measurement point is represented as (x,y, z). x, y and z have a longitudinal value, a latitudinal value and a depth value of a depth measurement point respectively. These points are prepared by Japan Hydro-graphic Association. The triangles are obtained by the following procedure. Firstly Delaunay triangulation is applied to the sea level points which are generated by projection of depth measurement points to sea level. After that, seabed polyhedron is composed of triangles, vertex of which are depth measurement points corresponding to the sea level points generated above procedure. Delaunay triangulations maximize the minimum angle of all the angles of the triangles in the triangulation. (Golias 1997).

Using seabed polyhedron contour lines, the depths of which are draughts of representative ships, are made. The process of obtaining such contour lines is shown conceptually in Figure.8. Moreover several depth contour lines corresponding to the draught values of representative ships and sea level projection of seabed polyhedron is shown in Figure 9 with lines of sea shores which are obtained by analyzing radar images. There are some discrepancies between lines of sea shores and outer edges of the projection of seabed polyhedron. Main reason of this is that as sea level values of depth measurement points are expressed by world geodesic system and these values must be transformed into the values of co-ordinate defined on the plane of radar images.

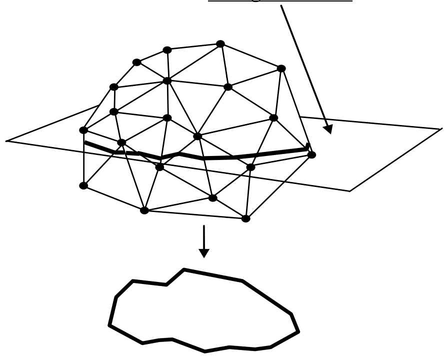

Figure 8 Seabed polyhedron and contour lines at draught of a ship.

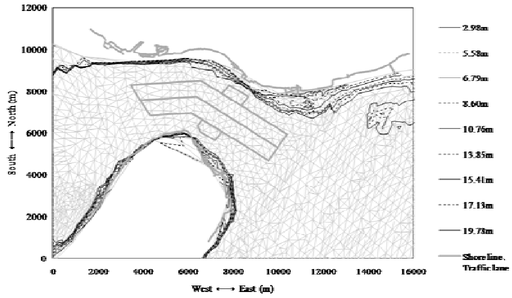

Figure 9 Sea level projection of seabed polyhedron and contour lines of some groups of ships in Akashi Channel (Kaneko 2007)

Grounding candidate and grounding frequency in Akashi Channel

Estimation of grounding candidate frequency (Model A)

Number of grounding candidates of all ship groups during 49 hours which estimated using Equation(5) varying time without corrective action as a parameter are shown in Table 3.

In order to estimate K_{out}(i,collision avoidance) in Equation 5,which represents number of deviations by collision avoidance manoeuvre of ship i, it is assumed that two ships are involved in a collision candidate and in Akashi Channel the number of collision candidates during 49 hours is 707(Kaneko,2007). Then K_{out}(i,collision avoidance) during 49 hours is estimated as follows.

$K_{out}(i, \text{collision avoidance}) = 707 \times 2/3179 = 0.44$ (for all i). Annual grounding candidate frequency, which is estimated as a multiplying number of grounding candidates during 49 hours by $365 \times 24/9$, is also shown in Table 3. As a p.d.f. of directional deviation the normal distribution in Figure 7 was used. In addition, $h_i(t)$, that is a p.d.f. of time without corrective action, is defined as a lognormal distribution, mean value of which is set to position fixing interval and the standard deviation is set to 5 minutes. Using the p.d.f.

the annual grounding candidate frequencies are obtained varying position fixing interval from 5 to 15 minutes which are means of the p.d.f. As a cause of deviation from planned routes only collision avoidance manoeuvre is considered. That is, only category 3 of Pedersen's model is considered.

Table 4 shows annual grounding numbers in Akashi Channel from 1989 to 1996, which are extracted from the casualty statistics (JCG 1989-1996). The casualty statistics describes number of groundings at which rescue was required and not required separately. Required number here is both numbers. Unfortunately this statistics does not describe number of groundings at which rescue was not required in Akashi Channel. Only the number in Seto Inland Sea which includes Akashi Channel is described. In this circumstances the number of groundings at which rescue was required and not required in Akashi Cannel is estimated as the way shown in Table 4. From table 4 average annual grounding frequency estimated as 1.91, using this value probability of failing to avoid grounding was estimated varying position fixing interval. The probabilities are shown in Table 5. In real sea area as causes of deviation from planned route, drifting by tidal current, failure of turning at way points etc. are considered. For Model A, K_{out} which are based on such causes except collision avoidance should be estimated for accurate estimation of grounding candidate frequency.

Table 3 Occurrence frequencies of grounding candidates varying time without corrective action Akashi Channel, where the mean of h(t) is 10 minutes.(Model A)

Group No.	Draught (m)	Time without corrective action (Ti (min))										
		1	2	3	4	5	10	20	30	40	50	60
1	0.96	1.99E+00	8.67E+00	2.09E+01	3.66E+01	5.28E+01	1.05E+02	1.48E+02	1.55E+02	1.57E+02	1.57E+02	1.57E+02
2	1.80	1.07E+00	3.07E+00	6.93E+00	1.09E+01	1.46E+01	2.33E+01	3.31E+01	3.72E+01	3.84E+01	3.88E+01	3.91E+01
3	2.49	5.82E+00	1.57E+01	2.81E+01	4.41E+01	5.81E+01	8.16E+01	1.14E+02	1.27E+02	1.31E+02	1.32E+02	1.33E+02
4	2.98	5.55E-03	1.18E-01	4.27E-01	1.34E+00	3.42E+00	1.12E+01	3.31E+01	4.35E+01	4.72E+01	4.94E+01	5.03E+01
5	3.36	3.51E-02	3.83E-02	1.01E-01	2.50E-01	6.67E-01	1.95E+00	7.19E+00	9.51E+00	9.78E+00	9.84E+00	9.87E+00
6	3.67	1.02E-04	7.12E-02	3.37E-01	2.50E+00	7.68E+00	2.65E+01	7.85E+01	9.01E+01	9.08E+01	9.09E+01	9.09E+01
7	4.39	1.54E+00	3.98E+00	6.48E+00	9.01E+00	1.19E+01	2.03E+01	3.31E+01	3.47E+01	3.48E+01	3.48E+01	3.48E+01
8	5.58	9.72E+00	2.14E+01	3.31E+01	4.43E+01	5.10E+01	6.39E+01	7.20E+01	7.31E+01	7.31E+01	7.31E+01	7.31E+01
9	5.67	0.00E+00	0.00E+00	7.50E-02	3.39E-01	9.78E-01	4.84E+00	8.70E+00	9.31E+00	9.32E+00	9.32E+00	9.32E+00
10	5.75	0.00E+00	3.65E-02	5.33E-01	1.46E+00	2.76E+00	9.98E+00	1.36E+01	1.41E+01	1.41E+01	1.41E+01	1.41E+01
11	5.84	0.00E+00	1.07E-02	2.24E-01	8.49E-01	1.58E+00	6.49E+00	1.02E+01	1.05E+01	1.05E+01	1.05E+01	1.05E+01
12	5.96	7.57E-09	6.35E-02	3.24E-01	1.33E+00	2.38E+00	9.53E+00	1.32E+01	1.35E+01	1.35E+01	1.35E+01	1.35E+01
13	6.13	0.00E+00	0.00E+00	0.00E+00	2.07E-05	4.00E-02	2.55E-01	7.89E-01	8.44E-01	8.60E-01	8.60E-01	8.60E-01
14	6.30	0.00E+00	0.00E+00	0.00E+00	0.00E+00	1.70E-03	1.20E-01	5.15E-01	6.49E-01	6.52E-01	6.52E-01	6.52E-01
15	6.46	0.00E+00	2.84E-08	1.23E-04	1.89E-01	3.07E-01	1.61E+00	2.57E+00	2.67E+00	2.67E+00	2.67E+00	2.67E+00
16	6.63	0.00E+00	0.00E+00	3.74E-02	1.36E-01	2.37E-01	1.14E+00	1.44E+00	1.44E+00	1.44E+00	1.44E+00	1.44E+00
17	6.79	0.00E+00	0.00E+00	0.00E+00	8.70E-02	3.20E-01	1.11E+00	1.46E+00	1.48E+00	1.48E+00	1.48E+00	1.48E+00
18	6.95	0.00E+00	0.00E+00	3.25E-05	9.84E-02	3.30E-01	1.27E+00	1.68E+00	1.73E+00	1.74E+00	1.74E+00	1.74E+00
19	8.60	0.00E+00	0.00E+00	1.07E-02	2.17E-01	6.06E-01	2.94E+00	6.88E+00	7.92E+00	8.25E+00	8.37E+00	8.44E+00
20	10.76	0.00E+00	0.00E+00	2.58E-07	5.79E-02	1.51E-01	7.26E-01	2.03E+00	2.39E+00	2.60E+00	2.62E+00	2.62E+00
21	12.07	0.00E+00	0.00E+00	1.26E-09	1.70E-02	8.85E-02	4.77E-01	1.33E+00	1.66E+00	1.71E+00	1.75E+00	1.75E+00
22	13.85	0.00E+00	0.00E+00	5.18E-08	5.36E-02	9.93E-02	4.70E-01	1.17E+00	1.28E+00	1.32E+00	1.32E+00	1.33E+00
23	15.41	0.00E+00	0.00E+00	0.00E+00	0.00E+00	1.33E-09	2.87E-02	2.03E-01	3.94E-01	4.45E-01	4.45E-01	4.45E-01
24	16.32	0.00E+00	0.00E+00	0.00E+00	6.74E-07	6.81E-03	1.21E-01	3.77E-01	4.45E-01	4.45E-01	4.45E-01	4.45E-01
25	17.13	0.00E+00	0.00E+00	9.94E-09	1.91E-02	7.45E-02	2.17E-01	3.91E-01	4.40E-01	4.45E-01	4.45E-01	4.45E-01
26	19.78	0.00E+00	0.00E+00	0.00E+00	2.10E-08	4.99E-05	7.11E-02	3.55E-01	3.96E-01	4.30E-01	4.44E-01	4.45E-01
Total(49hour)		2.02E+01	5.32E+01	9.75E+01	1.54E+02	2.10E+02	3.76E+02	5.85E+02	6.41E+02	6.54E+02	6.58E+02	6.60E+02
1 Year		3.61E+03	9.51E+03	1.74E+04	2.75E+04	3.75E+04	6.71E+04	1.05E+05	1.15E+05	1.17E+05	1.18E+05	1.18E+05
h(Ti)		1.41E-16	7.46E-10	8.08E-07	4.54E-05	5.90E-04	1.38E-01	7.14E-01	1.36E-01	1.01E-02	6.72E-04	4.94E-05
Number of grounding candidates		5.10E-13	7.10E-06	1.41E-02	1.25E+00	2.21E+01	9.26E+03	7.48E+04	1.56E+04	1.18E+03	7.91E+01	5.84E+00

In table 3 $h(T_i) = \int_{T_{i-1}}^{T_i} \text{p.d.f.of Lognormaldistribution}(t\,;\text{mean} = 15\text{min},\text{standarddeviation} = 5\text{min})\,dt$

Table 4 Number of grounding accidents in Akashi Channel (JCG 1989-1996)

A.D.	Akashi Channel: Number of ships that required rescue (A1)	Akashi Channel: Number of ships that required or did not require rescue (B1) (Estimation : B1=A1*B2/A2)	Seto Inland Sea: Number of ships that required rescue (A2)	Seto Inland Sea: Number of ships that required or did not require rescue (B2)	B2/A2
1989	2	2.29	97	111	1.14
1990	1	1.11	105	117	1.11
1991	0	0.00	153	170	1.11
1992	2	2.16	111	120	1.08
1993	0	0.00	107	118	1.10
1994	0	0.00	76	82	1.08
1995	5	5.56	124	138	1.11
1996	4	4.18	89	93	1.04
Total	14	15.31	862	949	1.10
Average	1.75	1.91	107.75	118.63	

Table 5 Grounding candidates' number and probability of failing to avoid grounding (Model A)

Average of position fixing interval (min)	5	10	15
Number of Grounding candidate	3.95E+04	7.91E+04	1.01E+05
Probability of failing to avoid grounding	4.83E-05	2.42E-05	1.89E-05

Table 6 Grounding frequencies varying time without action in Akashi Channel, where omission error probability is 0.001(ε) and position fixing interval is 2 minutes. (Model B)

Group No.	Draught (m)	Time without corrective action (min): 2	4	6	8	10	12
1	0.96	2.16E+01	7.21E+01	8.23E+01	6.18E+01	5.39E+01	3.68E+01
2	1.80	7.39E+00	2.23E+01	2.09E+01	1.42E+01	1.44E+01	8.53E+00
3	2.49	3.75E+01	7.56E+01	7.38E+01	3.30E+01	3.39E+01	2.10E+01
4	2.98	4.31E-01	4.20E+00	1.93E+01	1.23E+01	2.03E+01	1.17E+01
5	3.36	6.85E-02	8.33E-01	4.13E+00	2.95E+00	4.35E+00	2.90E+00
6	3.67	1.67E-01	9.70E+00	4.69E+01	3.76E+01	5.59E+01	3.91E+01
7	4.39	8.91E+00	1.17E+01	1.63E+01	1.33E+01	2.09E+01	1.22E+01
8	5.58	4.76E+01	5.25E+01	2.69E+01	1.25E+01	1.40E+01	8.05E+00
9	5.67	0.00E+00	1.32E+00	3.78E+00	4.26E+00	7.92E+00	3.59E+00
10	5.75	1.54E-01	5.21E+00	8.81E+00	7.77E+00	8.57E+00	3.41E+00
11	5.84	4.57E-02	3.30E+00	4.76E+00	6.20E+00	7.08E+00	4.10E+00
12	5.96	1.43E-01	4.56E+00	6.81E+00	8.54E+00	9.42E+00	3.11E+00
13	6.13	0.00E+00	0.00E+00	6.55E-01	4.53E-01	3.91E-01	1.61E-01
14	6.30	0.00E+00	0.00E+00	1.92E-01	3.27E-01	2.81E-01	6.24E-01
15	6.46	0.00E+00	8.08E-01	1.23E+00	1.82E+00	3.01E+00	1.16E+00
16	6.63	0.00E+00	5.20E-01	5.08E-01	7.60E-01	1.34E+00	5.02E-01
17	6.79	0.00E+00	3.04E-01	1.34E+00	1.19E+00	8.85E-01	1.70E-01
18	6.95	0.00E+00	3.61E-01	1.34E+00	1.33E+00	9.13E-01	5.22E-01
19	8.60	0.00E+00	7.57E-01	2.40E+00	3.75E+00	3.00E+00	1.79E+00
20	10.76	0.00E+00	2.47E-01	5.36E-01	7.47E-01	6.72E-01	8.56E-01
21	12.07	0.00E+00	7.20E-02	4.48E-01	4.70E-01	4.14E-01	5.71E-01
22	13.85	0.00E+00	2.28E-01	3.43E-01	2.49E-01	4.16E-01	2.54E-01
23	15.41	0.00E+00	0.00E+00	0.00E+00	0.00E+00	6.67E-02	1.33E-01
24	16.32	0.00E+00	0.00E+00	2.80E-01	1.43E-01	0.00E+00	1.43E-01
25	17.13	0.00E+00	8.00E-02	2.40E-01	2.34E-01	1.27E-01	1.27E-01
26	19.78	0.00E+00	0.00E+00	8.00E-02	1.07E-01	1.40E-01	3.37E-03
Total(49hour)		1.24E+02	2.67E+02	3.24E+02	2.26E+02	2.62E+02	1.62E+02
1 Year		2.22E+04	4.77E+04	5.80E+04	4.04E+04	4.69E+04	2.89E+04
$\varepsilon, \varepsilon^2, \varepsilon^3$, ---		1.00E-04	1.00E-08	1.00E-12	1.00E-16	1.00E-20	1.00E-24
Grounding numbers		2.22E+00	4.77E-04	5.80E-08	4.04E-12	4.69E-16	2.89E-20

Table 5 suggests that shortening of position fixing interval would enable to make the grounding candidates frequency small.

Estimation of grounding frequency (Model B)

Omission error probability is obtained as from 1.0×10^{-3} to 3.0×10^{-3} per item when use of written procedure is specified from a literature (Swain 1983).

These values are used in nuclear power plants. Omission error in the middle of action for route correction when officers recognize deviation from planned route and follow a modified route is assumed as smaller than that in normal operation of nuclear power plant here. The reason is that level of consciousness at such emergency operation for correction of route when officers recognize deviation is thought to be higher than that in usual operation of nuclear power plant. However this assumption has not been verified yet.

Table 6 shows grounding frequencies at every value of time without corrective action and its calculation process where omission error probability is 0.001. Table 7 shows annual grounding frequencies estimated varying omission error probability and position fixing interval. The combinations of time without corrective action and omission error probability which make estimated annual grounding frequency near the statistical data in Table 4 can be found in Table 7. Table 7 indicate that for good agreement between the statistical data of grounding frequency in Akashi Channel and the estimated grounding frequency, rather smaller omission error probability than that used in nuclear plant and rather shorter position fixing interval than the usual value are necessary.

Table 7 Annual grounding frequency varying omission error probability and position fixing interval

		Position fixing interval (min)				
		1	2	3	4	5
Omission occurrence probability	3.0E-03	2.49E+01	6.69E+01	1.28E+02	2.11E+02	2.99E+02
	1.0E-03	8.25E+00	2.22E+01	4.25E+01	7.00E+01	9.93E+01
	5.0E-04	4.12E+00	1.11E+01	2.12E+01	3.50E+01	4.96E+01
	1.0E-04	8.23E-01	2.22E+00	4.24E+00	6.99E+00	9.91E+00

Discussion

Most of estimation methods of grounding frequency developed until now are based on the modelling which uses a position distribution of a ship along lateral direction of the route of the ship. Different from those methods, this method is based on the directional deviation from planned routes or realized trajectories after dealing with deviations from planned routes, therefore the developed methods can be said to be new approaches of estimating grounding frequencies. Moreover these method can deal with ships of optional draughts and optional seabed all together.

Some problems and possible improvements to the model were discussed in the followings.

On Model A

Trajectories are different from initially planned routes, therefore assuming trajectories as planned routes is not reasonable basically. However if similarity between planned routes and trajectories will be verified the assumption can be considered to be rational. But to obtain planned routes of thousands of ships are very difficult. A possible way of this is thought to be inquiring mariners. As trajectories of deviation were not classified by their causes, to use obtained deviation distribution of Figure 7 and Table 6 as deviation distribution by collision avoidance is not appropriate. Classification of deviation distribution by their cause is too difficult to be done. If it will be done and planned routes of all ships in a considered sea area will be obtained Model A will become reasonable.

On Model B

Trajectories obtained from radar images includes the trajectories when coping with deviations, and the view that deviation from trajectories leads a ship to grounding presents a practical way for estimating grounding frequency because Model B does not need planned routes. The point is the merit of Model B comparing Model A.

For good agreement between the statistical data of grounding frequency in Akashi Channel and the estimated grounding frequency, rather smaller omission error probability than that used in nuclear plant and rather shorter position fixing interval are necessary. To overcome this problem a few assumptions are introduced. However they should be verified in the future.

Common problem

In these methods a ship is expressed as a point. However in order to improve accuracy of frequency of grounding candidate frequency and that of grounding frequency to obstacles in sea areas where heavy traffic exists such as established traffic lane, it is necessary to consider shape of a ship. Moreover for improving accuracy it is necessary to estimate tide level.

Conclusion

The followings are dealt with in this paper. New grounding models were developed. The models use trajectories and geometry of seabed. One of them(Model A) is based on the assumption that differences between trajectories and corresponding planned routes are small enough for considering trajectory as planned routes. However this assumption is not true basically. The other model(Model B) is based on the assumption that deviation from trajectory by omission error leads a ship to grounding.

These grounding models were applied to Akashi Channel in Japan. The reasonableness of the two models are not fully justified by the result. However if some improvements will be done these models would be verified as suitable for grounding model. Though they need great computing power to handle large data, recent personal computer is powerful enough to handle ship trajectories and seabed polyhedron in the sea area like Akashi Channel. Therefore these models are considered to be effective method to estimate grounding frequency in real sea area.

Acknowledgement

This research was carried out as a part of the research project, title of which is "Research on general safety assessment of ships(RR-S7)" of Japan Ship Technology Research Association, which carried out during 2002 fiscal year of Japan. (JSTRA 2003) The project was supported by Nippon Foundation. The author is grateful to those association, foundation and people concerned for their cooperation and support.

The used data of trajectories in Akashi Channel in this paper were offered by the Kobe Marine Casualty Prevention Institute. Dr. Daich Hara of Japan Marine Science Inc. taught the author how to use the trajectory data. The author is also grateful to them.

References:

Lloyd's Register Fairplay (LRFP). 1998-2007. Casualty and ship characteristics database. London. England.

Mazaheri A. 2009. Probabilistic Modeling of Ship Grounding – A review of literature, Helsinki University of Technology Faculty of Engineering and Architecture. Department of Applied Mechanics. Series AM. TKK-AM-10. Espoo, Finland.

Jutta Y. et al. 2008. Accident Probabilities in Selected Areas of the Gulf of Finland, Helsinki University of Technology Faculty of Engineering and Architecture. Department of Applied Mechanics. Series AM. TKK-AM-6. Espoo, Finland.

Fujii, Y.,et al., 1974. Some Factors Affecting the Frequency of Accidents in Marine Traffic: I-The Diameter of Evasion for Crossing Encounters, II-The probability of Stranding,III-The Effect of Darkness of the Probability of Collision and Stranding, Journal of Navigation.Vol.27(2):239-247.

Pedersen, P.T.1995. Collision and Grounding Mechanics. Proceedings of WEMT '95'. Copenhagen. Denmark. The Danish Society of Naval Architecture and Marine Engineering.

Golias N.A.,and Dutton R.W. 1997. Delaunay triangulation and 3D adaptive mesh generation. Finite Elements in Analysis and Design. Vol.25:331-341

Kaneko F. 2007. Estimation of dangerous encounters' number from observed ship trajectories, Proceedings of 3rd ICCGS Conference.:187-193. Hamburg. Germany.

Japan Dredging and Reclamation Engineering Association(JDREA). Navigation method. Umidas #13, http://www.umeshunkyo.or.jp/207/257/data.html

Japan Coast Guard(JCG). 1989-1996. Rescue Needed Casualty Statistics.

Japan Ship Technology Research Association(JSTRA). 2003. Report of Research on general safety assessment of ships.

A.D.Swain,H.E.Guttman. 1983. Handbook of Human Reliability Analysis with Emphasis on Nuclear Power plant Applications(Final Report). NUREG/CR-1278. SAND80-0200:15-14

Influence of coupling in the prediction of ship collision damage

Kristjan Tabri

Tallinn University of Technology, Department of Civil Engineering, Faculty of Mechanical Engineering

Abstract:
The paper studies the influence of coupling between the ship motions and the structural resistance in predicting the ship collision damage. Several collision scenarios are simulated using coupled and decoupled approaches. A coupled approach implies a time-domain simulation, where a precise description of the whole collision process together with the full time histories of the motions and forces involved, is achieved. There, the ships' motions are evaluated in parallel to the structural deformations i.e. the coupling between external dynamic and inner mechanics is preserved. A decoupled approach is based on the conservation of momentum and allows fast estimation of deformation energy without providing exact ship motions. The method is based on the ship masses and velocities, and there is no coupling from the structural behaviour. The extent of deformation is defined by applying some external routine to evaluate the penetration depth along some prescribed path required to absorb this energy. The comparison of the outcomes of two methods reveals that while the deformation energy is predicted at reasonable accuracy with both methods, the difference in penetration path is significant. The decoupled approach precisely predicts the penetration in symmetric collision, but in non-symmetric collisions under oblique angle the results differ from those of decoupled solution and also from the experimental measurements. The forward velocity of the struck ship does not significantly influence the precision of the decoupled approach.

Introduction

It is a common approach in ship collision studies to decouple the analysis of inner mechanics from the external dynamics. Decoupling implies that there is no interaction between the ship motions and structural deformations i.e. the actual ship motions in collision are not considered. Decoupling can be done both in the analytical models and in finite element simulations, where it allows significant reduction of simulation time due to time step scaling. In a decoupled analysis the structural response is evaluated in so-called displacement controlled manner the struck ship is kept fixed and the striking ship collides with it at a constant velocity along a prescribed path, see Figure 1 for a general principle. The contact force as a function of this prescribed penetration path is obtained. The actual extent of the penetration is obtained by comparing the area under the force-penetration curve, the deformation energy, to the deformation energy evaluated with some calculation model that gives the energy based on the conservation of momentum in collision (Minorsky, 1959; Pedersen and Zhang, 1998). Such a model uses only ship mass properties, collision velocity, location and angle for input. External fluid forces due to the surrounding water are included only through a constant added mass and the velocity dependent forces are neglected as the actual ship motions cannot be evaluated.

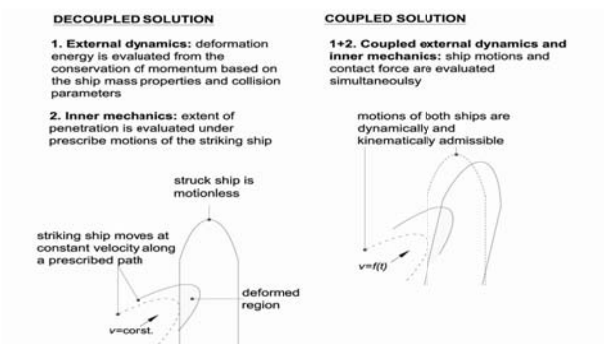

Figure 1. Decoupled and coupled solution procedure

The accuracy of the decoupled method depends mainly on the level of precision on predicting the penetration path. This can be done rather precisely for a symmetric collision, where the striking ship collides under a right angle at the amidships of the initially motionless struck ship and only few motion components are excited. Statistical studies (Lützen, 2001; Tuovinen, 2005) have, however, indicated that the majority of collisions are non-symmetric in one way or another. Often the collision angle deviates from a right angle, the contact point is not at the amidships or the struck ship has initial velocity. As in non-symmetric ship collisions more motion components are excited, the penetration path cannot always be predefined with reasonable precision, but it should be evaluated in parallel with the ship motions, i.e. a coupled approach has to be applied.

The coupled approach considers actual ship motions in the evaluation of the contact force; see Figure 1. The contact force influences the ship motions and vice versa, thus the name coupling. The contact force is evaluated along the actual, physically correct penetration path. No preliminary predictions are required and the external fluid forces can be precisely included. The coupled models of Petersen (1982) and Brown (2002) considered the motions in the plane of water surface only, while Tabri et al (2010) also included the third dimension.

Brown (2002) and Tabri (2010) compared the coupled and decoupled approaches and revealed that while the total deformation energy is predicted rather precisely by the decoupled approach, associating this energy with the deformations at certain directions cannot be done at the same precision for all the collision scenarios. In some scenarios this results in erroneous prediction of damage length and depth. In this paper, we compare the two approaches and assess the influence of coupling in a wide variety of collision scenarios. The differences in the deformation energy and in the longitudinal and transversal extend of penetration are studied in order to define the limits where the decoupled approach can still be applied. For the decoupled approach the deformation energy is obtained from Pedersen and Zhang (1998) and the extent of damage with the contact model of Tabri et al (2010). For the coupled approach the same contact model is applied together with the time domain collision simulation model of Tabri et al (2010). As both approaches share the same model to evaluate the contact force, the differences analysed in this paper arise due to the neglected coupling and velocity dependent external fluid forces in the decoupled model. In all the simulations the striking ship is assumed rigid and the deformations are limited to the struck ship.

Influence of coupling in collision experiments

First, we exploit the model-scale collision experiments to illustrate the predictions we can obtain with different approaches. The model-scale experiments were performed to extend the physical understanding of ship collisions. The large-scale experiments were scaled to model scale using a scaling factor of 35 (Tabri et al, 2008). In this, Froude's scaling law was used to assure physical similarity. This scaling resulted in ship models with the following main dimensions: length $L^A = L^B$ = 2.29 m, depth $D^A = D^B$ = 0.12 m, and breadth B^A = 0.234 m for the striking ship and B^B = 0.271 m for the struck ship. Hereafter, the superscript characters A and B denote the striking and the struck ship, respectively. The striking ship model was equipped with a rigid bulb in the bow and it collided with the side structure of the struck ship model; see Figure 2. At the contact location a block of homogeneous polyurethane foam was installed. The force-penetration curve from the large-scale experiment was used to scale down the structural response of the struck ship and, thus, maintain dynamic similarity. The scaling was based on the crushing strength of the foam and on the geometry of the bulb (Tabri et al, 2008; Ranta and Tabri, 2007).

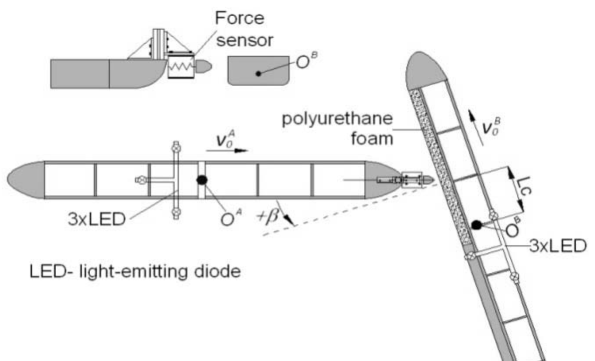

Figure 2. Model-scale test setup with the definitions of the collision angle β and eccentricity L_C

During the collision all six motion components of both ships were recorded with respect to an inertial coordinate system using a Rodym DMM non-contact measuring system. Depending on the collision scenario, the contact force was recorded either in a longitudinal or in the longitudinal and transverse directions with respect to the striking ship model (Tabri et al, 2008). Given the ship motions, the penetration time history was calculated based on the relative position between the ships, see Eq. (3) in Tabri et al (2010). Combining the measured contact force and the penetration history results in a force–penetration curve, and the area under that curve gives the deformation energy E_D of the collision process.

The deformation energies and penetration paths are calculated for four non-symmetric model-scale collision tests, which main parameters are given in Table 1. Deformation energy for the decoupled analysis is evaluated with the external dynamics model of Pedersen and Zhang (1998). This model evaluates the deformation energy based on the conservation of momentum in collision and uses as input the ship mass properties and the collision parameters such as ships' velocities, collision angle β and eccentricity L_C, see Figure 2 for the definitions. It should be noted that no information on structural resistance is required to evaluate the deformation energy with this model. In Table 1 this energy is compared to the energies obtained from the model-scale experiments and by the coupled approach of Tabri (2010). For the decoupled approach only the total deformation energy is presented while for the other two methods also the pure plastic energy is presented. In the decoupled model the decomposition of the total energy to plastic and elastic components requires the knowledge of the ships' velocities immediately after the contact, which can not be defined based on the decoupled approach alone.

According to Table 1, the computational models tend to overestimate the total deformation energy approximately by 10% and both methods give a similar outcome, except in test 309 where there is significant sliding between the ships. In the decoupled model the total deformation energy is the only outcome and the penetration is assumed to follow the direction of the initial velocity of the striking ship (Zhang, 1999). To solve the final value of the penetration corresponding to the obtained deformation energy, the contact force model from of Tabri et al (2010) is exploited. The penetration paths evaluated by two computation models are presented in Figure 3 for different model-scale tests. There, the penetration paths of the bulb into the side of the struck ship are presented. It should be noted that when talking about the penetration path, we only consider the path of the point that first contacts with the other ship and the extent of damage due to the shape of the impact bulb is not presented, even though it is obviously considered in the calculations. The longitudinal extent of damage is denoted with x^B and correspondingly the transverse extent with y^B. For the test 202 presented in Figure 3a, results of both methods agree well with the measured one, even though the longitudinal penetration is slightly underestimated. In other tests with oblique angle the differences between the results of different methods are larger. The coupled method estimates the penetration paths at good accuracy, while the decoupled approach yields to

Table1. Test data

Test	β	L_C	m^A	m^B	v_0^A	$\max(E_D)/E_{D,P}$ [J]		
	[deg]	[m]	[kg]	[kg]	[m/s]	Experimental	Decoupled*	Coupled model
202	0	0.83	28.5	30.5	0.71	2.36/2.28	2.50/-	2.51/2.14
301	30	0.37	28.5	20.5	0.87	4.20/4.14	4.31/-	4.62/4.21
309 (sliding)	55	0.46	28.5	20.5	0.87	3.19/3.19	4.3(2.9*)/-	3.60/3.60
313	-30	0.29	28.5	20.5	0.76	3.14/3.09	3.7/-	3.45/3.14

m^A, mass of the striking ship; m^B, mass of the struck ship; v_0^A, initial velocity of the striking ship; E_D, deformation energy; $E_{D,P,}$ plastic deformation energy; * based on Pedersen and Zhang (1998).

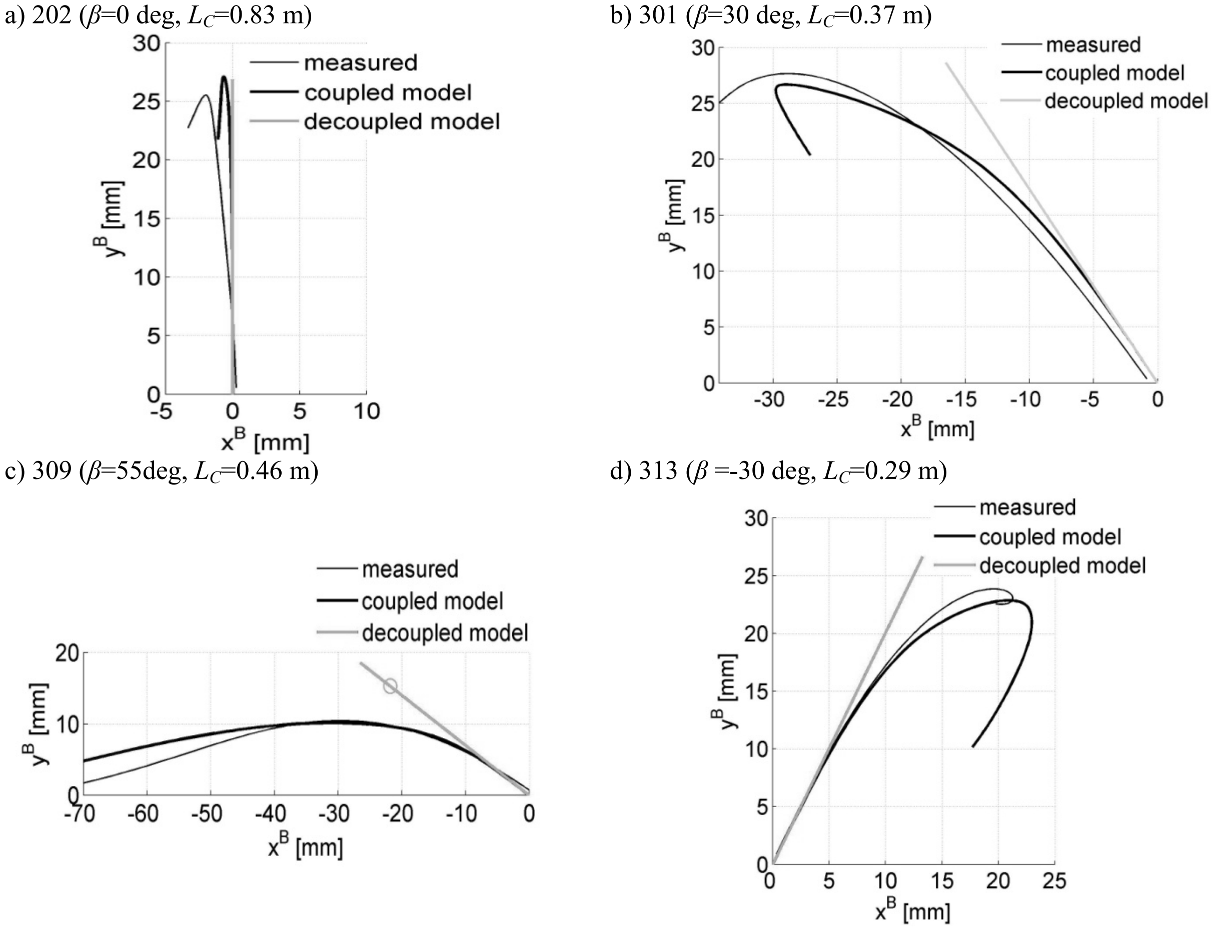

Figure 3. Penetration paths of the bulb in the struck ship (see Appendix B in Tabri et al (2010) for test matrix).

deeper penetration with shorter longitudinal extent. This becomes especially clear from the results of the test 309 in Figure 3c, where the striking ship slides along the deformation energy when the sliding contact is assumed to occur in the model of Pedersen and Zhang (1998), as this model makes a clear difference whether the ships side of the struck ship and thus the penetration path deviates significantly from the direction of the initial velocity. A circular marker in the Figure 3c denotes the stick together during the contact or whether they slide along each other.

Influence of coupling in different collision scenarios

Above examples only covered four points in the wide spectrum of possible collision scenarios. Having obtained confidence in the numerical model through experimental validation, we use it to study the influence of coupling in a wider range of collision scenarios. The simulations are carried out using the mass and structural properties of the ship models used in the experiments. As we simply compare the outcomes of two methods, the scale where the comparison is conducted does not affect the outcome. The relative difference between the two approaches is defined as

$$diff. = \frac{x_C - x_{DC}}{x_C}, \qquad (1)$$

where x_C and x_{DC} are the values in question from the coupled and decoupled analysis, respectively.

Collision scenarios and parameters

In total, 126 different collision scenarios are studied. Mass and inertia properties of the ship models used are kept unchanged and are given in Table 2. Also the structural resistance and the shape of the impacting bow are assumed to be the same in all the scenarios. Seven different collision angles β=0°, ±30°, ±45°, ±60° and nine collision locations L_C/L^B=0, ±0.1, ±0.2, ±0.3, ±0.4 are studied. The striking ship has a velocity of v_0^A =0.75 m/s and the struck ship is either initially motionless of also has a forward velocity of v_0^B=0.75 m/s. In all the simulations with the decoupled approach it is assumed that the penetration follows the direction of the relative velocity between the ships. All the collisions are assumed to occur at parallel middle body. In the decoupled analysis it is assumed that $\alpha=\beta$ and μ_0=0.6 in Pedersen and Zhang's (1998) model. The value μ_0=0.6 was chosen as this resulted in most precise prediction of energy as revealed in Figure 4, which presents the averaged difference $\overline{diff.}$ in the deformation energy for the collision scenarios where the struck ship is initially motionless. The difference $\overline{diff.}$ is evaluated by averaging the differences over nine collision locations as

$$\overline{diff.} = \frac{1}{9}\sum_{n=1}^{9}\frac{x_{C,n} - x_{DC,n}}{x_{C,n}} \tag{2}$$

Table 2. Physical parameters of the models

Model	Draft [cm]	Mass [kg]	KG [cm]	k_{XX} [cm]	k_{YY} [cm]	k_{ZZ} [cm]	μ_{sway} [%]	μ_{heave} [%]	μ_{roll} [%]	μ_{pitch} [%]	μ_{yaw} [%]
Striking	4	20,5	7,4	19	70	70	17	300	12	220	14
Struck	4	20,5	7,4	19	77	77	16	376	20	231	10

KG, vertical height of the mass centre of gravity from the base line; k_{XX}, k_{YY}, k_{ZZ} the radii of inertia in relation to the x, y and z axes; μ, non-dimensional added mass (Tabri et al, 2010)

This averaged difference is evaluated for all 7 different collision angles and presented in Figure 4 for a number of μ_0 values. Relatively larger differences occur at β=±45° as there the decoupled analysis predicts sliding contact while in reality it is neither pure sliding nor sticking. This implies that the outcomes of decoupled analysis are strongly dependent on the μ_0 value, especially when the sliding between the ships occurs. However, the precise determination of μ_0 value just based on the parameters describing the collision scenario is not possible.

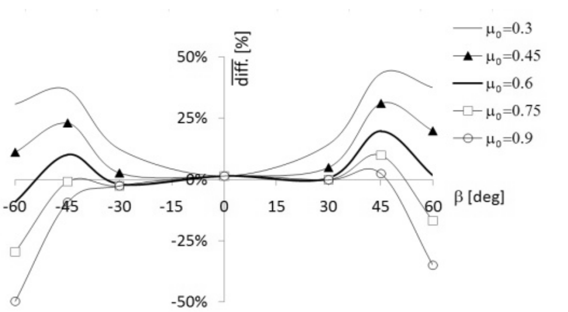

Figure 4. Averaged difference in deformation energy as a function of collision angle β and with μ_0 as a parameter.

Influence of coupling

We first study the scenarios where the struck ship is initially motionless. The difference between the total deformation energy is presented in Figure 5 as a function of β. The difference due to the collision eccentricity is described by the error bars. Collision scenario is visualized on the top of the graph for β=-60, 0 and 60 deg. In this, and also in the coming graphs, dashed lines are drawn for the difference of ±15%, which can be considered as well acceptable difference. The energy plot reveals that in most of the scenarios the energy is predicted within the margin of ±15%. In the case of a right angle collisions (β=0°) there were only neglectful differences between the two approaches. Again, larger differences occur in the case of β=±45° as the decoupled analysis cannot precisely predict the scenarios where the sticking and sliding occur simultaneously.

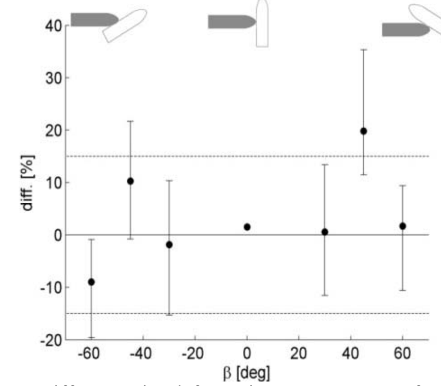

Figure 5. Difference in deformation energy as a function of β $v_0^A = 0.75\,m/s.,\ v_0^B = 0$.

Differences in the deformation energy change as the struck ship has a forward velocity, see Figure 6. With β<0°, the energy is well predicted with the decoupled approach, the difference is even smaller compared to scenarios where the struck ship was initially motionless. In the scenarios with β<0° the velocity of the struck ship reduces the sliding between the ships and thus, the decoupled analysis yields to precise estimation of energy. Contrary, for β>0°, the sliding becomes more extensive and the difference between the two methods increases significantly.

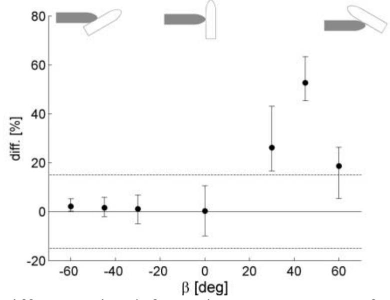

Figure 6. Difference in deformation energy as a function of □ $v_0^A = v_0^B = 0.75\,m/s$

Differences increase when looking at the penetrations in Figures 7 and 8. With the decoupled approach the longitudinal penetration is underestimated as much as 80%, see Figure 7a. It should be noted that in Figure 7a, and later also in Figure 8a, the longitudinal penetration is not presented for β=0 as the comparison would be ill-conditioned. This is because the decoupled analysis will predict zero longitudinal penetration for all the scenarios where β=0 and the struck ship is initially motionless, while in the coupled analysis the longitudinal penetration still obtains some value mainly due to yaw motion of the ships. Their comparison would always lead to very large differences even if neglectfully small values are compared. The largest differences again occur in the scenarios where there is significant sliding between the ships. In the case of sliding not only the deformation energy is poorly predicted, but also the direction of the penetration deviates from that of the relative velocity. This is further confirmed when looking at the longitudinal penetration in the scenarios where the struck ship has a forward velocity. For β<0° the sliding becomes less due to the velocity of the struck ship and the penetration is predicted more precisely compared to the initially motionless struck ship. With β>0° the sliding increases and the error in predicting the penetration path in the decoupled manner increases.

a) b)

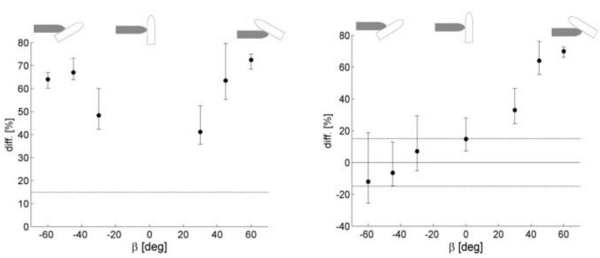

Figure 7. Difference in longitudinal penetration for (a) $v^A = 0.75\,m/s$, $v^B = 0$ and (b) $v^A = v^B = 0.75\,m/s$.

The trends are similar in the case of the transverse penetration in Figure 8. Decoupled analysis overestimates the transverse penetration up to 45% for the scenarios with the initially motionless struck ship. The overestimation increases as the collision angle deviates from a right angle. When the struck ship has some forward velocity the transverse penetration is predicted relatively precisely, except for β =60°, where the overestimation is up to 45%.

In general, the differences in transverse extent are smaller as the deformation energy increases rapidly with the increasing transverse penetration. In the longitudinal direction the increase in energy is moderate and already small differences in energy appear large in the longitudinal extent of damage.

a) b)

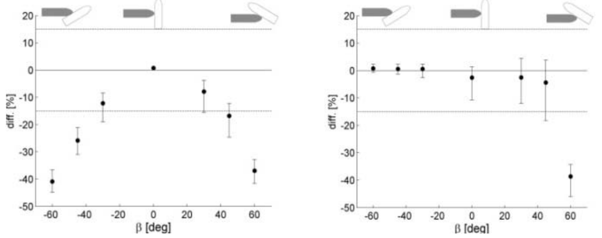

Figure 8. Difference in transverse penetration for (a) $v^A = 0.75\,m/s$, $v^B = 0$ and (b) $v^A = v^B = 0.75\,m/s$.

Conclusions

Ship collisions are numerically simulated using two different approaches: a coupled and a decoupled approach. In this paper, Tabri's method (Tabri et al, 2010) is used for the coupled approach, and Pedersen and Zhang's method (1998) is used to evaluate the deformation energy in the decoupled approach. For both approaches the contact force as a function of penetration is evaluated with the contact model of Tabri et al, 2010. The differences in the collision energy, in the longitudinal and transverse penetration depths have been compared for a wide range of collision angles and locations. The approaches were compared for the scenarios where only the striking ship had a forward velocity and where both ships had a forward velocity of the same magnitude.

It was revealed the two methods yield to different outcomes, especially when looking at the penetration depths. When the struck ship is initially motionless the deformation energy can be predicted at good accuracy. Larger differences occur at large collision angles, where both the sticking and sliding occur simultaneously. The coupled analysis can well cope with such a scenario, while the decoupled analysis always assumes just one of these processes occurring. Despite well predicted energy, the exact penetration path is not known in the decoupled analysis and it is assumed to follow the direction of the relative velocity between the ships. This holds true for the collision angles close to a right angle, but for larger angular deviations the longitudinal penetration tends to become overestimated and contrary, transverse penetration becomes underestimated. The velocity of the struck ship improves the estimations in the scenarios where, as a result of this forward velocity, there is less sliding between the ships. In majority of the collision scenarios the forward velocity of the struck ship did not lower the precision of the decoupled approach. The larger difference in the penetration depth compared to the deformation energy implies that the neglected coupling yields to larger error compared to the neglected velocity dependent external fluid forces in the decoupled model. The decoupled approach can be used with full confidence in right angle collisions, where both the deformation energy and the penetration bath are well determined despite the collision eccentricity and velocities. When the angles deviate from a right angle, the errors increase and for some scenarios the results become unacceptable, especially in the case of penetration depth.

Differences presented here arise mainly as with different methods the penetration paths become different. In this paper the side structure of the struck ship was assumed homogeneous and did not influence the outcome. Homogeneous side structure misses structural hard points such as web-frames and bulkheads for example. A numerical study with ships of different sizes and structural configurations is to be conducted to assess whether the conclusions drawn here are valid in more realistic scenarios and ship structures.

Acknowledgement

This work has been performed in the scope of the project MARSTRUCT, Network of Excellence on Marine Structures (www.mar.ist.utl.pt/marstruct/), which has been financed by the European commission. This help is kindly appreciated.

References:

Brown A. 2002. Collision scenarios and probabilistic collision damage. Journal of Marine Structures. Vol. 15, pp. 335-364.

Lützen M. 2001. Ship Collision Damage. Ph.D. Thesis, Technical University of Denmark.

Minorsky VU. 1959. An Analysis of Ship Collision with Reference to Protection of Nuclear Power Plants. J Ship Research, 3(1):1-4.

Pedersen PT, Zhang S. 1998. On Impact Mechanics in Ship Collisions. Journal of Marine Structures. Vol. 11, pp. 429-449.

Petersen MJ. 1982. Dynamics of Ship Collisions. Journal of Ocean Engineering. Vol. 9, pp. 295-329.

Ranta J, Tabri K. 2007. Study on the Properties of Polyurethane Foam for Model-Scale Ship Collision Experiments. Helsinki University of Technology, Report M-297, p. 44.

Tabri K. 2010. Dynamics of Ship Collisions. Doctoral dissertation. Aalto University, available at http://lib.tkk.fi/Diss/2010/isbn9789522482730/

Tabri K, Määttänen J, Ranta J. 2008. Model-scale experiments of symmetric ship collisions. J Marine Science and Technology, 13:71-84.

Tabri K, Varsta P, Matusiak J. 2010. Numerical and experimental motion simulations of non-symmetric ship collisions, Journal of Marine Science and Technology, 15:87 - 101.

Tuovinen J. 2005. Statistical Analysis of Ship Collisions. Master’s Thesis, Helsinki University of Technology. p. 93.

Zhang S. 1999. The mechanics of ship collisions. Ph.D. thesis, Technical University of Denmark, p. 262.

Rapid Assessment of Ship Grounding over Large Contact Surfaces

Lin Hong and Jørgen Amdahl

Department of Marine Technology, Norwegian University of Science and Technology

Abstract:
A simple method for rapid assessment of ship bottom structures subjected to grounding over seabed obstructions with large contact surface is proposed in this paper. It has been recognized that the shape and size of the seabed obstruction is of crucial importance in relation to the characteristics of bottom damage. Most studies of ship grounding are concerned with "rock" type sharp obstruction, where plate tearing is the dominating failure mode. However, very few studies are found related to grounding over blunt obstructions with large contact surface such as "shoal". Denting rather than tearing is more likely for bottom plating as observed from actual grounding incident. The sharp obstruction may cause earlier penetration, and result in very unfavorable consequences such as compartment flooding. In contrast, the bottom plating may not fracture when moving over blunt type sea floor. But it may threaten the global hull girder resistance and give rise to even worse consequences such as hull collapse. The proposed simple method is established on the basis of a series of closed-form solutions for individual structural members developed from plastic mechanism analysis. The primary deformation modes for the major bottom structural members are: sliding deformation of longitudinal girders, denting and crushing of transverse members, indentation of bottom plating. The effect of friction is considered and estimated in a simple manner. The vertical resistance which governs the vertical ship motion is derived. It is found that the vertical resistance is free of friction. The proposed simple method for bottom strength is verified against large-scale nonlinear finite element analyses where good correlation is obtained.

Introduction

In the last two decades, significant effort has been put into understanding the response of ships subjected to collision and grounding, due to the continuously increasing public concern over several catastrophic accidents. As a result, a large body of tools and analysis procedures has been developed. Some novel ship structures have been proposed, as summarized by, e.g. NRC (1991), Paik (2003), which are capable of mitigating or preventing potential accidental consequences, such as oil spill. This has partly been based on analysis of structural crashworthiness using techniques widely applied by the automobile industry. Recently, there is seen a clear trend to adopt more rational design procedure for collision and grounding rather than the prescriptive regulations. The following four items are considered elementary in such a rational design procedure, see, for example Amdahl et al (1995): scenario definition, global and local structural performance calculation, post-accident evaluation, acceptance criteria. If such a design procedure is used, especially in the preliminary design stage, it is essential that the structural performance of various designs can be checked and compared quickly for a large number of potential accident scenarios. Also, in risk analysis, it is required to predict the consequences related to various scenarios. In this context, calculation tools with high efficiency are required. Apparently, experiments or non-linear finite element method (NLFEM) is not an option in such situations. Full- or large-scale physical experiments with ship structures on collision or grounding are usually too expensive and risky to be executed, though they have been conducted (Carlebur 1995, Rodd 1996). Small-scale tests may be difficult to be interpreted to real scale events due to the intricate scaling laws involved. The NLFEM is often considered to be "numerical experiments", but it implies intensive effort on both modeling and calculation. On the other hand, the results of numerical simulations depend significantly on the skill and knowledge of the user, which makes it difficult for application by ship designers. Therefore, development of simple methods or tools with reasonable accuracy is motivated and precipitated because of their characteristic of fast estimation. Compared to empirical methods, as pioneered by Minorsky (1959) for assessment of high-energy collisions, it is advantageous to apply plastic methods of analysis in developing simplified methods (ISSC 1997, ISSC 2003), since mechanism analysis can provide significant insight into the governing physical processes. Many simplified analytical formulae have been developed based on the construction of realistic deformation mechanisms identified during either actual ship accidents or model tests (Amdahl 1983, Wang 1995, Simonsen 1997, Zhang 1999, Wierzbicki and co workers 1992-2000). For a ship bottom structure, beside the structural arrangement, the characteristics of the structural behavior are determined by the definition of the accident scenario, among which loading condition and seabed topology are of crucial importance. The grounding action may be in the vertical direction, longitudinal direction, or a combination. The mechanics of vertical action is referred to as "stranding" (Amdahl and Kavlie 1992). If the ship grounded with forward speed, it is often referred to as "powered grounding" (Simonsen and Friis-Hansen 2000). The mechanics involved in the "powered grounding" varies due to the "powered grounding" varies due to the variety of seabed topologies.

Three major types of seabed topologies have been defined in the grounding scenarios by Alsos and Amdahl (2007), namely "rock", "shoal" and "reef" (Figure 16). The shape and size of the seabed is evaluated in relation to the characteristic resistance of the double bottom. Different deformation mechanisms may be triggered by seabed obstructions with different shape and size.

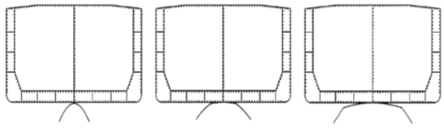

(a) (b) (c)

Figure 16: Seabed topology with reference to bottom size: (a) rock; (b) reef; (c) shoal (Alsos and Amdahl, 2007).

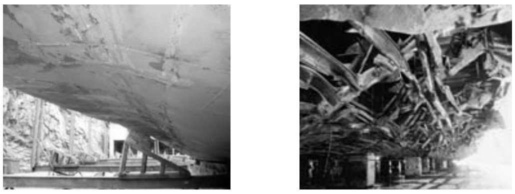

(a) sliding damage (Courtesy of Hagbart S. Alsos)

(b) raking damage of Sea Empress (Courtesy of www.archive.official-documents.co.uk)

Figure 2: Ship bottom damage due to grounding.

Most studies on ship grounding to date are subjected to the "rock" type seabed obstructions. Consequently, bottom plate cutting or tearing have been investigated extensively. Various simplified methods have been formulated for the plate tearing failure mode, refer e.g. Vaugnan (1980), Jones and Jouri (1987), Ohtsubo and Wang (1995), Simonsen and Wierzbicki (1997), Simonsen (1997), Paik and Wierzbicki (1997) and Zhang (2002). This type of grounding is commonly referred to as "*raking*" (Wang et al 1997). The bottom damage due to raking is demonstrated by the grounding of Sea Empress (Figure b). Indeed, the sharp rock may cause earlier penetration of the bottom plating, and result in very unfavorable consequences such as compartment flooding. In contrast, the bottom plating may not fracture when moving over "shoal" type seabed obstructions which have large contact surfaces. In this situation, denting rather than tearing is a more likely deformation mode for bottom plating, as witnessed by an actual grounding incident, see Figure 2a. Such type of grounding may be termed as "*sliding*". During sliding, it is more likely to damage a significant part of the ship bottom and thereby threaten the global hull bending resistance (Pedersen 1994, Alsos and Amdahl 2008b).

Figure shows an example where the global hull girder capacity is exceeded after running aground. It has been recognized that relatively flat seabed and blunt obstructions are by far the most common in practice, see Amdahl et al (1995), Wang et al (2000, 2002). However, it has been overlooked. This necessitates studies on the response of ship bottom structure subjected to grounding over seabed obstructions with larger contact surfaces.

Figure 3.: Hull collapse of a container ship (Courtesy of www.shipspotting.com)

It is a general understanding that the process of ship grounding can be divided into external dynamics and internal mechanics, see e.g. Simonsen and Wierzbicki (1996). The present study is concerned with the internal mechanics of ship grounding in relation to sliding damage. A simple method is proposed and developed, which can be used to assess the force and energy dissipation of ship bottom structure during powered grounding, when seabed obstructions with large contact surfaces such as "shoal" are considered. The simple method is constructed by assembling various simplified analytical formulae for individual structural members developed by using plastic methods of analysis. The primary deformation modes identified in the sliding process are: sliding deformation of longitudinal girders, denting and crushing of transverse members and indentation of bottom plating, respectively. The effect of friction is considered and estimated in a simple manner. The proposed method is applied to a double bottom structure, and verified by large-scale nonlinear finite element analyses. The results are encouraging, however, further work is still required to fully understand the structural response. Some significant features of the structural behavior of the double bottom subjected to sliding are observed and described. The simplified method developed will contribute substantially to the establishment of efficient methods for fast and reliable assessment of the outcome of accidental grounding events. It is also essential for probabilistically based formal safety assessment procedures or quantitative risk analysis (Friis-Hansen and Simonsen 2002, Bognaert and Boon 2007). The method may in turn be incorporated into decision support tools (Amdahl and Hellan 2004) for crisis handling in emergency situations, e.g. for tankers in disabled conditions.

Studies on ship grounding

During stranding ship bottom structures behave similarly to ship side structures subjected to right-angle collisions. Punching and perforation of shell plating, denting of supporting members, crushing of intersections are the main deformation modes involved in stranding. Amdahl and Kavlie (1992) reported model experiments for double bottom stranding. Wang et al (2000) conducted a series of nine tests to investigate the behavior of a double hull under a wide range of collision or stranding scenarios. The penetration of the double bottom was designed to start at shell plating, main supporting members and intersections of main supporting members respectively. Simplified formulae for predicting the resistance of various structural members are proposed and verified. Alsos and Amdahl (2008a) recently performed a series of 1:3 scale panel penetration tests, representing the double hull stranding actions, with the aim of investigating the onset of fracture. This is a key issue regarding the strength of the ship structure and remains as a challenge in crashworthiness analysis (ISSC 2003, ISSC 2006, Törnquist 2003, Törnquist and Simonsen 2004, Alsos et al 2008a, 2008b). Through a benchmark study, Elhers et al (2008) revealed that the effect of mesh size sensitivity might be more important than the failure criterion itself. Considering “powered grounding”, most studies are focused on the “raking” type damage. In early 1990s, the Carderock Division of Naval Surface Warfare Center, USA, conducted a series of 1:5 scale grounding tests. The results were partly reported by Rodd (1996). Kuroiwa et al (1992) reported static and dynamic 1:3 scale bottom raking tests conducted in Japan. This is also reported by Ohtsubo et al (1994). ASIS (Association for Structural Improvement of Shipbuilding Industry) in Japan sponsored a series 1:4 scale bottom raking tests conducted in Netherlands, see Vredeveldt and Wevers (1995). Thomas and Wierzbicki (1992) proposed a grounding damage prediction model including plate cutting, plate tearing and girder tearing for double hull tankers. Wang et al (1997) proposed a simple method for damage prediction of ship raking over a rock by assembling four primary failure modes: stretching failure for transverse members, denting, tearing and concertina tearing for bottom plates. Simonsen (1997) conducted a comprehensive study on the mechanics of double bottom structures during raking.

Apparently, most existing experimental studies and simplified methods are concerned with “rock” type sharp seabed obstacle. In stranding situation, it is often represented by conical type indenter characterized by spreading angle. While in raking situation, the obstacle is often represented by wedges characterized by semi-wedge angle and its breadth, or cones expressed by apex angle and tip radius.

Since the seabed topology has been regarded as one of the dominating factors for the structural response during grounding, it is far from sufficient to consider grounding with respect to rock type obstruction only. Consider, for example, the structural response of a longitudinal web girder. If the bottom is subjected to grounding over a rock, the girder or bulkhead will normally be deformed to the side of the rock due to shear straining corresponding to the global deformation mode of the bottom plating (Simonsen 1997). However, if grounding takes place over an obstruction with large flat contact surface, a repetitive wave-like deformation pattern is observed (Midtun 2006; Samuelides et al 2007a, b). A theoretical model has been established and a simple formula has been derived for this sliding deformation pattern by Hong and Amdahl (2008b). In this context, the mechanics involved in the sliding process must be investigated. Subsequently, a simple method, such as that established for raking by Wang et at (1997), should be developed. Concerning simple methods for bottom sliding, it is noticed that Alsos and Amdahl (2008b) found the sliding resistance of a double bottom in the steady state phase is about half of the resistance during stranding. A semi-analytical procedure has been proposed to find the steady state horizontal grounding force.

A simple method for assessment of the resistance of ship bottom structures during sliding type grounding accident over large contact surfaces, is presented. It is based on an assembly of various simplified analytical formulae for major structural members.

Primary structural deformation modes

Figure 4. shows a simple model of the typical double bottom structure. For simplicity, it is assumed that the ship under consideration moves in the horizontal plane, disregarding pitch and heave movement. The response of the ship bottom can be considered periodic because of the repetitive arrangement of structural members. Three types of structural components are of major concern in the grounding process:

1. longitudinal girder, including longitudinal bulkhead;
2. transverse member, including bottom floor, transverse bulkhead;
3. bottom plating.

The tertiary stiffeners or cutouts on the web girder and the bottom floor are not considered in this study. They may be taken into account by the method of smearing which has been proved effective for cutting of longitudinally stiffened plates by Paik (1994). The seabed obstacle is represented by a rigid indenter with flat contact surface and trapezoidal cross-section. For simplicity the middle web girder is assumed to be impacted at the center of the indenter.

Figure 5. shows the deformation of bottom structures after grounding over obstructions with large flat surface. The deformation of bottom plating is seen in Figure 6.The primary deformation modes for individual structural members are: sliding deformation of longitudinal girders, denting and crushing of transverse members, indentation of bottom plating. The mechanisms introduced hereafter are formulated in such a way that they are mathematically tractable, but at the same time as realistic as possible. Some significant features of the structural behavior of the double bottom subjected to grounding over seabed obstructions with large flat contact surface are also described.

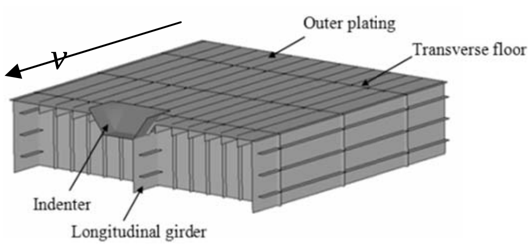

Figure 4: A simple model of ship grounding analysis.

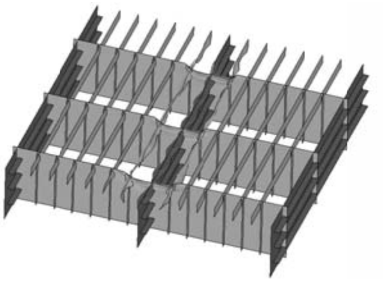

Figure 5: Deformation of the bottom structure after grounding.

Simplified method for longitudinal girder

A longitudinal girder connects the inner and outer bottom plating in a double bottom structure. The longitudinal girder will be subjected to a continuous sliding process, in which it will be crushed both vertically and horizontally. Hong and Amdahl (2008b) proposed a theoretical model (Figure 6) for the girder crushed by a flat indenter during horizontal sliding. The accuracy of the mechanism model has been verified by series of numerical simulations in terms of energy absorption and resistance force.

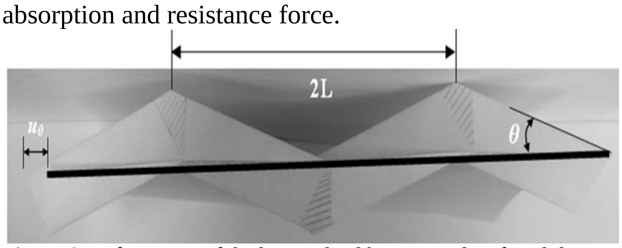

Figure 6: Deformation of the longitudinal bottom girder after sliding (paper model).

The intersection with the transverse floor can be considered to form a plated cruciform. In this context, the theory for axial crushing of intersections may be applied. However, this part of the longitudinal girder is very limited and exhibits similar deformations as proposed for steady-state sliding. For simplicity, the horizontal sliding deformation model is applied to the whole longitudinal girder. According to the proposed mechanism, the energy absorption in a half-wave is derived to be

$$E_{girder} = M_0 \pi H \left(1 + 2\sqrt{1+\tan^2\theta}\right) \cdot \frac{1-\tan^2\theta}{\tan\theta} + \frac{4N_0H^2}{\sqrt{3}}\sqrt{\frac{1}{4}+\tan^2\theta} \, . \tag{1}$$

The mean horizontal crushing force is:

$$F_{mH,girder} = M_0 \pi \left(1 + 2\sqrt{1+\tan^2\theta}\right) + \frac{4N_0H}{\sqrt{3}} \frac{\tan\theta}{1-\tan^2\theta}\sqrt{\frac{1}{4}+\tan^2\theta} \, . \tag{2}$$

M_0 represents the fully plastic bending moment capacity of a plate strip, N_0 is the plastic membrane force of a plate strip. H and θ are half of the vertical crushing distance and the crushing wave angle of the mechanism respectively (Figure 6). According to the upper bound theory, it is postulated that the free parameters should adjust themselves in the deformation process to obtain the least energy dissipation. However, due to the complexity of the problem and the simplicity of the theoretical model, it is not possible to get analytical solutions for H and θ currently. Even so, such approach still has been proved to work well in a large number of simplified analyses, see for example Wierzbicki and Culbertson-Driscoll (1995). In the first place, empirical expressions are introduced to make the calculation possible. H and θ are expressed as

$$2H = 1.0836D + 0.0652 \, , \tag{3}$$

$$2\theta = 0.94\alpha \text{-} 0.0048\alpha^2 \, , \tag{4}$$

where D is the indentation depth from the indenter, α represents the crushing angle of the indenter. The detailed description and derivation of the mechanism for the longitudinal web girder can be found in Hong and Amdahl (2008b, 2008c).

Simplified method for transverse members

In the literature, sharp wedges have been widely used to represent the grounding condition. Ship grounded over rocks has been the major subject over decades. Regarding the failure mode of transverse members by a concentrated load, Wang et al (1997) applied a beam model dominated by membrane force. Simonsen (1997) modified the denting model of transverse members for application to the bottom raking process.

A flat indenter with trapezoidal cross-section is employed to represent the shape of the seabed. As a result, the response of the transverse member can be divided into two parts (Figure 7). The central part of the transverse member of the intersection, which has the same breadth as the contact surface from the indenter, is pushed horizontally by the indenter. One buckle is formed. The crushing behavior is similar to the axial crushing of a cruciform, but with a horizontal displacement. The remaining part of the transverse member deforms simultaneously with the central part. The deformation mode is similar to the local denting mode of a web girder subjected to a concentrated load. However, from the simulation, it is observed that the deformation zone of the transverse floor does not extend to the boundary of the member, i.e. adjacent longitudinal girders.

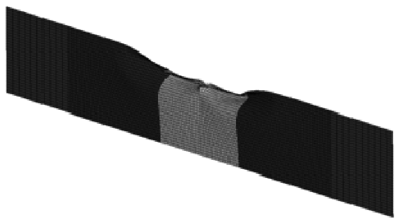

Figure 7: Transverse floor after horizontal crushing (central part is colored yellow with the same breadth as the contact surface with indenter).

From numerical simulations, the central part of the transverse floor is observed to be crushed to form a wrinkle or buckle. This is especially apparent from the edge type view of the transverse floor after sliding (Figure 8).

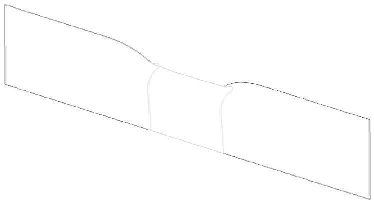

Figure 8: Transverse floor after horizontal crushing (edge type figure).

Another characteristic feature of the horizontal crushing is that the crushing distance cannot be simply characterized by one parameter, such as crushing distance in axial crushing. The total crushing depth is separated into a short and a long component, i.e. *ab* and *bc*, refer Figure 9. The energy is dissipated through the three plastic hinge lines and by the stretching of the vertical material fibers beyond the lower hinge line. Once the elongation of the material line *ab* or *bc* is found, the energy dissipation by the central part of the transverse floor can be calculated.

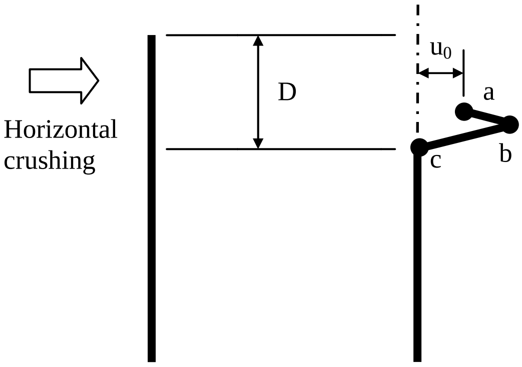

Figure 9: Cross-section of the central part of the transverse floor before and after horizontal crushing.

The horizontal displacement of the top edge of the central part of the transverse floor, u_0, can be determined from the theoretical model for longitudinal girder (Hong and Amdahl 2008b), refer Figure 6,

$$u_0 = 2H\tan\theta\,. \tag{5}$$

However, because of the sophisticated interaction between transverse and longitudinal members, a new mechanism for the central part of the transverse member has not been developed in the present study. This may be done in a future study. Therefore, to simplify the problem and proceed with the establishment of the simple assessment tool, the existing theory for axial crushing of intersections is applied to estimate the response of the central part of the transverse floor. Amdahl (1983) proposed a symmetric deformation mode for predicting the average crushing strength of a cruciform. The plastic energy is mainly dissipated in triangular regions I and II by in-plane deformation and plastic bending at inclined and straight hinge lines (Figure 10). Assuming that the collapse pattern is determined at an early stage of crushing and remains constant during further crushing, Amdahl (1983) calculated the parameter to be k=0.573. This has been widely accepted by other authors on the problem of crushing of plated structures, for example, Kierkegaard (1993), Paik and Pedersen (1995). The central part of the transverse member with breadth 2C, which equals the span of the contact surface with the indenter, is considered to be two flanges of a cruciform. The energy dissipated by the collapse of the two flanges is

$$E_{trans,central} = 4M_0\left(2.58\frac{H^2}{t} + \left(\frac{\pi}{2}\right)^2 t + \pi C\right). \tag{6}$$

This amount of energy is dissipated over u_0, the horizontal displacement of the web girder, given by Eq. (5). Consequently, the mean horizontal crushing force is obtained by dividing Eq. (6) by Eq. (5):

$$\begin{aligned} F_{mH,trans,central} &= \frac{E_{trans,central}}{u_0} \\ &= \frac{2M_0}{H\tan\theta}\left(2.58\frac{H^2}{t} + \left(\frac{\pi}{2}\right)^2 t + \pi C\right) \end{aligned}. \tag{7}$$

The response of the rest of the transverse member may be calculated by the denting mode. The local denting mode was proposed for plates subjected to a load which moves in the plane of the plate. This type of load is often seen in stranding or collision. In a horizontal sliding process, the indenter moves in the longitudinal direction perpendicular to the plane of the plate. Despite the difference, the denting mode can be consistently applied to the analysis of the raking process, see Simonsen (1997). Hong and Amdahl (2008a) reviewed the existing theoretical models for local denting, and proposed an improved theoretical model with two folding elements. The model captures more precisely the deformation process of a web girder under concentrated load. The simplified formula agrees satisfactorily with small and large scale experiments. This will be applied to evaluate the strength of the transverse member outside the intersection region.

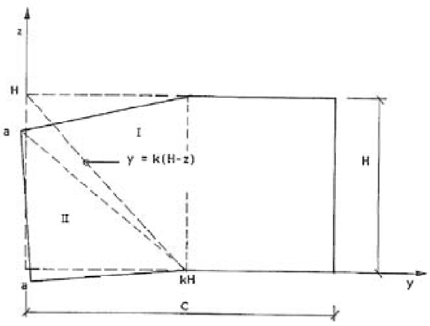

Figure 10: Basic folding element in a symmetric mode for a cruciform (Amdahl 1983).

The energy absorbed during the crushing of the remaining part of the transverse member is

$$E_{trans,side} = \frac{14}{3}\pi M_0 b + 29.68\frac{N_0 H^3}{b}\,, \tag{8}$$

where b is the half length of the deformation extension in transverse direction, H is the characteristic vertical crushing distance. This energy is dissipated over a distance u_0, the horizontal displacement of the web girder, i.e. Eq. (5). Consequently, the mean horizontal crushing force is obtained by dividing Eq. (8) by Eq. (5):

$$F_{mH,trans,side} = \frac{E_{trans,side}}{u_0} = \frac{7}{3}\pi M_0 \frac{b}{H\tan\theta} + 14.84\frac{N_0 H^2}{b\tan\theta} \quad (9)$$

In this case, the vertical crushing distance is determined by the crushing depth of the indenter. The optimality condition should be applied to determine the extension of the deformation in the transverse direction:

$$\frac{\partial F_{mH,trans,side}}{\partial b} = 0\ , \quad (10)$$

which yields

$$b = 2.85H\sqrt{\frac{H}{t}}\ . \quad (11)$$

Up to now, no restriction has been imposed on the deformation extension of the transverse member. However, it is noted that b in any case should be larger than the shoulder breadth of the indenter, B, refer Figure 11. Since the deformation of the transverse member will be restrained by the neighboring longitudinal web girders, the girder spacing should constitute an upper limit.

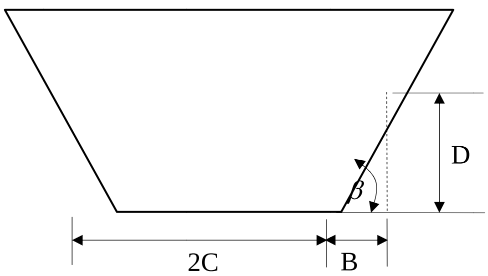

Figure 11: The transverse section of the indenter.

In order to have a better understanding, Figure 12-15 give some impression on how the nodes around the bottom intersection displace. It reveals significant interaction between longitudinal and transverse members of a ship bottom. The nodes of the top edge of the longitudinal girder displace horizontally with the same magnitude (Figure 12). But the inward nodes exhibit different phenomena. The node located on the intersection has the maximum horizontal displacement. In this specific case, it is about 2.5 times the displacement of the nodes in longitudinal girder at the same height (Figure 13).

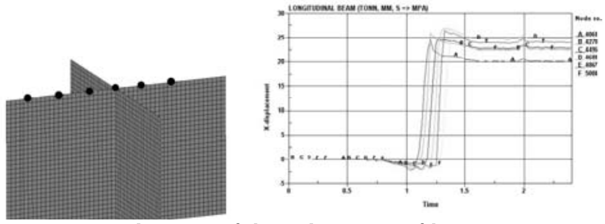

Figure 12: Displacement of the nodes on top of bottom intersection. (A-F denotes the nodes from left to right.)

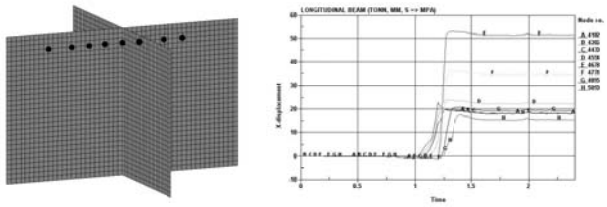

Figure 13: Displacement of the nodes inward from the top of the bottom intersection. (A-H denotes the nodes from left to right.)

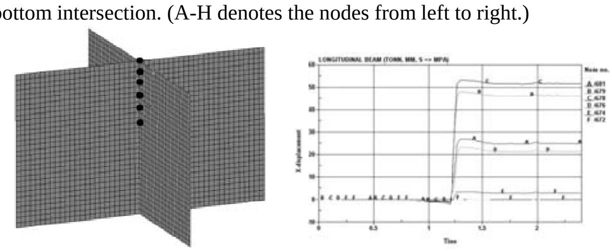

Figure 14: Displacement of the nodes of the intersection. (A-F denotes the nodes from the top.)

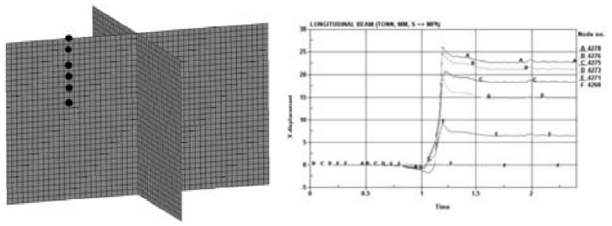

Figure 15: Displacement of the nodes outside the intersection. (A-F denotes the nodes from the top.)

The horizontal displacement of the nodes of the intersection line increases from the top of the intersection, after reaching a maximum displacement, it starts to decrease to zero (Figure 14). The points that constitute the second hinge line have the maximum horizontal displacement. However, this is not the case elsewhere in the longitudinal girder. The displacement decreases from the top node in cross sections other than the intersection line of the longitudinal girder (Figure 15). It is thus concluded that there is significant interaction between the longitudinal and transverse members.

Simplified method for bottom plating

Plastic deformation in the form of membrane straining of ship bottom plating constitutes a significant part of energy dissipation during grounding process. Rather than being torn open by a sharp rock type obstacle, the bottom plate is indented horizontally by the blunt seabed with no tearing as long as the weld is capable of resisting the horizontal grounding force. The widely developed plate cutting/tearing mode which has been discussed in section 1 is not appropriate in the present situation. Figure 16 illustrates the horizontal displacement of bottom plate. The bottom plate within the breadth of the flat indenter has the same magnitude of horizontal displacement. The horizontal displacement is determined from the model developed for horizontal crushing of longitudinal bottom girder, given by Eq. (5). Then the horizontal displacement vanishes gradually when it is contacted with the shoulder of the indenter.

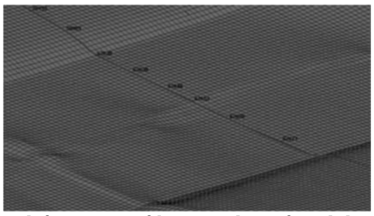

Figure 16: The deformation of bottom plate after sliding (the red line highlights the horizontal deformation of the plate).

The energy is dissipated by bottom plate through three major modes:

1. Plastic bending at four longitudinal hinge lines;
2. Membrane stretching of the material between the longitudinal hinge lines;
3. Plastic rolling and membrane stretching of the plate in contact with the front surface of the indenter.

In reality, there is no clear distinction between these modes. They are presumed to contribute independently to the total energy absorption. In this way the theoretical analysis is significantly simplified.

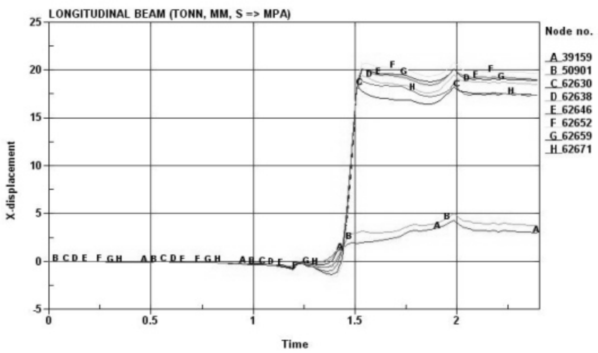

Figure 17: The displacement of various nodes of bottom plate along transverse direction.

After being indented by the sliding object, four longitudinal hinge lines are formed with the bending angle $\Delta\varphi$

$$\Delta\varphi = \arctan\left(\frac{D}{b}\right). \tag{12}$$

The transverse extension of the bottom plate, b, is assumed to be determined from the crushing of the transverse floor.

The energy dissipated by plastic bending of the four longitudinal hinge lines is

$$E_{b,\,plating} = 4M_0 l \Delta\varphi\ . \tag{13}$$

As for the membrane energy, it is assumed that all stretching takes place in the area which is in contact with the side surface of the indenter (indicated by the shaded area between the longitudinal hinge lines in Figure 18).

The deformation of the plate can be described by

$$u = u_0 \frac{y}{b}, u_0 = D\tan\theta\ , \tag{14}$$

$$v = v_0 \frac{y}{b},\ v_0 = \sqrt{D^2 + b^2} - b\ . \tag{15}$$

u_0 and v_0 are the horizontal and transverse displacement of the plate respectively. Then, the energy dissipated by membrane stretching can be derived as

$$E_{m,\,plating} = \frac{4}{\sqrt{3}} N_0 l \sqrt{{u_0}^2 + {v_0}^2}\ . \tag{16}$$

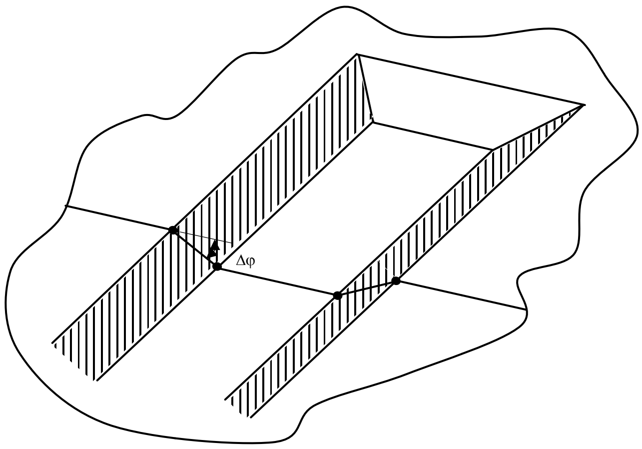

Figure 18: Damage model for bottom plate during sliding.

The plating forward of the tip of the indenter is assumed to conform to the front surface of the indenter. The energy is dissipated through plastic rolling and membrane stretching if friction force is accounted for. When the indenter travels through the plating, a curvature will be imposed on the plate initially, and the curvature will be removed when the plate leaves the rolling surface (figure 19). In addition, when the friction force builds up during the rolling process, membrane stretching will take place in the second rolling surface.

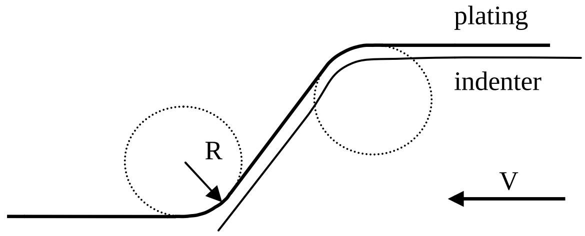

Figure 19: Plastic rolling process at the contact surface between plate and indenter.

The rate of the plastic energy dissipation of a plate strip in contact with the front surface of the indenter is established as

$$\dot{E}_{tip,plastic} = M_0 \frac{2}{R} V + M_0 \left(1 - \left(\frac{N}{N_0} \right)^2 \right) \frac{2}{R} V + N \dot{u} . \quad (17)$$

R is the rolling radius, N denotes the axial force. The first term of Eq. (17) comes from the bending at the first roller, the second term is the bending at the second roller in which the bending moment capacity is reduced because of the presence of axial force due to the friction. The last term represents the contribution of membrane tension in the second roller. $\dot{u}$ is the rate of material elongation in the second roller, and it will be decided from the plastic interaction function

$$\Gamma = \frac{M}{M_0} + \left(\frac{N}{N_0} \right)^2 - 1 , \quad (18)$$

and the normality criterion

$$\begin{Bmatrix} \dot{\theta} \\ \dot{u} \end{Bmatrix} = \dot{\lambda} \begin{Bmatrix} \frac{\partial \Gamma}{\partial M} \\ \frac{\partial \Gamma}{\partial N} \end{Bmatrix} . \quad (19)$$

Then, $\dot{u}$ can be related to $\dot{\theta}$ as

$$\dot{u} = \frac{2M_0}{N_0} \frac{N}{N_0} \dot{\theta} . \quad (20)$$

$\dot{\theta}$ is the rate of rotation, and is expressed constantly as

$$\dot{\theta} = \frac{V}{R} \quad .(21)$$

Substituting Eq. (20) into Eq. (17), the second order term of the axial force is eliminated due to the interaction between bending and axial forces. The rate of the plastic energy dissipation is reduced to a single term as

$$\dot{E}_{tip,plastic} = M_0 \frac{4}{R} V . \quad (22)$$

This is independent of the friction force. Once the plastic rolling radius is determined, the energy dissipation due to rolling and stretching of the front contact surface can be obtained. Normally, the rolling radius should adjust itself to give the minimum energy dissipation. Obviously, this could not be done at present. The influence of the rolling radius on the total energy absorption capacity will be investigated later. Subsequently, the horizontal resistance from the tip rolling and stretching is

$$F_{H,tip} = M_0 \frac{4}{R} (2C) . \quad (23)$$

Energy absorption due to the rolling and stretching, when being crushed a distance, l, is

$$E_{p,tip} = M_0 l \frac{4}{R} (2C) . \quad (24)$$

The total energy absorbed by the bottom plating when being crushed a distance, l, is obtained as

$$E_{plating} = 4l \left(M_0 \Delta\varphi + \frac{N_0}{\sqrt{3}} \sqrt{u_0^{\,2} + v_0^{\,2}} + \frac{2M_0 C}{R} \right) . \quad (25)$$

Subsequently, combining Eqs. (2, 7, 9 and 25), the total horizontal reaction force due to plastic deformation is obtained as

$$F_{H,plasticity} = F_{mH,girder} + F_{mH,trans,central} + F_{mH,trans,side} + F_{mH,plating} \quad (26)$$

Friction and vertical resistance

Generally, friction will play a significant role during grounding. For example, in the plate tearing model for bottom raking proposed by Ohtsubo and Wang (1995), the factor representing the effect of friction on the plate resistance is

$$g(\mu,\theta) = 1 + \frac{\mu}{\tan\varphi} . \quad (27)$$

μ is the Coulomb friction coefficient, φ is semi-wedge angle. Assuming θ=45^o and μ=0.3, the resistance will increase 30% due to friction. More increasing can be obtained for wedges with smaller semi-wedge angle. In the study of steady-state plate cutting by Simonsen and Wierzbicki (1998), a more complicated expression for the factor accounting for friction is derived. It was shown that when μ=0.3 and wedge inclination angle 10^o, the friction factor is 2.8, 1.7 and 1.5 for semi-wedge angle equal to 10^o, 30^o and 45^o respectively. The contribution of friction to total grounding resistance is of considerable magnitude.

Consequently, the effect of friction shall be considered and included in a consistent manner. As general, it is postulated that the external work equals the total internal work due to plasticity, friction, and fracture if applicable

$$F_H \cdot V = F_{H,plasticity} \cdot V + F_{H,fracture} \cdot V + \mu V' \int_S p dS . \quad (28)$$

F_H is the total horizontal resistance of the structure, V is relative velocity between ship and obstruction, $F_{H,plasticity}$ and $F_{H,fracture}$ denotes the resistance due to plasticity and fracture respectively, V' the relative velocity between the plating element dS and obstruction during contact, p the pressure distribution on the contact surface, S the contact surface. Last term of Eq. (28) represents the energy dissipation by friction forces on the contact surface.

For calculating the friction force, it is assumed that all the contact pressure is acting on the front plane surface of the indenter for simplicity. The shoulders of the indenter also transmit some force. However, it is believed that the major part of the force is taken by the front surface. Thus, the influence from the shoulders maybe neglected. The irregularities of the sharp edges of the indenter are also omitted due to their minor effect.

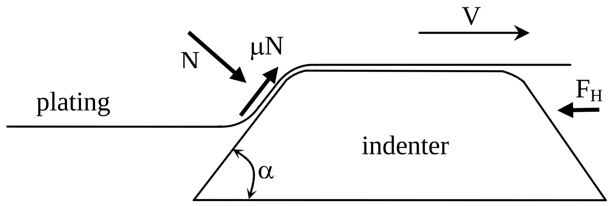

Figure 20: Relative motion of bottom plate and indenter for friction factor calculation.

Considering the present problem, Eq. (28) can be rewritten as

$$F_H \cdot V = F_{H,plasticity} \cdot V + \mu N V' . \quad (29)$$

N is the normal force on the contact surface, see Figure 20. The relative velocity $V'=V/\cos\alpha$. The equilibrium in the horizontal direction referred to the indenter is established as

$$F_H = N \sin\alpha + \mu N \cos\alpha . \quad (30)$$

Combining Eq. (30) and Eq. (29), eliminating N, an expression for the total horizontal resistance F_H in terms of $F_{H,plasticity}$ is given as

$$F_H = g(\mu,\alpha) \cdot F_{H,plasticity} , \quad (31)$$

where $g(\mu,\alpha)$ is the friction factor which is the ratio between F_H and $F_{H,plasticity}$. It is derived as a function of the friction coefficient μ and the inclination angle of the flat indenter relative to the bottom plate α, expressed as

$$g(\mu,\alpha) = \frac{F_H}{F_{H,plasticity}} = \left(1 - \frac{\mu}{(\sin\alpha + \mu\cos\alpha)\cos\alpha}\right)^{-1} \quad (32)$$

Subsequently, the vertical equilibrium gives the expression for vertical resistance

$$F_V = k(\mu,\alpha) \cdot F_H = k(\mu,\alpha) \cdot g(\mu,\alpha) \cdot F_{H,plasticity} , \quad (33)$$

$k(\mu,\alpha)$ is employed to represent the ratio of vertical resistance F_V to horizontal resistance F_H

$$k(\mu,\alpha) = \frac{F_V}{F_H} = \frac{1-\mu\tan\alpha}{\tan\alpha + \mu} . \quad (34)$$

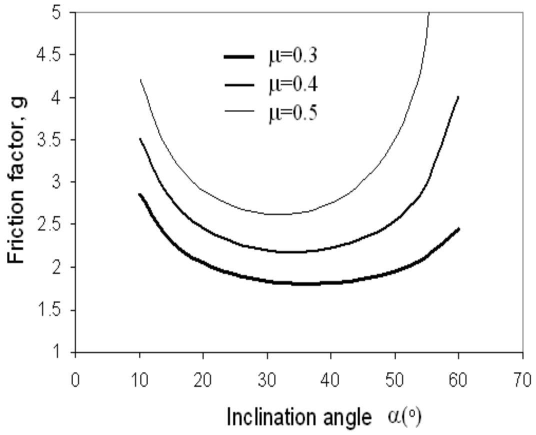

(a) friction factor as a function of α and μ

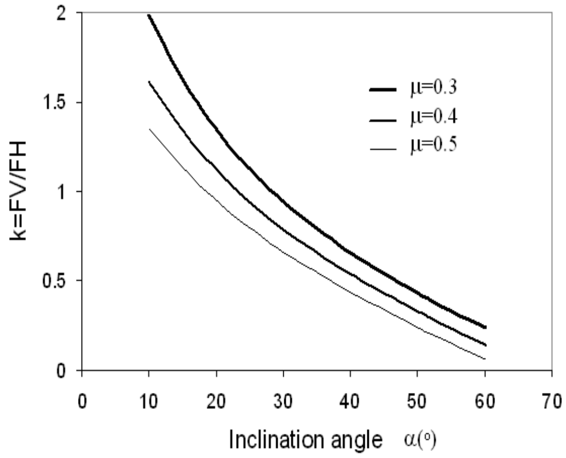

(b) ratio of F_V and F_H as a function of α and μ

Figure 21: Illustration of friction factor g and ratio of $k=F_V/F_H$.

It is interesting to find that the vertical resistance, F_V, is free of the friction coefficient μ with reference to $F_{H,plasticity}$. This is evident from the product of $g(\mu,\alpha)$ and $k(\mu,\alpha)$, which determines the magnitude of F_V

$$k(\mu,\alpha) \cdot g(\mu,\alpha) = 1/\tan\alpha . \quad (35)$$

This is also in accordance with the observations from numerical simulations. Once the horizontal resistance due to plastic deformation is obtained, the total horizontal resistance which takes into account of the effect of friction between contact surfaces can be consistently derived. The same applies to vertical resistance which governs the vertical motion and the magnitude of penetration.

As illustrated in Figure 21(a) for friction factor, if μ=0.3 is assumed, g will be 2.05, 1.84 and 1.94 for α=20°, 30° and 50° respectively. This indicates a prominent increasing for the total horizontal resistance due to the effect of friction. Figure 21(b) shows k as a function of α and μ. For large inclination angles, the vertical component of the frictional force dominates over the normal force. The total vertical force acting on the ship may become negative for very large inclination angles.

Application examples

The major structural deformation modes for longitudinal web girders, transverse members and bottom plating have been identified. Subsequently, simplified solutions have been derived in the previous section. Simplified formulae for individual structural components are assembled and applied to a simple ship bottom structure as shown in Figure 4. Compared to the bottom structure in Figure 4, only two transverse floors are included in the calculation hereafter. The stiffeners on the longitudinal web girders and bottom plating are smeared into their parental members. The grounding scenario is set up as in Figure 4. The major scantlings of the bottom structure are listed in Table 1. The bottom structure is subjected to four grounding processes with a shallow indentation depth of 150mm, an intermediate depth of 450mm and a relatively small sliding angle of 24.4^0 and an intermediate angle of 51.3^0.

Table 1: Major parameters of the simple bottom structure.

Material flow stress [MPa]	355
Spacing of transverse floors [mm]	4200
Spacing of longitudinal web girders [mm]	3750
Bottom height [mm]	900
Breadth of flat indenter [mm]	1500
Plate thickness [mm]	16

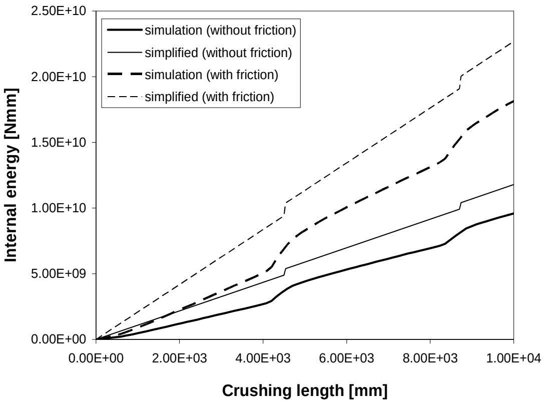

Case 1: α=24.4°, D=150mm

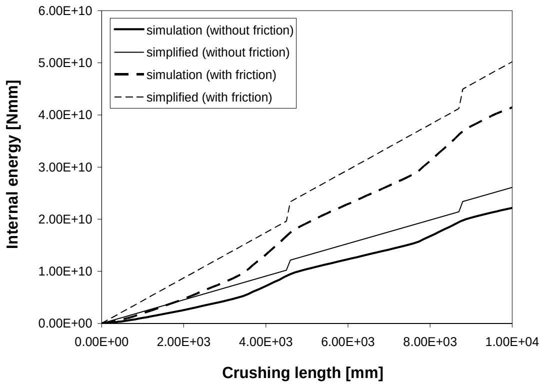

Case 2: α= 24.4°, D=450mm

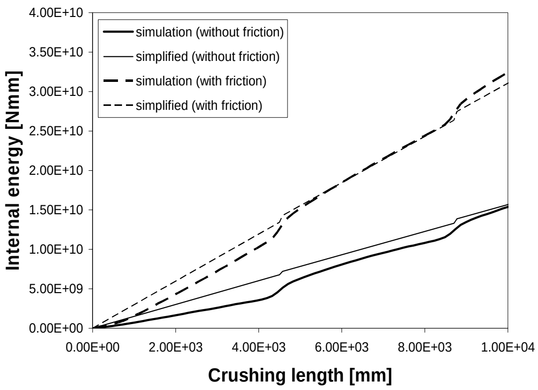

Case 3: α=51.3°, D=150mm

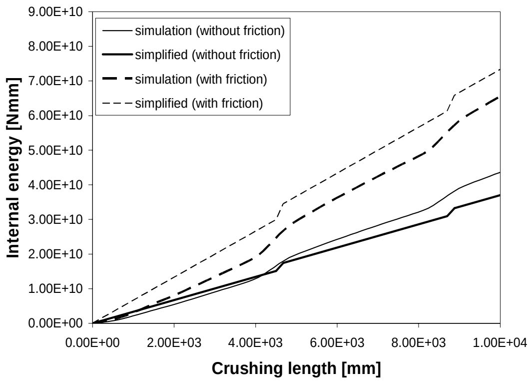

Case 4: α=51.3°, D=450mm

Figure 22: Simplified method vs. numerical simulation in terms of total bottom energy absorption.

The grounding processes have been analyzed numerically using the explicit non-linear finite element software, LS-DYNA (Hallquist, 1998), which is suitable of analyzing contact and transient impact problems. The results of numerical simulations are compared to the prediction by using simplified method proposed in this study. Energy dissipation curves obtained from numerical simulations and predicted from the present simplified method when assuming R=1000mm are compared in Figure 22.

The friction coefficient is assumed as 0.3 when the effect of friction is taken into account. The simplified method agrees satisfactorily with the results of numerical simulations in case 3 and case 4 when α=51.3°. For α=24.4°, the internal energy is overestimated considerably especially in case 1.

The present method gives better results when friction effect is not taken into account which implies further improvement of the present model for considering friction effect.

The increased strength due to a transverse member, associated with a hump in the energy absorption curve, is reasonably captured. However, the strength predicted by the simplified method tends to increase slightly slower. This is mainly due to the neglect of the interaction between longitudinal girder and transverse member.

The longitudinal girder near the intersection deforms somewhat differently compared to its steady-state mode. It consumes more energy than during the steady-state. If this can be treated separately, the hump of the energy absorption curve may be predicted with better accuracy. A new model for the crushing of central part of the transverse floor may also contribute to an improved prediction.

This may be the subject of future studies. Because the rolling radius R cannot be determined analytically according to the present method, it is of interest to investigate how it affects the total energy dissipation. Figure 23shows the comparison of total energy absorption for the grounding scenario “case 4” when R is assumed to be 200mm, 500mm, 1000mm, 1500mm and 2000mm respectively.

It is observed that the energy estimated by the present method for large rolling radius approaches the result from numerical simulation. When R is larger than 500mm, the effect of rolling radius on the total energy dissipation becomes stabilized. Therefore, an experienced based value such as R=1000mm may be assumed for the rolling radius.

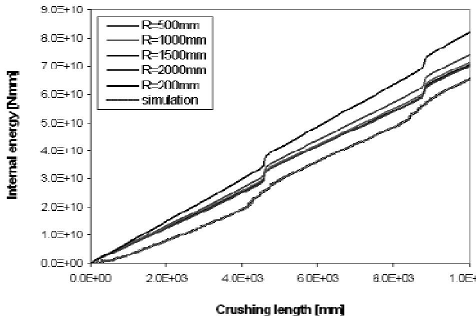

Figure 23: Total bottom energy absorption when different rolling radius is assumed.

Despite of the discrepancies, the results are encouraging. However, further studies are required to fully understand the structural response of ship grounding over large flat contact surface. Further improvement and more verification examples are needed before the model is generally accepted.

Conclusion

Compared to grounding over sharp underwater obstructions such as “rock”, the ship bottom structure behaves quite differently when grounded over obstructions with large flat contact surface. The mechanics in connection with this type of grounding is termed as “sliding” in the present study. In this situation, denting rather than tearing is more likely for bottom plating. Also, the longitudinal girder behaves in a sliding deformation mode compared to its behavior during raking. A simple method for assessing the resistance of ship bottom structure during grounding over obstructions with large flat contact surface has been presented in this study. The method is constituted by assembling primary deformation/failure modes of three major bottom structural members, which are longitudinal bottom girders, transverse members and bottom plating. The effect of friction is included in a simple manner. The vertical resistance is derived, and is found to be free of friction. The proposed method has been applied to a simple ship bottom structure subjected to sliding. The proposed method is considered to be a rational analysis tool, although it overestimates the energy absorption capacity to some extent in some cases. When coupled with a model for external dynamics, the present theory can be used to calculate ship motions and damage in a given grounding scenario. Such a coupled analysis has been conducted by, e.g. Simonsen and Wierzbicki (1996).

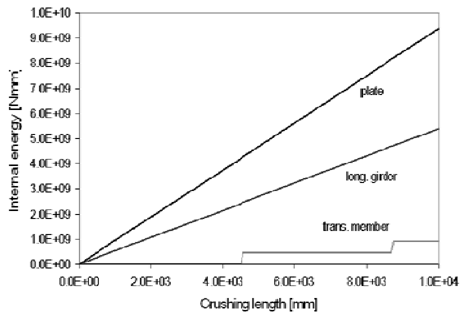

Figure 24: Contribution of bottom plating, longitudinal girder and transverse member to the total energy dissipation.

The results are encouraging, however, further work is required to increase the accuracy of the present simplified method. Figure 24 shows the energy partition between the three major structural members in the grounding scenario “case 3” which is considered representative for the present method. The bottom plating absorbs the most significant amount of energy during the sliding process. Whereas the energy consumed by transverse members is much lower. This indicates that further improvement of the present method should be focused on the bottom plating and longitudinal girders.

Blunt seabed obstructions with different types of contact surfaces such as spherical or cylindrical surface need to be considered for generality. Their influence on the strength of the ship bottom shall be investigated. Moreover, the global hull girder resistance should be checked along with the structural damage during sliding. The simplified method developed is considered to contribute substantially to the establishment of efficient methods for fast and reliable assessment of the outcome of accidental grounding events. It is also essential for probabilistically based formal safety assessment procedures or quantitative risk analysis.

Acknowledgement

The present work is initially carried out within the scope of the Strategic University Programme ‘‘ScenaRisC&G’’ in Norwegian University of Science and Technology

(NTNU). The support from the Research Council of Norway is acknowledged. In addition, some of the work embedded is generated according to the project - European Framework for Safe, Efficient and Environmentally-Friendly Ship Operations (abbreviated as FLAGSHIP). The financial support from European Commission is also acknowledged gratefully.

References:

Alsos HS, Amdahl J. 2007. On the resistance of tanker bottom structures during stranding. Marine Struct, 20(4):218-237.

Alsos HS, Amdahl J. 2008a. On the penetration resistance of stiffened plates Part I – Experiments. Int J Impact Eng, 36(6):799-807.

Alsos HS, Amdahl J. 2008b. Resistance of ship bottom structures during steady state sliding. Submitted to Marine Struct.

Alsos HS, Hopperstad OS, Törnqvist R, Amdahl J. 2008a. Analytical and numerical analysis of local necking using a stress based instability criterion. Int J of Solids and Struct ,45:2042–2055.

Alsos HS, Amdahl J, Hopperstad OS. 2008b. On the penetration resistance of stiffened plates Part II – Numerical analysis. Int J of Solids and Struct, 36(7):875-887.

Amdahl J. 1983. Energy absorption in ship-platform impacts. PhD thesis, Department of Marine Technology, Norwegian University of Science and Technology.

Amdahl J, Kavlie D. 1992. Experimental and numerical simulation of double hull stranding. DNV-MIT workshop on Mechanics of Ship Collision and Grounding, Oslo, Norway.

Amdahl J, Kavlie D, Johansen A. 1995. Tanker Grounding Resistance. Proc. of the 6th International Symposium on Practical Design of Ships and Mobil Units (PRADS1995), vol. 2, Sept 17-22, Seoul.

Amdahl J, Hellan Ø. 2004. Intentional grounding of disabled ships- on-board and shore based decision support system. In: Proc 3rd ICCGS, IZU, Japan.

Bognaert H, Bart Boon. 2007. New collision damage calculation tool used for quantitative risk analysis for LNG import terminal. In: Proc 4th ICCGS, Hamburg, Germany.

Carlebur AFC. 1995. Full-scale collision tests. Safety Science, 19:171-178.

Ehlers S, Broekhuijsen J, Alsos HS, Biehl F, Tabri K. 2008. Simulating the collision response of ship side structures: A failure criteria benchmark study. International Shipbuilding Progress, 55(1-2): 127-144.

Friis-Hansen P, Simonsen BC. 2002. GRACAT: software for grounding and collision risk analysis. Marine Struct, 15:383-401.

Hallquist JO. 1998. LS-DYNA: theoretical manual. Livermore Software Technology Corporation.

Hong L, Amdahl J. 2008a. Crushing resistance of web girders in ship collision and grounding. Marine Struct, 21:374-401.

Hong L, Amdahl J. 2008b. Plastic mechanism analysis of the resistance of ship longitudinal girders during grounding and collision. Int J Ships Offshore Struct, 3(3):159-171.

Hong L, Amdahl J. 2008c. Plastic behavior of web girders during ship collision and grounding. OMAE2008, 15-20 June, Lisbon, Portugal.

[ISSC]. 1997. Specialist Panel V.4: Structural design against collision and grounding. 13th International Ship and Offshore Congress, Trondheim, Norway.

[ISSC]. 2003. Committee V.3-collision and grounding. 15th International Ship and Offshore Structures Congress 2003, San Diego, USA.

[ISSC]. 2006. Committee V.1-collision and grounding. 16th International Ship and Offshore Structures Congress 2006, Southampton, UK.

Jones N, Jouri WS. 1987. A study of plate tearing for ship collision and grounding damage. J Ship Res;31(4):253–68.

Kierkegaard H. 1993. Ship bow response in high energy collisions. Marine Struct, 6:359-376.

Kuroiwa T, Kawamoto Y, Yuhara T. 1992. Study on damage of ship bottom structures due to grounding. Proc. Conf. on prediction methodology of tanker structural failure.

Midtun HO. 2006. Analysis of tankers during grounding and collision. Master Thesis, Norwegian University of Science and Technology.

Minorsky VU. 1959. An analysis of ship collision with reference to protection of nuclear power plants. J Ship Res, 3(1):1-4.

[NRC] National Research Council, Marine Board, Committee on Tank Vessel Design. 1991. Tanker spills: prevention by design. National Academy Press, Washington D.C., USA.

Ohtsubo H, Kawamoto Y, Kuroiwa T. 1994. Experimental and numerical research on ship collision and grounding of oil tankers. Nuclear Engineering and Design, 150:385-396.

Ohtsubo H, Wang G. 1995. An upper-bound solution to the problem of plate tearing. J Mar Sci Technol;1:46–51.

Paik, JK.1994. Cutting of a longitudinally stiffened plate by a wedge. J Ship Res, 38(4): 340-348.

Paik, JK, Pedersen, PT. 1995. Ultimate and crushing strength of plated structures. J Ship Res, 39(3): 250-261.

Paik JK, Wierzbicki T. 1997. A benchmark study on crushing and cutting of plated structures. J Ship Res; 41(2):147–60.

Paik JK. 2003. Innovative structural designs of tankers against ship collisions and grounding: a recent state-of-the-art review. Marine Technology, 40(1):25-33.

Pedersen PT. 1994. Ship grounding and hull-girder strength. Marine Struct, 7:1-29.

Rodd JL. 1996. Large scale tanker grounding experiments. Proceedings of 6th International Offshore and Polar Engineering Conference (ISOPE), Los Angeles, USA.

Samuelides MS, Amdahl J and Dow R. 2007a. Studies on the behaviour of bottom structures during grounding. In: Proc Int Conference on Advancements in Marine Structures, Glasgow, UK.

Samuelides MS, Voudouris G, Toulios M, Amdahl J, Dow R. 2007b. Simulation of the behaviour of double bottoms subjected to grounding actions. In: Proc of 4th ICCGS, Hamburg, Germany.

Simonsen BC, Wierzbicki T. 1996. Grounding bottom damage and ship motion over a rock. Proceedings of 6th International Offshore and Polar Engineering Conference (ISOPE), Los Angeles, USA.

Simonsen BC, Wierzbicki T. 1997. Plasticity, fracture and friction in steady state plate cutting. Int J Impact Eng;19(8):667–91.

Simonsen BC. 1997. Ship grounding on rock-I Theory. Marine Structures, 10:519-562.

Simonsen, B.C., Friis-Hansen, P. 2000. Theoretical and statistical analysis of ship grounding accidents. Journal of Offshore Mechanics and Arctic Engineering, Transactions of the ASME 122:200–207.

Thomas PF, Wierzbicki T. 1992. Grounding damage to double hull tank vessels. Proceedings of 2nd International Offshore and Polar Engineering Conference (ISOPE), San Francisco, USA.

Törnqvist R. 2003. Design of Crashworthy Ship Structures. Ph.D. thesis, DTU.

Törnqvist R, Simonsen BC. 2004. Experimental and Numerical Modelling of Ductile Crack Propagation in Large-scale Shell Structures. Marine Struct, 17:1-27.

Vaughan H. 1980. The tearing strength of mild steel plate. J Ship Res, 24(2):96-100.

Vredeveldt AW, Wevers LT. 1995. Full scale grounding experiments. Conference on Prediction methodology of tanker structural failure and consequential oil spill, Tokyo, Japan.

Wang G, Ohtsubo H, Liu D. 1997. A simple method for predicting the grounding strength of ships. J Ship Res, 41(3):241-47.

Identification of ship damage conditions during stranding

Tan-Hoi Nguyen, Jørgen Amdahl, Luca Garrè and Bernt J. Leira

Department of Marine Technology, NTNU Trondheim, Norway

Abstract:
This study outlines a new procedure for the estimation of stranding forces and their contact positions. The method is based on few on-site measurements, namely the draughts and the bending moments acting on the stranded ship. Additionally, also a procedure to estimate penetrations into the ship bottom based on knowledge of the resistance of the ship bottom to penetration is presented. The developed method can be a useful tool for quick decision making during critical situations. The ultimate goal of the analysis is to allow near real time prediction of the risk of penetration into cargo tanks with oil spill as well as hull girder failure. The method is illustrated by means of simulation of a realistic stranding scenario which demonstrates the effectiveness of the proposed model.

Introduction

Groundings and collisions are certainly recognized as the most relevant accidents to ships. According to the International Oil Pollution Compensation Fund (IOPCF 2005), grounding accidents are responsible for grossly 23% of the oil release into sea waters worldwide. Following the Maritime Accident Review (EMSA 2008), statistics show that during the last five years the likelihood of a ship being involved in a serious grounding, collision or contact accident has doubled and the same increase can be estimated also for the costs associated with these accidents. This figure clearly urges to a better understanding and modeling of the response of ships for various grounding scenarios, both towards the prevention of these events and the mitigation of the possible consequences. In this respect, much effort has been devoted in the last decades to the analysis of ship's performance during grounding, and nowadays the literature available on the topic is rather comprehensive. The main aim of the work made in this respect is to provide the topology, position and extension of the bottom damage under a certain set of parameters defining the stranding scenario, i.e. type of ship, speed, structural arrangements, characteristics of the sea floor and so on. A complete and thoroughly review of this family of procedures can be found in (Wang et al. 2002).

It is also noted that, in order to perform a satisfactory assessment of the safety of a ship against grounding, this set of procedures must be considered in a wider framework considering the whole category of possible consequences which are due to a specific event. In this respect, Formal Safety Assessment (FSA) introduced by the International Maritime Organization (IMO 2002), requires a risk-based approach. Departing from a risk-based assessment of the design of a ship, the approach is aimed at evaluating, for a given accident scenario, the cost-to-benefit impact of each Risk Control Option (RCO) on the design. In line with this scope, a first set of probabilistic and risk analyses have been pursued and remarkable efforts in this respect can be found (see for instance Hauke et al. 1999; Friis-Hansen et al. 2002; Sven et al. 2002; Ravn et al. 2008). Within the wide extent of risk-based evaluation of safety against grounding, also a proper assessment of the post-grounding or stranding scenario, i.e. when the grounded ship has come to a complete stop and rests at a given position along the bottom, becomes important. From analysis of past accidents, it is in fact observed that this situation might become critical as consequences can escalate if appropriate counteractions, to be considered by all means as potential effective RCOs, are not taken in due time. This would generally imply the definition of standardized intervention patterns tailored for each possible scenario, such as for instance those envisaged within the Decision Support System for Ships in Degraded Condition program (DSS_DC, see Amdahl and Øyvind 2004). It is however clear, as also outlined by (Amdahl et al. 1995), that in this respect a reliable identification of the scenario, i.e. definition of the main characteristics of the damage, is of primary importance to build up a proper decision model for intervention purposes. This becomes important in the light of a scenario-based risk assessment of groundings, possibly aimed at supporting an emergency decision framework for immediate accident recovery or, additionally, in the planning of intentional grounding as envisaged by (Amdahl and Øyvind 2004). Additionally, this identification must be established on the basis of a limited number of measurable quantities and be built upon fast and efficient computational procedures, if practical use and possible industrial implementation is foreseen.

According to this background, the present work proposes a new and simple procedure for quick identification of the number and longitudinal position of the points of contact with the seabed, together with an estimate of the stranding reaction forces. This set of variables is in fact considered to be of outmost importance in the evolution of the accident scenario, as they play a primary role in both determining the local penetration in the bottom structure and the characteristics of longitudinal shear and bending distributions acting on the hull girder. Moreover, an estimate of the longitudinal position of contact can in principle provide insights regarding the behavior of the bottom features where the ship is resting. This information could be useful with respect to safety against penetration and prevailing margins before fracture of the cargo tanks. The proposed procedure is based on a limited set of on-site measurable quantities, namely the aft and fore readings of draught, and measurements of the bending moment acting on the stranded ship girder as provided by an onboard stress monitoring system, if available. An illustrative example of the possible extension of the proposed procedure to estimate the local indentation at the stranded position, provided the resistance versus penetration behavior of the bottom is known, is also given.

Clearly, the complete determination of the actual state of the ship during the considered stranding scenario is associated with significant variability, involving for instance the possible structural arrangements of the bottom and the detailed topology of the ground. Moreover, available measurements are affected by uncertainties, mainly related to reading errors or, for the present case, deflection of the hull beam and its influence on measured draughts. While these effects are not explicitly considered in the present study, it is believed that the proposed procedure can be further extended to account also for their influences.

The considered stranding scenario

As mentioned in the introduction, a new and simple approach to the characterization of a stranding scenario is proposed. The scenario considered is depicted in Figure 1. After grounding, the ship has come to a complete stop and strands at a given single position X_1 on the bottom. The characteristics of the damage which occurred along the hull up to X_1 are related to the first dynamic development of the grounding event and are not further considered here. From this moment on, the scenario can be divided into two distinct phases: in the first phase the ship floats with a given trim, corresponding to rotation equilibrium around X_1, which can be thought of as a pivot point of the ship. In thissituation, the main displacement of the ship is rotation around this point. Assuming an ebb tide at the time of grounding, the ship changes trim until she eventually comes to rest when the clearance Z_0 (refer to Figure 1) is closed and the seabed is touched at a second position X_2. This situation corresponds to the second phase. It must be remarked that the present study is limited to contacts located on the keel line, with reaction forces lying in the longitudinal plane of symmetry of the ship. Accordingly, only longitudinal rotation of the stranded ship is accounted for while roll effects are not considered.

The prevailing stress regime in the girder and, in turn, the intervention countermeasures to be undertaken, strongly relies on which stranding phase is taking place. In fact, the evolution of the global loads acting on the girder as a function of ebb tide depends on the number and position of the stranding point(s). As the performance of the hull girder changes considerably depending on the type of global loads, the stranding scenario should be carefully assessed in an emergency situation.

According to this outline, a procedure is sought to assess the following items:

1) Determination of position X_1 and ground reaction F_1 in the first phase of stranding;
2) Additional determination of X2 and ground reaction F2 in the second phase of stranding;
3) Possible discrimination between the first and the second phase, if unknown;

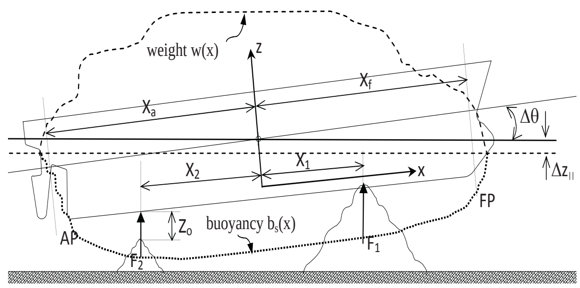

Figure 1. Analytical procedure for stranding scenario

Finally, the number of contacts with the seabed could be higher than two, if considerable deflection of the hull girder takes place. This case is however not considered at the present stage of the analysis.

Outline of the proposed procedure

The proposed procedure requires knowledge of the ship's weight and buoyancy longitudinal distributions acting on the stranded hull girder, $w(x)$ and $b_s(x)$ respectively, in which x denotes the longitudinal axis in the body-fixed reference coordinate system. The first distribution can be inferred from the voyage data and the information contained in the loading master or, in case of tankers, in the Ullage Reports. The second distribution is directly obtained from measurements of the aft and fore draughts of the ship in the stranded condition, respectively $Z(X_a)$ and $Z(X_f)$, in which X_a and X_f identify the positions of the aft and fore perpendiculars.

Let us consider the longitudinal load distribution $l_s(x) = w(x) - b_s(x)$. It is here noted that $l_s(x)$ does not include the stranding reactions F_1 and F_2. For the common case of a ship floating still in the sea ($F_1 = F_2 = 0$), $l_s(x)$ corresponds to the actual longitudinal load distribution acting on the hull girder at equilibrium. In the frame of a beam analysis of the hull girder, in this situation $l_s(x)$ satisfies both the translational (vertical) and rotational equilibrium of the ship. This means that both the shear and bending moment distributions, $Q_s(x)$ and $M_s(x)$, computed respectively as single and double integration of $l_s(x)$ along the girder axis:

$$Q_s(x) = \int_{X_a}^{x} l_s(x)dx \tag{1}$$

$$M_s(x) = \int_{X_a}^{x} Q_s(x)dx \tag{2}$$

are null in correspondence of the foremost section of the girder, assumed in the present case corresponding to the fore perpendicular ($x = X_f$): $Q_s(X_f) = 0$, $M_s(X_f) = 0$

(a null value of these distributions at the aftmost section, $x = X_a$, is given as no constant is provided in Eqs. (1) and (2). However, since $l_s(x)$ does not include F_1 and F_2 acting in the present stranding case, these distributions for this case does not reflect the rigid body translational and rotational equilibrium of the stranded girder. As a consequence of this, $Q_s(X_f)$ and $M_s(X_f)$ computed according to Eqs. (1) and (2) are not null. On the contrary, it is possible to show that these values are respectively equal to (these relationships can be derived reintroducing the translational and rotational equilibrium accounting also for the contributions of F_1 and F_2):

$$Q_s\left(X_f\right) = F_1 + F_2 \tag{3}$$

$$M_s\left(X_f\right) = F_1\left(X_f - X_1\right) + F_2\left(X_f - X_2\right) \tag{4}$$

In words, the terms given by Eqs. (3) and (4) represent the translational and rotational contributions of F_1 and F_2 required to balance $l_s(x)$ and to realize the equilibrium of the ship. The basic concept of the present procedure takes advantage from this conclusion. More specifically, with knowledge of $w(x)$ and of the distribution $b_s(x)$ derived from the measurements $Z(X_a)$ and $Z(X_f)$ on the stranding site, $l_s(x)$ and the values $Q_s(X_f)$ and $M_s(X_f)$ are computed. From these values, Eqs. (3) and (4) can be solved for the variables characterizing the stranding scenario, i.e. X_1, X_2, F_1 and F_2. As illustrated in the following, the way in which the solution is achieved depends on the phase of stranding.

Finally, it should also be noted that $w(x)$ and $b_s(x)$ are, in a real case, perpendicular to the water line. In the integrals, however, these distributions are assumed to be perpendicular to the x-axis. This assumption is reasonable for small angles θ, which, however, are considered to be the most likely to occur in stranding of long ships.

First phase

Computation of the stranding forces and their positions simply requires solution of Eqs. (3) and (4) with F_2 set equal to zero. The solution is trivial, as the two equations represent a linear system in two unknowns which is immediately solved once $Q_s(X_f)$ and $M_s(X_f)$ are known.

Second phase

In the second phase the two unknowns F_2 and X_2 are added in the system of equations. In this case a unique solution of the problem requires, in principle, two new equations. It is not immediately clear which additional parameters should be considered to supply the missing equations, especially as the set of measurable quantities in a real situation is rather limited. As a first simplification, the number of additional equations is reduced by assuming that X_1 is known. This could be either the result of a previous determination of this variable during the first phase or, alternatively, the range of this variable is estimated by expert judgment and a simplified analysis of the previous dynamic grounding event. The third equation needed is obtained accounting for the possibility to measure the bending distribution with a hull stress monitoring system. This technology is in fact becoming more and more common for new vessels, especially for large tankers, and usually returns readings of the bending effects in correspondence of the ship's quarter lengths $x_j = j \cdot L/4$, $j = 1, 2, 3$. Further description and examples of these applications can be found, for instance with reference to existing systems (HMON, HullMon+). For the present case, bending measurements are used to define the following error function:

$$\hat{E} = \sqrt{\sum_{j=1}^{3}\left[M_R\left(x_j\right) - M_H\left(x_j, X_2\right)\right]^2} \tag{5}$$

in which $M_R(x_j)$ represents the "real" bending moment distribution acting on the stranded ship as measured by the monitoring system, and $M_H(x,X_2)$ is a fictitious bending distribution which corresponds to choosing the position X_2 arbitrarily. It is in fact noted that, once a value of X_2 is assumed, Eqs. (3) and (4) are uniquely solved for F_1 and F_2 and $M_H(x,X_2)$ can be determined, including also the effect of the two ground reactions. The correct position X_2 is then found according to a minimization of Eq. (5).

Minimization of this error requires an iterative scheme of solution. However, thanks to the limited complexity of the involved formulations, the resulting computational burden of the problem is relatively low. Given this, one can avoid the implementation of solution schemes and simply adopt a screening of the full range of possible X_2.

Clearly, there are uncertainties related to measurements. One of these regards the bending moment distribution as returned by the monitoring system, $M_R(x)$. In this respect, it is worth to mention that readings of the monitoring system are calibrated upon the design section modulus of the intact ship. This means that, when the ship is damaged, the estimates of the moment are biased by a quantity which is proportional to the damage itself. This effect, which introduces an additional uncertainty of the readings, has been not accounted for at the present stage of the study.

Identification of phase

A third aspect regards the possibility to identify which of the two phases is taking place. A possible approach can be based on the previous development. It is first assumed that the ship rests on only one stranding point. Accordingly, Eqs. (3) and (4) are solved for X_1 and F_1 and the corresponding distribution $M_H(x,X_1)$, i.e. the fictitious bending distribution assuming only one stranding position at X_1, is computed. The hypothesis of having one stranding point is then tested against the error moment given by Eq. (5).

Solution Scheme

The previous procedure can be summarized according to the following step by step scheme:

1) Determination of $w(x)$ from available cargo and ship data;
2) Computation of $b_s(x)$ from on site measurements of draughts;
3) Determination of $M_R(x_j)$ from the stress monitoring system;
4) Computation of $Q_s(X_f)$ and $M_s(X_f)$ from Eqs. (1) and (2);
5) Hypothesis: one single contact point;
6) Computation of X_1 and F_1 from Eqs. (3) and (4);
7) Computation of the error $\hat{E}$ from Eq. (5); Is $\hat{E}$ within tolerable limits? Yes: X_1 and F_1 are the solution; No: proceed to the following steps;
8) Determination of X_1 analysis of previous stranding phase or expert judgments;
9) Tentative value for X_2 – start of the iterative scheme;
10) Solution of Eqs. (3) and (4) and computation of F_1 and F_2;
11) Computation of $\hat{E}$;
12) Is $\hat{E}$ within tolerable limits? Yes: X_2, F_1 and F_2 are the solution. No: restart from step 9).

Case study

In order to illustrate the proposed procedure, a given stranding scenario is first generated. A fully loaded shuttle tanker is considered. The ship has a total length of approximately 265 m, a molded breadth of nearly 42.5 m, and a design draught of 15 m.

The tanker is initially stranded at X_1 = 40 m. Ebb tide is assumed to take place at the moment of stranding, causing the ship to undergo the two phases previously described. After the ship has covered a clearance Z_0 of approximately 0.6 m (refer to Figure 1), the ship is assumed to rest upon the second stranding position, X_2 = -50 m. The origin of the reference system is located amidship.

In a real situation, the development of the stranding scenario is determined by the temporal variation of the sea level due to tide. More specifically, let the sequence z^1, z^2, , z^i, , z^n identify a given set of tide levels. For each level, a corresponding pair of the aft and fore draughts, $Z(X_a)^i$ and $Z(X_f)^i$, is measured. According to the proposed procedure, trim and corresponding distributions $l_s(x)^i$, $Q_s(x)^i$ and $M_s(x)^i$ are identified by each pair $Z(X_a)^i$ and $Z(X_f)^i$ measured for each variation of tide. As it will be detailed in the following sections, these distributions are then used to compute the magnitudes of the stranding forces F_1^i and F_2^i at each *i-th* tide level and their locations X_1 and X_2.

It must be also noted that, in a real stranding case, discrepancies will be observed between the variation of the tide level, $\Delta_{tide}{}^i = z^i - z^{i-1}$, and the measured variations in draughts, $\Delta_{aft}{}^i = Z(X_a)^i - Z(X_a)^{i-1}$ and $\Delta_{fwd}{}^i = Z(X_f)^i - Z(X_f)^{i-1}$. Disregarding the influence of the deflection of the hull girder, these discrepancies are due to the local penetrations δ_1 and δ_2 of the obstructions into the bottom of the ship, generated by the relative increase of the stranding forces F_1^i and F_2^i as the tide level decreases. Accounting for these penetrations, the variation Δ_{tide} will be higher than the measured Δ_{aft} and Δ_{fwd}.

For the present purpose of generating a scenario to validate the identification procedure, the measurements corresponding to a real stranding case have been necessarily simulated according to a backward approach which departs from assumed sequences of the stranding forces F_1^i and F_2^i. The main outcomes of this generation, which is detailed in Appendix 1, are the histories of $Z(X_a)^i$ and $Z(X_f)^i$ and the associated temporal change of tide Δ_{tide}. In Table 1 these values are reported as a function of time.

Table 4: Assumed measured draughts and corresponding tide

Time [hour]	$Z(X_a)^i$ [m]	$Z(X_f)^i$ [m]	Trim [m]	Δ_{tide} [m]
0	14.21	13.94	0.27	0
0.37	14.23	13.62	0.61	0.26
0.76	14.25	13.30	0.94	0.53
1.58	14.01	12.92	1.08	1.07
2.47	13.77	12.55	1.21	1.61
3.55	13.26	12.44	0.82	2.14
6.00	12.90	12.20	0.69	2.67

Now, the simulated draughts are assumed to be the ones measured at the stranding site. Departing from them, the proposed procedure is applied in order to derive the (known) values of the contact forces and their (known) positions. The distributions $l_s(x)^i$, $Q_s(x)^i$ and $M_s(x)^i$ corresponding to a given pair $Z(X_a)^i$ and $Z(X_f)^i$ have been computed using an in-house code for load and hydrostatic computations of ships.

It is additionally recalled that, in case of two stranding positions, the readings of the bending moment $M_R(x)^i$ as provided by the hull monitoring system are also required. In the generation of the present scenario, these readings have been simulated by simply assuming them equal to the bending distribution computed by the code at each *i-th* application of the forces.

Finally, in the last section of this paper, the discrepancies occurring between the measurements in draughts and the variation in tide have been used to present a possible approach to establish the bottom penetrations δ_1 and δ_2.

Validation of the proposed procedure

First phase of stranding

The first phase corresponds to the ship stranded only at X_1. For a pair of measured draughts $Z(X_a)^i$ and $Z(X_f)^i$, the distributions $Q_s(x)^i$ and $M_s(x)^i$ are calculated using Eqs. (1) and (2). These distributions, according to the concepts previously outlined, must not be zero at the foremost section of the girder. This because they are derived from the load distribution $l_s(x)$, which does not include the reaction forces from the seabed. Therefore, the unknown stranding reaction acting on the ship bottom yields nonzero values of $Q_s(X_f)^i$ and $M_s(X_f)^i$.

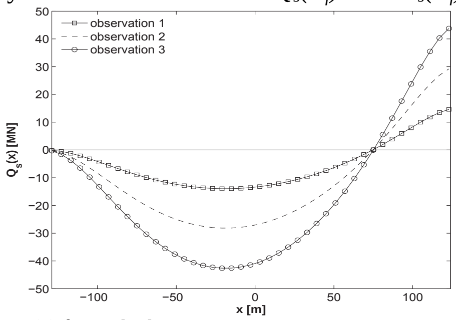

Figure 2. $Q_s(x)$ for each observation.

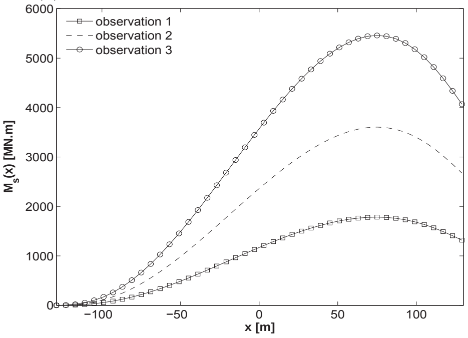

Figure 3. $M_s(x)$ for each observation.

These two distributions are shown in Figures 2 and 3. As expressed by Eq. (3), the unbalance in shear force must be equal to the contact force. Hence, the resulting contact force F_1 for the first step is 15 MN, in the second step is 30 MN and in the third step is 45 MN (see $Q_s(X_f)$ in Figure 2. These values are equal to the values simulated in the generation of the scenario and reported in Appendix 1).

The stranding position, X_1, is computed from the unbalance in bending moment, Eq. (4):

$$X_1^i = \frac{M_s(X_f)^i}{Q_s(X_f)^i} \tag{6}$$

The computed value X_1^i for each *i-th* observation is plotted in Figure 4. It is seen that X_1^i coincides with the correct value (40 m) for the first three observations, i.e. i = 1, 2, 3 in Table 1. However, when computed from the fourth observation on, this value changes. This is a clear indication that ship has also made contact with the seabed at a second location. Additionally, the very same effect can be captured in terms of the error $\hat{E}$, Eq. (5). This error, plotted in Figure 4, departs from zero when the hypothesis of having just one stranding position is no longer valid, and is a useful metric to assess the elapse of the stranding.

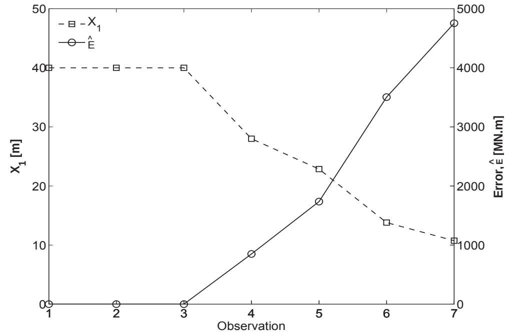

Figure 4. X_1 and $\hat{E}$ for each observation.

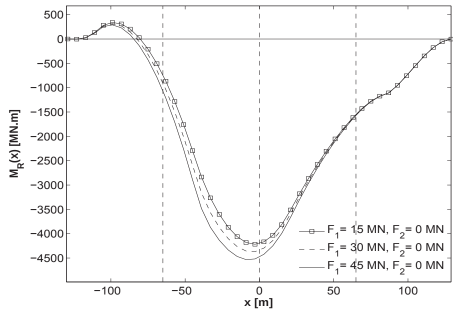

Figure 5. $M_R(x)$ for each observation.

The assumed monitored values $M_R(x_j)^i$ required to compute $\hat{E}$ are shown in Figure 5. They correspond to the magnitude of the distribution $M_R(x)$ at the three vertical dashed lines. In a real case, only these three values are likely to be known from readings of the monitoring system, while the entire distribution as plotted in Figure 5 can be computed only after solution of X_1 and F_1.

Second phase of stranding

During the second phase the ship strands at X_1 and X_2. The distributions $Q_s(x)^i$ and $M_s(x)^i$ corresponding to the measurements of the draughts in this phase (fourth to seventh row of Table 1) are plotted in Figures 6 and 7.

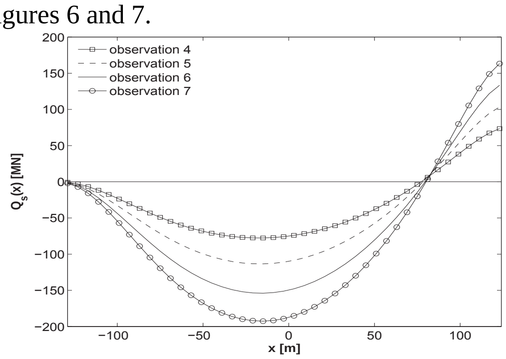

Figure 6. $Q_s(x)$ for each observation

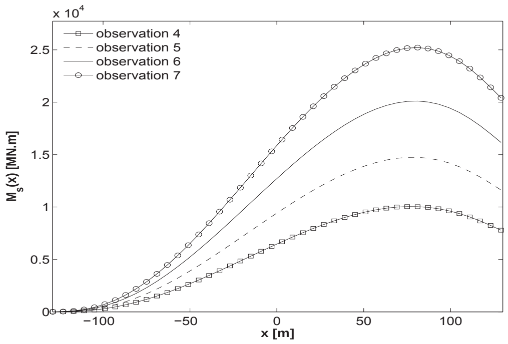

n

Figure 7. $M_s(x)$ for each observation.

In the second phase, there are three unknowns, X_2, F_2, and F_1, while X_1 is known from solution of the previous phase. The resultant of the contact forces, i.e F_1+F_2, is equal to the non-zero shear value at the fore perpendicular, $Q_s(X_f)^i$. The condition that the moment of the two contact forces about the fore perpendicular shall be equal to $M_s(X_f)^i$, Eq. (4), provides the second equation. The third equation to determine all the three unknowns is provided, in principle, by the actual bending moment distribution $M_R(x)^i$ measured for each *i-th* observation at any of the three monitoring locations x_j. However, as the solution will not be exact in a practical application due to uncertainties in the readings, and in order to make the procedure more general, the error function $\hat{E}$, introduced in Eq. (5), is computed from the measurements at all the monitoring points. In Figure 8, this function is plotted for each observation as a function of the (assumed) location of the second contact point. It is observed that it becomes zero at the exact position of the second contact point, X_2 = -50 m. Of course, the error vanishes completely because the process is calculated in a reverse way disregarding possible uncertainties. In a real application, measurements and calculation inaccuracies will not give perfect results and the minimum error will be used.

After identification of X_2, the problem reduces to a system of two equations and two unknowns (F_1 and F_2), which is immediately solved for the forces.

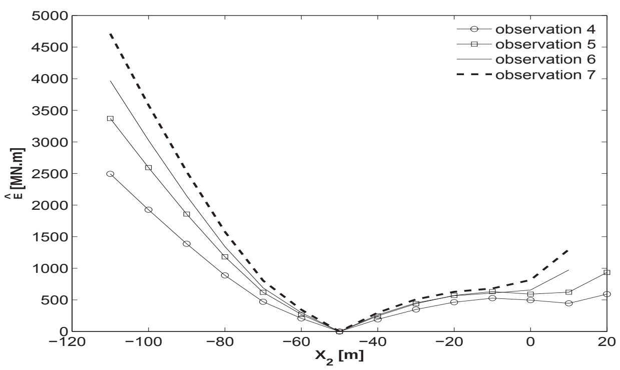

Figure 8. for each observation and different X_2.

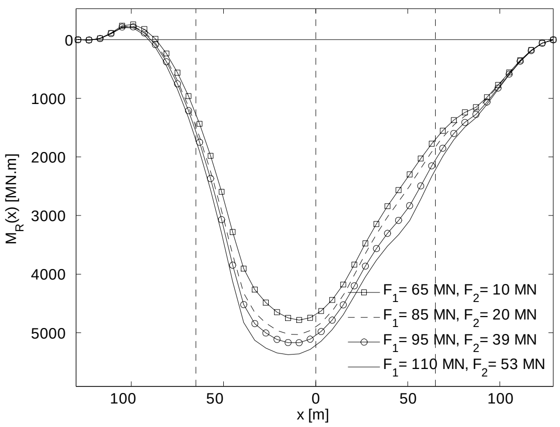

Figure 9. $M_R(x)$ for each observation

The assumed monitored values $M_R(x_j)^i$ required to compute $\hat{E}$ are shown in Figure 9. Again, in a practical application only these values are known from readings of the monitoring system and the entire distribution can be computed only after solution of X_2, F_1 and F_2.

Computation of penetration and identification of seabed topology

In the last section of this paper, a possible extension of the present procedure to identify the main characteristics of the stranding damage is illustrated. A convenient way to characterize stranding damages is by means of force versus penetration curves. In this respect, (Alsos and Amdahl 2007) introduced a useful categorization of the possible seabed topologies, namely “rock”, “reef”, and "shoal”, based on possible different structural responses of the bottom to penetration. Following the same line of reasoning as in (Alsos and Amdahl 2007), the identification of the proper force versus penetration curve can in principle characterize the topology of obstruction and, to a second extent, the structural elements of the bottom involved in the stranding.

As a first step of the proposed method, penetrations into the bottom δ_1 and δ_2 at the stranding positions X_1 and X_2 are computed. As previously mentioned, these are responsible for discrepancies between the tidal and the measured draught changes. Owing to this, they can be assessed as the difference between the known actual tide change, $\Delta_{tide}{}^i$, and the change in measured draughts $\Delta Z(X_j)$ at location X_j of stranding, j =1,2:

$$\delta_j^{\,i} = \Delta^i_{tide} - \Delta Z\left(X_j\right)^i \qquad (7)$$

This quantity can be directly measured at the position of stranding or, alternatively, can be in principle assessed from the changes at the fore and aft perpendiculars, $\Delta_{fwd}{}^i$ and $\Delta_{aft}{}^i$. The value δ_j^i provided by the above formula must be considered as the differential increment occurring between an observed tide level z^i and z^{i-1}. Therefore, the entire penetration up to a certain level is returned by summing up the previous increments, and the whole sequences of penetrations constitute the temporal evolution of these variables as the stranding scenario develops. Together with this, also the stranding forces F_1^i and F_2^i are estimated for each measured pair of draughts $Z(X_a)^i$ and $Z(X_f)^i$ at each z^i tide level. This provides the temporal evolution of forces. The histories of penetration and forces considered jointly provide a “tracking” of the force versus penetration curve at the given stranding position X_j. Application of the procedure for the considered scenario yields the force penetration curve given in Figure 10. The so-found curve can then be compared with a set of reference curves (obtained for instance with Finite Element Analysis such as Alsos (Alsos and Amdahl 2007), or Plastic Analysis such as Hong (Hong and Amdahl 2008)), each representing a given different stranding situation, identified in terms of the type of obstruction and the bottom structure topology involved in the stranding. From this, the stranding scenario under monitoring can be characterized.

From the curves of the present example, it is concluded that the shape of the sea floor characterizing the first stranding location (in Figure 10a) corresponds to reef. There is substantial deformation of the girders in the bottom, but the outer shell is far from fracture. The second contact point is obviously a rock type obstruction, which penetrates easily into the ship bottom and affects the hydrostatic conditions very little. For this second case, rupture of the outer plate (identified by the square point of Figure 10b) may be easily originated if proper counteractions are not taken in due time. The presented results are obtained with a simplified simulation of the scenario (as outlined in Appendix 1)

(a)

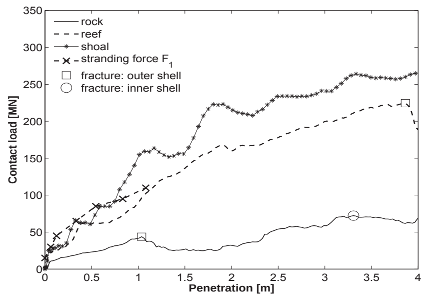

(b)

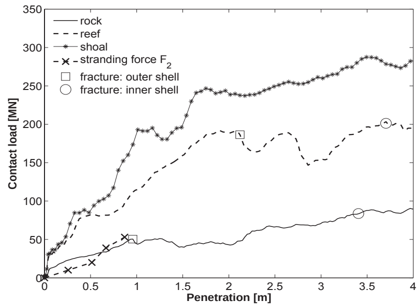

Figure 10. Contact force versus penetration δ: (a) at X_1; (b) at X_2

and must be considered as an illustration of the proposed approach. Generally, in a real application the reported curves will easily have mixed behavior corresponding to a combination of possible shapes, thus not clearly fitting any of the standard curves at hand. For this general case, the proper identification needs to be extended accounting also for these intermediate situations. The potential of the present approach is however noted, with special reference to identification of stranding in real-time. This identification represents an important element in the definition of countermeasures and emergency intervention plans.

It is finally remarked that, since the present approach concerns only with increments of penetration during ebb tide (Eq. 7), uncertainties are related to the first penetration already affecting the first measurements (i = 1). This value determines the placement of the curve (starting point) onto the plots in Figure 10. In this respect, this initial value can be tentatively assessed with a best fit of the obtained curve onto the available ones.

Conclusions

A new and simple approach for the characterization of a stranding scenario is proposed. The procedure is aimed at the identification of relevant parameters defining the scenario, namely the positions of stranding along the ship bottom and the corresponding stranding forces. The procedure is based on on-site measurements of the draughts of the stranded ship and on readings of the bending moment distribution acting on the girder as provided by a hull monitoring system.

With the aim to validate the proposed procedure, a possible stranding scenario has been generated. The scenario accounts also for ebb tide occurring at the moment of grounding, responsible for the evolution of the stranding scenario in terms of the number of stranding points, here limited to a maximum of two. It is seen that application of this procedure leads to a correct estimation of the values characterizing the stranding. Moreover, it is noted that detection of multiple stranding points along the ship bottom is made possible.

A simplified approach to the estimation of the penetrations into the ship bottom during stranding is also presented. This is done monitoring the changes in draughts as the tide level decreases, together with the increasing stranding forces. From these measurements, force versus penetration curves are obtained, which are then used to characterize the on-going stranding in terms of possible types of obstruction and involved structural arrangements. Clearly, a number of uncertainties affect the actual application of the present procedure. These are mainly related to the accuracy of the measurements and to effects neglected at the present stage such as deflection of the girder.

Moreover, the wide number of possible combinations of ground topologies and bottom structural arrangements realizable in a real case further complicates the analysis. It is however believed that both the uncertainties and the variability of the scenario can be consistently tackled in future developments, accounting also for a probabilistic modeling of the various variables involved.

Acknowlegments

The authors gratefully acknowledge the support of the Strategic University Program (SUP) in Norwegian University of Science and Technology (NTNU). A special gratitude goes to the Research Council of Norway for providing the funding for this research. Part of the study is generated within European Framework for Safe, Efficient and Environmentally-Friendly Ship Operations (FLAGSHIP). The financial support from European Commission is gratefully acknowledged.

Appendix 1

As previously anticipated, two increasing sequences of the reaction forces F_1^i and F_2^i, acting at X_1 and X_2, are first assumed. These two sequences, reported in Table A-1, are meant to reproduce the increase of reactions from the seabed at each decreasing level of tide z^i. For each application of the forces, the equilibrium condition is computed (mean draught and trim for each level) and identified in terms of $Z(X_a)^i$ and $Z(X_f)^i$.

Table A-1: Assumed sequences for F_1^i and F_2^i

i	F_1^i [MN]	F_2^i [MN]
1	15	0
2	30	0
3	45	0
4	65	10
5	85	20
6	95	39
7	110	53

The tide change associated with each application of the forces is generated with the following formula:

$$\Delta^i_{tide} = k\,\frac{\Delta^i_{aft} + \Delta^i_{fwd}}{2} \tag{8}$$

in which $\Delta_{tide}^i = z^i - z^{i-1}$, $\Delta_{aft}^i = Z(X_a)^i - Z(X_a)^{i-1}$ and $\Delta_{fwd}^i = Z(X_f)^i - Z(X_f)^{i-1}$. Moreover, k is a factor higher than 1 whose magnitude determines the level of discrepancies between these quantities. In turn, this value determines the level of penetrations δ_1 and δ_2 into the bottom. It is noted that, in principle, the value of k depends on the actual response of the bottom structure in the considered stranded scenario. This effect however requires appropriate analysis of the local stranding conditions, such as the identification of the components of the bottom involved and the topology and geometry of the seabed, (see Alsos and Amdahl 2007). In the present case, this value is simply assumed equal to 1.75.

References:

Alsos HS, Amdahl, J. 2007. On the resistance of tanker bottom structures during stranding. Marine Structures 20:218-237.

Amdahl J, Kavlie D, Johansen A. 1995. Design of tankers for grounding and collision. In: Proceedings of International Conference on Technologies for Marine Environment Preservation, Tokyo, Japan, Vol. 1, p. 167-174.

Amdahl J and Oyvind H. 2004. Intentional grounding of disabled ships - on-board and shore based decision support system. In: International Conference on Collision and Grounding of Ships (ICCGS), Izu, Japan, 25 - 27 October.

[EMSA] Maritime Accident Review, issued by European Maritime Safety Agency 2008.

Friis-Hansen P, Simonsen BC. 2002. GRACAT: software for grounding and collision risk analysis. Marine Structures 15:383–40.

Hauke L Kite-Powell, Di Jin et al. 1999. Investigation of potential risk factors for groundings of commercial vessels in US ports. International Journal of Offshore and Polar Engineering 9(1):16-21

HMON, Hull Monitoring System, available from www.dnv.com

Hong L, Amdahl J. 2008. Plastic mechanism analysis of the resistance of ship longitudinal girders in grounding and collision. Ships and Offshore Structures. 3(3):159-171.

HullMon+ 2000. Marintek project, Tronheim, Norway.

[IMO] Guidelines for formal safety assessment (FSA) for use in the International Maritime Organization rule-making process, 5 April 2002.

[IOPCF] Report from The International Oil Pollution Compensation Funds (IOPC Funds) 2005.

Ravn ES, Hansen PF, Engberg P. 2008. User Manual for the GRISK program.

Sven Otto, Preben T. Pedersen, Manolis Samuelides, et al. 2002. Elements of risk analysis for collision and grounding of a RoRo passenger ferry. Marine Structures 15:461–474.

Wang G, Spencer J, Yongjun Chen. 2002. Assessment of a ship's performance in accidents. Marine Structures 15:313–333.

Elements of risk analysis for collision and grounding of oil tankers in the selected areas of the Gulf of Finland

Jakub Montewka[1], Przemysław Krata[2] and Pentti Kujala[3]

[1,3] *Aalto University, School of Science and Technology, Espoo, Finland, Department of Applied Mechanics, Marine Technology;*
[2] *Gdynia Maritime University, Poland, Faculty of Navigation, Department of Ship Operation*

Abstract:
The navigational risk assessment process plays a key role in a marine traffic management especially in congested and narrow waterways. The Gulf of Finland is considered one of the most dense place in the world in terms of marine traffic, which increased rapidly in the recent years, mostly due to growing oil export from Russia and import of other goods. Heavier traffic means that potential dangerous situations are not uncommon; therefore the appropriate risk analysis is of great importance. This paper presents two models of risk analysis for vessels grounding and colliding in the busy waterways with emphasis put on tankers. Two new adaptations of pre-existent physical models are presented, the MDTC model for probability of collision assessment and field theory based, gravity model for probability of grounding assessment. The consequences of an accident are expressed in the monetary terms. They concern the costs due to an oil spill, and are based on a recent research carried out in Japan, and officially submitted by this country to IMO Marine Environment Protection Committee. Neither loss of humans' life nor structural damages were considered in the risk model. The considered sea areas are: the waterways junction between Helsinki and Tallinn and the fairway leading to the biggest Finnish oil terminal in Sköldvik.

Introduction

The Baltic Sea is a unique and extremely sensitive ecosystem. Large number of islands, routes that are difficult to navigate, slow water exchange and lengthy annual periods of ice cover render this sea an especially vulnerable sea area. The Gulf of Finland is said to be one of the most dense operated sea areas in the world, with dense passenger and cargo traffic of which petroleum conveyances have a share of over 50 %. It is widely believed that the growth of maritime transportation will continue also in the future (Kuronen et al., 2008). The huge rise in traffic is far beyond what experts had forecast. At the beginning of the decade, it was estimated that by year 2010, an annual amount of oil transported through these sea lanes would be like 75 million tones.

Last year more than 150 million tones were shipped through the Gulf of Finland and the latest estimate for 2010 is 250 million tones (Nikula & Tynkkynen, 2007; Kuronen et al., 2008). As it may be noticed, the traffic in the Baltic area has not only increased, but the nature of the traffic has also changed rapidly, the increase of oil transportation strongly increases the risks for oil spills, and this is predicted to continue as well (Mäkinen, 2003; Rytkönen, 2005).
Last but not least, which can not be neglected while analyzing the risk of maritime traffic in the Gulf of Finland are the harsh winter conditions, which significantly influences the number and types of accidents (Kujala et al., 2009).

In this paper authors took up the challenge of marine traffic risk description in selected areas of the Gulf of Finland, with emphasis put on accidents which involve tankers. Therefore the following sea areas were considered: the junction between Helsinki and Tallinn, and a fairway to Sköldvik oil terminal. The risk calculated in this study is given in the yearly perspective for the whole analyzed areas and is expressed as a product of an accident probability and its consequences, where the latter are the product of an oil spill probability given the accident and costs of the oil spill. Innovative use of two models for accidents probabilities assessment may be recognized in this paper.

Traffic profiles in the analyzed area of the gulf of finland

The sea area under consideration in this study is the junction of two main waterways in the Gulf of Finland; one leads N-S and the other E-W. The N-S stream consists mainly of passenger vessels cruising between Helsinki and Tallinn, whereas the E-W stream consists of cargo vessels bound for and from harbours located in the Gulf of Finland. The vessel traffic profiles over the area under analysis are described using data derived from the AIS transmissions recorded in March and July 2006. To estimate the number of vessels that arrive in and depart from the Gulf of Finland, counting gate number 1 was established along meridian 023.5°E. To compute the traffic volumes of the streams in the junction, another two counting gates were established. Gate number 2 was established along parallel 60°N to count N-S traffic, and gate number 3 along the meridian 026°E to count E-W traffic (Figure 1). The marine traffic in this area was assumed to consist of four main flows: east, west, north, and south, while the north and south flows are assumed to contain passenger vessels only. Each flow was modelled with the following input parameters: overall number of vessels, type of vessels, number of vessels of a given type, size of vessel of a given type, speed of vessels of a given type, course of vessel, and position of vessel across the waterway. For modelling purposes most of these values were approximated by continuous distribution or by histograms. The distribution of the features being analysed was chosen according to the results of a chi-square test. Those which fitted best (obtained the highest value of chi-square test) were selected as inputs for the model. In some cases, if none of the available distributions fitted then recorded discrete values were taken into the model, by random sampling.

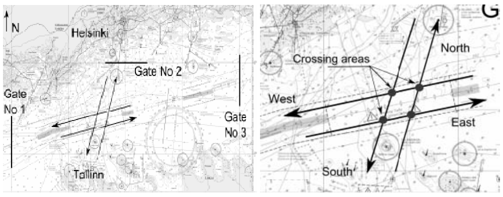

Figure 1: Waterways junction that was analysed with counting gates (to left) and main traffic flows (to right) marked.

The types of vessels and their percentage share of the traffic in the Gulf of Finland are presented graphically in Figure 2. The diagram constitutes the results of two months of AIS transmission recordings, carried out in March and July 2006 at counting gates numbers 1 (all vessels) and 2 (passenger vessels only). The traffic recorded in March was considered the winter profile of traffic, whereas the traffic registered in July was a summer profile of marine traffic in the Gulf of Finland.

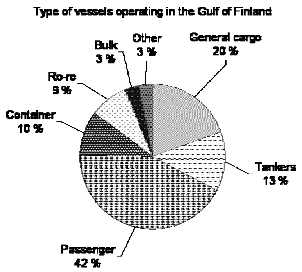

Figure 2: Types of vessels operating in the Gulf of Finland in the year 2006 (Montewka et al., 2009).

The total number of vessels registered at gates 1 and 2 is presented in Table 1. There are no significant differences in the number of vessels passing gate 1 during each season (winter, summer), except tankers, the traffic composition of which is presented in Figure 3. However, such differences exist for gate 2, where the number of vessels in summer is marked with an asterisk and for winter with double asterisks. The main reason for the difference is that during wintertime the operations of high-speed craft between Helsinki and Tallinn were suspended, and therefore the number of passenger vessels on the above route was reduced.

Table 1: Number of vessels passing gate 1 (E-W traffic) and gate 2 (N-S traffic), registered in March (**) and July (*) 2006 (Montewka et al., 2009).

Vessel type	Gate number 1		Gate number 2	
	East	West	North	South
Ro-Ro	397	400		
Tankers	618	607		
Container carrier	470	464		
Passenger ship	505	502	1140* 488**	1140* 488**
General cargo ships	895	929		
Bulk carriers	153	145		
TOTAL	3038	3047		

Although the number of vessels passing gate 1 was similar throughout the year, the spatial distribution of traffic varied this depended mostly on icing conditions in the area. The differences in the distributions were significant and could not be omitted in risk analysis (Montewka et al., 2009). The above relations hold true for the other gates as well. For the purposes of safety assessment and traffic modelling the traffic spatial distributions may be approximated either by statistical distribution, or by histograms, if the recorded traffic fits any common distribution poorly.

Tankers traffic profile

Tankers traffic in the Gulf of Finland was assumed to consist of two major types of vessels: crude oil tankers (25%) and oil product tankers (70%), the remaining 5% includes chemical and gas tankers which are not considered in the present analysis. The numbers of tankers recorded in the March and July 2006 differed, therefore the assumption was made, that tanker traffic was season dependent, but it hold true in terms of number of vessels not their dimensions. The dimensions of vessels were not affected by the season of the year. The distribution of tanker types and numbers according to season is presented in Figure 3.

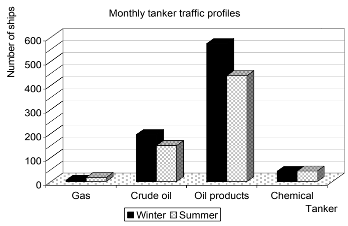

Figure 3: The seasonal tanker traffic profile in the Gulf of Finland.

It was assumed, for modelling purposes that the main dimensions of tankers (their length, breadth and maximum design draught) were estimated with use of triangle distributions, and the minimum, maximum and mean values adopted are presented in Figure 4. The triangle distributions were the ones that fitted best the observed discrete data.

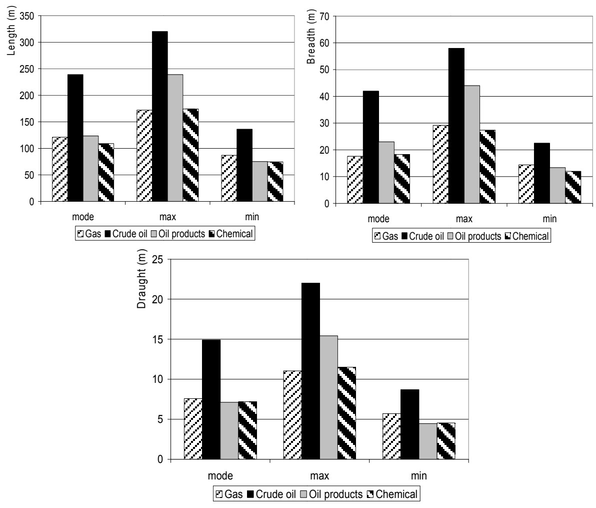

Figure 4: Distributions of length, breadth and draught of different types of tanker navigating in the Gulf of Finland.

Velocity of the tankers was modelled by a Logistic distribution, which fitted best the recorded values (Figure 5), and follows the formula:

$$v = f(x) = \frac{\operatorname{sech}^2\left(0.5\left(\frac{x-\alpha}{\beta}\right)\right)}{4\beta}, \tag{1}$$

where *sech* is a hyperbolic secant function, x is a random variable (velocity), α is a location parameter and equals 12.7, and β is a scale parameter which equals 1.2. The courses of the vessels were modelled by either distributions or a sampling method from the recorded AIS data.

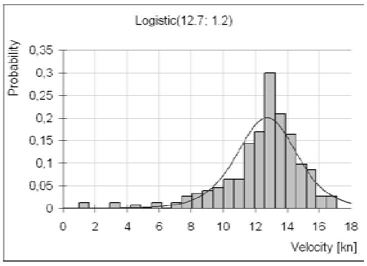

Figure 5: Histogram of tankers' velocities with Logistic distribution as the probability density function, which fitted best.

Probability of collision and grounding modelling

Probability of ship colliding and grounding was modelled by means of two original models, which have been developed by the authors. A model which assesses the probability of collision is called the MDTC model and was described in details in (Montewka et al., 2010). Therefore this chapter contains only limited description of the model, and only the main ideas are mentioned. The MDTC model defines the probability of a collision as follows:

$$P = N_A P_C, \tag{2}$$

where N_A is the geometrical probability of a collision course and P_C is the causation probability, also called the probability of failing to avoid a collision when on a collision course. A ship on a collision course is called a collision candidate, which may end up as a collision as a result of technical failure or human error. The causation probability quantifies the proportion of cases in which a collision candidate ends up as a collision. The value of the causation probability for this analysis is adopted from a state-of-the-art model based on a Bayesian Belief Network developed in earlier research (Det Norske Veritas, 2003; Hanninen & Kujala, 2009). The following values were adopted for collision cases: 1.3E-04 for vessels being on crossing courses and 4.9E-05 for head-on and overtake situations (Kujala et al., 2009). The MDTC model used in this study estimates the geometrical probability of vessels colliding, taking into consideration ships manoeuvrability, which is a novel approach in the field.

A grounding model is a gravity model, which considers ship and surrounding her obstacles the imaginary masses which affect each other, the detailed description was given in (Krata, 2007). The grounding probability is considered here a probability of a situation occurrence in which vessel breaches a "safety contour". A novelty of this method is a process of "safety contour" assessment. In previous models a depth curve as a boundary was commonly used (Montewka, 2008), the "safety contour" calculated by means of the gravity model, includes some elements of human factor like influence of sea bathymetry (density and distribution of obstacles).

Gravity model for probability of grounding modelling

A ship at a seaway and navigational obstructions may be perceived as a system. The formal description of a system notion as a set of elements and relations between them may have the form of an ordered pair (Jacyna, 2009):

$$\mathbf{S} = \langle \mathbf{A}, \mathbf{R} \rangle, \tag{3}$$

where S is a system, A is a set of system elements $A=\{a_s\colon s=1, 2, \dots, n\}$, and R is a set of relations $R=\{R_r\colon r=1, 2, \dots, m\}$, $R_r \subset A \times A$, where n denotes number of elements of the system, and m number of relations between system elements. Instead of the discrete formulation, locally defined continuous functions are applied in the proposed model. The spatial distributions of values of the functions create the continuous fields in the considered space. The field concept is understood as a feature of the considered space and the sufficient descriptor defining the field is the possibility to attribute specific characteristic to every selected point of the space, for instance the draught. The main features describing essential ships' characteristics are: maximum draught (T), turning circle radius (R), coefficient of the effective distance of obstruction detecting (d), coefficient describing a technical equipment of a ship (e), coefficient of ship's manoeuvrability (m). Thus, the field of characteristics of ships location is described by the formula:

$$S = S(T_{(j,i)}, R, d_{(R,e.m)}), \tag{4}$$

where S denotes a field of ships' characteristics, T, R, d are the fields which describe the ships, and (j, i) denotes coordinates of ships. It is assumed that obstructions' features describing fair enough the source of their threat in the investigated area are: water depth (H), coefficient of soundings accuracy (s), coefficient of ship's hull destruction when contacted with the seabed (b), coefficient of soundings position accuracy (c). The function describing the obstructions' features field is given by the formula:

$$P = P(H_{(j',i')}, b_{(j',i')}, s_{(j',i')}, c_{(j',i')}), \tag{5}$$

where P means a field of obstructions characteristics, H, b, s, c denote fields describing obstructions, and (j', i') the coordinates of obstructions. The functions (4) and (5) representing the fields of ships and navigational obstructions in a gravity type model of grounding threat. The key foundation of gravity models is that elements of considered system may be treated as imaginary masses distributed in the space and interacting with each other (Rosenberg, 2009). The core notion regarding obstructions and ships distribution is the concept of the distance between them (r). The spatial aspect of description of the distance influence on the relation ship-obstruction may be given by the distance decay curve (Rodrigue et al., 2009). The curve applied in the model presents a threat impact of any obstruction in inverse proportion to the distance. Considering the fields S and P of the system effecting ships tracks and taking into account the distance decay function r^{-1}, the vector function of a grounding threat $\overline{F}$ is constructed in a form given by the formula:

$$\overline{F} = \overline{F}\left[S(T_{(j,i)}, R, d_{(R,e,m)}), P(H_{(j',i')}, b_{(j',i')}, s_{(j',i')}, c_{(j',i')}), r_{(j,i)}\right] = M \cdot \frac{T}{H \cdot r} \cdot \overline{e_r}, \quad (6)$$

where M is a coefficient defined as follows:

$$M = \frac{R \cdot b}{d \cdot s \cdot c} \quad (7)$$

The interactions modelled by the grounding threat function are deterrents to ship from navigating in close proximity of shallow. It is one-way relation with no feedback. The postulate of including all important system features and optimization criteria in the ship-obstruction system analysis, which is equivalent to the requirement of multiobjective optimization, is fulfilled in the paper by the use of multiattributive method based on the American inspiration and applying a utility function (Jacyna, 2009). The method may be also called the method of synthesis to the single criterion omitting incomparability and it consists in the aggregation of all particular criteria (points of view) to one utility function, which is the base for optimization process later on (Jacyna, 2009). The utility function applied in the model is based on the grounding threat field described by the vector function (6). It is transformed into the grounding threat intensity field. The grounding threat intensity field is a kind of field description focused on navigational obstructions characteristics. The grounding threat intensity $\bar{E}$ is defined similarly to the classical intensity definition and may be presented in the following form (Orear, 1979):

$$\overline{E} = \lim_{T \to 0} \frac{\overline{F}}{T} \quad (8)$$

where $\overline{F}$ is a vector of a grounding threat, and T means a ship draught. The vectors of the grounding threat intensity may be superposed, so the grounding threat intensity at any arbitrarily chosen point of the researched space containing any number of sources of a threat can be obtained as a vector sum of grounding threat intensities coming from every single obstruction according to the formula:

$$\overline{E}(j,i) = \sum_{k=1}^{n_p} \overline{E_k}, \quad (9)$$

where $\bar{E}(j,i)$ denotes a grounding threat intensity field in the point (j, i), $\bar{E}_k$ grounding threat intensity vector generated by k-numbered obstruction, and n_p is a number of obstructions located in considered area. For the purpose of the model presentation the exemplary sea area is depicted in Figure 6. It comprises some shallows of different characteristics.

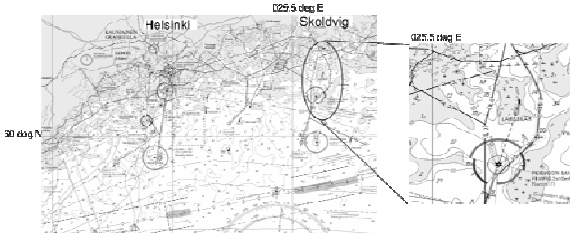

Figure 6: A fragment of a sea chart presenting the considered fairway to Sköldvik harbour.

For the modelling purposes the bottom profile of the area in question was needed. Therefore the sea chart has been digitalized and the bathymetry data were derived and converted into a grid, which is presented in Figur 7.

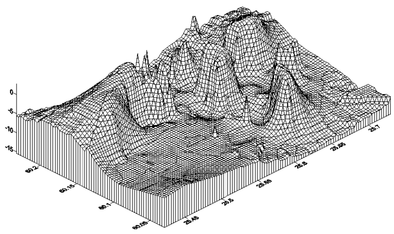

Figure 7: A profile of a bottom of the analyzed area.

The distribution of the grounding threat intensity vectors $\bar{E}$ on the modelled exemplary area is determined with regard to the formulas (8) and (9). The resultant spatial distribution of values of the grounding threat intensity vectors (applied utility function) is shown in Figure 8. A grey scale used in the Figure 8 expresses the magnitude of the utility function; the more intense colour the higher value of the utility function, and the higher grounding threat to ship. Therefore light grey areas represent the safety areas, whereas dense grey or black areas consider no-go areas. Some single white spots inside dark grey areas may be noticed, they were constructed artificially, by truncating utility vectors, which were extremely high at these points. Therefore these areas shall not be considered safety, despite their "safety" colour.

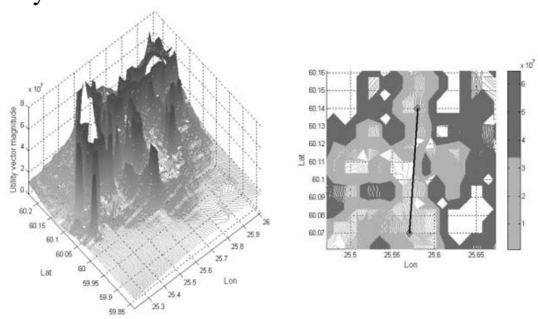

Figure 8: Spatial distribution of values of utility function vector filed.

A shape of a safety contour (light grey) depends on the assumption regarding the acceptable value of the grounding threat intensity vectors in the closest point of shallow approach. The critical value adjustment was performed on the basis of a minimum under keel clearance (UKC) requirement. The minimum allowed value of UKC was obtained according to the following formula (Jurdzinski, 1998):

$$UKC = \sum R_S + \sum R_D \,, \tag{2}$$

Where ΣR_S is a sum of static corrections and ΣR_D is a sum of dynamic corrections. The static corrections included an accuracy of bathymetric data (0.52m), an uncertainty of actual sea level (0.2m), and an error of draught estimation (0.1m) (Jurdzinski, 1998). The dynamic corrections comprised a squat (1.2m) and changes in ship's draught due to heave and pitch motions (0.4m) with presence of 1m height wave (Pettersson & Hammarklint, 2006). The maximum squat for analyzed area, and tankers considered was calculated with the following equation (Millward, 1990):

$$\delta_{MAX} = 0.01 v^2 C_B \text{ [m]}, \tag{3}$$

where C_B is a block coefficient, and v ship's linear speed [kt]. It was assumed, that tankers were laden to 9 meters draft, which was maximum allowed draft on this fairway, and they were proceeding with maximum allowed speed of 12 knots, and their block coefficient was equal to 0.8. The computed value of the required UKC was 2.4m, which roughly corresponded to the 2m value set by the port regulations (Finnish Maritime Administration, 2007).

Modelling of accidental oil outflow from tankers

The process of modelling an accidental oil spill from tankers presented in this paper consists of four steps as follows:

- on the basis of AIS the fleet of tankers operating in the Gulf of Finland was described,
- on the basis of tanker sizes the probability of oil outflow in case of accident was calculated,
- the probability of no spill in case of accident was estimated,
- the costs of spill were estimated.

The deadweight of a tanker as a function of her length is presented in Figure 9 these data were derived from the AIS records carried out in March and June 2006. Therefore it was assumed, that the size of the tankers was irrespective of a season of the year. A function that fitted best the discrete recorded data was a power function, which form is as follows:

$$DWT = f(Lpp) = 0.0015 Lpp^{3.3008}, \tag{4}$$

where DWT is a tanker's deadweight, Lpp is a tanker's length between perpendiculars.

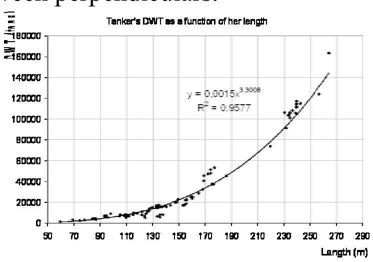

Figure 9: Baltic Sea tankers DWT as a function of the length, observed data with power function fitted.

Probability of oil outflow was calculated for double hull tankers only and it was assumed that the lognormal distribution provided an adequate representation of oil spill volume data (Maxim & Niebo, 2001). When performing the calculations mean outflow considering there is a spill was computed by means of modified IMO methodology (Smailys & Česnauskis, 2006; Seppälä, 2010) and standard deviation was calculated based on the assumption that one in 100 casualties where a cargo tank is damaged would lead to loss of entire cargo deadweight. The parameters of lognormal distribution for certain types of tankers are presented in Table 2 (Seppälä, 2010).

Table 2. The parameters of distribution oil outflow for certain types of tankers (Seppälä, 2010).

Tankers DWT (tons)	Mean value for side damage (tons)	Standard deviation	Mean value for bottom damage (tons)	Standard deviation
10000	811	2.94	539	3.52
35000	3423	2.70	2093	3.37
50000	5231	2.64	2971	3.38
75000	8643	2.53	4345	3.42
115000	15143	2.36	6309	3.52
150000	21881	2.29	7791	3.61

The regression formulae used for the calculation of the mean value of oil outflow volume in case of collision and grounding are presented in Figure 10. The discrete data for five typical sizes of tanker obtained by means of the IMO modified methodology in case of collision and grounding was plotted and the best fits were found. In both cases the polynomials of second order showed a good agreement with calculated data, and were used for further modelling.

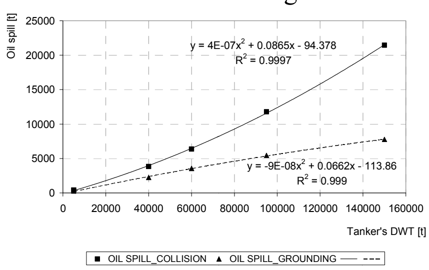

Figure 10: The values of mean oil outflow from tanker due to collision or grounding, considering there is a spill

On the basis of tabulated value of the standard deviations for certain types of tanker presented in Table 2, the general formula to calculate this value in case of collision was derived as follows:

$$\sigma_{COLL} = 6.99 DWT^{-0.092} \tag{5}$$

In case of grounding the following equations were applied:

$$\sigma_{GRND} = \begin{cases} 9 \cdot 10^{-12} DWT^2 + 5 \cdot 10^{-7} DWT + 3.34 & for DWT > 10000 \\ 3.52 & for DWT < 10000 \end{cases} \tag{14}$$

In the next step, on the basis of formerly defined parameters of the lognormal distributions as a functions of tanker's deadweight, the Monte Carlo simulations with 10000 iterations were run. As a result the discrete values were obtained which described the probability of an oil spill of certain size, taking into account the size and frequency of tankers of given size navigating in the Gulf of Finland. The continuous distributions that fitted best these discreet data were Pareto2 distributions, both for collision (summer and winter traffic) and grounding cases, but with different parameters. Henceforth the probability density function of oil spill volume (P_{OS}) in the Gulf of Finland is expressed as follows:

$$P_{OS} = f(x) = \frac{qb^q}{(x+b)^{q+1}}, \tag{6}$$

where q in case of collision is 1.9 for summer, 8.4 for winter and in case of grounding 1.5, b in case of collision is 9009.1 for summer, 49459.0 for winter, and 3847.6 in case of grounding, x is a volume of spill size in tons. The appropriate probability density functions are depicted in Figure 11and Figure 12.

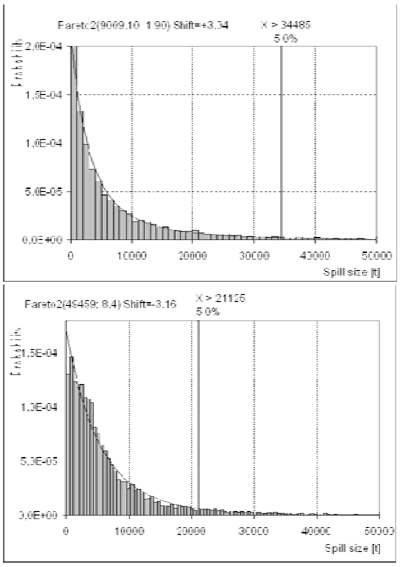

Figure 11: The probability of an oil spill from the tankers operating in the Gulf of Finland in case of collision, estimated by Pareto2 distributions for summer (to left) and winter traffic (to right).

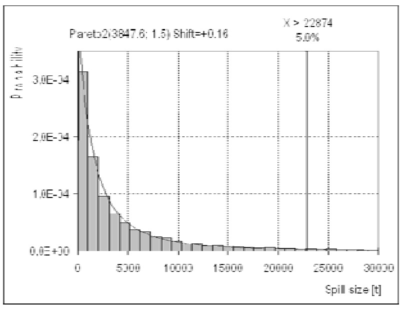

Figure 12: The probability of an oil spill from the tankers operating in the Gulf of Finland in case of grounding, estimated by Pareto2 distribution for summer traffic.

The probability of no spill (P_{ZERO_OS}) refers to the likelihood of no spill in all potential collision and grounding scenarios, and the following values were adopted (Marine Board & Transport Research Board, 2001):

- for collision: 0.86 irrespective of tanker's size,
- for grounding:
- for tankers of 40000 DWT: 0.94,
- for tankers of 150000 DWT: 0.73.

In the risk analysis process, it is more useful to use the conditional probability of spill given an accident ($P_{OS|A}$) instead of the probability of no spill (P_{ZERO_OS}), and it is expressed as follows:

$$P_{OS|A} = 1 - P_{ZERO\_OS}, \tag{7}$$

In the last decade many studies have been carried out to investigate the various factors that influence the cost of oil spill. Most of these studies point out that oil type, spill weight and the location of an oil spill are the most significant factors influencing the cost of an oil spill. An approach utilized in this paper is based on a recent research of oil spill costs computation carried out by Yamada and Kaneko, and officially submitted by Japan to IMO Marine Environment Protection Committee (IMO, 2008) as an alternative method for oil spill cost assessment. Based on historical data of major oil spill incidents from tankers reported by International Oil Pollution Compensation Funds the regression analysis between the cost of an oil spills and the volume of the oil spilled was carried out (Yamada, 2009). A nonlinear regression formula was estimated from the data, and the following equation for a mean level of oil spill cost estimation was arrived at, which shows relatively good agreement with analyzed historical data:

$$C = 35951W^{0.68} \tag{8}$$

where C denotes a total cost of an oil spill in USD, and W a weight of the oil spill in tons. This approach documents the non-linearity of oil spill costs, which seemed to be neglected in previous researches. It is also important to point out that costs that IOPCF reports to the public are not real oil spill costs. They refer to the amount of money that was paid for compensation to claimants (Kontovas & Psarafitis, 2008). Although the IOPCF compensation figures are real and cannot be disputed, a question is if these figures can be taken to reasonably approximate real spill costs.

Risk assessment

Risk may be expressed in several ways, by distribution, expected values, or single probabilities of specific consequences, but probably the most commonly used is the expected values (Vinnem, 2007). Approach presented in this paper uses the latter that describes the risk, which was considered a random variable. Expressing the random variable risk as a distribution is very useful, it takes into account uncertainties of input values, and seems mode accurate than single value. The risk that tankers colliding or grounding posed to the environment was calculated using the following formula:

$$R = P_A \cdot P_{OS|A} \cdot P_{OS} \cdot C \tag{9}$$

where P_A means a probability of accident (collision or grounding), and the others factor were defined in chapter 4. The generic diagram of the risk assessment process implemented in this study is shown in the Figure 13.

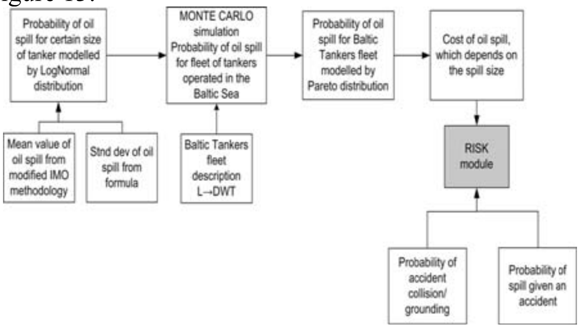

Figure 13: Block diagram of risk assessment process applied in presented study.

Risk due to collision

The expected numbers of collision candidates, collision probability, and a mean time between collisions are shown in Table 3. The estimated yearly mean volumes of oil accidentally spilled to the sea due to collision are shown in Table 4. Presented data concerns the annual volume of traffic in the junction between Helsinki and Tallinn only, and were computed separately for summer and winter traffic conditions. The oil spill volume concerns double hull tankers.

Table 3. Estimates of collision candidates number, collision probability and collision reoccurrence for tankers in the crossing between Helsinki and Tallinn.

Area	Number of candidates per year		Causation probability	Probability of collisions per year		Collision reoccurrence in years	
	Summer	Winter		Summer	Winter	Summer	Winter
Crossing S-E	111.0	92.3	$1.3 \cdot 10^{-4}$	0.014	0.012	76.6	90.3
Crossing S-W	79.0	65.8	$1.3 \cdot 10^{-4}$	0.010	0.010	112.2	131.8
Crossing N-E	88.5	79.2	$1.3 \cdot 10^{-4}$	0.012	0.010	101.0	110.0
Crossing N-W	111.3	106.2	$1.3 \cdot 10^{-4}$	0.014	0.014	82.3	87.5
Overtaking E	155.4	153.7	$4.9 \cdot 10^{-5}$	0.0077	0.0075	131.0	133.3
Overtaking W	197.5	199.5	$4.9 \cdot 10^{-5}$	0.010	0.010	105.0	103.5
Head-on for W-bound tankers	265.0	251.3	$4.9 \cdot 10^{-5}$	0.011	0.011	106.0	91.0
Head-on for E-bound tankers	195.5	219.8	$4.9 \cdot 10^{-5}$	0.011	0.011	95.0	92.0

Table 4. Estimate of annual accidental oil spill volume for double hull tankers in the crossing between Helsinki and Tallinn.

Meeting type	Accidental oil spill volume [t]	
	Summer traffic	Winter traffic
Crossing S-E	15.8	12.3
Crossing S-W	10.7	8.7
Crossing N-E	12.1	10.9
Crossing N-W	15.5	14.5
Overtaking E	7.0	6.7
Overtaking W	9.1	8.9
Head-on for W-bound tankers	4.4	4.5
Head-on for E-bound tankers	4.2	4.3
Total	78.8	70.8

The probability of spills of given magnitude were estimated from distribution described by equation (15), and the obtained results are presented in Table 5. To estimate the costs of oil spill of certain size the Monte Carlo simulations were adopted, and the continuous distributions that fitted best the obtained data and used for further modelling are tabulated below. The risk that was posed by tankers involved in collisions in the analyzed area, in the yearly perspective, calculated for summer traffic is presented in Figure 14 and for winter traffic in Figure 15. The risk is expressed in USD, and distributions that fitted best the calculated discrete data were as follows:

- the LogNormal distribution for summer traffic,
- the Gamma distribution for winter traffic.

The parameters of these distributions and the distributions are presented in the graphs below.

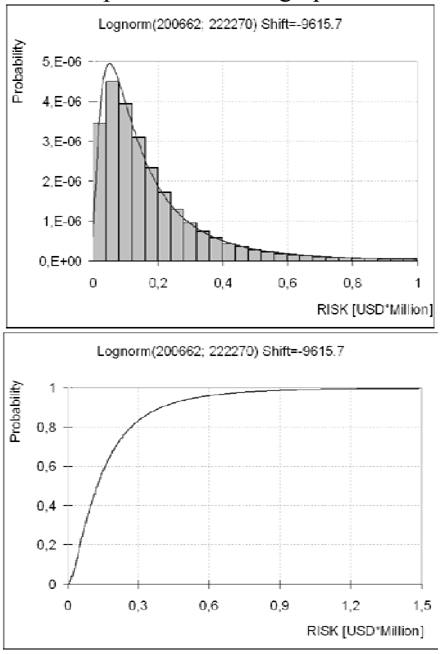

Figure 14: Probability and cumulative density functions of variable “risk” in case of collision in the Gulf of Finland, summer traffic.

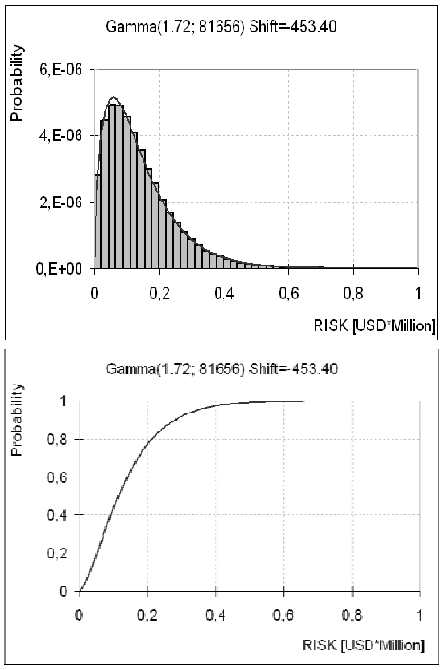

Figure 15: Probability and cumulative density functions of variable “risk” in case of collision in the Gulf of Finland, winter traffic.

Table 5. The parameters of distribution oil outflow in case of collision for certain types of tankers.

Oil spill size in tons	Probability of oil spill of given size P_{OS}	Cost of oil spill of given size modelled by following distribution:		Probability of collision P_A		Probability of spill given accident $P_{OS\|A}$
		Summer	Winter	Summer	Winter	
0-500	0.098	Beta Generalized	Beta Generalized	0.091	0.076	0.14
500-1000	0.084	Uniform	Uniform	0.091	0.076	0.14
1000-5000	0.388	Beta Generalized	Uniform	0.091	0.076	0.14
5000-10000	0.190	Beta Generalized	Beta Generalized	0.091	0.076	0.14
10000-30000	0.179	Triangle	Beta Generalized	0.091	0.076	0.14
30000-60000	0.061	LogNormal	Exponential	0.091	0.076	0.14

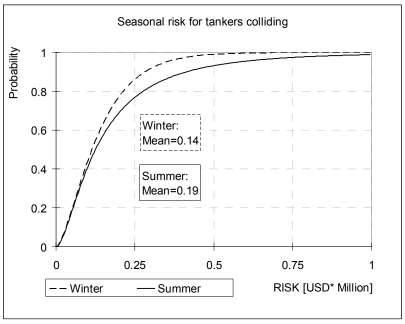

Figure 16: Cumulative density functions of risk due to tankers collisions in the Helsinki-Tallinn crossing for summer and winter traffic.

The risk of collision for tankers in case of summer traffic (R_S) was defined by Lognormal distribution, which satisfies the following equations:

$$R_S = f(x) = \frac{1}{x\sqrt{2\pi\sigma'}} e^{-0.5\left[\frac{\ln x - u'}{\sigma'}\right]^2}, \tag{10}$$

where x is a random variable "risk" in case of collision, μ' and σ' were defined as follows:

$$u' \equiv \ln\left[\frac{\mu^2}{\sqrt{\sigma^2+\mu^2}}\right], \text{ and } \sigma' \equiv \sqrt{\ln\left[1+\left(\frac{\sigma}{\mu}\right)^2\right]}, \tag{11}$$

where μ equals 200662, and σ equals 222270. Whereas the risk of collision in case of winter traffic (R_W) was described by Gamma distribution, which follows the equation:

$$R_W = f(x) = \frac{1}{\beta\Gamma(\alpha)}\left(\frac{x}{\beta}\right)^{\alpha-1} e^{-\frac{x}{\beta}}, \tag{12}$$

where β equals 81656, $\Gamma(\alpha)$ is the Gamma Function, and α equals 1.72.

Risk due to grounding

Probability of grounding (P_G) was obtained from the formula:

$$P_G = \int_{d\_\max}^{+\infty} f(y)dy, \tag{13}$$

where *d_max* is a distance from a waterway centre to the safety contour and *f(y)* is a probability density function of ship lateral distribution across a waterway. The waterway centre line and safety contours for the analyzed leg of approach channel to Sköldvik are presented in Figure 16. The safety contours depicted in Figure 17 are a simplification of original safety areas obtained by means of gravity model presented in Figure 8.

The lateral distribution of tankers across the leg of a waterway was described by the normal and uniform distributions mixture, but the distributions' parameters varied for southbound and northbound traffic, therefore these two mixture distributions were overlaid as depicted in Figure 17, and as such were used for modelling.

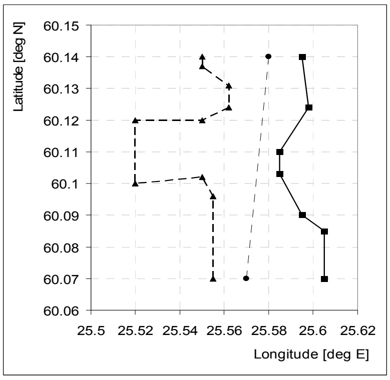

Figure 17: The safety contours of the analyzed fairway to Sköldvik (triangles and rectangles joint with lines) and the fairway centre line (thin dotted line joining two circles).

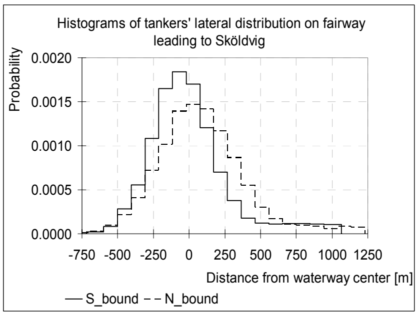

Figure 18: The overlaid two histograms of tankers' lateral distribution on the fairway to Sköldvig, a black dotted line represents north bound traffic whereas a solid black line is south bound traffic.

The zero value on the x axis in Figure 18 represents the centre of a fairway; negative values refer to port and positive to starboard side of a fairway. The following were assumed: ship location along the analyzed leg did not change, there were no other ships in the fairway, and only summer traffic for the year 2008 was considered. The probabilities of grounding were calculated for seven distinctive locations to starboard and ten locations to port, as marked in Figure 19. In the next step, a maximum value of grounding probability for a distinctive location was found, and multiplied by a product of the probability of an oil spill and the costs. Thus the maximum value of risk that a tanker posed to the given leg was yielded. The results are presented in Table 6.

At the end Monte Carlo simulations with 10000 iterations were adopted to get the distribution of random variable "risk", the input was the maximum risk value obtained formerly.

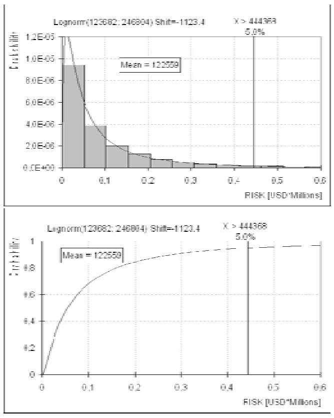

Figure 19: Probability and cumulative density functions of variable "risk" in case of grounding in the Sköldvik harbour approach, summer traffic.

Table 6. The discrete risk values due to tankers grounding in the Sköldvik harbour approach.

	Location	Grounding probability P_G	Probability of oil spill P_{OS}	Probability of spill given grounding $P_{OS\|G}$	Product $P_G\, P_{OS}\, P_{OS\|G}$	Risk [USD]
Port	1 – south	0,0E+00			0,0E+00	0
	2	0,0E+00			0,0E+00	0
	3	0,0E+00			0,0E+00	0
	4	0,0E+00			0,0E+00	0
	5	0,0E+00			0,0E+00	0
	6	0,0E+00			0,0E+00	0
	7	0,0E+00		1-0.94	0,0E+00	0
	8	0,0E+00	Pareto2 distribution	DWT=40000t	0,0E+00	0
	9	0,0E+00			0,0E+00	0
	10 - north	0,0E+00		1-0.73	0,0E+00	0
Starboard	1 – south	0,0E+00		DWT= 150000 t	0,0E+00	0
	2	0,0E+00			0,0E+00	0
	3	6,0E-04			6,0E-04	208
	4	5,9E-02			5,9E-02	20565
	5	7,0E-02			7,0E-02	24422
	6	4,4E-03			4,4E-03	1529
	7 - north	3,0E-02			3,0E-02	10248

The maximum risk that may be expected due to tankers grounding on one leg of the fairway leading to Sköldvik oil terminal was described by Lognormal distribution that follows the equation:

$$R_G = f(x) = \frac{1}{x\sqrt{2\pi\sigma'}} e^{-0.5\left[\frac{\ln x-\mu'}{\sigma'}\right]^2}, \tag{14}$$

where x is a random variable "risk" in case of grounding, μ' and σ' were defined in the previous chapter, μ equals 123682, and σ equals 246804.

Conclusions

The paper presents the risk models for marine traffic in general and for oil transportation in particular. The risk is expressed as a product of probability of accident (collision or grounding of tanker) and its consequences (costs of an oil spill given the accident).

The probabilities of accidents were assessed by means of two innovative models, the MDTC model in case of collision and the gravity model in case of grounding. The model that assesses the probability of an oil spill size is based on modified IMO methodology, which was adjusted to the tankers fleet that operates in the Baltic Sea. The costs of an oil spill are estimated with use of the state-of-the-art, statistic based model.

The risk was calculated for two chosen locations in the Gulf of Finland. One was a busy waterways junction in front of Helsinki harbour, where east-west waterways crossed north-south lines, which comprised mostly of passenger ferries. The other location was a part of a fairway to the oil terminal in Sköldvik. The risk was assessed for accidents that involved tankers, thus collisions in which at least one tanker was involved and tankers running aground.

The risk calculated in this study was given in the yearly perspective separately for two analyzed areas.
The obtained risk values for tankers involved in collision in the waterways junction were assessed for summer and winter traffic profiles individually, and the seasonal differences may be noticed. The risk was expressed in a form of probability density functions, obtained by means of Monte Carlo simulations, thus the uncertainties of the input values were taken into account.
The risk values obtained for tankers running aground in the approach fairway to Sköldvik concerned summer traffic. The analysis was carried out for one of two legs of the outer fairway, which was able to accommodate ships of maximum draft of 9 meters. The main factor that influenced the probability of grounding was “the safety contour” which was a value that determined the allowed navigable width of a waterway for a certain type of vessel and area, and was obtained by means of the gravity model of grounding. The gravity model in the form presented in this study is at its preliminary stage, and is still being developed. It is to some extent subjective in terms of the safety contour determination, therefore further improvement works are carried out, to make the model as much as possible objective.
The cost model applied did not take into consideration the season of a year, thus the traffic composition was the only factor that made a difference between winter and summer risk values. Due to a significant difference between summer and winter navigational conditions in the Gulf of Finland it shall be investigated if the oil spill costs are not season dependent, and if it is justified to consider them equal for summer and winter conditions.

Acknowledgments

DSc Erik Sonne Ravn from Danish Maritime Administration is thanked for his help to evaluate the ship traffic pattern in the approach to Sköldvik harbour.
The authors appreciate the financial contributions of the following entities: the EU, Baltic Sea Region (this research was partly founded by EfficienSea project), the city of Kotka and the Finnish Ministry of Employment and the Economy.

References:

Det Norske Veritas (2003) Formal Safety Assessment - Large Passanger Ships, ANNEX II: Risk Assesment - Large Passenger Ships - Navigation.

Finnish Maritime Administration (2007) Fairway Chart - Sköldvig Channel (15.3 M).

Hänninen M, Kujala P. (2009) The effect of causation probability on the ship collision statitics in the Gulf of Finland. In: Weintrit A, editor. Marine navigation and safety of sea transportation. London: Taylor & Francis, pp. 267-72.

IMO, Marine Environment ProtectionCommittee. (2008) Formal Safety Assessment, relevant information in relation to the Draft Environmental Risk Evaluation Criteria, submitted by Japan. London, MEPC 58/17/1.

Jacyna, M. (2009) Modelling and assessment of transportation system. Waraw, Publishing house of Technical University of Warsaw (in Polish).

Jurdzinski, M. (1998) Navigational planning in confined waters.Maritime University of Gdynia, Publishing House of Maritime University of Gdynia (in Polish).

Kontovas, C. & Psarafitis, H. (2008) Marine Environment Risk Assessment: A Survey on the Disutility Cost of Oil Spills. In: *2nd Int. Symposium on Ship Operations,Management and Economics*. Athens, Society of Naval Architects and Marine Engineers.

Krata, P. (2007) A model of selected effects during SAR operations. In: *Marine Traffic Engineering*. Świnoujście, Maritime University of Szczecin (in Polish).

Kujala, P., Hänninen, M., Arola, T. & Ylitalo, J. (2009) Analysis of the marine traffic safety in the Gulf of Finland. *Reliability Engineering & System Safety*, 94 (8), pp.1349-1357.

Kuronen, J., Tapaninen, U., Helminen, R. & Lehikoinen, A. (2008) *Maritime transportation in the Gulf of Finland in 2007 and in 2015*. Turku, Center for Maritime Studies, Turku.

Marine Board & Transport Research Board (2001) *Environmental Performance of Tanker Designs in Collision and Grounding: Method for Comparison -Special Report 259*. Washington D.C., National Academy Press.

Maxim, L. & Niebo, R. (2001) *Oil Spill analysis for North Slope Oil Production and Transportation Operations*. In: Environmental report for Trans Alaska Pipeline System Right-of-Way Renewal.

Millward, A. (1990) A preliminary design method for the prediction of squat in shallow water. *Marine Technology*, 27 (1), pp.10-19.

Montewka, J. (2008) Determination of a ship's manoeuvring area by field studies - verification of simulation and analytical methods. PhD Thesis. Maritime University of Szczecin.

Montewka, J., Kujala, P. & Ylitalo, J. (2009) The quantitative assessment of marine traffic safety in the Gulf of Finland, on the basis of AIS data. Scientific Journals, Maritime University of Szczecin, 18(90), pp. 105-115.

Montewka J., Hinz T., Kujala P., Matusiak J. (2010) Probability modelling of vessel collisions; Reliability Engineering and System Safety, doi: 10.1016/j.ress.2010.01.009

Mäkinen, A. (2003) WWF Suomi [Internet]. Available from: <http://www.wwf.fi/tiedotus/tiedotteet/tiedotteet_2003/ccb_itamerelle_saatava.html>.

Nikula, P. & Tynkkynen, V. (2007) *Risk in oil transportation in the Gulf of Finland. Not a question of if - but when.* Helsinki, University of Helsinki & Nordic Centre for Spatial Development.

Orear, J. (1979) *Physics*. MacMillan Publishing Company.

Pettersson, H. & Hammarklint, T. (2006) Wave climate in the Baltic Sea 2005. Available from: <http://www.helcom.fi/environment2/ifs/archive/ifs2006/en_GB/Waveclimate/>.

Rodrigue, J.P., Comtois, C. & Slack, B. (2009) *The geography of transport system*. 2nd ed. New York, Routledge.

Rosenberg, M. (2009) Gravity model [Internet]. Available from: <http://geography.about.com/library/weekly/aa031601a.htm>.

Rytkönen, J. (2005) Archive 2005 < Expert articles < Baltic Rim Economies < Economic monitoring < Pan-European Institute < Special Units < Units < Turku School of Economics [Internet].

Seppälä, T. (2010) *Assessment of accidental oil outflow from tankers due to collision and grounding.* In: Study of algorithm development using data mining. Research report, Aalto University, Espoo (not published).

Smailys, V. & Česnauskis, M. (2006) Estimation of expected cargo oil outflow from tanker involved in casualty. *Transport Vilnius*, 21 (4), pp.293-300.

Vinnem, J. (2007) *Offshore Risk Assessment*. 2nd ed. Springer London.

Yamada, Y. (2009) The Cost of Oil Spills from Tankers in Relation to Weight of Spilled Oil. *Marine Technology*, 46, pp.219-228.

A homogenized cohesive element ice model for simulation of ice action a first approach

Jimmy Forsberg[1], Daniel Hilding[1] and Arne Gürtner[2]

Engineering Research Nordic AB[1], Sweden; Statoil ASA, Research Centre Trondheim, Norway[2]

Abstract:
Cohesive element based ice material models have applications in realistic simulations of ice crushing against offshore installations. In this article we propose an improvement of the cohesive element based ice model. The proposed improvement consists of the introduction of a homogenization approach for the ice fracture modeling of sub-element size cracks.
Finally a test of the improved method is made by comparing simulated and measured force levels from an ice sheet crushing event against the Norströmsgrund lighthouse. The work presented in here was conducted for Statoil Research Centre.

Introduction

A general ice model that could be used in transient large deformation finite element simulations to calculate the forces from ice sheets and icebergs on structures and ships would be a most useful engineering tool. In this article we describe an improved cohesive element based ice model. The model aims at modeling ice undergoing severe crushing such as when drifting ice sheets are crushed to rubble against offshore installations. The forces on the structure and ice deformations in this type of event are considerable. The improvement consists of the introduction of a first approach to treat the ice fracturing and deformation as a homogenization problem. The improved ice model is a result of a recent research project for Statoil Research Centre on simulation of the action from drifting ice sheets on offshore structures.The work presented here builds upon the work by Konuk, Gürtner & Yu (2009a, 2009b), Konuk (2009), and Gürtner et al. (2009). No review is given here on the use of the cohesive element method for ice modeling; instead we refer the reader to the review in Gürtner et al. (2009).

Outline

First an overview of the basic ideas of the cohesive element method for ice modeling is given in Section 2. Section 3 describes the new homogenization approach. In Section 4 a short description of the used simulation tools is given. To test the new method, simulation results of an actual ice crushing event together with a comparison to measured ice forces is given in Section 5. The final section contains the conclusions.

The basic cohesive element ice model

A more in depth description of the Cohesive Element Method (CEM) for ice modeling can be found in Konuk, Gürtner & Yu (2009a). The CEM is not a new method, it is well known within the field of fracture mechanics for modeling crack propagation in solids, such as metals and concrete. There are many publications on the use of the CEM for finite element crack propagation simulations. However, its extended application to modeling ice fracture during complex ice-structure interaction is new and was pioneered by Gürtner (2009). Usage of a cohesive zone model for the pure study of ice fracture was first described by Mulmule & Dempsey (1998). The basic ideas are as follows for using CEM for ice modeling. It is assumed that ice is essentially an elastic continuum. A perfectly elastic ice however cannot realistically model large deformations. It follows that in order to be able to model large irreversible processes such as ice crushing something must be added. In the CEM, in its most basic form, the addition is that one assumes that all non-reversible or non-elastic behavior is caused by cracks forming in the ice1 (For CEM the ice is actually always modeled as an elasto plastic material with hardening. Here, for the sake of not complicating the matter, we assume the ice is elastic as the exclusion of plasticity does not matter for the presentation of the homogenization approach which is the main topic of the paper.) As cracks are formed the ice can slide along the crack-planes, developing a frictional ice mass.

In the CEM as described here, a fixed pattern of potential cracks is assumed. The implementation is typically as follows: The ice block is discretizised using standard solid finite elements, e.g. hexahedral elements. Each individual element is attached to its neighbors using so called cohesive elements. A cohesive element is a zero thickness element that when subject to tension or shear responds by deforming according to a given traction-separation curve. When the force or deformation reaches a limit value the cohesive element is removed and thus a crack is formed and energy is dissipated or released. A crack can grow by the deformation and failure of neighboring cohesive elements. Note that contact conditions are added to the crack faces so that friction can occur if sliding occurs in a closed crack. Figure 1 shows an illustration of a block of ice built up by elastic hexahedral elements connected with cohesive elements. One can say that the cohesive elements act as the glue that holds the ice block elements together.

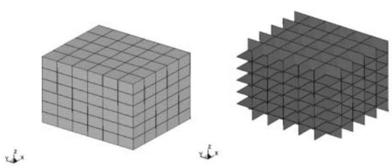

Figure 1. A block of ice built up by elastic hexahedral elements is shown to the left. To the right the cohesive elements that hold together the hexahedral elements in the block are shown.

By setting a proper traction-separation curve one can have the cohesive elements release a physically correct amount of energy as the crack is formed either due to a mode I or mode II deformation(Definition for deformation modes of crack in a plate: Mode I is an in-plane opening of the crack, mode II in-plane shear deformation, and mode III out of plane shear deformation.)
Typically the energy release for ice cracks is on the order of 10 – 50 J/m^2.

CEM with homogenization
Derivation

Here we will derive the CEM with homogenization, CEMH. Assume a situation where a block of ice is crushed to rubble, i.e. very small pieces with a diameter D. An example would be the crushing of the point of a not too pointy ice-cone against a hard surface. Assume CEM is used to model the ice block in a simulation of the event with a side length H of the finite elements. Here we are interested in the situation where H>>D. Under the latter assumptions the basic CEM as described in Section 2 might not be able to model the event properly because the smallest particle size possible is given by the element size H, which is much larger than D.

To remedy the latter situation one can either refine the mesh so that H<D, or try to model the macroscopic effect of the sub elements size cracks by modifying the material properties of the ice on the macroscopic level. Here the latter approach is used. An approach were the effect of sub-element size or microscopic phenomena are modeled through material models on the macroscopic level involving observable macroscopic state variables, i.e. stress and strain, is referred to as homogenization.

The simplistic approach proposed here can be seen as a first test of the usefulness of such an approach for ice modeling.

The first step is to make the following ad hoc assumptions about a representative volume or ice finite element that is to be crushed and thus contain internal cracks:

1. Until the first crack arises the element is elastic.
2. The volume of the element is preserved during the deformation. Note: This is reasonable if the ice is subject to constraints from surrounding elements.
3. The cracks occur on planes with maximum shear stress. Note: This corresponds to mode II and III cracks.
4. The process is irreversible, i.e. cracks cannot disappear or mend.
5. The macroscopic effect of more cracks in the element is that it softens.
6. When the element is totally crushed to rubble it behaves as a viscous incompressible fluid.

It is reasonable to assume that the amount of cracks is proportional to the amount of deformation of the element. Under assumption 2 this implies that the effective shear strain can be a reasonable deformation measure, as a shear deformation is volume preserving. Thus, here we will simply use the effective shear strain as the measure of the amount of cracks or damage to the ice element.

A well known material model that fits assumptions 1 to 6 and the choice to measure deformation using the effective shear strain is isotropic elasto plastic theory with a Tresca yield condition. To implement assumptions 5 and 6 a hardening curve like in Figure 2 should be used.

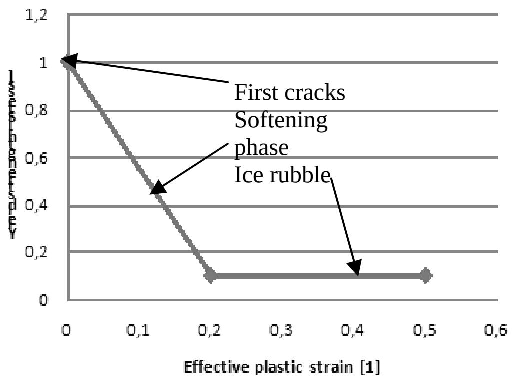

Figure 2. Schematic hardening curve for ice elements with a homogenized crack model.

Summary of CEMH

In summary we have shown that, under suitable assumptions, it is plausible that one can actually model the macroscopic effect of the sub-element size cracks in the CEM mesh using a homogenization approach. What is more, it turns out that a standard elasto plastic material model with a non-standard hardening curve, see Figure 2, could be sufficient as a first attempt. We will refer to the CEM with the described homogenization as CEMH.

The potential advantages of CEMH compared to CEM follows from that it is aimed at accounting for the macroscopic effect from sub element size cracks. This implies the potential that larger elements could be used with CEMH compared to CEM, given the same requirements on accuracy, leading to reduced simulation run times. Note: The Tresca yield condition can be difficult to handle numerically, thus in the simulations we approximate the Tresca yield condition with von Mises.

Software tools

All simulations were performed using the MPI parallel version of LS - DYNA 971, Hallquist (2007). The simulations were run on a cluster (Intel Xeon CPUs) with a fast interconnect (Infiniband). To include the effect from the buoyancy, i.e. that the ice floats on the water, and drag on the ice a special drag and buoyancy subroutine was implemented in LS-DYNA as an UDF (User Defined Module). The drag model is a simple drag model for fully developed turbulent flow according to Reynolds, see e.g. Batchelor (2000).

Test case Norströmsgrund ice force measurements

A test is needed to determine if the CEMH has the potential to mimic a physical event where the ice is crushed to fairly small particles. Here we use the same test case as is used for a previous CEM simulation by Gürtner et al. (2009). In two EU projects, LOLEIF, see Jochmann & Schwarz (2000), and STRICE, several load measurements were made on the Norströmsgrunds lighthouse. From the test data an event was chosen were a state of continuous crushing of the ice sheet occurred as the sheet drifted towards the lighthouse. In such an event, the ice is crushed or milled to small particles, giving rise to high non-synchronized and stationary ice forces around the contact surface and involving low stationary structural response of the lighthouse. An image of the simulation set up showing the Lighthouse and the ice sheet is shown in Figure 4.

Simulation set up

An outline of the simulation set up is a follows. Material parameters according to Tables 1 and 2 were used. The increase of the yield curve, see Figure 3, for strains above 0.5 is only to avoid excessively distorted elements and would ideally not be needed. In the simulation the ice floats on the water using a buoyancy model, see Section 4.

The ice and lighthouse have a relative velocity of 0.15 m/s. The ice has a thickness of 0.69 m. The lighthouse is rigid. The finite element size for the ice is about 0.13x0.2x0.2 m. An illustration of the simulation model is given in Figure 4. To simulate the fact that the ice sheet is in fact much larger than in the simulation, fixed boundary conditions were added along the edges of the ice sheet except on the side with the lighthouse.

Table 1. Material parameters used for water and ice elements

Ice density	910 kg/m^3
Ice elastic modulus	5 GPa
Ice Poisson's ratio	0.3
Ice element yield curve	See Figure 3.
Water density	1000 kg/m^3
Coefficient of friction ice to ice	10 % static, 5 % dynamic
Coefficient of friction ice to steel	20 % static, 10 % dynamic

Table 2. Material parameters used for the cohesive elements

Parameter	Vertical cohesive elements	Horizontal cohesive elements
Shear strength	1 MPa	1.1 MPa
Tensile strength	1 MPa	1.1 MPa
G_{IC}	5200 J/m^2	5200 J/m^2
G_{IIC}	5200 J/m^2	5200 J/m^2

Note: Artificially high values are used for G_{IC} and G_{IIC}. The motivation for this is not presented here, but will be presented in a coming paper by Gürtner et al. (2010).

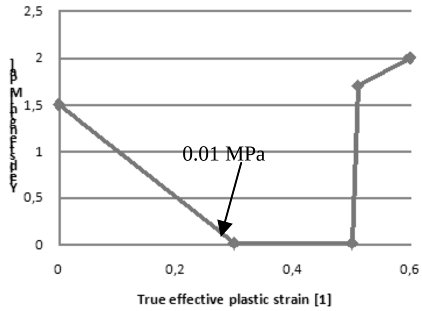

Figure 3. Yield curve for the ice elements.

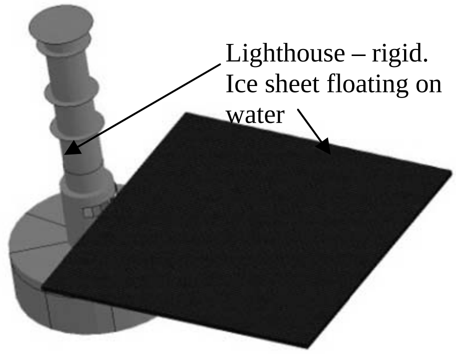

Figure 4. Simulation model for the continuous ice crushing simulation.

Comparing simulations with measurements

Images from the simulations are given in figures 5 and 6. Figure 7 shows the calculated ice force from the simulation of the continuous crushing event. An achievement is the fact the CEMH simulation reaches a stationary process state with a nearly constant mean force value like in reality. The stationary mean force level from the test is around 3.5 MN, which is higher than the about 2.5 MN obtained in the simulation. The mode of deformation of the ice and the piling up of ice rubble around the tower is similar to what can be observed on the video images from the measurements at the lighthouse.

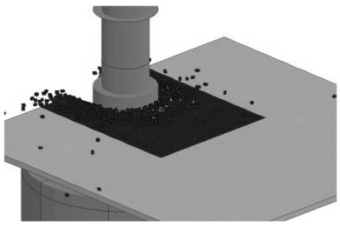

Figure 5. Deformations from the ice crushing simulation – top view. Ice rubble piles up around the lighthouse.

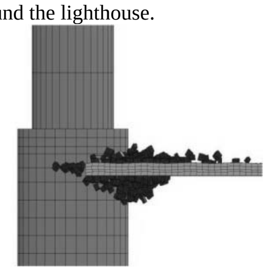

Figure 6. Deformations from the ice crushing simulation – cross section. Ice rubble floating below the surface and piling up around the lighthouse.

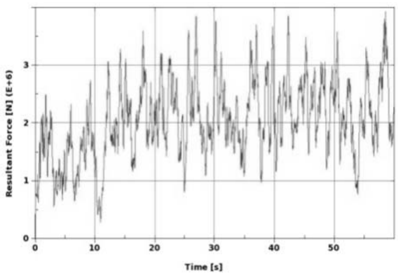

Figure 7. Simulated force on the lighthouse. Mean force is about 2.5 MN.

Conclusions

An improved ice model including a homogenization approach, CEMH, is proposed. The new model is able to mimic the behavior of ice in a process where the ice is subject to severe crushing (almost milling). It is evident that the present homogenization represents a first approach to the very complex problem and should be supplemented with a deeper theoretical analysis. Still we believe that using a homogenization approach is a promising addition to ice material modeling in combination with the CEM for ice-structure interaction simulations.

Acknowledgment

The work presented in this report was conducted for Statoil Research Centre. The authors thank Statoil for allowance to present data and simulation results from the project.

References:

Batchelor G (2000). An introduction to fluid dynamics. Cambridge University Press, Cambridge.

Gürtner A (2009). Experimental and Numerical Investigations of Ice-Structure Interaction. Doctoral thesis, Norwegian University of Science and Technology, No. 2009:26.

Gürtner A, Bjerkås M, Kühnlein W, Jochmann P, Konuk I (2009). Numerical simulation of ice action to a lighthouse. Proceedings of the ASME 2009 28th International Conference on Ocean, Offshore and Arctic Engineering.

Gürtner A, Forsberg J, Bjerkås M, Hilding D (2010). Numerical modeling of full scale ice events. Submitted for publication in the proceedings of the 20th IAHR International Symposium on ice 2010, Finland.

Hallquist J (2007). LS-DYNA Keyword User's Manual, version 971. Livermore Software Technology Corporation, Livermore.

Jochmann P & Schwarz J (2000). Ice Force Measurement at Lighthouse Norströmsgrund – Winter 1999. Validation of Low Level Ice Forces on Coastal Structures: LOLEIF, Report No.:5, Hamburg.

Konuk I, Gürtner A, Yu S (2009a). A cohesive element framework for dynamic ice-structure interaction problems – Part I: Review and Formulation. Proceedings of the ASME 2009 28th International Conference on Ocean, Offshore and Arctic Engineering.

Konuk I, Gürtner A, Yu S (2009b). A cohesive element framework for dynamic ice-structure interaction problems – Part II: Implementation. Proceedings of the ASME 2009 28th International Conference on Ocean, Offshore and Arctic Engineering.

Konuk I (2009). Study of dynamic ice and cylindrical structure interaction by the cohesive element method. The 20th Intl. Conference on Port and Ocean Engineering under Arctic Conditions, June 9-12, 2009 – Luleå, Sweden.

Mulmule S V & Dempsey J P (1998). A Viscoelastic Fictitious Crack Model for the Fracture of Sea Ice. Mechanics of Time-Dependent Materials 1:331-356. Klüwer Academic Publishers,Netherlands

Integrated Analysis of ship/iceberg collision

Zhenhui Liu, Jorgen Amdahl and Sveinung Løset

Norwegian University of Science and Technology, Trondheim, Norway

Abstract:
The Arctic area has probably a huge amount of oil and gas stored, and is attracting more and more attention. Ice loads and ice robust design will become an important task in Arctic engineering projects. As the ice is melting merchant ship traffic north of Siberia is expected to increase radically and accidental collisions with icebergs are to be expected. In this context icebergs refer to so-called bergy bits or growlers with small area above sea surface, and hence, hard to detect by radars.
This study is divided into external mechanics and internal mechanics. Both issues are discussed. First, the external mechanics, which is based on the work done by Pedersen and Zhang (1997) and Stronge (2000), is considered. An improved model is derived, which deals with the 12 DOF problems for ship and iceberg. Second, the internal mechanics which involves deformation and energy dissipation in the ship structure and iceberg is studied. In order to simulate the correct behavior of the ice feature in a collision scenario, a new ice material model is proposed. It is shown to give adequate pressure-area relationships when simulating ice impact on a rigid body. Finally, integrated analysis of the iceberg and ship is described. The analysis is carried out within the accidental limit state (ALS) framework; i.e. the side shell and frames may be severely damaged, but penetration of cargo tanks with subsequent oil spill and/or global hull girder failure should not be accepted. Different scenarios are considered including various characteristic iceberg shapes. The ice resistant properties of various side shells designs are investigated.

Introduction

Due to the large amount of oil and gas reserves in the Arctic area, offshore activities are going to increase. It is quite necessary for engineers to undertake a first investigation about the ice impact loads prior to the practical engineering projects. The present paper gives a comprehensive description of a project on ship/iceberg collision carried out at NTNU.

The draft of ISO/CD 19906, e.g. ISO (2008), categories ice actions as being an Extreme Level Ice Event (ELIE) or an Abnormal Level Ice Event (ALIE). The ALIE corresponds to the Accidental Limit State (ALS) in modern codes for the offshore structures. In the ALIE check, the ship should survive with no spill of cargo to the environment and associated pollution etc. The present study deals with ship/iceberg collision within the ALIE (or ALS) domain. As to the structural response, significant plastic deformation is acceptable. Fracture of steel plating should be taken into consideration This has been studied by a number of authors, e.g Peschmann (2001), Tornqvist (2003) and Ehlers and Varsta (2009). This study is based upon work carried out by Alsos H. S. (2008a, 2008b). The in-house experience and fracture material model could be seamless applied to present integrated analysis. The challenging parts of this project are the external mechanics of the ship/iceberg collision and the development of an adequate ice material model in order to facilitate integrated analysis.

Like ship/ship collision, it always convenient to split the collision mechanics into external mechanics and internal mechanics, see Terndrup Pedersen and Zhang (1998). External mechanics deals with momentum and energy balance while the internal mechanics deals with large deformation of structures in local areas. Both mechanics are connected through the dissipated energy, see Zhenhui L. (2009a). The external mechanics of ship/iceberg collision is more complicated than that of ship/ship collision, as it is a fully 3D problem (totally 12 DOF) based on observation, see Johnston, Timco et al. (2008). It is believed that in the ALIE state, a Pressure-Area relationship description of ice actions is not sufficient, see Zhenhui L. (2009c). In order to assess accurately the iceberg impact loads in the ALIE domain, both the offshore structure and the iceberg should be modeled “correctly”, and integrated analysis is called for. The integrated analysis here is corresponding to the Shared-energy design method according to the NORSOK code N-004 App. A, if we treat the iceberg as the striking object and the ship as the struck one, see Figure 1.

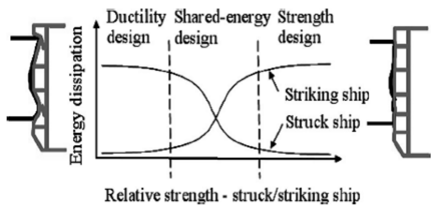

Figure 1 Strength, Ductility and shared-energy design, NORSOK N-004, App. A.

Most attempts to analyze iceberg impacts are within the domain of Ductility design, in which the iceberg is simplified as a rigid body and all energy dissipation stems from deformation of the ship structure, e.g. Han S. (2008), Bo Wang (2008). However, ductility design is conservative and often far way from the real case. In present study, the ship and iceberg are both ductile and may undergo large deformations.
In the following sections details of the solutions to the external and internal mechanics respectively will be described.

External Mechanics

The external mechanics of ship/iceberg collision is a further development of the work done by Terndrup

Pedersen and Zhang (1998) and Stronge (2004). Zhenhui L. (2009a) proposed a new formulation of the impact mechanics to ship/ship and ship/iceberg collision. In this method, a closed form solution is obtained. In this paper, the main are presented.

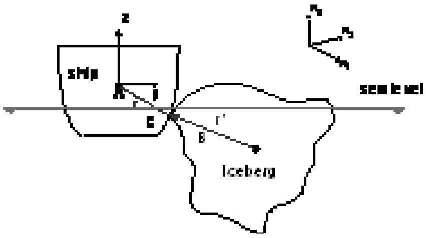

Figure 2 Illustration of ship/iceberg collision

It has to be pointed out that, all the equations are derived in the so called local frame, which is located at the impact point, the $n_1 n_2 n_3$ in Figure 2. Based on the equation of motion, (for details, please refer to the original paper), we finally have following expression:

$$dv_i = m_{ij}^{-1} dp_j \qquad (0.3)$$

where dv_i is the incremental velocity on each direction of the local frame, m_{ij}^{-1} is the inverse of equivalent mass and dp_j is the incremental impulse on each direction of the local frame.
Based on the above equation, the dissipated energy on each direction can be explicitly obtained as follows:

$$E_i = \int_0^t f_i ds_i = \frac{1}{m_{ij}^{-1} \frac{f_j}{f_i}} \frac{dv_i}{2}(dv_i + 2v_i^0) \qquad (0.4)$$

In order to solve Eq.(0.4), the Amontons-Coulomb theory for friction, see e.g. Johnson (1985), is considered. The theory is based on the assumption that the friction force is proportional to the normal component of reaction. Two friction factors, are introduced, namely the normal friction factor and tangential friction factor, μ_n, μ_t, respectively.

$$\sqrt{f_1^2+f_2^2} < \mu_n f_3 \qquad if \qquad (v_1^t)^2+(v_2^t)^2 = 0 \qquad \sqrt{f_1^2+f_2^2} = \mu_n f_3 \qquad if \qquad (v_1^t)^2+(v_2^t)^2 > 0$$

$$f_2 = \mu_t f_1 \qquad (0.5)$$

$$f_1 = \frac{\mu_n}{\sqrt{1+\mu_t^2}} f_3 \qquad (0.6)$$

$$f_2 = \frac{\mu_t \mu_n}{\sqrt{1+\mu_t^2}} f_3 \qquad (0.7)$$

where v_1^t, v_2^t are the velocity components on n_1, n_2 direction respectively at the time t, when the collision finishes. The normal friction factor μ_n is calculated by the impulse ratio in order to determine whether the sticking or sliding case applies, see Eq.(0.8).

$$\mu_n = sign(dp_1)\frac{dp_3}{\sqrt{dp_1^2 + dp_2^2}} \qquad (0.8)$$

μ_0 is the actual friction factor between two collision objects, ship to ship or ship to iceberg.

The relative velocities between two collision objects are needed. Assuming:

$$v_3^t = -ev_3^0 \qquad (0.9)$$

then

$$dv_3 = v_3^t - v_3^0 = -(1+e)v_3^0 \qquad (0.10)$$

where $e(0 \le e \le 1)$ is the coefficient of restitution. For an entirely plastic collision, $e = 0$, and for a perfectly elastic collision, $e = 1$.
For the case where two collision objects stick together after collision, we have:

$$dv_1 = v_1^t - v_1^0 = -v_1^0 \qquad (0.11)$$

$$dv_2 = v_2^t - v_2^0 = -v_2^0 \qquad (0.12)$$

For the case where the sliding happens, the relative velocities will be discussed later.

a. Sticking case $|\mu_n| \le |\mu_0|$
b. In this case,:

$$dv_i = -v_i^0,\ i = 1,2 \qquad (0.13)$$

and Eq. (0.3)can be solved to obtain dp_i and μ_n, then:

$$\mu_t = \frac{dp_2}{dp_1} \qquad (0.14)$$

Substituting (0.13) and (0.14) and using the relationship in Eqs. (0.5),(0.6),(0.7)- into Eq.(0.4), the dissipated energy in each direction is obtained:

$$E_1 = \int_0^t f_1 ds_1 = \frac{-1}{m_{11}^{-1} + m_{12}^{-1}\mu_t + m_{13}^{-1}\frac{\sqrt{1+\mu_t^2}}{\mu_n}} \frac{(v_1^0)^2}{2} \qquad (0.15)$$

$$E_2 = \int_0^t f_2 ds_2 = \frac{-1}{m_{21}^{-1}\frac{1}{\mu_t} + m_{22}^{-1} + m_{23}^{-1}\frac{\sqrt{1+\mu_t^2}}{\mu_n \mu_t}} \frac{(v_2^0)^2}{2} \qquad (0.16)$$

$$E_3 = \int_0^t f_3 ds_3 = \frac{-(1-e^2)}{m_{31}^{-1}\frac{\mu_n}{\sqrt{1+\mu_t^2}} + m_{32}^{-1}\frac{\mu_t \mu_n}{\sqrt{1+\mu_t^2}} + m_{33}^{-1}} \frac{(v_3^0)^2}{2} \qquad (0.17)$$

c. Sliding case, $|\mu_n| > |\mu_0|$

In this case
$$dv_3 = -v_3^0 \qquad (0.18)$$

$$\mu_n = \mu_0 \qquad (0.19)$$

where μ_0 is the actual friction factor. μ_t can be estimated by using Eq. (0.14) assuming tentatively that the sticking case applies. On this basis equation (0.3) can be solved to obtain dp_3, dv_1, dv_2.

Substituting (0.18) and (0.19) and using the relationship in Eqs. (0.5),(0.6),(0.7) into Eq.(0.4), the following relationships apply:

$$E_1=\int_0^t f_1 ds_1=\frac{1}{m_{11}^{-1}+m_{12}^{-1}\mu_t+m_{13}^{-1}\dfrac{\sqrt{1+\mu_t^2}}{\mu_0}}\frac{dv_1}{2}(dv_1+2v_1^0) \tag{0.20}$$

$$E_2=\int_0^t f_2 ds_2=\frac{1}{m_{21}^{-1}\dfrac{1}{\mu_t}+m_{22}^{-1}+m_{23}^{-1}\dfrac{\sqrt{1+\mu_t^2}}{\mu_0\mu_t}}\frac{dv_2}{2}(dv_2+2v_2^0) \tag{0.21}$$

$$E_3=\int_0^t f_3 ds_3=\frac{-(1-e^2)}{m_{31}^{-1}\dfrac{\mu_0}{\sqrt{1+\mu_t^2}}+m_{32}^{-1}\dfrac{\mu_t\mu_0}{\sqrt{1+\mu_t^2}}+m_{33}^{-1}}\frac{(v_3^0)^2}{2} \tag{0.22}$$

Thus the total dissipate energy is calculated as

$$E=E_1+E_2+E_3$$

Using the procedure described above, Zhenhui L. (2009a) calculated the dissipated energy during the foreship and iceberg collision. It was found that the energy dissipation is sensitive to the shape of the hull of the ship at the collision location as well as the iceberg properties. Using "worst case" parameters, the following formula was recommended for design purposes;

$$r_E=0.3-0.027r_M+9.0r_M^2,\quad r_M\le 0.125$$

where r_E is the energy ratio, $r_E=E/E_0\le 1$, r_M is the mass ratio, $r_M=M_{iceberg}/M_{ship}$. Generally, 30% of maximum collision energy E_0, where E_0 corresponding to the dissipated energy due to central and plastic collision.

$$E_0=\frac{1}{2}M_{iceberg}v_{ship}^2\frac{1-\left(\dfrac{v_{ice}}{v_{ship}}\right)^2}{1+\dfrac{M_{iceberg}}{M_{ship}}}$$

v_{ship} is the velocity of ship, v_{ice} is the velocity of iceberg, $M_{iceberg}, M_{ship}$ are the mass properties of iceberg and ship respectively (the added mass should be included).

Internal Mechanics

Ice model

As stated before, the challenging part of this project is the ice model. This model should be able to describe the ice behavior reasonably accurate when it is applied to the integrated analysis. In a previous paper, Zhenhui L. (2009b) has presented a promising user defined ice material model. This model has been successfully implemented into the commercial explicit code, LS-DYNA, see Hallquist (2007). A general description of the ice model is presented below.

Ice is categorized as first-year ice and multi-year ice. The first category means floating ice of no more than one year's growth, developing from young ice and thickness from 0.3 to 2 meters, like level ice. The latter category is normally defined to be ice which has survived at least two summer seasons, like ice ridges and icebergs. In order to understand the ice mechanical properties, researchers have carried out series of uniaxial and triaxial experiments. In ship/iceberg collision, see Figure 3, crack and damage of ice are happening depending on the stress state of ice particles.

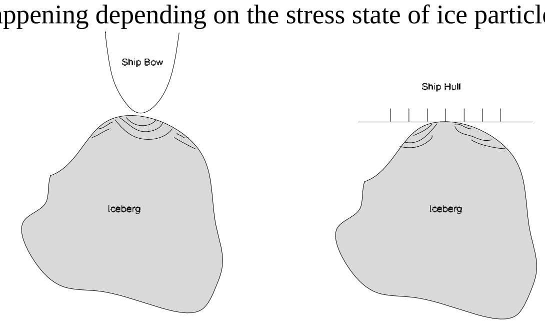

Figure 3 Illustration of ship/iceberg collision scenarios

Due to the relative large contact area compared to that of level ice, the ice in the contact area is in a triaxial stress state. The neighboring ice provides confinement and somehow increases the strength of the ice. Another problem in ship/iceberg collision is the strain rate influence because ice strength is quite sensitive to the strain rate. It is likely that in the ship/iceberg collision, the associated strain rate is larger than $10^{-3}s^{-1}$, Derradji-Aouat Ahmed (2005). Thus, the ice will behave elastically with a brittle failure mode. As discussed by Zhenhui L. (2009c), this property is accounted for by adopting a quasi-brittle material ice model. First, the constitutive relationship of stress and strain is described by the yield surface and associated flow rule, see Belytschko (2000). Second, a user defined failure criterion based on accumulated plastic strain is proposed, see Zhenhui L. (2009b). All the parameters involved should be calibrated with respect to experimental data. In order to the yield surface of the ice, triaxial experiments should be carried out in first place. Unfortunately, few experiments are available at this moment. Nadreau and Michel (1986) analyzed the triaxial experimental data by J.Jones (1982), see Figure 4. An elliptical shaped failure curve is derived.

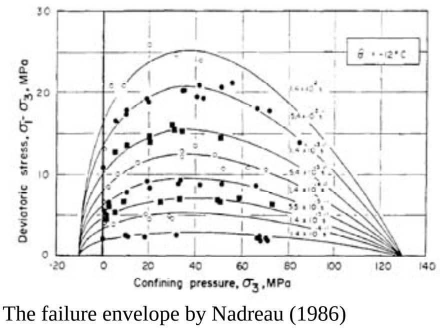

Figure 4 The failure envelope by Nadreau (1986)

Derradji-Aouat (2000) investigated the experimental data by J.Jones (1982) and Gagnon R.E. (1995) and proposed a unified elliptical failure envelope both for the isotropic fresh ice and iceberg ice, see Figure 5.Again, an elliptical shaped failure curve is obtained.

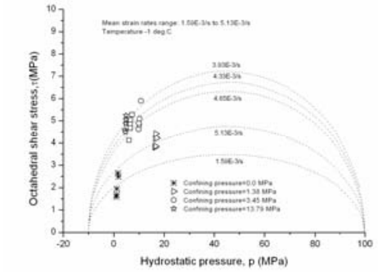

Figure 5: Elliptical failure envelope by Dhajaaji (2000)

As concerns numerical simulations, Sveinung Løset (1994) first used a similar elliptical failure curve based material model to simulate iceberg impacts with offshore structures. This failure curve is termed the Tsai-wu failure criterion. This model is also adopted in the present research. The Tsai-wu failure criterion is calibrated with the elliptical failure envelope proposed by Derradji-Aouat (2000) for iceberg. Plasticity theory is applied to describe the constitutive behavior of ice treating the failure criterion as a yield surface.

The basic assumption of the Tsai-wu strength criterion is that there exists a failure surface in the stress space in the following scalar form, (see S.Tsai (1971).

$$f(\sigma_k) = F_i\sigma_i + F_{ij}\sigma_i\sigma_j = 1$$

If the ice material is assumed isotropic, the failure criterion is reduced, see Riska K. (1987).

$$f(\sigma_k) = F_1 I_1 + \frac{1}{3}(F_{11} + 2F_{12})I_1^2 + 4F_{33}J_2 = 1$$

where I_1 is the first invariant of the stress tensor, and J_2 is the second invariant of deviatoric stress tensor, $J_2 = (\frac{1}{2}s_{ij})^{1/2}$, s_{ij} is the deviatoric stress tensor.

We may rewrite the above expression in the so called $J_2 - p$ space, see Figure 6.

We have:

$$f(p, J_2) = J_2 - (a_2 p^2 + a_1 p + a_0)$$

where p is the hydrostatic pressure, $p = \frac{1}{3}\sigma_{ii} = \frac{1}{3}I_1$ and q is the deviatoric stress, $q = (\frac{3}{2}s_{ij})^{1/2}$,$a_2$,$a_1$,$a_0$are constant which should be fitted through experimental data.

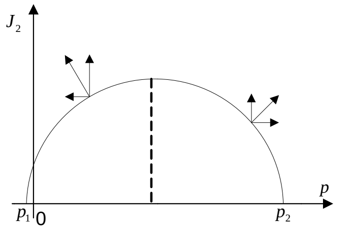

Figure 6: Tsai-Wu yield surface in $p - J_2$ space

One interesting point of the ship/iceberg collision is the influence of so called HPZ (high pressure zone) in ice mechanics, see Jordaan (2001). It is reported that pressures as high as 70 MPa HPZs are generated during the ice and structure interaction. The present ice material model follows the Tsai-wu yield surface and the user defined failure criterion is designed to let the elements stay alive if they are in the high pressure stress state.

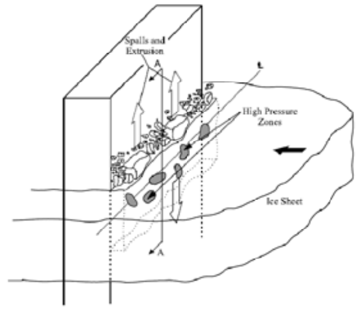

Figure 7: Schematic illustration of ice-structure interaction (Jordaan (2001).

The failure criterion is based on the equivalent plastic strain, which is defined as follows:

$$\varepsilon_{eq}^p = \sqrt{\frac{2}{3}\varepsilon_{ij}^p : \varepsilon_{ij}^p}$$

One of the proposed failure criterions is defined in the following format:

$$\varepsilon_f = \varepsilon_0 + (\frac{p}{p_2} - 0.5)^2$$

where ε_0 is a constant, to be determined by experiments, p_2 is the right root of the yield surface, see Figure 8 for example. If $\varepsilon_{eq}^p > \varepsilon_f$, element erosion is initiated. Both ε_0 and cutoff pressure should be calibrated through comparing the experimental data.

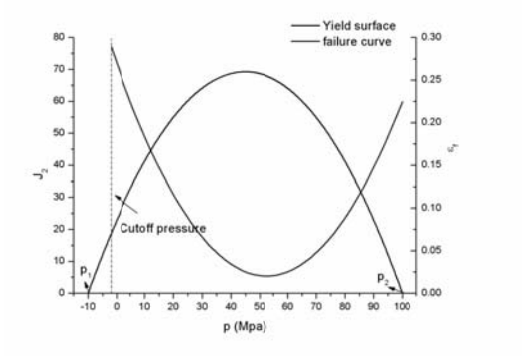

Figure 8: Yield surface and failure curve example

Integrated analysis

The integrated analyses are carried out with the commercial code LS-DYNA. The ice material model and the steel fracture model developed by Alsos (2008b) are implemented as user defined subroutines. The erosion technique is used to delete failed elements.

Scenarios of interest include iceberg collisions with

- Ship side in the bow area
- Ship side in the mid ship area
- Bulbous bows

Two of the scenarios are illustrated in Figure 9

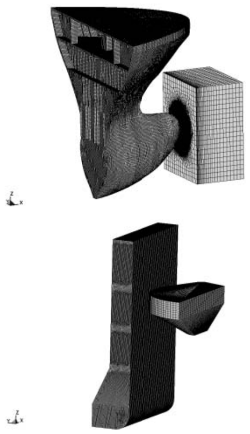

Figure 9: Iceberg collision scenarios

Figure 10 and 11 illustrate results of bulbous bow impact. With the given choice of bow and iceberg parameters, the bow undergoes substantial deformations, but is capable of penetrating significantly into the iceberg

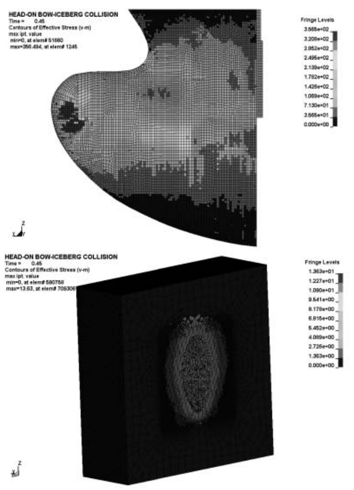

Figure 10: Screen shot for the Case a

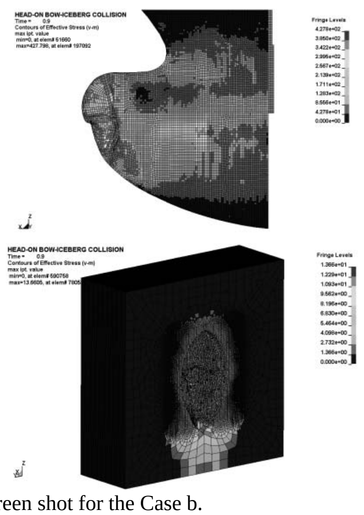

Figure 11: Screen shot for the Case b.

For side impact in the bow and midship area, a key issue is that the side shell may be severely damaged, but the inner shell containing hazardous cargo shall not be penetrated. In previous study of side shell impact, e.g. Zhenhui L. (2009c), it was found that the energy to cause the maximum deflection of inner shell in the midship area is 22 MJ. This figure is probably conservative and further investigations are carried out. This comprises parametric variation of structural layout and scantlings, so as to determine improved impact resistant design.

Conclusions

A method for assessment of structural damage in ship ice berg collision has been described. It is based on de-coupling the external and internal collision mechanics. The approach adopted for calculation of external mechanics takes all six degrees of freedom into account. Analyses show that typical ships size and hull shape show gives an energy dissipation ratio of 30%-45% with respect to the maximum possible demand for energy dissipation if the collision happens in the foreship area, see Zhenhui L. (2009a).

The internal mechanics model is based upon Tsai-wu yield model and element erosion. Despite its simplicity the material model is capable of simulating the crushing mechanics of the ice fairly well. Preliminary calculations show the importance of taking ice-structure interaction into account. In the integrated analysis, the total dissipated energy is initially larger than that of the ductile analysis because the energy is dissipated mostly through crushing of the ice at this stage. As the resistance of the ship structure and the contact area increase, the ship side is severely damaged and whereas the ice is comparatively stiff.

Finally, the dissipated energy from the quasi-static analysis is evaluated against the results obtained from the external mechanics analysis. In this manner a framework for analyzing ship/iceberg collision is established. In further work focus will be placed on how various structural lay-out and side scantlings affect the resistance of ships side to penetration for abnormal level ice impacts.

Acknowledgement

The present work is carried out within the scope of the Strategic University Programme (SUP) “ScenaRisC&G” in Norwegian University of Science and Technology (NTNU) which is funded by the Research Council of Norway (NFR). The authors wish to thank the Research Council of Norway for the funding of the study.

References:

Alsos H. S., A. J. a. H. O. S. (2008a). "On the resistance to penetration of stiffened plates." International Journal of Impact Engineering.

Alsos Hagbart S., A. J. a. H. O. S. (2008b). "On the resistance to penetration of stiffened plates Part II - Numerical analysis." International Journal of Impact Engineering..

Belytschko, T. (2000). Nonlinear finite elements for continua and structures.

Bo Wang, H.-C. Y. a. R. B. (2008). Ship and Ice collision modeling and strength evaluation of LNG ship structure. OMAE, Portugal.

Derradji-Aouat, A. (2000). A Unified failure envelope for isotropic fresh water ice and iceberg ice. OMAE, New Orleans.

Derradji-Aouat Ahmed, M. L. (2005). Ice loads on electric power generating stations in the bell isle strait. POAC, Postdam, New York.

Ehlers, S. and P. Varsta (2009). "Strain and stress relation for non-linear finite element simulations." Thin-Walled Structures 47(11): 1203-1217.

Gagnon R.E., G. P. H. (1995). "Triaxial experiments on iceberg and glaciers ice." Journal of Glaciology 41(139): 528-840.

Hallquist, J. O. (2007). Ls-dyna Keyword User's Manual (version 971), Livermore software.

Han S., J.-Y. L., Y-I Park and J Che (2008). "Structural risk analysis of an NO96 membrane-type liquified natural gas carrier in Baltic ice operation." Proceedings of the Institution of Mechanical Engineers. Proceedings part M, Journal of engineering for the maritime environment 222(4): 179.

ISO (2008). Petroleum and natural gas industries - Arctic offshore structures. ISO/DIS 19906, ISO TC 67/SC 7.

J.Jones, S. (1982). "The confined compressive strength of polycrystalline ice." Journal of Glaciology 28(98): 171-177.

Johnson, K. L. (1985). Contact Mechanics, Cambridge Unv.

Johnston, M., G. W. Timco, et al. (2008). "Measuring global impact forces on the CCGS Terry Fox with an inertial measurement system called MOTAN." Cold Regions Science and Technology 52(1): 67-82.

Jordaan, I. J. (2001). "Mechanics of ice-structure interaction." Engineering Fracture Mechanics 68(17-18): 1923-1960.

Nadreau, J.-P. and B. Michel (1986). "Yield and failure envelope for ice under multiaxial compressive stresses." Cold Regions Science and Technology 13(1): 75-82.

NORSK STAND N-004 App. A (2004) Design of steel structures.

Peschmann, J. (2001). Energy absorption computations of ship steel structures under collision and grounding (Germany). Doctoral Dissertation. Technical University of Hamburg.

Riska K., F. R. (1987). Modelling ice load during penetration into ice., Joint report of the technical research center of Finland and the National Research Council of Canada.

S.Tsai, E. W. (1971). "A General theory of strength for anisotropic materials." Composite Materials 1.

Stronge, W. J. (2004). Impact mechanics.

Sveinung Løset, T. K. (1994). Iceberg/structure interaction-effects of ice temperature on the impact force. IAHR Ice Symposium, Trondheim.

Terndrup Pedersen, P. and S. Zhang (1998). "On Impact mechanics in ship collisions." Marine Structures 11(10): 429-449.

Tornqvist, R. (2003). Design of crashworthy shop structures. PhD Dissertation. Technical University of Denmark.

Zhenhui L., a. J. A. (2009a). "A new formulation of impact mechanics of ship/ship and ship/iceberg collisions." submitted to Marine Structures.

Zhenhui L., J. A., Sveinung L. (2009b). Application of plasticity theory in the simulation of iceberg impacts. Marine 2009. Trondheim.

Zhenhui L., J. A., Sveinung L. (2009c). Numeric simulation of collisions between ships and icebergs. POAC, Lulea.

Experimental Investigations on Collision Behaviour of Bow Structures

Ingo Tautz, Martin Schöttelndreyer, Wolfgang Fricke and Eike Lehmann

Hamburg University of Technology (TUHH), Germany

Abstract:
Dimensioning of bow-structures is mainly based on loads like slamming, ice load and hydrodynamic pressure. At present, steel designers do not have any upper limits regarding the stiffness of bow-structures. That means bow-structures could have arbitrary stiffness even if this would lead to disastrous consequences for optional collision partners.
The authors are currently engaged in a collaborative research project which - amongst others - deals with the comparison of different structures of bulbous bows and corresponding effects on collision behaviour. This paper gives an account of the project background and focuses on collision experiments with bulbous bows against rigid wall. The experiments were carried out on the test facility of the Institute for Ship Structural Design and Analysis of TUHH in March 2010. Because the project is still ongoing more results will be published in future.

Introduction

This paper reports on actual research work carried out in the collaborative project ELKOS (German acronym, meaning: „Improving collision safety by integrating effects of structural arrangements in damage stability calculations“). Superior research objective is to develop a method, that allows adequate consideration of structural arrangements that significantly increase collision safety in damage stability calculations. The project is funded by German Federal Ministry of Economics and Technology (BMWi). TUHH is engaged with its institutes „Ship Structural Design and Analysis“ and „Ship Design and Ship Safety“. Industrial partner is the German yard Flensburger Schiffbau-Gesellschaft. The authors focus on experimental investigations of inner mechanics concerning several designs of ship side structures and following numerical simulations. Further more, stiffness of bulbous bows will be considered in a realistic manner and corresponding effects on collision mechanics with side structures will be investigated. In addition to collision experiments with bulbous bow and ship side structures, pre-tests will be carried out which will take deformable bow structures against a rigid wall into consideration. Experimental results will provide the basis to validate simplified simulation approaches needed to realize a reasonable coupling between collision simulation and damage stability calculation.
Most of experimental investigations of the past focused on the struck ship. There have been just a few experiments that took also the behaviour of the striking ship into consideration and fewest that were carried out especially to investigate inner mechanics of bulbous bows during collision.
Amdahl[1] simplified bulbous bow structures in several tests as tubes with circular and elliptical cross-section. The tubes have been stiffened in several different ways and have been set under axial compression. Yamada[2] tested models of bulbous bows under axial load as well as under a collision angle of 72°. Because of shape and size of his models very realistic behaviour could be achieved. The experiments described within this paper have been carried out against rigid wall. In this point they indeed follow the above mentioned tests of Yamada and Amdahl but additionally, tests that consider the side structure of the struck ship as well, will be carried out in the future. Influences of deformable bulbous bow structures on the whole collision procedure will then also be experimentally verified.

Experimental Conditions

Collision tests are carried out on the existing test plant of the institute of Ship Structural Design and Analysis of TUHH that is adequately supplemented and modified for this purpose. (Figure 1).

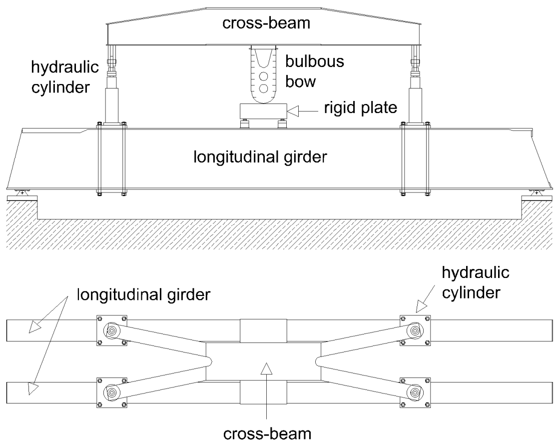

Figure 1. Test plant, configuration bow against rigid plate

Collision forces are applied by four hydraulic cylinders. They are connected with the longitudinal girders of the test plant and with a cross-beam. Thereby a closed flow of forces is provided. The test model of the bulbous bow is located underneath the cross-beam. It is driven against a counter plate that can be assumed as rigid. Collision forces are measured at the hydraulic cylinders as well as at pressure load cells underneath the rigid counter plate. The maximum loading capacity is 4000 kN. Hydraulic cylinders are limited at 400 mm regarding the maximum range of displacement. Thus larger displacements will be realized by using appropriate interim pieces between the bulbous bow and the cross-beam. This approach is permissible because the whole test procedure is quasi-static with maximum speed of 0.5 mm/s. Therefore the interruption of the test is feasible and permissible at any time. Nevertheless it should be observed if the original load path will be reached after re-loading.

The test plant offers possibilities to integrate ship side structures with moderate effort instead of using the rigid plate. Side structures will be supported adequately to measure collision forces as well as membrane forces (Fig.2) Regarding dimensions, test models of side structures will be comparable with those investigated in a very realistic manner in the research project „Life Cycle Design“[3] in 1998 in the Netherlands (scaling ca. 1:3).

Regarding the steel design, the test model will be comparable with side structures of RoRo-vessels. The start of these experiments is scheduled for January 2011. Therefore this paper in the following focuses on experiments with bulbous bow against rigid plate according to Figure 1 only.

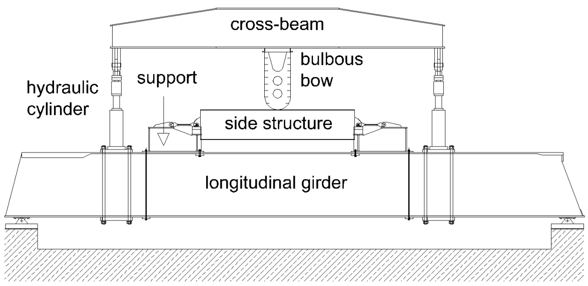

Figure 2. Test plant, configuration bow against side structure

Test Model

There will be a total of two bulbous bows tested against rigid wall. The first one is designed in conventional design, the second one will be set up with collision friendly deformation behaviour. At present, experimental results are just available for the first test model. Therefore descriptions in this and the following chapters concentrate on the first model (conventional design). Principle considerations regarding the second model are described in chapter 6.

The length of the test model amounts to 1800 mm. Its assembly was carried out in two blocks. The block joint lies between #4 and #5 in the middle of the length (Figure 3). The aft end of the test model is of cylindric geometry with a diameter of 813 mm. The geometry of the fore end is derived from the bulbous bow of an actual newbuilding of a RoRo-vessel. This derivation is done first by adjusting the section at center line to a rotation symmetric contour, second by scaling the aft diameter of the adjusted contour down to 813 mm (to be compatible with the load transmission in the cross-beam). The stiffening of the test model can only approximately be comparable with typical steel design of bulbous bows. The reason for this are restrictions regarding manufacturing requirements resulting from narrow geometric conditions. For the realization of the stiffening system of the test model (Figure 3) a longitudinal bulkhead, a stringer deck and a transversal framing with a distance of 200 mm were taken. The most important structural elements are considered with this approach. The material to be used for manufacturing was specified to be ordinary shipbuilding steel with a thickness of 5 mm and a yield stress of 235 N/mm².

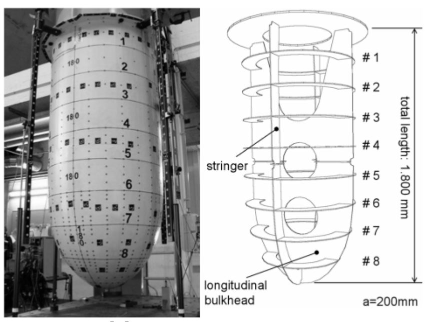

Figure 3. First test model

Experimental Results

The collapse behaviour is a typical progressive folding as described and examined e.g. in [4].

The history of the collision force shows a comparable periodic appearance of peaks in a range between 2900 kN and 3200 kN about every 160 mm, which amounts to approximately 80% of the framing distance. After reaching a force-peak, folding occurs straight behind the ring frame being next to get into contact with the rigid plate. This typical folding mechanism is shown in Figure 4. The corresponding status in the load-displacement curve is marked.

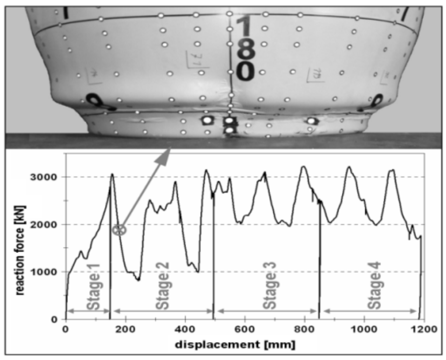

Figure 4. Load-displacement curve of experiment with one corresponding state of deformation

Figure 4 also shows unloading and reloading carried out before, respectively after, mounting the next interim piece. Complete unloading of the test model appears to be unproblematic. The original load path was reached with sufficient accuracy after reloading at any time.

Comparison with Numerical Analysis

For dimensioning purposes the FE-Model shown in Figure 5 was built up. It was fixed at its aft end in all degrees of freedom (#0 according to Figure 3). A rigid wall was driven against the model in axial direction with constant velocity and mass. Calculations are performed with the finite element code LS-DYNA. In contrast to Figure 3 which shows the real geometry of the test model, some simplifications have been made in the FE-Model. In particular lightening holes as well as constructional details in the area of the block joint are neglected. Because tensile tests have not been performed yet the material model is based on a true stress-strain curve resulted from material tests carried out in another context. No criterion of failure and no strain rate effects are integrated.

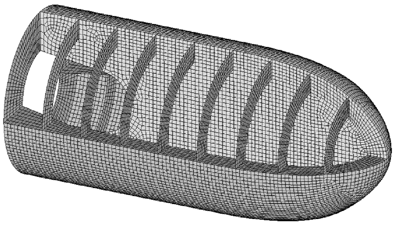

Figure 5 FE-Model BB1

The comparison of experimental and numerical results in Figure 6 shows that experimentally determined reaction forces are generally on a level above the results from the FE-calculation. A spot check of material thickness of the test model showed that there is evidence to suggest that it was built with plate thickness of about 5.5 mm which is 10% higher than specified, respectively than calculated in the FE-model. Furthermore, it was found that the diameter of the test model is about 10 mm greater than the numerical model. Both of these effects are likely to be fundamentally responsible for the differences in reaction forces between experiment and calculation.
The real geometry of the test model was captured by a photogrammetric measurement and will be integrated in ongoing corrections of the FE-model. Furthermore, the true stress-strain relationship of the materials used for manufacturing of the test model will be integrated but it has not yet been available for this paper.

Apart from the above mentioned differences according to the absolute value of forces, there is good correlation in the course of reaction forces in principle. Hence the calculation approach also will be used for the dimensioning of the second test model.

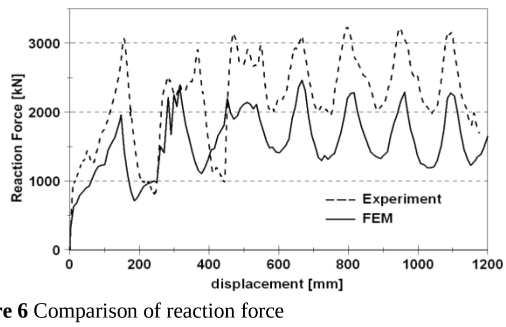

Figure 6 Comparison of reaction force

Considerations Regarding Collision Friendly Test Model

The second test model shall be designed with collision friendly deformation behaviour. In particular low energy level at small displacements, that means, at the very beginning of the collision, shall be reached. Flattening of the bow tip with the least resistance possible shall be achieved in order to enlarge the contact area. Former investigations [5] have shown that the flattening of the bow tip leads to a less sharp penetration of the bow in the side structure. Hence the whole process will have an increased collision friendliness.
Because geometry of the shell as well as the plate thickness, will be identical for both test models, changes of the collision behaviour can only be achieved by changing the stiffening system. In particular the longitudinal bulkhead of the FE-model BB1 is characterized by a comparable high rate of absorbed energy. Therefore it shall be examined if a design with a corrugated longitudinal bulkhead will have positive effects on collision behaviour (Figure 7).
Furthermore a FE-model with no longitudinal stiffening elements will be examined (Figure 8).

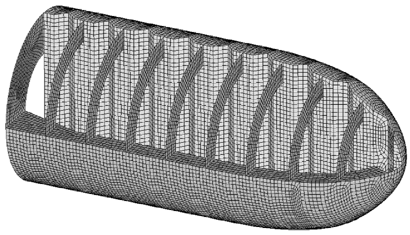

Figure 7 FE-Model BB2-corrugated

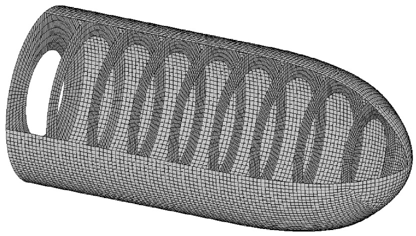

Figure 8 FE-Modell BB2-no-longitudinals

Comparing the computed energy absorption capacity of the three structural designs of bulbous bows mentioned so far, it becomes obvious, that corrugating the longitudinal bulkhead (BB2-corrugated) does not lead to significant differences in the course of collision energy compared with the geometry of the first test model (BB1). Hence it can be assumed that corrugating longitudinal elements do not have a significant positive impact in order to increase collision friendliness.

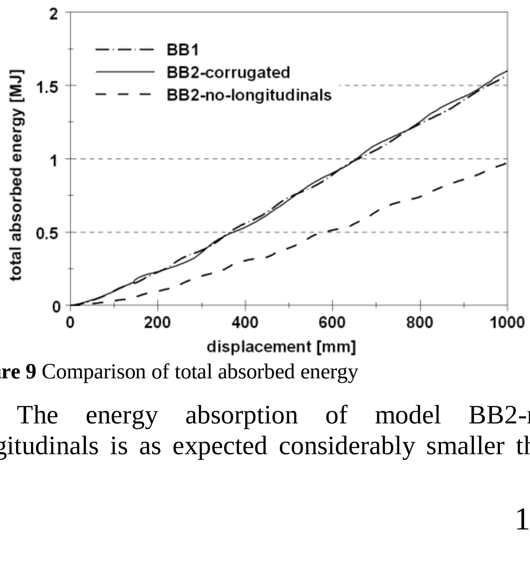

Figure 9 Comparison of total absorbed energy

The energy absorption of model BB2-no-longitudinals is as expected considerably smaller than those of the other two calculations used for comparison. A more differentiated impression can be achieved by relating the absorbed energy of model BB2-no-longitudinals to the absorbed energy of model BB1 (Figure 10). At the end of the process, the energy level of the model without longitudinals is turning into approximately 60% of the comparative calculation. It is of particular interest that this level is reduced to values below 30%, especially at the very beginning of the collision up to displacements of about 200 mm.

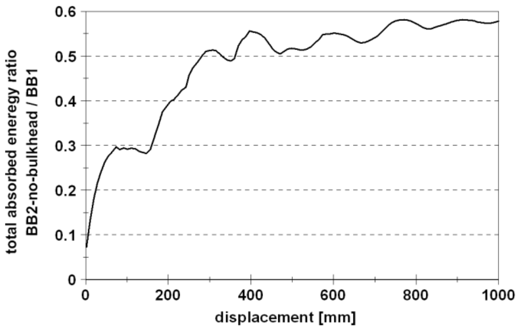

Figure 10 Energy ratio

The steel design of real bulbous bows without longitudinals of course has to be in line with applicable classification rules and also has to consider typical operational loads. It is possible, that realizing the above mentioned proposal without longitudinals will lead to unrealistic large plate thicknesses of the outer shell.[6] e.g. showed that outer shell does absorb the largest amount of collision energy, so this would relativize the above described effect.

Longitudinal structural elements of course are of particular importance to provide sufficient bending stiffness of the bulbous bow structure. Therefore longitudinal bulkheads and decks are well established and reasonable.

The above mentioned results however lead to the recommendation to leave away these longitudinal elements in the area of some few frames behind the tip of the bulbous bow (Figure 11). In the foremost area the required bending stiffness is comparably small in general. With this approach, a collision friendly design according to the proposal BB2-no-longitudinals will be easier to realize because it just concentrates on the foremost part of the bulbous bow.

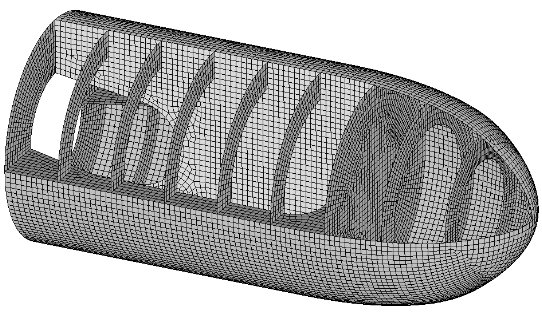

Figure 11 FE-Model BB2-hybrid-type

Comparing the energy absorption capacity of model BB2-hybrid-type with model BB1 and model BB2-no-longitudinals (Figure 12), it can be observed that the course of absorbed energy of model BB2-hybrid-type is identical to BB2-no-longitudinals. This is the case up to a displacement of about 500mm. This is approximately the point when longitudinal elements are getting into contact. Subsequently the absorbed energy passes into the gradient of the curve belonging to BB1.

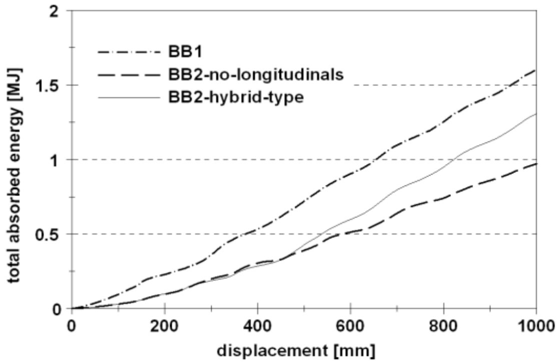

Figure 12 Comparison of total absorbed energy

The total level of absorbed energy of model BB2-hybrid-type indeed is considerably higher than the one of the model without any longitudinal element. However this is acceptable because of the good accordance of both models at small displacements.

Project Outlook

The described experiments with bulbous bows against rigid plate are pre-tests. Beside the investigations of the tested models, they are used to prepare quasi-static collision tests against scaled-down ship side structures of RoRo-vessels.

Actual planning is to carry out a total number of four experiments beside the pre-tests. Objective of the investigations will be two different designs of ship side structures. A first series of experiments will be with rigid bow as collision partner. A second series of experiments with test models of the same kind (regarding the side structure) will be tested with a bulbous bow that will deform to a certain extend. This will lead to a comparison of collision scenarios under the established assumption „rigid bow" with scenarios that consider the deformation behaviour of bulbous bows.

Conclusion

This paper described experimental and numerical results of bulbous bow collisions with rigid plate. Although exact model geometry and material parameters of the test model are not yet included in FEM-calculations, the simulation results are in sufficient correlation with the experiment for further considerations regarding a second test model. These considerations have been described and led to a preliminary solution of a test model with collision-friendly behaviour, especially at low levels of displacements. Effects of such collision-friendly bow structures on the whole collision scenario are going to be investigated in the future. The principle project planning of the corresponding experiments and calculations was described, some more information of the project background was given.

Acknowledgement

The work was performed within the research Project ELKOS, funded by German Federal Ministry of Economics and Technology (BMWi) under project no. 03SX284B. The authors are responsible for the content of this paper and wish to thank for supporting this project. The authors' gratitude also goes to German yard Flensburger Schiffbau-Gesellschaft that delivered the cross-beam for the test plant as well as the test model.

References:

J. Amdahl, Energy Absorption in Ship-platform Impacts, Department of Marine Technology, The University of Trondheim, Report No. UR-83-34, 1983

Y. Yamada, Bulbous buffer bows: a measure to reduce oil spill in tanker collisions, Ph.D. thesis, Danish University of Technology (DTU); 2006

TNO-report 98-CMC-R0359, Full scale ship collision experiments 1998, TNO, 1999

E. Lehmann and X Yu, Progressive folding of bulbous bows, PRADS 95, Volume 2, Seoul, 1995

I. Tautz, Predetermined breaking points in a ships double hull, Proceedings of ICCGS, Hamburg 2007

E. Lehmann and X. Yu, Inner Dynamics of bow collision to bridge piers, International Symposium on Advances in Ship Collision, Proceedings, Copenhagen, 1998

On the Derivation of $CATS_{thr}$ within the Framework of IMO environmental FSA studies

Yasuhira Yamada and Fujio Kaneko

National Maritime Research Institute, 6-38-1, Shinkawa, Mitaka-shi, Tokyo, Japan

Abstract:
The purpose of this paper is to investigate reasonable cost benefit criteria within the framework of environmental formal safety assessment (FSA). In this study a statistical analysis of oil spill data was carried out based on the report of International Oil Pollution Compensation Funds (IOPCF, 2007). According to the statistical study of actual oil spill from tankers, it is found that collisions and groundings are the most probable causes of the oil spills from tankers. Probability distributions of costs of oil spill and oil spill amount are investigated, and a non-linear regression formula between costs of oil spills and oil spill volume are derived. Using the regression formula, an oil spill volume dependent $CATS_{thr}$ is proposed. Moreover in order to apply the volume dependent $CATS_{thr}$ to cost benefit analysis (CBA), a new cost-effective criterion is newly proposed with considering its concrete application to environmental.

Introduction

Collision and grounding are main causes of oil spill accidents. In order to protect maritime environment from disastrous oil spill accidents it is very important to develop cost effective counter measures against oil spill accidents. However, since resource of shipping and shipbuilding are limited, the balance between costs and effectiveness of risk reduction counter measures is also important. For such purpose "environmental risk evaluation criteria" (EREC) is under discussion in IMO within the framework of Environmental Formal Safety Assessment (FSA). EREC to protect the maritime environment from oil spills from ships is under development as a first step of the environmental FSA. In order to establish the criteria a concept of CATS (Cost to Avert Tonne of oil Spilt) is proposed to judge cost-effectiveness of an arbitrary Risk Control Option (RCO). In this study, the IOPCF (International Oil Pollution Compensation Funds) data (2007) is analyzed and causes of oil spills from tankers are investigated. According to the statistics of actual oil spill from tankers, it is found that collisions and groundings are the most probable causes of the oil spills from tankers. A regression formula between costs of oil spills and oil spill volume is statistically derived by carrying out regression analysis based on the IOPCF data. Using the regression formula several possible ways to establish reasonable CATS criteria are proposed and these ways are discussed in detail considering its application to environmental FSA. It is noted that from its meaning it might be appropriate to use "Formal Environmental Assessment (FEA)" instead of "environmental FSA" with regards to formal risk assessment of oil spill from tankers. However in this paper latter wording is used since "FSA" is widely used in many papers and IMO documents as well as is widely recognized.

Statistical Analysis

In this section distribution of oil spill weight (W) as well as oil spill costs (C) are investigated using "oil spill database" created from the annual report of IOPCF (2007), where oil spill incidents resulting from spills of persistent oil from tankers are treated. Similar analysis was carried out by Friis-Hansen & Ditlevsen (2003) using 101 oil spill incidents which took place from 1979 to 1999 based on the report of IOPCF (2000). In this study, slightly updated database is used including the disastrous oil spill incident of Prestige in 2002. Consequently the database includes 136 oil spill incidents from tankers which took place between 1970 and 2007. Since W and/or C are unknown for some incidents, 114 incidents are used for oil spill weight (W), 129 incidents are used for oil spill costs (C) among 136 incidents. In the present study C denotes costs of oil spill which have actually been paid by IOPCF. The IOPCF report uses 9 categories for costs of oil spill such as costs of cleaning up oil, fishery/tourism compensation, loss of income, property damage indemnification as shown in Table 1. Table 1also shows subtotal costs [US$] of all accidents in each category as well as its ratio, where average currency exchange rate between 2002-2007 in IOPCF report is used. It is interesting to note that ratio of cleaning up costs is much higher than others, and that more than 90% of total costs are occupied by top 3 categories (cleaning up costs, fishery/tourism compensation) as far as IOPCF data. It is also noted that present results are obtained by limited amount of data, therefore in order to derive general tendency more oil spill data is necessary. More details about created database are also described in Yamada (2009). Figure 1 shows cause of oil spill from tankers derived from IOPCF (2007), where 136 major oil spill accidents in all over the world treated by IOPCF are included. It is seen in Figure 1 that collision is the most probable cause of oil spill accidents from tankers followed by grounding. It is interesting to note that collision and grounding occupy more than 50% of causes of oil spill accidents from tankers. Therefore it can be said that it is important to reduce risk of collisions and groundings of tankers in order to reduce oil spill risk from tankers.

Friis-Hansen & Ditlevsen (2003) pointed out that positive correlation can be seen between costs of oil spills and oil spill amount in double logarithmic axis. Yamada (2009) confirmed this correlation using updated database of IOPCF (2007).

Table 1 Subtotal costs and ratio for compensation category

Category	Subtotal Costs [US$]	Ratio [%]
Clean-up	1,934,008,770	71.8%
Fishery	393,065,064	14.6%
Tourism	147,391,359	5.5%
Environmental damage	63,450,396	2.4%
Indemnification	39,577,915	1.5%
Others	38,954,507	1.4%
Loss of income	35,664,386	1.3%
PropertyDamage	24,820,957	0.9%
Preventive Studies	15,936,290	0.6%
Total	2,692,869,645	100.0%

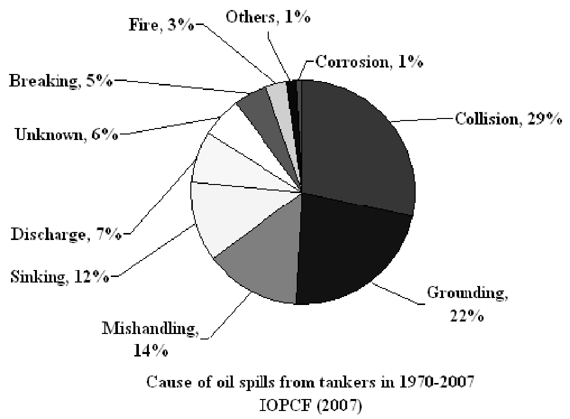

Figure 1: Cause of oil spills from tankers (IOPCF , 2007)

Figure 2 shows probability density function (PDF) of Log10(W) where samples (IOPCF data) and normal distribution are compared. Figure 3 shows cumulative distribution function (CDF) where samples and normal distribution are also compared. Log10(W) is assumed to follow normal distribution in Figure 2 and Figure 3. It can be seen in Figure 2 that histogram of sample data and normal distribution has a good correlation. Common logarithm (Log10) is used in the previous investigation (Yamada, 2009) considering consistency with frequency index (FI) and severity index (SI), where common logarithm is also used. However it is found that it might be beneficial from statistical and mathematical point of view to use natural logarithm since log-normal distribution function and its related formula can be directly used. Therefore natural logarithm of oil spill weight is calculated and similar figures are made as shown in Figure 4 and Figure 5 where LN(W) is used as horizontal axis instead of Log10(W). As shown in Figure 4 and Figure 5 good correlation can also be seen between samples and normal distributions in case of LN (W). It is interesting to note that slightly different shape can be seen in histogram of sample probability between PDF (Figure 2 and Figure 4) while similar tendency can be seen between CDF (Figure 3 and Figure 5). Statistical parameters Log10(W) and LN(W) are shown in Table 2.

Chi-square test of goodness of fit is also carried out for both Log10(W) and LN(W). An assumed distribution is regarded as suitable if following formula is satisfied (Miyazawa, 1954).

$$\chi^2 < \chi_\alpha{}^2(k-s-1) \tag{1}$$

where, χ^2, k and s are a chi-square value, number of categories in histogram and number of parameters respectively. χ is a significance level and, in this study, Chi=5% is adopted. χ^2 can be calculated as:

$$\chi^2 = \sum_{i=1}^{k} \frac{\left(f_i - np_i\right)^2}{np_i} \tag{2}$$

where f_i and p_i are frequency of samples in category i and probability of assumed distribution in category i respectively. n is a number of samples. It is noted that number of categories (k) has an effect on the results of chi-square test. Therefore based on Miyazawa (1954), several categories are merged if expected frequency of samples is less than 5 until expected frequency of samples becomes larger than 5 in calculating χ^2. Consequently number of categories (k) might be changed as compared with the value used in PDF and CDF figures. It is confirmed by carrying out sensitivity analysis that, as far as present data, adjustments of categories do not affect the results of chi-square test significantly and gives stable results.

In case of Log10(W), χ^2 = 9.00 < 12.59 is obtained using k= 9, s=2. In case of LN(W), χ^2 = 11.30 < 16.92 is obtained using k=12, s=2. Therefore it can be said that both Log10(W) and LN(W) would follow the log-normal distribution with a significance level of 5%. Considering benefit described above, natural logarithm is used for statistical investigation of W, C and C/W in the present study hereafter.

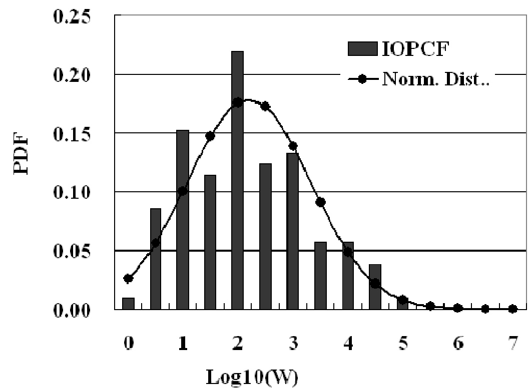

Figure 2:PDF of Log10(W)

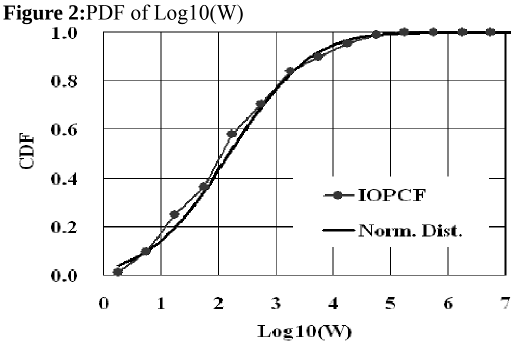

Figure 3:CDF of Log10(W)

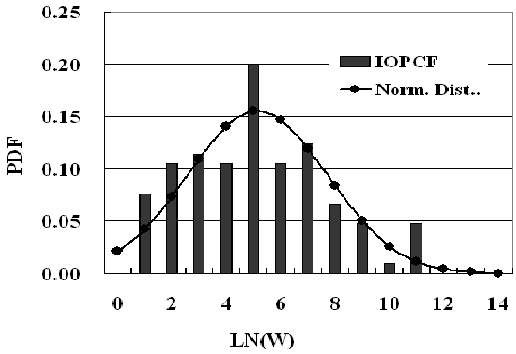

Figure 4:PDF of LN(W)

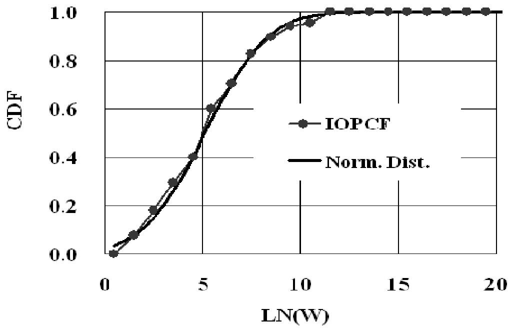

Figure 5:CDF of LN(W)

Table 2: Parameters for distributions of W estimated by IOPCF data

	Log10(W)	LN(W)
mean	2.45	5.64
stddev.	1.11	2.55
median	2.30	5.30

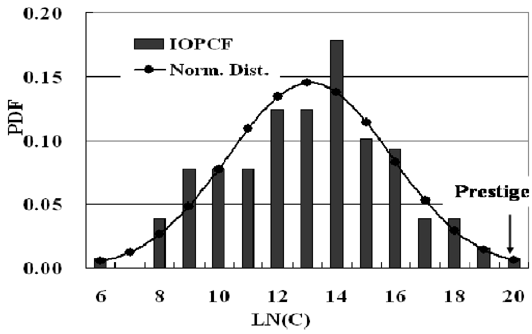

Figure 6:PDF of LN(C)

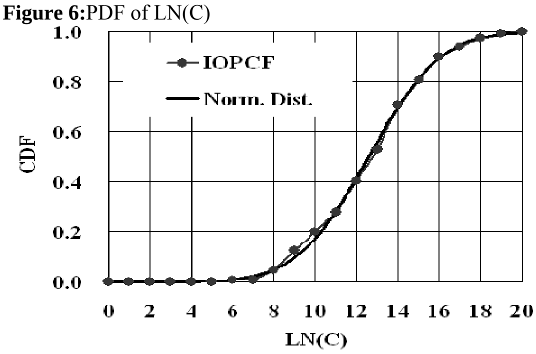

Figure 7:CDF of LN(C)

Figure 8 and Figure 9 show PDF and CDF of Ln(C/W) respectively, where samples (IOPCF data) and normal distribution are compared. It can be seen in Figure 8 and Figure 9 that samples and normal distribution has a good correlation. Figure 10 shows scatter plot of Ln(C) and Ln(W). Median and Expected value assuming lognormal distribution is also described in Figure 10. It can be seen in Figure 10 that Ln(W) and Ln(C) has a positive correlation. It is interesting to note that expected value of lognormal distribution is located not center of plots (distribution) but relatively at large value while median is located at almost center of distribution. This is mainly due to that expected value of lognormal distribution is largely affected by a few very large data. That is, as pointed out by many statistics text book, median might be suitable to represent lognormal distribution although an expected value of lognormal distributions also has its meaning.

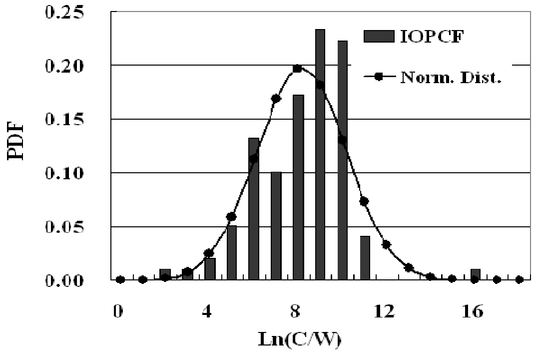

Figure 8:PDF of **LN(C/W)**

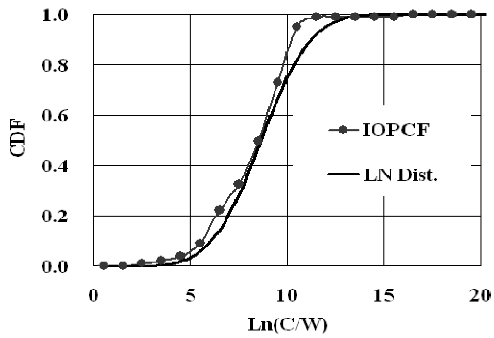

Figure 9:CDF of LN(C/W)

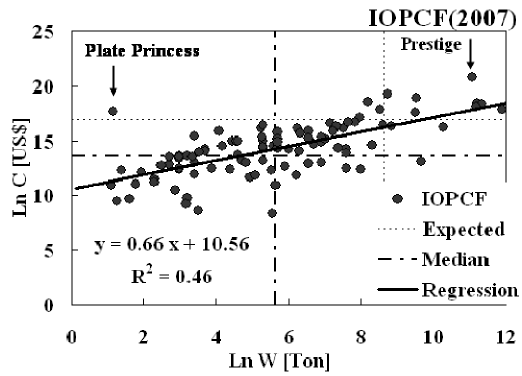

Figure 10: Relation between costs of oil spill and weight of spilt oil

CATS Criteria

Within the framework of safety FSA in IMO, a risk control option (RCO) is judged as cost-effective (IMO, 2007; Vanem et al, 2007; Vanem et al, 2008) if following formula is satisfied:

$$CAF < CAF_{thr} \quad (3)$$

where CAF and CAF_{thr} denote Cost of Averting a Fatality and its threshold value respectively.
Following safety FSA criteria, a concept of CATS (Cost of Averting a Ton of oil Spilt) is proposed for FSA for oil pollution (Skjong et al, 2005; Vanem et al, 2008) and CATS is defined as:

$$CATS = \frac{\Delta S}{\Delta W} = \frac{S_{new} - S_{org}}{-(W_{new} - W_{org})} \tag{4}$$

where
ΔS=Snew-Sorg:(>0) Costs of introducing RCO (Risk Control Option) [US$/ship].
ΔW= Worg -Wnew:(>0) Reduction of oil spill risk by RCO [ton/ship].
Sorg : Costs of building a ship before introducing RCO [US$/ship]
Snew : Costs of building a ship after introducing RCO [US$/ship]
Worg : Risk of oil spill before introducing RCO [ton/ship]
Wnew : Risk of oil spill after introducing RCO [ton/ship]

Usually it can be expected that ΔS>0 and ΔW>0 if RCO is effective. According to Eq.(4), CATS means how much cost increases is required in order to reduce unit ton of oil spill by a RCO. If the following formula is satisfied, a RCO is judged as cost-effective (Skjong et al, 2005; Vanem et al, 2008).

$$CATS < CATS_{thr} \tag{5}$$

where $CATS_{thr}$ is a threshold value to judge CATS for arbitrary RCO. It is important to distinguish the term “CATS” and the term “$CATS_{thr}$” since $CATS_{thr}$ is a kind of criteria (threshold value) to judge cost-effectiveness of arbitral RCOs while CATS can be estimated for various RCOs. CATS is specific for a RCO under investigation and, different RCOs usually have different CATS values. According to definition of CATS, $CATS_{thr}$ can be expressed as

$$CATS_{thr} = \frac{dC}{dW} \tag{6}$$

where C and W denotes costs of oil spill [US$] and weight of spilt oil [ton] respectively.
Substituting Eq.(4) and Eq.(6) into Eq.(5) , following relation can be derived as:

$$\frac{\Delta S}{\Delta W} < \frac{dC}{dW} \tag{7}$$

Figure 11 illustrates the relation between CATS and CATSthr as well as meaning of Eq.(7), where Eq.(9) is assumed as a cost function of oil spill. It can be seen in Figure 11 that a RCO is cost-effective if slope of □S/□W is smaller than slope of tangential line (dC/dW).

Figure 12 illustrates relation between dC/dW and RCOs, where three RCOs (RCO1, RCO2 and RCO3) are shown. Usually several RCOs can be proposed to reduce risk of oil spill. Each RCO has different □W, □S and □W/□S respectively. According to CATS criteria of Eq.(7) a RCO which has smaller slope than dC/dW is regarded as cost-effective. That is, RCO1 whose arrow is above tangent line of dC/dW is regarded as cost-effective.

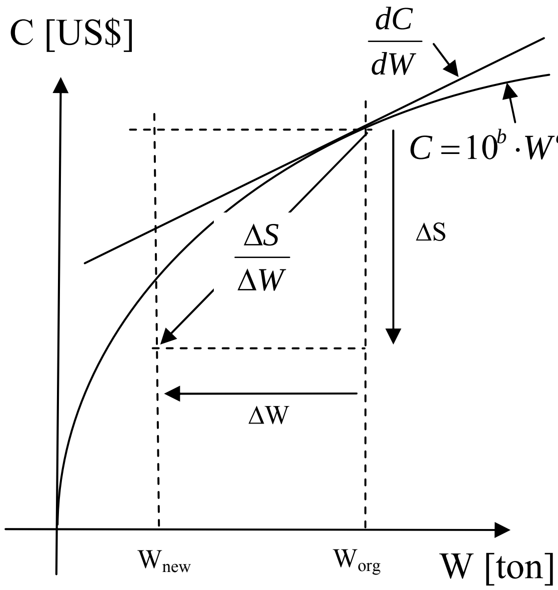

Figure 11: Illustration of oil spill risk reduction (**ΔW**) and costs of introducing RCO (**ΔS**)

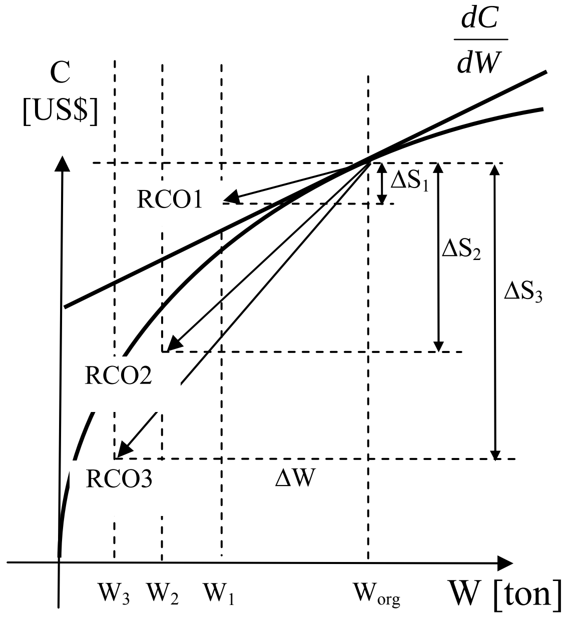

Figure 12: Illustration of dC/dW and various RCOs

$CATS_{thr}$

Constant CATSthr

Skjong et al (2005) and Vanem et al (2008) proposed $CATS_{thr}$ = 60,000US$/ton within the framework of EU project “SAFEDOR”. This value was estimated as:

$$CATS_{thr} = Ave[C/W] \cdot F_e \cdot F_a \tag{8}$$

where Ave [C/W] denotes average costs of oil spill per unit ton. F_e denotes environmental factor and is used in order to take into account oil spill costs other than cleaning up oils, that is, costs of natural resource damage, fishery/tourism compensations and so on. F_a

denotes assurance factor, reflecting the fact that spending resources on preventing oil spills is always preferable to accepting similar costs related to an actual spill (prevention better than cure). Ave[C/W] = 16,000 [US$ / ton], Fe= 2.5 and Fa = 1.5 were estimated, and consequently 60,000 (=16,000 x 2.5 x 1.5) [US$/ton] was estimated as $CATS_{thr}$. See detail in Skjong et al (2005) and Vanem et al (2008).

Volume dependent CATSthr (Function Type)

Yamada (2009) proposed a new regression formula between costs of oil spills and oil spill weight as:

$$C = 10^b \cdot W^a \equiv C_0 \cdot W^a \tag{9}$$

where, a and b are regression parameters and a=0.66, b=4.59 were estimated from regression analysis of IOPCF data (Yamada, 2009). C_0 denotes 10^b (=38,735). This formula indicates that costs of oil spill do not linearly increase as oil spill weight increases, but nonlinearly increase mainly due to that initial costs effects reduce as oil spill weight increases (See Etkin, 2000). Substituting these coefficients, Eq.(9) becomes as:

$$C = 10^{4.59} \cdot W^{0.66} = 35951 \cdot W^{0.66} \tag{10}$$

Yamada (2009) derived $CATS_{thr}$ by deviating Eq.(9) as:

$$CATS_{thr} = \frac{dC}{dW} = a \cdot W^{a-1} \cdot 10^b \tag{11}$$

Substituting a and b Eq.(11) becomes as:

$$CATS_{thr} = \frac{dC}{dW} = 25441 \cdot W^{-0.34} \tag{12}$$

Equivalent $CATS_{thr}$

It is one of the reasonable ways to directly use Eq.(12) as a $CATS_{thr}$ in order to carry out an FSA for oil spill pollution. However, in safety FSA, one single value of CAF_{thr} is widely used as a simple criterion. Therefore in this study an attempt to derive one single value of $CATS_{thr}$ is carried out corresponding to CAF_{thr} within the framework of IMO FSA methodology. However it is noted that to use volume dependent $CATS_{thr}$ (Eq.(10)) is supposed to be reasonable as well as practical. Details are discussed in later section.

In order to derive a single value of $CATS_{thr}$ from the nonlinear formula, an equivalent $CATS_{thr}$ value ($CATS_{thr,eq}$) can be proposed by the following formula (see also Fig. 1).

$$CATS_{thr,eq} = \frac{A}{W_2 - W_1} = \left(\int_{W_1}^{W_2} \frac{dC}{dW} dW \right) / (W_2 - W_1) \tag{13}$$

where A denotes an area under the regression curve. W_1 and W_2 are the lower and upper bounds of the integral respectively. W_2 is the maximum oil spill weight [ton] which we are considering as a risk of oil spill. This formula means that the area under the nonlinear curve, divided by the range of weight of spilled oil is equal to the value of $CATS_{thr,eq}$. In other words, $CATS_{thr,eq}$ is obtained by letting area1 = area2 in Figure 13.

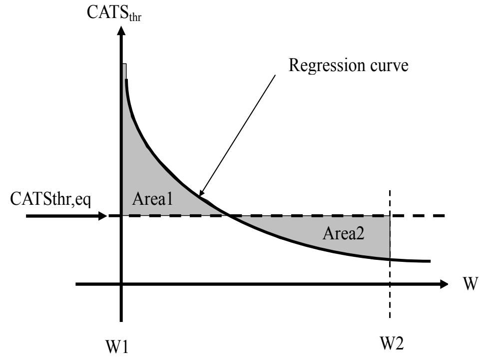

Figure 13: Regression curve and equivalent $CATS_{thr}$

Substituting Eq.(9) to Eq.(13),$CAT^{thr,eq}$ can be analytically obtained as:

$$CATS_{thr,eq} = \frac{C_0\left(W_2{}^a - W_1{}^a\right)}{W_2 - W_1} \tag{14}$$

Considering that the minimum oil spill is nearly equal to 0, W_1 = 0 can be substituted to the equation. Consequently, Eq.(14) becomes:

$$CATS_{thr,eq}(W_2) = \frac{C_0 \cdot W_2{}^a}{W_2} = C_0 \cdot W_2{}^{a-1} = \frac{C}{W_2} \tag{15}$$

Substituting a=0.66, C0=38,735 (based on the latest IOPCF data,), Eq.(15) becomes:

$$CATS_{thr,eq}(W_2) = C_0 \cdot W_2{}^{a-1} = 38735 \cdot W_2{}^{-0.34} \tag{16}$$

Therefore the $CATS_{thr,eq}$ becomes a function of W_2, the maximum possible spill weight. Figure 14 shows the relation between $CATS_{thr,eq}$ and W_2. It is seen in Figure 14 that $CATS_{thr,eq}$ becomes smaller as the W_2 gets larger. Thus, if W_2=10,000[ton] is assumed, $CATS_{thr,eq}$ becomes 1,642 [US$/ton] as shown in Figure 14. If W_2 = 300,000 [ton] is assumed as a maximum size of spilled oil considering that the whole cargo of a VLCC is spilled out, $CATS_{thr,eq}$ becomes 511 [US$/ton]. Moreover if W_2 = 600,000 – 700,000[ton] is assumed considering that a collision of two VLCC tankers takes place, $CATS_{thr,eq}$ of 403 [US$/ton] can be derived according to the present method. The black line in Figure 14 shows the $CATS_{thr,eq}$ dependency on the W_2 value.

As is described, two kinds of scale factor Fe (=2.5) and Fa (=1.5) are proposed by Skjong et al (2005). Although reasonable values of these factor should be more carefully discussed in the future, a kind of resultant scale factor F (=Fe x Fa = 3.75) can be considered. In order to investigate the effect of the scale factor F on the $CATS_{thr}$ curve, a curve with taking into account the effect of F (=3.75) is also plotted inFigure 14. It is noted that the scale factor F=3.75 is used as an illustrative purpose only since the value of F has not yet

been approved in the IMO. A dot line in Figure 14 shows the $CATS_{thr,eq}$ multiplied by the scale factor depending on W_2 value. Values at the left end of curves in Figure 14 show the values of $CATS_{thr,eq}$ in case W_2=10,000 [ton]. It can be seen in Figure 14 that even in the case of W2=10,000 and considering F=3.75, $CATS_{thr,eq}$ becomes 6,156 US$/ton, which is one order of magnitude lower than the value of 60,000 US$/ton as is described. It is also noted that the $CATS_{thr,eq}$ is an averaged value of $CATS_{thr}$ and we should be careful in judging cost-effectiveness of the arbitrary RCO using the $CATS_{thr,eq}$. If the IMO is discussing mostly large oil spills, $CATS_{thr,eq}$ might cause an overestimate of the oil spill cost as shown inFigure 13. On the other hand, if the IMO is discussing only small oil spills, such as mishandling in the port and operational spills, $CATS_{thr,eq}$ might be an underestimate of the oil spill cost (Figure 13).
Therefore it is recommended that the regression formula (Eq.(12)) can be directly used in FSA for oil spills. If the IMO is considering to prevent relatively larger oil spills by large crude oil tankers (such as in MEPC58/17/2, MEPC58/INF.2), it might be reasonable to use the $CATS_{thr,eq}$ corresponding to the larger value of W_1 and W_2.

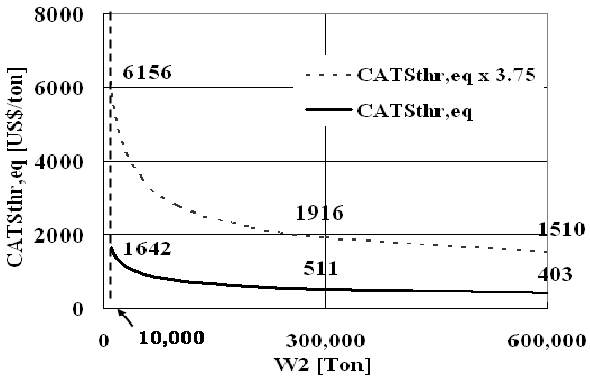

Figure 14: Relation between CATSthr,eq and W_2 (Fa=2.5x1.6=3.75)

Figure 15 and Figure 16 show relation between $CATS_{thr}$ and oil spill weight (W). It is interesting to note that according to the present analysis $CATS_{thr}$ becomes lower than 10,000 US$/ton if W > 20ton as shown in Figure 15. Therefore it might be one solution to use $CATS_{thr}$ =10,000US$/ton for oil spills larger than 20ton with considering safety factor for larger oil spills.

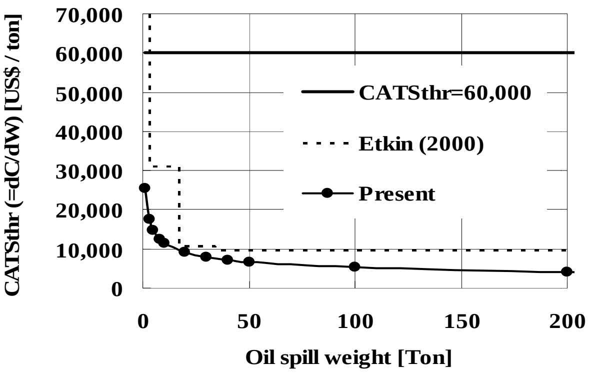

Figure 15: Relation between CATSthr and oil spill weight (W)

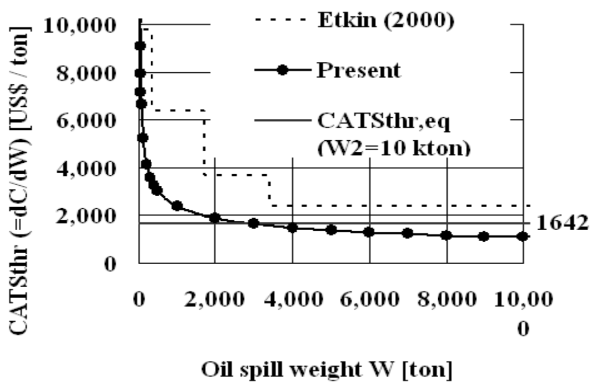

Figure 16: Relation between $CATS_{thr}$ and Oil spill weight (W)

Several types of $CATS_{thr}$ is considered and its applicability to FSA is shortly discussed. The author thinks it is reasonable to directly use volume-dependent $CATS_{thr}$ in function type (Eq.(12)) since this would directly reflect the characteristics of oil spill costs in relation to oil spill weight. This function can be updated with more oil spill data. However it is pointed out that the scale factor F which can be multiplied to Eq.(12) as a kind of safety factor is not discussed in the present study since this is under investigation and discussion in IMO. Even considering the effect of the scale factor F, the author believes that to use volume dependent $CATS_{thr}$ is reasonable as well as effective, and does not loose its characteristics. In the following chapter new cost-effective criteria to use volume dependent $CATS_{thr}$ is proposed.

New cost-effective criteria

In this section a new cost-effective criteria is proposed to apply a volume dependent CATS to the FSA framework.

Application of volume dependent $CATS_{thr}$

Substituting Eq.(4) into Eq.(5) the formula becomes as:

$$\frac{\Delta S}{\Delta W} < CATS_{thr} \tag{17}$$

Considering that $CATS_{thr}$ is volume dependent Eq.(17) can be further transformed as:

$$\frac{S_{new} - S_{org}}{W_{org} - W_{new}} < CATS_{thr}(W) \tag{18}$$

In applying a volume-dependent $CATS_{thr}$ in Eq.(18), we come to the fork that what kind of W value is appropriate to substitute in the right hand term of Eq.(18). As a value of W to use W_1, W_2 or average of W_1 and W_2 can be considered. If W_1 and W_2 are both relatively large, or W_1 and W_2 are relatively close, $CATS_{thr}(W_1)$ and CATSthr (W_2) can be close considering characteristics of volume dependent $CATS_{thr}$ (See Figure 16). Consequently the effect of using W_1 or W_2 on the $CATS_{thr}$ value can be small or negligible. That is, we could use either W_1 or W_2 and the results of cost-effectiveness can be same regardless of using W_1 or W_2.

However if W_1 and W_2 are both relatively small, or difference of W_1 and W_2 is large, $CATS_{thr}(W_1)$ can be quite different from $CATS_{thr}(W_2)$, consequently the effect of using W_1 or W_2 on the $CATS_{thr}$ value is significant. That is, the results of cost-effectiveness might be different depending on the W value substituted to a volume-dependent $CATS_{thr}$.

As a third candidate we can use average of W1 and W2, but it seems to be difficult to find out a reasonable reason to adopt this solution. In order to solve this issue, new cost-effective criteria is proposed in the next section.

New cost-effective criteria

A RCO can be regarded as cost-effective if following formula is satisfied (MEPC58/17, ANNEX, p5).

$$\Delta B - \Delta S > 0 \tag{19}$$

where ΔB (>0) denotes a benefit by implementing arbitrary RCO which can be calculated as a risk reduction [US$]. ΔS denotes a cost of implementing a RCO. Eq.(19) indicates that the RCO is regarded as cost-effective if benefit (ΔB= risk reduction [US$]) by implementing arbitrary RCO is larger than costs of implementing this RCO (ΔC [US$]). Eq.(19) can be transformed as:

$$\Delta S < \Delta B = E\left[C_{org}\right] - E\left[C_{new}\right] \tag{20}$$

where E[Corg] and E[Cnew] denote an expected cost of oil spill [US$] before RCO is introduced and that after RCO is introduced respectively, where E [ ] indicates an expected value. E[Corg] and E[Cnew] can be calculated using an risk model such as an "event tree" in the FSA framework. According to the definition of a risk, E[C] can be described as:

$$\begin{aligned} E[C] &= \sum (P_i \times C_i) \\ &= \sum (P_i \times W_i \times f_{cost}(W_i)) \\ &= \sum (E[W_i] \times f_{cost}(W_i)) \\ &= \sum (E[W_i] \times CATS_{thr}(W_i)) \end{aligned} \tag{21}$$

where Pi , Ci and Wi denote probability of oil spill, costs of oil spill [US$] and weight of oil spilt for a sequence i of an event tree. fcost(W) [US$/ton] denotes a kind of factor or function to convert oil spill weight (Wi [ton]) to a corresponding cost [US$] of oil spill depending on Wi (C [US$] = W[ton] x fcost(W)[US$/ton]). As a function of fcost (W), CATSthr can be considered. However in order to produce costs of oil spill for oil spill weight of W [ton], it might be reasonable to use following function as fcost (W).

$$f_{cost}(W) = \frac{C}{W} = C_0 \cdot W^{a-1} = 35951 \cdot W^{-0.33} \tag{22}$$

Once an event tree is established in FSA study, P_i and W_i are known in each sequence, and therefore $E[W_i]$ can be easily calculated for each sequence. By summing up $E[C_i]$(= $E[W_i]$ x $f_{cost}(W_i)$) for each sequence, E[C] for all the sequences can be calculated. It is noted that an event tree is usually established in Excel file and $E[W_i]$ has already been calculated as shown in MEPC58/INF.2 (described as "PLC" in the table), and that $E[C_i]$ can be calculated effectively and relatively easily by copying the first cell to other cells vertically (See Figure 17).

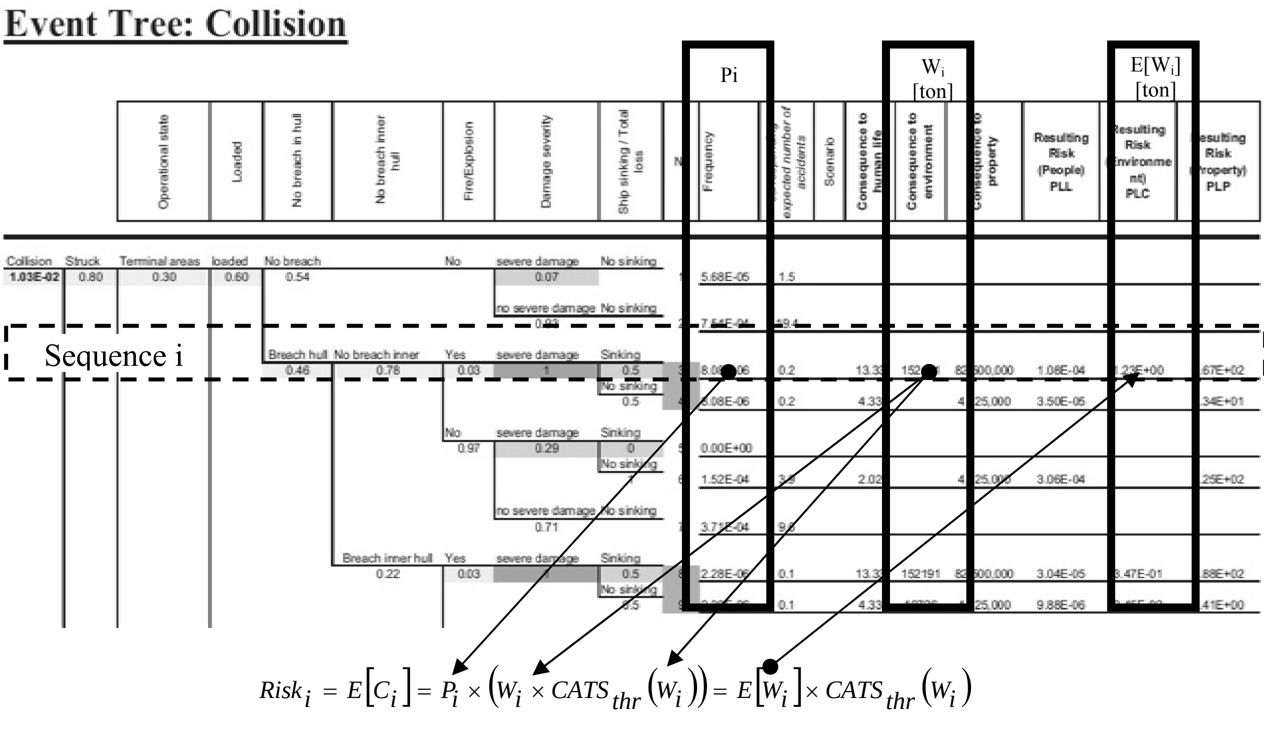

Figure 17: Illustration of application of volume-dependent CATS in relation to an event tree (Event tree is referred from MEPC 58/INF.2, E[Ci] denotes an expected costs[US$] for sequence i. E[C] [US$] can be estimated by summing up E[Ci] for all sequences.)

Applying Eq.(21) into Eq.(20), the formula can be transformed as:

$$\Delta S < \sum \left\{ E\left[W_{org,i}\right] \cdot CATS_{thr}\left(W_{org,i}\right) \right\} - \sum \left\{ E\left[W_{new,i}\right] \cdot CATS_{thr}\left(W_{new,i}\right) \right\} \tag{23}$$

where $E[W_{org,i}]$ and $E[W_{new,i}]$ denote a expected weight of oil spill [ton] for sequence i before RCO is introduced and that after RCO is introduced respectively, which are calculated from an event tree.

If i=1 is considered the formula can be simplified as:

$$\Delta S < E\left[W_{org}\right] \cdot CATS_{thr}\left(W_{org}\right) - E\left[W_{new}\right] \cdot CATS_{thr}\left(W_{new}\right) \tag{24}$$

Eq.(23) can be a promising equation to judge cost-effectiveness of a RCO to prevent oil pollution since this equation is in more general form than the present criteria (Eq.(29)) in the sense that Eq.(23) can be applicable to not only volume dependent CATS but also constant CATS. Moreover it is noted that we could easily and practically calculate Eq. (23) using an event tree which is usually used to carry out FSA studies. Eq.(23) is one of reasonable and practical solutions to use a volume dependent CATS within a framework of FSA.

Equivalency of new criteria and present criteria

Present criteria (Eq.(17)) can be derived as a special case of new criteria (Eq.(23)). In the special case that $CATS_{thr}(W)$ is constant ($=CATS_{thr}$), following formula can be derived.

$$CATS_{thr}\left(W_{org,i}\right) = CATS_{thr}\left(W_{new,i}\right) = CATS_{thr} = const. \tag{25}$$

Substituting Eq. (25) into Eq.(23) the formula can be transformed as:

$$\Delta S < \Sigma \left\{ E\left[W_{org,i}\right] \cdot CATS_{thr} \right\} - \Sigma \left\{ E\left[W_{new,i}\right] \cdot CATS_{thr} \right\} \tag{26}$$

$$\Delta S < CATS_{thr} \cdot \Sigma \left\{ E\left[W_{org,i}\right] - E\left[W_{new,i}\right] \right\} \tag{27}$$

Considering {E[Worg,i]-E[Wnew,i]}ΔW Eq. becomes as:

$$\Delta S < \Delta W \cdot CATS_{thr} \tag{28}$$

where ΔW denotes oil spill risk reduction [ton]. Considering ΔW >0, Eq.(29) is derived and coincides Eq.(17).

$$\frac{\Delta S}{\Delta W} < CATS_{thr} \tag{29}$$

where $CATS_{thr}$ denotes a constant CATS threshold. Therefore it can be said that both criteria is equivalent in the sense that both Eq.(29) and Eq.(23) are derived from Eq.(19). However it is noted that the CATS criteria of Eq.(29) is applicable only to the special case that CATS is a constant value. On the other hand CATS criteria of Eq.(23) can be used for constant CATS as well as volume-dependent CATS, therefore it can be said that CATS criteria of Eq.(23) is a more general criteria.

Conclusion

Within the framework of IMO FSA studies, cost of oil spill, cost of oil spill is investigated using IOPCF data, and cost-effective criteria as well as $CATS_{thr}$ are considered and following conclusion can be achieved. Costs of oil spill from tankers are largely dependent on weight of oil spill. Therefore it is reasonable to use a volume-dependent $CATS_{thr}$ proposed based on IOPCF data.In order to apply volume-dependent $CATS_{thr}$ a new cost-effective criteria for FSA for oil pollution is newly proposed.

It is expected that new criteria can be easily applied to FSA studies of oil pollution although it has not yet been carried out in the present study. The applicability and practicability of new criteria to actual FSA studies would be investigated in the future study.

Acknowledgement

Present research is a part of research project on evaluation methods for environmental standards at the Japan Ship Technology Research Association (JSTRA) funded by Nippon Foundation. The author is grateful to Nippon Foundation and JSTRA for funding and supporting the present research. The author thanks to all the members of the committee of research project as well as to whom it may concern.

Reference:

Etkin, D.S., (2000). “Worldwide analysis of oil spill cleanup cost factors”, Proceedings of 23rd Arctic & Marine Oils pill Program Tech. Seminar.

Friis-Hansen, P. and Ditlevsen, O. (2003). “Nature Preservation Acceptance Model Applied to Tanker Oil Spill Simulations”, Structural Safety, 25, pp.1-34.

IMO (2007), “Consolidated text of the Guidelines for Formal Safety Assessment (FSA) for use in the IMO rule-making process (MSC/Circ.1023−MEPC/Circ.392), MSC 83/INF.2.

IMO (2008), “FORMAL SAFETY ASSESSMENT, FSA – Crude Oil Tankers, Submitted by Denmark”, MEPC58/INF.2

IOPCF (2000). “Annual Report 2000”, International Oil Pollution Compensation Funds.

IOPCF (2007). “Annual Report 2007”, International Oil Pollution Compensation Funds.

Miyazawa (1954), “Theory of modern mathematic statistics”, Kyoritsu shuppan CO., LTD.

Skjong R, Vanem E and Endresen O (2005). “Risk Evaluation Criteria”, Report of SAFEDOR D.4.5.2

Vanem E., Eide, M.S., Gravir, G. and Skjong, R (2007). “Cost-Effectiveness of Preventing Grounding with ECDIS”. Proceedings of PRADS.

Vanem E., Endresen O. and Skjong (2008), R. “Cost-Effectiveness crieteria for marine oil spill preventive measures. Reliability Engineering and System Safety Vol.93, pp1354-1368.

Y.Yamada, 2009, "The Cost of Oil Spills from Tankers in Relation to Weight of Spilled Oil", Marine Technology, Vol. 46, No. 4, pp. 219-228

Incident reporting and continuous improvement: poor utilisation of safety measures in maritime industry

Lappalainen Jouni, Salmi Kim, Kujala Pentti and Tapaninen Ulla

University of Turku - Centre for Maritime Studies/Kotka office;The Aalto University School of Science and Technology

Abstract:
Human errors are considered the most important reason for maritime accidents. The international safety management code (the ISM Code) has been established to clarify the responsibilities of safety on vessels and to cut down the occurrence of human errors by creating a safety-oriented organizational culture for the maritime industry. According to the ISM Code shipping companies are required to report adequately near-misses, hazardous occurrences and other incidents.

An intensive interview study was made within Finnish shipping companies followed by accident analysis. The study consists of two literature studies, statistical analyses, and in-depth interviews which were carried out in 2008 and 2009. In this study, it was discovered that near-misses are not perfectly reported. Mariners are still reluctant to report their mistakes. One of the most common deficiencies in the safety management systems concerns the reporting of the nonconformities and occurrences of accidents.

The poor reporting practises cause further problems. The information about the non-conformities, accidents and hazardous occurrences does not cumulate at any level of the maritime industry. The personnel of the other ships cannot learn from the experiences of the other vessels. There are no possibilities to interchange information about incidents between the vessels. The company cannot utilize the cumulative information when improving its safety performance. Companies do not have the opportunity to learn from other companies' mistakes. The national maritime administrations are powerless in their attempts to develop the maritime safety. The fundamental philosophy of the ISM Code is the philosophy of continuous improvement. The procedures for reporting the incidents and performing the corrective actions are the essential features of the continuous improvement. By developing these processes the probability of maritime accident could be decreased.

Introduction

Background

Human errors are considered the most important reason for maritime accidents. The international safety management code (the ISM Code) has been established to clarify the responsibilities of safety on vessels and to cut down the occurrence of human errors by promoting philosophy of continuous improvement in the maritime industry.

The foundation of the ISM Code was laid in the late 1980s, when numerous fatal accidents had occurred. Particularly the capsizing of the Herald of the Free Enterprise in 1987 awoke broad concern in the maritime community about maritime safety (Anderson 2003). The Herald of Free Enterprise capsized because the bow door was left open without anyone noticing the imminent danger. This was not the first occasion on which such an incident had occurred. Her sister vessel the Pride of Free Enterprise had left the port with the bow door open. Fortunately, the accident was avoided in the case of the Pride of Free Enterprise.

The accident of the Estonia had similar features that the accident of the Herald of Free Enterprise. The fact is that other bow visor failures had occurred even before the Estonia accident (Hänninen 2007). Hänninen supposed that there might have been opportunities to avoid the bow visor failure of the Estonia if an industrial-level system for handling incidents such as bow visor failures had existed. There was no cumulative information about the other bow visor incidents in the industrial level so shipping companies could not learn from the other companies' mistakes. Even national maritime administrations were reported inadequately by the shipping companies.

The lack of safety management system was seen as a reason for the both accidents (Anderson 2003; Hänninen 2007). According to Hänninen there is a lack of risk handling measures and that the risk management systems are underdeveloped in the maritime industry. Due to these deficiencies in the risk management systems, the maritime industry has poor procedures for handling incidents and safety warnings.

The fundamental philosophy of the ISM Code is the philosophy of continuous improvement. Investigating incidents is an integral component the process of continuous improvement in safety management systems. Learning the lessons from incidents should help to improve safety performance since incidents can share the same underlying causes as losses. (IMO 2008b).

According to the ISM Code, the safety management system should be based on the philosophy of continuous improvement. The ISM Code requires that the company should actively improve the skills of personnel and enhance the preparedness for emergencies. In addition, the ISM Code requires that the shipping companies should establish procedures which ensure that non-conformities, accidents and hazardous occurrences are reported to the company. Naturally, the companies should ensure that corrective actions are implemented. (IMO 2008a)

Furthermore, the IMO has emphasised the importance of continuous improvement by providing guidance on near-miss reporting (IMO 2008b). According to the IMO, investigating near-misses is an integral component of continuous improvement in the safety management system.

Purpose and methodology of the study

The research questions of this paper are:

- Are there established and actively working processes for continuous improvement in the maritime industry?

- Can safety and the impact of ISM Code on maritime safety, be measured?

In order to evaluate processes of continuous improvement and whether these processes function properly in Finnish shipping companies, an interview study (Lappalainen and Salmi 2009) was made.

A semi-structured questionnaire was provided in order to examine the research area. The purpose of the questionnaire was to assist the interviewer and serve as a reminder. The interview sessions were structured as discussions. The interviewees were encouraged to express themselves freely in order to find out the most important issues from their point of view. In order to focus on research theme, following type of questions were posed: How are incidents and near-miss situations reported and analysed in your company and how are corrective actions performed? In addition, the designated persons (DP; safety managers of shipping companies required by the ISM Code) were asked about the numbers of reported incidents per year and per vessel. The designated persons were asked about the existence of quantitative targets or indicators, or usage of statistical methods for evaluating the safety performance of the company.

Target group

A total of 94 people were interviewed in this interview study. All those who were interviewed were actively working in the Finnish shipping business. Almost all had a maritime education and maritime working experience. Every person interviewed had worked with the ISM Code based safety management system. Almost all were Finnish citizens.

The seven shipping companies involved in this study comprehensively represent the Finnish maritime industry. All important shipping business areas were represented. 16 ships were visited during the project. These were passenger ships, ROPAX ships and all types of cargo ships. The combined fleet of the shipping companies represents a large proportion of the total Finnish fleet.

The other stakeholder organisations are involved in safety management on a daily basis. They have a comprehensive idea of the current safety culture of the Finnish shipping business due to their close co-operation with Finnish shipping companies and their personnel. Other interest groups that have participated in the study are the Finnish Maritime Administration (FMA), Finnpilot, and the Accident Investigation Board Finland.

A total of 94 interviewees were involved in the interview study (see Table 1. below). The main group of interviewees were active seafarers: masters, deck officers, engineering officers, deck hands and engineering operators, and hotel and catering staff. Whenever it was considered relevant to group the responses of the interviewees, the results were categorised into three groups. These groups were the group of masters, that of officers including deck officers and engineering officers, and that of other crew members, including deck hands, engineering operators, and hotel and catering staff. The anonymity of the maritime personnel could be secured by grouping the results into larger categories. The total number of active seafarers was 62.

Table 1. Table of interviewees

Active Seafarers	
Officers	
Masters	15
Deck officers	21
Engineering officers	10
Crew Members	
Deck hands/eng. Operators	5
Hotel and catering staff	11
Subtotal	**62**
Management (DPA's and top management)	
Maritime working experience	10
No maritime working experience	4
Subtotal	**14**
Other interviewees	
Pilots	4
FMA Maritime Inspectors	8
FMA* (other officers)	4
FAIB*	2
Subtotal	**18**
Total of Interviewees	**94**

Note: * the semi-structured questionnaire was not applied

The management group includes safety managers (DPAs) and managing directors of the shipping companies involved in the study. The management group consisted of 14 interviewees, including both people who have maritime working experience and people who have no maritime working experience. The group with no maritime working experience is small. From that point of view, the overwhelming majority of the interviewees have maritime working experience. Almost all managers have worked at sea and applied the ISM Code in practice. In order to ensure the anonymity of the interviewees, the responses of the DPA's were processed together with other management representatives.

The personnel of vessels under the Finnish flag were mostly Finnish. The personnel of vessels under the Dutch and Gibraltar flag represented various nationalities, such as Russian, Latvian and Filipino. The personnel members who were interviewed were mostly Finnish, including one Estonian citizen.

Eight maritime inspectors of the FMA and four pilots were interviewed. The maritime inspectors of the FMA had conducted external ISM Audits in shipping companies and on vessels. These inspectors were responsible for carrying out the Port State Control inspections of foreign ships visiting Finnish ports. All of the pilots and maritime inspectors who were interviewed had been active seafarers before their engagement in Finnpilot or the FMA. The answers of the pilots were included in the maritime personnel's results due to the small number of interviewees.

Four other officials of the Finnish Maritime Administration and two maritime accident investigators of the Accident Investigation Board were also interviewed. The officials of the FMA provided useful background information about issues relating to the ISM Code. The officials of the FMA and the accident investigators of the AIB were not interviewed using the semi-structured questionnaire (marked * in Table 1.). These interviews were carried out as open discussions.The results of the interviews with representatives of public administration concern the entire maritime sector, not only the shipping companies involved in the research project.

Contents of the paper

This paper is composed of two different approaches to evaluate the impacts of the ISM Code. The state of the process of continuous improvement is evaluated through the qualitative approach which uses the results of interview study focused on the Finnish maritime industry. The quantitative approach is used to evaluate measurably the impact of the ISM-code to Finnish maritime accident frequency and severity. In chapter 2 the problems with incident reporting and continuous improvement is explained in the light of literature studies. The concept of risk is induced as a method to describe safety and the choice of tools for statistical approach is explained in the light of the literature review. In Chapter 3, the subjective view, acquired by the interview study, of seafarers and maritime administration officials concerning incident reporting and continuous improvement, is presented. The state of actual use of statistical tools in Finnish maritime is presented. After the qualitative approach, the quantitative approach using accident statistics is presented. Accident analysis is induced as one of the tools for evaluating risk evolution. At the end the results of both approaches, qualitative and quantitative, are used for conclusions in Chapter 4.

Literature reviews

Impacts of the ISM Code on maritime safety and problems with incident reporting

In order to evaluate the impacts of the ISM Code on maritime safety a literature review of previous studies concerning the ISM Code was made. The literature review showed that the ISM Code has brought a significant contribution to the progress of maritime safety in recent years. Shipping companies and crews are more environmentally friendly and more safety-oriented than 12 years ago. (Lappalainen 2008) Othman (2003) states that most (80%) of Malaysian shipping companies have implemented their safety management systems effectively according to the requirements of the ISM Code. The member states of the Paris MoU conducted a Concentrated Inspection Campaign (CIC) which focused on the effectiveness of the ISM Code. The Paris MoU discovered that most of the shipping companies and crews on vessels understand safety and implement it (Paris MoU 2008). British Maritime and Coastguard Agency (MCA) carried out an assessment of the British fleet in the winter of 2007 - 2008. The basic result of the MCA research was that the shipping industry is a safer and a more environmentally friendly industry than it was 12 years ago when the ISM Code became mandatory. The study indicated that there is a common consensus about the positive contribution of the ISM Code to the maritime safety. (ReportISM 2008) Nevertheless, the direct effect and influence of the ISM Code on maritime safety could not be very well isolated. No quantitative measurement (statistics/hard data) could be found in order to describe the impacts of the ISM Code on maritime safety (Mejia 2001; Anderson 2003; IMO 2005, ReportISM 2008). The studies referred by Lappalainen (2008) show that one of the most serious shortcomings concerns the process of continuous improvement and incident reporting. Several studies have concluded that incidents are not perfectly reported. Mariners are still reluctant to expose their mistakes. In the literature, reporting of non-compliance and deficiencies by the ships' personnel has been seen as a significant indicator of a properly functioning safety culture (Anderson 2003; IMO 2005; Mejia 2001). According to Mejia, willingness to report is an indication of whether the ISM Code is functioning as it should. The main focus of the study by Anderson was to investigate how the incidents, near-misses and other hazardous occurrences were reported. According to Anderson, a properly working reporting process indicates the cycle of continuous improvement in an outstanding manner. Unfortunately, the procedures for incident reporting do not work properly. The Paris MoU (2008a) reported that one of the most common ISM-related deficiencies was the lack of reporting nonconformities, accidents and hazardous occurrences. Also Anderson (2003) discovered that the reporting of incidents was quite insufficient within the seafarers. Especially the minor incidents were not regularly reported. Particularly, Anderson was surprised that most of the seafarers were more or less reluctant to report the incidents. Furthermore, Anderson discovered that in certain cases, further analysis of and corrective actions on the reported incidents were not properly carried out. In this case, the no-blame culture did not prevail. Withington considered the means of measuring the progress of the improvement of the safety management system (Withington 2006). According to Withington, accurate reporting of incidents could provide the fundamental basis for evaluating the effectiveness of the ISM Code. Unfortunately, he recognized that in practice severe insufficiencies in the reporting of the shipping companies can be found, regardless of the requirements of the ISM Code that necessitate establishing a proper reporting system for incidents. The level of the reporting varies significantly between companies, flag States and port States. Withington (2006) noticed that neglected reporting is due to the fear of blame and criticism. Withington was seeking possibilities to a global measurement of the safety progress by utilising data provided by the safety management systems based on the ISM Code.

Literature study on safety measuring

Safety is complicated and subjective matter and thus its measuring is a challenge. To measure the impact of ISM-code, the following statement (Kiuru and Salmi 2009) has to be acknowledged: to do the evaluation of impact of one factor, the whole field of safety with its multiple factors has to be evaluated and for this, the set of appropriate indicators have to be developed.

To reply this demand a statistical approach was initiated with literature study (Jalonen and Salmi 2009) in order to find appropriate measuring methods. The Formal Safety Assessment (FSA) was considered as appropriate frame to approach safety. In FSA, safety can be measured trough evolution of risks.

To evaluate risks all the factors behind them have to be evaluated, this is to say that to be able to count the risks; all the influencing factors have to be measurable. To measure distributing factors of risk a set of corresponding indicators have to be developed.

By investigating the use of indicators in several other industries and traffic forms; such as aviation, nuclear power, off-shore industry and road traffic; following conclusions were made:

- The free flow of correct incident information is the key element of working risk analysis.
- The basic set of indicators can be relatively general, thus some indicators already in use on other industry branches are adoptable to maritime safety.
- The use of LEADING indicators (such as traffic flows and speeds measured with cameras, or the quantity of drunken drivers stopped by the police) should be adapted from road traffic to maritime traffic. This would permit a proactive approach.

The traditional approach to measure risks is to use LAGGING indicators: indicators which can be developed and used after realised accidents. These indicators tell what went wrong and where the safety barriers failed. Presentation of LEADING and LAGGING indicators, illustrated to Reasons "Swiss-cheese" accident model, in Figure 1. (Jalonen and Salmi 2009)

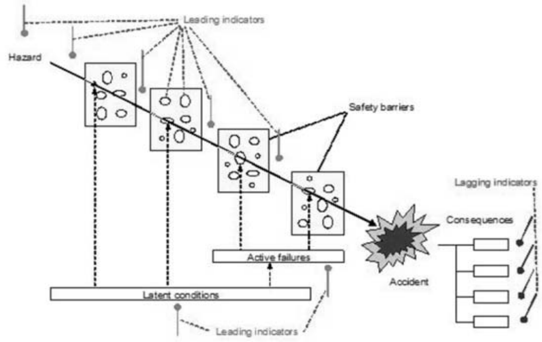

Figure 1: Leading and Lagging safety performance indicators in the context of the "Swiss-cheese" accident model of Reason (1990). (Jalonen and Salmi 2009)

A model of safety can be produced by using together statistics, acquired from leading and lagging indicators. The model has to be monitored also qualitatively to eliminate anomalies introduced by uncertainties in these indicators. These uncertainties may occur for example, due subjectivity if indicators are build on information acquired from human interface.

The interview study and the Use of statistical methods IN safety measuring

The state of the incident reporting in the Finnish maritime industry

In this section, subjective views of seafarers and maritime administration officials concerning incident reporting and continuous improvement will be presented.

In order to evaluate the processes of continuous improvement, questions were posed: How are incidents and near-miss situations reported and analysed in your company, and how are corrective actions performed? In addition, the safety managers were asked about the quantities of reported incidents per year and per vessel. The designated persons were asked about the existence of quantitative targets, indicators or usage of statistical methods for evaluating the safety performance of the company.

The safety managers (DP's) and the masters of the vessels were asked about the number of reported incidents and near-misses per year. The average number of reported incidents and near-misses varied greatly depending on the vessel. Typically, the number of written reports was low; just a few reports per year and per vessel. On some vessels, only 1 to 3 cases were reported per vessel per year. In some vessels, the reported number was as much as 20 – 30 incidents per year per vessel.

The interviewees shared a common opinion that incidents are reported defectively. Regardless of how many incidents were reported per year, the majority of the interviewees hold the view that compliance should be improved in reporting incidents.

Some interviewees (8) considered that over-reporting occurs. According to the interviewees, the reason for over-reporting was a system that rewarded active reporting. These interviewees said that there also have been cases where under-reporting was apparent.

The public administration also considered incident reporting a problem. Four of the maritime inspectors brought up incident reporting. They considered that incident reporting has been poorly applied by the maritime personnel. According to one maritime inspector, the ISM Code has not been successful in that respect. One maritime inspector added that the older seafarers have often neglected to report incidents. According to the inspectors who were interviewed, the ordinary crew members' attitude to incident reporting is poor. The ratings and hotel and catering staff do not report incidents at all.

When executing an ISM Audit in a shipping company, the maritime inspectors go through the reports of internal audits and records of non-conformities, accidents and hazardous situations (incidents). They considered that very few incidents were reported per vessel and per year. One inspector added that it was hard to believe that more situations which should have been reported have not occurred. According to one maritime inspector, alarm bells should start ringing, if no reports on incidents or non-conformities can be found onboard. The inspectors that were interviewed consider that those ships that reported the largest numbers of incident were the safest ones. The large number of reported incident shows that these ships and companies are interested and willing to learn from their mistakes and to develop their operations towards a safer course. The inspectors that were interviewed considered that poor reporting practices were also a problem at the international level. The interviewees said that this does not depended on the nationality of the ship. Their shared opinion of foreign ships was no better than that of ships under the Finnish flag. The maritime inspectors confessed that even the maritime administration itself has been unwilling to report it if something went wrong. Reasons for this unwillingness to report were mentioned. Some (5 answers) interviewees thought that people are ashamed if something goes wrong. One interviewee told the researchers that some masters discourage reporting because they think that nothing should happen on their ship. Especially older seafarers considered that minor incidents should not be reported, as they felt this was bureaucratic. According to some interviewees minor mistakes and all the technical problems are reported (due these problems are wanted to noticed by the management), but mistakes that cause near-accident situations are not reported unless forced by circumstances. Notwithstanding, some interviewees thought that unreported incidents and near-miss situations are discussed onboard. Improvements are made, although written reports do not exist. One maritime inspector also believed that corrective actions have been executed onboard quietly without official reporting. One interviewee added that when a close shipmate makes a mistake, they usually fail to report it. People are reluctant to put blame on their shipmates. However, when a foreign ship has caused a near-miss situation, the report of this incident is much easier to compose. In a case where bonus salaries were based on a safety target (for example target = zero defects of occupational casualties), this could be an obstacle to drawing up an incident report. If the casualty has been minor, the report has often been neglected. Some mariners felt that the concept of incident was not specific. They suggested that the descriptions of non-conformities, accidents and hazardous situations should be clarified and standardised in the maritime industry. Some mariners supposed that the maritime personnel have perceived the significance of incident reporting poorly. In such a case, the negligent person has not understood the positive consequences of reporting incidents for safety.

The analysis of statistical methods of measuring safety in Finnish shipping

The interview study was used to evaluate the present state and methods used for measuring safety in Finnish shipping. The use of quantitative analyses and statistical methods in general for safety purposes greatly varies between the companies studied. In some companies, a highly detailed reporting system regularly feeds information to a databank. This saved information can then be used statistically to evaluate present and future risks and the level of safety. At the other end of the scale, in some companies the statistical approach is seen as futile due to the small number of reports, or statistical information was not found to give added value when a statistical approach was tried. The administration itself is not exploiting potential safety measuring tools in its disposition. An example of this is the incident/violation reporting made by Finnish Maritime Administration VTS-operators, about vessels in their observation areas. The statistical use of information from ISM-audits made by maritime inspectors is also completely neglected. Both of these examples contain information that could produce a set of leading indicators. The attitude towards continuous improvement has developed and can be seen in the way some companies are nowadays using their accident and incident reports for developing safety. The continuous improvement in reporting can be seen to progress in steps, the first of which is the development of efficient reporting methods and routines. The second phase is when responding to reports changes from time-consuming individual analyses to overall analyses of incident types. The final step seen in some of the companies that were interviewed is a statistical approach, where trends are used to estimate risks in advance, making preventive actions possible. Safety managers considered that there is a lack of suitable indicators and felt that such indicators should be developed. According to the interviewees, some quantitative or statistical measures should be developed. The types and causes of non-conformities should be recorded in some manner in order to analyse the phenomenon/data more comprehensively. According to the maritime inspectors, the use of statistical methods is not common in Finnish shipping companies. The inspectors could not name a single shipping company that utilises statistical methods in order to evaluate the progress of safety management. One representative of the public administration considered that quantitative measurement of safety progress is quite difficult. Suitable statistical measures have not been established. One should establish a practical indicator in order to evaluate the progress of safety.Some interviewees discussed the fundamental problems of quantitative measurement. For example, the quantity of incident reports is arguably an indicator. Which option should be preferable: a low rate of reports or a high rate of reports? A lower rate of reports could indicate that the safety level has increased, but it could also indicate poor attention to reporting. Likewise bonus systems based on a quantitative indicator were discussed. On the one hand, the maritime personnel have been rewarded for active reporting of incidents. According to some interviewees, this could cause over–reporting, where insignificant defects are reported. On the other hand, the personnel have been rewarded for zero defects, which could counteract active reporting, especially that of minor incidents or near misses.

Accident analysis as a tool for development of LAGGING indicators

Accident analysis (Kiuru and Salmi 2009) was performed using accident reports made by the Accident Investigation Board of Finland. In this analysis accidents were scrutinized and a set of accident leading factors was induced along with the accident severity factor. These factors were used to evaluate risk levels of individual accident causes as well as the development of risk levels during the period of 1994 to 2008.

Accident leading factors are developed from different causes for accidents. The causes for accidents were sorted to the table of accidents. Then all the causes were weighted based on their impact in arising of the accident. All the accidents were also weighted by their severity. The Analytic Hierarchy Process (AHP) (Saaty 1980) was used for weighting. List of causes in Table 2.

Table 2:. Accident causes

ACCIDENT CAUSES
Tiredness or other human related cause
Co-operation (concerns mainly bridge)
Technical failure
Lack of education
Route planning
Actions and mental resources
Layout / Devices of bridge
Weather
Other ISM related cause (organizational, missing instructions etc.)
Other

The risk appraisal is presented in Figure 2. where both, the "accident leading factor" on horizontal axe and "accident severity factor" on the vertical axe, are equal distributors of the risk.

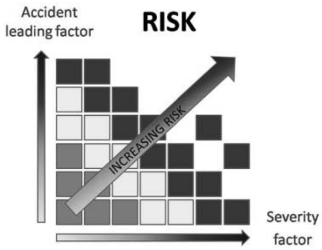

Figure 2:. Risk presented by Accident leading factor and Severity factor

As result from the approach presented in figure 2, the evolution of risk by leading causes can be observed from Table 3 and Figure 3.

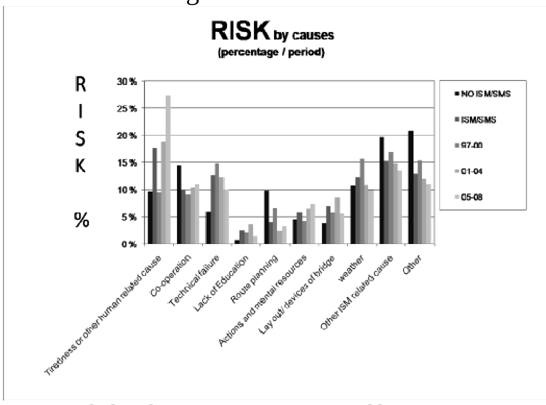

Figure 3:.Risk distribution percentage / period by Cause

Table 3: Risk by accident leading cause

RISK BY ACCIDENT LEADING CAUSE										
	Tiredness or other human related cause	Co-operation	Technical failure	Lack of Education	Route planning	Actions and mental resources	Lay out/ devices of bridge	weather	Other ISM related cause	Other
NO ISM/SMS	5.22	7.81	3.23	0.38	5.32	2.42	2	5.75	10.64	11.23
ISM/SMS	45.76	26.18	32.83	6.65	10.44	15.34	17.99	31.89	39.45	33.46
97-00	8.34	8.01	13.03	1.83	5.78	3.73	5.12	13.9	14.83	13.43
01-04	21.26	11.71	13.91	4	2.79	7.31	9.6	12.14	16.69	13.59
05-08	16.16	6.45	5.89	0.82	1.88	4.3	3.27	5.85	7.92	6.45
Percentage /period										
NO ISM/SMS	9.67 %	14.46 %	5.98 %	0.69 %	9.85 %	4.49 %	3.70 %	10.66 %	19.71 %	20.79 %
ISM/SMS	17.60 %	10.07 %	12.63 %	2.56 %	4.02 %	5.90 %	6.92 %	12.27 %	15.17 %	12.87 %
97-00	9.48 %	9.11 %	14.80 %	2.08 %	6.57 %	4.23 %	5.82 %	15.79 %	16.85 %	15.26 %
01-04	18.81 %	10.37 %	12.31 %	3.54 %	2.47 %	6.47 %	8.50 %	10.75 %	14.77 %	12.02 %
05-08	27.39 %	10.94 %	9.99 %	1.39 %	3.18 %	7.29 %	5.55 %	9.92 %	13.42 %	10.93 %

The distribution of realized risks by leading cause has evolved significantly during the last 15 years:

- Route planning, co-operation and "other ISM related causes" have decreased which could be considered as, and contributed to, the successful implementation of ISM code.
- On the other hand the alarming growth of "Tiredness and other human related causes" could be seen as a failure of ISM, but it could also be interpreted in a more positive way: - The safety culture is improved and thus the accident investigators are finally getting correct information about accident events. (This is also supported by literature estimations about human factor influence on accident deriving)
- Technical failures and "layout / devices of bridge" have increased severely which could be due fast development of technology that have lead to situation where equipment is so complicated, that ordinary seafarer don't understand how they function. This leads to situations were malfunctions of the equipment are not recognised or they are recognised but their use is continued due to the understanding is not adequate to develop a replacing method. The new equipment makes also the work of

safety service personnel, such as the pilots, more challenging. Sometimes pilots have to learn to use new equipment within minutes of boarding the ship: even though pilots job is to “assist the ship crew” in many cases pilot is forced to take the “control” (but not the responsibility) of the vessel to assure its safety.

The evolution of accident leading causes can be used as safety indicators, but when doing this, a broad view has to be used. In this view the influence of change in safety culture has to be taken into account.

The risk data combined with traffic quantities for evaluating the evolution of severity of accidents in Finnish maritime traffic, Figure 4.

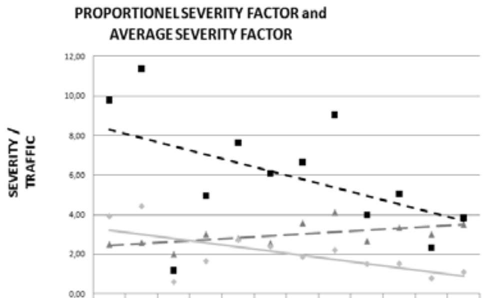

	1997	1998	1999	2000	2001	2002	2003	2004	2005	2006	2007	2008
■ Severity factor (accumulated)*10^4/traffic	9,79	11,38	1,18	4,95	7,64	6,08	6,65	9,05	3,98	5,05	2,32	3,83
▲ Severity factor (yearly average)	2,50	2,57	2,00	3,00	2,80	2,56	3,57	4,11	2,67	3,33	3,00	3,50
◆ (Accidents/Traffic)*10^4	3,92	4,42	0,59	1,65	2,73	2,38	1,86	2,20	1,49	1,51	0,77	1,10

Figure 4: Evolution of accident severity in Finnish maritime traffic

Following conclusions can be made from Figure 4:

- The accident frequency has **decreased** to one third during the observed time period of 1997-2008.
- The total severity of yearly accident has **decreased** to one third during the observed time period of 1997-2008.
- The average severity of accidents has **increased** by one third during the observed time period of 1997-2008.

The lack of near accident reporting in comparison to other incident reporting (information acquired from the interview study) could explain the figure 4: While accident frequency and severity versus quantity of traffic is decreasing the average severity of accident is increasing. This is also an indicator.

Conclusions

According to the IMO, the safety management system should be based on the philosophy of continuous improvement. The investigation of near-misses is an integral component of continuous improvement in the safety management system. (IMO, 2008b).

Several previous studies concerning the impacts of the ISM Code found insufficiencies in the reporting of incidents (Lappalainen, 2008). The findings of our interview study were similar. The study showed that the maritime personnel’s attitudes towards incident reporting were unsatisfactory. The mariners who were interviewed admitted that reporting is often neglected. The low number of reported incidents supports this conclusion. In spite of the fact that some interviewees felt that apparent over reporting has sometimes occurred, the under reporting of incidents is a much more serious problem.

The poor reporting practises cause further problems. Information about non-conformities, accidents and hazardous incidents does not cumulate at any level of the maritime industry. The personnel cannot learn from the experiences of other vessels. There are no possibilities of interchanging information about incidents between the vessels. The company cannot utilize cumulative information to improve its safety performance. Companies do not have the opportunity to learn from the mistakes of others. The national maritime administrations are powerless in their attempts to develop maritime safety.

Hence, there is still room for improvement in the reporting of incidents in the maritime industry. Under these circumstances, a successful cycle of continuous improvement could not function.

The level and evolution of safety in maritime can be measured by using the concept of RISK. The risk can be measured by using multiple indicators and combining the acquired results.

The administration should also present more active approach to incident reporting. The use of different tools such as VTS-operator reports, Port State Control reports, ISM-audit information and accident reports in a combined analysis should give administration a set of indicators to use for safety development. Results of this administrations analysis should also be used by the whole maritime industry to evaluate and develop the use of their own safety indicators.

The accident analysis (Kiuru and Salmi 2009) demonstrated that ISM have had positive impact on accident frequency and accident causes related to ISM, but it also highlighted the non functioning near accident reporting as significant reason behind increasing average severity of accidents.

To conclude measurable impact of ISM to safety of Finnish maritime, the results of interview study and the accident analysis have to be combined with results of future statistical analysis of data gathered from administration and private companies.

Certainly there are also other useful tools for the implementation of continuous improvement. The ISM Code also provides other tools for continuous improvement. These tools include procedures for internal audits and reviews. The functioning of the other tools was not examined in our study. These tools have also not been comprehensively examined in previous studies concerning the IMS Code.

The fact that incident reporting producers have not functioned properly in the maritime industry is a good reason to investigate also other tools for continuous improvement. The suitability and feasibility of the other tools for the purposes of the maritime industry should be investigated in the future.

Nevertheless, mutual activities of the entire maritime community are needed in order to promote the incident reporting as crucial for successful continuous improvement of the maritime safety - for the best of all mariners.

Acknowledgements

This article has been written as a part of the METKU research project that evaluates the impacts of the ISM Code (the International Safety Management Code) on the maritime safety culture in Finland (METKU – Developing Maritime Safety Culture). The project attempts to find the best practices for the shipping companies while improving their operations by implementing and developing their safety management systems.
This project was funded by the European Union and several private partners. The Centre for Maritime studies in the University of Turku and Helsinki University of Technology express its gratitude to the European Community, Regional Council of Päijät-Häme, City of Kotka and all the member companies of the project corporate group.
Writers want to express their gratitude also to all the interviewees and the companies they present.

References

Anderson P. 2003. Cracking the Code – The Relevance of the ISM Code and its impacts on shipping practices. The Nautical Institute. London.

Hänninen H. 2007. Negotiated Risks: the Estonia Accident and the Stream of Bow Visor Failures in the Baltic Ferry Traffic. Helsinki school of economics. Helsinki

IMO 2008a International Safety Management (ISM) Code 2002, International Maritime Organization. Available at: http://www.imo.org/HumanElement/mainframe.asp?topic_id=287

IMO 2008b. MSC-MEPC.7/Circ.7. Guidance on near-miss reporting. International Maritime Organization. London

Jalonen R. and Salmi, K. 2009. Safety Performance Indicators for Maritime Safety Management. Helsinki University of Technology. TKK-AM-9. Espoo

Kiuru H. and Salmi K. 2009. Accident analysis the tool for RISK evaluation. Helsinki University of Technology. TKK-AM-11. Espoo

Lappalainen J. 2008. Transforming Maritime Safety Culture, Publications from the Centre for Maritime Studies. A46/2008. Turku

Lappalainen J and Salmi K. 2009. Safety Culture and Maritime Personnel's Safety Attitudes, Publications from the Centre for Maritime Studies. A48/2009. Turku

Othman M. R. 2003, Effectiveness of Safety Management Systems (SMS) BY Malaysian Shipping Companies in Compliance to the International Safety Management (ISM) Code. Available at:
http://www.ismcode.net/research_projects/wmd_2003_paper.pdf

Paris MoU 2008. Evaluation CIC on ISM in 2007. Paris MoU on Port State Control. Port State Control Committee 41st session. 19-23 May 2008 Loutraki. Greece

Pun K. Yam R. Lewis W. 2003. Safety management system registration in the shipping industry. International Journal of Quality & Reliability Management; Volume 20. Issue 6. 2003

Reason. J. 1990. Human Error, Cambridge University Press, New York

ReportISM. May 2008. Available at: http://www.consultism.co.uk/ReportISM_May_2008_PDF.pdf

Saaty T. 1980. The Analytic Hierarchy Process. McGraw-Hill. New York

Withington S. 2006. ISM – What has been learned from marine accident investigation? Available at: http://www.he-alert.com/documents/published/he00475.pdf

Damage tests of the single shell ship fuel tank with additional elastic protective coating

Janusz Kozak

Gdansk University of Technology Faculty of Ocean Engineering and Ship Technology

Abstract:
Grounding or collision of medium size cargo ship like containership or ferry can lead to pollution of sea environment by fuel released from failured fuel tanks usually single skinned and partially located in double bottom space. Amount of such fuel can be sufficient to destroy sea ecosystem on large scale. In the paper, background of idea of reducing of risk of oil spill from ship fuel tanks is presented. Such idea based upon introduction into tank space additional semi-elastic, polyurethane based fuel resistant layer, supported on passive or active core made of light concrete, to form second barrier protected of fuel spill in case of failure of steel shell. In the paper natural scale laboratory test of the penetration of the single skin as well as coated bottom structure are presented. Test stand, geometry of models and measurements is described. Results of test of two variants of shell covering are discussed and compared.

Introduction

For increase of amount of cargo shipped by sea and associated increase of number of cargo ships, observed in the world fleet for several last years, many sea regions of the world have become more busy and hazardous for navigation. Small closed navigation regions are specially endangered by possible sea disasters. One of them is the Baltic Sea [1]. The high traffic intensity, difficulty in navigation through the straits leading from the North Sea, often occurring bad weather conditions and other factors make that the Baltic is a sea region where many ship accidents occur year by year. The map of particular kinds of the accidents together with indication of places of their occurrence is presented in Fig. 1.

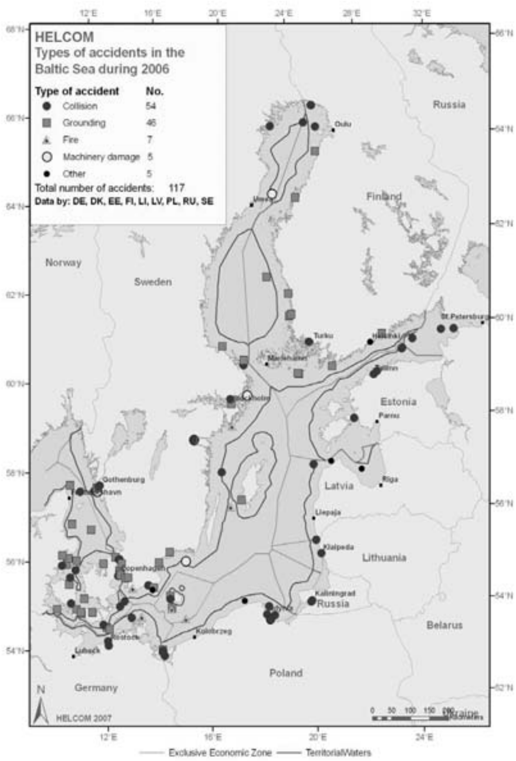

Fig. 1. Type of sea accidents registered with indication of places of their occurrences [2].

In the connection with the increasing risk of ecological disasters associated with sea transport, in the last years the European Union adopted some legal instruments dealing with safety at sea. Only basic design regulations concerning stability and floatability of damaged ships or amount of spill of liquid load from damaged hull are commonly adopted. However in 2004 Germanischer Lloyd (GL) introduced to its rules the notation COLL which determines degree of ship hull resistance (strength) against collisions [3]. The resistance is measured by comparing the strength against impact of strengthened ship side structure with that not strengthened of single plating. The regulations directly concerning collisions are the requirements for ships intended for inland navigation on the Rhine (Switzerland, Germany, the Netherlands), introduced in 2003. The ADNR regulations require to design structural elements of gas tankers as to make them able to absorb the energy of 22 MJ released during collision against ship side structure [4]. The basic philosophy of the approval procedure to compare the critical deformation energy in case of side collision of a strengthened design to that of a reference double hull design complying with the damage stability calculations is presented in the chapter II-1 of SOLAS [5]. Though for cargo tanks of oil cargo tankers the legal requirements have been recently made much more stringent, similar ones for fuel oil tanks are still introduced, nevertheless amount of fuel oil contained in them is often comparable with that of liquid cargo carried by a small tanker. The hazard becomes greater by the fact that most of such tanks are located in double bottom, i.e. in the zone very susceptible to failure both in the case of ship-to-ship collision and the taking of ground or rock. This is also why part of ship hull new regulations has been introduced [6]. One of possible acceptable solution proposed is to minimise theoretical spill of oil in case of accident.

Idea of the semi-elastic fuel tank barrier

For above mentioned reasons a research work was undertaken aimed at elaboration of a way of lowering the risk of releasing protection barrier. The idea of the project consists in adding an internal elastic oil-resisting coating placed inside of the tank on a core material, in such a manner, that in the case of tank plating failure occurring as a result of a collision - tightness of the tank by means of the elastic coating able to be displaced to some distance is fulfilled and thus to prevent against oil spill in emergency, Fig. 2 and Fig 3.

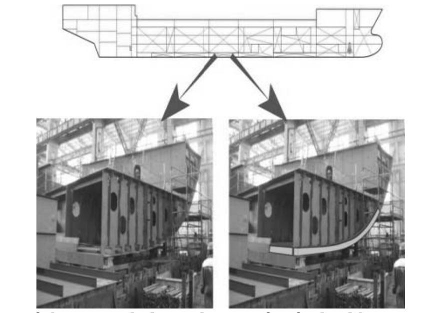

Fig. 2. Idea of the second elastic barrier for fuel oil bottom tank.

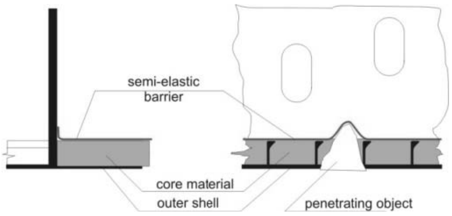

Fig. 3. Behaviour of the second elastic barrier during shell penetration for fuel oil bottom tank.

In order to elaborate such novel solution many problems was investigated including the following:

- elaboration of recipe for an oil resistant plastic material, inexpensive and suitable for coating it inside closed spaces in shipyard's conditions.
- selection of a material for intermediate filling layer,
- elaboration of an engineering process of applying the components of the barrier in industrial conditions with special taking into account difficult places such as corners, bends etc,
- selection of the dimensions of the second barrier components: depth of the filling layer and thickness of the protection coating,
- influence of the additional coating and filling material on corrosion rate of steel structure,
- elaboration of a method for control of state of hidden surfaces,
- making agreement with classification societies as to principles of implementation and use of the novel solution.

The mentioned problems constitute the subject of work carried out in the frame of the research project EUREKA E!3614 „CORET": *"Elastic protection coatings for ship tanks to increase environment protection level"*.

As results of search of recipe for an oil resistant plastic material, inexpensive and suitable for coating it inside closed spaces in shipyard's conditions as well as of selection of a material for intermediate filling layer, the combination of polyurethane coating supported by light concrete core was chosen. To raise adhesion between steel, concrete and polyurethane layers, a special surface treatment was elaborated and tested also. In the same time engineering process of applying the components of the barrier in industrial conditions with special taking into account difficult places such as corners, bends etc, was elaborated.

Natural scale collision tests

For final verification of detail design introduced, the laboratory, natural scale tests of behaviour of new design was planned. It was assumed to compare test results for "classical" (single-skinned) with new, improved structure. As test part of bottom shell of fuel tank of medium scale containership was designated. For real modelling of interaction of body of ship hull, relatively large model was assumed. Due to such reason model of three beams span was selected and clamping both of beams as well as shell plating – as boundary conditions – were introduced. Geometry of the test model, boundary conditions applied as well as loading point is presented in Fig. 4.

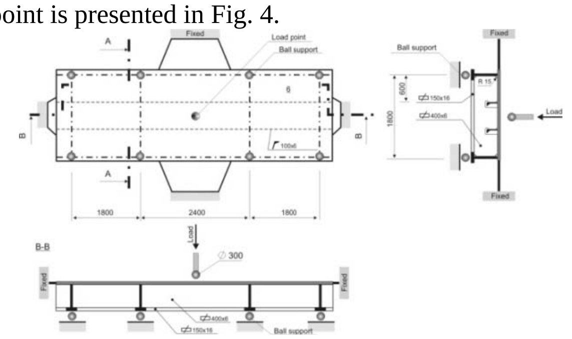

Fig. 4. Model for test with boundary conditions and load application details indicated

The same structure was used for verification of elaborated technology for application on industrial scale of the components of second, semi-elastic barrier. In Fig.5. process of application of the second barrier is shown.

Fig. 5. Preparation of the tested model

To compare effect of applying of the additional protective barrier, two models assumed to be tested: one without any improvements and second with second layer applied.

As model of penetrator ("artificial rock") imitating interaction of the external body, steel ball diameter of 300mm was used. During the test permanent registration of load versus displacement of loading point was performed, and visual checking of presence of cracks in shell plate was done. Additionally for given steps of loaded ball displacements, measurement of transverse deformations of shell plate was made by three methods: geodetic and by electronic displacement transductors in given points as well as by laser scanning techniques.

For test versatile test stand with hydraulic actuator of 1000kN load and 250 mm displacement was used. In Fig.6 test stand with model ready for test is presented.

Fig. 6. Test stand with model ready for test

During the test, penetrator was moved perpendicularly to shell plane with constant speed of 0,1 m/sec, moved by actuator controlled by displacement. After each step of displacement, movement was stopped and procedure of registration of deformations was done. The visual inspection of both sides of shell plate was performed also. During the test, as failure criterion, moment of loosing of leak tightness was assumed. Reaching of such stage was obtained by visual inspection.

Differences in qualitative behaviour of two tested model one can observe in Fig. 7.

(a) (b)

Fig. 7. Way of destruction of tested models: a) single skinned, b) with additional layer.

One can see here, that depth of penetration of external body to moment of loosing of leak tightness for both models differs significantly. Observed and registered depth of penetration for that moment is 7 times higher for model with second, additional layer.

During the preparation of the test, precise calculation with using numerical model under LS-Dyna software was made [7]. The numerical model reflected real model geometry with some simplifications. Due to fact, that the simulation was performed for a load applied to the plate midway between two stiffeners, geometrical details of stiffeners and girders crossings as well as welds were not modelled. The penetrating ball with a diameter of 0.3m was modelled as a rigid body. Boundary conditions of the numerical model corresponded to the real model mounting during the experiment (Fig. 4). Finally a model with a mesh of 18,000 shell elements was used. As a material, a 24-Piecewise Linear Plasticity model from the Ls-Dyna library was used, which includes strain rate effect and failure. During the simulation the internal algorithm ‘Contact_Automatic_Single_Surface‘ was applied. Failure criterion applied assumed, that mesh elements whose strain exceeded rupture strain were automatically removed from the model, and calculations were continued with the eroded mesh [8].

Results of calculation shows very good agreement with test results both if failure picture is analysed – Fig.8, but also when load changes characteristics during the test is compared – Fig.9. However maximum load carrying by structure prior to rupture was 1,25 times higher when estimated by numerical modelling in relation to as measured during the experiment. It shows, how important is correct definition of failure criterion during modelling, what is related with proper obtaining of the critical stress-strain relationship.

(a) (b)

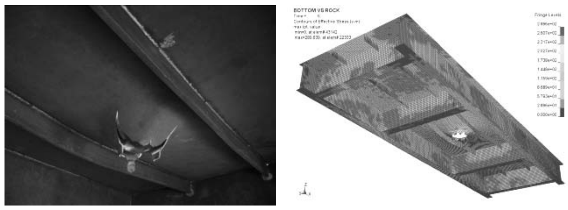

Fig. 8. Comparison of the way of failure: a) tested model; b) numerical results.

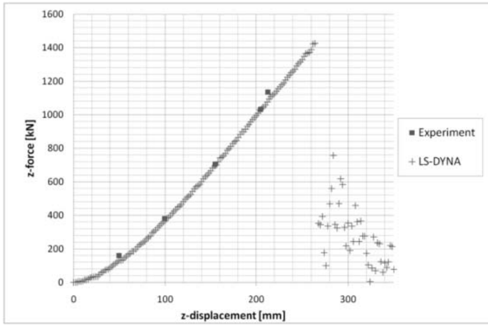

Fig. 9. Relationship between loading force and displacement of loading point during failure process: for tested model and numerical results.

Conclusions:

In the paper, background of idea of reducing of risk of oil spill from ship fuel tanks is presented. Such idea based upon introduction into tank space additional semi-elastic fuel barrier polyurethane based, supported on passive or active core layer made of light concrete. This was the aim of EU-supported EUREKA project CORET. Presented paper is based upon research carried out within frame of the project.

As verification natural scale laboratory test of the penetration of the bottom structure was designed. Test stand, geometry of models, boundary conditions and measurements are described. Results of test of two variants of shell geometry are discussed and compared. It was observed during the test, that registered depth of penetration for moment of loosing of leak tightness is 7 times higher for model with second, additional layer compared to pure metallic shell one.

Due to fact, that results of the numerical modeling are strongly affected by way of modeling (model of material, material parameters, accuracy of meshing, failure criterion etc.), natural scale laboratory test seems to be most credible way for checking of the structure behavior against failure. But preparation and performing of such test is time-consuming and expensive, such test should usually is performed on single or small amount of tested models. From this reason, numerical calculation is the best way for proper preparation of such tests.

References:

Maritime Transport in the Baltic Sea. Draft HELCOM Thematic Assessment in 2006. HELCOM Stakeholder Conference on the Baltic Sea Action Plan Helsinki, Finland, 07.03.2006.

Report on shipping accidents in the Baltic Sea area for the year 2006, HELSINKI COMMISSION, August 2007.

Rules for Classification and Construction I Ship Technology Part-1 Seagoing Ships Chapter 1 Hull Structures Section 33 Strengthening against Collisions, Germanischer Lloyd 1992, Hamburg, Germany

Rules for the Transport of Dangerous Cargo on the Rhine (in German,French and Dutch), http://www.ccr-zkr.org, ADNR 2003.

IMO, SOLAS 2009 MSC 80/24/Add.1 (June 2005)

Resolution MEPC.141(54): Amendments to the Annex of the Protocol of 1978 relating to the International Convention for the Prevention of Pollution from Ships, 1973 (MARPOL 73/78)

Niklas K., Numerical calculations of behavior of ship double-bottom structure during grounding, Polish Maritime Research Special Issue 2008, ISSN 1233-2585.

Sajdak, A.W. (2004), Analyses of Ship Collisions: Determination of Longitudinal Extent of Damage and Penetration, Dissertation of Doctorate of Philosophy in Naval Architecture and Ocean Engineering, 2004

Collision Analysis of Stiffened Plates

Amier AlAli, Yehia Abdel-Nasser and Aly Aliraqi

The Public Authority for Applied Education &Training College of Technological Studies Automotive & Marine Engineering Department

Abstract:
Structural design of ships against collision requires prediction of the extent of damage to stiffened plates subjected to impact. In ship structures, stiffened plates are furnished with vertical or horizontal stiffeners to sustain conventional loads such as shearing, bending and local buckling. The consideration of collision in ship structural design is especially important for tankers where accidents may cause serious environmental pollution. In predicting the extent of collision damage, FE modeling of stiffened plates using ABAQUS software is applied to demonstrate collision scenario. Typical stiffened plates of tankers in service with different configurations of stiffeners are used to examine absorbed energy for each one. The aim of this paper is to select the proper stiffener shape for absorbing more deformation energy. These analyses of stiffened plates will guide ship designers to properly select effective stiffener absorbing higher deformed energy when simulate full scale ship against collision.

Introduction

The serious consequences of ship grounding and collision necessitate the development of structural design and requirements for subdivision to reduce damage and environmental pollution and improve safety. The consideration of the crashworthiness in design is necessary for tankers where accidents may cause serious environmental damage. As Kuwait is a major exporting member of OPEC, and Kuwait's economy depends on crude oil production and other oil products which provide well over 80% of Kuwaiti's national revenues, the transportation of such products is very important to the economy, and as Kuwait Oil Tanker Company (KOTC) is the main carrier for such shipments it is very important to keep the company's vessels in good working condition and reduce probability of collision.

There are two ways in dealing with ship collisions, the first one is to prevent the occurrence of extreme loads and accidents. This can be achieved by using onboard monitoring equipment and well-trained crews. In addition, the surveillance of sea routes, especially in high traffic areas near harbors, channels and offshore structures contributes a lot in minimizing accident occurrence. The second aspect is to increase the absorbed energy of structural components. This is done by developing stiffening systems that may bear damage within the limits of a required safety of the structure and environment.

The International Maritime Organization (IMO) is responsible for regulating the design of oil tankers and other ships to provide for ship safety and environmental protection [1]. Collision analysis models were first developed for analyzing the design of ships transporting nuclear materials. The crashworthiness of these ships under worst case conditions was the primary concern. A totally inelastic, right angle collision with the struck ship at rest was considered the "worst case". The most popular of these approaches is the one proposed by Minorsky [2]. Hutchison generalized the Minorsky method to include all horizontal degrees of freedom (surge, sway, yaw) and hull membrane resistance [3]. The virtual masses of both struck and striking ships were developed in matrix form, including the added mass terms. The computer program DAMAGE can be used to predict structural damage in the different accident scenarios [4]. Pedersen and Zhang derive expressions for absorbed energy uncoupled from internal mechanics [5]. They apply three local coordinate systems to the striking ship, the struck ship and the impact point separately. Since most deformation in collisions is local, instead of modeling the whole struck ship, they developed a collision model for analyzing minor collisions, which are defined as collisions without rupture of cargo boundaries. A similar model is used by Crake and Brown [6]. A simplified collision model (SIMCOL) performs a collision scenario [7]. There are three major ship-to-ship collision classifications: puncture, raking and penetrating. Servis et al and Naar [8] also provide some excellent general guidance. They used LSDYNA to model full-scale collision tests. Their work identifies variable values that provide results consistent with their test results. Paik provides many techniques for modeling crushing of ships experimentally and numerically [9]. Kitamoura O. et al [10], and Lee J.W. et al [11] have developed very large FE element models and compared results with experimental results. In the field of material failure, the selection of material behavior until fracture is important, where this behavior influences the accuracy of non-linear finite element simulation. Ehlers, S. [12] has introduced material relation to assess the crashworthiness of ship structures. In the framework of selecting an efficient FE code for simulating ship collisions, several criteria should be met. These criteria relate to the modeling capabilities for both the internal and the external collision mechanics. In this aspect, the code must be capable of modeling ship motions during and after the collision (external mechanics), as well as the deformation and collapse of the structures (internal mechanics).

Finite Element Analysis

The paper addresses the numerical simulation of impacts on ship structural components by applying FEM. This research work is concerned with the internal deformation of structural components. It aims to know which stiffener arrangement absorbs higher internal energy, when large-scale impact is modeled. The FE simulation of a collision encompasses a number of individual problems, which should be given appropriate attention. These problems are: The selection of a mesh and type of element, which should be fine enough, especially at the contact areas to acquire accurate results and to represent real failure modes during impact. Coarse mesh may apply for areas located far from collision region to reduce CPU time. Other problem such as modeling of the material damage criteria is explained in Refs. [12 and13].

ABAQUS/Explicit Version 6.8-4 code is used to simulate the stiffened panel of a struck ship with different stiffening systems when subjected to accidental load. The stiffened plates are modeled using four nodes, thin shell double curved elements (S4R). The accidental load from a striking ship is simulated by assuming the ship' bow as a V-shape and modeled with rigid elements. This assumption is chosen because we are interested in comparing the effect of the collision on the different stiffened plates with no reference to the striking body. Different configurations of stiffening systems of struck ship are considered. The absorbed energy and contact force for each stiffening system are calculated after damage.

Simulation of Impact on Ship Structural Components

Structural components such as stiffened plates of ship side or bulkheads may be used to investigate the effect of impact on structural behavior. In this work, stiffened plates with vertical stiffeners and horizontal stiffeners are examined. Various FE models for such configurations have been developed. The purpose of these models is to predict the extent of damage observed in real collision and to investigate the effect of the selection of stiffening system on the absorbed internal energy due to collision.

The stiffened panel considered here consists of 3.4x4m plate, stiffened transversely or longitudinally with L-shaped stiffener having scantling of 150x100x9.5mm as shown in Fig.1. and the plate thickness is to be taken 15mm. The material is assumed elastic-plastic of yield strength steel of 340 N/mm^2 with isotropic hardening to a strength of 347 N/mm^2 at plastic strain of 0.025. In this aspect, the damaged response depends on element dimensions so fine mesh is recommended at the region of contact.

Different boundary condition may be selected around edges of stiffened panel and for each boundary condition, result of simulation will change. In this work, the stiffened panel is constrained from all movements along its longitudinal edges (only one rotation in z direction is allowed) while it is free on its ends. This assumption of boundary condition is similar to a real behavior of stiffened panels in ship sides during collision. The striking bow is rigid and free to move in right angle with a translational velocity along the -y-axis equal to 3.6 m/sec. This velocity is applied at the reference point of the bow. Point masses are assumed to model the mass of the ship and the added mass. Virtual mass for the striking ship is acting at the reference point of the striking bow.

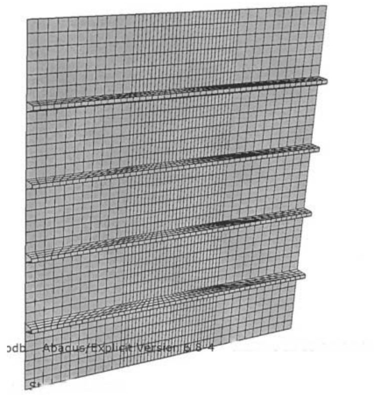

a)Longitudinally stiffened plate

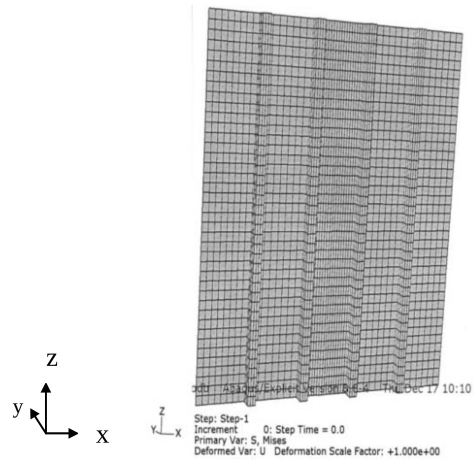

Fig.1b)Transversely stiffened plate

However, this mass is not representing real mass of striking ship, real higher masses will be investigated. The contact surface during collision, elements based surface are applied to define contact region. Middle region of both stiffened panel and rigid bow are considered as surfaces contact. A dynamical explicit analysis at a time 0.25 sec is running.

Collision Analyses of Transversely Stiffened Plates

In the first analysis three configurations of transversely stiffened plates are modeled with L, flat and box stiffeners, in addition to modeling of the smeared plate (T=17.8 mm). Scantlings of stiffeners are determined on the basis of keeping cross sectional area and flexural rigidity for each stiffener are equal to those of L-stiffeners. Four stiffeners with equal frame space are furnished in the stiffened plate. Fig. 2 shows scantlings configuration for the stiffeners.

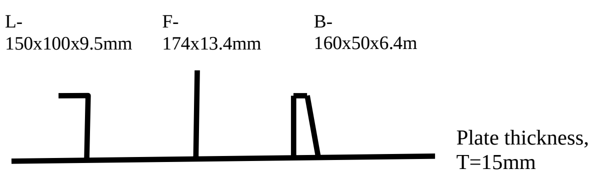

Fig.2 Scantlings of stiffeners

Figure 3 shows deformed shape and internal energy for the analyses of transversely stiffened plates for all configurations. It is noticed that the three stiffened panels absorb small amount of the internal energy till their failure. This is because the stiffeners in the transverse direction have negligible contribution to the impact load. Consequently the panel absorbs small internal energy. In contrast, the smeared plate absorbs higher internal energy. Stiffened plates for three configurations are collapsed at a time about 0.15sec due to plastic deformation. The failure is observed when the stiffness of element of the contact region has reached zero value. The displacement of point at the center of gravity of rigid bow is calculated for all stiffened panels as shown in Fig.4. Almost same values of displacement are observed for the three stiffened plates. Figure 5 shows contact force against time for all configurations. The force-time relationship has same behavior for all configurations. However, the smeared plate shows higher contact force than other stiffened plates.

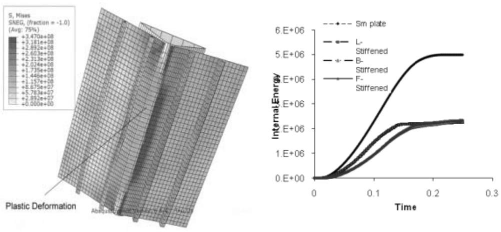

Fig.3 Internal energy –time relationship of a transversally stiffened panel

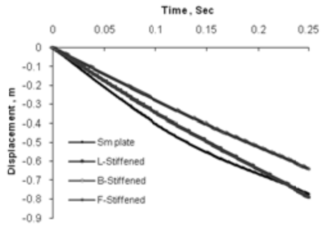

Fig.4 Displacement-Time relationship

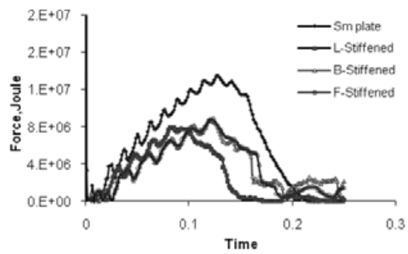

Fig.5 Force-Time relationship

Figure 6 shows effect of mass of striking bow on the internal energy. It is noticed when increasing mass of striking bow; deformed internal energy will slightly increase.

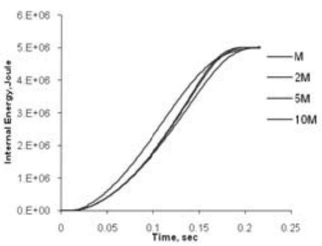

Fig. 6 Effect of mass of striking bow

Collision Analyses of Longitudinally Stiffened Plates

In the second analysis, the stiffened plates are longitudinally stiffened with L, flat and box stiffeners, in addition to the modeling of the smeared plate. As mentioned before scantlings of stiffeners are determined on the basis of keeping area and flexural rigidity are equal to those of L-stiffener. Also, fine mesh for contact elements in the region of collision is applied. Figure 7 shows absorbed internal energy for longitudinally stiffened plates. Small difference is noticed in the absorbed internal energy for all configurations as shown in Fig.7.However, Figure 8 shows higher contact force for smeared plate than other stiffened plates. Stiffened plates furnished with Box or L stiffeners attained similar behavior of contact force.

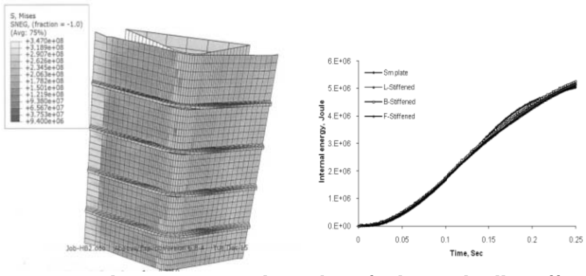

Fig.7 Internal energy –time relationship of a longitudinally stiffened panel

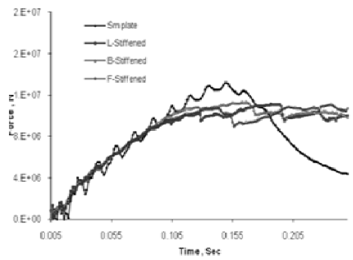

Fig.8 Force-Time relationship

Figure 9 shows penetration displacement of the striking bow into the stiffened plates through period of collision time. Same penetration depth of striking bow is observed for both stiffened plates and the smeared plate .

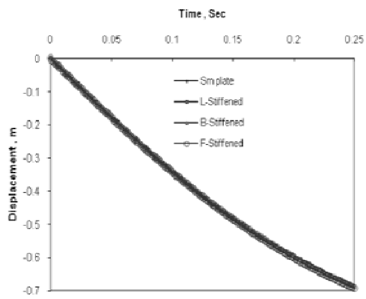

Fig.9 Displacement-Time relationship

Conclusions

The paper refers to the simulation of stiffened plates collisions. The following related aspects are considered to be essential for such a research work:

- The selection of boundary condition to simulate real collision scenario is necessary to investigate failure modes observed in real impact.

- The striking mass is important to generate kinetic energy required to generate deformed energy on struck ship.
- The longitudinally stiffened of the struck ship using different stiffeners configurations shows little difference in the absorbing energy. However, the modeling with smeared plate shows higher contact force.
- The validation of this study have to be executed onto real scale ship.

Acknowledgments

This research is carried out for the part of (research No. TS-08-05) of PAAET (Public Authority for Applied Education & Training, Kuwait). The authors are grateful for PAAET for their financial support.

References:

IMO, 1995, "Interim Guidelines for Approval of Alternative Methods of Design and Construction of Oil Tankers under Regulation 13F(5) of Annex I of MARPOL 73/78", Resolution MEPC.66 (37), September 14.

Minorsky, V.V., 1959 "An Analysis of Ship Collisions with Reference to Protection of Nuclear Power Plants ", Journal of Ship Research.

Hutchison, B.L., 1986, "Barge Collisions, Rammings and Groundings an Engineering Assessment of the Potential for Damage to Radioactive Material Transport Casks", Report No. SAND85-7165 TTC-05212.

Simonsen, B.C.,1999, "Theory and Validation for the DAMAGE Collision Module", Joint MIT Industry Program on Tanker Safety, Report No. 67, June.

Pedersen, P.T. and Zhang, S., 1998. "On Impact Mechanics in Ship Collisions", Marine Structures, Vol. 11, pp. 429-449.

Rawson, C., Crake, K. and Brown, .J., 1998, "Assessing the Environmental Performance of Tankers in Accidental Grounding and Collision", SNAME Transactions 106, 41-58.

Chen, D., 2000, "Simplified Collision Model (SIMCOL)", Dept. of Ocean Engineering, Virginia Tech, Master of Science Thesis, May.

Servis, D. et. al., 2001, "The Implementation of Finite Element Codes for the Simulation of Ship- Ship Collision", 2nd International Conference on Collision and Grounding of Ships, Copenhagen, Denmark, July.

Paik, J.K., 2007, "Practical Techniques for FE Modeling to Simulate Structural Crashworthiness in Ships", Ship and offshore structures, Vol. 2 ,pp 69-80.

Kitamura, O., July, 2001, "FEM Approach to The Simulation of Collision and Grounding Damage", 2nd International Conference on Collision and Grounding of Ships, Copenhagen, Denmark .

Lee J. W., Petershagen, H., Rorup, J., Paik, H. Y. & Yoon, J. H., "Collision Resistance and Fatigue Strength of New Oil Tanker With Advanced Double Hull Structure", Practical Design of Ships and Mobile Units, 1998, Elsevier Science B.V.

Ehlers, S. "Material Relation To Assess The Crashworthiness Of Ship Structures", Doctoral Dissertation, Helsinki University of Technology, Faculty of Engineering and Architecture, Department of Applied Mechanics, Nov.,2009.

Lehmann, E. & Yu, X., 1998," On Ductile Rupture Criteria for Structural Tear in The Case of Ship Collision and Grounding", Practical Design of Ships and Mobile Units, Elsevier Science B.V.

Simulation of Grounding Damage using the Finite Element Method

Anuar AbuBakar[1] and Robert S. Dow[2]

Department of Maritime Technology, University Malaysia Terengganu, Malaysia.[1];School of Marine Science and Technology, Newcastle University, England, UK.2

Abstract:
This paper presents an initial comparison with experimental data on the resistance of stiffened panels to penetration damage. The author's use the finite element method and FEA software to predict the penetration damage and then extend this modelling simulation to investigate the grounding damage to a double bottom structure investigating different grounding scenarios. The progressive failure of the double bottom is investigated considering both, the effect of damage due to plastic deformation of the double bottom and also damage evolution including material rupture. The double bottom structure was modelled using three different levels of complexity, these were: modelling of inner and outer shell plating; modelling of shell plating including longitudinal stiffeners, and modelling of structure including stiffening on longitudinal floors. The analysis was carried out in the ABAQUS explicit code.
The Results presented includes the crushing force as a function of time and also an investigation of the energies involved in plastic deformation and rupture of the double bottom structure.

Introduction

In the past, most of the studies involving collisions and grounding were carried out by a combination of mathematical and experimental approaches. Since the late 90's (Kitamura 2002) the rapid progress of computer technology has made large-scale finite element analysis (FEA) practicable, while further progress in analytical methods has been relatively slow. In order to meet the increasing demands from the shipbuilding industry for reliability and cost-efficiency, FEM approaches are being applied more in the direct quantitative estimation of crashworthiness and also for validation and verification of simplified analytical methods. Although, previous studies have been carried out using either theoretical, experimental and numerical approaches, currently there are a range of different approaches and codes available in the market that are capable of predicting the damage to ships structures during grounding. These approaches include damage modelling such as Forming limit Diagram (FLD) explained by (Keeler and Backofen 1964; Jie, Cheng et al. 2009), Rice-Tracey, and Cockcroft-Latham (RTCL) described in (Alsos and Amdahl 2007; Alsos, Amdahl et al. 2009), Bressan, Williams and Hill (BWH) explained by (Alsos, Hopperstad et al. 2008; Alsos, Amdahl et al. 2009) and many other approaches. In this analysis the forming limit diagram method will be used as material failure model for dynamic loading using properties as described in the material failure section.

The present analysis is divided into two parts: firstly the comparison of numerical and experimental results with (Alsos, Hopperstad et al. 2008; Alsos and Amdahl 2009; Alsos, Amdahl et al. 2009) for penetration of a double bottom structure, secondly extending the analysis to a typical double bottom application using the same material failure model and looking at vertical penetration followed by longitudinal movement along the compartment.

Material properties

The Materials used in this analysis are mild steel (S235JR-EN10025) and high strength steel (S355NH-EN10210) the material properties are describe in table 1 below;

Table 1: The properties of steel are taken from (Alsos and Amdahl 2009; Alsos, Amdahl et al. 2009) and were obtained experimentally.

Material types	K (MPa)	n	ε_{plat}	ε_f	σ_y (MPa)	σ_u (MPa)
S235JR-EN10025 (A)	740	0.24	-	0.35	285	416
S235JR-EN10025 (B)	760	0.225	0.015	0.35	340	442
S355NH-EN10210 (C)	830	0.18	0.01	0.28	390	495

The material is assumed to be isotropic and to exhibit strain hardening properties as described by Ludwik's strain hardening power law;

$$\sigma = K\varepsilon^n$$

To describe the time dependence of the material response, the following true stress-natural strain relation was employed using deformation theory. Where K, m and n are material parameters, where m lies between 0 and 0.05 from (Hutchinson and Neale 1978).

$$\sigma = K\varepsilon^n\ \dot{\varepsilon}^m$$

Hence, the true stress-strain relation is approximated by the equation below assuming isotropic material properties, where ε_{plat} is the plateau strain proposed by (Alsos, Amdahl et al. 2009).

$$\sigma = \begin{cases} \sigma_y if \varepsilon \le \varepsilon_{plat} \\ K(\varepsilon + \varepsilon_0)^n \dot{\varepsilon}^m otherwise \end{cases}$$

and

$$\varepsilon_0 = \left(\frac{\sigma_y}{K}\right)^{1/n} - \varepsilon_{plat}$$

Where a quasi-linear stress-strain relationship described in (Jie, Cheng et al. 2009) can be approximately written as:

$$\dot{\varepsilon} = \left[\frac{\varepsilon}{(m+n)} - s(\sigma,\varepsilon)\right]\frac{\dot{\sigma}}{\sigma} + \left(\frac{\sigma}{K\varepsilon^n}\right)^{1/m}$$

Where:

$s(\sigma,\varepsilon) = \frac{-c\sigma}{\varepsilon^{n/m}}$ and $\dot{\sigma} = E_t \dot{\varepsilon}$ where, E_t is tangent modulus for plastic deformation and C is integration constant, which can be determined from uniaxial testing at various strain rates.

Material Failure

The material failure is based on forming limit diagram (FLD) method which is a concept introduced by (Keeler and Backofen 1964) to determine the amount of deformation that a material can withstand prior to the onset of necking instability. The maximum strains that a sheet material can sustain prior to the onset of necking are referred to as the forming limit strains Abaqus documentation. Considering the forming limit strains including rate-dependant effects in FLD, details of which can be found in (Jie, Cheng et al. 2009) the following relationships are used

$$\varepsilon_1 = \begin{cases} \frac{(m+n)}{1+r_\varepsilon} + \frac{\sqrt{3}(m+n)s(\sigma_{eq},\varepsilon_{eq})}{2\sqrt{1+r_\varepsilon+r_\varepsilon^2}} & if\ r_\varepsilon \le 0 \\ \frac{3r_\varepsilon^2+(m+n)(2+r_\varepsilon)^2}{2(2+r_\varepsilon)(1+r_\varepsilon+r_\varepsilon^2)} + \left(\frac{(m+n)s(\sigma_{eq},\varepsilon_{eq})}{2(2+r_\varepsilon)(1+r_\varepsilon+r_\varepsilon^2)}\right)[(2+r_\varepsilon)\sqrt{3(1+r_\varepsilon+r_\varepsilon^2)}\ \varepsilon_{eq} - 3r_\varepsilon^2\ ] & if\ r_\varepsilon > 0 \end{cases}$$

Where ε_{eq} is the equivalent strain which, for the Von Misses, criterion is $\varepsilon_{eq} = \frac{2}{\sqrt{3}}\varepsilon_1\sqrt{1+r_\varepsilon+r_\varepsilon^2}$

where:$r_\varepsilon = \frac{\varepsilon_2}{\varepsilon_1}$ is strain ratio, $r_\varepsilon = 0$ for plain strain, $r_\varepsilon = -0.5$ for simple tension and $r_\varepsilon = 1$ biaxial tension which is the basis for localised necking failure.

This FLD material failure will be compared with experimental results, RCTL and BWH failure models in predicting the resistance of stiffened panels to penetration damage.

Briefly, the RCTL damage criterion is a combination of modified Rice Tracey and Cockcroft-Latham damage criterion. Both of these functions are based on hydrostatic stress state, express by the stress triaxiality:

$$T = \frac{\sigma_m}{\sigma_{eq}},$$

Where σ_m is the hydrostatic stress and

is hydrostatic stress and σ_{eq} is the equivalent stress

The value of T lies between -1/3 < T < 1/3, damage ceases when T < -1/3 which is referred to as the cut-off value where fracture will not occur below this value. The BWH criterion is based on the onset of local necking as a failure mechanism. The model describes an analytical forming limit curve in stress space and is employed by several authors. Both of these failure models are described in detail in (Alsos and Amdahl 2009; Alsos, Amdahl et al. 2009).

The element characteristic length

The accuracy of FEA analysis results depends upon the mesh density which for material failure and rupture energy dissipation will occur when the material exhibits strain-softening and necking due strain localization. Material failure is normally expressed in terms of stress-strain relationships, see Figure 1a. During loading the material will undergo a damage processes which will follow a damage evolution law where damage will start to initiate at point D=0 and full damage degradation will occur when D reaches at maximum where $D_{max} \le 1$. The equivalent plastic stress and strain at the onset of necking are denoted by σ_{y0}, $\bar{\varepsilon}_0^{pl}$ respectively where $\bar{\sigma}$ is true stress curve in absence of damage or fully plastic condition and σ_0 yield stress. Finally, elements which fail are removed from the model when they satisfy the maximum damage evolution law as $D_{max} \le 1$.

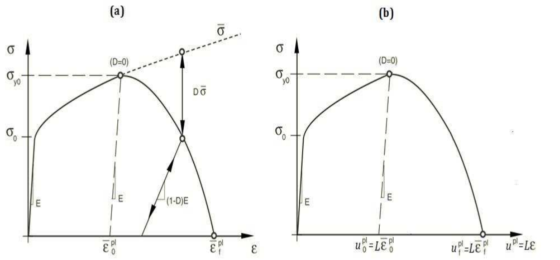

Figure 1: (a) Abaqus documentation-Stress-strain curve with progressive damage degradation. (b) Stress-strain curve with progressive damage degradation dependent on mesh density, (Jeong, Yu et al. 2008).

The available literature comes to no real conclusion about the characteristic element length required for solution accuracy, hence the need for mesh convergence studies e.g. (Wisniewski and Kolakowski 2003; Zhang and Suzuki 2005; Alsos, Amdahl et al. 2009). Abaqus Explicit tries to resolve the problem by introducing an element characteristic length which is related to the element size. Figure 1b shows the damage evolution law embedded with mesh dependency where u^{pl}, is the fracture work conjugate of the yield stress after the onset of damage (work per unit area of the crack), $u_0^{pl}$is damage initiation point, u_f^{pl} is fully degraded material where the elements will be removed from the model and L is mesh element characteristic length. For shell and 2D elements, L is the square root of the integration area and for 3D elements, it is the integration of volume, where $\bar{\varepsilon}_f^{pl}$ is determined from uniaxial tension tests and assumed to be same as ε_f in table 1.

Mesh Convergence Studies

Mesh convergence studies were conducted in order to find the most suitable mesh for using in grounding damage studies for both stiffened panels and double bottom structures. The chosen mesh is always a compromise between accuracy of intended result, computer resources and reasonable computational time. The chosen meshes, as previously stated, were 35mm, 25mm and 15mm. The study found that the best results for the FLD failure model, which give good correlation with the experimental data from (Alsos and Amdahl 2009) which was achieved with a 15mm mesh size, see figures 2a, 2b and 2c.

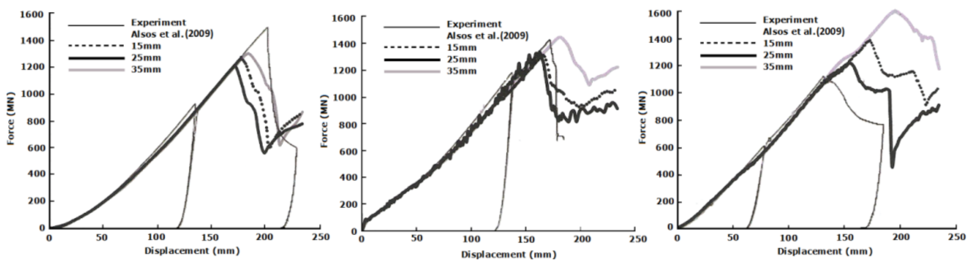

(a) No Stiffener (b) Single Stiffener (c) Two Stiffeners

Figure 2: Mesh Convergence Studies

Although the results shown in figure 2a using a 35mm element size is the best result when compared to the experimental values, overall the 15mm element size is the best when considering all of the simulation results for the different structural models.

On the resistance of stiffened panels to penetration damage

A series of experiment tests were carried out by (Alsos and Amdahl 2009) under quasi-static conditions, which were compared with FEA simulations in reference (Alsos, Amdahl et al. 2009), using both RTCL and BWH damage evolution criterions. The results of (Alsos and Amdahl 2009; Alsos, Amdahl et al. 2009) are shown in Figures 2a, 2b and 2c where they are compared with current FEA analysis using FLD damage failure model. The current FEA simulations use 15mm element mesh size and only require simple damage input parameters, also the results produced are consistent and reliable when compared to the actual experiment results.

The FEA analysis was conducted without consideration of strain rate effect ,which under quasi-static loading conditions, which mean m=0 and s=0 in the above FLD equations expressed in (Jie, Cheng et al. 2009), the FLD failure model then becomes;

$$\varepsilon_1 = \begin{cases} \dfrac{\mathrm{n}}{(1+\mathrm{r}_\varepsilon)} & if\ r_\varepsilon \le 0 \\ \dfrac{3\mathrm{r}_\varepsilon^2 + (2+\mathrm{r}_\varepsilon)^2\mathrm{n}}{2(2+\mathrm{r}_\varepsilon)(1+\mathrm{r}_\varepsilon+\mathrm{r}_\varepsilon^2)} & if\ r_\varepsilon > 0 \end{cases}$$

Stiffened Panel Analysis

The panels identified were manufactured and tested by (Alsos and Amdahl 2009) in order to provide a simulation and analysis of the grounding scenario (see Figure 3a, 3b and 3c). The tests were carried out by laterally forcing an "indenter" to a depth of about 0.25m as shown in Figure 3d into the centre of a plate of size of 720 x 1200 x 5mm made form material Type A from Table1.

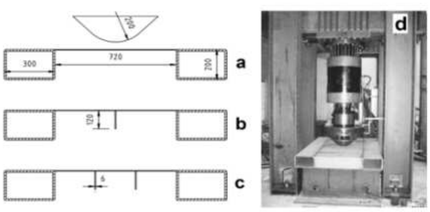

Figure 3: Flat panel, stiffened plate configurations and experimental setup from (Alsos and Amdahl 2009).

The configurations of structure are as below;

a. Penetration of flat panel

b. Penetration on stiffener of single stiffened panel

c. Penetration of stiffened panel between two stiffeners.

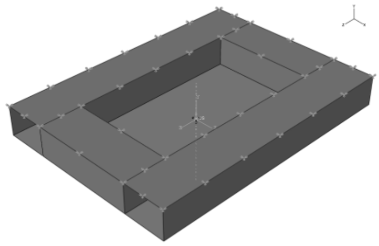

Figure 4: The boundary condition for penetration of stiffened plate and flat panel.

For the stiffened panel cases the plate stiffeners (120 x 6mm flat bars) were made from material Type B from Table 1 and were evenly space as shown in Figures 3b and 3c. The 300 x 200 x 12.5mm hollow square frame supporting the test panels was assumed to be fully fixed as shown in Figure 4. Figure 3d shows the penetration of the "indenter" in the experiment taken from (Alsos and Amdahl 2009). Both the experiment and numerical simulations were carried out under quasi-static conditions.

Finite Element Procedure

The FE analysis was performed using Abaqus explicit with general surface contact and S4R elements. Through thickness integration was carried out using Simpson rule with 5 integrations point through the thickness.

For this problem the load was applied in terms of the lateral displacement of the indenter which is applied at a uniform rate of 0.6m/s. When the speed of application of the load was slower than 2m/s, (Yamada, Endo et al. 2005) or 10m/s, (Ehlers 2009) then there are no significant inertia effects apparent. The penetration depth was set at 0.234 meters and a friction coefficient of 0.3 was used. The analysis didn't take into account strain rate effects therefore the constants *m* and *s* in material properties section will be zero. If required these parameters could be obtain from material tensile tests. The modelling of the material plastic behaviour was carried out using a power law expression previously discussed in material properties section. The relationship between fracture strain and element size is discussed by various authors. (Alsos, Amdahl et al. 2009) using a scaling law included results from uniaxial tensile tests to establish expressions for a predicted value fracture strain of 0.71. (Lehmann and Peschmann 2002) predicted fracture strains of up to 0.25 for 12-20mm thick steel and 0.18-0.30 for steel of thickness 5mm. (Ehlers 2009) predicted fracture strains in the region of 0.50-0.60. For the purposes of this study the fracture strain listed in Table 1 have been adopted. However to investigate the effect of failure strain versus element size mesh convergence studies were run until the FE results gave good agreement with the experimental results. Additionally some further analysis were run with larger values of rupture strain (0.704) in the true stress/strain relationship modelled in ABAQUS. The results for this analysis demonstrated little effect on the local necking and fracture behaviour observed in the analysis. The materials A, B and C were used for flat panels, stiffeners, and frame respectively.

Simulation Results

(a) Unstiffened Flat Panel

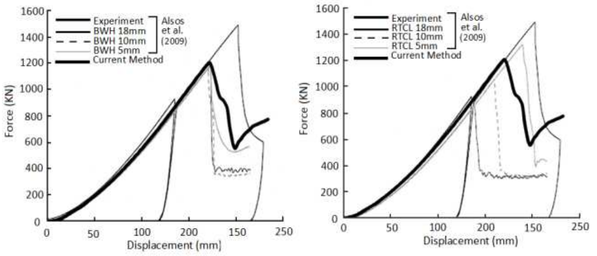

(a) **(b)**

Figure 5: Penetration of flat panel

The results for the penetration of the flat panel using different damage criterion are shown in Figures 5a and 5b, the current method using the FLD damage model coupled with the progressive failure model previously discussed, predicts the rupture at a vertical displacement of the penetrator of 180mm which is higher than that obtained using the BWH and most of RTCL simulations. The BWH failure method predicts the rupture at 175mm which is constant for most of element mesh sizes; the RTCL failure method predicts a scattered rupture at 120, 170 and 190mm for 18mm, 10mm and 5mm mesh size respectively. These predictions compare with 200mm obtained in the experiment. The numerical simulations would appear to give a good prediction of rupture initiation when compared to the experimental result. Figure 8a shows the rupture damage predicted by the FE simulation which compares well with the experimental damage levels for this panel.

(b) Single Stiffened Panel

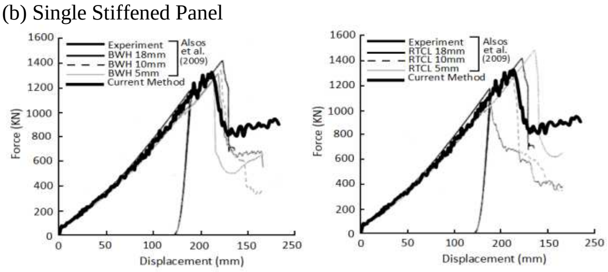

(a) **(b)**

Figure 6: Penetration on stiffener of single stiffened panel

The results for the penetration of a single stiffened panel are shown in Figures. 6a and 6b, where the current simulation predicts rupture at about the same level with both BWH and RTCL failure models. Depending on mesh size, the rupture occurred at about 170mm for current FLD failure method using 15mm mesh and similar results were obtained for BWH and RTCL failure models using 10mm mesh. The simulation using the current FLD method gives good agreement with the experiment leading to the conclusion that a 15mm mesh size is likely to be the most effective mesh size which can be used in this type of simulation, using the progressive damage model described previously. Figure 8b again shows the rupture damage pattern predicted by the FE solution.

(c) Panel with two Stiffeners

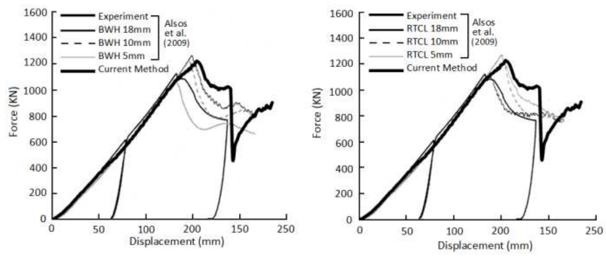

(a) (b)

Figure 7: Penetration of stiffened panel between two stiffeners

Results are shown in Figures 7a and 7b, these show for the case of penetration of a stiffened panel between two stiffeners, graphs of penetrator force vs. displacement comparison for both RTCL and BWH failure models are presented. The RTCL and BWH models always give variable results depending on the mesh size used in the simulations. The figures compare numerical predictions with experiment for both BWH and RTCL failure models using 5mm and 18mm element mesh sizes respectively.

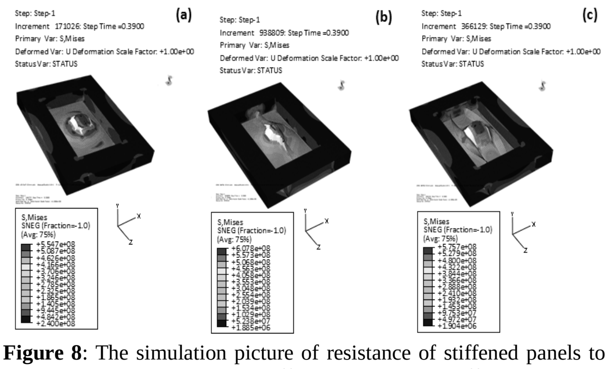

Figure 8: The simulation picture of resistance of stiffened panels to penetration damage: (a) no stiffener, (b) Single stiffener, (c) Two stiffeners

The rupture predicted by the current FLD method, using 15mm element size, occurs at about 162mm penetration which compares well with both the BWH and RTCL for 18mm and 5mm element sizes, respectively. In the current simulation as shown in Figure 8c, the stiffeners seem to be tripping in the opposite direction to that observed in the experiment, this could be because the current simulations fail to consider the effects of welding and HAZ on stiffened panel or it could be caused by slight offsets of in the position that the impactor strikes the plating experimentally.

Discussion

As normal in FEA, accurate results depend on the element type and mesh size, finer meshes normally produce more accurate results. This is because the finer mesh usually gives a better representation of the stress concentrations and also gives a better prediction of the onset of failure. In the current numerical simulations this is not always the case. For the RTCL damage criterion, in almost all the simulations carried out, the finer mesh produces less accurate results than the courser mesh when compared with experiment. The current FLD failure criteria and the BWH criterion produce consistently similar results where finer meshes give better correlation with experimental results as shown in Figures 2a, 2b and 2c. The comparison between numerical simulation and experimental results in this study are obviously valid for the mesh chosen and the material and rupture model used. Much more work needs to be carried out before any conclusion can be made about the applicability to other types of simulation. It is easy for researchers to produce accurate results from numerical simulations when we know the answer we are trying to achieve is known. The mesh density can be varied as well as the modelling parameters until reliable results are achieved. Overall the current method demonstrates good convergence and a good correlation when compared to experimental results. Also, the FLD method requires less complexity of input parameters than some other failure models

Grounding damage of double bottom

The use of FEA on crashworthiness analysis for double bottom structure has been studied by various authors e.g (Amdahl and Kavlie 1992; Naar, Kujala et al. 2002; Zhang and Suzuki 2005) most of them using both course and fine mesh densities to demonstrate convergence of the results. Recently (Samuelidies, Georgios et al. 2007; Zilakos, Toulios et al. 2009) carried out an analysis of a similar structure but using flat bar stiffeners instead angle bar stiffeners on the outer and inner shell of double bottom as used in the current model. The simulation by (Samuelidies, Georgios et al. 2007; Zilakos, Toulios et al. 2009) used von-mises stress failure criteria, which did not account for the rupture failure of the model, instead only looking at the extreme condition of the strength of the structure using fully plastic deformation.

In the current simulation both, von-mises plastic deformation and rupture damage models are considered when investigating both vertical grounding and longitudinal crushing along the compartment. In the vertical grounding simulation all the complexity of the structure and simulation of impact location as mentioned in the previous numerical simulations are considered. For longitudinal crushing only the structure including all inner and outer stiffeners, is considered during the analysis due to the very long simulation times.

Structure geometry

The double bottom structure geometry which has been modelled is an idealised version of a real ship. Its particulars are as follows: LOA 265m, LBP 256m, Beam 42.5m draught 15.65m, GT (ITC 69) 72.449T, and DWT 126.355T. The midship compartment was selected with a length of 32 metres and a beam of 42.5 meters. Nine transverse frames were included with a frame spacing of 4.0 meters being assumed as constant throughout the compartment. The height between outer plating and inner plating is 2.97 metres and spacing between vertical floors ranging from 4.65, 4.98, and 5.81 metres as shown in Figure 9. All structural members are included in the numerical models including: outer plating, inner plating, longitudinal floors, transverses, outer plating stiffeners, inner plating stiffeners and longitudinal floors stiffeners.

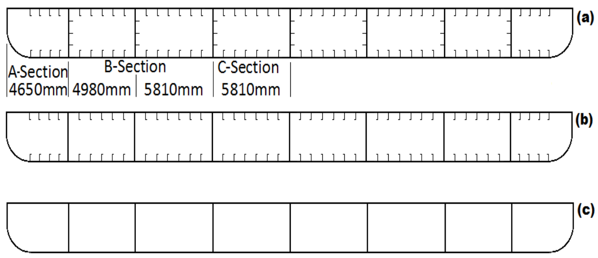

Figure 9: Simplified models of double bottom.

Three alternative FE models were used to carry out the numerical simulations and are shown in Figure 6, these were:

i. Model A: All longitudinal stiffeners included in the model (ALLSI)
ii. Model B: All longitudinal stiffeners included except stiffeners on longitudinal floors (SI)

Model C: No longitudinal stiffeners included (ALLSNI)

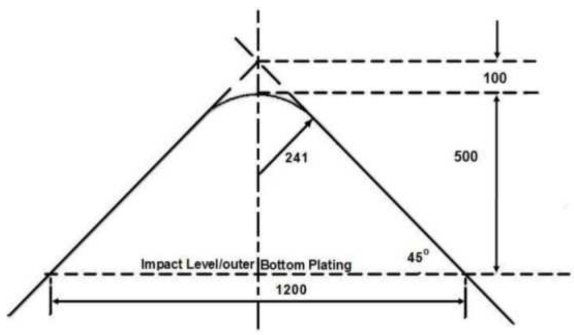

Figure 10: Simplified rock with conical shape from (Zilakos, Toulios et al. 2009)

The details of the model arrangement and thickness of all plating and stiffeners are presented in Figures 9a, 9b and 9c and table 2.The rock geometry model was taken from (Zilakos, Toulios et al. 2009) and is shown in Figure 10.

Numerical approach

A mesh size of 15mm was chosen based on the convergence study carried out in the previous simulation. The structure arrangement and location of crushing impact

Table 2: The thickness of double bottom hull plating

Types of structure member	Material	Thickness (mm)
Floor-1	C	15
Floor-2	C	15
Floor-3	C	15
Floor-4	C	16
Floor-5	C	15
Floor-6	C	15
Floor-7	C	15
A-Section Stiffeners-16 of 400x14mm	C	14
B-Section Stiffeners-44 of 430x15mm	C	15
C-Section Stiffeners-24 of 400x16mm	C	16
Floors stiffeners-21 of 300x14mm	C	14
9 of Transverses	C	17
Inner plate	A	17
Outer plate	A	18

are both taken into consideration during the numerical simulations. The main impact locations considered were: impact on main transverse frame (IoMG) and (IbMG) impact between the main transverse frames as shown in Figure 11.

For all the simulations the friction coefficient was set at 0.3 which is applicable for most cases of mild steel surface contact, the analyses utilised a structured quadrilateral dominated mesh for fine as well as coarse mesh regions and unstructured mesh for the transition region. The speed of the vessel was taken as being a typical ship in service speed of 10m/s or 19.4 knots, and assumed to be constant during grounding simulation. This speed has been used by other researchers, (Samuelidies, Georgios et al. 2007; Zilakos, Toulios et al. 2009) in similar studies.

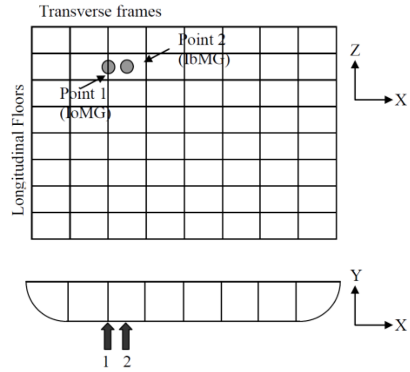

Figure 11: Impact location on Midship compartment (42.5m x 32m)

There are two different phases of impactor movement during these analyses: phase 1 is vertical movement or penetration of the double bottom of 0.5 metre depth in Y-direction, this is followed by phase 2, which is horizontal movement, travelling about 13 meters in Z direction (-ve). Phase 1 will simulate the early stage of rupture which happens during grounding of the double bottom. Phase 2 will simulate the significant damage and rupture which occurs in the structure as the ships momentum moves it forwards.

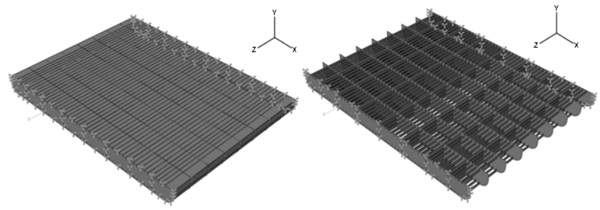

(a) Midship compartment (42.5 x32m) (b) Internal Structure members

Figure 12: Boundary condition set as ECANSTRE in red colour

All the analysis was carried out using a strain based failure criterion as described previously in the material failure model. The boundary conditions were set as ESCANTRE (fully fixed) for both ends of the transverse frames see Figure 12. This was modelled in this way due to the presence of transverse watertight bulkheads at these positions. The analysis was run without considering the strain rate effect due to the lack of uniaxial tensile test data for the material, the effect of this is estimated to be about 2-4% compared to fully static condition (Alsos and Amdahl 2009).

The analysis were carried out by two types of desktop computers which are using single processor Intel Core i7, 12 GB RAM, and dual Intel Xeon E5540, 24GB RAM systems. Most of the analyses generated file sizes ranging from 25-40 GB, running time between 300-360 hrs, and using range of elements between 154229 and 254790 for the complete simulation; this includes vertical penetration and horizontal crushing during grounding. The dual Intel Xeon processor was faster during simulations compared to single processor when the same analysis was run on both machines.

Simulation Results

In this section, the progressive failure of the double bottom will be discussed considering both, the effect of damage due to plastic deformation of the double bottom and also damage evolution including material rupture. In phase 1, the extreme grounding simulation vertical penetration of the double bottom is carried out by looking at force displacement and energy displacement relationships for all models. In phase 2, the main focus is mainly looking at fully plastic deformation and material degradation against time due to grounding, only for model A (ALLSI).

The results for impact on the main floor are shown in Figure 13. Figure 13a, shows that the structure for model C is capable of resisting a higher force and displacement before rupture, followed by model B and then Model A. Material rupture takes place at 0.30m, 0.32m and 0.45m of penetration for models A, B and C respectively. The figure also indicates the significant effect of modelling stiffeners and their contribution to the failure during impact.

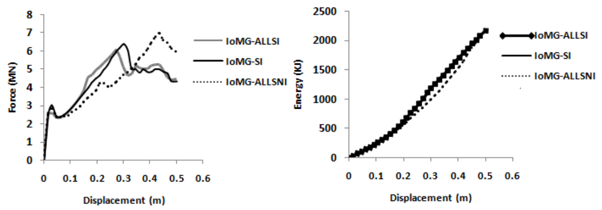

(a) Force Penetrator Displacement (b) Energy Penetrator Displacement

Figure 13: Impact on Main Floor

This shows that the stiffness of the structure plays an important part in the onset of rupture, a more rigid structure will give less crashworthiness capability compared to more flexible structure from the point of view of hull rupture. Looking at Figure 13b, we can see that the energy absorbed by the structure is of a similar magnitude for all three models. The model without any longitudinal stiffeners, Model C, slightly deviates from models A and B, but ends up at same point at 0.5m of displacement and 2.2MJ crushing energy.

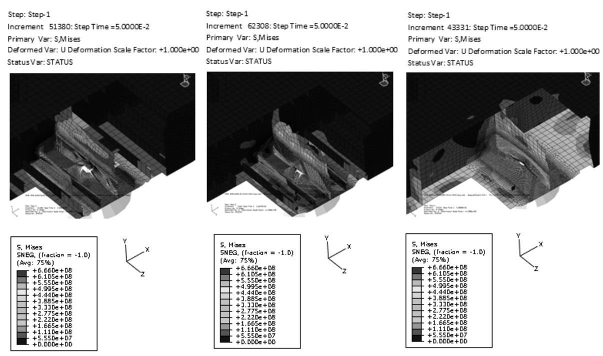

(a) Model A (b) Model B (c) Model C

Figure 14: Phase 1-The simulation picture of vertical grounding displacement for model impact on main floor.

The response of the models to vertical grounding on the main transverse floor is shown in Figures 14a, 14b and 14c, these clearly show that damage starts to occur on the bottom plating during grounding due to the large local deformation and strain being generated by the penetrator.

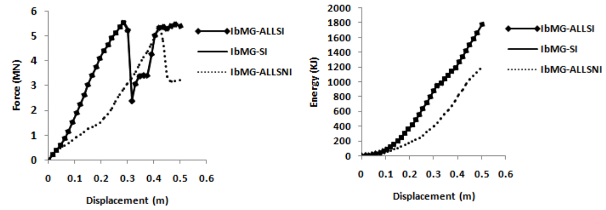

(a) Force - Penetrator Displacement (b) Energy - Penetrator Displacement

Figure 15: Impact between Main Floors

The forces generated during phase 1 grounding between the main transverse floors are shown in Figure 15a for model A and B, and are almost identical, rupture occurring at 0.31m vertical displacement and 5.6MN maximum force. This indicates that stiffeners on the main longitudinal floor do not appear to contribute significantly to the strength to the structure for this phase of grounding. But, when all the stiffeners on the structure are removed the penetrator is able to cause greater deformation of the structure before rupture initiates, rupture occurring at 0.44m vertical displacement. Figure 15b shows a similar pattern, where the energy for model A and B are the same giving 1.78MJ at a vertical displacement of 0.5m. The energy for model C is a lower than for models A and B giving 1.20 MJ at the same displacement.

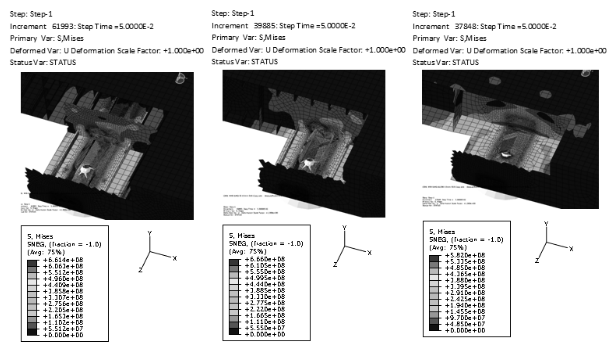

(a) Model A (b) Model B (c) Model C

Figure 16: Phase 1-The simulation picture of vertical grounding displacement for model impact between main floors.

The behaviour of the structure during the simulations are show in Figure 16a, 16b and 16c, where model A and B again behave in the same manner and show similar rupture propagation tendencies. For model C the rupture pattern displays similar patterns to that shown in the simplified experiment carried out by (Alsos and Amdahl 2009).The depth of penetration and subsequent grounding damage has been chosen is to consistent with the result of (Samuelidies, Georgios et al. 2007; Zilakos, Toulios et al. 2009), since this is part of the same study.

Phase 2: Horizontal Crushing during grounding

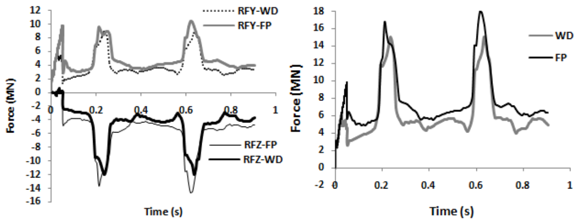

(a) The grounding force in Y and Z direction (b) The resultant force.

Figure 17: Impact on Main Floor

The next stage in the simulation is to investigate horizontal crushing of the double bottom after rupture due to the forward momentum of the ship. Both Figures 17a and 17b show the grounding force on the double bottom for the midship compartment. Both figures also show, the fully plastic (FP) force which would be obtained if the simulation had been carried out without modelling material failure, this demonstrates that higher forces are produced for this simulation than when material damage (rupture) (WD) modelling is included in the simulation. In Figure 17a we can see that, the maximum grounding force during crushing of the transverse floors are: RFY: 10.4MN, RFZ: -14.6MN, for fully plastic, and RFY: 8.74MN, RFZ: -12MN and when material failure properties are included.

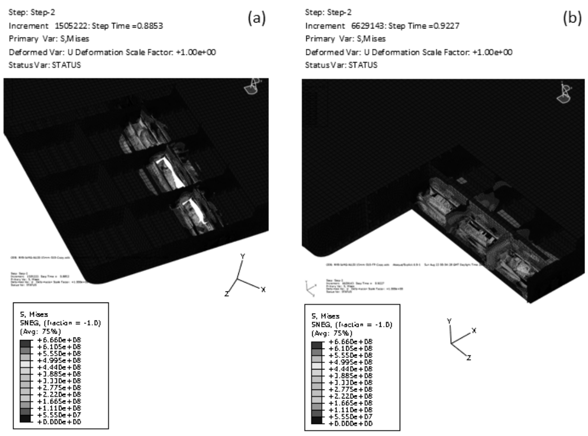

Figure 18: Impact on Main Floor (a) With damage (b) without damage

When we look at the resultant crushing force on the double bottom as shown in Figure 17b, the grounding force when neglecting material failure (rupture) (FP) is always higher than when we include material rupture (WD). The difference between them is estimated at about 15-50%, the peak forces for phase 1 and phase 2 are 9.69MN, 17.96MN and 6.18MN, 15.01MN for FP and WD failure models respectively. The performance of the structure, for both conditions, can be seen clearly in Figures 18a and 18b. In Figure 18a, tearing of plate during grounding due to high stress concentrations which occur at the joint of plate between floor and bottom plate can be observed. In Figure 18b, the elements display only stretching without showing any tearing or rupture.

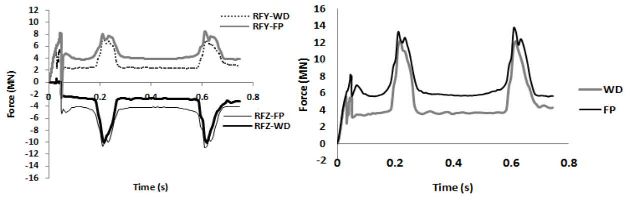

(a) The grounding force in Y and Z direction (b) The resultant force.

Figure 19: Impact between Main Floors

Figure 19 shows the response of the structure when the grounding occurs between the main transverse floors followed by longitudinal tearing of the structure. The same behaviour as before is shown in Figure 19a and 19b, where a larger force is generated without modelling rupture of the structure (FP) than when rupture ((WD) is modelled.

The different between FP and WD failure modelling produces differences in the force in the range of 11-40% for both. In Figure 19a, RFY and RFZ forces peak at 8.47MN and -10.84MN respectively for FP, and, 6.86MN, -10MN respectively for WD. The resultant force for phase 1 and phase 2 maximums, shown in Figure 17b, are 8.2MN, 13.76MN and 5.54MN, 12.22MN for FP and WD respectively.

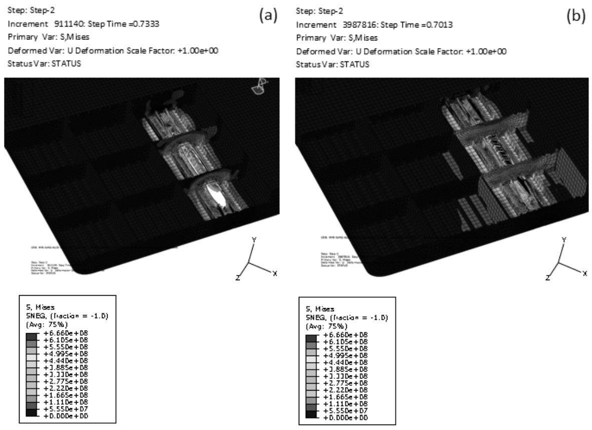

Figure 20: Impact between Main Floors, (a) With damage (b) without damage

The failure mechanisms of the structure are clearly shown in Figures 20a and 20b. Figure 20a, shows the failure of the structure during grounding and the plate tearing close to longitudinal stiffeners. Figure 20b, shows the bottom plate elements stretching in a middle of span between longitudinal bottom plate stiffeners without any rupture.

Discussion

In this analysis it has been demonstrated that more rigid structure is less crashworthy than more flexible structure when considering hull rupture. This phenomena clearly shown in Phase 1 of the simulation, where the penetration of the indenter shows higher displacements before initiation of rupture when comparing model C with models A and B. This simulation also showed that not modelling rupture (FP) always produces higher failure loads than when rupture is modelled (WD), where simulations demonstrate higher results by about 30-50% for Phase 1 and 11-35% for Phase 2.

The results in Phase 2 also show good correlation when compared to (Zilakos, Toulios et al. 2009) where, the maximum force for RFY-FP and RFZ-FP during crushing of the transverse floors demonstrates an almost constant level of force throughout the simulation irrespective of the number of transverse floors. The results obtained for RFY-FP and RFZ-FP simulations are also higher than (Zilakos, Toulios et al. 2009), which is reasonable due to higher plastic material properties being used, (Zilakos, Toulios et al. 2009) used 245MPa as the material yield stress where the current model is using properties as defined in Table1. The analysis also found that estimated onset of material rupture in Phase 1 is very sensitive to the material failure model adopted, compared to phase 2. The differences between fully plastic and material failure models in Phase 1 clearly show significant differences as mention above. It has also been demonstrated that the effect of grounding is very localised in all simulations this can be seen by observing the localisation of high stress contours which only occur in the area close to the impact location.

Conclusion

The purpose of this analysis was to investigate and understand the behaviour of the double bottom structure during grounding. This is a very complex process and computational calculations are dependent on mesh size, types of loading, crushing location, boundary conditions and the software that is being used in the analysis. Although many papers have been published on this topic, there still exists considerable variability in the results that still require a significant amount of discussion and explanation with regard to the accuracy and reliability of results.

Nevertheless, FEA is an appropriate tool which can be used to investigate the local and global behaviour of a ship structure during grounding. Overall numerical simulations are cheaper to run than experimental studies, but there is still a significant requirement to carry out good quality experimental studies. Results from good quality experiments are necessary for validating numerical simulation models for predicting the structural response during collisions and grounding. Comparisons between experiment and numerical modelling studies will help establish suitable numerical models for carrying out future assessments of collision and grounding scenarios.

Overall the results obtained from the FEA simulations of penetration are acceptable when compared to the actual experiments. The grounding simulation also showed good correlation with previous published results (Samuelidies, Georgios et al. 2007; Zilakos, Toulios et al. 2009) where the comparisons of the penetration force gave very close correlation.

Acknowledgements

This work has been partially performed within the context of the Network of Excellence on Marine Structures (MARSTRUCT) partially funded by the European Union through the Growth Programme under contract TNE3-CT-2003-506141.

Reference:

Alsos, H. S. and J. Amdahl 2007. On the resistance of tanker bottom structures during stranding. Marine Structures 20(4): 218-237.

Alsos, H. S. and J. Amdahl 2009. On the resistance to penetration of stiffened plates, Part I - Experiments. International Journal of Impact Engineering 36(6): 799-807.

Alsos, H. S., J. Amdahl, and O. S. Hopperstad. 2009. On the resistance to penetration of stiffened plates, Part II: Numerical analysis. International Journal of Impact Engineering 36(7): 875-887.

Alsos, H. S., O. S. Hopperstad, R. Tornqvist and J. Amdahl. 2008. Analytical and numerical analysis of sheet metal instability using a stress based criterion. International Journal of Solids and Structures 45(7-8): 2042-2055.

Amdahl, J. and D. Kavlie 1992. Experimental and numerical simulation of double hull stranding. DNV-MIT Workshop on Mechanics of Ship Collision and Grounding.

Ehlers, S. 2009. A procedure to optimize ship side structures for crashworthiness. Engineering for the maritime environment. J. Engineering for the Maritime Environment 224: 1-11.

Hutchinson, J. W. and K. W. Neale 1978. Sheet necking-III. Strain-rate effects Mechanics of Sheet Metal Forming: 269-285.

Jeong, D. Y., H. Yu, J. E. Gordon and H. Tang. 2008. Finite Element Analysis of Unnotched Charpy Impact Tests. Materials Science and Technology Conference and Exhibition, MS and T'08 1: pp. 579-590

Jie, M., C. H. Cheng, L. C. Chan and C. L. Chow. 2009. Forming limit diagrams of strain-rate-dependent sheet metals. International Journal of Mechanical Sciences 51(4): 269-275.

Keeler, S. P. and W. A. Backofen 1964. Plastic Instability and Fracture in Sheets Stretched over Rigid Punches. ASM Transactions Quarterly 56: 25–48.

Kitamura, O. 2002. FEM approach to the simulation of collision and grounding damage. Marine Structures 15(4-5): 403-428.

Lehmann, E. and J. Peschmann 2002. Energy absorption by the steel structure of ships in the event of collisions. Marine Structures 15(4-5): 429-441.

Naar, H., P. Kujala, B. C. Simonsen and H. Ludolphy. 2002. Comparison of the crashworthiness of various bottom and side structures. Marine Structures 15 (4-5): 443-460

Samuelidies, M. S., V. Georgios, M. Toulios and R. Dow. 2007. Simulation of the behaviour of double bottoms subjected to grounding actions. 4th International conference on collision and grounding of ships. Hamburg, Germany.

Wisniewski, K. and P. Kolakowski 2003. The effect of selected parameters on ship collision results by dynamic FE simulations. Finite Elements in Analysis and Design 39(10): 985-1006.

Yamada, Y., H. Endo, and P. T. Pedersen. 2005. Numerical study on the effect of buffer bow structure in ship-ship collision. Proceedings of the International Offshore and Polar Engineering Conference. Seoul, Korea.

Zhang, A. and K. Suzuki 2005. Numerical simulation the bottom structure grounding test by LS-DYNA. 5th European LS-DYNA Users Conference. Birmingham, Birmingham.

Zilakos, I., M. Toulios, M. Samuelides, T. H. Nguyen and J. Amdahl. 2009. Simulation of the response of double bottoms under grounding actions using finite elements. Proceedings of MARSTRUCT 2009, 2nd International Conference on Marine Structures-Analysis and Design of Marine Structures.

The strength characteristics of different types of double hull structures in collision

Chen-Far Hung, Kun-Ping Wu and Yun-Tzu Huang

Department of Engineering Science and Ocean Engineering, National Taiwan University

Abstract
Metal sandwich panels have the advantage of weight-strength efficiency. The advanced fabrication technology is continuously under developing. In this paper the strength characteristic of five different types of double hull structures and one conventional single hull structure struck by conical body were examined. The buckling load and the crashworthiness between them were compared. Some mechanical behaviors in the damage process during impact were discussed. Five different types of double hull structures investigated here are (1) the honeycomb type, (2) the lattice-core type, (3) the flat plate core type, (4) The X-type core type and (5) The Y-type core double hull. For comparison purpose the investigated structures are designed to keep about the same dimensions and overall stiffness characteristics. The damaged states, buckling load, the reaction force and the energy dissipation of different types of structures struck by a solid conical body were analyzed by non-linear FE-method.

Intrudction

Although the velocity of ship motion is not very fast, the huge ship mass possesses enormous momentum and kinetic energy. During the collision the kinetic energy will redistributed in short time, portion of kinetic energy of striking ship will be transferred to struck vessel, and the velocity of striking ship will be reduced very quickly and it also induces very high impact loading between two colliding vessels, and may cause serious damage on striking vessel and struck structures. The catastrophe of oil pollutions on the sea may take place consequently. In order to prevent the calamity induced by ship collision and grounding the double hull and mid-deck design concepts were requested to avoid the oil escaping from tank while the ship hull was struck since last 20 years. The impact force of ship structures subjected to collision and grounding became an important issue; and numerous researches about the crashworthiness were carried out in different approach, e.g. theoretical, experimental, and numerical approaches (Jones and Jouri 1987; Pedersen et al 1993; Pedersen and Zhang 2000; Wang 2000; Kitamura 2002; Lehmann and Peschmann 2002). The large scale experiments for ship collision and grounding are very expensive, and it was performed only in some special projects used as benchmarks for other researches (Rodd 1996; Wevers and Vredevelt 1999, Ehler et al 2008).

The sandwich structure has superiority over the traditional stiffened plates structures in uniformly distributed stiffness, and have the advantage of light weight (Wadely et al 2003), and anti-shock performance (Fleck and Deshpande 2004). It has been applied to ship and offshore structures, e.g. deck, double shell, double bottom, and also applied to anti-shock or anti-blast structures (Xue and Hutchinson 2004; Rathbun et al 2006). The advanced fabrication technology are continuously under developments (Wadely et al 2003; Kolsters and Wennhage, 2009), and different types of core structures have been examined, e.g. honeycomb panel by Rathbun et al 2006, pyramid core by Chiras et al 2002 and Zok et al 2004. The research approaches to the strength problems for metal sandwich structures can be categorized into theoretical study, derivation of approximate method, and experiments. Most of the theoretical study has specific assumptions; its results were verified by experiments.

Due to the progress of laser welding technology and the improvement of its investment advantage in past years, the European ship industries attach great importance to the application of advanced laser welded steel sandwich structures.

The impact responses of marine structures subjected to under water explosion or blast load becomes an interesting topic in past years, the anti-blast sandwich panel design concepts examined by different field may be considered as possible application for marine structures (Xue and Hutchinson 2004; McShane et al 2006)

The damages of double hull structures during collision can be classified into four fundamental damage modes, which are the stretching mode, the tearing mode and the penetration mode of plates, as well as the denting mode for single girder and crossing girders. The simplified formulae for approximation of energy dissipation and impact force of four fundamental damage modes were derived (Pedersen and Zhang 2000; Wang 2000; Hung and Chen 2007; Yamada and Pedersen 2008). The overall energy dissipation and impact force of a stuck double-hull structures can be estimated by assembly of these fundamental failure mechanisms (Hung and Chen 2007, Paik and Seo 2007). The damage states of double-hull structures analyzed by nonlinear FEM become a principle approach in past years.

This paper investigated the strength, deformation and crashworthiness of five different types of double hull structures subjected to low speed impact; for comparison purpose the impact analysis of a stiffened plate structures was performed. The different type of structures shown in Figure 1 was examined in this paper; comparison of strength and crashworthiness between them were carried out. Figures 1(a) and 1(b) have been used for light structures and figures 1(c) to 1(e) are possibly used for ship and offshore structures.

Investigated model of different types of sandiwish structures

Model

This paper investigated lattice core panel examined by McShane (2005), the honeycomb core panel examined by Paik(1999), the X-plate core, Y-plate core and flat plate core double hull structures examined by Klanac et al (2005) shown in figure 1.

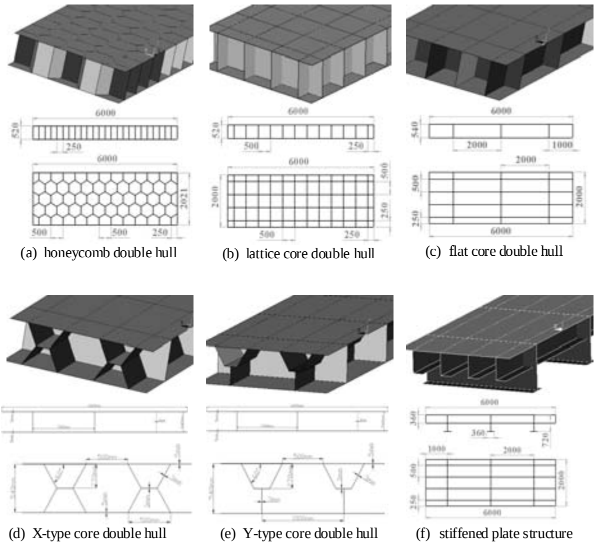
(a) honeycomb double hull (b) lattice core double hull (c) flat core double hull
(d) X-type core double hull (e) Y-type core double hull (f) stiffened plate structure

Figure 1 Different type of structures (dimension in mm).

The plate thickness of each model is shown in the lower part of each sub-figures and also listed in Table 1. The analysis domain of each model is length x breadth = 6m x 4m. The stiffened plate with girder structure was selected as reference for comparison. About the same global moment of inertia was set for each model, and the mass and depth of each model has difference, shown in table 1. The thickness of the top and bottom plate for each double hull structures and stiffened plate is 5mm.

Table 1. Plate thickness of different type of structures

structure type	double hull					girder + stiffened plate	
component	honeycomb	lattice-core	flat-core	x-core	y-core		Thickness (mm)
plate thickness(mm)	5	5	5	5	5	top plate	5
core plate thickness(mm)	3.5	3.5	3.5	3	3	stiffener	web: 5 flange: 10
web thickness (mm)	-	-	4	4	4	girder web	5
						girder flange	9
Depth (mm)	520	520	540	540	540		720
overall I (mm^4)	4.53E+9	4.53E+9	4.53E+9	4.53E+9	4.53E+9		4.54E+9
mass (kg)	1606	1630	1402	1451	1352		1770

The boundary conditions were specified as shown in figure 2(a); two opposite sides are symmetrical boundary conditions to represent the un-supported sides, the another two are considered as one constrained side to simulate the support of bulkheads, the other is symmetrical condition.

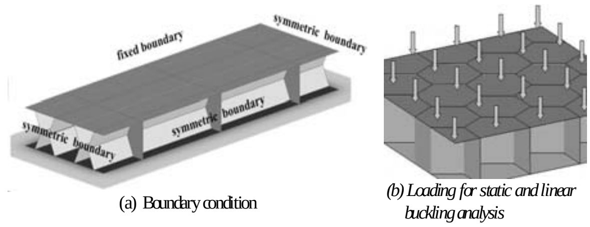

(a) Boundary condition (b) Loading for static and linear buckling analysis

Figure 2 Boundary and loading conditions for FE-analysis.

The material constants of steel are listed in Table 2. The Belytschko-Tsay shell element is used for the FE-model of the double hull and stiffened plate structures; the element size in this paper was set as 50mm. The effect of stain rate on yield strength is modeled using the Cowper and Symonds strain rate model (1957).

$$\frac{\sigma_0'}{\sigma_0} = 1 + \left(\frac{\dot{\varepsilon}}{D}\right)^{1/n}$$

where $\dot{\varepsilon}$ = strain rate, σ_0' = dynamical yield stress, σ_0 = static yield stress, D and n are the strain rate parameters and taken as 40.4sec^{-1} and 5, respectively.

Table 2. The material constants of steel

Young's modulus	210 GPa
density	7860 kg/m^3
yield stress	300 MPa
tangent modulus	355 MPa
rupture strain	0.34
ultimate strength	420 MPa
friction coefficient	0.2
Poisson's ratio	0.3
Strain rate parameters	n=4, D=40.4

Analysis items

The following analyses were performed in this paper.

1. Static analysis: 1kN/m^2 uniformly distributed load was applied on top plate of each model to examine their global stiffness and relative stress levels, and then their yield loading was determined.
2. Linear buckling analysis: The buckling loads of different structures under uniformly distributed load applied on top plate were examined.
3. Impact analysis: The top plate was struck by a steel conical body with 45^o half conic angle and with a sphere head of 200mm diameter. The crashworthiness of each structure was evaluated.

Results of static analysis

The static analysis was performed with ANSYS code. 1kN/m^2 uniformly distributed load was applied on the top plate of each model as shown in figure 2(a). The distribution of equivalent stress on the top plate for honeycomb, lattice core and flat core type double hull structures are shown in figure 3.

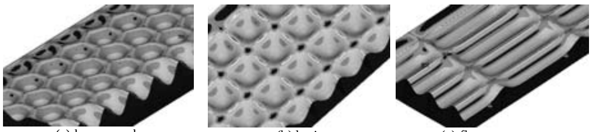

Figure 3 Distribution of equivalent stress on top plate of different type of structures.

Distributions of equivalent stress on the top plate for other three structures are similar to lattice core type. The maximum stress of top plate for honeycomb and lattice core type appeared at both longitudinal and transverse core supports, for other four types structures appeared at core supports. The maximum von Miese's stress at the connection of plate to core for different types of structures is shown in Table 3.

Table 3 Results of static analysis for different structural types

structural type	uniformly distributed loading = 1kN/m^2			yield loading (kN/m^2)
	max. displacement (mm)		max. von Mises stress (MPa)	
	top plate	lower plate		
honey comb	0.0699	0.0114	3.85	77.9
lattice core	0.0446	0.0112	2.75	109.1
Flat core	0.103	0.0358	4.49	66.8
X-type core	0.104	0.034	4.54	66.1
Y-type core	0.111	0.0323	4.55	65.9
stiffened plate	0.0936	0.0197	4.43	67.7

The honeycomb and lattice core type has the smaller stress level due to uniformly distributed plate panels; the other four types have about the same stress levels. The yield stress of steel used in this investigation was 300MPa; and the uniformly distributed load applied on top plate to cause the maximum stress to achieve yield stress is termed as yield loading. The right column of table 3 shows the yield loading of six different types of structures. The maximum displacement at bottom plate shows the global deformation of each structure, the honeycomb and lattice core type double hulls have relative smaller deflections, i.e. their global stiffness is higher than others.

Results of linear buckling analysis

The linear buckling analysis was performed with ANSYS code. The loading was applied on the top plate as the static analysis shown in figure 2(b). The buckling load of first four modes for different type of structures is shown in Table 4.

Table 4. The buckling load for different type of structures

structural type	Buckling load (kN/m^2)			
	mode 1	mode 2	mode 3	mode 4
honeycomb	300.25	304.84	313.86	328.92
lattice core	257.35	257.36	257.38	257.41
Flat core	101.99	101.99	101.99	112.42
X-type core	125.17	125.17	125.17	129.15
Y-type core	88.231	88.237	88.251	105.22
stiffened plate	201.46	201.57	201.66	253.99

Figure 4 shows the shape of first mode of each structural model. The first buckling mode for honeycomb is a coupling deformed shape of plat and core plate and has the highest buckling load. For other four types of double hull structures the mode shape appeared in web plate. The lattice core type has smaller web panel and its buckling loading is higher than other three types. The Y-type core has larger web panel, and has lower buckling load. The mode shape of stiffened plate structure appeared on the coupling deformation of webplate and flange of girders.

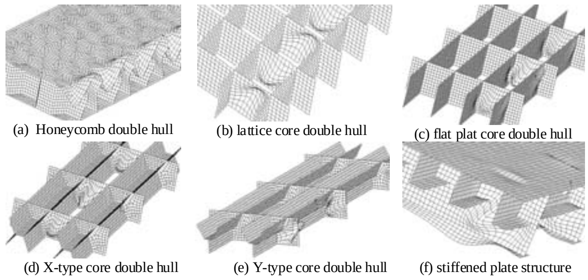

Figure 4 Deformed shape of first mode for different types of structures.

Results of impact analysis

The top plate was struck by a conical body with 45^o half conic angle. The conical body contains a spherical impact head with 200mm diameter shown in figure 5(a). The conical body was specified as a steel solid body with very high density (1000 times of steel density) to simulate a striking body with about 1000tons mass, which dropped with initial velocity of 6m/s, i.e. the initial kinetic energy is about 16MJ. The Impact analysis was performed with LS/DYNA code, and the analysis of impact duration was set for 0.3 second. Two impact conditions were taken into consideration:

Case A: The conical body strikes on the center of top plate panel shown in figure 7(b), the damage started from plate stretch mode.

Case B: The conical body strikes on the top of girder center shown in figure 7(c), the damage started from dent mode of webs, the top plate and the web were ruptured simultaneously.

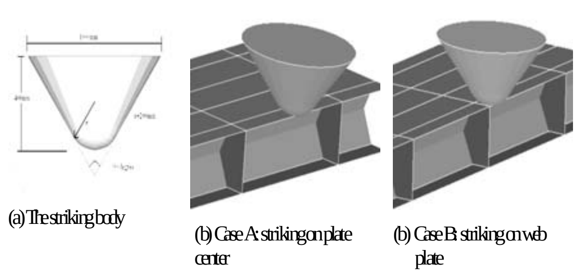

Figure 5 The striking solid body and striking points for impact analysis.

Figure 6 shows the damage states of honeycomb, lattice-core, Y-type core double hull and the stiffened plate structures under case A when top plate began to rupture. In the lower four subfigures the top plate was removed to display the damage states of core and web plates as well as stiffeners. The damage modes of honeycomb and lattice core plate are plate denting. The damage modes of Y-type core and stiffener plate are the combined mode of core plate (or stiffener) denting and webplate buckling.

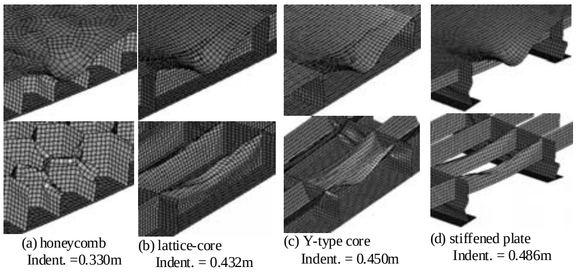

Figure 6 The damage states of different type of structures under Case A when the top plate began to rupture**.**

The damage state of flat plate core and X-type core structures are similar to Y-type core structure, therefore they were not shown in this figure. Figure 7 represents the damaged states of core, web and bottom plate of honeycomb, lattice-core, Y-type core and X-type core double hull structures under case A when the bottom plates started to rupture. The damage states of lattice core double are similar to honeycombs.

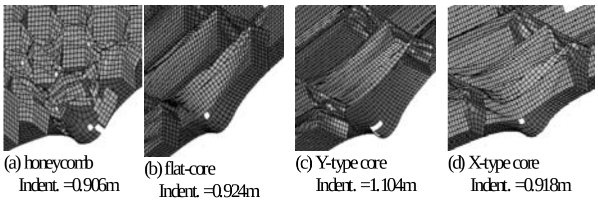

Figure 7 The damage states of different type of structures under Case A when the bottom plate began to rupture.

Similar damage states of different type of structures under case B are shown in figure 8 and figure 9.

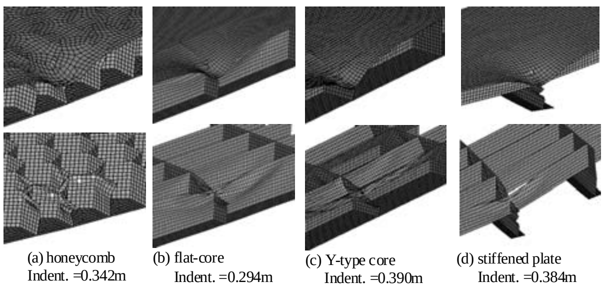

Figure 8 The damage states of different type of structures under Case B when the top plate began to rupture.

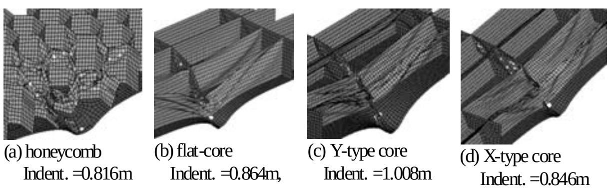

Figure 9 The damage states of different type of structures under Case B when the bottom plate began to rupture.

The calculated reaction force and energy dissipation of different types of structures when the top plate and bottom plate began to ruptured are listed in Table 5.

Table 5 Comparison of the results of impact analysis between different types of structures

impact case	Case A						Case B					
structural type	top plate ruptured			bottom plate ruptured			top plate ruptured			bottom plate ruptured		
	I	R	E	I	R	E	I	R	E	I	R	E
honey comb	0.330	2205	303	0.906	4474	1335	0.342	2125	339	0.816	4160	1147
lattice core	0.324	2121	329	0.918	4950	1490	0.270	1823	210	0.822	3877	1081
flat core	0.432	1715	345	0.924	3477	1022	0.294	1460	210	0.864	3302	1016
X-type core	0.432	1713	323	0.918	3454	1017	0.360	1818	308	0.846	3382	992
Y-type core	0.450	1532	358	1.104	3416	1516	0.390	1644	339	1.008	3566	1335
Stiffened plate	0.486	3289	801	--	--	--	0.384	2768	614	--	--	--

Note: I = Indentation (m), R = total reaction force (kN), E = energy dissipation (kJ)

The reaction force and energy dissipation of different type of structures versus displacement of striking body (or indentation depth of structures) for Case A and Case B are shown in figure 10 figure 11, respectively.

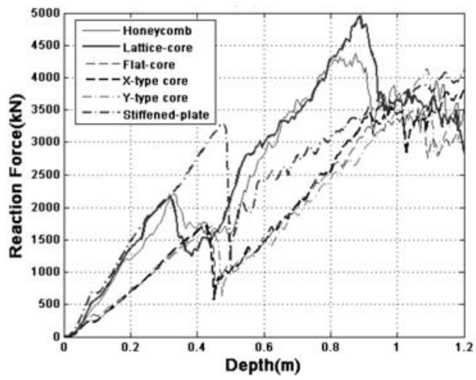

(a) Case A: striking point at plate center

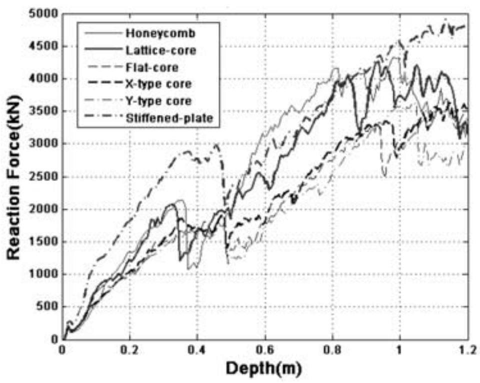

(b) Case B: striking point at top of webplate

Figure 10 Total reaction force of six different types of structures vs. indentation depth.

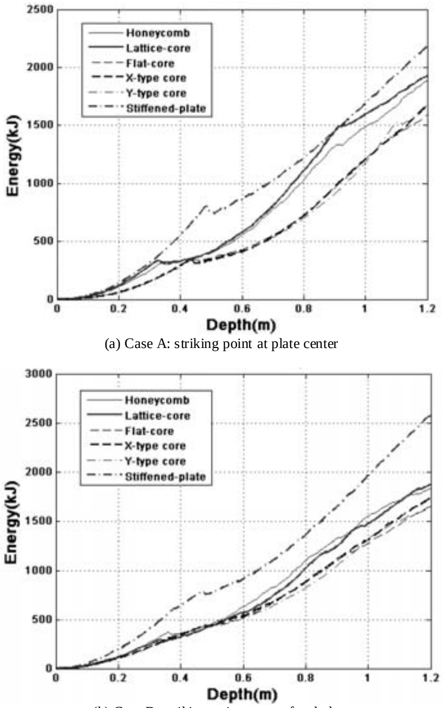

(a) Case A: striking point at plate center

(b) Case B: striking point at top of webplate

Figure 11 Eenergy dissipation of six different types of structures vs. indentation depth

From the results of figure 6 to figure 11 and Table 5, following points can be summarized:

a. Top plate ruptured under Case A: The first rupture of top plate appears at core support and the support core plates were also buckled. The honeycomb and lattice core type double hull have higher stiffness and buckling load; they possess higher total reaction forces and lower indentation depth than other structures when the top plate started to rupture. The damage mode of stiffened plate structure is the denting stiffener combined with buckling of girder, its indentation depth and energy dissipation are higher than other structures.

b. Bottom plate ruptured under Case A: When the bottom plate began to rupture, the core plates of the honeycomb and lattice core type double hull were broken before rupture of bottom plate; for other three double hulls the core plate were buckled without broken. The Y-type core double hull had higher indentation depth and energy dissipation than others.

c. Top plate ruptured under Case B: the first rupture of top plate appear at core support and the support core plates were dent simultaneously. The honeycomb and lattice core type double hull have no significant higher stiffness and buckling load for crossed support plate. In stiffened plate, the dent of girder top combines with its lower part buckling; its total reaction force and energy dissipation are higher than other structures.

d. Bottom plate ruptured under Case B: similar to CASE A.

e. Crashworthiness of struck structures depends on the arrangement of core structure and its correlated damaged modes. Different damaged mode possesses different level of reaction force and energy dissipation.

The results show that the variation of indentation, the reaction force and the energy dissipation for Case A and Case B differed between different types of structures.

Although the stiffened plate structure has higher reaction force and energy dissipation combined with higher indentation when the top plate started to rupture, the single hull ship will be flooded when the hull plate is damaged. The double hull structure provides an additional protection, and has higher reserved reaction force and energy dissipation correlated with higher indentation until bottom plate ruptured.

The honeycomb and lattice core type double hulls have higher global stiffness and also higher reaction force; The Y-type core double hull has relative flexible in reaction force, and has higher energy dissipation and higher indentation when bottom plate is ruptured.

Conclusions

This study performed static and impact response analysis for five different types of double hull and one stiffened plate structures by nonlinear FE-analysis, which were designed to have about the same global stiffness. Based on the results, the following conclusions are drawn:

1. For the same static loading, the honeycomb and lattice core type double hulls have higher global stiffness and also have smaller stress level and displacement; the other four structures have almost the same stress level. The flat-core, X-type core and Y-type core structures are relative more flexible, and have also higher displacement responses. Comparison studies of the indentation depth, the reaction force and the energy dissipation between the stiffer and more flexible structures before rupture of hull plate in ship collision will be the important issues for design of ship hull to reduce the damage of structures and its consequent catastrophe of environmental pollutions.
2. The honeycomb and lattice core type double hulls have higher buckling load; the X-type core and Y-type core double hull have relative larger web panel, and have lower buckling load. The stiffened plate structure has higher buckling load than flat core, X-type core and Y-type core double hulls.
3. Before the top plate ruptured, the damage mode of stiffened plate structure showed the web plate of girder was dented combined buckling of lower part of girder, its reaction force and energy dissipation are higher than the double hulls, the double hull structure provides an additional protection, and has higher reserved reaction force and energy dissipation correlated with higher indentation until bottom plate ruptured.

4. The Y-type core double hull is relative more flexible during the collision, and has higher indentation depth and energy dissipation before the bottom plate began to rupture.
5. The double structure has superiority over the traditional stiffened plate structures with deep girder not only in uniformly distributed stiffness, smaller depth, and lighter weight. Although the stiffened plate structure has higher reaction force and energy dissipation than double hull structures when top plate damaged; nevertheless, the double hulls provides an additional protection, and has higher reserved reaction force and energy dissipation correlated with higher indentation depth until the bottom plate ruptured.

Acknowledgements

The authors would like to acknowledge that this work was supported by the National Science Council of ROC under grant NSC96-2221-E-002-307-MY3.

References

Chiras S, Mumm DR, Evans AG, Wicks N, Hutchinson JW, Dharmasena K, Wadley HNG, Fichter S. 2002. The structural performance of near-optimized truss core panels. Int. J. of Solids and Structure. 39(15):4093–4115.

Cowper GR, Symonds PS. 1957. Strain hardening and strain rate effects in the impact loading of cantilever beams, Brown University Division of Applied Mathematics Report. No 28.

Ehlers S, Broekhuijsen J, Alsos H S, Biehl F and Tabri K. 2008. Simulating the collision response of ship side structures: A failure criteria benchmark study. International Shipbuilding Progress. 55(1-2):127–144.

Fleck NA, Deshpande VS. 2004, The resistance of clamped sandwich beams to shock loading. J Appl Mech. 71:386-401.

Hung CF, Chen CP. 2007. [Approximate method to predicate the crashworthiness of ship double hull structures]. (in Chinese) J. Taiwan SNAME. 26(3):139-150.

Jones N, Jouri WS. 1987. A Study of Plate Tearing for ship Collision and Grounding Damage, Journal of Ship Research. 31(4):253-268.

Kitamura O. 2002. FEM approach to the simulation of collision and grounding damage. Marine Structures 15(4-5):403-428.

Klanac A, Ehlers S, Tabri K, Rudan S, Broekhuijsen J. 2005. Qualitative design assessment of crashworthy structures. In Int. Congress of international Maritime Association of the Mediterranean (IMAM), Lisboa, Portugal. 26-30, September 2005.

Kolsters H, Wennhage P. 2009. Optimisation of laser-welded sandwich panels with multiple design constraints. Marine Structures 22(2):154–171.

Lehmann E, Peschmann J. 2002. Energy absorption by the steel structure of ship in the event of collisions. Marine Structures, 15(4-5):429-441.

McShane GJ, Radford DD, Deshpande VS, Fleck NA. 2006. The response of clamped sandwich plates with lattice cores subjected to shock loading. European Journal of Mechanics, A/Solids. 25(2):215-229.

Paik JK. 1999. The strength characteristics of aluminum honeycomb sandwich panels. Thin-Walled Structures. 35:205-231.

Paik JK, Seo JK. 2007. A method for progressive structural crashworthiness analysis under collisions and grounding. Thin-Walled Structures. 45(1):15-23.

Pedersen PT, Valsgaad S, Olsen D, Spangenberg S. 1993. Ship impact: bow collision. International J. Impact Engineering. 13 (2):163-187.

Pedersen TP, Zhang S. 2000. Absorbed Energy in Ship Collisions and Grounding-Revising Minorsky's Empirical Method. Journal of ship Research, 44(2):140-154.

Rathbun HJ, Radford DD, Xue Z, He MY, Yang J, Deshpande V, Fleck NA, Hutchinson JW, Zok FW, Evans AG. 2006. Performance of metallic honeycomb-core sandwich beams under shock loading. Int. Journal of Solids and Structures. 43(6):1746-1763.

Rodd JL. 1996. Observation on Conventional and Advanced Double Hull Grounding Experiments. in Int. Conf. On Design and Methodologies for Collision and Grounding Protection of Ship, San Francisco, USA, 1996, pp. 13.1-13.13.

Wadley HNG, Fleck NA, Evans AG. 2003. Fabrication and structural performance of periodic cellular metal sandwich structures. Composites Science and Technology 63(16):2331-2343.

Wang G. 2000. Behavior of a double hull in a variety of stranding or collision scenarios. Marine structures 13(3):147-187.

Wevers LJ and Vredevelt AW. 1999. Full Scale Ship Collision Experiment. TNO, Report, Delft.

Xue Z, Hutchinson JW., 2004, A comparative study of impulse-resistant metallic sandwich plates. Int J Impact Eng 2004;30:1283–305

Yamada Y, Pedersen P. 2008. A benchmark study of procedures for analysis of axial crushing of bulbous bows, Marine Structures 21(2-3):257–293.

Zok FW, Rathbun HJ, Wei Z, Evans AG. 2003. Design of metallic textile core sandwich panels. Int. Jour. of Solids and Structures. 40(21):5707– 5722.

Numerical simulation of grounding experiment

Karol Niklas

Gdansk University of Technology, The Faculty of Ocean Engineering and Ship Technology

Abstract:
One of the possible solutions to increase the ship structure crashworthiness is to design it in such a way to absorb the highest possible amount of energy during collision. One of the new ideas, a subject of the CORET project (EUREKA E!3614), is to increase ship structure resistance to rupture during collision and grounding by addition of an extra semi-elastic protective barrier. The suitable design of ship structure with the use of the new solution, and its optimization requires a number of experiments and numerical simulations. The subject of this paper is a numerical simulation of ship grounding (double bottom structure without additional protective barrier). Data collected during the real scale experiment allowed for its verification. Additionally, the influence of selected parameters of numerical model on results was analysed. The verified numerical model can be the basis for future development of hull structure with additional semi-elastic barrier.

Introduction

In shipbuilding industry a steadily growing interest in increasing ship structure safety in the event of collision and grounding can be observed. The need for increased safety applies first of all to the ships carrying environmentally hazardous cargo, but not only. Numerous actions (active and passive) are undertaken to enhance this safety. Active methods concentrate on preventing accidents (new traffic control systems, early warning systems, etc.), passive mainly on reducing the effects of collisions. Statistics presenting ship density on restricted areas (Figure 1) and the number of accidents clearly show that passive methods of reducing the effects of accidents still are, and in future will remain very important.

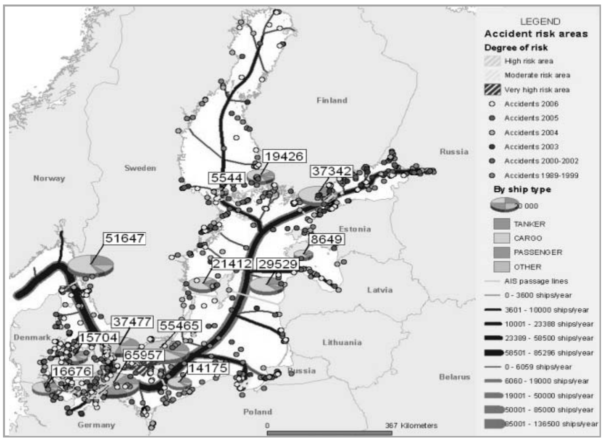

Figure 1 Ship density on the Baltic Sea and accidents until year 2006, based on [21,22]

The most important step in increasing passive safety was introducing the requirements for double bottom and double sides for oil tankers. By about 2020 world oil transportation fleet is expected to have double hulls. Much effort was also put into creating new concepts of solutions distinguished by their ability to absorb more energy during collision. The most important ones are innovative double hull structures [1, 2], sandwich structures [3, 4], and a special type of bow bulb so called Buffer bow [5, 6, 7]. One of the new innovative solutions (the topic of the EU founded CORET project) aiming at increasing environmental safety in the event of collision is introducing an additional, semi-elastic protective barrier to the currently used single plate structure [11]. The solution allows to reduce the risk of fuel leak in the event of collision or grounding, when the fuel is carried in the double bottom of the ship. The problem of large quantities of fuel carried in the double bottom of a ship was observed before, but only the newly introduced IMO directive (MEPC.141-54) toughens the fuel tank capacity and location requirements [20]. Dynamic changes in ship structures lead to increase in marine environment safety. The CORET project is based on the idea that watertightness is ensured by elasticity of polymer layer and energy absorption of lightweight concrete used for the additional protective barriers (sandwich: steel-lightweight concrete-polymer). In the course of the project it was proved experimentally that the structure with the elastic polymer layer (compared with classical structure) remains watertight even if penetration during collision is 10 times deeper. The most efficient methods of designing new types of structures are numerical simulations. In those simulations the contact area of bottom structure is the most demanding fragment to be modelled. Elements of structure in the area become heavily distorted, buckled, plastic deformed and torn.

The presented model includes simulations of the experiment of pressing a hypothetical rock into a ship bottom structure. It simulates ship grounding. The numerical model is a fragment of a ship double bottom identical to the one used during the experiment (the one without additional semi-elastic barrier). Experimental results allowed for verification of the model. By changing selected parameters, mainly material model parameters, the numerical model was calibrated to simulate real structure behaviour accurately. In the future the verified numerical model of steel structure can be used for further simulations of structures with additional protective layers.

Numerical Model

The simulation of pressing a steel sphere into a ship double bottom structure was conducted with the use of explicit solver in LS-DYNA software. The numerical model geometry is similar to the real model geometry (Figure 2) with minor simplifications.

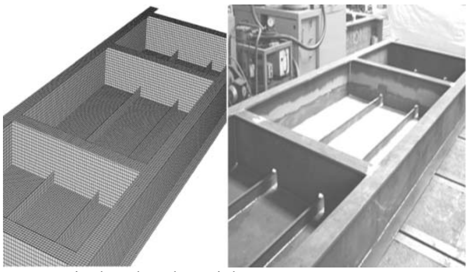

Figure 2 Numerical and real model geometry

Geometrical details of stiffeners and girders crossings were omitted, since the simulation concentrates on a case when a load is applied to the plate halfway between two stiffeners. For the same reasons also welds were not modelled. Applying a load to the plate between stiffeners is the most adverse case when talking about the tearing resistance of the structure. The steel sphere with a diameter of 0.3 m was modelled as a rigid body. Boundary conditions of the numerical model corresponded to the real model mounting during the experiment (Figure 3).

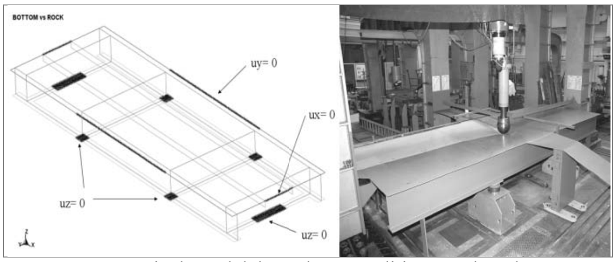

Figure 3 Numerical model boundary conditions and real structure mounting

During the experiment, as well as the simulation, the load was applied quasi-statically. However, to accelerate calculations sphere speed was increased to 0.8 m/s. It was verified that at this speed the influence of dynamic effects on results is insignificant. Simulation time was set for 5 s. Owing to contact instability the maximum time step was 0.18e-5 s. After applying the mass scaling technique calculation time was reduce significantly. The influence of mass scaling ratio (scaled mass/physical mass) on results is discussed in paragraph 4. In the simulation a model with a mesh of 18,000 shell elements was used. Mesh refinement in the contact area would have been ineffective, since by shortening the time step it would lead to increasing calculation time. The benefit of reducing total number of elements in the model would have been counteracted by shortening of the time step, which is dependent on the smallest mesh element side length.

Heavy deformations are expected during the simulation including plating tears. Therefore, a specific minimal number of finite elements per span of structural element must be used. The smallest element of the mesh is dimensioned by the stiffener. When modelling deformations within elastic range it is sufficient to use one element per stiffener span. Taking buckling effects and ultimate strength into consideration four elements per stiffener span must be used. The greatest number of elements is required with models used to analyse large plastic deformations, especially in the area of a 'plastic hinge' — 16 elements per span [8]. Another important aspect of a model is selection of the shell element type. The default Belytschko-Tsay (BT) element has a very high computing efficiency, however relies on a perfectly flat geometry. The BT element uses the local coordinate system, which deforms along with the element and that increases computing efficiency. When calculating linear and nonlinear deformations the BT element accurately simulates thin-walled structures behaviour in collision simulations [9, 10]. Another element used in calculations was type 16, for the reason of potentially smaller numerical errors (especially hourglassing). It was checked that Hourglass energy of the calculated model was below 1% of the internal energy. The influence of the choice of the element on results is discussed in paragraph 4. Up to 16 integration points through thickness were used. Increasing the number of integration points above 4 did not change the results in any way. Owing to the effect of plating tare the influence of elements shape and their distribution should also be analysed (regular or irregular pattern). When the model is covered with a regular mesh of quadrilateral elements the number of elements is lower, and the elements are more favourable numerically. In the other hand regular meshes have a predefined node line, which is a drawback since it can distort the actual shape of the structure tear [8,9].

During the simulation the occurrence of sphere and bottom structure plating contact is observed. The applied algorithm 'Contact_Automatic_Single_Surface' tracks the mutual distances of nods in every time step. The algorithm includes shell thickness, and its implementation is easy due to the lack of shell orientation. In calculations the accepted friction coefficient was steel to steel (static 0.74 and dynamic 0.57 according LSDYNA user's manual) [19]. Depending on the author the value of the static friction coefficient is between 0.5 and 0.8, and of dynamic — most often about 0.3 [18].The influence of static and dynamic friction coefficient values is not analysed in this model. It is assumed that for the analysed load case (force perpendicular to the shell) the influence is not significant. In the event of the sphere sliding in one of the horizontal directions the influence of the friction coefficient values on results would have been greater (strong influence of friction coefficients on contact forces).

One extremely important element of a model is the choice of material model. For the simulation a 24-Piecewise Linear Plasticity model from the Ls-dyna library was used, which includes strain rate effect and failure [19]. Material data of the model are presented in Table 1.

Table 1 Steel material data [12]

Yield Strength [MPa]	Ultimate Strength [MPa]	Rupture Strain [-]	Young's Modulus [MPa]	Poisson Ratio [-]
282	400	0.35	2e5	0.3

First calculations were carried out without scaling yield stress. Additionally, calculations were performed with strain rate effect which was calculated using Cowper-Symonds model with different formulation for rate effect: deviatoric strain rate, yield stress scaling and viscoplastic formulation. Cowper-Symonds model scales yield stress with factor dependent of strain rate (equation 1).

$$\sigma_d = \sigma_Y \left[1 + \left(\frac{\varepsilon_r}{C}\right)\right]^{1/p} \qquad (1)$$

σ_d — dynamic yield stress
σ_y — material static yield stress
ε_r — plastic strain rate
C, p — material constraints

The fundamental aspect in the analysed model is a tear criterion. Then the plastic strain of any element of the model reaches the value of rupture strain it is automatically deleted from the mesh.
The value of rupture strain parameter differs considerably depending on the reference (see Table 2). At the same time, it can be proved that the value of rupture strain depends on the size of the element used by each author. Generally speaking, the larger the model mesh elements, the lower the value of rupture strain (Figure 4).

Table 2 Rupture strain value by different authors

Author	Wisniewski [13]	Naar [14]	Simonsen, Lauridsen [15]	Kitamura [16]	Servis [17]
Rupture strain [-]	0.17	0.18	0,19	0.3	0.46

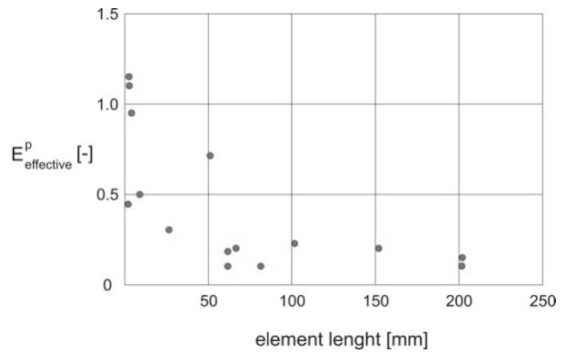

Figure 4. Reported failure strains vs. element size [18]

Mesh elements whose strain exceeded rupture strain were automatically removed from the model, and calculations were continued with the eroded mesh. The influence of the critical value of strain on the analysis results is discussed in paragraph 4.

As can be seen, a numerical model that includes numerous non-linearities requires a particular attention in the aspects outlined above. The influence of some chosen model elements on results is presented in paragraph 4.

Results

To ensure correctness of calculations, first energy equation related results should be analysed (equation 2). The internal energy includes elastic deformation energy and work consumed for plastic deformations. The external work includes work performed by the applied forces, pressures, as well as work performed by the given boundary conditions (displacement, speed, acceleration).

$$\underbrace{E_{kin} + E_{int} + E_{si} + E_{rw} + E_{damp} + E_{hg}}_{\boxed{\text{Total Energy } E_{total}}} = E_{kin}^{0} + E_{int}^{0} + W_{ext} \qquad (2)$$

E_{kin} — kinetic energy
E_{int} — internal energy
E_{si} — sliding energy
E_{rw} — rigidwall energy
E_{damp} — damping energy
E_{hg} — hourglassing energy
E_{kin}^{0} — kinetic energy (t=0)
E_{int}^{0} — internal energy (t=0)
W_{ext} — external work

Internal energy constitutes the greatest percentage of total energy (Figure 5). Up to the moment of shell tearing the energy grows very rapidly. Before tearing sliding energy is an insignificant component of total energy. The growth of kinetic energy of the rigid body caused by increasing the sphere speed (to reduce calculation time) has no influence on the results. Quasi-static conditions of the real experiment were modelled correctly.

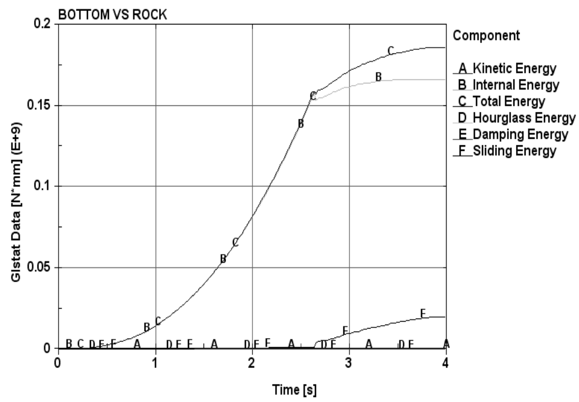

Figure 5 Changes in total energy and its components

The damage is local on account of the sphere dimensions and the place of force application between stiffeners. Nonetheless, both the stiffeners and girders were plastic deformed. The character of the damage obtained during the experiment and simulation is similar (Figure 6). The differences result from the experiment conditions in its last stage. Probably the more accurate plating tear shape can be achieved when using additionally irregular mesh in the greatest deformation area. Shell tearing in the simulation happens after covering 266 mm counting from the moment of sphere and plating contact. The maximum reaction force in supports in z-axis direction is 1.15 MN.

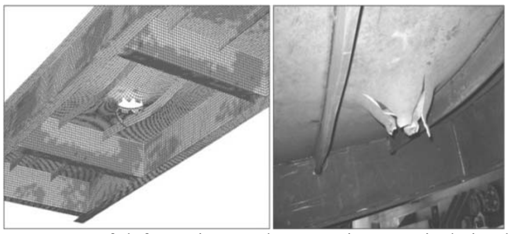

Figure 6 Image of deformations and rupture in numerical simulation and real damage photograph

On the force-displacement chart from the experiment numerical simulation results were marked (Figure 7). The chart illustrates results from both the model without yield stress scaling and the models which include strain effect according to Cowper-Symonds model (three different formulation for rate effects options). A great agreement between experimental and numerical results can be observed. However, for calculations without scaling yield stress the curve obtained from the simulation is less steep and less tilted to the right with the growing number of plastic deformations in the structure. For the model which includes strain rate the simulation represents real structure behaviour during the experiment very accurately. The influence of the way of strain rate inclusion on results is discussed in paragraph 4. Additionally, between experimental and numerical results there is a difference in points there tearing starts. The difference results from the way of loading the model in the last stage of the experiment. The numerical model can be calibrated using the data registered during the real experiment. The analysis of chosen parameters influence on results is helpful in selection of optimal values for those parameters.

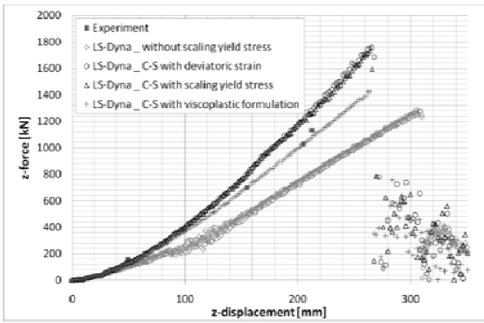

Figure 7 Experiment and numerical simulation force-displacement chart, influence of formulation for rate effects option for material model

Parameters influence on results

The influence of chosen parameters changes is presented with the use of force-displacement charts (in z-axis direction) against a background of experimental results. Figure 7 presents the influence of choosing the formulation for rate effects option in material model. As can be seen, including scaling of yield stress in the model and selecting the adequate Cowper-Symonds (C-S) model has a great influence on results. In the first stage of the experiment deviatoric strain and simple yield stress scaling overlap with empirical results. However, with the increase of plastic deformations they raise the value of the force (the curves are over the experimental curve). The most accurate results were obtained from the model material with the viscoplastic formulation of rate effect. The results from the model in which the yield stress was not scaled along with the element strain are the least accurate and underrate the value of force.

All the simulations were carried by displacing the sphere by 400 mm in the plating direction. At the beginning the calculations were carried with 10 mm/s sphere movement speed with the use of mass scaling technique (attempts, to shorten the calculations time). In later simulations the sphere movement speed was 100 mm/s, therefore the total sphere movement time has decreased ten times. The influence of mass scaling in calculations for the speed of 10 mm/s and the influence of increasing the sphere speed to 100 mm/s is presented in Figure 8. For considered speeds strain rate effect does not influence results. For higher strain rates (not only in high speed impact cases) material strain rate sensitivity should be analysed carefully [24]. Stress-strain curves for various strain rates differ significantly (especially for higher strengths steels).

The calculations were carried out on a PC with Intel Core2 Quad Q6600 2.4GHz processor and the use of mass scaling technique has reduced the calculations time significantly (Figure 9). However, application of any ‘trick’ aimed at altering calculations speed has to be analysed thoroughly with attention to its influence on the results. Adding nonphysical mass to increase the timestep in quasi-static simulations does not affect results since the velocity is low and the kinetic energy is very small in comparison with the internal energy. In dynamic simulations inertia of mass plays an important role therefore it is a common practice to increase mass no more than 5%. Every use of a mass scaling technique requires careful consideration of the influence on results.

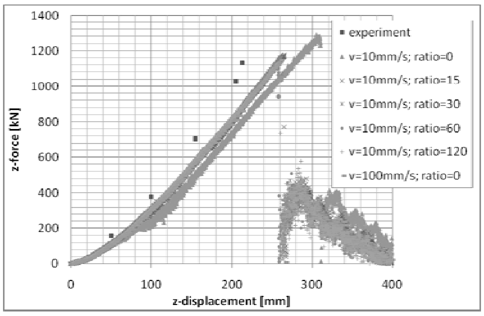

Figure 8 Influence of mass scaling and increasing speed from 10 mm/s to 100 mm/s

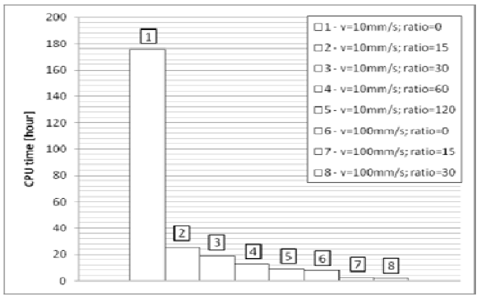

Figure 9 Influence of mass scaling and changing sphere motion speed for calculations

The analysis included also the influence of potentially very important parameter the critical value of an element strain. Simulations were conducted for three values of critical strain: 0.25, 0.35 and 0.45 (Figure 10). On the chart points where structure tear occurred for a given criterion are marked with arrows. As it was expected the influence of this parameter on results is very big. In the model the element side length was 25 mm and the value of rupture strain equal 0.35 gave results corresponding to values from real scale experiment.

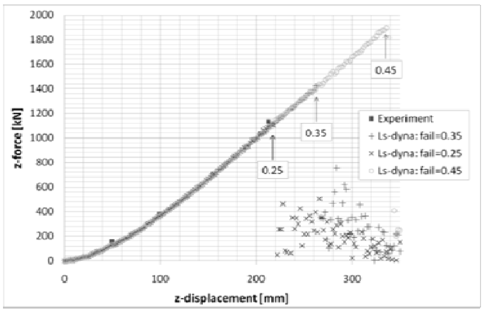

Figure 10 Influence of failure criterion value on results

There were also conducted some calculations with the use of finite elements which were simpler than the aforementioned type 16 element (fully integrated shell). The results for Belitsko-Tsay (BT) and Belytsko-Wong-Chiang (BWC) type elements are presented on Figure 11. The influence of the mentioned finite element type on results in this model until the appearance of plating tear is insignificant. Calculations time for the above elements is given in the legend. In this case usage of simpler elements instead of a fully integrated shell makes it possible to shorten the calculations time for 50% without compromising the accuracy. In analyzed numerical models 4 integration points over the element thickness were used.

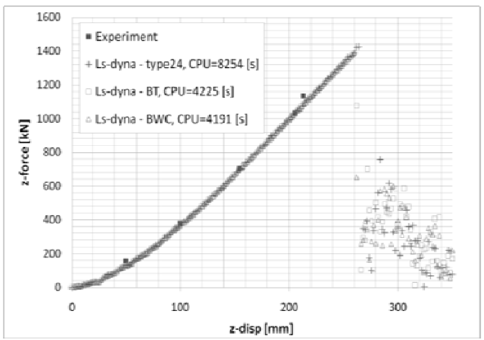

Figure 11 Influence of element selection on results

During calculations the influence of model mesh elements distribution in the area of greatest deformations was not analysed. However, it can be stated that the regular mesh of quadrilateral elements models the structure behaviour very accurately until the moment of plating tear. This is an important fact due to numerical advantages of regular, quadrilateral elements mesh. Additionally, if there is a necessity to analyse paths of tears, probably the mesh of irregularly distributed elements will model it more accurately.

Conclusions

Ship density on restricted areas such as the Baltic Sea increases the risk of accident occurrence. Despite a number of actions aiming at minimising their number, collisions and groundings will still happen. Especially in the case of ships carrying hazardous materials it is very important to reduce the effects of such accidents. Many actions were already taken to increase safety [5-10]. The introduction of the requirements for double bottom and double sides for oil tankers was the greatest step towards increasing safety. With the growth of ship size the danger connected with carrying large quantities of fuel in the double bottom of a ship was also spotted. In this case fuel was separated from the environment only by single plating. Since recently the directive IMO (MEPC.141-54) is in effect and restricts the amount and location of carried fuel. The direction of all those changes dynamically leads to more and more safety solutions. One of the new proposed solutions (being topic of EU funded CORET project) decreasing leakage risk was an idea of applying additional half-elastic protective barriers. The process of designing such innovative structures includes complex numerical simulations. In this paper a numerical model of pressing a sphere into a standard ship double bottom was presented (the one without additional semi-elastic barrier). The numerical calculations were conducted with the same assumptions as the real experiment simulating ship grounding. Numerical results corresponded with the experimental ones. The influence of chosen parameters on the results was also analysed. The results are most affected by the choice of material model, and its key parameter is the formulation for rate effects option. When using Cowper-Symonds model with yield stress scaling with viscoplastic formulation the results were highly correlated with the experimental ones. Failure criterion is the second very important parameter of the model. For the element size of 25 mm the correct value of critical strain is 0.35. The use of mesh with predefined node-lines correctly simulates forces and deformations, however the pattern of tearing differs from the real one.

The verified numerical model allow the most effective way of designing structures to increase safety during collision through numerical simulations.

Reference

[1] Konter, A., Broekhuijsen, J., Vredevelt, A. (2004), A quantitative assessment of the factors contributing to the accuracy of ship collision predictions with finite element method, ICCGS, 2004

[2] Hu, Z., Gu, Y., Gao, Z. (2005), Research on crashworthiness of Y-shape side structure design for FPSO, ISOPE, 2005

[3] Naar, H., Kujala, P., Simonsen, B.C., Ludolphy, H. (2002), Comparison of the crashworthiness of various bottom and side structures, Journal of Marine Structures 15, 2002

[4] Klanac, A., Ehlers, S., Tabri, K., Rudan, S., Broekhuijsen, J. (2005), Qualitative design assessment of crashworthy structures, IMAM, 2005

[5] Kitamura, O. (2000), Buffer Bow design for the improved safety of ships, Ship Structure Symposium, 2000

[6] Endo, H., Yamada, Y., Kawano, H. (2004), Verification on the effectiveness of buffer bow structure through FEM simulation, ICCGS, 2004
[7] Yamada, Y., Endo, H., Pedersen, P.T. (2005), Numerical study on the effect of buffer bow structure in ship-to-ship collisions, ISOPE, 2005
[8] Wu, F., Spong, R., Wang, G. (2004), Using numerical simulation to analyze ship collision, ICCGS, 2004
[9] Simonsen, B.C., Lauridsen, L.P. (2000), Energy absorption and ductile failure in metal sheets under lateral indentation by a sphere, International Journal of Impact Engineering, 2000
[10] Tornqvist, R. (2000), Numerical prediction of ultimate strength of steel structures, Department of Naval Architecture and Offshore Engineering, 2000
[11] Kozak, J. (2008), Elastic protection coatings for ship fuel tanks, intended for the increasing of environment protection level, Polish Maritime Research, Nr S1/2008, ISSN 1233-2585, 2008
[12] Salmon, C. G., Johnson, J. F. (1996), Steel structures: Design and Behavior, HarperCollins, 1996
[13] Wisniewski, K., Kolakowski, P. , Rozmarynowski, B., Gierlinski, J.T. (2001), Dynamic FE simulation of damage in ships collision, ICCGS, 2001
[14] Naar, H. (2001), Comparison of the Crashworthiness of Various Bottom and Side Structures., ICCGS, 2001
[15] Simonsen, B. C., Lauridsen, L. P. (2000), Energy Absorption and Ductile Failure in Metal Sheets Under Lateral Indentation by a Sphere, International Journal of Impact Engineering, ISSN 0734-743X, 2000
[16] Kitamura, O. (2001), FEM Approach to the Simulation of Collision and Grounding Damage, ICCGS, 2001
[17] Servis, D. (2001), The Implementation of Finite Element Codes for the Simulation of Ship- Ship Collision, ICCGS, 2001
[18] Sajdak, A.W. (2004), Analyses of Ship Collisions: Determination of Longitudinal Extent of Damage and Penetration, Dissertation of Doctorate of Philosophy in Naval Architecture and Ocean Engineering, 2004
[19] LS-DYNA Keyword user's manual version 971, Livermore Software Technology Corporation, ISBN 0-9778540-2-7, 2007
[20] IMO Resolution MEPC.141(54), Annex 2, Amendments to the annex of the protocol of 1978 relating to the International Convention for the Prevention of Pollution from Ships 1973, 2006
[21] Helsinki Commision (2007), Report on shipping accidents in the Baltic Sea area for the year 2006, , 2007
[22] http://62.236.121.189/website/MARIS1/viewer.htm
[23] http://www.marinetraffic.com/ais/
[24] Minamoto, H., Kawamura, S. (2009), Effects of material strain rate sensitivity in low speed impact between two identical spheres, International Journal of Impact Engineering 36 p.680–686, Elsevier Ltd., 2009

Analysis of sloshing interaction in ship collisions by means of ALE finite element method

Smiljko Rudan [1], Kristjan Tabri [2] and Ivan Klarić [1]

[1] *Faculty of Mechanical Engineering and Naval Architecture, University of Zagreb*
[2] *Faculty of Civil Engineering, Tallinn University of Technology*

Abstract:
Ship collisions are marine accidents with potentially large impact on the safety of human lives, environment and ship structural damage. Large- and model-scale experiments have revealed that the sloshing of fluid in partially filled tanks influences the collision dynamics and lowers the energy available for structural deformations. This paper presents a numerical analysis of sloshing interaction in collision. The model is based on the arbitrary Eulerian-Langrangian (ALE) finite element method with multi-material option. Free-surface elevation and motions evaluated numerically are compared to those from the model-scale experiments. Comparison reveals that the free-surface elevation inside the partially filled tanks is well predicted with the numerical approach. The difference in the rigid body velocity indicates however that the amount of energy in the sloshing fluid is somewhat overestimated.

Introduction

Ship collisions, as well as groundings, are marine incidents with significant consequences on structural integrity of the ships, environment and, in the worst case, lives of the people involved. Collision between ships or ship and other object are being extensively studied due to, among other reasons, advances in numerical analysis methods and awareness on environmental issues. Crashworthiness of the ship structure is being a matter of significant research effort ranging from the better understanding of external ship dynamics and internal damage mechanics to the application of novel structural design involving sandwich structures. The aim of the research in progress is to minimize the collision consequences through structural design that is able to absorb as much as possible energy before rupture, see for example (Klanac et al, 2005).

Particular attention is paid to the crashworthiness of tankers carrying crude oil, LNG, LPG, chemicals and other liquids worldwide. Several famous collisions and groundings have shown to wide audience the enormous impact on environment due to oil spills. So far the LNG and LPG fleet has an excellent record with no significant or disastrous incidents, but by constant increase of the fleet and ship size the risk of incident will inevitably rise. Due to a nature of its cargo, tankers are prone to sloshing of liquid in the tanks when they are partially filled. Sloshing may have significant effect on the ship stability or structural integrity of the tank itself. Due to the sudden change of ship velocity in collision or grounding incident a violent sloshing in the partially filled tanks may be expected.

Large-scale and model-scale experiments have indicated that sloshing in partially filled tanks affects collision dynamics in a way that deformation energy is being reduced compared to a no-sloshing scenario. In another words, less damage may be expected in the cases where the amount of water in partially filled tanks is significant compared to the ship's mass. Influence of the sloshing on collision dynamics has been studied analytically and experimentally by Tabri et al. (2009) and numerically using the arbitrary Lagrangian-Eulerian (ALE) finite element method by Zhang and Suzuki (2008). Experimentally validated numerical study has not been presented yet.

This paper presents a numerical simulation model based on a set of model-scale collision experiments presented by Tabri et al (2009). The numerical model is based on the ALE FE method and aims to evaluate both the water elevation inside the partially filled tanks and the sloshing interaction with collision dynamics. First, a study on the mesh sensitivity is presented. Three models with different mesh resolution are created and experimentally measured ship motions are used as moving boundary conditions. Water elevation inside the tank is studied under these conditions and compared with the experimental measurements. A sufficient mesh resolution is determined and applied to create a complete configuration of the striking ship model used in the model-scale experiments. The collision is simulated in a simplified manner, where the striking ship is accelerated to the desired velocity and the contact is modelled by applying the experimentally measured contact force. Thus, the struck ship model is excluded from the analysis and the investigation is based on the striking ship alone. Ensuing ship motions and the water elevation in the tanks is compared to those measured experimentally. Comparison is extended to ship motions occurring well after the contact between the ships has vanished.

Sloshing interaction in ship collision

Colliding ships are subjected to the rapid change in their motions due to the contact force. In turn, the change. In ship motions excites fluid sloshing inside the partially filled tanks. If the amount of sloshing fluid is significant compared to the total mass of the ship, the distribution of energy components in the collision is changed significantly.

In a collision, the momentum of the striking ship is transmitted to the struck ship through contact loading. If there are no partially filled tanks, the change in momentum is predominantly caused by the change in ships' velocities. If one of the ships, or both, has partially filled liquid tanks the fluid inside the tank starts to slosh during the collision, Figure 1, and interacts with the containing structure over a longer time span than would a rigidly fixed mass. Thus, the participation of the sloshing mass in the momentum transmission is delayed, the ship carrying fluid appears lighter and the resulting collision damage becomes lower. This was presented with the model-scale experiments in which the direct influence of sloshing was evaluated by comparing the results of tests with and without water in tanks (Tabri et al, 2009). The deformation energy in the tests with partially filled tanks was only about 80% of that in the equivalent tests where fixed masses were used instead of fluid. Therefore, in the presence of partially filled tanks, a collision analysis has to account for the sloshing interaction.

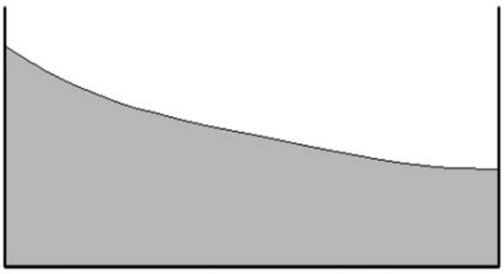

Figure 1: Sloshing of liquid in partially filled tank

Model-scale collision experiments with sloshing interaction

An understanding of the sloshing physics has been gained through a series of model-scale collision experiments, Figure 2. The experiments were conducted both with onboard tanks partially filled with fluid and with the fluid replaced by a rigidly connected mass. Hereafter, these experiments are referred to as wet or dry tests. In all the tests the striking ship model collided at a right angle to the amidships of the initially motionless struck ship model. An elaborated description of the ship models and their scaling is given in Tabri et al (2009).

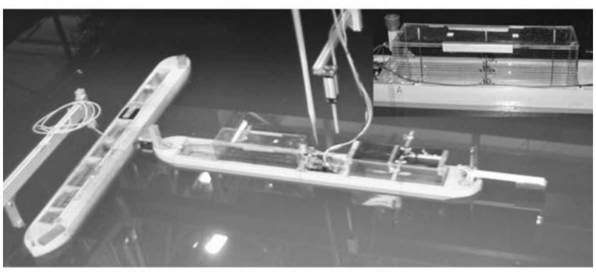

Figure 2: Ship models with sloshing tanks on board of the striking ship (Tabri et al, 2009)

The model tests were designed to be physically similar to the large-scale experiments (Wevers and Vredeveldt, 1995) with the scaling factor of □= 35. The ship models had the following main dimensions: length $L^A = L^B = 2.29$ m, depth $D^A = D^B = 0.12$ m, and breadth $B^A = 0.234$ m and $B^B = 0.271$ m, with the superscript A referring to the striking ship and B to the struck ship.

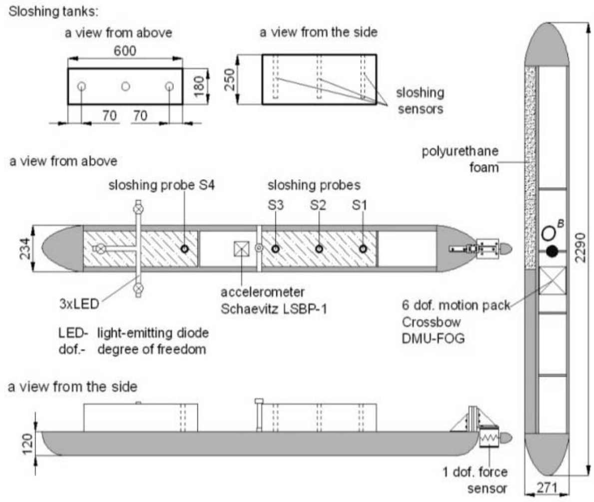

Figure 3: Test setup with two sloshing tanks

Two fluid tanks were installed on board of the striking ship model, as shown in Figure 2 and Figure 3. In the model tests the length of each tank was about 1/4 of the total length of the model. The striking ship model was equipped with an axi-symmetric rigid bulb. In the struck ship model a block of polyurethane foam was installed at the location of the collision. The model-scale force-penetration curve was built up on the basis of this value and the shape of the contact surface. The striking model was connected to the carriage of the test basin and it was accelerated smoothly to the desired collision velocity u_0^A to prevent sloshing before the collision. The struck model was fixed to the basin with line reels. Both models were released just before the contact. All six motion components of both ships were recorded. The free surface elevation in the sloshing tanks was measured with four resistive wave probes made of steel wire. Three probes were installed in the fore tank and one in the aft tank; see Figure 3. The rigid bulb was connected to the striking ship via a force transducer. The force was measured only in the longitudinal direction with respect to the striking ship model as the other components were expected to be negligible in symmetric collisions.

Given the ship motions, the penetration time-history was calculated based on the relative position between the ships, see Eq. 3 in (Tabri et al 2008). Combining the measured contact force and the penetration history results in a force–penetration curve, and the area under that curve gives the deformation energy ED at the end of the collision process.

ALE finite element method

Several methods exist for analyzing sloshing problems and, in general, fluid-structure interaction (FSI) problems. Finite element method, finite difference method and smoothed particle method may be distinguished, among others. A comparative review of numerical approaches to sloshing and FSI problems is presented in (Rebouillat, 2010). The Arbitrary Langrangian-Eulerian (ALE) finite element method

solves the transient equations of motion of the fluid and structure using the explicit time integration method (Zhang et al, 2007). A brief introduction to the method is presented here.
A Lagrangian finite element formulation describes the motion of the body using spatial coordinate system fixed to the centre of the mass of the body. In addition, material is fixed to finite elements of the body. As a consequence, Lagrangian mesh moves with the material making it easy to track changes and apply boundary conditions. Mesh distortions correspond to material distortions, and, if excessive, lead to reduction in calculation time step and/or solution breakdown. Using the Eulerian formulation, on the other hand, the mesh remains fixed in space while material moves through it. Mesh distortion is therefore not a problem but interfaces and boundary conditions are difficult to be tracked (Aquelet et al, 2003). An ALE formulation contains both the Lagrangian and the Eulerian formulations and have the capability of providing either Lagrangian or Eulerian solution, or an arbitrary combination of both. ALE method may be applied in two different ways. The first one solves the fully coupled equations for computational fluid mechanics and is able to handle only a single material in an element. The second one consists of two-step calculation in each time step. First a Lagrangian step is performed. Mesh moves with material and eventually becomes distorted. Changes in the velocity and energy equilibrium are calculated in this step. Mass is conserved as there is no material flow between elements. Then a so-called advection step is performed. Node positions are remapped to reduce mesh distortions, and mass, velocity, internal energy and momentum across cell boundaries are restored. A pure Eulerian process is produced if the nodes are remapped back to their initial positions. Multi-material elements are easily formed in this way and elements that are partially filled define the free surface.
Three different advection methods can be used in LS-Dyna code (LS-Dyna Keyword Manual, 2006):

1) donor cell + HIS (half-index-shift, first order accurate,)
2) van Leer+ HIS (second order accurate, conserving internal energy and momentum over each advection step)
3) donor cell+HIS, (first order accurate, conserving total energy over each advection step instead on internal energy, thus conserving total energy of the system).

Several authors have successfully applied the ALE finite element method in analysing sloshing and FSI problems. Zhang et al (2007) presented a comparative study of the numerical simulations for FSI of liquid-filled tank during ship collision. ALE FE model, Lagrangian FE model and linear/mechanical model results were compared for a 95% filled tank in a two global FEM ship models collision. Anghileri et al (2003) used ALE finite element and three other numerical models to validate crashworthiness of a water filled tank during the impact with the ground. Nonlinear FSI interaction in seismic analysis of anchored and unanchored tanks was performed using ALE FE method by (Ozdemir et al, 2010).

Numerical analysis

Recent advances in the finite element codes offer a possibility to perform a numerical simulation of the highly nonlinear phenomena as is the case of sloshing in the partially filled tanks. A motivation for numerical analysis presented here is to verify the capability of commercial software to model a complex fluid behaviour due to interaction with tank structure in a collision event.
Sloshing analysis was performed using LS-Dyna FEM software applying ALE finite element method with multi-material option. Numerical model is made in a way that its geometrical properties, water level heights in both fore and aft tanks and overall mass distribution resemble as much as possible to the experimental setup. The experiment studied here is referred as S1_v7 in Tabri et al, 2009. The main parameters defining the collision scenario are presented in Table 1 and the physical properties of the participating ships in Table 1. First, the mesh sensitivity is studied by investigating the water elevations in the cases of three different mesh resolutions. There, the experimentally measured velocity depicted in Figure 5 is used as a moving boundary condition.

Table 1. Collision parameters

Test	u_0^A	m_{LS}^A	Water mass		h_W/l_T		amount of water	m^A/m^{B*}	E_D	
			fore	aft	fore	aft			exp.	calc
	[m/s]	[kg]	[kg]	[kg]	[-]	[-]	[%]	[-]	[J]	
S1-V7	**0.7**	**22.1**	**5.0**	**8.0**	**0.08**	**0.13**	**37%**	**1.15**	**3.3**	**3.6**

u_0^A -collision velocity; m_{LS}^A -lightship mass of the striking ship; h_w -water height inside the tank, l_T -tank length, E_D -deformation energy.

Table 2. Physical parameters of the ship models during the test

Model	Draft	Total mass	KG	L_{COG}	k_{XX}	$k_{YY}=k_{zz}$	2	3	4	5	6
	[cm]	[kg]	[cm]	[cm]	[cm]	[cm]	[%]	[%]	[%]	[%]	[%]
Striking (wet)	6.75	35.0	7.5	-6.6	18	82	28	195	6	99	15
Struck ship	6	30.5	7.3	0	17	83	21	238	14	128	12

KG -vertical height of the mass centre of gravity measured from the base line of the model; L_{COG} -longitudinal centre of gravity measured from the amidships; k_{XX}, k_{YY}, k_{ZZ} the radii of inertia in relation to the *x*- and *y*-axes, μ_i hydrodynamic added masses (see Tabri et al, 2009).

Sensitivity study

First, a single tank test models were generated to study the influence of mesh sensitivity on the water elevation under the prescribed tank motions. Test models scantlings are 600x250x180mm (length x height x width). Three different test models were generated, see Figure 4:

1. Mesh_50 model with 50 finite elements along tank length, element dimensions 12x12mm
2. Mesh_100 model with 100 finite elements along tank length, element dimensions 6x6mm
3. Mesh_150 model with 150 finite elements along tank length, element dimensions 4x4mm.

In all the models the element width is equal to the tank width.

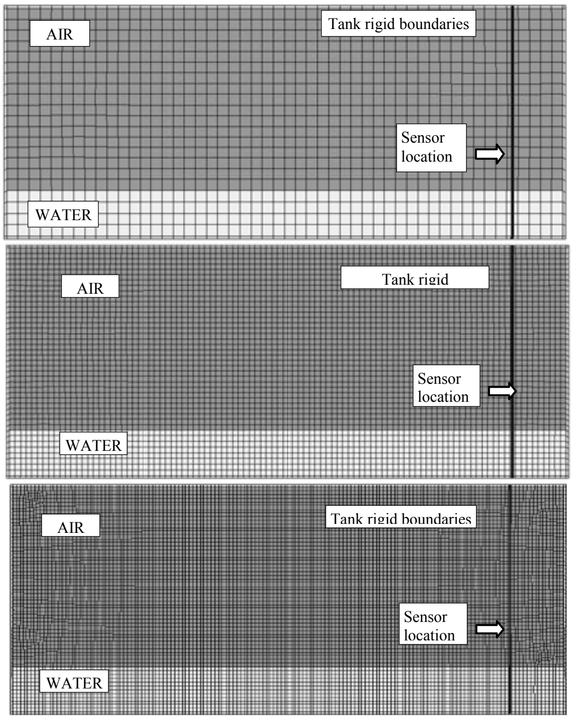

Figure 4: Mesh_50, Mesh_100 and Mesh_150 test models (from up down)

Test models materials are presented in Figure 4. Vertical line indicates water level height sensor in the experimental setup. At the same location free surface height will be evaluated in numerical analysis.

The water level height in the test models is 47.6mm and is therefore 2.8% higher than experiment water level height, being 46.3mm. Consequently, the same applies to the mass of water in the tank. The difference arises due to uniform element distribution along height of the tank and is considered to be insignificant. The rest of the tank is filled with air. The tank boundaries are modelled with the rigid solid elements with z translation and rotation around x- and y-axis fixed. In such a way motion of the model was restricted to the x-y plane. The water and the air properties were described by *EOS_LINEAR_POLYNOMIAL command. EOS parameters used were 1.0E+05 and 2.2E+09 for water and 1.0E+05 and 1.42E+05 for air. Both materials were defined using a *MAT_NULL command with density 1000 kg/m^3 for water and 1.29 kg/m^3 for air. A gravity acceleration of 9.81 m/s was applied. Donor cell + HIS advection method was used.

Motion of the model was set by prescribed velocity time-history depicted in Figure 5. Collision on this, and all the other figures, occurs at t=0s. The test model was slowly accelerated for 6 seconds, so that no initial sloshing is present when the collision occurs. At t=0s and onwards velocity measured during experiment was set to control the motion of the tank.

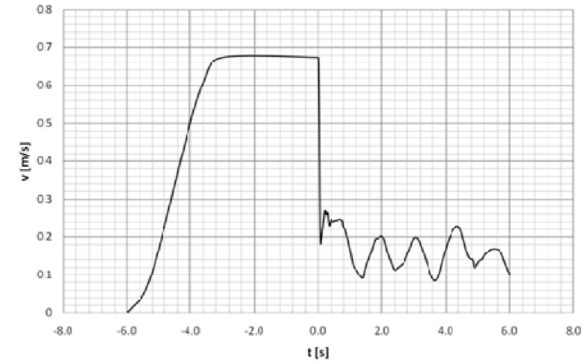

Figure 5: Test model prescribed velocity

A test model analysis revealed numerical instabilities requiring certain control measures. Single precision solver led to severe hourglassing, which was significantly reduced by using a double precision solver.

Figure 6 presents comparison of the experimental and numerical results for the mesh_50 test model. Although numerical results seem to be reasonably accurate in comparison to the experiment, it was concluded that mesh_50 density was not fine enough. Figure 7 and Figure 8 present comparison of the mesh_100 and mesh_150 models with experimental results, respectively. Comparison of the ALE FEM and experimental results is very good for both mesh resolutions.

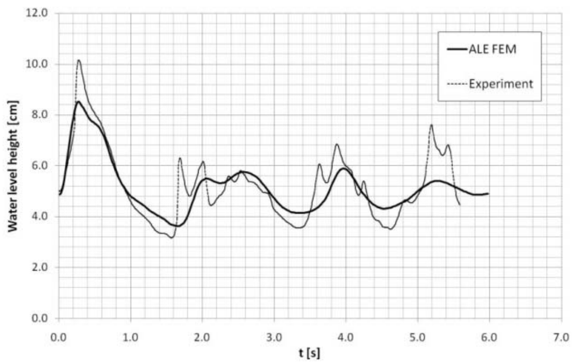

Figure 6: Test model Mesh_50 Comparison of results

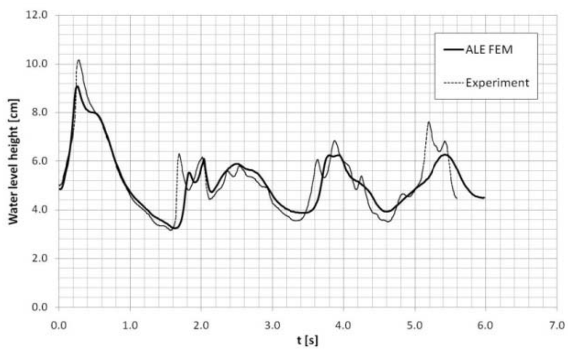

Figure 7: Test model Mesh_100 Comparison of results

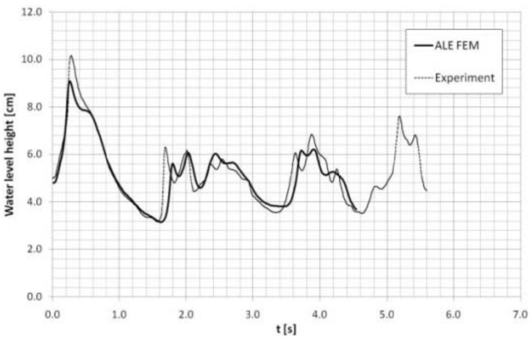

Figure 8: Test model Mesh_150 Comparison of results

The calculation time increased with the mesh refinement. Since no obvious advantages of using mesh_150 were noticed, the reference resolution of mesh_100 model was used in the subsequent analysis. It should be noted that numerical instabilities were noticed using mesh_150 density in a form of non-realistic velocity peaks. This was controlled by setting TSSFAC parameter in *CONTROL_TIMESTEP command to 0.67, as recommended by LS-DYNA support.

Numerical analysis of sloshing interaction

By taking into account the test model analysis, a complete S1_v7 model configuration was generated, Figure 9. S1_V7 model consists of the aft tank filled with 8kg of water, the fore tank filled with 5kg of water and the lightship mass of 22.1kg located in the ship centre of gravity. The remaining part of the tanks was filled with air. Material parameters were the same as in the test model.

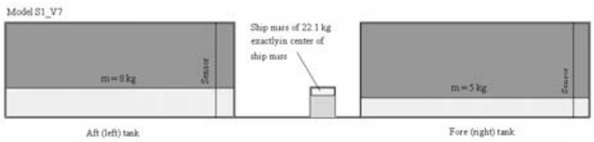

Figure 9:S1_V7 model Mass distribution

The motion of the model was restricted to x-y plane in the similar manner as the test model. The model was accelerated first by prescribed velocity so that at the moment of collision it had a velocity of 0.7 m/s.

At t=0s collision occurs and the model is free to move in the x-y plane. Sloshing in tanks is not limited otherwise. The contact with the struck ship is simulated by imposing the measured contact force to the centre of gravity of the ship. The time-history of the contact force is presented in Figure 10.

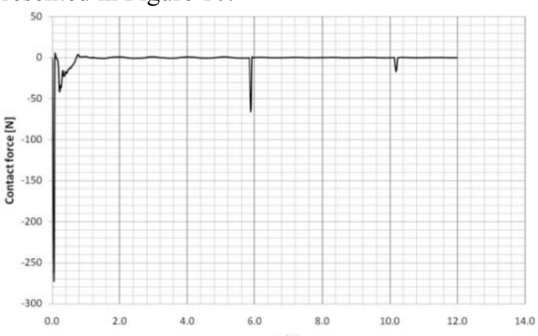

Figure 10:S1_V7 model Prescribed force

Figures 11 and 12 present comparison of ALE FEM and experimental results. Water elevation in time is presented for fore tank in Figure 11 and for aft tank in Figure 12.

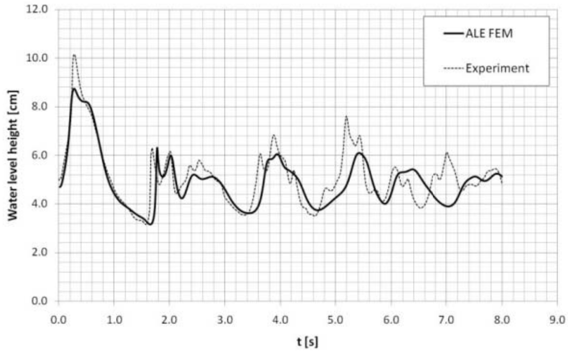

Figure 11:S1_V7 model Comparison of ALE FEM and experimental results, fore tank

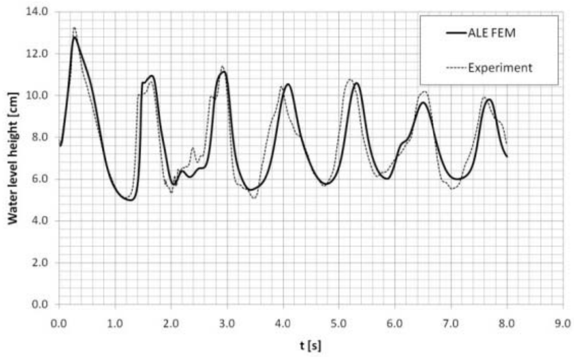

Figure 12: S1_V7 model Comparison of ALE FEM and experimental results, aft tank

A comparison of the results shows very good agreement of numerical and experimental results for both fore and aft tank. The underestimation of approx. 15% may be noticed in the case of fore tank where initial, and highest, sloshing height is lower than the one measured by experiment. The aft tank calculations, having more water inside, match experimental results almost perfectly.

The sloshing period is well estimated numerically and most of the peaks coincide in time. Differences are somewhat higher in the fore tank, while aft tank behaviour is in very good correlation with the experimental results. As the sloshing progresses in time, the numerically estimated sloshing period gets slightly longer compared to the experimental measurements.

A comparison of the rigid body surge velocity is presented on Figure 13. A certain underestimation of rigid body velocity is present in the numerical simulation, indicating too high proportion of the kinetic energy in the sloshing motion. However, both numerically evaluated and measured velocities are well in phase.

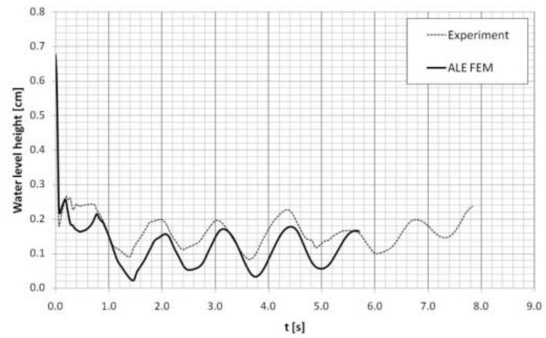

Figure 13: S1_V7 model Velocity

The rigid body surge acceleration is presented in Figure 14. A small underestimation of the initial peak deceleration can be noticed in the numerical result. This again indicates that in the numerical simulation the striking ship appears too light and there is too much energy in the fluid motion.

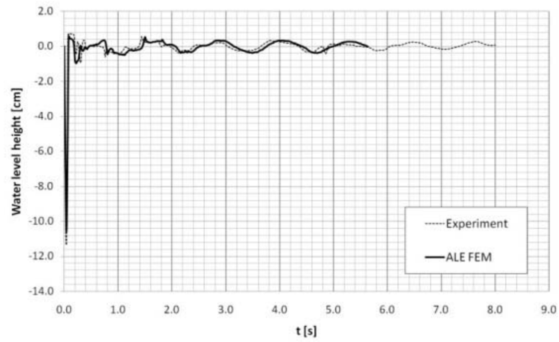

Figure 14: S1_V7 model Acceleration

Calculation time was approx. 61 hours on a standard dual core PC, using double precision LS-Dyna solver.

Conclusion

A numerical model to study the sloshing interaction in ship collisions has been presented and validated experimentally. Numerical simulations were conducted exploiting multi-material ALE finite element method.

A numerical model was found to be mesh sensitive so proper mesh size needs to be determined considering precision/cost ratio. Also, a numerical model needs to be verified against numerical instabilities and controlled in the case of unrealistic model behaviour.

Underestimation of approx. 15% in initial sloshing height was noticed in the case of fore tank (lower water level height), while the overall liquid sloshing was captured very well. For the aft tank (higher water level height) a comparison of ALE FEM and experimental results is excellent.

The rigid body motion of the ALE FEM model, i.e. velocity and acceleration, resembles to the motion measured during experiments. Motions are in phase while some velocity underestimation of 20% in the average is noticed for the ALE FEM model.

It may be concluded that the ALE finite element method is able to capture sloshing in dynamic events such as collision with very good precision.

Based on this findings future research may examine sensitivity analysis regarding different water level heights (i.e. water masses in tanks) and model speeds. The observed underestimation of ALE FEM model velocity and corresponding difference in sloshing energy should be studied. Finally, a comparison of energies for fluid and rigid mass models should be evaluated.

References

Anghileri M., Castelleti L.-M.L., Tirelli M., Fluid-structure interaction of water filled tanks during the impact with the ground, International Journal of Impact Engineering 31 (2005), p. 235-254.

Aquelet N., Souli M., Gabrys J., Olovson L., A new ALE formulation for sloshing analysis, Structural Engineering and Mechanics, Vol. 16, No. 4 (2003).

Klanac A., Ehlers S., Tabri K., Rudan S., Broekhuijsen J., Qualitative design assessment of crashworthy structures, Proceedings of the 12th International Congress of the International Maritime Association of Mediterranean (IMAM 2005), p.461-470, Lisboa, Portugal.

Lloyd's Register, Structural Design Assessment – Sloshing Loads and Scantling Assessment, LR, 2004.

Ozdemir Z., Souli M., Fahjan Y.M., Application of nonlinear fluid-structure interaction methods to seismic analysis of anchored and unanchored tanks, Engineering Structures 32 (2010), p. 409-423.

Rebouillat S., Liksonov D., Fluid-structure interaction in partially filled liquid containers: A comparative review of numerical approaches, Computer & Fluids 39 (2010), p. 739-746.

Tabri K., Määttänen J., Ranta J. (2008) Model-scale experiments of symmetric ship collisions, Journal of Marine Science and Technology, 13, pp. 71-84.

Tabri K., Matusiak J., Varsta P. (2009) Sloshing interaction in ship collisions An experimental and numerical study, Journal of Ocean Engineering, 36, pp. 1366-1376.

Zhang A., Suzuki K., A comparative study of numerical simulations for fluid-structure interaction of liquid-filled tank during ship collision, Ocean Engineering 34 (2007), p. 645-652

Comments on Geometrical Modeling of Ship Grounding

Arsham Mazaheri and Jutta Ylitalo

Aalto University, School of Science and Technology Department of Applied Mechanics, Marine Technology

Abstract:
More than 30 years have passed since Macduff and Fujii expressed their first ideas about the modeling of ship grounding. The probability of ship grounding is usually calculated by multiplying two probabilities named geometrical and causation probabilities. Geometrical probability gives the probability of a ship being a grounding candidate, which means a ship that will run aground if no evasive action is performed. Consequently, the causation probability will give the probability of a grounding candidate not to do any evasive action and then goes aground.Many geometrical models have been presented during these years for estimating the probability of grounding. However, after all these years, there is still lack of a well-defined geometrical model for analyzing the probability of ship grounding.This paper represents four of the most cited geometrical probability models (the models of T. Macduff, Y. Fujii, P.T. Pedersen and B.C. Simonsen) and discusses about their weaknesses and strengths. In the third part of the paper, some improvement for Macduff and Fujii's models are suggested. In the fourth part of the paper, the capability and sensitivity of all four models are assessed by calculating the probability of ship grounding with real traffic information from the AIS (Automatic Identification System) data of the Gulf of Finland in 2008.

Introduction

Ship grounding accounts for about one-third of commercial ship accidents (Jebsen and Papakonstantinou 1997; Kite-Powell et al. 1999). To give few examples, about 20% of all tanker losses between 1987 and 1991 were due to grounding (Amrozowicz et al. 1997). Zhu et al.(Zhu L., James P., Zhang S., 2002, Statistics and damage assessment of ship grounding, Marine Structure, 15:115-530) [cited in (Samuelides et al. 2009)] have reported that the total losses of all ships during the period 1995-1998 were 674 in numbers and 3.26 M in Gross Tonnage (GT), where 17% in number and 24% in GT were due to grounding. Also more than half of all the accidents in the Gulf of Finland are grounding accidents (Kujala et al. 2009). Moreover, 47% of all accidents of the Greek ships larger than 100 GT all over the world between years 1992-2005 were reported as grounding (Samuelides et al. 2009).

Nowadays most of the risk assessments on ship grounding are done by the help of Macduff's (Macduff 1974) and Fujii's (Fujii et al. 1974) first ideas. They both used the concept of multiplying the number of ships being on a grounding course (grounding candidate) and the probability of not making evasive maneuvers (causation probability) to calculate the number or the probability of grounding accidents.*Grounding candidates* are those ships that go aground if nothing, internally or externally, changes; it means that if nobody onboard does any evasive actions or the environmental situation does not change(some say that "if the ship navigates blindly"). Some models give grounding candidate probability whereas some others yield the number of grounding candidates. The *number of grounding candidates* is the number of the ships that are grounding candidates through the analysis area; and if this number is multiplied by the causation probability, it will yield the number of groundings. *Grounding candidate probability* is the probability that a ship is a grounding candidate during one passage through the analysis area; and if this probability is multiplied by the number of vessels in the traffic, it will yield the number of grounding candidates.

Causation probability informs how probable it would be that the situation (internally or externally) does not change in favor of the ship, in different given scenarios.

Therefore, according to present knowledge, for finding the probability of grounding in a given location or scenario, it is needed to have both the number of grounding candidates and causation probability. There are different internal and external factors that affect both probabilities. *Internal factors* are those that are related to the ship, herself; and *external factors* are those that will appear depending on the environmental situation related to the location of the ship.

Different factors like human factors, vessel and route characteristics, atmospheric and situational factors should be statistically analyzed to get the clear contribution of each specific factor affecting the causation probability (Mazaheri 2009). However, the grounding candidate probability can be obtained via so-called geometrical model. Although the contributing factors in geometrical modeling and also the level of models' precision is still a matter of question (Mazaheri 2009), there are plenty of useful geometrical models available in the literature.

This paper includes three main parts. In the first part the most cited geometrical models in the area of grounding probability (models of T. Macduff, Y. Fujii, P.T. Pedersen and B.C. Simonsen) have been represented and their strengths and weaknesses are discussed. In the second part, some improvements are suggested for the models of Macduff and Fujii. In the last part the discussed models have been used for analyzing the grounding probability in a real case in the Gulf of Finland (near Sköldvik). At the end, the conclusion is presented.

Dominant Models

The existing models in the literature can be divided into two groups as *analytical* and *statistical* models (Mazaheri 2009). Analytical models include Fujii's and Macduff's models together with those who have followed them in their modeling like (Fowler and Sørgård 2000) and (Kristiansen 2005). None of them use *ship traffic distribution*, which is the probability density function of the lateral position of ships on a waterway (see Figure 3). On the other hand, the models of Pedersen and his followers like (Simonsen 1997), (Karlsson et al. 1998), (Otto et al. 2002), (Gucma 2006) and (Quy et al. 2007) can be called statistical, as the ship traffic distribution has been used in the models. On the other hand, the existing models deal with two different major scenarios as stranding and grounding. (Kristiansen 2005; Mazaheri 2009) "*Stranding* is the event that a ship impacts the shore line and strands on the beach or coast. It happens when the track of the ship intersects the shoreline by either navigational error or drifting. However *grounding* is the event that the bottom of a ship hits the seabed. It happens when a ship is navigated through an individual shoal in a fairway while her draft exceeds the depth." (Mazaheri 2009).

Analytical Models

(Macduff 1974)

Macduff argued that the real probability of grounding (P_{RG}) would be the product of geometrical probability (P_G) and causation probability (P_C):

$$\mathrm{P_{RG}} = \mathrm{P_G} \times \mathrm{P_C} \tag{1}$$

Then, by the help of Buffon's needle problem, he calculated the geometrical probability of random grounding (assuming random navigation through the channel) as:

$$P_G = \frac{4s}{\pi C} \tag{2}$$

where:

s is the track length of the ship or stopping distance

C is the width of the channel or waterway

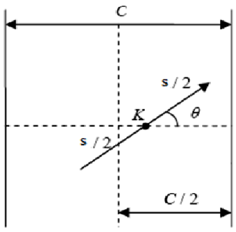

Figure 1: Probability of hitting the wall of the channel according to (Macduff 1974).

Macduff's model does not consider any shoal in the middle of the channel, so it just yields the probability of stranding. A matter for consideration in Macduff's model is that the width of the channel should be assumed not to change significantly when moving along the channel. Since the number of natural channels that meet this criterion is, if not say zero, very few, the scope of the formula will be limited to just some manmade channels. In addition Macduff's model does not take into consideration the length of the studied waterway, which is questionable as logically ships have more possibilities to run aground in a longer channel than in a shorter one.

Another considerable point about Macduff's model is that he has used Buffon's needle problem, which is a 2D model, to find a geometrical probability of stranding (hitting walls of a channel). In his model, the ship has been considered as a needle or a line, which is one dimensional. When applying this approach, two matters need to be considered. First, vessels (unlike needles) are not dropped into the channel from the sky, so their positions and headings do not fit into the uniform distribution (Kunkel 2009). Also one may argue that the path of the ship (unlike the needle) is not straight either. However it should be noticed that a straight line from the starting point to the end point of the path is enough as a criterion. The second matter is that since needles (as line), contrary to ships, have one dimension, it could be understood that the breadth and the draft of the vessel and the depth of the channel have not been taken into the attention. However, it can be argued that hitting the wall of a channel, itself, means the draft has exceeded the depth of the channel; and therefore it can be understood that the draft and the depth has been taken into account.

(Fujii et al. 1974)

Fujii's model together with Macduff's was one of the earliest geometrical models designed for grounding risk modeling, and most of the researches in this area have been done based on their works.

Fujii has argued that the approximate number of ships going aground in a waterway would be:

$$N = P_C(D + B)\rho V \tag{3}$$

where:

V is the average speed of the traffic flow

ρ is the average density of the traffic flow

D is the linear cross-section of the obstacle shallower than the [*average*] draft

B is the [*average*] ship width

D+B is the effective width of the obstacle or shoal

P_C is the probability of mismaneuvering or causation probability

Fujii brought into attention that since D is usually much larger than B, B can be ignored.

$$N = P_C D\rho V \tag{4}$$

Also he has mentioned that when D is much larger than W, width of the route, the formula can be rewritten as:

$$N = P_C Q \tag{5}$$

where:

Q is the traffic volume and is equal to ρWV

W is the width of the channel

However, the question is how possibly D could be larger than W? The only possibility is when the ship omits a turn in vicinity of a shoal and grounds on the shoal; otherwise D could be maximally equal to W and in this case all ships would be grounding candidates.Although Fujii has showed that he has taken the draft into consideration by mentioning that "… *obstacle shallower than the draft*", like Macduff's model, the channel's depth and the vessels' drafts have not been considered directly for calculating the grounding candidates. In addition, Fujii's grounding model is similar to his model on collision with fixed object (Fujii 1983). Therefore, contrary to Macduff, he has not considered the probability of hitting the wall of the waterway, and his model just yields the probability of grounding and not stranding. On the other hand, Fujii, like Macduff, did not take the length of the waterway into account.

Statistical Models
(Pedersen 1995; Simonsen 1997)

Pedersen's model is the most used geometrical grounding model in recent years. Simonsen's model is actually a revised version of Pedersen's work. Their models have been used in two recent risk analysis software [GRACAT (Hansen et al. 2000; Hansen and Simonsen 2001) and GRISK (Ravn et al. 2008), currently called as IWRAP Mk2 (2009)] for analyzing grounding and collision probabilities.

Pedersen has defined an imaginary route with a bend in the navigation route around an area where ships with a draft above a certain level may ground (Figure 2). Again, does it mean that he has considered the ship's draft and the depth of the channel in his model? Like what has been posed, do we really need to think about how these factors (draft and depth) can affect the model; or going aground, by its own, means that those factors have been considered into the model?

Pedersen and Simonsen have categorized the grounding scenarios into 4 different categories (Pedersen 1995; Simonsen 1997), and the estimated frequencies of grounding on the shoal can be obtained as a sum of the four different accident categories. The third and forth categories are about grounding due to evasive maneuvers and drifting ships; and they are not represented here in this paper.

In category I, ships follow the ordinary and direct route at normal speed. The accidents are due to human error and unexpected problems with the propulsion/steering system which occur in the vicinity of a shoal. The simplified expression of this category, according to Pedersen is:

$$F_{Cat.1} = \sum_{Ship\ class\ i=1}^{n\ class} P_{Ci} Q_i \int_L f_i B_i ds \qquad (6)$$

and according to Simonsen is:

$$F_{Cat.1} = \sum_{Ship\ class,i} P_{C,i} Q_i \int_{Z_{min}}^{Z_{max}} f_i(z) dz \qquad (7)$$

The simplified expression for the category of ships which fail to change course at a given turning point near the obstacle (category II), according to Pedersen is:

$$F_{Cat.2} = \sum_{Ship\ class\ i=1}^{n\ class} P_{Ci} Q_i P_0^{(d-a_i)/a_i} \int_L f_i B_i ds \qquad (8)$$

and according to Simonsen is:

$$F_{Cat.2} = \sum_{Ship\ class,i} P_{C,i} Q_i e^{-d/a_i} \int_{Z_{min}}^{Z_{max}} f_i(z) dz \qquad (9)$$

where:

- F_{Cat} is expected number of groundings per year
- i is the index for ship class, categorized by vessel type and dead weight or length
- P_{ci} is the causation probability, i.e. ratio between [*actual*] ship groundings and ships on a grounding course
- Q_i is the number of movements per year of vessel class (i) in the considered lane
- L is the total width of the considered area perpendicular to the ship traffic
- B_i is the collision indication function, which is one when the ship strikes the structure or shoal and zero when the candidate colliding ship does not hit the obstacle, that is, passes safely or grounds prior to collision or grounding on the considered shoal.
- P_0 is the probability of omission to check the position of the ship
- d is the distance from obstacle to the bend in the navigation route, varying with the lateral position of the ship
- a_i is the average length between position checks by the navigator
- z is the coordinate in the direction perpendicular to the route
- (z_{min},z_{max}) are the transverse coordinates for an obstacle
- f_i or $f_i(z)$ is ship track distribution

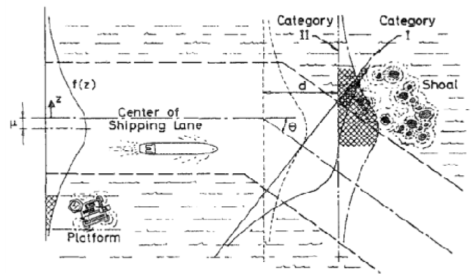

Figure 2: Distribution of ship traffic on a navigation route [source (Pedersen 1995)].

As is seen, Simonsen has replaced the Pedersen's B factor by integration boundaries Z_{Max} and Z_{Min}. Either B factor or integration boundaries let us to consider those ships that are in grounding or collision courses only (Figure 3).

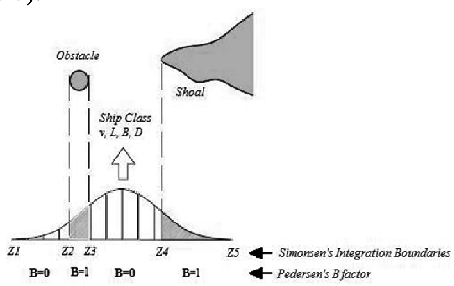

Figure 3: Grounding candidates for ships on straight route [adapted (Rambøll 2006)].

Pedersen's and Simonsen's models include the parameter a_i, average distance between position checks by the navigator. The parameter depends on navigational environment and ship characteristics as type and size. It should be estimated separately for every location and ship group. To get indicative results, some global values can be used. Nonetheless, the mentions of numerical values of a_i are very rare in the literature.

Simonsen has assumed the event of checking the position of the ship is a Poisson process; thus he replaced P_0 in Pedersen's equation Eq.(8) by an exponential function Eq.(9) This has made Simonsen's model less sensitive to the values of a_i, which will be shown later. Simonsen has mentioned that the theoretical result achieved by the model is quite sensitive to both the causation probability, P_C, and the distance between each position checking, a_i.

The most important advantage of their models is that instead of traffic volume and traffic densities, which have still some vagueness in their definitions, Pedersen and Simonsen used traffic distribution. Since the traffic distribution also shows the location of the vessels in the waterway, it is more precise than traffic volume or density for estimating the grounding candidates. In addition, it has made their models suitable for analyzing both grounding and stranding accidents. However, the main issue in using the traffic distribution is that in practice it needs a complete AIS database about the traffic to be precise; otherwise it is just traffic estimation, which decreases the accuracy of the method.

Improvements

Suggested Improvements for Macduff's Model

The probability should always be less than or equal to 1, and it is so for geometrical probability of grounding (P_G). Therefore it is obtained from Eq.(2) of Macduff's model that $\frac{s}{C} \leq \frac{\pi}{4}$; which is not always the case.

By reconsidering the Macduff's first idea about using Buffon's problem and also by applying the Buffon's needle problem's criteria differently, the authors suggest the geometrical probability of hitting the wall of a channel (stranding) to be estimated by Eq.(10). The equations are inspired from the presented solution for Buffon's problem by Wolfram MathWorld. The angle should be presented in Radian.:

$$P_G = \begin{cases} \frac{2s}{\pi C} & for\ \frac{s}{C} \leq 1 \\ \frac{2}{\pi} \times \left(\frac{s}{C} + \cos^{-1}\left(\frac{C}{s}\right) - \sqrt{\left(\frac{s}{C}\right)^2 - 1} \right) & for\ \frac{s}{C} \geq 1 \end{cases} \qquad (10)$$

The Buffon's problem is defined and solved for a needle laying down on just one line, while for grounding it should be solved for two parallel lines. Also it is not important if the needle intersects the line with its tail or head, while the direction of the hitting is another important matter for grounding event. Nevertheless, by assuming that ships always move forward (hitting with bow) and also in a channel (two parallel lines), the Buffon's equations Eq.(10) still can be applied for grounding event without any changes.

According to Figure 4, which is based on Eq.(10), P_G is almost equal to 1 for $\frac{s}{C} \geq 30$. Since Macduff has mentioned that "*it is estimated that ships are capable of stopping within a distance equal to 20 times their length*", s is equal to $20L$, where L is the length of the ship. Therefore by accepting Macduff's definition, ships are certainly grounding candidates for cases that $L \geq 1.5\,C$.

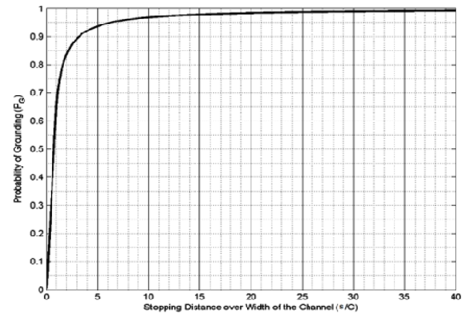

Figure 4: Probability of Grounding v.s. $\frac{s}{C}$

As has been mentioned, the geometrical model should present the candidate ships for grounding. In other words, it should present the probability of ships running aground while they are navigating in blind situation. Blind situation or blind navigation means not to do any action to avoid grounding; or in other words, not to adjust the course and speed over ground during the voyage in the channel. If it is so, does the stopping distance (s) has any meaning in blind navigation? The ship is supposed not to do any evasive action to avoid grounding; while stopping distance means that somebody on board has did some efforts to stop the ship before going aground. Moreover, the grounding can be avoided not only by stopping but also by changing the course. For instance, in high speed (usually more than 12 knots) the accident can be avoided more readily by turning than by stopping (Mandel 1967).

On the other hand, navigating under blind situation cannot be well defined; always there would be the risk of going aground in blind navigation, even in safe routes. For instance in Figure 5, there would always be risk of grounding for a ship navigating under blind situation, even for ships navigating between two region 1s (safe transit channel). However, in reality those ships that have entered the region 1 are those who are candidates for going aground; if they do evasive action, they will survive. Still for some reasons with different probabilities, all of them will not be able to avoid entering region 2. Most probably those ships that have entered region 2 will run aground, because the maneuvering ability of the ship to avoid grounding will be decreased (Amrozowicz et al. 1997). The widths of the regions 1 and 2 are dependent on different parameters such as vessel's characteristics and environmental conditions.

Macduff's model can be modified by the help of Figure 5. If C is considered as the width of the safe transit channel (Figure 5), then Macduff's P_G would be the probability of being a grounding candidate. In this case a new definition for s is needed, which with the help of

Simonsen idea (assuming as a Poisson process) can be defines as:

$$s = L \times e^{\left(\frac{-C}{V \times a}\right)} \quad (11)$$

where:

V is the (average) speed of the ship(s)

a is the (average) time between each position checking by the navigator(s)

L is the (average) length of the ship(s)

C is the (average) width of the channel

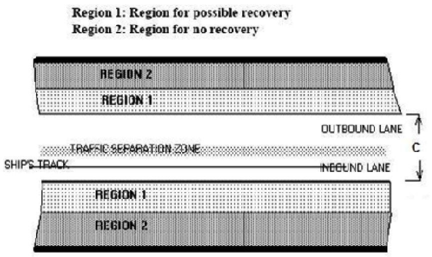

Figure 5: Hypothetical waterway [adapted (Amrozowicz et al. 1997)].

Since the probability in Macduff's improved model is very sensitive to the changes of $\frac{s}{C}$ where $0 < \frac{s}{C} < 5$ (Figure 4), it is very sensitive to any changes of s. This shows the need of having a reasonable definition for s. A question still remains whether s should be the stopping distance or something else like Eq.(11)?

A better method for describing the situation (for both grounding and stranding accidents) could be ship domain, as demonstrated in Figure 6. If the vessel does not turn before the region 1 of the domain hits the channel's wall or a shoal, the vessel will be a grounding candidate. However, she still can survive if an evasive action takes place. If the evasive action is not performed and the region 2 of the domain hits the wall or shoal, most probably the ship will go aground.

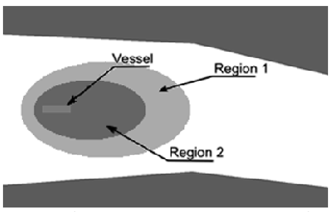

Figure 6: An example of hypothetical ship domain for grounding.

According to (Zhu et al. 2001) the ship domain should be defined according to the navigator's sense of safety. The fact is that in the case of grounding, the safe area cannot be separated from the dangerous area by a simple line; so that passing the line would mean the ship is in danger, and not passing would mean she is safe. Thus, to improve the above idea, an interesting tool could be fuzzy theory by Zadeh (Zadeh L. A., Fuzzy sets (1965), Information and control, No. 8, 338). By applying fuzzy logic method on different affecting factors, the above theory can be modified in order to give a better estimation of grounding probability. This method can be applied for every single factor affecting the size and the shape of the ship domain. The resulted domain is *fuzzy ship domain* (Figure 7). Using fuzzy boundary for ship domain is proposed by (Zhao et al. 1993) and is developed by (Pietrzykowski and Uriasz 2009) for ship-ship collision; however it has never been used for ship grounding.

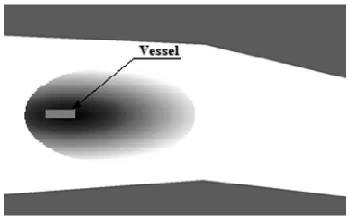

Figure 7: An example of fuzzy ship domain for grounding.

The main issue here is to define and calculate the shape and the size of the domain's regions. They are related to many factors such as size and the speed of the vessel and topography of the sea bed. Also a suitable ship domain for grounding is a 3D domain; and a 2D domain does not work properly for grounding.

The fuzzy ship domain is suitable for both geometrical probability modeling and also for real time grounding probability analysis of an individual ship, which could be useful for Decision Support Systems (DSS) on board the ships or at VTS (Vessel Traffic Service) centers [Cited in (Pietrzykowski 2002)]. However, the geometrical models are just practical for analyzing the whole traffic in a specific area, which is useful for predicting future risks and precautionary plans.

Comments on Fujii's Model

Referring to Eq.(3), since the number of grounding (N) has an inherent time factor[1], its dimension is $\frac{Number\ of\ the\ ships}{T}$. By this definition, the dimension of the density of the traffic flow according to (Fujii et al. 1974) would be gained as:

$$[\rho] = \frac{Number\ of\ the\ ships}{(L)^2} \quad (12)$$

if[2]:

[N] = Number of the ships / T

[D] and [B] = L

[V] = L / T

$[P_C]$ = *Dimensionless*

If it is so, referring to Eq.(5), the dimension of traffic volume (Q) would be gained as:

$$[Q] = [\rho][W][V] = \frac{Number\ of\ the\ ships}{T} \quad (13)$$

Fujii has mentioned that "*the traffic flow density is equal to the traffic volume per unit width of waterway*" (Fujii et al. 1974), which makes the authors to reach to the conclusion that the traffic volume (Q) should be equal to the product of the traffic flow density (ρ) and width of the waterway (W):

$$Q = \rho \times W \Rightarrow [Q] = \frac{Number\ of\ the\ ships}{L} \quad (14)$$

[1] The number of groundings or grounding candidates should always be accompanied by the term of "*per time unit*"; otherwise it would be confusing.

[2] Square brackets are used to show the dimension of an element

On the other hand, Fujii has mentioned another definition for traffic volume in his paper as "*the product of the traffic density and the average speed*" (Fujii et al. 1974). Therefore:

$$Q = \rho \times V \Rightarrow [Q] = \frac{Number\ of\ the\ ships}{LT} \quad (15)$$

As is showed, three different dimensions for traffic volume could been extracted from his paper, while he has actually mentioned the dimension for traffic volume as "*the number of the ships per km^2*" (Fujii et al. 1974) or

$$[Q] = \frac{Number\ of\ the\ ships}{(L)^2} \quad (16)$$

which does not match none of them above, and also is similar to what is extracted for traffic density. As is seen, there is no clear definition neither for traffic volume nor for traffic density according to (Fujii et al. 1974).

Suggested Improvements for Fujii's Model

In authors' opinion, the traffic density should be defined as the number of ships per unit area of the waterway. However, there are two points that should be considered:

1. Since the traffic is compressible and is not stationary, the time is an inherent factor for traffic density. Thus the time window has to always be considered when defining the traffic density. To overcome this barrier, the length of the area, within which the traffic density is going to be defined, will be connected to the desired time window. It means that the length of the studied area is equal to the distance that the traffic (ships) travels within the desired time window.
2. Since traffic of, for instance two small boats differs from traffic of two VLCCs (Very Large Crude Carrier), the dimensions of the vessels also should be considered in traffic density definition. Therefore a dimensionless parameter, size factor, should affect the traffic density.

Thus the authors recommend defining the traffic density as:

$$\rho = \frac{Number\ of\ the\ ships}{(W \times L^*)_{Waterway}} \times \overbrace{\left(\frac{(\sum(L \times B))_{Vessels}}{(W \times L^*)_{Waterway}}\right)}^{Size\ Factor} \quad (17)$$

where

L^* is the distance that traffic travels within desired time window

As a result the dimension of the traffic density would be the same as what is extracted from (Fujii et al. 1974) and then, with the help of mass flow rate concept in fluid dynamic, the *traffic flow rate* could be defined as:

$$Q = \rho W V \quad (18)$$

where V and W are the average velocity of the vessels and the width of the waterway, respectively.

If it is so, the dimension for the traffic flow rate would be gained as:

$$[Q] = [\rho][W][V] = \frac{Number\ of\ the\ ships}{T} \quad (19)$$

(Kristiansen 2005) named this traffic flow rate (Q) as the "*arrival frequency of meeting ships*", when he was analyzing the expected number of head-on collisions in his book. General believe about the traffic volume is the number of the vehicles passing an imaginary line during a specific period of time (Jacobson 2007). Therefore, regarding to Eq.(19) the traffic flow rate cannot be taken as traffic volume. However, can traffic volume be compared with a fluid dynamic concept so-called flux? If it is so, traffic volume (or traffic flux) could be defined as the number of vessels navigating through a unit line per unit time; or the product of the traffic density and the average speed Eq.(20), which is similar to one of the Fujii's definitions for traffic volume.

$$\emptyset = \rho V \Rightarrow [\emptyset] = \frac{Number\ of\ the\ ships}{LT} \quad (20)$$

Since the used density in this formula has been redefined by Eq.(17), the size of the vessels also affects the traffic volume.

In this regard, the traffic flow of ships towards a shoal with the effective width of D+B and average speed of V can be defined as:

$$\varphi = \int_{T_1=0}^{T_2=T} \rho V(D+B)dt = \emptyset(D+B)T \quad (21)$$

where:

T is the time window in which the traffic flow is desired to be calculated

Thus, the number of grounding candidates per time unit would be calculated as:

$$N_G = \frac{\varphi}{T} = \emptyset(D+B) \xRightarrow{B \ll D} N_G = \emptyset D \quad (22)$$

As a result, the number of groundings (N) per time unit could be calculated by using the probability of mismaneuvering (causation probability):

$$N = \emptyset D \times P_C \quad (23)$$

As is seen, the result is similar to what Fujii presented in his paper, but with changes in the definitions of traffic density and traffic volume. Without those changes, the yielded annual number of groundings would be different if different time windows were used.

It should be borne in mind that the traffic density has been considered constant during the time window for calculating the traffic flow. If the average traffic density is not used, or the time window is not small enough so that the traffic density could be considered constant in it, then traffic density (ρ) should be defined as a function of time:

$$\varphi = \int_{T_1}^{T_2} \rho(t)V(D+B)dt \quad (24)$$

The question is that how easily the traffic density can be defined as a function of time? There are many factors that should be considered, like the season, day time, weather condition, economic situation, and some of them are hard to predict. However, even if the traffic density can be defined as a function of time, still using traffic density in geometrical modeling of grounding means that the traffic has been considered uniformly distributed. Thus, it may unnecessarily decrease the accuracy of the yielded results. This could be considered as the main disadvantage of using traffic density (analytical models) instead of actual ship traffic distribution (statistical models) in geometrical modeling of grounding.

Application of Dominant Models

For calculation of grounding frequency, a waterway on the way to Sköldvik (Figure 8) has been chosen. Two locations have been indicated from the area for two different types of calculations. First type of calculation is about Pedersen's category I of groundings; and the chosen location for this purpose is the waterway between islands on the way to Sköldvik (Location 1 inFigure 8,Figure 9). For this type of calculation, the models of Macduff, Fujii and Pedersen are used. It should be noted that for type I calculation the models of Pedersen and Simonsen do not differ. The second type is about Pedersen's category II of groundings (Location 2 in Figure 8,Figure 12). For the second type of calculation, just the models of Pedersen and Simonsen are used, as other models do not consider the scenario of omitting a turn in vicinity of a shoal.

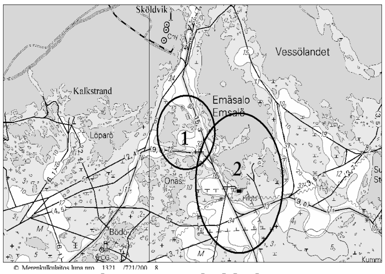

Figure 8: Waterway on the way to Sköldvik.

Majority of vessels navigating to Sköldvik port are tankers, so only tankers are taken into account in the calculations. AIS data of year 2008 is used to get traffic characteristics as tanker length and draft.

All the calculations yield either the number of grounding candidates or the grounding candidate probability. It means that the causation probability does not affect the calculations or in other words, P_C has been considered as equal to 1.

Type I Calculations

The number of tankers that navigated northward along the waterway, for the location 1, was 1176 in 2008. The longest tankers on the waterway were 277 m long. The average length of tankers was approximately 147 m and the average breadth was 22.9 m. The studied channel was approximately 900 m wide and 2000 m long. The ship distribution on the waterway was combined normal (66 %) and uniform (34 %) distribution.

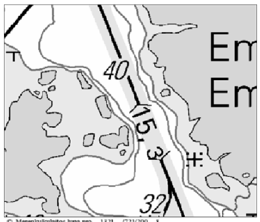

Figure 9: Location 1 (see Figure 8) between islands on the waterway to Sköldvik.

Macduff's Model

As it is mentioned before, to apply Macduff's model a waterway has to be approximated as a channel of which width is assumed not to change significantly when moving along the channel. No such channels exist in the Gulf of Finland. However, Macduff himself used his model for the Dover strait that is a natural channel as well; so its width is not constant either.

The modified equation of Macduff's model Eq(10) with C=900m, L=147m and s=20L gives the geometrical grounding probability of P_G=0.9018 or 1061 annual grounding candidates, which is a quite high probability. However, if the definition of s is replaced by the new definition Eq.(11) and V=11.78 kn and a=180s, the probability would be P_G = 0.0456 or 54 annual grounding candidates. The original equation of Macduff's model Eq.(2) gives the geometrical grounding probability of P_G = 4.16, which is not acceptable.

As is seen, the probability in Macduff's model is very sensitive to definition of s, which requests further attention to be rational. However, since there were no registered grounding accidents for the mentioned area during the past 12 years (1996-2008) in the database of Accident Investigation Board of Finland the new definition for s seems more reasonable.

Fujii's Model

To apply Fujii's model, it needs to be considered that the channel has shoals in the middle of it. For that reason, the islands on the western side of the channel are considered to be part of the channel. Thus the new width of the channel is 1960 m (D=850 m).

According to the new definition Eq.(17), traffic density (ρ) for the mentioned location is $3.32 \times 10^{-8}\ \frac{Ships}{km^2}$, when the time window is set to one year. Then, according to Eq.(20), the traffic volume (Φ) is $1.42 \times 10^{-6}\ \frac{Ships}{km \times h}$. Thus, by the help of Eq.(22), 0.0055 annual grounding candidates are obtained for the studied location; which would mean one grounding candidate every 182 years.

Pedersen's and Simonsen's Models

It is said that the model of Pedersen is implemented to the program called IWRAP Mk2. However for the event of checking position of the ships, it seems that the theory of Simonsen is used in the program. Nevertheless, the following calculations are made with IWRAP Mk2.

Depth curves of 10 m, 6 m, 3 m and 0 m of the area were inserted to the program. Figure 10 presents the waterway in question as it was defined for calculations in IWRAP Mk2, and Figure 11 presents the riskiest locations in the area. For the area in question, IWRAP Mk2 gave of 0.00544 grounding candidates annually when a blackout frequency of 1.75 was assumed and 0.00233 candidates if the blackout frequency of 0.75 was assumed. All grounding candidates are drift grounding candidates. Drift speed was assumed to be 1 knot. Interestingly, the first mentioned result is similar to what comes out from Fujii's improved model. However, it should be borne in mind that Fujii's presents just the annual grounding candidates, while IWRAP Mk2 presents both the annual grounding and stranding candidates together.

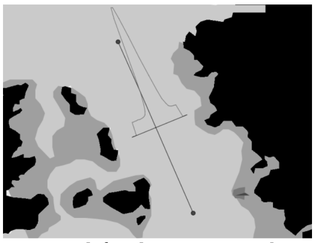

Figure 10: Location 1 as defined in IWRAP Mk2: grounds in black, 10 m depth curve in light gray, 6 m depth in medium gray, and 3 m depth curve in dark gray.

Figure 11. Results of grounding frequency calculation of IWRAP Mk2. The depth curves are shown white here for more clarity. A scale from light gray to dark gray is used to illustrate the grounding probability for different locations: dark gray signifies the highest number of grounding candidates in the analyzed area.

Type II Calculations

For type II calculations, an example location on the way to Sköldvik was chosen (Location 2 in Figure 8,Figure 12). Ships have to turn or they will run aground on an island about 1000 m after they have omitted to turn. On this waterway, 893 tankers navigated northwards in 2008. The largest tankers heading to Sköldvik cannot use the waterway in question and thus the length of all tankers is less than 175 m and the most common length group of tankers is 125-150 m. The average speed of the tankers approaching the island is 19.2 knots.

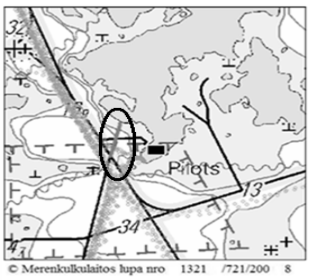

Figure 12: Location 2 on the waterway to Sköldvik (grounding scenario is marked with black ellipse).

Table 1 presents the number of annual grounding candidates in the studied waterway according to Pedersen's and Simonsen's models for different mean times between position checking, which results different values of a_i. From Table 1, it is obvious that Pedersen's model is very sensitive to the value of a_i. Simonsen has assumed the event of checking the position of the ship to be a Poisson process, and this made his model less sensitive to a_i compared to Pedersen's model. Still, Simonsen has claimed that his model is also sensitive to the value of a_i. However, the sensitivity of Simonsen's model will decrease when the larger values are used for a_i; which was predictable as he uses Poisson process. As a conclusion, it should be noted that hardly even professional navigators can estimate a_i so exactly that it would not give a large uncertainty to the results. (Ylitalo et al. 2008)

Table 1: Number of type II grounding candidates with different time interval of checking the position.

Mean time between position checking	30s	60s	90s	120s	150s	180s	210s
Annual grounding candidates according to Pedersen's model	0.02	37.68	502.38	1834.37	3989.88	6697.94	9697.12
Annual grounding candidates according to Simonsen's model	30.57	165.21	289.94	384.10	454.7	508.84	551.41

Conclusion and Further Research

Calculations of type I have showed that four used models give different results for the number of annual grounding candidates. Since, for the studied area, there are no available databases about the near-missed cases and no registered actual groundings in the database of Accident Investigation Board of Finland for years 1996-2008, it is hard to say which model gives more accurate results than the others. In general, it seems that the chosen location is not a high risk area for grounding accident. Thus low probability for grounding candidates seems more sensible.

Calculations of type II show Pedersen's approach gives more grounding candidates than the actual traffic (893 tankers) for mean times between position-checking longer than 100 s. Although it is hard to define an exact value for mean time between position-checking, using larger values than 100 s is not rare; for instance IWRAP Mk2 uses 180 s as its default value. In addition, Simonsen's model is less sensitive to the values of a_i. Thus Simonsen's approach is more rational than Pedersen's.

The main issue in analyzing the risk of grounding is that by today's knowledge, a holistic and precise model which could describe the reality, if not say impossible, is at least a really hard goal to achieve. Although Macduff and Fujii were the pioneers in the geometrical analysis of the grounding probability, it is shown in this paper that their methods have some weaknesses. So far, it can be said that Simonsen's model, which is based on Pedersen's first idea, is a more rational and completed geometrical model than other mentioned models. Simonsen considers (like Pedersen) not only the class, dimensions and velocity of the vessels, but also the distance between position-checking, which is more or less a human factor in navigation. One another important issue is that geometrical probability and causation probability are closely linked to each other when calculating the grounding probability. When estimating causation probability, the used geometrical model has to be taken into consideration. The simplest way to calculate the causation probability is to divide the number of actual groundings by the number of grounding candidates, like what (Macduff 1974) and (Fujii et al. 1974) did. Thus, the causation probability includes a close link to the used geometrical model. Therefore, the causation probability cannot be directly used with other geometrical models. Nor can it be compared with other causation probabilities without paying attention to the geometrical models they are made to be used with.

It seems there is no place for more improvement in Macduff’s and Fujii’s models, based on their first theories. Thus, in order to find a better model for estimating the ship grounding probability, either Simonsen’s model should be improved or another method, for instance using fuzzy ship domain, should be introduced. Introducing a 3D fuzzy ship domain, with proper shape and size, for ship grounding probability analysis is the idea that authors consider as their next step in their researches.

Acknowledgment

The authors wish to thank the financial contribution of the European Union and the city of Kotka. This research is carried out within SAFGOF project and in association with Kotka Maritime Research Center.

References:

2009. "IWRAP Wiki site." IALA Waterway Risk Assessment Programme.

Amrozowicz, Michael D., Alan Brown and Michael Golay. 1997. "A Probabilistic Analysis of Tanker Groundings." In 7th International Offshore and Polar Engineering Conference. Honolulu, Hawaii.

Dziedzic, T., Pietrzykowski, Z., Uriasz, J., (2000), ”Knowledge-based system for evaluation of ship’s navigational safety”, In Proc. of 1st Conf. COMPIT 2000, Potsdam, 132-140

Fowler, Timothy G. and Eirik Sørgård. 2000. "Modeling Ship Transportation Risk." Risk Analysis 20(2):225-244.

Fujii, Yahei. 1983. "Integrated Study on Marine Traffic Accidents." In IABSE Colloquium. Copenhagen, Denmark.

Fujii, Yahei, Ryozo Oshima, H. Yamanouchi and N. Mizuki. 1974. "Some Factors Affecting the Frequency of Accidents in Marine Traffic: I- The Diameter of Evasion for Crossing Encounters, II- The probability of Stranding, III- The Effect of Darkness of the Probability of Collision and Stranding." Journal of Navigation 27(2):239-247.

Gucma, Lucjan. 2006. "The method of navigational risk assessment on waterways based on generalised real time simulation data." In Proc. International Conference on Marine Simulation and Ship Maneuvaribility. Terschelling, Netherlands.

Hansen, Peter Friis, Anders Melchior Hansen and Bo Cerup Simonsen. 2000. "User Manual for GRACAT- Grounding and Collision Analysis."

Hansen, Peter Friis and Bo Cerup Simonsen. 2001. "GRACAT: Software for Grounding and Collision Risk Analysis." In International Conference on Collision and Grounding of Ships (ICCGS). Copenhagen, Denmark.

Jacobson, Sandra. 2007. "The Role of Traffic Volume in Habitat Connectivity and Mortality."

Jebsen, Johan Jarl and Vassilis Constantine Papakonstantinou. 1997. "Evaluation of the Physical Risk of Ship Grounding." In Department of Ocean Engineering: Massachusetts Institute of Technology.

Karlsson, Max, Finn M. Rasmussen and Lars Frisk. 1998. "Verification of ship collision frequency model." In Ship Collision Analysis. Balkema, Rotterdam.

Kite-Powell, Hauke L., Di Jin, Johan Jebsen, Vassilis Papakonstantinou and Nicholas Patrikalakis. 1999. "Investigation of Potential Risk Factors for Groundings of Commercial Vessels in U.S. Ports." International Journal of Offshore and Polar Engineering 9(1):16-21.

Kristiansen, Svein. 2005. "Traffic-Based Models." In Maritime Transportation-Safety Management and Risk Analysis.

Kujala, Pentti, Maria Hänninen, Tommy Arola and Jutta Yliato. 2009. "Analysis of the marine traffic safety in the Gulf of Finland." Reliability Engineering & System Safety.

Kunkel, Paul. 2009. "Buffon's Needle Problem." ed. Arsham Mazaheri. Personal Communication.

Macduff, T. 1974. "The Probability of Vessel Collisions." Ocean Industry 9(9):144-148.

Mandel, Philip. 1967. "Ship Maneuvering and Control." In Principles of Naval Architecture, ed. John P. Comstock. New York.

Mazaheri, Arsham. 2009. "Probabilistic Modeling of Ship Grounding A review of the literature." In TKK-AM-10. Espoo: Helsinki University of Technology.

Otto, Sven, Preben T. Pedersen, Manolis Samuelides and Pierre C. Sames. 2002. "Elements of Risk Analysis for Collision and Grounding of a RoRo Passenger Ferry." Marine Structure 15:461-474.

Pedersen, Preben Terndrup. 1995. "Collision and Grounding Mechanics." In Proceedings of WEMT '95'. Copenhagen, Denmark: The Danish Society of Naval Architecture and Marine Enginerring.

Pietrzykowski, Zbigniew. 2002. "The analysis of a ship fuzzy domain in a restricted area." In IFAC Conference Computer Applications in Marine Systems CAMS'2001. Elsevier Science Ltd. 2002.

Pietrzykowski, Zbigniew and Janusz Uriasz. 2009. "The Ship Domain - A Criterion of Navigational Safety Assessment in an Open Sea Area." Journal of Navigation 62(1):93-108.

Quy, N.M., J.K. Vrijling, Pieter van Gelder and R. Groenveld. 2007. "Identification and Estimation of Ship Navigational Limits for Waterways Designs Using Simulation." In 4th International Conference on Collision and Grounding of Ships. Hamburg, Germany.

Rambøll. 2006. "Navigational safety in the Sound between Denmark and Sweden (Øresund)." Denmark: Rambøll Danmark A/S.

Ravn, Erik Sonne, Peter Friis Hansen and Per Engberg. 2008. "User Manual for the GRISK program." 1.0.10 Edition.

Samuelides, M.S., N.P. Ventikos and I.C. Gemelos. 2009. "Survey on grounding incidents: Statistical analysis and risk assessment." Ships and Offshore Structures 4(1):55-68.

Simonsen, Bo Cerup. 1997. "Mechanics of Ship Grounding." In Department of Naval Architecture and Offshore Engineering. Kongens Lyngby: Technical University of Denmark.

Ylitalo, Jutta, Maria Hänninen and Pentti Kujala. 2008. "Accident probabilities in selected areas of the Gulf of Finland." In TKK-AM-6. Espoo: Helsinki University of Technology.

Zhao, Jingsong, Zhalin Wu and Fengchen Wang. 1993. "Comments on Ship Domains." Journal of Navigation 46(3):422-436.

Zhu, Xiaolin, Hanzhen Xu and Junqing Lin. 2001. "Domain and its model based on neural networks." Journal of Navigation 54(1):97-103.

SAFGOF a cross-disciplinary modelling approach to minimizing the ecological risks of maritime oil transportation in the Gulf of Finland

Annukka Lehikoinen

University of Helsinki, Department of Environmental Sciences, Fisheries and Environmental Management group (FEM)

Abstract:
The maritime traffic in the Gulf of Finland (GoF) is predicted to rapidly grow in the near future, which increases environmental risks through both direct environmental effects and by increasing the accident risk. This paper describes a multidisciplinary oil accident risk modeling approach which is under development in the EU funded project SAFGOF. Based on varying growth predictions, three alternative scenarios concerning maritime traffic of the GoF in year 2015 have been produced by the project and the probability for a major oil accident and its likely effects on the ecosystem in the light of spatial biodiversity are under modeling. In the future, this model can be conditioned to selected management actions which provides for comparing their effects on the accident probabilities and total ecosystem risk. In the modeling work, Bayesian belief networks (BBNs) are applied. The approach will produce unique information on the environmental oil accident risks separately for most accident-prone areas in the GoF, which would enable efficient local risk control actions to be analyzed by the decision makers e.g. to decrease the probability of accidents.

Introduction

Environmental issues are typically multidisciplinary by nature, dealing with natural interactions as well as societal and economic issues (Burgman, 2005). Thus, when evaluating the environmental risks aroused by human society, we operate with very complex and multidimensional system. Cause-effect chains beginning from the human needs (“drivers”) to business that harms or has a potential to harm the ecosystem (“pressures”) and further on, to their actual impacts on the ecosystem “state”, is long and complicated. Each part of the chain is related to either stochasticity (aleatory uncertainty) or knowledge-based (epistemic) uncertainty in many cases both of them. Decision-makers should still be able to manage and evaluate these huge entities and make justifiable decisions despite the uncertainty. They should also assess the cost-effectiveness of different management actions (“responses”) as well as the costs (“impacts”) for the kind of ecosystem elements that are somewhat impossible to put a price on. A common problem in environmental management is that decisions should be made based on fragmented data sets and models, or possibly competing expert opinions (Burgman, 2005). Decision-makers are typically faced with a flood of information, in which the comparability of results is poor and uncertainties high. An optimal solution based on point estimates of the state of nature may not be the safest one when compared with an optimal solution based on the best expected utility, taking the total uncertainty into account. The expected utilities of various options are uncertain; thus, choosing the “best” action is not self-evident (Burgman 2005). Often, a “one-answer” scenario is not enough, and a conclusion based on “many answers” derived from a series of decision support models is more realistic (Power and McCarty 2000).

Decision analyses and decision support systems are terms for methods that provide a quantitative means to study alternative decisions in the presence of multiple aims (e.g. Clemen, 1996). They ease the work of decision-makers by helping them to make consistent and justifiable choices. As more and more complicated and multifaceted evaluation problems arise in the field of environmental issues, it is essential to develop operational decision support tools that can readily support and evaluate “what-if” scenarios by altering parameters used in different decision support methods (Power & McCarty, 2000). The evaluation of the nature and extent of uncertainty should always be included in these tools to make the process transparent and to give the decision-makers a realistic picture of the uncertainty and the range of the possible outcomes of the management actions (Burgman, 2005; Power and McCarty, 2006). Modeling aims at finding out optimal decisions; when and where these investments on the future state of our environment are most effective?

The purpose of this paper is to present a risk assessment and decision support tool that is under construction in the EU funded project (2008-2010) “SAFGOF Evaluation of the traffic increase in the Gulf of Finland during the years 2007-2015 and the effect of the increase on the environment and traffic chain activities”. From the viewpoint of maritime accident research, the point of this presentation is to describe an idea how ship accident modeling can - and should - be exploited when evaluating the environmental risks towards marine ecosystems caused by human activities. It also describes an idea how probabilistic Bayesian networks can be used as helpful tools when integrating different types of models and multidisciplinary knowledge.

Problem description: environmental risks arising from the oil transportations in the Gulf of Finland (GoF)

The Gulf of Finland (GoF), a large basin of the brackish Baltic Sea, is one of the world’s most stressed sea areas with substantial nutrient loading and intensive maritime traffic that is predicted to strongly increase in the near future (see Klemola et al., 2009; Kuronen et al.

2008). The increasing amount of oil transport in addition to the increase of ships navigating in the GoF, will inevitably lead to a raised probability of a large scale oil accident. The International Maritime Organization (IMO) has designated the Baltic Sea, including the Gulf of Finland, as a Particular Sensitive Sea Area (PSSA) needing special protection (IMO, 2005). Since many organisms and communities are negatively affected by other anthropogenic activities, the ecosystem effects of an oil tanker accident and a resulting oil spill would most probably be serious, especially on rare and endangered species (Ihaksi et al.; 2007; Juntunen et al., 2005; Kokkonen et al., 2010). The need for comprehensive, sub-regional risk assessment tools and evaluation methodology targeting the minimization of the oil accident probability and the negative effects of them in the Baltic Sea is commonly recognized (e.g. HELCOM, 2007; Steiner, 2004). Such tools would be of great aid in trying to reach international consensus of the best ways to manage the risks. So far, the oil spill risk management work in the Baltic Sea and GoF has focused mainly on the minimization of the negative impacts through efficient oil recovery organization. In addition, it is still essential to assess alternative precautionary strategies. The unfinished modeling approach described here is designed to help in investigation of the overall probability for an oil accident and its ecosystem-level consequences as well as the efficiency of different management policies under alternative (uncertain) future scenarios. Commercial software Hugin Expert ® (Madsen et al., 2005) is used to build a probabilistic meta-model structure that integrates latest maritime traffic statistics, predictions based on alternative growth scenarios, modern accident modelling techniques, ecosystem models and a spatial map-based valuation interface. This paper focuses on describing the methodology and techniques used for the integration of this kind of multidisciplinary information and the information flow between multiple sub-models. As the work is still going on, the actual end results gained with the model are not reported here.

Bayesian Belief Networks (BBN) and Influence Diagrams (BID)

Bayesian belief networks (BBN) are models for reasoning under uncertainty through computing our updated beliefs about (unobserved) events given observations on other events (Kjærulff and Madsen, 2005). They were originally developed as a formal means of choosing optimal decision strategies under uncertainty (Pearl, 1986). Since then, BBNs have been successfully exploited in modeling complex environmental questions and interactions containing significant uncertainties (Borsuk et al., 2004; Marcot et al., 2001; Reckhow, 1999) as well as in decision analysis under uncertainty (e.g. Kuikka and Varis, 1997; Uusitalo et al., 2005; Varis et al., 1990).

A BBN is a probabilistic model in which each variable has a particular number of mutually exclusionary states of outcome and where its relation to the other variables is defined with links (Jensen, 2001; Kjærulff and Madsen, 2005). Each random variable having incoming links has a conditional probability table (CPT). A CPT contains the information on conditional probability distributions specifying a probability of a variable being in a certain state depending on the configuration of its parents. Unconditional variables (without parents), in turn, have only one prior distribution describing the relative credibilities of the states. Divergent ways to produce these probability distributions can be used, from simulations and data analyses (e.g. Gilks et al., 1994; Mäntyniemi, 2006) to interviews of one or more experts (e.g. O'Hagan et al., 2006; Uusitalo et al. 2005).

BBNs enable the combination of data sets of different forms and with different precision to a single analysis, and the assessment of the origin, type and magnitude of the uncertainties related to the cause-effect relationships and decisions. They provide a possibility to integrate qualitative knowledge with quantitative data, which makes them extremely useful in multidisciplinary questions. BBNs enable the incorporation of social values, expert assessments, and scientific data or statistics into the same analysis (Bromley et al., 2005; Klemola et al. 2009; Marcot et al., 2001). Afterwards, the BBN can be used to evaluate the functioning of the system by manipulating the state of some variables and calculating the effects on others. The inference within a BBN follows the rules of probability calculus. When one or more of the variables are observed, the marginal probability distributions of other variables are updated according to the Bayes' rule

$$P(\Theta|X)=P(X|\Theta)P(\Theta)/P(X) \qquad (1)$$

where $P(\Theta)$ is the prior distribution of unobserved variables, $P(X|\Theta)$ is the CPT of observed variable X conditional on unobserved variables Θ, $P(X)$ is the probability of the observed evidence, and $P(\Theta|X)$ is the result of learning: the conditional distribution of unobserved variables given the observed evidence.

BBNs augmented with decision variables including alternative actions to take, and utility functions specifying our preferences concerning the output, are called Bayesian Influence Diagrams (BID) (Kjærulff & Madsen 2005). The objective of a BID is to identify the action d_i of the decision node D that produces the highest expected utility (*EU*), being calculated as

$$EU(d_i) = \sum_j U(d_i, h_j) P(h_j \mid X) \qquad (2)$$

where h_j is a state of the (outcome) variable *H*, $U(d_i, h_j)$ is the value or utility gained if h_j comes true (when action d_i has been taken), and *X* represents our data or evidence. A BID can compute the EUs of all combinations of decision options given the state of uncertainty at the time of the decision, thus they are found to be flexible tools in the construction of different kinds of DSS's (e.g. Borsuk et al., 2004; Marcot et al. 2001;Varis, 1997). Because of their understandability and clarity, BBNs and BIDs are found to be accessible also to decision-makers without earlier modeling experience (Cain et al., 2003).

Risk assessment and decision analysis model (SAFGOF)

Plenty of studies have been conducted on the short and long term impacts of oil on marine species and communities around the world (e.g. Brown et al., 1996; Peterson et al., 2003), some of which particularly on the organisms and ecosystem of the Baltic Sea (e.g. Carr and Lindén, 1984; Tedengren and Kautsky, 1987). Juntunen et al. (2005) have earlier constructed a BBN model, which was developed for combining the results of these studies and predicting biological consequences of a random oil accident in the Gulf of Finland given different environmental and intervention scenarios. Its main purpose is to study the effects of the interventions (management of maximum tanker size and oil recovery capacity) on biological impacts given the details of an accident (accident type, tanker capacity and oil type), location (coastal area or open sea) and environmental conditions (season and wave height). The biological consequences are evaluated in terms of disturbance caused by the oil on different groups of organisms (aquatic and terrestrial plants, aquatic invertebrates, fish, birds and seals living in the Gulf of Finland) and the recovery of the disturbed populations afterwards. The iterative nature of Bayes' theorem (Ellison, 2004) allows us to use certain parts of this existing BBN by linking them to new variables and updating their state accordingly. The current approach is a BID that describes how different future oil transportation growth scenarios affect the biological risks, i.e. the probability and severity of an accident in the Gulf of Finland and how well the risks can be controlled by different management actions, given the growth scenario (Fig. 1). The model integrates several, uncertain future scenarios on maritime traffic with advanced accident models for spatial collision and grounding probabilities, all of which can be manipulated through a selection of management actions. The biological risk is evaluated by linking the BBN to nature value software OILECO, developed for the purposes of coastal oil combating prioritization (Kokkonen et al. 2010).

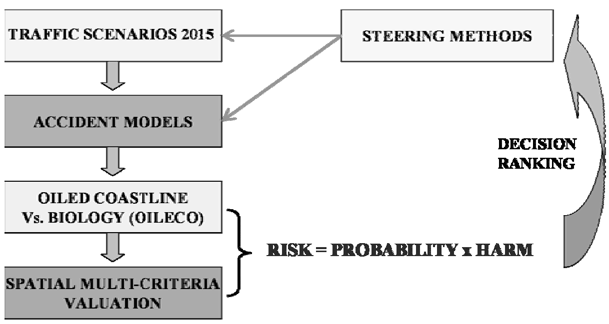

Fig. 1: Principle of the SAFGOF risk and decision analysis meta-model.

The BID structure includes decision variables defining the future maritime traffic scenario for year 2015, alternative accident probability management actions (preventative risk management) and alternative oil recovery design solutions (secondary risk management) (Fig. 2). In addition, the user will be able select one of the five accident prone "hot spots" on the map, for which the model can be run separately. The decision variables are providing input both to traffic pattern variables and directly to the sub-models of different accident types and factors. Accident types modeled are collisions and groundings. Separate sub-models for geometric and causation (human factor) probabilities will be included (Hänninen, 2008; Kujala et al., 2009; Mazaheri, 2009; Ylitalo et al., 2008).

Three probabilistic future growth scenarios for the maritime traffic in the GoF have been created based on earlier forecasts, current statistics and expert interviews (Kuronen et al. 2008). The main factors behind these scenarios are economic, industrial and transportation trends in the GoF's coastal countries as well as on European Union and global level. In the current model, the probability distributions of traffic amounts in different locations, ship types and sizes and also the amount and type of the oil transported are conditioned scenario-specifically. These all are affecting the oil accident probabilities and consequences and providing input for the collision and grounding models (Fig. 2).

Preventative management actions aim for preventing the oil accidents and damages caused by them beforehand. They can be grouped to regulatory, economic and information guidance policy instruments (Kuronen & Tapaninen, 2009). In the current study, the actions will be selected so that they affect different parts of the BBN: either the traffic parameters related to the geometric accident probabilities or the human factors affecting the causation probabilities given the growth scenario and location (Fig. 2). Despite the preventative actions, whenever the oil is transported, the possibility for an oil accident still exists. If a tanker collision or grounding happens, the spill occurrence and size are dependent on variety of factors, e.g. the size and speed of the tanker as well as the magnitude of damage to the hull, arrangement of the tanks, height of the oil column in the tanks, oil type etc. (see e.g. Devanney, 2006). Leak size modeling is a field so far quite poorly studied. In the current work, probability distributions for the likely spill size is modeled basing on the approach of Maxim & Niebo (2001) given the tanker size (dwt) and type of the accident (grounding or collision) (Tapio Seppälä & Yakub Montewka, unpubl.). However, the contents and structure of BBN are easily updatable whenever more sophisticated leak models - that are also under construction for the GoF - will be available.

In the case of a realized oil accident, effective oil combating plays a major role in minimizing the negative impact of oil on the vulnerable ecosystem of the GoF. Current oil combating is mainly based on mechanical recovery as recommended by Helsinki Commission (HELCOM, 2001), thus the efficiency depends not only on the arrangement, amount and capacity of existing recovery vessels in relation to the accident location but also environmental conditions and oil type (Helle, 2009). In the ongoing project, different oil recovery design and capacity alternatives are tested and the mechanical open sea recovery efficiency, given the accident location, evaluated. This BBN model will be linked to the main BID as a sub-model as well (Fig. 2).

The final product of the leak size and recovery efficiency sub-models (given the accident scenario) is variable (final amount of) *"Oil in water"* producing the probability distribution for the amount of oil that will be washed ashore (Fig. 2). For simplification, the offshore oil combating is not included into this study so far. The oil drifting model SpillMod (Ovsienko, 2002) is used for producing scenario-specific probability maps to evaluate the magnitude and spatial distribution of the Finnish coastal areas that are in greatest risk to be oiled. It models trajectory and fate of oil in different hydro-meteorological conditions sampled from historical weather statistics. SpillMod produces probability maps with the grid resolution of 2 x 2 km, in which a point estimate for percentual contamination probability of each cell is modeled. In the current study, the SpillMod maps are produced given the states of random variables *location of accident area* (five locations), *type of oil spilled* (three alternative viscosities: heavy, medium and light oil), *season* (weather statistics during last 10 years – three alternative states: spring, summer and autumn; winter and ice conditions are so far excluded) and *oil amount in water* (six alternative intervals). Duration of the spill (8 hours) and drifting time (10 days) are standardized. Total amount of possible accident location - scenario combinations - i.e. also the SpillMod model runs to be produced – is thus 270.

The concept of risk contains both the probability of a certain event and the magnitude of harm caused if it becomes true. The magnitude of harm or utility is always somewhat subjective a question, thus being problematic to be defined unambiguously (Burgman 2005). The current approach SAFGOF aims for producing risk assessments that are commonly acceptable and follow the current concerns and decisions of the society. The Gulf of Finland is geographically and ecologically unique area and hundreds of local – even unique – occurrences of threatened species living in the vicinity of Finnish shoreline have been detected. Leaked oil washing to the beaches might have irretrievable effects on the biodiversity if these unique populations are destroyed. Protection of the biodiversity and threatened species is an international objective regulated and supported by several laws, acts and conventions (e.g. Council directive 92/43/EEC; Council directive 79/409/EEC; Rassi et al., 2001). Evaluation of the harm caused by a random oil accident in the GoF is thus based on these commonly accepted rules and values also in the SAFGOF risk model.

Kokkonen et al. (2010) have developed decision support software OILECO for the prioritization of coastal oil combating in the GoF. It is based on mapped knowledge concerning spatial distribution of the detected threatened species occurrences on the Finnish coastline. For each occurrence, indexes of conservation value and recovery potential (resulting from several sub-factors, such as exposure and mortality indexes), ranging between 0 -1, are defined. In SAFGOF model, the "harm-value" of each SpillMod -map cell is determined by summing up the product of these two indexes for each of the occurrences included in that area. The higher the value in a cell, the greater the harm caused in the case that this particular cell would be contaminated by oil.

Finally, when both the integrative BBN model - including the traffic scenarios, accident and leakage models - and the SpillMod maps have been produced, they will be integrated by a GIS-software to run as one risk model (Fig. 2). Each of the cells on map will have a CPT including the contamination probability distribution resulting from the SpillMod run for each of the 270 combinations of scenario components in that particular cell. As the information concerning the scenarios is served in the form of probability distributions, the contamination probability of a cell will in practice have a corresponding scenario-specific distribution as well. The expected risk (*ER*) in each cell (c_j) can thus be calculated according to the formula of the expected utility (eq. 2) by giving negative values for the states of the utility parameter $U(d_i, h_j)$. We could also present the formula of ER as:

$$ER(c_j) = \sum_i R(c_j, s_{i,j}) P(s_{i,j} \mid Sc) \quad (3)$$

where $s_{i,j}$ is a state i of the (outcome) variable "*contamination probability"* in cell j (i.e. the probability of a cell to be oiled), $R(c_j, s_{i,j})$ is the "harm" caused if state $s_{i,j}$ comes true (in this particular cell c_j). Sc, in turn, represents our data or "knowledge" – in this case the selected scenario or settings in the decision variables. As ER values of all the cells will be summed up we end up to a single total risk –value (Fig. 2).

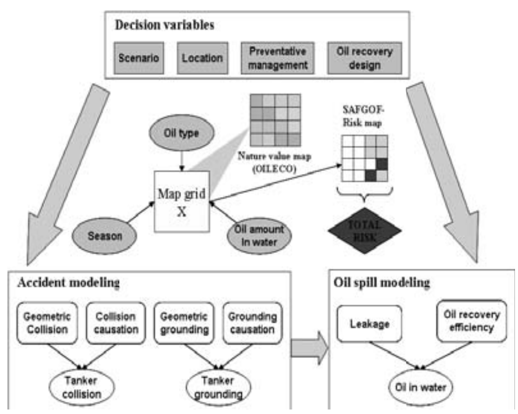

Fig. 2: Simplified model structure of SAFGOF risk assessment and decision support model. Pink squares illustrate decision variables, round cornered boxes are sub-models and green round nodes input information transformed from BBN to GIS.

Discussion and conclusions

The assessment of the total risk provides for summarizing the probabilistic information from multiple models and spatial distribution of both oil contamination probability and harm into one value. As such this value does not tell us much, but it is rather meant to be compared with the end results of the other scenarios. By comparing the total risks of alternative scenarios, it is possible to evaluate the effectiveness of different preventative management actions and oil recovery design solutions against each other. This can be done e.g. by choosing certain future growth scenario and / or accident location as starting points for the analysis or in the light of overall uncertainty concerning the future development and the place where the accident happens. This also enables assessing the robustness of the ranking order of management actions when the uncertainty in certain part of the model is manipulated something which can also be utilized for directing the further research work most cost-effectively.

Remarkable uncertainties are related to each of the model components: the future development of maritime transportations, the effect of the management actions, the severity of a possible accident and the biological consequences as well as the response of the ecosystem. A probabilistic approach enables providing a realistic picture of the accuracy of the current knowledge. In addition, with BBNs it is possible to integrate the best available knowledge of different forms. Results can be given in a graphic form that is relatively easy to understand. This provides an excellent base for planning of future actions, although careful orientation to the underlying ideology and discussion on the acceptable risk levels are first demanded to avoid gratuitous misconceptions.

As this type of a decision model covers such scenarios and states of the system that have never been observed but which are possible (and of high interest in the future) it cannot be validated with data in a traditional sense. Alternative ways to assess the goodness of BBN models still exist, e.g. learning from additional data, model testing against adaptive management, asking third party expert opinion or performing sensitivity analyses (see e.g. Barton et al., 2008).

The maritime traffic in the Gulf of Finland is expected to greatly increase in the future. At the same time, the indirect environmental effects of the traffic will increase. At the current phase of this ongoing study it seems that this kind of cross-disciplinary, probabilistic approach could help in creating more holistic view of the process and the related risks. Efficient risk management actions are in the first place typically dependent on the political will prevailing in the society. By compiling the existing multi-disciplinary knowledge and clearly and realistically showing the risks and our potential influence over them as well as the possible consequences of passivism, we can not only help the decision-makers in their demanding work, but also to rise public awareness and discussion on the situation. The magnitude of increasing knowledge and more holistic understanding on the system should not be undervalued either. By integrating accident probability modeling and ecological risk assessment and updating them with the latest statistics and forecasts, this model while fnalized will enable the evaluation of e.g. alternative shipping route plans and logistic re-organization as well as new legislation from the environmental point of view.

Acknowledgements

Author wish to thank the financers of the SAFGOF project: European Regional Development Fund, Regional Council of Kymenlaakso, City of Kotka, Kotka-Hamina Regional Development Company Cursor, Port of Hamina, Finstaship, Machine Technology Center Turku Ltd and Kotka Maritime Research Centre.

References:

Barton, D.N., Saloranta, T., Moe, H.O. & Kuikka, S. (2008): Bayesian belief networks as a meta-modeling tool in integrated river basin management Pros and cons in evaluating nutrient abatement decisions under uncertainty in a Norwegian river basin. Ecological Economics 66, p. 91-104.

Borsuk, M.E., Craig, A.S. & Reckhow, K.H. (2004): A Bayesian network of eutrophication models for synthesis, prediction and uncertainty analysis. Ecological Modeling 173, p. 219-239.

Bromley, J., Jackson, N.A., Clymer, O.J., Giacomello, A.M. & Jensen, F.V. (2005): The use of Hugin® to develop Bayesian networks as an aid to integrated water resource planning. Environmental Modeling and Software 20, p. 231-242.

Brown, E.D., Norcross, B.L. & Short, J.W. (1996): An introduction to studies on the effects of the Exxon Valdez oil spill on early life history stages of Pacific herring, *Clupea pallasi*, in Prince William Sound, Alaska', *Canadian Journal of Fisheries and Aquatic Sciences* 53, p. 2337-2342.

Burgman, M.A. (2005): Risks and decisions for conservation and environmental management. Ecology, biodiversity and conservation. Cambridge University Press, 488 pp.

Cain, J.D., Jinapalab, K., Makinb, I.W., Somaratnab, P.G., Ariyaratnab, B.R. & Pererab, L.R. (2003): Participatory decision support for agricultural management: A case study from Sri Lanka. Agricultural Systems 76, p. 457-482.

Carr, R.S. & Lindén, O. (1984): Bioenergetic responses of *Gammarus salinus* and *Mytilus edulis* to oil and oil dispersants in a model ecosystem, *Marine Ecology Progress Series* 19, p. 285-291.

Clemen, R.T. (1996): Making hard decisions: an introduction to decision analysis. 2nd edition, Belmont, CA,Duxbury Press, 696 pp.

Council Directive 92/43/EEC of 21 May 1992 on the conservation of natural habitats and of wild fauna and flora.

Council Directive 79/409/EEC of 2 April 1979 on the conservation of wild birds.

Devanney, J. (2006): The tankship tromedy: the impending disasters in tankers. Tavernier, Fla : The CTX Press, 401 pp.

Ellison, A.M. (2004): Bayesian inference in ecology, *Ecology letters* 7, p. 509-520.

Gilks, W.R., Thomas, A. & Spiegelhalter, D.J. (1994): A language and program for complex Bayesian modeling. The Statistician 43, p. 169-177.

HELCOM (2001): HELCOM Recommendation 22/2. Restricted use of chemical agents and other non-mechanical means in oil combating operations in the Baltic Sea.

HELCOM (2007): Baltic Sea Action Plan. Available online at: http://www.helcom.fi/stc/files/BSAP/BSAP_Final.pdf

Helle, I. (2009): Modelling the effectiveness of oil combating from an ecological perspective – a Bayesian network approach for the Gulf of Finland. MSc thesis, Helsinki University of Technology, Faculty of Engineering and Architecture, 98 pp.

Hänninen, M. (2008): Analysis of human and organizational factors in marine risk modelling – Literature review. Faculty of Engineering and Architecture, Department of Applied Mechanics, TKK-AM-4, 51 pp. Available online at: http://www.merikotka.fi/safgof/Hanninen_2008_Analysis.pdf

Ihaksi, T., Helle, I., Lecklin, T., Ryömä, R., Kokkonen, T. & Kuikka, S. (2007): Using biological knowledge and decisions of society in spatial prioritization of oil combating, ICES CM 2007 / C:02.

Jensen, F.V. (2001): Bayesian networks and decision graphs. Springer-Verlag, NY, 268 pp.

Juntunen, T., Rosqvist, T., Kuikka, S. & Rytkönen, J. (2005): How to model oil combating technologies and their impacts on ecosystem: a Bayesian network application in the Baltic Sea, ICES CM 2005 / S:02.

Kjærulff, U.B. & Madsen, A.L. (2005): Probabilistic Networks - An Introduction to Bayesian Networks and Influence Diagrams. Unpublished, 133 pp. Available online at: http://www.cs.aau.dk/~uk/papers/pgm-book-I-05.pdf

Klemola, E., Kuronen, J., Kalli, J., Arola, T., Hänninen, M., Lehikoinen, A., Kuikka, S., Kujala, P. & Tapaninen, U. (2009): A cross-disciplinary approach to minimizing risks of maritime transport in the Gulf of Finland. World Review of Intermodal Transportation Research 2(4), p. 343-363.

Kokkonen, T., Ihaksi, T., Jolma, A. & Kuikka, S. (2010): Dynamic mapping of nature values to support prioritization of coastal oil combating. Environmental Modelling & Software 25, p. 248-257.

Kuikka, S. & Varis, O. (1997): Uncertainties of climatic change impacts in Finnish watersheds: a Bayesian network analysis of expert knowledge. Boreal Environmental Research 2, p. 109-128.

Kujala, P., Hänninen, M., Arola, T. & Ylitalo, J. (2009): Analysis of the marine traffic safety in the Gulf of Finland. Reliability Engineering and System Safety 94(8), p. 1349-1357.

Kuronen, J., Helminen, R., Lehikoinen, A. & Tapaninen, U. (2008): Maritime transportation in the Gulf of Finland in 2007 and in 2015. Publications from the Centre for Maritime Studies, University of Turku A45, 110 pp. Available online at: http://www.merikotka.fi/julkaisut/Kuronen_Maritime_transportation_20 08_v2.pdf

Kuronen, J. & Tapaninen, U (2009): Maritime safety in the Gulf of Finland – Review on policy instruments. Publications from the Centre for Maritime Studies, University of Turku A49, 86 pp. Available online at: http://www.merikotka.fi/safgof/Kuronen_Tapaninen_SAFGOFWP6.pdf

Madsen, A.L., Jensen, F., Kjærulff, U.B. & Lang, M. (2005): The Hugin tool for probabilistic graphical models. International Journal on Artificial Intelligence Tools 14, p. 507-543.

Marcot, B.G., Holthausen, R.S., Raphael, M.G., Rowland, M.M. & Wisdom, M.J. (2001): Using Bayesian belief networks to evaluate fish and wildlife population viability under land management alternatives from an environmental impact statement. Forest Ecology and Management 153, p. 29-42.

Maxim, L. & Niebo, R. (2001): Oil spill analysis for North Slope oil production and transportation operations. In: Trans Alaska Pipeline System Owners 2001. Environmental Report for Trans Alaska Pipeline System Right-of-Way Renewal. Appendix B. 36 pp.

Mazaheri, A. (2009): Probabilistic modelling of ship grounding – a review of the literature. Faculty of Engineering and Architecture, Department of Applied Mechanics, TKK-AM-10, 72 pp. Available online at: http://www.merikotka.fi/safgof/ProbabilisticModelingofShipGrounding.pdf

Mäntyniemi, S. (2006): Bayesian fisheries stock assessment: integrating and updating knowledge. Academic dissertation, Rolf Nevanlinna Institute, Department of mathematics and statistics, University of Helsinki.

O'Hagan, A., Buck, C.E., Daneshkhah, A., Eiser, J.R., Garthwaite, P.H., Jenkinson, D.J., Oakley, J.E. & Rakow, T. (2006): Uncertain judgements: eliciting experts' probabilities. Wiley, Chichester, UK, 338 pp.

Ovsienko, S. (2002): An updated assessment of the risk for oil spills in the Baltic Sea area. 77 pp. Available online at:http://www.helcom.fi/stc/files/shipping/RiskforOilSpillsReport2002.pdf

Pearl, J. (1986): Fusion, propagation, and structuring in belief networks, Artificial Intelligence 29, p. 241-288.

Peterson, C.H., Rice, S.D., Short, J.W., Esler, D., Bodkin, J.L., Ballachey, B.E. & Irons, D.B. (2003): Long-Term Ecosystem Response to the Exxon Valdez Oil Spill, Science 302, p. 2082-2086.

Power, M. & McCarty, L.S. (2000): Risk-cost trade-offs in environmental risk management decision-making. Environ Sci Policy 3, pp.31-38.

Power, M. & McCarty, L.S. (2006): Environmental risk management decision-making in a societal context. Hum Ecol Risk Assessm 12, p.18-27.

Rassi, P., Alanen, A., Kanerva, T. & Mannerkoski, I. (2001): The Red List of Finnish Species. Ministry of the Environment & Finnish Environment Institute, Helsinki, 432 pp. (In Finnish, summary in English).

Reckhow, K.H. (1999): Water quality prediction and probability network models. Canadian Journal of Fisheries and Aquatic Sciences 56, p. 1150-1158.

Steiner, R. (2004): Gulf of Finland Oil Transport / Spill Issues: Summary and Recommendations from May 2004 visit. Available online at: http://www.ccb.se/newsletters/2004/summer/gulf_of_finland_oil_transport.pdf

Tedengren, M. and Kautsky, N. (1987): Comparative stress response to diesel oil and salinity changes of the blue mussel, *Mytilus edulis* from the Baltic and North Seas, Ophelia 28, p. 1-9.

Uusitalo, L., Kuikka, S. & Romakkaniemi, A. (2005): Estimation of Atlantic salmon smolt carrying capacity of rivers using expert knowledge. ICES Journal of Marine Science 62, p. 708-722.

Varis, O. (1997): Bayesian decision analysis for environmental and resource management. Environmental Modeling and Software 12, p. 177-185.

Varis, O., Kettunen, J. & Sirviö, H. (1990): Bayesian influence diagram approach to complex environmental management including observational design. Computational Statistics and Data Analysis 9, p. 77-91.

Ylitalo, J., Hänninen, M. & Kujala, P. (2008): Accident probabilities in selected areas of the Gulf of Finland. Faculty of Engineering and Architecture, Department of Applied Mechanics, TKK-AM-6, 49 pp. Available online at: http://www.merikotka.fi/safgof/Ylitalo_2008_Accident.pdf

Estimating ship-ship collision probability in the Gulf of Finland

Maria Hänninen and Jutta Ylitalo

Aalto University School of Science and Technology,Department of Applied Mechanics, Marine Technology

Abstract:
In this paper the overall ship-ship collision probabilities for the Gulf of Finland over open water season are estimated. The estimates are obtained as a product of the so-called number of collision candidates in head-on, crossing, merging, bending, and overtaking encounters on the waterways and causation probabilities describing the probabilities of not making an evasive maneuver in various meeting situations. The numbers of collision candidates are estimated based on Automatic Identification System data from the Gulf of Finland in the year 2008. Causation probability is modeled with a Bayesian Network. The modelling results in 0.3 ship-ship collisions per year, which is well comparable with recent accident statistics from the area. The estimated causation probability values for crossing and head-on encounters are of the same order as the probabilities presented in the literature. Most of the collision candidates are ships about to collide after omitting a turn in a bending waterway section and ships in an overtaking situation. The most accident-prone waterway is the main route from the entrance to the Gulf of Finland to St. Petersburg through the whole gulf. Collision probability is high especially in the eastern part of the route.

Introduction

The Gulf of Finland is one of the most heavily trafficked sea areas in the world. Marine traffic has been continuously increasing in the Gulf of Finland and especially the increasing number of oil tankers is raising concern in the coastal countries. Moreover, the growth of marine traffic is expected to continue within the near future (Kuronen et al. 2008). Unfortunately, the increasing ship traffic increases the probabilities of accidents, which could lead to oil spills. An oil disaster would most probably have serious effects on the Gulf of Finland ecosystem (Ihaksi et al. 2007), and the Baltic Sea, including the Gulf of Finland, has been categorized as a Particularly Sensitive Sea Area (PSSA) by the International Maritime Organization (IMO 2005).

18 major and several smaller ports are located on the shores of the Gulf of Finland (Kuronen 2008). Figure 1 presents the marine traffic in the Gulf of Finland on 1st and 2nd of July 2008 based on recordings of Automatic Information System (AIS) sent by the ships. From Figure 1 it can be seen that the busiest route is the waterway from the entrance to the Gulf of Finland to the eastern ports and back, and that intersecting traffic is especially high where the traffic between Helsinki and Tallinn crosses the main waterway.

The approach most commonly applied in mathematical estimation of the probability of ship-ship collisions in certain location is to calculate the accident frequency as a product of a so-called number of collision candidates and a causation probability (e.g., Fujii et al. 1971, 1974; Macduff 1974, Pedersen 1995). The number of collision candidates describes the number of ships that would collide, if no evasive manoeuvres are made, i.e., "blind navigation" is assumed. The number of collision candidates depends on the properties of ship traffic such as the lateral traffic distribution over the studied waterways, meeting angle, ship sizes and speeds. The causation probability denotes the probability of not making evasive manoeuvres while the ships are on a collision course, and it is conditional on the blind navigation assumption. The causation probability value has been estimated based on the difference between accident frequencies according to accident statistics and the estimated number of collision candidates (Fujii 1971, 1974; Macduff 1974), or by applying risk analysis tools such as fault tree analysis (Pedersen 1995, Rosqvist et al. 2002). In 2006, a document submitted by the Japanese agency for maritime safety to the IMO Maritime Safety Committee (2006) suggested the utilization of Bayesian networks in Step 3 of the Formal Safety Assessment, definition of risk control measures. Bayesian networks are directed acyclic graphs which consist of nodes representing variables and arcs representing the dependencies between variables (e.g. Jensen 2007). Each variable has a finite set of mutually exclusive states. For each variable A with parent nodes B_1, B_n, there exist a conditional probability table P(A | B_1, B_n). If variable A has no parents, it is linked to unconditional probability P(A). More recently, Bayesian networks have also been applied in causation probability estimation (Friis-Hansen and Simonsen 2002, Det Norske Veritas 2003, Det Norske Veritas 2006, Rambøll 2006, Hänninen and Kujala 2009). Regardless of the estimation method, causation probability values for crossing encounters in the literature have varied within $6.83 \cdot 10^{-5}$ $6.00 \cdot 10^{-4}$ (Macduff 1974, Fujii 1983, Pedersen 1995, Fowler and Sørgård 2000, Otto et al. 2002, Rosqvist et al. 2002) and for meeting ships within $2.70 \cdot 10^{-5}$ $6.00 \cdot 10^{-4}$ (Macduff 1974, Fujii 1983, Pedersen 1995, Karlsson et al. 1998, Fowler and Sørgård 2000, Rosqvist et al. 2002).

According to marine traffic accident statistics, groundings and collisions are the dominant accident types in the Gulf of Finland. Based on DAMA accident database and HELCOM's accident registrations in the Gulf of Finland within 1997-1999 and 2001-2006, there had been approximately 12 groundings and 5 ship-ship collisions per year (Kujala et al. 2009). Several studies on estimating the collision or grounding risks in the Gulf of Finland have been published (Hänninen et al. 2002, Rosqvist et al. 2002, Nikula and Tynkkynen 2007, Hänninen and Kujala 2009, Kujala et al. 2009), but none of these has been examining the overall ship-ship collision probability based on combining the accident probabilities of all the major waterways in the Gulf of Finland. In this study the focus is on collisions, but the grounding risk estimation for the Gulf of Finland has also begun (Mazaheri and Ylitalo 2010). The purpose is to estimate the overall ship-ship collision probabilities for the Gulf of Finland during open water season. The calculated collision candidates for head-on, crossing, merging, bending, and overtaking encounters on the waterways are combined with a causation probability model describing the probability of not making an evasive maneuver in various meeting situations. The resulting accident-prone areas are described, and accident databases are examined in order to compare the results of the models to the accident statistics.

The study is a part of a cross-disciplinary approach for minimising the risks of maritime transport in the Gulf of Finland (Klemola et al. 2009). The aim is to model the maritime traffic in the Gulf of Finland in the year 2015, and evaluate the resulting accident risk, the direct environmental effects and the risk of environmental accidents. The final aim is to model and compare the effects of legislation and other management actions on reducing marine traffic risks.

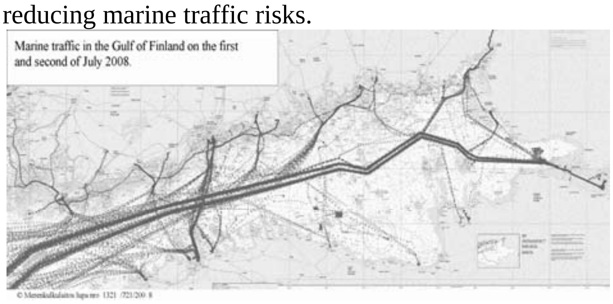

Figure 1. Marine traffic in the Gulf of Finland during on the 1st and 2nd of July 2008 based on AIS recordings.

Data and models

Automatic Identification System data [1]

The main data source for estimating the number of collision candidates was Automatic Identification System (AIS) recordings collected from the studied area for the year 2008. According to the studied AIS data, 39 511 ships had entered or exited the Gulf of Finland in 2008 and the most heavily trafficked internal waterway in the gulf was located between Helsinki and Tallinn. In 2008, 15 965 ships had navigated south or north between Helsinki and Tallinn. Seasonal variation of traffic volume is significant in the Gulf of Finland. The most heavily trafficked month had been July, both at the entrance to the Gulf of Finland as well as between Helsinki and Tallinn. In both locations, February had been the month with the least traffic. On the other hand, seasonal variation is more important between Helsinki and Tallinn than at the entrance to the Gulf of Finland: in February, the traffic volume was only 37 % of the traffic volume of July. At the entrance to the Gulf of Finland, the corresponding percentage was 77.

The ice season 2007-2008 was exceptional in the Gulf of Finland as it was the mildest winter since 1720 – the beginning of ice winter statistics gathering (Baltic Sea Portal 2008). Ice breaking was not needed at all. Thus, the AIS data of the year 2008 does not provide information concerning navigating in ice and does not help in estimating how winter affects traffic and accident probability. Therefore, in this study the winter time 2008 was treated as if it was a prolonged autumn.

Example Data of One Analyzed Waterway

As an example of the data applied in the analysis, the data of one waterway is presented here. The chosen waterway is located at the east side of Gogland and it is part of the route through the Gulf of Finland. Figure 2 presents histograms of lateral positions of ships on the waterway in question during the year 2008 (2a), and the applied fitted distributions (2b). The numbers and types of ships on the waterway are presented in Table 1. For the analysis, the ship type groups were divided further into size groups by ship length.

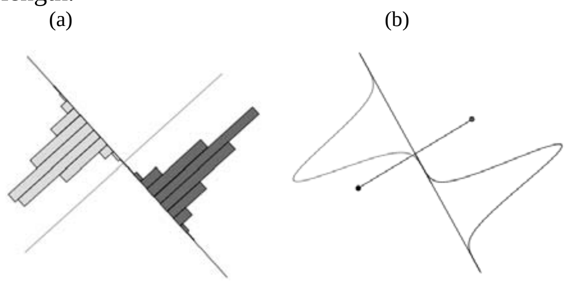

Figure 2. (a) Histograms of the lateral position of ships on the waterway at east side of Gogland; dark beams represent traffic to northeast and light beams traffic to southwest. (b) Distributions fitted to lateral position of ships on the waterway at east side of Gogland.

Table 1: Ship types and volumes in the waterway at east side of Gogland in 2008.

Ship type	Northeastbound	Southwestbound	Total
General cargo ship	3127	3108	6235
Container ship	2480	2455	4935
Oil products tanker	1005	1008	2013
Crude oil tanker	704	709	1413
Ro-Ro cargo ship	622	622	1244
Bulk carrier	533	541	1074
Passenger ship	426	390	816
Support ship	131	135	266
Chemical tanker	26	25	51
Pleasure boat	23	24	47
Fishing ship	19	20	39
Fast ferry	6	1	7
Gas tanker	0	0	0
Other ship	265	296	561
Total	9367	9334	18701

Collision candidates

The number of geometrical collision candidates was estimated with IWRAP Mk II software, which is recommended for evaluating grounding and collision probabilities by International Association of Marine Aids to Navigation and Lighthouse Authorities (IALA) (IALA 2009). IWRAP utilizes collision probability model presented by Pedersen (1995) (Friis-Hansen 2008). The most important waterways in the Gulf of Finland were modelled into IWRAP based on a density plot of traffic as presented in Figure 4. Areas within the

[1] Note: the chapters 2.1-2.3 and the results acquired with the IWRAP software are based on a Master's thesis submitted by the second author (Ylitalo 2010).

vicinity of ports were not included in this study. Similarly to the example waterway presented in chapter 2.2, traffic volume and lateral traffic distributions as well as traffic characteristics such as ship types and lengths were analysed for each waterway segment. The number of ships continuing to different directions was considered for each waypoint.

In IWRAP the collision frequencies are provided separately for head-on, overtaking, merging, crossing, and bend collisions. Head-on and overtaking collisions occur at waterway segments, whereas merging, crossing, and bend collisions occur near waypoints. The relative risk of each waterway and waypoint is marked on the result map (Figure 4). The scale is from light to dark where dark represents the areas of the highest probability of a collision. It is also possible to examine collision frequencies at certain waterway or waypoint.

Although IWRAP includes default values for causation probabilities of various collision types, more detailed evaluation of suitable causation probabilities is left to the software user. In this study the causation probabilities were modelled separately, and the causation probability estimates for the various collision types were then inserted into IWRAP in order to obtain the final collision frequency estimates. Causation probability modelling is described in the following subchapter.

Causation probability

For acquiring the collision frequency estimates, the number of collision candidates was multiplied with causation probability, i.e. the probability of not making evasive maneuvers. The causation probability for the Gulf of Finland was estimated with a Bayesian network model. The model was based on fragments of a collision model network in the Formal Safety Assessment of large passenger ships (Det Norske Veritas 2003) and a grounding model in the FSA of ECDIS chart system (Det Norske Veritas 2006). Network variables were related to navigational aids, conditions, safety culture, personnel factors, management factors, other vigilance, and technical reliability. The network structure can be seen in Figure 3.

In the model a collision occurs, if the ships are on a collision course, at least one of them has lost control due to human or technical failure, and none of the ships makes evasive maneuvers. The loss of control resulting because of OOW's wrong action in a meeting situation depends on the correctness of OOW's situation assessment, his/her performance level, and possible danger detection by others such as the 2nd officer, pilot or VTS operator. Variables "time of year", and "collision type" were added to the network in order to be able to examine certain season or collision type alone. Because the network applied to the analysis included multiple ship types, "Own ship type" node was added. "Location" was added because of technical reasons: it was impossible to obtain ship type distributions based on all AIS recordings in the Gulf of Finland. Because the majority of ship traffic not exiting the Gulf of Finland consisted of the passenger vessels and high speed crafts navigating between Helsinki and Tallinn, ship type distributions were constructed for the ships entering and exiting the Gulf of Finland as well as for a location between Helsinki and Tallinn, and weight factors of 0.8 and 0.2 were assigned to these distributions, respectively.

The majority of the probability values of the Bayesian network node states were derived from the original DNV models (2003, 2006). They had mainly been based on expert judgment. Ship type and length distributions were obtained from AIS-data described in chapter 2.1. The probabilities of "Weather" states were based on Finnish Meteorological Institute's statistics on the average number fog days at Isosaari in 1961-2000, the average number of storm days at Finnish sea areas in 1990-2008 thinned by the average portion of storm observations from the Gulf of Finland in 2006-2007, and the average number of strong wind days at Isosaari in 1961-2000 (Finnish Meteorological Institute 2008). The daylight distributions describing the probabilities of a ship navigating in the dark for the times of year were based on AIS information and sunrise and sunset times outside Helsinki at 15.1.2008, 15.4.2008, 15.7.2008, and 15.10.2008. The probability of state "yes" of the node "VTS" was set to 1.0 because it was assumed that all the waterways belong to Vessel Traffic Service monitoring areas or to the Mandatory Ship Reporting System in the Gulf of Finland (GOFREP) area. The distribution of collision types (head-on, crossing and merging, overtaking) in the node "Collision type" was based on the number of collision candidates calculated with IWRAP as mentioned in chapter 2.3 but using causation probability value of 1.0. It should be noted that the collisions caused by omitting a turn in a bending waterway segment were not considered in the network.

The overall causation probability for the Gulf of Finland was derived when there was no other evidence on collision type except the distribution of collision candidate types estimated with IWRAP in the node "Collision type". The separate causation probabilities for crossing, head-on, and overtaking encounter types were achieved by instantiating "Collision type", i.e., setting the probability of the state describing the encounter type in question to 1.0. The network was built and the probability calculations were performed with Bayesian network software Hugin Researcher.

Accident statistics

Accident statistics were studied for validating the modeling results. As in the analysis, the focus was to consider the number of collisions in the Gulf of Finland not been caused by ice conditions or otherwise not related to navigating in ice channels and which had not been occurred in the vicinity of ports. The ship-ship collision registrations from DAMA accident database and accident registrations acquired from the Baltic

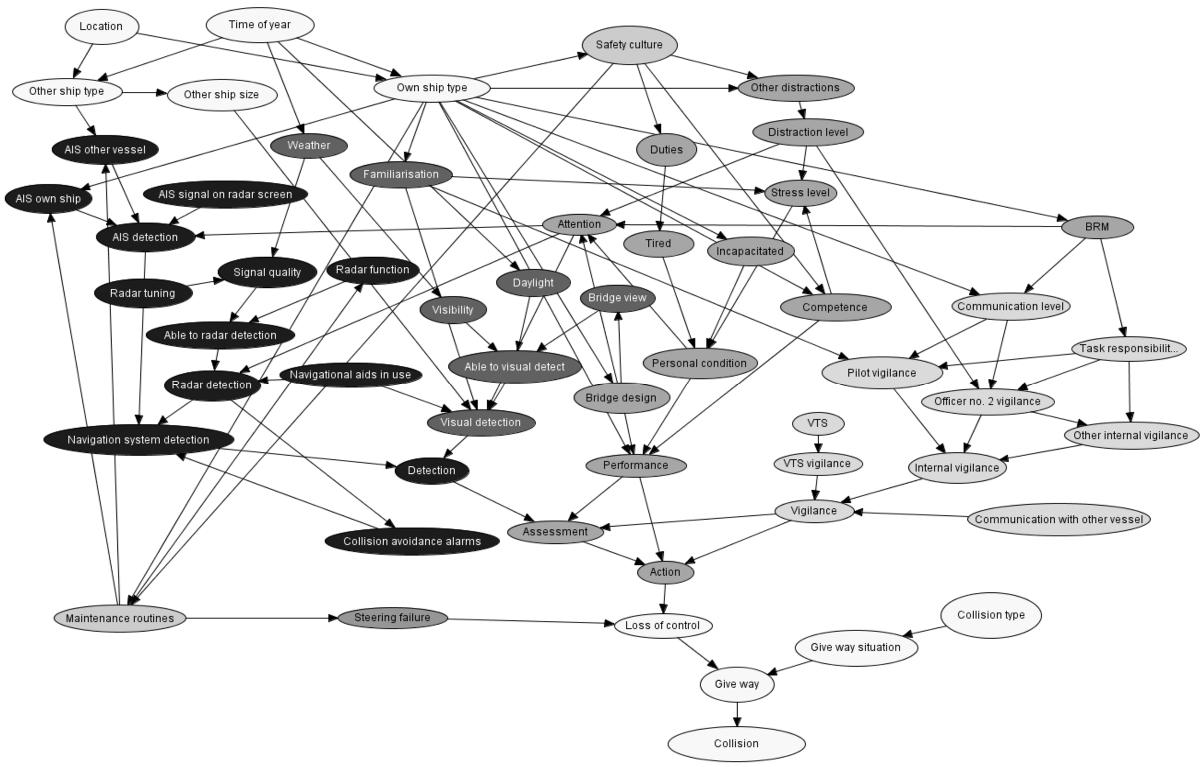

Figure 3. The applied Bayesian network model for causation probability estimation.

Marine Environment Protection Commission HELCOM (Helsinki Commission) in the Gulf of Finland within 1997-1999 and 2001-2006 were examined. DAMA database consists of marine casualty reports given to the Finnish Maritime Administration (FMA), and HELCOM registrations also include the accidents occurred in Russian and Estonian waters. Additionally, accident descriptions (Heiskanen 2001, Laiho 2007) were studied for those accidents for which DAMA database or HELCOM data did not include enough information on the causes and/or location.

Results of the analysis

In total, the number of collision candidates in the Gulf of Finland was estimated to be 1890. The applied causation probability model did not include collisions occurring because omitting a turn in a bending waterway location. If this collision type was omitted, an overall causation probability value of $6.12 \cdot 10^{-5}$ was obtained for the Gulf of Finland. However, if bend collision candidates were included in the causation probability model as additional crossing candidates, the overall value was $1.39 \cdot 10^{-4}$. This difference describes how the distribution of collision types weights the overall causation probability.

Separate causation probabilities, collision candidates, and the estimated number of collisions for the various encounter types are presented in Table 2. From Table 2 it can be seen that the models estimated approximately 0.26 collisions per year. Figure 4 presents the relative number of collisions of each waterway as well as of each bend, merging and crossing point. According to the accident statistics and descriptions, there had been two collisions within the eight years i.e., 0.25 collisions per year which were not caused by ice conditions or otherwise related to navigating in ice channels or which had not occurred in the vicinity of ports. Both of the collisions had occurred in the eastern part of the gulf. According to the analysis, the most collision-prone waterway was the waterway at east side of Gogland (number 2 in Figure 4). The second probable waterway for collisions was the waterway to St. Petersburg (number 5 in Figure 4). The most collision-prone waypoint was where the waterway from Primorsk merges to the main route through the Gulf of Finland (point 4 in Figure 4). The collision probability per year of that waypoint was 15.5 % of the collision probability of the analyzed area in the Gulf of Finland. The collision probability of the most collision-prone waterway was 1.6 % of the overall collision probability. Collision probability values of the waterways and waypoints with the highest collision probabilities are presented in Tables 3 and 4.

Table 2. The estimated values of causation probability, the number of collision candidates, and the number of collisions per year for the studied encounter types in the Gulf of Finland. *For merging and bend encounters, the causation probability of crossing encounters was applied.

Encounter type	Causation probability	Collision candidates	Collisions
Bend*	2,56E-04	757,76	1,94E-01
Overtaking	5,62E-05	629,79	3,54E-02
Crossing	2,56E-04	72,95	1,87E-02
Merging*	2,56E-04	43,61	1,12E-02
Head-on	1,01E-05	385,93	3,89E-03
		Total	**2,63E-01**

Table 3. The collision probabilities of the two most risky waterways.

Waterway location	Number in Figure 4	Overtaking collision probability	Head-on collision probability	Overall collision probability
East side of Gogland	2	4.73E-03	2.41E-09	4.73E-03
To St. Petersburg	5	3.54E-03	1.10E-06	3.54E-03

Table 4. The collision probabilities of the three most collision-prone bending, merging and crossing points

Number in Figure 4	Bend collision probability	Merging collision probability	Crossing collision probability	Overall collision probability
1	3.74E-02	0	0	3.74E-02
3	3.78E-02	0	0	3.78E-02
4	4.33E-02	3.40E-03	1.26E-04	4.68E-02

Figure 4. Indication of more and less collision-prone waterways and bend, merging and crossing points based on modeling results. The legs and points with the darkest colour are areas of the highest collision probability.

Conclusions

The collision probability estimated with IWRAP and the Bayesian network model was 0.26 collisions per year, which is reasonable when compared to the 0.25 collisions per year derived from the accident statistics. However, it should be noted that it is difficult to compare the results to statistics since analyzed time interval should be long but the traffic would have to remain constant. Traffic in the Gulf of Finland has increased significantly after the beginning of the studied accident statistics period. Thus, it is reasonable that the modeling estimates higher collision probability than what is obtained from statistics. Further, the studied area in the Gulf of Finland did not cover the whole gulf, which suggests the actual number of collision candidates in the gulf being larger than the number obtained from this analysis. However, area limitations were taken into account when studying accident statistics.

As can be seen from Table 4, bend collision probability is 75 % of the overall collision probability. However, the bend collision model used in IWRAP assumes that 1 % of ships arriving to a bend of a waterway do not turn as they should and thus become collision candidates (Friis-Hansen 2008). The authors have not found any reasoning for the assumption of 1 % of the ships omitting a turn at a bend. The probability of not to turn is, for example, considerably larger than causation probability although its reasons seem to be similar.

Overall, the route from the entrance to the Gulf of Finland to St. Petersburg through the whole gulf seems the most risky waterway. This route gets narrower towards east, which can be easily seen from Figure 1. Ships navigate closer to each other and thus the route segments are more dangerous in the eastern part of the gulf than in the western part even though the traffic volume is higher in western part. Likewise, the registered non-ice related collisions had also occurred in the eastern part. Surprisingly, the crossing area between Helsinki and Tallinn does not seem to be particularly prone to accidents. It is one limited area, whereas the route through the gulf is long and its importance results from its length and from the number of ships navigating all the way along it. However, if the most important consequences are considered to be lost human lives, then the relative risk is higher in the crossing area between Helsinki and Tallinn. A large number of passenger vessels and high speed crafts with many passengers is navigating in the area, as opposed to only a few passenger vessels navigating in the eastern Gulf of Finland.

In 2009, IWRAP is the best available tool for the analysis of collision candidates or collision frequency in the Gulf of Finland, but it still has weaknesses: Daytime and time of year are assumed not to influence traffic volumes, which is not realistic for the Gulf of Finland. IWRAP also uses lateral traffic distributions without distinguishing individual ships for estimating the number of collision candidates, which can produce situations in where a ship colliding with herself will be interpreted as a collision candidate. This is relevant especially for passenger ships making frequent passages in a waterway. Additionally, in IWRAP ice season can be included in the calculations only through causation probability.

The estimates of the causation probability derived with the Bayesian network were reasonable when compared to the values presented in the literature. However, it should be noted that the model depends heavily on the network parameters. In an ongoing research project the network model will be developed further and validated with expert judgment. This way the special characteristics of the traffic in the Gulf of Finland can be taken into account. It should also be noted that this study included only open water season. According to accident statistics, many of the ship-ship collisions occur in winter navigation, and wintertime traffic should be included in the modeling in the future.

Acknowledgement

Authors would like to European Union, European regional development fund, Regional Council of Kymenlaakso, City of Kotka, Kotka-Hamina regional development company Cursor Ltd., Kotka Maritime Research Association Merikotka, and Kotka Maritime Research Center Corporate Group for making this analysis possible as a part of SAFGOF-project. Ph.D. Erik Sonne Ravn from Danish Maritime Safety Administration and M.Sc. Markus Porthin from VTT Research Centre of Finland are thanked for the help to evaluate the traffic flows in the Gulf of Finland based on the AIS data.

References:

Baltic Sea Portal: Ice winter 2007/2008 [Internet]. Baltic Sea Portal; [updated 2008 Sep 16; cited 2009 Aug 19]. Available from: http://www.fimr.fi/en/tietoa/jaa/jaatalvi/en_GB/2008/

[DNV] Det Norske Veritas. 2003. Formal Safety Assessment – Large Passenger Ships, ANNEX II.

[DNV] Det Norske Veritas. 2006. Formal Safety Assessment of Electronic Chart Display and Information System (ECDIS). Technical Report No. 2005-1565, rev. 01.

Finnish Meteorological Institute. (n.d.) Weather statistics [Internet]. FMI; [cited 2009 Sep 28] Available from: http://www.fmi.fi/

Fowler TG, Sørgård E. 2000. Modeling Ship Transportation Risk. Risk Analysis 20(2): 225-244.

Friis-Hansen P, Simonsen BC. 2002. GRACAT: software for grounding and collision risk analysis. Marine Structures 15(4): 383-401.

Friis-Hansen P. 2008. Basic modelling principles for prediction of collision and grounding frequencies. Technical University of Denmark. Working document.

Fujii Y, Shiobara R. 1971. The Analysis of Traffic Accidents. Journal of Navigation 24(4): 534-543.

Fujii Y, Yamanouchi H, Mizuki N. 1974. Some factors affecting the frequency of accidents in marine traffic. II - The probability of stranding and III - The effect of darkness on the probability of collision and stranding. Journal of Navigation 27(2): 239-247.

Fujii Y. 1983. Integrated Study on Marine Traffic Accidents. IABSE Colloquium on Ship Collision with Bridges and Offshore Structures; Copenhagen 42: 91-98.

Heiskanen M. 2001. Accident analysis 1990-2000 (in Finnish). Finnish Maritime Administration. 66 p. Merenkulkulaitoksen julkaisuja 7/2001.

Hänninen S, Nyman T, Rytkönen J, Sonninen S, Jalonen R, Palonen A, Riska K. 2002. Preliminary study of risk factor in the Gulf of Finland marine traffic (in Finnish). Espoo: VTT Tuotteet ja tuotanto. 106 p. BVAL34-021198.

Hänninen M, Kujala P. 2009. The effects of causation probability on the ship collision statistics in the Gulf of Finland. Paper presented at: TRANS-NAV 2009. 8th International Navigational Symposium on Marine Navigation and Safety of Sea Transportation; Gdynia, Poland.

Ihaksi T, Helle I, Lecklin T, Ryömä R, Kokkonen T, Kuikka S. 2007. Using biological knowledge and decisions of society in spatial prioritization of oil combating. ICES CM 2007/C:02.

[IALA] International Association of Marine Aids to Navigation and Lighthouse Authorities. 2009. IALA Recommendation O-134 on the IALA Risk Management Tool for Ports and Restricted Waterways, Edition 2.

[IMO] International Maritime Organization. 2005. Revised Guidelines for the Identification and Designation of Particularly Sensitive Sea Areas (PSSAs), Resolution A.982(24).

[IMO] International Maritime Organization. 2006. Formal Safety Assessment. Consideration on Utilization of Bayesian Network at Step 3 of FSA, Maritime Safety Committee 81st Session, MSC 81/18/1.

Jensen FV, Nielsen TD. 2007. Bayesian networks and decision graphs. 2nd ed. New York: Springer.

Karlsson M, Rasmussen FM, Frisk L. 1998. Verification of ship collision frequency model. In: Gluver H, Olsen D, editors. Ship Collision Analysis. Proceedings of the International Symposium on Advances in Ship Collision Analysis. Rotterdam: Balkema. p. 117-121.

Klemola E, Kuronen J, Kalli J, Arola T, Hänninen M, Lehikoinen A, Kuikka S, Kujala P, Tapaninen U. 2009. A cross-disciplinary approach to minimising the risks of maritime transport in the Gulf of Finland. World Review of Intermodal Transportation Research 2(4): 343-363.

Kujala P, Hänninen M, Arola T, Ylitalo J. 2009. Analysis of the marine traffic safety in the Gulf of Finland. Reliability Engineering and System Safety 94(8): 1349-1357.

Kuronen J, Helminen R, Lehikoinen A, Tapaninen U. 2008. Maritime transportation in the Gulf of Finland in 2007 and in 2015.Turku: University of Turku, Centre for Maritime Studies. 110 p. A 45: Publications from the Centre for Maritime Studies.

Laiho A. 2007. Ship accident analysis 2001-2005 (in Finnish). Finnish Maritime Administration. 23 p. Merenkulkulaitoksen julkaisuja 5/2007.

Macduff T. 1974. The probability of vessel collisions. Ocean Industry 9(9): 144–148.

Mazaheri A, Ylitalo J. 2010. Comments on Geometrical Modeling of Ship Grounding. Paper accepted to ICCGS 2010.

Nikula P, Tynkkynen VP. 2007. Risks in Oil Transportation in the Gulf of Finland: ”Not a Question of If – But When”. Aleksanteri Institute, University of Helsinki, Nordregio, Nordic Centre for Spatial Development. CIVPRO Working paper vol. 7.

Otto S, Pedersen PT, Samuelides M, Sames PC. 2002. Elements of risk analysis for collision and grounding of a RoRo passenger ferry. Marine Structures 15(4): 461-474.

Pedersen PT. 1995. Collision and Grounding Mechanics. Proceedings of WEMT'95. Copenhagen: The Danish Society of Naval Architects and Marine Engineers. 125-127.

Rambøll. 2006. Navigational safety in the Sound between Denmark and Sweden (Øresund); Risk and cost-benefit analysis. Rambøll Danmark A/S.

Rosqvist T, Nyman T, Sonninen S , Tuominen R. 2002. The implementation of the VTMIS system for the Gulf of Finland - a FSA study. Proceedings of the RINA International Conference Formal Safety Assessment; 2002 Sep 18-19; London,UK. 151-164.

The effectiveness of maritime safety policy system in prevention of groundings, collisions and other maritime incidents

Jenni Kuronen and Ulla Tapaninen

University of Turku - Centre for Maritime Studies/Kotka office, Finland

***Abstract*:**
The topic of the paper is policy instruments, which are or could be used to prevent groundings and collisions. Various international, regional and national policy instruments aim at minimizing the risks of accidents.
This paper presents the current situation and future sights of maritime policy. The maritime policy instruments include administrative (e.g. regulation on the structure and operation of ships, supervision of ship conditions, ship reporting systems and routeing), economic (e.g. waterway dues, marine insurances, liability and compensation issues) and information guidance instruments (e.g. voluntary training). The maritime safety regulation is to great extend international, the most important actor being International Maritime Organisation (IMO). However, the European Union has shown increasing interests to regulate maritime safety, and there are also other international actors in the field such as HELCOM. In addition, some of maritime safety related matters belong to the sphere of national regulation, for example piloting.
This paper addresses the following questions: what are the criteria for effective policy, what are the strengths and weaknesses of the maritime safety policy system, how effective is the maritime safety policy system,what could be the alternatives for the current system.

Introduction

Accidents at sea and increasing amount of maritime traffic, especially the transportation of dangerous cargoes, have awakened the growing awareness about the safety of maritime traffic. International and national maritime safety regulation has a long history and regulation is revised and developed further continuously in numerous maritime safety related issues by numerous actors. Instead of looking at the single policies it is sometimes important to think about the system as a whole. Does it achieve the goals it is meant to achieve, is it effective, should it be changed?
This paper presents criteria for effective policy instruments and it evaluates the current maritime safety policy system as a whole in the light of those criteria. The paper includes the review of the maritime safety policy system and the critique of it. The paper is based on literary sources, largely on the articles published in the academic journals. The structure of the paper is as follows. First, the criteria for effective policy instruments are presented. Second, the regulatory bodies of maritime safety and maritime safety policy instruments are reviewed. After that, the critique and the weak points of the system are looked through. In the end, the maritime safety policy system is evaluated against the criteria for effective policy and the findings of the study are discussed. Also an alternative for the current system is presented.[1]

Effectiveness of policy instruments

Policy instruments can be grouped to three groups: regulatory control (jurisdiction and law based decrees, restrictions, licences etc.), economic control (taxes, subsidies, fees etc.) and information guidance (information, voluntary education, certification, awards etc.). Policy instruments can be also viewed from the viewpoint of what interests are to be protected: private goods (the competitiveness of companies) or public goods, which the market would otherwise neglect (the maintenance of safety and security in the shipping and protection of the environment from the harmful effects of shipping). Policy instruments can be either preventive measures or sanctions and consequences. Both preventive measures and consequences can be either private (e.g. insurances) or administrative measures (e.g. prohibitions) (Figure 1).

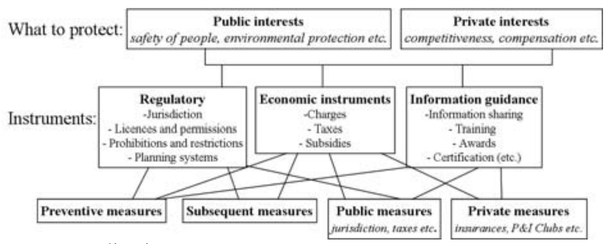

Figure 1. Policy instruments

Government, financial, administrative and community resources are limited and must be deployed where they are most likely to have the greatest positive impact. It is important to assess the strengths and weaknesses of the range of instruments in terms of the stated objectives and to identify the circumstances in which they are most likely to make a positive contribution to the outcome sought. (Greiner et al. 2000)

Vieira et al. (2007) have developed a system to assess transport policy instruments where the set of policies are evaluated against certain criteria and in relation to each other. Also Greiner et al. (2000) has had very similar criteria for transport policy evaluation. These criteria are presented below.

- **Effectiveness** refers to the potential improvement in the thing that is trying to be

[1] This research has been done as part of the cross-disciplinary research project "SAFGOF - Evaluation of the traffic increase in the Gulf of Finland during the years 2007-2015 and the effect of the increase on the environment and traffic chain activities" of Kotka Maritime Research Centre (http://www.merikotka.fi/uk/SAFGOF.php).

change. It relates to whether an instrument is technically suitable for achieving a goal. (Greiner et al. 2000; Vieira et al. 2007)

- **Economic efficiency** relates the effectiveness to the implementation costs of an instrument and to the economic efficiency of an instrument in a collective sense, assessing the total benefits of the associated change in risk minimizing against its total costs. (Greiner et al. 2000; Vieira et al. 2007)
- **Acceptability** refers to the stakeholders' level of agreement on a new policy instrument, and to the political and community acceptability of an instrument. Acceptability is a necessary condition for the durability of the policy. (Greiner et al. 2000; Vieira et al. 2007)
- **Enforcement** indicates how effectively a policy instrument can be implemented. Some instruments can be difficult to implement even though they would be probably effective. Vieira et al. (2007) presents the following types of barriers for implementation: legal and institutional (legal or regulatory conflicts, legal powers are spread through various institutions or organizations), resource or financial (lack of financial or physical resources to implement an instrument), political and cultural (some groups oppose policy) and technological (e.g. lack of suitable technology). (Greiner et al. 2000; Vieira et al. 2007)
- **Lateral effects** refer to possible spill over effects of an instrument for other sectors (e.g. reduce of air emissions can improve the health of people, which decreases health care expenses). (Vieira et al. 2007)
- **Incentive and innovation effects** relate to the question whether an instrument encourages experimentation and change and provides an ongoing incentive for improvement. (Greiner et al. 2000)

In comparison with regulatory and economic instruments, regulatory instruments are very effective and easy to enforce, because they are, by their nature, compulsory. The weaknesses of regulatory instruments can be their economic efficiency and public acceptance, and their enactment and implementation can be expensive, difficult or practically impossible. (Vieira et al. 2007) Regulatory policy instruments may not promote changes or innovations because there is no economic incentive (Klemmensen et al. 2007).

Economic instruments can reach environmental targets with good economic efficiency from the point of view of more social-efficient allocation of resources. However, economic instruments often face acceptance difficulties because they tend to increase prices. If they have lateral effects or in the combination of other policies they can be more acceptable if the price increase in the first is compensated by the price decrease of the other. Recently the popularity of economic regulation has been decreasing because it is seen to distort market competition and to reduce overall economic efficiency. (Vieira et al. 2007) Effective policy instruments should be coherent with overall policy orientations. Policies should not be evaluated separately. Some set of policies can together be more effective than any single policy would be. In their study on transport policy instruments, Vieira et al. 2007 found that most of the studied policy instruments had positive synergy effects, i.e. the effectiveness of instruments implemented together is potentially bigger than the effectiveness of each instrument separately. It is also important to look at which current policies might provide conflicting incentives and which should be removed. Policy instruments should also be reviewed if the context of maritime shipping system changes. (Greiner et al. 2000; Vieira et al. 2007; Walker 2000) One aspect of the effectiveness of jurisdiction based policy instruments is what happens in the case of non-compliance. Non-compliance should result in penalties or economic consequences severe enough to minimise the temptation of an actor to break the rules. (Greiner et al. 2000)

Regulatory bodies of maritime safety

Because ships can move around the world between different states, it is appropriate to have worldwide regulations on maritime safety matters in order to avoid the situation where each coastal state would have its own rules on issues like ship structure, manning etc. (Stopford 2009). Besides international level (UN, International Maritime Organisation IMO, International Labour Organisation ILO) maritime safety regulation is done also in supra-national (EU), in national (Finland, Estonia, Russia), and in regional (the Gulf of Finland) level (Figure 2). In principle these levels work in the so-called nested hierarchy, which means that the international level is the outmost circle and other levels are within each other in the circle, and inner circles should always be consistent with the outer levels of the circle. Otherwise the implementation of regulation is likely to be ineffectual. (Roe 2008) Besides regulatory bodies there are institutions which do not have legislative power but which are somehow affecting the maritime safety regulation, for example environmental organisations like WWF, classification societies and marine insurance companies. There are also cases where the United States have legislated maritime safety nationally and it has had an effect on the entire shipping industry, for example the Oil Pollution Act of 1990 (OPA 90) (Luoma 2009).

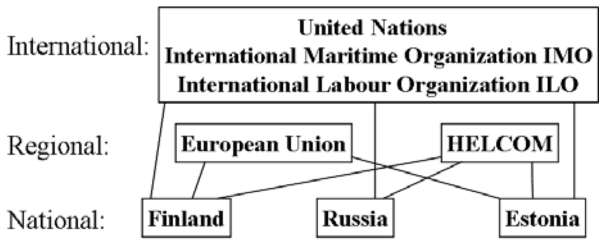

Figure 2. Example of main regulatory bodies of maritime safety the Gulf of Finland

United Nations has delegated maritime issues mainly to two UN agencies: International Maritime Organisation (IMO) and International Labour Organisation (ILO). IMO is responsible agency for ship safety, pollution and security, and ILO for the laws governing maritime personnel. The main instrument of both agencies is conventions, which become law when they are enacted by each member state. IMO and ILO also give codes, guidelines or recommended practices on important matters not considered suitable for regulation by formal treaty instruments.

The United Nations Convention on the Law of the Sea (UNCLOS) establishes the most fundamental rules governing all uses of the oceans and their resources including the movements of ships. UNCLOS, for example, defines the boundaries between sea zones and areas in which coastal state legislation is permitted. The rights of the port state are defined by dividing the sea into maritime zones: the territorial sea zone, the contiguous zone, the exclusive economic zone and high sea zones. (Stopford 2009)

In the past decades it was perceived in IMO that there was a need for a system which would take into the consideration also the local circumstances. As an answer to the problem, IMO developed the concept of Particularly Sensitive Sea Area (PSSA) in order to protect ecologically sensitive sea areas from the hazards of shipping Designation of PSSA is not a regulation in its own right, but it serves as a basis for the proposal for additional protective measures (APMs). (Roberts 2007) APMs given on the basis of PSSA status can include routeing systems of ships (traffic separation schemes, areas to be avoided, no anchoring areas, inshore traffic zones, deep water routes, precautionary areas, recommended routes), ship reporting systems, and discharge and emission control restrictions. (Mäkinen 2008)

In the past, the starting point in the European Union was that maritime safety matters should be negotiated at an international level and EU did not engage itself into this policy area. Neverthless, after maritime accidents in European waters, for example the capsizing of Herald of Free Enterprise, maritime safety issues became into the agenda of the EU. (Pallis 2006) At the moment there are over 40 Community regulations on maritime safety. National authority has shifted to the European Union in maritime issues where Community legislation exists. (Ministry of Transport and Communications 2009). European Union has been making attempts to gain full membership in IMO and to present all EU countries with one voice which is thought to be more effective than individual state representations in IMO. (Roe 2009)

Helsinki Commission's (HELCOM) aim is to protect the marine environment in the Baltic Sea and it deals also with pollution from maritime traffic. HELCOM gives recommendations to member states, which member states can implement although in legal sense they are not obliged to do so. In practise member states usually follow the recommendations (Karvonen et al. 2006). HELCOM has paid attention for example to the following shipping issues: proposals for additional safety measures (PSSA), decreasing of emissions and discharges from shipping, treatment of ballast waters, realisation of systematic hydrographical surveying in the main waterways, the development of electric navigation charts (ENC; Electronic Navigational Charts) and the harmonization of accident investigation procedures. (HELCOM 2009; Ministry of Transport and Communications 2009)

National policy level focuses on the implementation of the policies agreed at international and/or supra-national level (Roe 2008). Piloting, vessel traffic services, maintenance of waterways and safety devices, nautical charting and weather, water level, ice services, waterway maintenance related dues and port dues are issues that are usually governed nationally (Ministry of Transport and Communications 2009).

Maritime safety policy instruments

Regulatory instruments

Regulatory instruments include jurisdiction, restrictions, licences, permissions and standards (Vieira et al. 2007). Also planning systems can be included in regulatory instruments (Ekroos et al. 2002). Regulatory instruments are the most widely used policy instruments, also in the maritime world. Table 1 presents how maritime safety is regulated with regulatory instruments.

Table 1. Maritime safety regulatory instruments

Regulated sector		*Main legislator/actors*
Ship construction and equipment	• construction and subdivision • stability • equipment • stowage • navigation • handling of the cargo	→ IMO
Surveillance of ship conditions	• flag state control • port state control • host state control • classification societies • vetting inspections	→ IMO → IMO, PARIS MOU → EU → private companies → private companies
Mariners	• working conditions • employment conditions • manning of ship • safety management	→ IMO, ILO
Navigation	• VTS • ship reporting • traffic separation scheme and routing • traffic recommendations and restrictions • piloting • waterway safety • nautical charts • information supply about weather, water level, ice situation etc. • towage services	→ IMO → IMO, regional co-operation → IMO, regional co-operation → IMO, regional co-operation and nations → nations → IMO, IALA → IMO → IMO → nations, private companies

Economic instruments

The rationale behind economic instruments is to make unwanted behaviour more expensive or wanted behaviour cheaper so that companies will have economic incentive to change their activities in order to avoid extra costs. Economic instruments are used in society also to cover the costs of providing infrastructure, such as waterways, and to prevent the exploitation of common resources. Economic instruments can be charges, taxes, subsidies or market-based mechanisms such as emission trading. (Klemmensen et al. 2007) It is typical for maritime safety related economic instruments that they are set on the national level or they are used between private actors (Table 2).

Table 2. Maritime safety economic instruments

Regulated sector	*Main legislator/actors*
Dues related to maintenance of waterways	→ nations
Port dues	→ nations, private companies
Marine insurance	→ private companies, IMO (obligatory insurances)
P&I Clubs	→ private companies
Liability and compensation (oil pollution)	→ IMO
Incentives	→ private companies, e.g. GreenAward Certification System, nations

Information guidance

Information guidance is premised on the idea that justified information makes people, communities or companies to change their behaviour patterns. Information guidance includes, for example, information, standardisation, certification or awards. It is characteristic of information guidance that it is based on voluntary actions. When regulatory or economic instruments are in most cases based on legislation and there are consequences in the case of non-conformity, the effect of information guidance is totally depended on the voluntary interests of an actor. Information guidance instruments are in use also in maritime safety issues, for example besides legally binding conventions IMO gives codes, guidelines or recommended practices on important matters.

Future sights

New policies are developed both at many levels and in many issues to improve maritime safety further. Especially the development of navigational aids and decreasing the effect of the human factor in accident causation are issues where changes can be expected. Also the wider use of economic instruments to promote maritime safety, such as compensation or green port dues, seems to be in the interests of legislators. At the same time, existing regulation is also developed to be more effective and to be more up to date. In regard to existing regulation and to what is under development it can be concluded that maritime safety risks are at least at the political level taken seriously.

Critique of the current system

Problems of international maritime safety regulation

Although maritime safety regulation can be proven to have improved maritime safety when for example looking at the number of casualties and their seriousness, there are still unwanted phenomena in the shipping industry from the point of view of maritime safety. Shipping causes harmful effects, such as environmental pollution or accident caused deaths. Sub-standard or otherwise obscurely managed ships are able to sail in the world seas. Inability of international regulation to take into consideration local circumstances and special needs has lead to different kinds of regional arrangements, which erode the international legislation system.

According to Roe (2008, 2009) current policy-making fails in many ways on many fronts: it fails to have desired effect, it is generated by inappropriate bodies (national governments rather than international authorities), it is diffuse and partial (Port State Control and the failure to eliminate sub-standard ships), and many times it is unclear where it emerges, what are the motives behind it or what is the methodology for its application.

International regulation process is not easy. It is often slow and the result can become a compromise of compromises (Stopford 2009). At the regional level there would often be preparedness to react more quickly to the deficiencies in the maritime safety system. IMO does not support regional decision-making and regional systems are problematic from the point of view of global shipping industry. An example of such occasion where national or supra-national legislation has conflicted with the international level is the case of double-hull tankers, which were first required by the United States and the US Oil Pollution Act. Later in the EU the number of member states introduced legislation to enforce the use of double-hull oil tankers before it was agreed on the EU level and well before the date recommended by IMO. (Roe 2008; Roe 2009) The contradiction in the current maritime legislation system is manifested also in the PSSA system, where the principle of freedom of the high seas and uniform international legislation is challenged. The designation of PSSA area can be seen as an attempt to extend national and regional authority in the sea area (Uggla 2007). In fact, such regional arrangements can be regarded as a failure of the international system to make effective regulation in maritime industry (Goss 2008; Kaps 2004).

IMO legislation can be considered mostly as reactive regulation is revised or tightened after major sea accidents and preventive actions are still uncommon. This kind of "post accident" policy is often unsuccessful. Policy-making is not very comprehensive and one particular risk gets too much attention (Goulielmos 2001; Karvonen et al. 2006; Knapp & Franses 2009).

At international level national representatives make up the IMO, constructing maritime policies for globalized industry from a national perspective. Problems arise when national interests conflict with supra-national ideas. Failures of shipping policies derive from the development of internationalised ownership of industrial and capital operation resulting from national protectionist regulations. (Roe 2008; Roe 2009)

The role of third parties in promotion of maritime safety

Regulation depends also on the enrolment of the third parties, both public and private (financial firms, insurers, government agencies, auditors, consultants, etc.). The third parties have the power to influence the behaviour of the companies. They can implement incentives or sanctions on other parties, from the making or breaking of social and economic relationship to concrete financial penalties formalised in legally binding contracts. Still, the third parties are still rarely exploited in promotion of the public interests. In maritime regulation such third party actors such as associations of shipowners, cargo owners, insurers, classification societies and banks have potential to exert an influence over ship safety and environmental standards. (Bennett 2000)

The third parties could be enrolled to assist the public policy for instance by holding them liable for environmental damage caused by their clients, making it a legal requirement that the targets of regulators use the machinery of third parties (such as auditors or insurers). Governments can also create rights such as tradable permits and incentives like the less scrutiny by regulatory authors. It should also be discussed what is the liability of the cargo owner and the shipper in the cases of accidents. (Bennett 2000)

Hänninen (2007) has observed that the marine system is lacking egalitarian stakeholder groups which would monitor risks and risk taking behaviour in maritime transportation. In other industries, such as in the nuclear power production and in the forest industry, egalitarian watch and interest groups are common and they provide fresh and unconventional views on matters of safety thus creating pressures on other groups to pay attention and upgrade safety related risk classification and regulatory practises.

All the companies in the shipping industry are not the same. There are companies, which buy cheap second-hand ships, operate them as cheaply as possibly, do not mind on safety measures and when repairs become too expensive they abandon the ships and their crews in some obscure port. There are also companies, which are very active in promoting safe shipping: they are willing to test new technologies, act as good employers and achieve a high reputation among the public. The problem is that good and bad companies are competing in the same markets. (Goss 2008) The shipper plays a crucial role in the maritime safety. For example, in the case of Erika accident, it turned out that the ship was chartered because of the affordability of offered transportation and the shipper did not have much interest on the condition of the ship (Karvonen et al. 2006). If a shipper requires from a transporter high safety level instead of looking solely at a price of transportation, obscure firms are not able to operate in the markets and distort fair market competition.

Human factor and safety culture problem recognised, but not solved

Human factor has been identified as the most important cause to the maritime accidents (e.g. Hänninen 2008; Karvonen et al. 2006; Trucco et al. 2008) and in all shipping accidents human factor plays some role. The development of technology has lead to the reduction of failures in technology, which in turn has revealed the underlying level of influence of human error in accident causation (Hetherington et al. 2006). Also the influence of economic pressure in a strongly competitive industry may have added to the human factor causing shipping accidents (Trucco et al. 2008). If the human factor is seen to be the major cause for the accidents, effective policies should take into consideration how the effect of the human factor in accident causes could be diminished. It seems that in the shipping industry there is growing awareness about the role of human factor in maritime safety, but it appears to be difficult to find good policies, which would tackle the human factor. Safety management, including inspection and training, are commonly thought to be the key means of tackling the human factor contribution to the accidents (Trucco et al. 2008). Also working conditions, safety culture on board, and proper use of technological and other tools have a role in preventing the human factor caused accidents (Karvonen et al. 2006).

The human factor related errors can be of two kinds: active and latent errors. The active errors are the ones made by pilot, control room crew, ship officers or other operators. But, the biggest threat to a safety comes from latent errors, which are caused by poor design, incorrect installation, faulty maintenance, poor management decisions etc. The active error made by the operator is just a finish touch in human factor based error leading to the casualty (Hänninen 2008). In other words, the human factor based error can be said to be the final act of a long and complex chain of organisational and systemic errors. According to Hetherington et al. (2006), the fundamental error inducing character in shipping lies in the social organization, economic pressure and in the structure of industry.

Maritime safety is by its nature very complex issue and it is as much related to culture as is anything else. Such issues as language, authority and communication are all complex and are determined by individual and institutional relationships that may or may not be affected by jurisdiction and other policy instruments. Successful policies need to reflect the complexity of inter-relationships and the multiplicity of centres of authority that influence safety and environmental standards and the implementation of penalties in the shipping industry. (Roe 2009)

Effectiveness of maritime safety policy system

In chapter 2 the criteria for the effective maritime safety policy system were presented. In this chapter, each criterion is looked at in the light of the current maritime safety policy system in general – does it as a whole fulfil the criteria. Naturally there are differences between single policies but here the purpose is solely to look at the system as a whole.

Effectiveness - *policy instrument must be suitable for achieving a desired goal*

Most of the maritime safety policy instruments can be considered suitable for their purposes. They address the things which are straight connected to the operational circumstances of a ship and improvement of them is likely to have an impact on the safety of shipping. One of the problems is that the international legislation seems to lack the capability to take into consideration local circumstances and to make fast responses when needed. PSSA status system and the activity of the European Union to legislate maritime safety are signs of this problem. Another problem is that it seems difficult to find effective policies which would tackle the human factor when the human factor is the main cause to the most of the accidents at sea.

Economic efficiency - *the benefits versus the costs of implementing the policy instrument should be at balance*

Economic efficiency varies between different policies and it is difficult to estimate as a whole. For sure, some people say that safety regulation costs too much for the industry, because it is so extensive. Nevertheless, in principle the costs of implementing international regulation should not be the problem for the industry because all actors bear the same costs. However, we know that this is not the case in the real world. Implementation level varies and regional regulation and arrangements like PSSA can alter the costs. Still, economic efficiency is very important criteria. Resources should be allocated so that maximum benefit is obtained. There is no point to make regulation which costs a great deal to the industry and which has only a little impact. The problem is that costs and benefits are in many cases hard to calculate and it seems where is no comprehensive information about the cost-effectiveness of the maritime safety policy system. This is the area which needs further development.

Acceptability - *policy instrument must be accepted by stakeholders and community*

In a way, the slowness of the international regulation process reflects that such policy instruments which are not accepted by stakeholders cannot be legislated, because the slow process is a sign that the stakeholders have differing opinions on the matter and it takes long to negotiate the result which can be accepted by the sufficient number of the stakeholders. When looking at the broader community, it seems that it would be willing and ready to make tighter policies for maritime safety but which are not accepted by the industry or they are against the principles of maritime law. For example, in many instances it has been proposed that VTS system should be reached to the whole Baltic Sea area, but at the moment it is not possible due to the international legislation, which does not allow a coastal state to oblige VTS system in high sea zones. (e.g. Karvonen et al. 2006)

Enforcement - *policy instrument can be implemented effectively*

This seems to be the core problem of the current system. International regulation which is based on the nation-state implementation is not functioning properly. In the global scale, there are too large differences in the way of implementation of maritime safety regulation. The existence of the flags of convenience is the most visible sign of it.

Lateral - *effects positive spill over effects of the policy instrument to other sectors*

At its best, maritime safety policy has many positive spill over effects. Safer shipping means less human misery and less polluted seas. These achievements affect the further society positively in many ways. People are healthier, live and work long. Ecosystems of seas are protected which improves the possibilities to use sea both for commercial and recreational activities although these things depend on many other issues as well. Safe transportation also decreases transport damages and cargo losses.

Incentive and innovation – *good policy instrument encourages experimentation and gives incentives for improvement*

Maritime safety policy is in many aspects very detailed, for example with regard to ship construction and equipment. The more detailed is the legislation, the less there is room for experimentation and innovations. Often economic instruments are thought to be better in promoting innovations and they are not much used in maritime safety policy (e.g. Mickwitz et al. 2008). However, regulatory instruments can encourage innovation as well and economic instruments do not necessarily do that. For example, ISM Code includes the requirement for continuous improvement, but as it has been perceived in the study of Lappalainen (2008) that the shipping industry often lacks that kind of culture which would aim at the continuous improvement of safety culture. In sum, how well maritime safety policy instruments encourage experimentation and innovation varies from policy to policy, but it looks like that more attention has recently been paid to make policies to be more innovative and encouraging for continuous improvement.

The current maritime safety policy system is effective in many respects but the greatest weaknesses are the implementation and cost-effectiveness of policies and the failure of the system to diminish the role of human factor in accident causation. Implementation, which is based on the nation-state authorities, has not succeeded in the global scale and the problem with cost-effectiveness is that there is not reliable and comprehensive data about the costs of policies both of single policies and of policies in comparison with each other. The system allows substandard shipping in many respects: the implementation of international legislation has not succeeded, other companies and actors agree to co-operate with obscure shipping companies and consequences of substandard shipping for the shipping company are not severe enough.

Multi-level or polycentric governance system

Roe suggests that the problem of making effective policies lies in the failure to understand the relationships between jurisdictions operating at international, supra-national and national levels, which makes it possible for uncaring shipowners to take advantage of the failings of current regulation systems, and in the failure to incorporate the stakeholder interests into the jurisdiction process. (Roe 2008; Roe 2009)

New approaches to shipping policy at the international level have been proposed, such as multi-level governance or polycentric governance system. Multi-level governance means that central government authority is dispersed both vertically to locate at other territorial levels and horizontally to non-state actors. Multi-level governance is thus characterised by overlapping and multiple jurisdictions in contrast to the simple hierarchical approach, and it allows the integration of state and non-state actors and the dispersion of state activity to supra-national, regional and local authorities in a way that reflects the shipping industry itself. Polycentric governance systems go one step further: it is a more complex policy-making framework encompassing a variety of policy-generating origins across all types of institutions, both private and public (governments, interest groups, political parties, commercial companies etc.) International jurisdiction gives levels but the concrete measures can be decided locally in co-operation with different actors. These governance systems may offer a mechanism to reflect the actual activities within the maritime sector and the priorities of stakeholders involved. (Roe 2008; Roe 2009) However, such change in international legislation seems to be remote.

Summary and conclusions

Various international, regional and national policy instruments aim at minimizing the risks of accidents and other harmful effects of maritime traffic. This paper has presented a short summary on the maritime safety policy and the criteria for effective policies. Then, the effectiveness of the maritime safety policy system has been evaluated.

Policy instruments can be grouped to regulatory, economic and information guidance instruments. Maritime safety is enhanced with all these instrument types although most prominently with regulatory instruments. Due to the international character of shipping industry, the regulation of maritime safety is aimed to be done mostly at international level but there are also regional and national bodies involved.

According to literature, effective maritime policy instruments should fulfil at least following criteria: 1) effectiveness policy instrument must be suitable for achieving a desired goal, 2) economic efficiency the benefits versus the costs of implementing the policy instrument should be in balance, 3) acceptability policy instrument must be accepted by stakeholders and community, 4) enforcement policy instrument can be implemented effectively, 5) lateral effects the positive spill over effects of the policy instrument for other sectors, and 6) incentive and innovation good policy instrument encourages experimentation and gives incentives for improvement.

There is increasing amount of maritime safety regulation, and in overall, the number of maritime accidents has decreased during past decades. Most of the regulation has been effective in preventing accidents and incidents. Still accidents and incidents happen at sea and the current regulation system can be criticised for several points. Making international regulation is not easy: regulation processes in IMO tend to be slow and the result can become the compromise of compromises. Regulation is mostly reactive instead of preventive and regulation is revised after accidents. Work of IMO is based on the participation of nation-states and on the implementation of regulation by flag states and all flag states do not have the same implementation standards. This has lead to the situation that there are several inspection systems which aim at the eliminating operation of sub-standard ships and still sub-standard ships are able to sail in the world seas. The failure of IMO to provide fast responses and to take into consideration local circumstances in regulation has lead to the situation where for example European Union gives its own maritime safety legislation and there are such arrangements as Particularly Sensitive Sea Areas. When comparing the current maritime safety policy system as whole with the criteria of effective policies, it can be concluded that in many respects the current system is effective but the greatest problems are in implementation and in cost-effectiveness. The nation-state based implementation system is not functioning properly and the existence of the flags of convenience is the clearest sign of that. Cost-effectiveness of policies is hard to calculate, both of single policies and of the policies in comparison with each other. This is the area which needs further research and better methods. Maritime safety regulation is mostly regulatory and probably economic instruments could be used more. Also third parties, for example shippers, insurers or auditors, are an unused resource in the promotion of maritime safety. However, there are some inherent problems in the system: flag state based implementation, the difficulty of making truly global and effective regulation which can react fast to needs of change, and the problems of safety culture in the shipping industry. Before these problems are solved, the major improvements of maritime safety cannot be expected to happen and ultimately single policies will only be band-aid solutions to the problem not interfering in the actual causes of bleeding.

Acknowledgements

This paper was produced as part of the project "SAFGOF – Evaluation of the traffic increase in the Gulf of Finland during the years 2007-2015 and the effect of the increase on the environment and traffic chain activities". The authors wish to acknowledge the financers of the project: the European Regional Development Fund, the Regional Council of Kymenlaakso, the City of Kotka, the Kotka-Hamina Regional Development Company Cursor, Kotka Maritime Research Centre and the companies of Kotka Maritime Research Centre corporate group.

References:

Bennett, P. (2000). Environmental governance and private actors: Enrolling insurers in international maritime regulation. Political Geography, 19 (2000), 875-899.

Ekroos, A., Kumpula, A., Kuusiniemi, K., Vihervuori, P. (2002). Ympäristöoikeuden pääpiirteet. WSOY Lakitieto, Vantaa, Finland.

Goss, R. (2008). Social responsibility in shipping. Marine Policy, 32 (2008), 142-146.

Goulielmos, A. M. (2001). Maritime safety: facts and proposals for the European OPA. Disaster Prevention and Management, Vol. 10, No. 4, 278-285.

Greiner, R., Young, M.D., McDonald, A.D., Brooks, M. (2000). Incentive instruments for the sustainable use of marine resources. Ocean & Coastal Management, 43 (2000), 29-50.

Hetherington, C., Flin, R., Mearns, K. (2006). Safety in shipping: The human element. Journal of Safety Research, 37 (2006), 401-411.

Hänninen, H. (2007). Negotiated risks - the Estonia accident and the stream of bow visor failures in the Baltic ferry traffic. Doctoral Thesis. Helsinki School of Economics A-300.

Hänninen, M. (2008). Analysis of human and organizational factors in marine traffic risk modeling – literature review. TKK-AM-4. Available at: http://www.merikotka.fi/safgof/Hanninen_2008_Analysis.pdf.

Kaps, H. (2004). Quality shipping – Incentives, disincentives. WMU Journal of Maritime Affairs, Vol. 3, No. 1, 85-97.

Karvonen, T., Keltaniemi A., Sundberg, P., Tikkanen, R., Nyman, T., Porthin, M., Sonninen, S., Honka, H. (2006). Merenkulun turvallisuuden hallinta [Control of maritime safety]. Merenkulkulaitoksen julkaisuja 6/2006. Available at: http://portal.fma.fi/portal/page/portal/fma_fi/tietopalvelut/julkaisut/julkaisusarjat/2006/Merenkulun_turvallisuuden_hallinta_6_2006.pdf

Klemmensen, B., Pedersen, S., Dirkinck-Holmfeld, K., Marklund, A., Rydén, L. (2007). Environmental policy – Legal and economic instruments. The Baltic University Press, Uppsala, Sweden.

Knapp, S. & Franses, P. H. (2009). Does ratification matter and do major conventions improve safety and decrease pollution in shipping. Marine Policy, 33 (2009), 826-846.

Lappalainen, J. (2008). Transforming maritime safety culture – evaluation of the impacts of the ISM Code on maritime safety culture in Finland. Publications from the Centre for Maritime Studies University of Turku A46 2008. Available at: http://www.merikotka.fi/metku/Lappalainen_2008_transforming_maritime_safety_culture_v2.pdf

Luoma, E. (2009). Oil spills and safety legislation. The Centre for Maritime Studies, University of Turku. Available at: http://www.merikotka.fi/julkaisut/Luoma_2009_Oil_spills_2.pdf

Mickwitz, P., Hyvättinen, H., Kivimaa, P. (2008). The role of policy instruments in the innovation and diffusion of environmentally friendlier technologies: popular claims versus case study experiences. Journal of Cleaner Production, 16S1 (2008), S162-S170.

Ministry of Transport and Communications (2009). Ohjelma Itämeren meriturvallisuuden parantamiseksi: Työryhmän taustaraportti [Baltic Sea Maritime Safety Programme]. Liikenne- ja viestintäministeriön julkaisuja 13/2009. Available at: http://www.lvm.fi/c/document_library/get_file?folderId=339549&name=DLFE-7220.pdf&title=Julkaisuja%2013-2009

Mäkinen, A. (2008). More maritime safety for the Baltic Sea – what are the options? Baltic Rim Economies – Bimonthly Review 3/2008. Available at: http://www.tse.fi/FI/yksikot/erillislaitokset/pei/Documents/bre2008/3_2008_BRE.pdf

Pallis, A.A. (2006). Institutional dynamism in EU policy-making: The evolution of the EU maritime safety policy. European Integration, Vol. 28, No. 2, 137-157.

Roberts, J. (2007). Marine environment protection and biodiversity conservation: The application and future development of the IMO's particularly sensitive sea area concept. Springer, Berlin, Germany.

Roe, M. S. (2008). Safety, security, the environment and shipping: The problem of making effective policies. WMU Journal of Maritime Affairs, Vol. 7, No.1, 263-279.

Roe, M. (2009). Multi-level and polycentric governance: Effective policymaking for shipping. Maritime Policy & Management, 36, No. 1, 39-56.

Stopford, M. (2009). Maritime Economics. 3rd edition, Routledge, London, UK.

Trucco, P., Cagno, E., Ruggeri, F., Grande, O. (2008). A Bayesian Belief Network modeling of organizational factors in risk analysis: A Case study in maritime transportation. Reliability Engineering and System Safety, 93 (2008), 823-834.

Uggla, Y. (2007). Environmental protection and the freedom of the high seas: The Baltic Sea as a PSSA from a Swedish perspective. Marine Policy, 31, 251-257.

Vieira, J., Moura, F., Viegas, J.M. (2007). Transport policy and environmental impacts: The importance of multi-instrumentality in policy integration. Transport Policy, 14 (2007), 421-432.

Walker, W.E. (2000). POLSSS: Overview and cost-effectiveness analysis. Safety Science, 35 (2000), 105-121.